DURBAN UNIVERSITY OF TECHNOLOGY
INYUVESI YASETHEKWINI YEZOBUCHWEPHESHE

Exploring phenolics against penicillin-binding proteins as druggable targets in antibacterial therapy: a structure-activity relationship study

Jamiu Olaseni Aribisala
22175731

Submitted in fulfilment of the requirements for the degree of Doctor of Philosophy (PhD) in Biotechnology in the Department of Biotechnology and Food Science, Faculty of Applied Sciences, Durban University of Technology, Durban, South Africa

Supervisor: Prof. S. Sabiu
Co-supervisor: Dr. T.R. Makhanya

August 2024

DECLARATION

I, Jamiu Olaseni Aribisala herby declare that this thesis entitled "Exploring phenolics against penicillin-binding proteins as druggable targets in antibacterial therapy: a structure-activity relationship study" submitted for the Doctoral Degree in Biotechnology in the Department of Biotechnology and Food Science, Faculty of Applied Science, Durban University of Technology, Durban, South Africa, has not been submitted in any form to any other academic institution. The study present original work by the author and all sources used or cited have been duly acknowledged. The research work described in the thesis was carried out in the Department of Biotechnology and Food Science, Durban University of Technology, Durban, South Africa, under the supervision of Prof. S. Sabiu and Dr. T.R. Makhanya.

_____
Student's Signature

As the candidate's supervisor we agree to the submission of this thesis _____
Supervisor's Signature

Co-Supervisor's Signature

DEDICATION

To almighty Allah, for his goodness his mercies
To my parents, Mr and Mrs Aribisala
To my wife and jewel, Sikirat Aribisala
To my kids, Mr Khalid Aribisala and Mr Faiz Aribisala
To my siblings, Mrs Fausat Oyelakin, Mr Rasheed Aribisala and Mr Tomide Aribisala

ACKNOWLEDGEMENTS

My genuine and sincere acknowledgement to:

The Almighty Allah (SWT), for the gift of life and the Grace and Mercy of seeing me through this program.

My Supervisor (Prof. Saheed Sabiu), for his advice, open-mindedness, fatherly, supervisory and mentorship role right from the time he accepted to be my supervisor until the end of my Ph.D. study. His ardent enthusiasm and ability to foresee and provide solutions to problems even before they exist enabled the aim and objectives of my project to be easily attained. Many thanks for being a wonderful and visionary leader; I shall forever be thankful for the newfound optimism and passion you instilled in me during my program. My prayers are for uncommon breakthroughs in both your personal and professional lives, Prof.

My co-supervisor (Dr. T.R. Makhanya) for providing scholarly and professional expertise during the retrosynthesis and synthesis of my compound. Without his assistance and dedicated involvement, this aspect of my work would have been a bottleneck. Many thanks, Dr.

Dr. C. Pillay, for her suggestions and contribution toward the success of my project.

Dr. T. Ghazi and Prof. A. Chuturgoon of the Department of Medical Biochemistry, University of Kwa-Zulu Natal, for arranging the use of a fluorescence plate reader for the quantification of reactive oxygen species (ROS) in my project. Many thanks.

The entire members of the Computational and Systems Biology Research Group, Durban University of Technology, for your advice, suggestions and contribution towards the success of my project.

The lab technicians (Dr. Adash and Mr Melvin), the lab assistants, the cleaners, postdoctoral fellows (Dr. S. Karishma, Dr. C. Aruwa, Dr. Balogun and Dr. Y. Babalola) and my fellow students (Oga Dayo, Hajia Rukayat, Sister Betty, Athika, Ayesha, Grace, Hajia Halimah, Vivian, Nosipho, Dweba, Aunty Dunni, Pastor Abayomi and Kingstone) in the Department, whose contribution I cannot overestimate.

The Durban University of Technology for providing a conducive environment to carry out research and the entire staff members of the Department of Biotechnology and Food Science, Durban University of Technology, South Africa.

The National Research Foundation (NRF) for the NRF− TWAS Doctoral Scholarship given to me during my program.

My parents, Mr and Mrs Aribisala, for always being there right from the beginning. Your good upbringing, guidance, and teaching are of great importance in my life today. My prayers are that almighty Allah, keep you safe for me and my siblings in good health and wealth to enjoy the fruits of your labour to the fullest, in shaa Allah Amin.

My siblings, Fausat Bukola Oyelakin, Rasheed Aribisala, and Tomide Aribisala, your prayers and moral support during my program are duly appreciated.

My Jewel and wife, Sikirat Omotola Aribisala, the sacrifices of being away during the program is greatly appreciated. Your love, perseverance, care, prayer, understanding and encouragement

are greatly valued and will never be forgotten. May we live together till old age in good health, wealth and success Amin.

My beloved Khalid Aribisala and Faiz Aribisala, may you grow in knowledge and be a blessing to your parents and the society in shaa Allah. Thanks for your sacrifices; daddy loves you so much.

The Federal University of Technology Akure, Nigeria, for the study leave with pay granted to me during my program. Thank you for the opportunity to strengthen and add value to my future academic endeavours.

RESEARCH OUTPUTS

PUBLICATIONS: JOURNAL ARTICLES AND BOOK CHAPTERS

The following publications are directly related to the project:

Aribisala, J.O., Aruwa, C.E. and Sabiu, S. "Progressive approach of phenolic acids toward the advancement of antimicrobial drugs." Advancement of phenolic acids in drug discovery: Fundamentals and applications, edited by Kumar, N., Goel, N. and Gandara, J.S., Academic Press, 2024, 177-210, https://doi.org/10.1016/B978-0-443-18538-0.00004-4.

Aribisala, J.O., S'thebe, N.W. and Sabiu, S. (2024). *In silico* exploration of phenolics as modulators of penicillin binding protein (PBP) 2× of *Streptococcus pneumoniae*. *Scientific Reports*, 14: 8788. https://doi.org/10.1038/s41598-024-59489-3

Aribisala, J.O. and Sabiu, S. (2024). Cheminformatics identification of phenolics as modulators of penicillin-binding protein-3 of *Pseudomonas aeruginosa* towards interventive antibacterial therapy. *Journal of Biomolecular Structure and Dynamics*, 42: 298-313, https://doi.org/10.1080/07391102.2023.2192808

Aribisala, J.O., Idowu, K., Makhanya, T. R. and Sabiu, S. (2023). Cheminformatics identification of phenolics as modulators of key penicillin−binding proteins of *Escherichia coli* towards interventive antibacterial therapy. *Molecular Simulation*, 49: 1324–1340. https://doi.org/10.1080/08927022.2023.2228423

Aribisala, J.O. and Sabiu, S. (2022). Cheminformatics identification of phenolics as modulators of penicillin−binding protein 2a of *Staphylococcus aureus*: A Structure–Activity−Relationship−Based Study. *Pharmaceutics*, 14:1818. https://doi.org/10.3390/pharmaceutics14091818

Aribisala, J.O. and Sabiu, S. (2022). Redox impact on bacterial macromolecule: a promising avenue for discovery and development of novel antibacterials. *Biomolecules*, 12: 1545. https://doi.org/10.3390/biom12111545

CONFERENCE ATTENDANCE AND PRESENTATIONS

The following conferences were attended during the study:

Aribisala, J.O. Makhanya, T.R. Sabiu, S. (2024) Silicristin-mediated lethality towards *Staphylococcus aureus:* evidence from oxidative stress contribution and molecular dynamics simulation. Gordon Research Seminar on New Antibacterial Discovery and Development, Ventura Beach Marriott, California, United State of America, 16 - 17, March 2024

Aribisala, J.O. and Sabiu, S. (2022). Computational insights into phenolics as leads against bacterial penicillin-binding protein 3 of *Pseudomonas aeruginosa.* SASBMB 2022 Biochemistry matters congress, South Africa, held on the 23rd to 26th January 2022.

Aribisala, J.O. and Sabiu, S. (2022). Organic derivatives of silicristin elicited potent antibacterial activity against penicillin-binding protein 3 of *Pseudomonas aeruginosa in silico*. ESCMID/ASM Conference on Drug Development. Crowne Plaza hotel, Dublin, Ireland, 4-7 October 2022.

Aribisala, J.O., Yamkela, D. and Sabiu, S. (2021). Computational insight into shikimate pathway-derived phenolics as therapeutic leads against bacterial penicillin-binding protein 3. International Marmara Scientific research and Innovation Congress, Istanbul, Turkey, held from the 21st to 22nd of August 2021

OTHER PUBLICATIONS NOT DIRECTLY RELATED TO THE STUDY

Lukman, H.Y., **Aribisala, J.O**., Akoonjee, A., Sulyman, A.O., Wudil, A.M. and Sabiu, S. (2024). Modulation of dipeptidyl peptidase IV by Rooibos tea metabolites towards type 2 diabetes care: evidence from molecular dynamics simulation and density functional theory. *Scientific African*, 24: e02173. https://doi.org/10.1016/j.sciaf.2024.e02173

Aribisala, J.O., Oyefunke, M.M., Amusa, O.M. and Sabiu. S. "Dietary nutrients, antinutritional factors, and valorization of food waste." Food Science and Technology: Fundamentals and Innovation, edited by Ijabadeniyi, O.A., Berlin, Boston, De Gruyter, 2024, 281-320. https://doi.org/10.1515/9783111013107-011

Murali, M., Ahmed, F., Gowtham, H.G., **Aribisala, J.O**., Abdulsalam, R.A., Shati, A.A., Alfaifi, M.Y., Sayyed, R.Z., Sabiu, S. and Amruthesh, K.N. (2023). Exploration of CviR-mediated quorum sensing inhibitors from *Cladosporium* spp. against *Chromobacterium violaceum* through computational studies. *Scientific Reports*, 13: 15505. https://doi.org/10.1038/s41598-023-42833-4.

Rampadarath, A., **Aribisala, J.O**., Makunga, N.P., Mazibuko-Mbeje, S. and Sabiu, S. (2023). Molecular bioprospection of *Helianthus annuus* L. (sunflower) cypselae for antidiabetic therapeutics through network pharmacology, density functional theory and molecular dynamics simulation, *South African Journal of Botany*,162: 72-95. https://doi.org/10.1016/j.sajb.2023.08.045.

Aribisala, J.O. and Sabiu, S. "Synthetic toxicants and their health implications." Food safety and toxicology: present and future perspectives, edited by Ijabadeniyi, O.A., Walter de Gruyter GmbH and Co KG, 2023, 317.

S'thebe, N.W., **Aribisala, J.O**. and Sabiu, S. (2023). Cheminformatics bioprospection of sunflower seeds' oils against quorum sensing system of *Pseudomonas aeruginosa*. *Antibiotics*, 12: 504. https://doi.org/10.3390/antibiotics12030504.

Abdulsalam, R.A., **Aribisala, J.O.** and Sabiu. S. (2023). Cheminformatics validation of plazomicin and bioprospection of putative modulators of aminoglycoside modifying enzymes from *Gnaphalium affine* towards interventive antibacterial therapy. *Journal of Biological Regulators and Homeostatic Agents*. 37: 6295-6318. https://doi.org/10.23812/j.biol.regul.homeost.agents.20233711.599

Aribisala, J.O., Abdulsalam, R. A., Dweba, Y., Madonsela, K., and Sabiu, S. (2022). Identification of secondary metabolites from *Crescentia cujete* as promising antibacterial therapeutics targeting type 2A topoisomerases through molecular dynamics simulation. *Computers in Biology and Medicine*, 145: 105432. https://doi.org/10.1016/j.compbiomed.2022.

Kaka, M.O., **Aribisala, J.O.**, Karishma, S., Oyebamiji, A.K., Ajayeoba, T.A., Ohanaka, N.J. and Sabiu, S. "Computational Applications in the Drug Discovery and Development Processes." Therapeutic use of plant secondary metabolites, edited by Sabiu, S., Bentham Science, 2022, 365. https://doi.org/10.2174/9789815050622122010018

Aribisala, J.O., Aruwa, C.E., Uthman, T.O., Nurain, I.O., Idowu, K. and Sabiu, S. (2022). Cheminformatics bioprospection of broad-spectrum plant secondary metabolites targeting the spike proteins of omicron variant and wild-type SARS-CoV-2. *Metabolites*, 12: 982. https://doi.org/10.3390/metabo12100982

Balogun, F.O., Naidoo, K., **Aribisala, J.O**., Pillay, C. and Sabiu, S. (2022). Cheminformatics Identification and validation of dipeptidyl peptidase-iv modulators from shikimate pathway-derived phenolic acids towards interventive type-2 diabetes therapy. *Metabolites*, 12: 937. https://doi.org/10.3390/metabo12100937

Aribisala, J. O., Nkosi, S., Idowu, K., Nurain, I. O., Gaositwe, M. M., Shode, F. O., and Sabiu, S. (2021). Astaxanthin-mediated bacterial lethality: evidence from Oxidative Stress contribution and molecular dynamics simulation. *Oxidative Medicine and Cellular Longevity*, 2021: 7159652. **https://doi.org/10.1155/2021/7159652**

MANUSCRIPT SUBMITTED FOR PUBLICATION

Aribisala, J.O. and Sabiu, S. Beta-lactam resistance in pathogenic bacteria mediated through modifications in Penicillin-Binding Proteins (PBPs) (submitted to Current Pharmacology Reports for review and subsequent publication)

AWARDS AND RECOGNITION DURING THE PROGRAM

Durban University of Technology, 2022 Envision 2030 Institutional Award for Top Doctoral Student (Platinum Category)

GENERAL ABSTRACT

Alterations in penicillin binding proteins (PBPs) coupled with inactivation of beta-lactam scaffold by beta-lactamase remain the major basis for the broad clinical resistance to beta–lactam antibiotics. While enzyme modification is most common with Gram-negative bacteria, alteration in key PBPs is prevalent in Gram-positive organisms and increasingly being reported in Gram-negative bacteria. Modification of PBPs ensures that the interaction with beta-lactams occurs at a considerably higher antibiotic doses than with PBPs from susceptible strains, thus substantially reducing biological activity. Consequently, developing potent therapeutics with a different scaffold against PBP druggable targets represents a viable alternative strategy against resistance to beta-lactams. Phenolics, aside having a different scaffold from conventional beta-lactams, have been reported to be effective against various multidrug-resistant Gram-negative and Gram-positive bacteria. The characteristic hydroxyl group of phenolics are implicated in strong PBPs binding while having the capability to auto-oxidize in the presence of transition metals to generating reactive oxygen species (ROS) which have been implicated in the lethality of most conventional antibiotics, including beta-lactams. These intriguing characteristics of phenolics position them as a viable source of drug candidates that can be developed as alternative beta-lactams. Hence, this study employed a multifaceted *in silico* and *in vitro* approach in bioprespection for phenolics as modulators of PBPs and ROS in an effort to manage resistance to beta-lactams due to PBP modifications.

Using a structure-based drug design (SBDD) approach involving the use of pharmacophore screening and molecular docking, the over 10,000 currently known phenolics were screened at the active site of key PBPs of common and clinically important Gram-positive (*Staphylococcus aureus* and *Streptococcus pneumoniae*) and Gram-negative (*Escherichia coli* and *Pseudomonas aeruginosa*) bacteria. The identified top-20 phenolics against each of the investigated key PBPs (PBP2a of *S. aureus*, PBP2x of *S. pneumoniae*, PBP3 of *P. aeruginosa* and PBP3 and 5 of *E. coli*) had higher negative docking scores relative to the four beta-lactams (amoxicillin, cefotaxime, aztreonam and doripenem) reference standards suggesting effectiveness of the adopted SBDD approach. Subsequent filtering of the top-20 leads in each case based on their physicochemical, pharmacokinetic and toxicological profiles afforded top-five phenolics that are chemically diverse, orally bioavailable and with good synthetic feasibility scores (<5) appropriate for drug development. The profiled top-five compounds against the key PBPs in each case were further subjected to 120-ns molecular dynamic (MD) simulations using the in-house HEAL1361 programme with Amber 18 package of the CHPC (Centre for High Performance Computing), South Africa. The identified lead phenolics with the highest negative binding free energy (ΔG_{bind}) in each case of the essential PBPs, which include silicristin (PBP2a active site: −25.61 kcal/mol and PBP2x allosteric site: -50.54 kcal/mol), epicatechin gallate (PBP2a allosteric site: −47.65 kcal/mol), lysidicichin (PBP3 of *E. coli*: −41.66 kcal/mol), epigallocatechin 4-benzylthioether (PBP5 of *E. coli* −38.97 kcal/mol), catechin 3-rhamside (PBP3 of *P. aeruginosa*: -28.99 kcal/mol), and epicatechin 3-O-(3-O-methylgallate (PBP2x active site: -42.18 Kcal/mol), all had higher negative binding free energy than the reference standards. Except for silicristin with lesser stability [higher root means square deviation (RMSD)] against three of the essential PBPs [PBP2a (5.65 Å) of *S. aureus*, PBP3 (3.97 Å) of *E. coli* and PBP2x (4.90 Å), of *S. pneumoniae*], all the lead phenolics had better stability (< 3 Å), compactness and flexibility relative to the referenced standards and other top-five phenolics in each case of the investigated PBPs. However, silicrsitin remain the only lead phenolics with broad spectrum ΔG_{bind} for all the essential PBPs, suggesting that the lesser stability of the compound with three of the essential PBPs could be improved to enhance stability. Moreso, as the focus of this study is to identify lead phenolic with wide spectrum activity against the investigated bacteria. Thus, for subsequent analysis, silicristin was selected

for structural optimization against the essential PBPs for the possibility of yielding novel drug candidates with improved antibacterial efficiency, higher stability, reduced toxicity and favorable pharmacokinetic properties relative to silicristin.
Improved thermodynamic stability has been demonstrated to be critical in affinity/potency of a drug for a target and its subsequent efficacy *in vitro* and *in vivo*. This study employed hybridization of pharmacophore and structural simplification techniques in the enhancement of thermodynamic stability of silicristin against the key PBPs of the investigated bacteria. The knowledge of the interactions of silicristin with the key PBPs of the organisms was employed in designing 25 novel derivatives of chalcone bis-coumarin from easily synthesizable starting materials of coumarin moieties. Following molecular docking, pharmacokinetic screening, MD simulation and energy refinement of the 25 derivatives, RD2c (PBP3 of *E. coli*: -46.26 kcal/mol), RD1c (PBP3 of *P. aeruginosa*: -39.42 kcal/mol and PBP2x active site: -42.90 kcal/mol), RD1a (PBP2a active site: -37.56 kcal/mol), D1a (PBP5 of *E. coli*: -37.19 kcal/mol), D1h (allosteric site of PBP2a: -53.09 kcal/mol and PBP2x of *S. pneumoniae*:-38.53 kcal/mol), were identified as best derivatives with enhanced ΔG_{bind}, stability, and pharmacokinetics properties relative to silicristin. Quantum calculations using DFT B3LYP/6-31G+ (dp) techniques further showed that these derivatives are more reactive and with higher ability to form hydrogen bonds due to their higher electrostatic potential compared to silicristin. Except for PBP2x, this observation is consistent with the bond analysis of each complex post-MD simulation as the best derivative in each case of the PBP formed higher number of hydrogen bonds compared to silicristin. The exploration of catechol, resorcinol, and hydroquinone either alone or in combination with each other at either end of the derivatives promotes good pharmacological properties, while the presence of a pyrogallol and/or a benzene ring with more than two hydroxy group at one or both ends of the derivatives caused reduced oral bioavailability relative to silicristin. The synthetic accessibility of the derivatives was exploited by synthesizing the parent compound of the best derivative using Knoevenagel condensation, Vilsmeiers Haack, and Aldol condensation reactions. The successfully synthesized parent compound was subjected to nuclear magnetic resonance (NMR) for structural elucidation and was further validated using the gauge independent atomic orbital (GIAO) method. Expectedly, significant improvement in binding capacity and pharmacokinetic properties was observed with the best derivatives relative to silicristin; an observation that could translate to enhanced potency *in vitro* and *in vivo.*

Silicristin is one of the bioactive compounds of silymarin, a standardized extract from the dried seeds of milk thistle which has been shown for its PBP modulatory properties *in silico*. Thus, to understand the mechanism of action of silicristin *in vitro*, this study investigates the antibacterial properties of silicristin and the synthesized parent compounds of the best derivatives of chalcone bis coumarin (PSCB) derived from silicristin against sensitive and resistant strains of Gram-positive (*S. aureus* and *S. pneumoniae*) and Gram-negative bacteria (*E. coli* and *P. aeruginosa*). Also, the possible involvement of ROS in the lethality of silicristin, PSCB and reference beta-lactams (amoxicillin against Gram-positive organisms and cefotaxime against Gram-negative bacteria) was also investigated. The minimum inhibitory concentration (MIC) assessment showed that silicristin, PSCB and reference beta-lactams had higher MIC values against the resistant strains [cefotaxime (2 – 16 µg/mL), amoxicillin (4 – 32 µg/mL, silicristin (8 – 64 µg/mL) and PSCB (16 – 128 µg/mL)]. The highest MIC for silicristin, PSCB and reference beta-lactams was observed against the resistant and sensitive strains of *P. aeruginosa* [sensitive strains (8 – 64 µg/mL), resistant strains (16 – 128 µg/mL)], while the lowest MIC was found in *S. pneumoniae* [sensitive strains (0.5 – 8 µg/mL), resistant strains (2 – 16 µg/mL)]. Compared to silicristin (4 – 64 µg/mL), PSCB (8 – 128 µg/mL) exhibited higher MIC values against all the test strains and the antibacterial activities were

observed to occur in a concentration- and time-dependent manner. Except against the sensitive and resistant strains of *E. coli* where silicristin had a comparable killing effect as cefotaxime, silicristin had a better killing rate than PSCB and reference standards against all the test organisms with the best effect observed between 8 – 14 h after treatment. Except for the exploration of silicristin and amoxicillin against the resistant strain of *E. coli*, which was found to be addictive, the combinatorial therapy showed that silicristin had a synergistic effect with both amoxicillin and cefotaxime against all test organisms. This could mean that silicristin had other mechanism of antibacterial effect different from beta-lactams. In contrast, PSCB with cefotaxime and amoxicillin had only synergistic effects against resistant strains of Gram-positive organisms suggestive of a similar mechanism of action for PSCB and the test beta-lactams. A further probe into the ROS generating potential of the antibacterial agents using ROS-specific dyes, showed that while PSCB and reference beta-lactams caused significant ($P < 0.05$) higher generation of superoxide ion ($O_2^{\bullet-}$), silicristin conversely enhanced higher ($P < 0.05$) generation of the most toxic ROS form, the hydroxy radicals ($^{\bullet}OH$), which is often produced via the Fenton reaction. This observation with silicristin suggests its enhanced modulatory effect on Fenton reaction relative to PSCB and the standards and further facilitated increased NAD/NADH ratio, ADP/ATP ratio, lipid peroxidation, carbonyl content, propidium iodide (PI) uptake, and depletion of reduced glutathione as observed with silicristin-treated cells. This observation points to the enhanced involvement of oxidative stress in the modulatory effect of silicristin against all the test organisms compared to PSCB and the reference standards. This enhanced oxidative stress in silicristin-treated cells was substantiated with scanning electron microscopy (SEM) and transmission electron microscopy (TEM) micrographs with cell walls with more blisters, eruptions, and sores compared to the observed effects with other treatments and the untreated cells. Oxidative stress was also noted to facilitate SOS (Save Our Souls) response in upregulating *SordA* and *SoxR*, with the most prominent effect observed with silicristin in a manner that is more evident in the sensitive strains relative to the resistant strains. Taken together, these observations points to the enhanced redox effect of silicristin on the sensitive and resistant strains of both Gram-positive and Gram-negative organisms relative to PSCB and reference beta-lactams and could be explored to develop novel alternative therapeutics to beta-lactams in the treatment of infections caused by the test organisms. Additionally, since the best derivative in each case of the essential PBPs had a similar synthetic route as PSCB, it is recommended that the synthetic route be adopted in the synthesis of the best derivatives to enable the investigation of their *in vitro* and *in vivo* antibacterial activities for the possibility of subsequent development as beta-lactams.

Keywords: Antibiotic resistant; Beta-lactams; Cell wall; Molecular docking; Molecular dynamic simulation; Oxidative stress; Penicillin-binding protein; Phenolics; Reactive oxygen species; Silicristin

TABLE OF CONTENT

DECLARATION.....**i**

DEDICATION.....**ii**

ACKNOWLEDGMENTS……..**iii**

RESEARCH OUTPUTS.....**v**

GENERAL ABSTRACT.....**viii**

CHAPTER ONE

1.0 General Introduction 1

1.1 Introduction ……..**2**

1.2 Research problem and justification ……**19**

1.3 Aim and objectives ……..**20**

1.4 Structure of the thesis……...**21**

References……..**22**

CHAPTER TWO

2.0 Literature Review.....34

2.1 Introduction ……**35**

2.2 Beta-lactam resistance in pathogenic bacteria mediated through modifications in Penicillin-binding proteins (PBPs)…….**38**

2.3 Progressive approach of phenolic acids towards the advancement of antimicrobial drug……**63**

2.4 Redox Impact on bacterial macromolecule: a promising avenue for discovery and development of novel antibacterials……...**98**

References……....**125**

CHAPTER THREE

3.0 Identification of lead phenolic compounds against penicillin binding proteins (PBPs) druggable targets of common and clinically significant pathogenic bacteria using computational methods…….....128

3.1 Cheminformatics identification of phenolics as modulators of key penicillin−binding proteins of *Escherichia coli* towards interventive antibacterial therapy **…….129**

3.2 Cheminformatics identification of phenolics as modulators of penicillin-binding protein-3 of *Pseudomonas aeruginosa* towards interventive antibacterial therapy **……147**

3.3 *In silico* exploration of phenolics as modulators of penicillin binding protein (PBP) 2x of *Streptococcus pneumoniae* towards interventive antibacterial therapy…….....**164**

3.4 Cheminformatic identification of phenolics as modulators of penicillin-binding protein 2a of *Staphylococcus aureus*: a structure–activity-relationship-based study **…….186**

CHAPTER FOUR

4.0 Retrosynthesis and derivatization of lead phenolics and evaluation of their enhanced druggability relative to the parent compounds using *in silico* methods.....212

4.1 Structural optimization of silicristin against key penicillin-binding proteins of selected clinically important bacteria yielded putatively potent chalcone bis-coumarin derivatives……..**213**

CHAPTER FIVE

5.0 *In vitro* evaluation of the antibacterial activity and reactive oxygen species (ROS) involvement in lead compound and its derivative against common and clinically significant pathogens ……323

5.1 Silicristin and parent structure of novel derivatives of chalcone bis coumarin modulate Fenton reaction and facilitate membrane damage in Gram-positive and Gram-negative organisms……**324**

CHAPTER SIX

6.0 General discussion, conclusions and recommendations……..437

6.1 General discussion……**438**

6.2 Conclusion and recommendation …….**450**

References……...**455**

CHAPTER ONE

1.0 General Introduction

1.1 Introduction …….**2**

1.2 Research problem and justification ……**19**

1.3 Aim and objectives …….**20**

1.4 Structure of the thesis……..**21**

References…….**.....22**

1.1 Introduction

Antibiotic resistance is one of the most pressing public health challenges of the 21st century, posing a threat to efficient prevention and treatment of the ever-increasing infections caused by several microorganisms (Al-Orphaly *et al*., 2021, Howard *et al*., 2013). Antibiotic resistance in bacteria makes the problem even more significant as the bacteria implicated in common infections have gained resistance to each new antibiotic introduced into the drug market over several decades, to varying degrees resulting in high mortality (Nelson *et al*., 2017). Annually, an estimated 700,000 deaths are attributable to infections caused by multidrug-resistant microorganisms (MRM), and this figure is expected to rise to 10 million by 2050, if no effective therapeutic alternatives are discovered (WHO, 2019). Hence, rapid effort is required in developing novel antibacterial therapeutics with different mode of actions against infections caused by MRM.

Generally, infections caused by MRM have become particularly challenging in the developing countries. These infections are associated with high morbidity and mortality, accounting for over 45% of death and protracted hospital stay in Africa (Al-Orphaly *et al*., 2021; Magiorakos *et al*., 2012). For instance, *Enterobacteriaceae* including *Esherichia coli* (38% prevalence) and non-lactose fermenting bacteria such as *Pseudomonas aeruginosa* (with a >50% prevalence rate in hospitalized patients) (Al-Orphaly *et al*., 2021; Kibret and Abera, 2011) have been identified as major multi-drug resistant Gram-negative bacteria in Africa (Nelson *et al*., 2017). On the other hand, *Staphylococcus aureus*, with 72%, 52% and 29.6% prevalence in Cameroon, South Africa and Nigeria, respectively, remains the most common Gram-positive MRM causing hospital acquired infections in both healthy subjects and individuals with underlying health conditions (Gulumbe and Faggo, 2019), while *Streptococcus pneumoniae* with a prevalence of 7.0% in Africa (Aliberti *et al*., 2019), is accountable for many community-

acquired infections, including pulmonary infection, meningitis, sinusitis, and pneumonia (Nelson *et al*., 2017).

Of the different classes of antibiotics, the beta-lactams [monobactams, various derivatives of penicillin (e.g., ampicillin), carbapenems and cephalosporins in multiple spectra (Palacios *et al*., 2020; Hecker *et al*., 2015)] are very important in the treatment of several bacterial infections gulping a worldwide annual expenditure of approximately 15 billion USD which makes up 65% of the total antibiotics market (Eiamphungporn *et al*., 2018). Of the various classes of antibiotics, resistance to beta-lactams, the most frequently administered antibiotics because of their minimal side effects, remains a growing challenge (Klein *et al*., 2021; Palacios *et al*., 2020). Studies have shown reduced sensitivity or outright resistance of several bacteria to beta-lactams (Khalifa *et al*., 2021, Wu *et al*., 2021, Baker *et al*., 2015). For instance, a recent study by Wu *et al*. (2021), showed that *E. coli* had 85%, 65%, and 60% resistance to amoxicillin, cefuroxime, and cefatriaxone, respectively due to drug overprescription/overuse. Another study by Khalifa *et al*. (2021), reported that a significant 93.8% of *E. coli* isolate from clinical settings showed an elevated resistance to beta-lactam antibiotics. Hence, the development of novel therapeutic strategies against such resistance is imperative. Beta-lactam antibiotics bind and interact with the penicillin- binding proteins (PBPs) of bacteria which are essential for bacterial cell wall synthesis (Meroueh *et al*., 2003). Bacteria have a variety of PBPs (PBP1a, PBP1b, PBP2a, PBP2b, PBP2x, PBP3 PBP4 and PBP5) with molecular mass varying between 120,000 and 40,000 daltons (Zapun *et al*., 2008). The peptidase activity of PBPs is facilitated by a common penicillin-binding domain (PBD), which binds beta-lactam antibiotics (Meroueh *et al*., 2003). The PBD of PBPs functions as transpeptidases, which catalyze the last stage of cell wall production by connecting a pair of peptidoglycans (Josephine *et al*., 2006). However, inactivation of beta-lactam ring structure of beta-lactams by beta-lactamase coupled with PBPs modifications caused by multiple mutations are the major cause

of the widespread clinical resistance to beta-lactams (Alekshun and Levy, 2007; Lambert, 2005). Specifically, alteration to the PBD of PBP2a has been shown to be the basis for the broad clinical resistance to beta-lactam antibiotics in *S. aureus* (Farrell *et al*., 2014; Otero *et al*., 2013), while alterations of PBP3 in *E. coli and P. aeruginosa* as well as multiple mutation of PBP2x of *S. pneumoniae* have been shown to be critical to resistance of these organism to beta-lactams (Chowdhury *et al*., 2012; Kosowska-Shick *et al*., 2010). Consequently, PBP2a in *S. aureus*, PBP3 in *E. coli* and *P. aeruginosa* and PBP2x in *S. pneumoniae* have been identified as possible drug targets and developing novel therapeutics with different scaffold and mode of action against them could represent a viable alternative strategy against resistance to beta-lactam antibiotics. Aside the principal mechanisms of action of beta-lactams which involve prevention of cell wall synthesis, investigations have demonstrated that beta-lactams, like fluoroquinolones and aminoglycosides could instigate bacteria killing via reactive oxygen species (ROS) generation (Dwyer *et al*., 2007; 2014). While these antibiotics share different primary mechanisms of action, their secondary mechanism of action through ROS generation, is similar. This approach has historically been applied in disinfectants and antiseptics but has not been widely employed in therapeutics due to its perceived toxicity and unacceptable harm to host tissue (Lam *et al*., 2020; Vatansever *et al*., 2013). However, growing evidence of ROS function in therapeutic lethality has been strengthened in recent times allowing their therapeutic application in topical and systemic infections to be investigated (Aribisala and Sabiu, 2021; Dryden, 2018).

1.1.1 Involvement of reactive oxygen species (ROS) in the antibacterial lethality of antibiotics

Oxygen is very crucial for the survival of living organisms and forms the basis of cellular respiration which brings about aerobic respiration (Alvarado and Arce, 2016). However, oxygen in the form of free radicals acts as a substance or molecule which causes oxidative

stress (Fanjul-moles and López-Riquelme, 2016). Oxidative stress is a pathophysiological condition resulting from the imbalance between free radical generation and the antioxidant defence systems of the body (Alvarado and Arce, 2016). Classes of antibiotics such as beta-lactams, fluoroquinolones and aminoglycosides induce cell death by interfering with their primary targets and increasing the tricarboxylic acid (TCA) cycle and the electron transport chain (ETC) activities of the organisms, leading to superoxide anion radical and hydrogen peroxide generation which contributes to cellular damage and death (Dwyer *et al*., 2007). In establishing the importance of TCA and ETC in ROS mediated bacterial killing, studies have employed several indirect methods of monitoring oxidative stress biomarkers such as evaluating the increased cellular level of the reducing equivalents NAD^+/NADH fuelling the ETC and cellular contents of ADP/ATP ratio translating to high energy production which all signals increased ETC activity following treatment with antibacterial agents (Wang *et al*., 2010). Using this type of evaluation in substantiating antibiotic ROS mediated bacterial killing has been demonstrated to be problematic as some studies have even suggested that ROS production in antibiotics treatment is an epiphenomenon of the death process and not a causal contributor to drug lethality (Liu and Imlay, 2013). However, Imlay (2013) subsequently lent credence to the concept of antibiotics-mediated ROS bacterial killing through expression of genes identified to be most sensitive to oxidative stress and reported that *SoxR*S and *OxyR* were induced by superoxide ions and hydrogen peroxide (H_2O_2), respectively, following antibiotics treatment. Furthermore, Dwyer *et al*. (2014) used a set of broad high-throughput ROS quantification methods involving diverse panels of independent and specific fluorescent reporter dyes for different arrays of ROS to demonstrate that ROS generated by antibiotics treatment contributed directly to bacterial lethality. If bactericidal antibiotics potentiate ROS-mediated cellular damage as part of their lethality action, it would then be anticipated that oxidative damage to macromolecules such as nucleic acids, protein and lipid would be the most

susceptible to oxidative stress during drug treatment. Although, superoxide ion and H_2O_2 do not directly cause oxidative damage to macromolecules, Fenton chemistry does, through the formation of highly reactive hydroxyl radicals (Dwyer *et al*., 2014) and conditions such as treatments under an aerobic condition and in the presence of glutathione, a natural antioxidant known to protect bacteria cells from a variety of biological stresses have been demonstrated to inhibit Fenton reaction and protect bacteria cells from death induced by antibiotics (Dwyer *et al*., 2014). This unique mechanism of action of ROS is now finding practical application as therapeutics. For example, Surgihoney, is a modified wound-healing honey manufactured in the UK by the Healing Honey International whose potent antibacterial effects is attributed to high level of H_2O_2 generation as its main mechanism of action (Lam *et al*., 2020). Polymyxin B is a peptide-based antibacterial agent which has been shown to derives its potency against Gram-negative bacteria such as *P. aeruginosa* via the accumulation of hydroxyl radicals (Chua *et al*., 2015). Similarly, nitrofurantoin is a drug whose mode of activities has been unclear since it was discovered in the 1940s (Barber *et al*., 2013). However, recent studies have shown that the continuous relevance, effectiveness, and minimal resistance of organisms to nitrofurantoin might be due to its main mechanism of action which involve ROS generation via redox cycling (Vaishampayan *et al*., 2022, Aribisala *et al*., 2021). Hence, an advantage of ROS-inducing antimicrobial agents may be that they are less susceptible to antibacterial resistance and therefore further exploration of more potent ROS-producing antibacterial agents might help in the fight against antibacterial resistant. Interestingly, ROS generation have been reported in the bactericidal lethality of several natural products and plant secondary metabolites including phenolics (Vaishampayan *et al*., 2022, Aribisala *et al*., 2021; Yang *et al*., 2019; Ajiboye *et al*., 2016), and this is presenting an avenue for the discovery of novel drug candidates.

1.1.2 Phenolics as antimicrobial agents

Although, the use of some plant metabolites has been suggested to promote bacterial mutagenicity and cause deleterious effects to humans at high concentrations (Galati *et al*., 2002), evidence suggesting their safety and tolerability for treatment at high dosage than most conventional antimicrobials in humans also exist (Charradi *et al*., 2018). Hence, natural products of plant-origin represent an alternative source of less toxic candidates for antimicrobial development that will be readily available. Interestingly, these compounds have been reported to be effective against various multidrug resistant strains of Gram-negative and Gram-positive bacteria (Aldulaimi, 2017, Kyaw *et al*., 2012). Of these compounds, the phenolics have, more importantly been demonstrated to exhibit significant antibacterial activity but the associated mechanisms are not yet fully deciphered, but with existing evidence pointing towards the involvement of many sites of action at the cellular level (Table 1). Phenolics have been demonstrated to modulate bacterial druggable targets (Alhadrami *et al*., 2020), inhibit beta-lactamase (Zhao *et al*., 2002) while also increasing cell membrane permeability for antimicrobial absorption (Table 1). These characteristics potentiate phenolics as a leading source of antimicrobials that can work in synergy with conventional antibiotics, an approach which would not only help in strengthening the potency of existing conventional antibiotics such as the beta-lactam antibiotics but also help shorten the time, cost and high risk of failure associated with developing new drugs. Furthermore, while, the antioxidant potential of phenolics have been well-documented (Panat *et al*., 2016; Dai *et al*., 2006; Weinreb *et al*., 2004), scientific data demonstrating their pro-oxidant activity also exist (Ajiboye *et al*., 2017; Eghbaliferiz and Iranshahi, 2016). In the presence of oxygen and transition metals, phenolic compounds can act as redox cyclers, generating ROS and quinone species (Galati *et al*., 2002). The ROS generated damages the Fe-S (iron-sulphur) cluster in bacterial cells and reacts with ferrous ions to form hydroxyl radicals, which consequently may result in damaging cellular

macromolecules such as carbohydrates, proteins, and DNA in bacterial cell (Yang *et al*., 2019; Kato and Suga, 2018; Ajiboye *et al*., 20116). The quinone species generated on the other hand, might disrupt biological functions of protein through reaction with protein thiols and reverting to its catechol moiety (Figure 1) (Aribisala and Sabiu, 2022). The redox cycling potential of phenolics and their ability to modulate druggable target fit them as a class of compound that can be explored in the discovery of new drugs that would be lethal via ROS generation while having capability to modulate druggable target like PBPs. With over 10000 phenolics currently in existence in literature (Ofosu *et al*., 2020), the screening of lead phenolics with better capability to modulate druggable target might be facilitated using advanced computational techniques for further *in vitro* validation. The combination of these approaches in the identification and evaluation of lead have been demonstrated to reduce the rate of failure in the preclinical and clinical stage of drug development (Ohba *et al*., 2023; Waring *et al*., 2015).

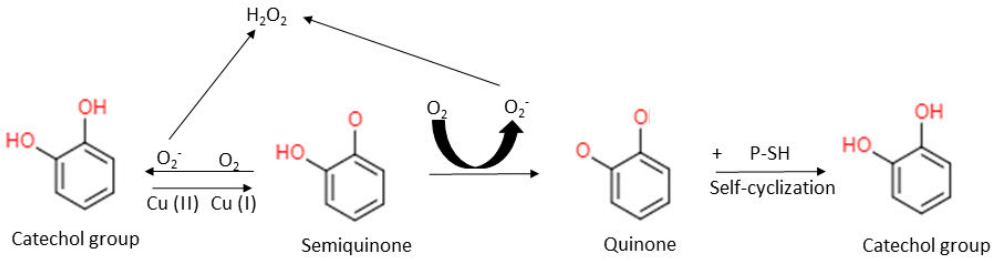
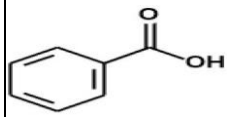
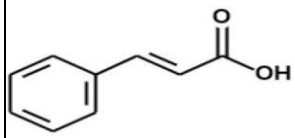
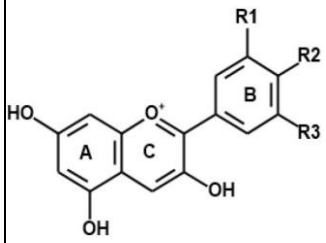
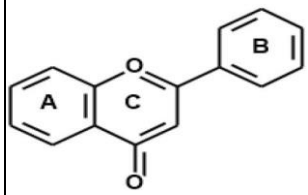


Figure 1: Prooxidant capabilities of phenolics through autooxidation, demonstrating the generation of ROS and quinone in the presence of transition-metals and oxygen, and subsequently transforming into catechol through self-cyclization (Aribisala and Sabiu, 2022).

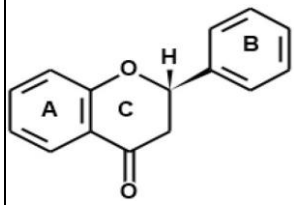
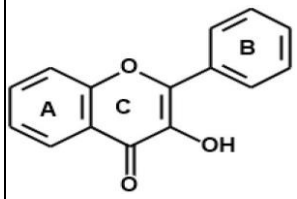
Table 1: Classification of phenolic compounds, their common sources, and reported mechanisms of antibacterial action

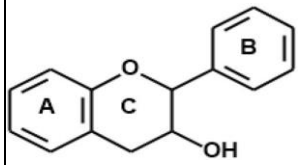
Class name and backbone structure	Examples	Sources	Reported antimicrobial mechanisms of action
1. Phenolic acids Benzoic acid  	Gallic acid Syringic acid Vanillic acid Protocatechuic acid	Fruits, vegetables, and cereals	Garlic acid was demonstrated to have minimum inhibitory concentrations (MIC) ranging between 500 and 2000 µ/mL against *P. aeruginosa, S. aureus, E. coli* and *L. monocytogenes* while implicating increase membrane permeability and linkage of intracellular potassium ion in the antibacterial activity (Borges *et al*., 2013) Ajiboye *et al*. (2017), showed protocatechuic acid to have MIC of between 600 and 800 µ/mL against *P. aeruginosa, S. aureus, and E. coli* while implicating the generation of ROS

			and the subsequent production of malondialdehyde and fragmentation of DNA in such antibacterial activity
 Cinnamic acid	*p*-coumaric acid Caffeic acid Ferulic acid Chlorogenic acid Sinapic acid	Fruits, vegetables, cereals, coffee	Ferulic acid was demonstrated to have minimum inhibitory concentrations (MIC) ranging between 100 and 1250 µ/mL against *P. aeruginosa*, *S. aureus*, *E. coli* and *Listeria monocytogenes* while implicating increase membrane permeability and linkage of intracellular potassium ion in the antibacterial activity (Borges *et al*., 2013) An MIC value ranging from 20 to 80 µ/mL was reported for chlorogenic acid against *S. aureus* 6538, *S. pneumoniae* ATCC49619, *Bacillus subtilis* 9372, *E. coli* ATCC25922, *Shigella dysenteriae* 51302, *and Salmonella typhimurium* 50013 linking the increased in outer membrane permeability

			and the loss of the barrier function in such activity (Lou *et al*., 2011).
2. Flavonoids  Anthocyanin	Cyanidin Pelargonidin Petunidin Malvidin Delphinidin Peonidin	Fruits such as cranberry, vegetables, cereals, red and blue flower petals	Although little or no information exist on the antimicrobial activity of pure anthocyanins, studies on fruit extract rich in anthocyanins showed that the extract had antibacterial effects on broad range of Gram-positive *(L. monocytogenes and E. faecalis*) and Gram-negative (*E. coli*) organism while associating morphological damage and loss of the structural integrity in the antibacterial effect (Wu *et al*., 2008; Lacombe *et al*., 2010)
Flavone  	Luteolin Apigenin Chrysin Baicalein	Alfalfa Indian trumpet flower	Luteolin has been shown to have good antibacterial activity against *B. subtilis, S. aureus, P. fluorescens, L. monocytogenes* and *E. coli.* The antibacterial mechanism of luteolin against *S. aureus* includes inhibition of nucleic acid and protein synthesis, impairment of bacterial cell

			membrane, induction of cell morphological changes and inhibition of biofilm formation (Qian *et al*., 2020; Wang *et al.*, 2010) Apigenin isolated from *Portulaca oleracea L.* was demonstrated to exhibit antibacterial activities against *P. aeruginosa*, *S. typhimurium*, *P. mirabilis*, *Klebsiella pneumoniae* and *Enterobacter aerogenes* at MIC ranging between 11.68 and 19.12 µ/mL (Nayaka *et al*., 2014). Another study by Kim *et al*. (2020) implicated the generation of ROS, damage of cell membrane and depletion of glutathione in the antibacterial activities of apigenin

 Flavanone	Hesperetin Naringenin	Citrus and grapefruit peels	Veiko *et al*. (2023) demonstrated the antibacterial activity of naringenin against *S. aureus* and implicated the disorderliness/damages at the cell membrane level as the main mechanism of action
Flavonol 	Quercetin Kaempferol Galangin Fisetin Myricetin Morin	Propolis, honey, fruits, vegetables, cereals	Quercetin has been shown to exert antibacterial effects against several gram-positive bacteria such as methicillin-resistant *S. aureus* (MRSA) and methicillin-susceptible *S. aureus* (MSSA) (Li *et al*., 2012) while working in synergy when combined with other antibiotics (Li *et al*., 2012). Veiko *et al*. (2023) also showed the antibacterial activity of quercetin against *S. aureus* and implicated the disorderliness/damages at the cell membrane level as the main mechanism of action.

			The antibacterial properties of kaempferol have been demonstrated against several Gram-positive and Gram-negative bacteria (Periferakis, *et al*., 2022). Although establishing its mechanisms of action has proven difficult due to the great diversity within the family of kaempferol derivatives, several studies suggest cell membrane disruption followed by activation of apoptosis and DNA fragmentation in some organisms (Li *et al.*, 2015; He *et al*., 2014)
 Flavan-3-ol	(+)-Catechin (–)-Epicatechin (–)-Epigallocatechin (–)Epicatechin-3-gallate (–)-Epigallogatechin-3gallate	Green tea, black tea, cocoa, cereals	Green tea extract has been proven to be more effective against gram-positive organisms such as *Enterococcus faecalis* (20 mg/ml) and *S. aureus* (10 mg/mL) compared to gram-negative organisms such as *E. coli* (35 mg/mL) (Liu *et al*., 2022). The antibacterial properties of the extract were attributed to catechins and subsequent study of its mechanisms of action showed that catechin damaged the

			cell membrane and increased the permeability of the cell membrane, resulting in changes in relative electrical conductivity and the release of certain components into the cytoplasm (Liu *et al*., 2022). Recent antibacterial evaluation of epigallocatechin against *S. flexneri*, a major intestinal pathogen in human, showed that the compound had effect at MIC of 400 μg/mL. and the investigation of its mechanism of actions showed that epigallocatechin interfered with protein synthesis and changed bacteria morphology via the generation of ROS (Zhang *et al*., 2023).

1.1.3 Computational techniques in drug discovery and development

While the traditional method of drug discovery and development is time-consuming and costly with possible high risk of failure rate, the use of modern and advanced technological approaches have been effective in alleviating these challenges (Harvey *et al*., 2015). More specifically, molecular computational methods with proven benefits and efficiency have been used over the years in identifying drug targets and drug candidates against degenerative diseases such as bacterial infections (Yuan *et al*., 2016; Harvey *et al*., 2015). Of the computational approaches, molecular docking has played an important role in computer-aided drug development and has established itself as a useful tool in the present scenario of structure-activity-relationship drug design. Docking techniques fit ligands into binding pockets of a protein by integrating and enhancing characteristics such as steric, hydrophobic, and electrostatic harmony, as well as determining the binding energy (Sethi *et al*., 2019). Although docking has become a popular method because of advancements in computational power, the prediction accuracy of the docking software is still rather limited (Durrant and McCammon, 2011). Consequently, molecular dynamics (MD) simulation has provided useful information in complementing docking predictions by understanding how each atom in a protein or other molecular structure moves over time, using the general model governing interatomic relationships (Sethi *et al*., 2019). MD simulations can detect an extensive range of critical biomolecular events, including structural changes, protein folding, ligand binding, displaying the locations of all the atoms at picosecond time precision. (Durrant and McCammon, 2011). Molecular dynamic (MD) simulation has been employed in understanding how bimolecular systems respond to perturbation in several studies. For instance, Sabiu *et al*. (2021) provided insights into the mechanism of the modulatory effect of phenolics on the activity of α-amylase and α-glucosidase using MD simulation. They reported based on the

findings from the binding free energy, structural stability, and compactness, that procyanidin and 1,3-dicaffeoxyl quinic acid were potent inhibitors of α -amylase, and α-glucosidase, respectively. Also, Malekshah *et al*. (2021) reported on the molecular dynamics of derivatised chitosan schiff base complexes against *S. aureus* enoyl-acyl carrier protein reductase (ENRs) and showed that all the derivatised compounds exhibited a higher binding affinity and stability against the protein than the parent compounds. Furthermore, using computational methods, Verma *et al*. (2021) screened 186 flavonoids against PBP2a and through MD simulation established five of the compounds as structurally stable with conformational versatility at the active site of PBP2a. Another important computational tool which has gained prominence in lead identification is the density functional theory (DFT). For several years, DFT has been established as a quantum mechanical (QM) method that is satisfactorily meticulous and competent for use in bioprospecting pharmaceuticals (Tandon *et al*., 2019). Biologically important molecular systems can be accurately described using DFT with less computational effort than other methods, making it a commonly used technique. The precision of DFT in studying the geometries of drug molecule and various important molecular properties has been extensively studied with findings showing good correlation with experimental data (Tandon *et al*., 2019, Zhan *et al*., 2003; Raghavachari, 2000). With the effectiveness of molecular docking, MD simulation and DFT and their ability in identifying leads from a library of compounds, these computational techniques have become an important tool in drug discovery and development.

A crucial step in drug discovery is establishing at the early phase the ADMET (absorption, distribution, metabolism, excretion, and toxicity) properties of drug compound, which has become an important consideration in the selection of compounds for further evaluation (Ohba *et al*., 2023; Waring *et al*., 2015). Over the past decade, online resources such as SwissADME and

Molinspiration, have facilitated drug-likeness studies in an economical and time-efficient manner. A study by Waring *et al*. (2015) on the attrition of drug candidates from four pharma giants (AstraZeneca, Pfizer, GlaxoSmithKline, and Eli Lilly and Company) confirmed that the control of physicochemical properties helps identify compounds of drug quality. The study also concluded that the optimisation of lead for improved physicochemical and pharmacokinetics properties might help reduce clinical failure due to safety issues. Other important benefit of lead optimization has been shown to include optimising target selectivity, defining secondary target and avoiding toxicity issues (Lim *et al*., 2023). One important technique for accelerating lead optimization is retrosynthesis, a process of "deconstructing" a desired molecule into easily accessible starting materials via imaginary bond breaking and the transformation of one functional group into another (Lim *et al*., 2023; Clara *et al*., 2012). This approach enables medicinal chemists to hybridize pharmacophore/skeleton (Pawełczyk *et al*. 2018) and simplified complex lead structure by shortening unnecessary groups/molecules/ring to improve synthetic accessibility, binding capacity and enhanced pharmacokinetic profiles (Wang *et al*., 2019). Hence, lead optimisation via hybridization and structural simplicity techniques have been identified as an effective strategy for obtaining active lead compounds and thus an appealing source of drug candidate in drug discovery. Hence, for the first time, this study screened a library of over 10,000 phenolic compounds currently in existence (Ofusu *et al*., 2020) against PBPs of common and clinically important bacterial using computational methods, and the lead phenolic was optimised for enhanced physicochemical and druggability through retrosynthesis for novel derivatives. The synthesis of the parent compound of the best derivative was exploited for authentication of their synthetic feasibility. The findings of the *in silico* studies were later validated *in vitro* for lead phenolics and parent compound of the best derivatives using different beta-lactam antibiotics as reference standard. Exploring natural

products via complementary *in silico* and *in vitro* evaluation as done in this study might help reduce the rate of failure of new chemical entities during the preclinical and clinical phases of drug development and especially, in this case, to identify potential antibacterial candidates for subsequent development as novel PBP inhibitors.

1.2 Research problem and justification

The beta-lactams are the most widely used antibiotics for the treatment of bacterial diseases, with a worldwide annual expenditure of approximately 15 billion USD, which makes up 65% of the total antibiotic market (Eiamphungporn *et al*., 2018). Unfortunately, bacteria have developed several mechanisms to combat these therapeutic agents, with one of the major resistance mechanisms involving modification of therapeutic target sites. Bacterial mutations in PBP have limited the potential of several beta-lactams in clinical practice, with the type of PBP being altered in an organism having implications on severity of resistance (Chowdhury *et al*., 2012). For instance, PBP2a mutations have been linked to the widespread clinical resistance to beta-lactam antibiotics in *S. aureus* (Farrell *et al.*, 2014; Otero *et al*., 2013), whereas PBP3 mutations in *E. coli* and *P. aeruginosa*, as well as PBP2x mutations in *S. pneumoniae*, are critical to resistance to beta-lactams against infections caused by these organisms (Chowdhury *et al*., 2012; Kosowska-Shick *et al*., 2010; Scheffers and Pinto, 2005). A previous study by Hecker *et al*. (2015) focused mostly on developing inhibitors (e.g., clavulanic acid, sulbactam, and tazobactam) of beta-lactamase (an enzyme that inactivates beta-lactams) which can be used in combination therapy with beta-lactams. However, bacterial resistance to this kind of combination therapy has evolved recently since the inhibitors share a common beta-lactams core structure with beta-lactam antibiotics (Palacios *et al.*, 2020; Eiamphungporn *et al.*, 2018). Also, the recently discovered beta-lactamase inhibitors with non-beta-lactam scaffolds (diazabicyclooctane derivatives) such as avibactam and relebactam,

approved by the Food and Drug Administration (FDA) in 2015 and 2019, respectively, inactivate beta-lactamase, but unlike beta-lactam-based inhibitors, this inactivation is slowly reversible, releasing an intact beta-lactamase and the inhibitor in the process, necessitating the need for other feasible alternative approaches in combating beta-lactam antibiotic resistance. The identification and development of potent therapeutics with diverse scaffolds against therapeutically important PBPs represents a viable alternative strategy. Phenolics due to their reported mechanisms of antibacterial actions (Table 1) represent a viable source of drug candidate that can be explored as potent PBP inhibitors. Hence, this study forms part of the ongoing efforts to address antimicrobial resistance consistent with beta-lactams through identification of potent lead phenolics and novel compounds against therapeutically important PBPs of common and clinically important pathogenic Gram positive (*S. aureus* and *S. pneumoniae*) and Gram-negative (*E. coli* and *P. aeruginosa*) bacteria.

1.3 Aim and objectives

Aim

The aim of this study was to explore phenolics against PBPs as druggable targets in antibacterial therapy of common and clinically significant pathogenic bacteria using *in silico* and *in vitro* experimental approaches.

The specific objectives are:

a. to identify lead phenolic compounds against PBPs druggable targets of common and clinically significant pathogenic bacteria using computational methods (molecular docking and molecular dynamic simulation) and determine their pharmacokinetics and ADMET properties;

b. to retro-synthesize and derivatize the identified lead phenolic compounds and evaluate their enhanced druggability relative to the parent compounds using *in silico* methods;

c. to determine the antibacterial activity of the lead compounds and their derivatives against common and clinically significant pathogenic bacteria using *in vitro* approaches; and

d. to evaluate the level of ROS contribution to the antibacterial activity of the lead compounds and their derivatives against common and clinically significant pathogenic bacteria using direct ROS quantification and indirect oxidative stress biomarker assays.

1.4 Structure of the thesis

This thesis is organized into six chapters and consists of contributions in the form of published articles, book chapters, and articles submitted for publication. Chapter one provides a general introduction to the topic, research problem and justification, the aim and objective of the research and the structure of the thesis while Chapter two elaborates on beta-lactam resistance in Gram positive (*S. aureus* and *S. pneumoniae*) and Gram-negative (*E. coli* and *P. aeruginosa*) bacteria mediated through modifications in PBPs, the progressive approach of phenolic acids towards the advancement of antimicrobial drugs (the advancement of computational techniques in the identification of active lead phenolics for drug development was highlighted) and redox impact on bacterial macromolecule as a promising avenue for the discovery and development of novel antibacterials. The cheminformatics identification of phenolics as modulators of key PBPs (PBP3 of *P. aeruginosa,* PBP3 and PBP5 of *E. coli*, PBP2a of *S. aureus*, and PBP2x of *S. pneumoniae*) towards interventive antibacterial therapy are presented in Chapter three. The structural optimization of silicristin (the lead phenolic compound with the best broad-spectrum effect against the essential PBPs of the investigated bacteria) and exploration of the synthetic routes of its best derivatives are presented in Chapter four, while the *in vitro* validation of the antibacterial activity and the possible involvement of ROS in the antibacterial activity of silicristin and the parent compound of the best derivatives are presented in Chapter five. In Chapter six, the general

discussion, conclusions and recommendation are presented to consolidate the overall results of the study.

References

Ajiboye, T.O., Habibu, R.S., Saidu, K., Haliru, F.Z., Ajiboye, H.O., Aliyu, N.O. Involvement of oxidative stress in protocatechuic acid-mediated bacterial lethality. *Microbiologyopen*. 2017, 6, e00472.

Ajiboye, T.O., Mohammed, A.O., Bello, S.A., Yusuf, I.I., Ibitoye, O.B., Muritala, H.F., Onajobi, I.B. Antibacterial activity of *Syzygium aromaticum* seed: studies on oxidative stress biomarkers and membrane permeability. *Microb. Pathog*. 2016, 95, 208-215.

Aldulaimi, O.A. General overview of phenolics from plant to laboratory, good antibacterials or not. *Pharmacogn.* 2017, 11, 123–127

Alekshun, M.N., Levy, S.B. Molecular mechanisms of antibacterial multidrug resistance. *Cell.* 2007, 128, 37–50

Alhadrami, H.A., Hamed, A.A., Hassan, H.M., Belbahri, L., Rateb, M.R., Sayed. A.M. Flavonoids as potential anti-MRSA agents through modulation of PBP2a: A computational and experimental study. *Antibiotics*. 2020, 9, 562,

Al-Orphaly, M., Hadi, H. A., Eltayeb, F. K., Al-Hail, H., Samuel, B. G., Sultan, A. A., Skariah, S. Epidemiology of multidrug-resistant *Pseudomonas aeruginosa* in the middle east and north Africa region. *Msphere.* 2021,6, 202-221.

Alvarado, A., Arce, I. Antioxidants in respiratory diseases: basic science research and therapeutic alternatives. *Clin Res Trials*. 2016, 3, 1-11.

Aribisala, J.O., Sabiu, S. Redox impact on bacterial macromolecule: a promising avenue for discovery and development of novel antibacterials. *Biomolecules*. 2022, 12, 1545.

Baker, K.S. Demystifying *Escherichia coli* pathovars. *Nat Rev Microbiol.* 2015, 13, 5.

Barber, A.E., Norton, J.P., Spivak, A.M., Mulvey, M.A. Urinary tract infections: current and emerging management strategies. *Clin. Infect Dis.* 2013, 57, 719 –724,

Borges, A., Ferreira, C., Saavedra, M.J., Simões, M. Antibacterial activity and mode of action of ferulic and gallic acids against pathogenic bacteria. *Microb Drug Resist*. 2013, 19, 256-65.

Chowdhury, C., Kar, D., Dutta, M., Kumar, A., Ghosh, A.S. Moderate decylation efficiency of DacD explains its ability to partially restore beta-lactam resisitance in *Escherichia coli* PBP5 mutant, *FEMS Microbiol Lett.* 2012, 337, 73 – 80

Chua, N.G., Zhou, Y.P., Tan, T.T., Lingegowda, P.B., Lee, W., Lim, T.P., Teo, J., Cai, Y., Kwa, A.L. Polymyxin B with dual carbapenem combination therapy against carbapnemase-producing *Klebsiella pneumonia*. *J. Infect.* 2015**,** 70, 309 – 311.

Charradi, K., Mahmoudi, M., Bedhiafi, T., Jebari, K., El May, M.V., Limam, F., Aouani, E. Safety evaluation, anti-oxidative and anti-inflammatory effects of sub chronically dietary supplemented high dosing grape seed powder (GSP) to healthy rat. *Biomed Pharmacother*. 2018, 107, 534 - 546.

Clara, D., Christ, M.Z., Jan, M.K. Mining electronic laboratory notebooks: analysis, retrosynthesis, and reaction based enumeration. *J. Chem Inf Model.* 2012, 52, 1745 – 1756.

Dai, Q., Borenstein. A.R., Wu, Y. Fruit and vegetable juices and Alzheimer's disease: the kame project. *Am J Clin Nutr*. 2006, 119, 751–759.

Dryden, M. Reactive oxygen species: a novel antimicrobial. *Int. J. Antimicrob Agents.* 2018**,** 51, 299 – 303.

Durrant, J.D., McCammon, J. A. Molecular dynamics simulations and drug discovery, *BMC Biol.* 2011, 9, 71 – 90

Dwyer, D.J., Belenky, P.A., Yang, J.H., MacDonald, I. C., Martell, J.D., Takahashi, N., Chan, C.T.Y., Michael A.L. *et al.* Antibiotics induce redox-related physiological alterations as part of their lethality. *PNAS*. 2014, 5, 100 – 109

Dwyer, D.J., Kohanski, M.A., Hayete, B., Collins J.J. Gyrase inhibitors induce an oxidative damage cellular death pathway in *Escherichia coli*. *Mol Syst Biol.* 2007, 3, 1–15.

Eghbaliferiz, S., Iranshahi, M. Prooxidant activity of polyphenols, flavonoids, anthocyanins and carotenoids: updated review of mechanisms and catalyzing metals. *Phyther. Res*. 2016, 30, 1379 –1391.

Eiamphungporn, W., Schaduangrat, N., Malik, A. A., Nantasenamat, C. Tackling the antibiotic resistance caused by class A β-lactamases through the use of β-lactamase inhibitory protein. *Int J Mol Sci.* 2018, 19, 2222.

Fanjul-Moles, M.L., López-Riquelme, G.O. Relationship between oxidative stress, circadian rhythms, and AMD. *Oxid Med Cell Longev*. 2016, 16, 7420637.

Farrell, D. J., Flamm, R. K., Sader, H. S., Jones, R. N. Activity of ceftobiprole against methicillin-resistant *Staphylococcus aureus* strains with reduced susceptibility to daptomycin, linezolid or vancomycin, and strains with defined SCC*mec* types. *Int J Antimicrob Agents.* 2014, 43, 323 – 327.

Galati, G., Sabzevari, O., Wilson, J.X., O'Brien, P.J. Prooxidant activity and cellular effects of the phenoxyl radicals of dietary flavonoids and other polyphenolics. *Toxicology.* 2002, 177, 91 – 104.

Gulumbe, B.H., Faggo, A.A. Epidemiology of multidrug-resistant organisms in Africa. *J Infect Microb Antimicrob*. 2019, 8, 25.

Harradi, K., Mahmoudi, M., Bedhiafi, T., Jebari, K., El May, M.V., Limam, F., Aouani, E. Safety evaluation, anti-oxidative and anti-inflammatory effects of sub chronically dietary supplemented high dosing grape seed powder (GSP) to healthy rat. *Biomed Pharmacother*. 2018, 107, 534 – 546.

Harvey, A.L., Edrada-Ebel, R., Quinn, R.J. The re-emergence of natural products for drug discovery in the genomics era. *Nat. Rev Drug Discov*. 2015, 14, 111–129.

He M., Wu T., Pan S., Xu, X. Antimicrobial mechanism of flavonoids against *Escherichia coli* ATCC 25922 by model membrane study. *Appl Surf Sci.* 2014, 305, 515 – 521.

Hecker, S.J., Reddy, K.R., Totrov, M., Hirst, G.C., Lomovskaya, O., Griffith, D.C., King, P., Tsivkovski, R., Sun. D., Sabet, M., Tarazi, Z., Clifton, M.C., Atkins, K. *et al*. Discovery of a cyclic boronic acid beta-lactamase inhibitor (RPX7009) with utility vs class a serine carbapenemases. *J Med Chem.* 2015, 58, 3682–3692.

Howard, S.J., Catchpole, M., Watson, J., Davies, S.C. Antibiotic resistance: global response needed. *Lancet Infect Dis*. 2013, 13, 1001– 1003

Imlay, J. A. The molecular mechanisms and physiological consequences of oxidative stress: Lessons from a model bacterium. *Nat Rev Microbiol.* **2013**, 11, 443 – 454.

Josephine, H.R., Charlier, P., Davies, C., Nicholas, R.A., Pratt, R.F. Reactivity of penicillin-binding proteins with peptidoglycan-mimetic beta-lactams: what's wrong with these enzymes?. *Biochemistry*. 2006, 45, 15873 – 15883.

Kato, Y., Suga, N. Covalent adduction of endogenous and food derived quinones to a protein: its biological significance, *J Clin Biochem Nutr.* 2018, 62, 213-220

Khalifa, S.M., Abd El-Aziz, A.M., Hassan, R., Abdelmegeed, E.S. β-lactam resistance associated with β-lactamase production and porin alteration in clinical isolates of *E. coli* and *K. pneumoniae*. *PLoS ONE*. 2021, 16, e0251594.

Kibret, M., Abera, B. Antimicrobial susceptibility patterns of *E. coli* from clinical sources in northeast Ethiopia. *African Health Sci.* 2011, 11, 40–45.

Kim, S., Woo, E.R., Lee, D.G. Apigenin promotes antibacterial activity via regulation of nitric oxide and superoxide anion production. *J Basic Microbiol*. 2020, 60, 862 – 872.

Klein, A.R., Sarri. E., Kelch, S.E. Basinska, J.J., Vaidya, S., Alristilde, L. Probing the fate of different structures of beta-lactam antibiotics: hydrolysis, mineral capture, and influence of organic matter. *ACS Earth Space Chem.* 2021, 5, 1511 – 1551

Kosowska-Shick, K., McGhee, P. L., Appelbaum, P. C. Affinity of ceftaroline and other beta-lactams for penicillin-binding proteins from *Staphylococcus aureus* and *Streptococcus pneumoniae*. *Antimicrob Agents Chemother.* 2010, 54, 1670– 1677

Kyaw, B.M., Arora, S., Lim, C.S. Bactericidal antibiotic-phytochemical combinations against methicillin resistant *Staphylococcus aureus*. *Braz J Microbiol.* 2012, 43, 938 – 945.

Lacombe, A., Wu, V.H., Tyler, S., Edwards, K. Antimicrobial action of the American cranberry constituents: phenolics, anthocyanins, and organic acids, against *Escherichia coli* O157:H7. *Int J Food Microbiol*. 2010, 139, 102 – 107.

Lam, P.L., Wong, R.S.M., Lam, K.H., Hung, L.K., Wong, M., Yung, L.H., Ho, Y.W., Wong, W.Y., Hau, D.K.P., Gambari, R., Chui, C.H. The role of reactive oxygen species in the biological activity of antimicrobial agents: an updated mini review. *Chem-Biol Interact.* 2020, 320, 109023.

Lambert, P.A. Bacterial resistance to antibiotics: modified target sites. *Adv Drug Deliv Rev.* 2005, 57, 1471 – 1485.

Li, X.M., Luo, X.G., Si, C.L., Wang, N., Zhou, H., He, J.F., Zhang, T.C. Antibacterial active compounds from *Hypericum ascyron* L. induce bacterial cell death through apoptosis pathway. *Eur J Med Chem.* 2015, 96, 436 – 444.

Li, K., Xing, S., Wang, M., Peng, Y., Dong, Y., Li, X. Anticomplement and antimicrobial activities of flavonoids from *Entada phaseoloides*. *Nat. Prod. Commun.* 2012, 7, 867 – 871.

Lim, P.K., Julca, I., Mutwil, M. Redesigning plant specialized metabolism with supervised machine learning using publicly available reactome data. *Comput Struct Biotechnol J*. 2023, 18, 1639 – 1650.

Liu, S., Zhang, Q., Li, H., Qiu, Z., Yu, Y. Comparative assessment of the antibacterial efficacies and mechanisms of different tea extracts. *Foods.* 2022, 11, 620.

Liu, Y., Imlay, J.A. Cell death from antibiotics without the involvement of reactive oxygen species. *Science.* 2013, 339, 1210 – 1213

Lou, Z., Wang, H., Zhu, S., Ma, C., Wang, Z. Antibacterial activity and mechanism of action of chlorogenic acid. *J Food Sci*. 2011, 76, 398 – 403.

Magiorakos, A.P., Srinivasan, A., Carey, R., Carmeli, Y., Falagas, M., Giske, C., Harbarth, S., Hindler, J., Kahlmeter, G., Olsson-Liljequist, B. Multidrug-resistant, extensively drug-resistant and pandrug-resistant bacteria: an international expert proposal for interim standard definitions for acquired resistance. *Clin Microbiol Infect.* 2012, 18, 268 – 281

Malekshah, R.E., Shakeri, F., Aallaei, M., Hemati, M., Khaleghian, A. Biological evaluation proposed molecular mechanism through docking and molecular dynamic simulation of derivatives of chitosan. *Int J Biol Macromol*. 2021, 166, 948 – 966.

Meroueh, S.O., Minasov, G., Lee, W., Shoichet, B.K., Mobashery, S. Structural aspects for evolution of beta-lactamases from penicillin-binding proteins. *J Am Chem Soc.* 2003, 125, 9612 – 9618.

Nayaka, H.B., Londonkar, R.L., Umesh, M.K., Tukappa, A. Antibacterial attributes of apigenin, isolated from *Portulaca oleracea* L. *Int J Bacteriol*. 2014, 14,175851.

Nelson, R.E., Slayton, R.B., Stevens, V.W., Jones, M.M., Khader, K., Rubin, M.A., Jernigan, J.A., Samore, M.H. Attributable mortality of healthcare-associated infections due to multidrug-resistant Gram-negative bacteria and methicillin-resistant *Staphylococcus aureus*. *Infect Control Hosp. Epidemiol.* 2017, 38, 848 – 856.

Ofosu, F.K., Elahi, F., Daliri, E.B., Chelliah, R., Ham, H.J., Kim, J.H., Han, S.I., Hur, J.H., Oh D.H. Phenolic profile, antioxidant, and antidiabetic potential exerted by millet grain varieties. *Antioxidants*. 2020, 9, 254.

Ohba, Y., Adachi, K., Furukawa, T., Nishimaru, T., Sakurai, K., Masuo, R., Inami, T., Orita, T., Akai, S., Adachi, T., Usui, K., Hamada, Y., Mori, M. et al. Discovery of novel NLRP3 inflammasome inhibitors composed of an oxazole scaffold bearing an acylsulfamide. *ACS Med Chem Lett*. 2023, 14, 1833 – 1838.

Otero, L.H., Rojas-Altuve, A., Llarrull, L.I., Carrasco-Lopez, C., Kumarasiri, M., *et al*. How allosteric control of *Staphylococcus aureus* penicillin binding protein 2a enables methicillin resistance and physiological function. *Proc Natl Acad Sci.* 2013, 110, 16808 – 16813.

Palacios, A.R., Rossi, M.A., Mahler, G.S., Vila, A.J. Metallo-beta-lactamase inhibitors inspired on snapshots from the catalytic mechanism. *biomolecule.* 2020, 10, 854.

Panat, N.A., Singh, B.G., Maurya, D.K., Sandur, S.K., Ghaskadbi, S.S. Troxerutin, a natural flavonoid bind to DNA minor groove and enhances cancer cell killing in response to radiation. *Chem Biol Interact.* 2016, 5, 34 – 44.

Pawełczyk, A., Sowa-Kasprzak, K., Olender, D., Zaprutko, L. Molecular consortia—various structural and synthetic concepts for more effective therapeutics synthesis. *Int J Mol Sci.* 2018, 19, 1104.

Periferakis, A., Periferakis, K., Badarau, I.A., Petran, E.M., Popa, D.C., Caruntu, A., Costache, R.S., Scheau, C., Caruntu, C., Costache, D.O. Kaempferol: antimicrobial properties, sources, clinical, and traditional applications. *Int J Mol Sci*. 2022, 30, 23, 15054.

Qian, W., Liu, M., Fu, Y., Zhang, J., Liu, W., Li, J., Li, X., Li, Y., Wang, T. Antimicrobial mechanism of luteolin against *Staphylococcus aureus* and *Listeria monocytogenes* and its antibiofilm properties. *Microb Pathog*. 2020, 142, 104056.

Raghavachari, K. Perspective on density functional thermochemistry. III. the role of exact exchange. *Theor Chem Acc.* 2000, 103, 361 – 363.

Sabiu, S., Balogun, F.O., Amoo, S.O. Phenolics profiling of *Carpobrotus edulis* (L.) N.E.Br. and insights into molecular dynamics of their significance in type 2 diabetes therapy and its retinopathy complication. *Molecules.* 2021, 26, 4867.

Scheffers, D.J. Pinho, M.G. Bacterial cell wall synthesis: new insight from localization studies, *Microbial Mol Biol Rev*. 2005, 69, 585 – 607

Sethi, A., Khusbhoo, J., Sasikala, K. Mallika, A. Molecular docking in modern drug discovery: principles and recent applications, *IntechOpen.* 2019, 21, 85991

Tandon, H., Chakraborty, T., Suhag, V. A Brief review on importance of DFT in drug design. *Res Med Engineer Sci*. 2019, 7, 00068

Vaishampayan, A., Grohmann, E. Antimicrobials functioning through ROS-mediated mechanisms: current insights. *Microrganisms*. 2022**,** 10, 61.

Vatansever, F., De Melo, W.C., Avci, P., Vecchio, D., Sadasivam, M., Gupta, A., Chandran, R., Karimi, M., Parizotto, N.A., Yin, R. *et al*. Antimicrobial strategies centered around reactive oxygen species—bactericidal antibiotics, photodynamic therapy, and beyond. *FEMS Microb Rev.* 2013, 37, 955 – 989.

Veiko, A.G., Olchowik-Grabarek, E., Sekowski, S., Roszkowska, A., Lapshina, E.A., Dobrzynska, I., Zamaraeva, M., Zavodnik, I.B. Antimicrobial activity of quercetin, naringenin and catechin: flavonoids inhibit *Staphylococcus aureus*-induced hemolysis and modify membranes of bacteria and erythrocytes. *Molecules.* 2023, *28*, 1252.

Verma, A.K., Ahmed, S.F., Hossain, M. S., Bhojiya, A. A., Mathur, A, Upadhyay, S.K., Srivastava, A.K., Vishvakarma, N.K., Barik, M., Rahaman, M.M., Bahadur, N.M. Molecular docking and simulation studies of flavonoid compounds against PBP-2a of methicillin-resistant *Staphylococcus aureus. J Biomol Struct Dyn.* 2021, 40, 10561 – 10577

Wang, Q., Xie, M.J. Antibacterial activity and mechanism of luteolin on *Staphylococcus aureus*. *Acta Microbiol Sin*. 2010, 50, 1180 –1184

Wang, S., Dong, G., Sheng, C. Structural simplification: an efficient strategy in lead optimization. *Acta Pharm Sin B.* 2019, 5, 880 – 901.

Waring, M.J., Arrowsmith, J., Leach, A.R., Leeson, P.D., Mandrell, S., Owen, R.M., Pairaudeau, G., Pennie, W.D., Pickett, S.D., Wang, J., Wallace, O., Weir, A. An analysis of the attrition of

drug candidates from four major pharmaceutical companies. *Nat Rev Drug Discov*. 2015, 14, 475 – 86.

Weinreb, O., Mandel, S., Amit, T., Moussa. B., Youdim, H. Neurological mechanisms of green tea polyphenols in Alzheimer's and Parkinson's diseases. *J Nutr Biochem.* 2004, 15, 506 – 516.

World Health Organisation (2019). International organizations unite on critical recommendations to combat drug-resistant infections and prevent staggering number of deaths each year. "Retrieved from https://www.who.int/news/item/29-04-2019-new-report-calls-for-urgent-action-to-avert-antimicrobial-resistance-crisis"

Wu, D., Ding, Y., Yao, K., Gao, W., Wang, W. Antimicrobial resistance analysis of clinical *Escherichia coli* isolates in neonatal ward. *Front Pediatr*. 2021, 9, 670470.

Wu, V.H., Qiu, X., Bushway, A., Harper, L. Antibacterial effects of American cranberry (*Vaccinium macrocarpon*) concentrate on foodborne pathogens. *LWT- Food Sci Technol*. 2008, 41, 1834 –1841.

Yang, L., Mih, N., Anand, A., Park J-O., Tan, J., Yurkovich, J.T., Monk, J.M., Lloyd, C.T., Sandberg, T.E., Seo, S.W., Kim, D. *et al*. Cellular responses to reactive oxygen species are predicted from molecular mechanisms. *PNAS*. 2019, 116, 14368 – 14373

Yuan, H., Ma, Q., Ye, L., Piao, G. The traditional medicine and modern medicine from natural products. *Molecules*. 2016, 21, 559 – 567.

Zapun, A., Contreras-Martel, C., Vernet, T. Penicillin-binding proteins and beta-lactam resistance. *FEMS Microbiol Rev.* 2008, 32, 361 – 385.

Zhan, C., Nichols, J.A., Dixon, D.A. Ionization potential, electron affinity, electronegativity, hardness, and electron excitation, energy: molecular properties from density functional theory orbital energies. *J Phys Chem A*. 2003, 107, 4184 – 4195

Zhang, Y., Zhang, Y., Ma, R., Sun, W., Ji, Z. Antibacterial activity of epigallocatechin gallate (EGCG) against *Shigella flexneri*. *Int J Environ Res Public Health.* 2023, 20, 4676.

Zhao, W.H., Hu, Z.Q., Hara, Y., Shimamura. T. Inhibition of penicillinase by epigallocatechin-gallate resulting in restoration of antibacterial activity of penicillin against penicillinase- producing *Staphylococcus aureus*. *Antimicrob Agents Chemother*. 2002, 46, 2266 – 2268.

CHAPTER TWO

2.0 Literature Review

2.1 Introduction ……**35**

2.2 Beta-lactam resistance in pathogenic bacteria mediated through modifications in Penicillin-Binding Proteins (PBPs) (**Currently submitted to Current Pharmacology Reports for review and subsequent publication)** ……**38**

2.3 Progressive approach of phenolic acids towards the advancement of antimicrobial drug (**Published as book chapter in Advancement of Phenolic Acids in Drug Discovery, Fundamental and Applications)** ……**63**

2.4 Redox Impact on bacterial macromolecule: A promising avenue for discovery and development of novel antibacterials **(Published in Biomolecules)** ……...**98**

References……...**125**

Two of the three review articles in this section have been published, one in Biomolecules and the other as a book chapter in Advancement of Phenolic Acids in Drug Discovery, Fundamental and Applications. The third review article is currently submitted for publication in Current Pharmacology Reports

2.1 Introduction

Antibiotic resistance in pathogenic bacteria has become a major public health concern, resulting in significant mortality and morbidity each year (WHO, 2019). Of great significance is the risk of infections posed by multidrug-resistant *Echerichia coli*, *Pseudomonas aeruginosa*, *Staphylococcus aureus* and *Streptococcus pneumonia* to both healthy individuals and patients with risk factors or underlying conditions, which are usually very difficult to treat and, as such, have drastically reduced treatment strategies (Al-Orphaly *et al*., 2021; Gulumbe and Faggo, 2019). Of the classes of antibiotics used in managing infections caused by MRM, resistance to beta-lactams, the most frequently administered antibiotics, remains a growing challenge (Klein *et al*., 2021; Thakuria and Lahon, 2013). Hence, the development of novel therapeutic agents against such resistance is imperative. The beta-lactam antibiotics have multiple PBPs as their targets which are essential for bacterial cell wall synthesis. Alteration at this site coupled with the inactivation of the beta-lactam by beta-lactamase has been demonstrated as the basis for the broad clinical resistance to beta-lactam antibiotics (Palacios *et al*., 2020; Eiamphungporn *et al*., 2018). Consequently, in this study, beta-lactam resistance in selected Gram positive (*S. aureus* and *S. pneumoniae*) and Gram negative (*E. coli* and *P. aeruginosa*) bacteria mediated through modifications in PBPs were appraised. One key approach identified in the review for tacking beta-lactam resistance mediated through modifications in PBPs is the discovery and development of novel broad-spectrum beta-lactam antibiotics with different scaffold from conventional beta-lactams.

From the earliest times, plant-derived compounds have been used in the treatment of human diseases thanks to their healing properties (Aldulaimi, 2017) and among these compounds, phenolics, have attracted considerable attention in the development of alternative natural antimicrobial agents (Bouarab-Chibane *et al*., 2019). Phenolic aside having a different scaffold

from conventional beta-lactams, have been reported to be effective against various multidrug-resistant strains of Gram-negative and Gram-positive bacteria (Alhadrami *et al*., 2020; Aldulaimi, 2017). Also, the ability of phenolic compounds to modulate bacterial druggable targets inhibit beta-lactamase while also increasing cell membrane permeability for antimicrobial absorption have been reported (Alhadrami *et al*., 2020; Araya-Cloutier *et al*., 2018). Additionally, the characteristic hydroxyl group of phenolics are implicated in autoxidation in the presence of transition metals (Ajiboye *et al*., 2017; Eghbaliferiz and Iranshahi, 2016), thus generating reactive oxygen species (ROS) which have been implicated in the lethality of most conventional antibiotics as a secondary means of action. These intriguing characteristics of phenolics positioned phenolic compounds as a viable source of alternative antimicrobials for the development of therapeutics that can exhibit direct antibacterial activity and/or act in synergy with antibiotics as resistance-modifying agents. Hence in this study, detailed information on the progressive approach of phenolic acids towards the advancement of antimicrobial drugs were discussed

Reactive oxygen species (ROS) generation has been implicated to contribute to bacterial killing of antimicrobials and the level of the contribution have been demonstrated to depends on compound type and exposure. Indeed, some quinolones and beta-lactams have been shown to rely fully on ROS generation for rapid killing, while others do not (Wang *et al*., 2010; Dwyer *et al*., 2014; Malik *et al*., 2007). Interestingly, the concept of ROS generation involvement/contribution to bacterial lethality has recently attracted research interests on the development of novel antimicrobials from plant secondary metabolites including phenolic compounds (Ajiboye *et al*, 2017; Eghbaliferiz and Iranshahi, 2016). Plant phenolics have been demonstrated to exhibit significant antibacterial activity by acting as a redox cycler thereby generating ROS and quinone species (Ajiboye *et al*., 2018; Eghbaliferiz and Iranshahi, 2016; Galati *et al*., 2002). The ROS generated damages the iron-

sulphur (Fe-S) cluster in bacterial cells and reacts with ferrous ion to form hydroxyl radicals, which consequently results in damaging cellular macromolecules such as carbohydrates, proteins and DNA (Ajiboye *et al*., 2018) while the quinone species generated, disrupt biological functions of protein through reaction with protein thiols and reverting to its catechol moiety (Ajiboye *et al*., 2018). Hence, stress-induced, ROS-mediated bacterial lethality represent an opened avenue for phenolics antimicrobial enhancement through identification of phenolic candidates whose mechanism of actions will rely majorly on ROS generation (Ajiboye *et al*., 2018; Eghbaliferiz and Iranshahi, 2016). Hence in this aspect of the study, redox impact on bacterial macromolecule as a promising avenue for discovery and development of novel antibacterials were appraised

This section of the thesis is divided into three parts comprising two review articles and a book chapter focussing on; (1) beta-lactam resistance in pathogenic bacteria mediated through modifications in PBPs, (2) the progressive approach of phenolic acids towards the advancement of antimicrobial drugs and (3) redox impact on bacterial macromolecule: a promising avenue for discovery and development of novel antibacterials.

2.2 Beta-lactam resistance in pathogenic bacteria mediated through modifications in Penicillin-binding proteins

Jamiu Olaseni Aribisala, Saheed Sabiu*

Department of Biotechnology and Food Science, Faculty of Applied Sciences, Durban University of Technology, PO Box 1334, Durban, 4000, South Africa.

*Corresponding author. e-mail: sabius@dut.ac.za

Abstract

Resistance of pathogenic bacteria to beta-lactams is facilitated majorly by two mechanisms, namely the production of beta-lactamases (an enzyme that inactivate beta-lactams) and the modification of essential high molecular weight penicillin-binding protein (PBPs). While the former is most common with Gram-negative organisms, modification in key PBPs is prevalent in Gram-positive organisms and becoming increasingly reported in Gram-negative organisms. Modification in key PBPs via multiple mutations produce PBP variants with low affinity for beta-lactams. Infections caused by organisms harboring such low affinity PBP variants are often very difficult to treat. Hence in this short overview, we discussed the role of PBPs in peptidoglycan production, mutation in PBPs of selected Gram-positive and Gram-negative bacteria and the approaches in tackling PBP modification-based resistance mechanisms. It is hoped that the review will help to reduce the continues resistance to beta-lactams due to mutation in the key PBPs of the profiled clinically significant bacteria.

Keywords: Beta-lactams, Cell wall, Mutation, Penicillin-binding protein, Resistance

1.0 Introduction

Beta-lactam antibiotics are among the most prescribed drug classes with a wide range of therapeutic uses (Bush, 2018). Their introduction since 1930s dramatically changed the fight against bacterial infections. The current annual expenditure on beta-lactam is around $15 billion, accounting for 65% of the total antibiotic market (Tooke *et al*., 2019; Fisher and Mobashery, 2016). However, due to the worrying development of antibiotic resistance, which remains a global public health concern, beta-lactam use in clinical practice has declined sharply (Bush, 2018). Beta-lactams exert their therapeutic effect via inactivation of penicillin-binding proteins (PBPs) that are implicated in cell wall synthesis (Cho *et al*., 2014). The bacterial cell wall is very crucial in bacteria, as it helps the pathogen to endure the internal pressure of its surroundings and also maintains its distinct shape that is replicated from generation to generation (Chen, 2017; Cho *et al*., 2014). The cell wall is composed of glycan chains linked by short stem peptides (Sethuvel *et al.*, 2023). PBPs facilitate both glycan strand elongation (transglycosylation) and glycan chain cross-linking (transpeptidation) (Sethuvel *et al*., 2023). However, modification/alteration in PBPs coupled with production of beta-lactamases, an enzyme which inactivate beta-lactams through the destruction of the beta-lactam ring represent the most prominent among the various mechanisms of resistance to beta-lactam (Sethuvel *et al*., 2023; Bush, 2018). While the resistance via the beta-lactamase generation is peculiar to Gram-negative bacteria, PBPs alteration in bacteria is common to Gram-positive bacteria and increasingly being reported in Gram-negative bacteria. Several reviews have documented the role of beta-lactamases in beta-lactam resistance (Tooke *et al*., 2019; Fisher *et al*., 2016), with only a few on PBP modification-based beta-lactam resistance and how it can be tackled. Here, we appraised previous studies on PBPs and their modifications that affect beta-lactam resistance in common and clinically significant Gram-positive (*S. aureus* and

Streptococcus pneumoniae) and Gram-negative (*Escherichia coli* and *Pseudomonas aeruginosa*) bacteria. Some promising approaches in tackling PBP modification-based beta-lactam resistant were also suggested. Sources including Google Scholar, the Nation Centre for Biotechnology Information (NCBI), Science Direct and PubMed were consulted in the collation of the review. Records cover from inception to June 2024 to assist in strengthening and evaluating resistance to beta-lactam mediated through modification in key PBPs and how it can be addressed in selected Gram-positive and Gram-negative bacteria. It is hoped that this review would be essential in the rational development of novel PBPs modulators that are effective against mutated key PBPs.

2.0 Classification and topology of PBPs

Bacteria have a variety of PBPs (Table 1) with molecular weight varying between 120,000 and 40,000 daltons (Zapun *et al*., 2008). The lower mass PBPs (LmPBPs), also referred to as class-C PBPs, perform the carboxypeptidases and/or endopeptidases, which are thought to promote the remodelling of cell wall in bacteria. Thus, LmPBPs are not too critical for bacteria growth, as their deletion had no significant impact on bacterial growth (Zapun *et al*., 2008; Josephine *et al*., 2006). The structure of the higher mass PBPs (HmPBPs) (Figure 1) contains a transmembrane anchor, a tail at the cytoplasmic region, and a linker (beta rich) that connect the two domains where the synthesis of peptidoglycan occurs at the outer layer of cytoplasmic membrane (Lovering *et al*., 2007; Macheboeuf *et al*., 2006). HmPBPs are categorized into class-A and class-B (Table 1) according to the arrangement and catalytic functions of the N2 domain (Figure 1). The C-terminal of the P-domain of Classes A and B has transpeptidase capability, which catalyses peptide linkage among neighbouring glycans (Figure 1). The N-terminal portion of class-A performs transglycosylation function, which catalyses the prolongation of yet to linked glycan chains (Lovering *et al*. 2007). On the other hand, the N-terminal section of class-B lacks

transglycosylation function but has been proposed to contribute to cell transformation by cooperating with other enzymes associated with cell cycle (Lovering *et al*., 2007). Due to the sequencing of several bacterial genomes, the number of PBPs of different bacteria has been determined, which also provides information about the binding region of beta-lactams in PBPs, which is believed to be similar in PBPs of different bacterial species (Figure 1). Differences only exist in the sequence of other regions and overall architectures (Figure 1). However, due to mutations, various bacteria have significantly changed their binding site to resist the activity of beta-lactams.

Table 1: Classifications of PBPs of selected Gram-positive and Gram-negative bacteria and their encoding genes

	CLASS-A PBPs (encoding genes)	**CLASS-B PBPs (encoding genes)**	**CLASS-C PBPs (encoding genes)**	**Key PBPs**
Escherichia coli	PBP1a (*ponA*), PBP1b (ponB), PBP1c (*pbpc*), MGT (*mgt*)	PBP2 (*pbpA*) PBP3 (*ftsl*)	PBP4 (*dacA*) PBP5(*dacC*) PBP6b (*dacD*) PBP7 (*dacG*) PBP4b (*yefw*) AmpH (*ampH)*	PBP3
Staphylococcus aureus (methicillin-resistant *S. aureus*)	PBP2 (pbp2), MGT (*mgt*)	PBP2a (*mecA*), PBP1 (*pbpA*) PBP3 (*pbp3*)	PBP4a (*daC*)	PBP2a
Streptococcus pneumoniae (resistant strain)	PBP1a (*pbpA*) PBP2a (*pbp2*) PBP1b (*pbp1b*)	PBP2x (*pypX*) PBP2b (*pbp2b*)	PBP3 (*pbp3*)	PBP2x
Pseudomonas aeruginosa	PBP1a (*ponA*), PBP1b (*ponB*)	PBP2 (*pbpA*), PBP3 (*ftsl*) and PBP3x (*pbp3*)	PBP4 (*dacB*), PBP5(*dacC*) and PBP7 (*dacG*)	PBP3

(adapted from Sauvage *et al*., 2008)

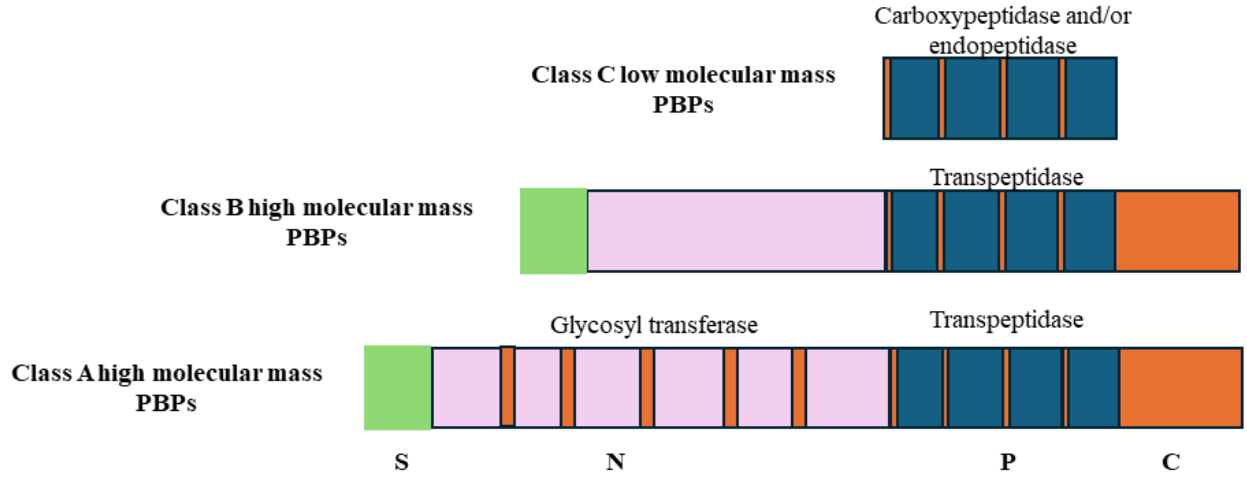


Figure 1: Domain arrangement of the class A, class B and class C PBPs. The class A and B HmPBPs include the S (green) region, N region (pink) responsible for glycosyl transferase activities in class A PBPs, P domain (dark green) region performing transpeptidase activities in both class-A and class-B PBPs and C domains (orange). The class-C low molecular mass PBPs have a single P domain (dark green) which performs carboxypeptidase and/or endopeptidase activity. The conserved orange regions of the P domain of all the classes of PBPs are fundamental to the active sites of each enzymatic activity and the target of beta-lactams.

3.0 Role of PBPs in transglycosylation and transpeptidation

Transglycosylation is the connection of the sugar moieties of peptidoglycan during cell wall biosynthesis, to form linear chains which are being crosslinked in a process know as transpeptidation (Banerjee *et al.*, 2010). For bifunctional PBPs (PBPs having transglycosylation and transpeptidation capabilities), transglycosylation can occur when the transpeptidase domain is blocked by beta-lactams, modification, or eliminated (Born *et al.*, 2006). Conversely, inhibition of transglycosylation functions by modification (Born *et al.*, 2006) or moenomycin totally inhibits polymerization. An investigation utilizing *E. coli* PBP1a found that transpeptidation requires transglycosylase activity on the same polypeptide (Born *et*

al., 2006). The N-terminal domain of class-A PBPs is associated with glycosyltransferase function, which catalyses the extension of peptidoglycan strands that are not yet linked (Figure 1). The glycosyltransferase domain of class-A utilizes undecaprenyl-P-P-MurNAc (pentapeptide)-GlcNAc lipid II as its primary substrate (Sauvage *et al*., 2008). The accessibility to considerable quantities of fluorescent substrate, has allowed for extensive kinetic analysis and the determination of the substances (DMSO, detergent, metal ions) required for PBP1b glycosyltransferase functionality (Schwartz *et al*., 2002). Most glycosyltransferases congregate in the midst of detergents, and proteolysis was frequently seen. In general, trypsin treatment of all class A PBPs results in an intact transpeptidase domain and full destruction of the glycosyltransferase domain (Di Guilmi *et al*., 2003).

During cell wall biosynthesis, following transglycosylation, the linear chains (glycan) formed are interlinked by transpeptidase activities using the short peptides attached to each sugar. Unlike transglycosylation, transpeptidation reaction without prior or simultaneous formation of glycan chains has only been reported in a few cases (Sauvage *et al*., 2008; Ghuysen, 1991). During crosslinking of glycan chains, the acylation of PBPs by D-alanine of the donor strand simultaneously release D-alanine while abstracting proton from the active site serine (Sethuvel *et al*., 2023). The lysine in the first motif perform deprotonation, and it is then given back to the departing D-alanine via the serine in the second motif (Sauvage *et al*., 2008; Macheboeuf *et al*., 2006). In the deacylation process, serine and lysine of the second and third motif, respectively, remove a proton from the amino group, allowing the active group to engage the carbonyl carbon of the acyl-enzyme's ester bond (Nicola *et al*., 2005; Goffin and Ghuysen, 1998). Thus, the transpeptidation region of the PBPs may be described as a twofold lysine-serine scheme that perform acylation and deacylation.

4.0 PBPs-mediated resistance in Gram-positive (*Staphylococcus aureus* and *Streptococcus pneumoniae*) and Gram-negative (*Escherichia coli* and *Pseudomonas aeruginosa*) bacteria

PBP-mediated resistance in Gram-positive bacteria

4.1 *Staphylococcus aureus*

Four intrinsic PBPs (PBP1, 2, 3 and 4) have been identified in susceptible strains of *Staphylococcus aureus* (Scheffers and Pinho, 2005). While PBP1, PBP3 and PBP4 have transpeptidases activities, PBP2 posses' dual peptidase's capabilities. Of the PBPs, PBP1 and PBP2 are the most critical for cell viability in *S. aureus* (Meisel *et al*., 2017). In addition to the native PBPs, mecA-encoded PBP2a is found in resistant strains of *S. aureus*, and its presences facilitates resistance in the organisms. According to Otero *et al.* (2013), PBP2a has a lesser affinity for beta-lactam antibiotics and can continue to facilitate cell wall production even after other native PBPs are inactivated. Beta-lactam decreased binding affinity for PBP2a is due to the inaccessibility of the active site of the protein which is always in a closed state (Dundas *et al.*, 2006). However, recent studies have been shown that the closed state of the active site is modulated by allosterism located 60° away from the active site (Alhadrami *et al.*, 2020; Meisel *et al*., 2017). Aside non-PBP2a-producing resistant strains of *S. aureus*, resistance due to mutation in other intrinsic PBPs have also been identified in *S. aureus*. Point mutations in the conserved penicillin-binding domains of PBP2 were discovered in two resistant strains of *S. aureus* (BB255R and CDC6), resulting in decreased binding affinity (Hackbarth *et al*., 1995). Another study by Xiaoliang *et al*. (2014), discovered four resistant isolates of *S. aurues* that lacked the encoding gene of PBP2a (*mecA*), but were still resistant to β-lactams suggesting resistance due to mutation in other intrinsic PBPs of *S. aureus*. However, structural basis of these type of alterations and their affect on beta-lactam binding need extra research work to be fully deciphered. Thus, going forward, it would be interesting to sequence intrinsic PBPs gene of several resistant strain of *S. aureus* relative to sensitive strains to discover mutation pattern.

4.2 *Streptococcus pneumoniae*

Streptococcus pneumoniae has three Class-A HmPBPs (PBP1a and b, and PBP2a), two Class-B HmPBPs (PBP2b and 2x), and a D, D-carboxypeptidase LmPBP (PBP3) (Scheffers and Pinho, 2017). Resistance to beta-lactams in *S. pneumoniae* has been associated with an alteration in all the PBPs (Beilharz *et al.*, 2012). Nevertheless, only the class-B HmPBPs (PBP2b and 2x) are key targets of beta-lactams, with resistance to beta-lactams in most clinical isolates majorly attributed to mutations in PBP2x. Clinical isolates harbouring PBP2x genes display low affinity for beta-lactams that may be passed on to susceptible strains (Meisel *et al*., 2017; Land *et al*., 2013; Dundas *et al*., 2006). Similarly, resistance caused by alterations in PBP1a and 2b was shown to arise only in *S. pneumoniae* strains with mutation in PBP2x, demonstrating the importance of PBP2x in the resistance of *S. pneumoniae* to beta-lactams (Meisel *et al.*, 2017). Another study by Mouz *et al*. (1999) showed that PBP2x isolated from the resistant strains of *S. pneumoniae* had a reduced affinity for beta-lactams due to the numerous alterations in the transpeptidase domain and most especially modification of Gln^{552} to Glu. Surprisingly, a PASTA region positioned close to the transpeptidase domain (27 Å), whose role had been deciphered for several years, has recently been shown to act as an allosteric site for promising transpeptidase action (Otero *et al.*, 2013). Bernardo-Garca *et al.* (2012) demonstrated that the binding of a pentapeptide at the PASTA region of PBP2x causes another pentapeptide from the same peptidoglycan strand to access the transpeptidase domain. Thus, the PASTA region of PBP2x could potentially act as a promising target for discovering new drugs that can function in combination with beta-lactams.

PBP-mediated resistance in Gram-negative bacteria

Although other mechanisms of antibacterial resistance in bacteria such as enzyme inactivation, cell impermeability, and efflux pump are less common, some reports have described the impact of PBP modifications on the emergence of beta-lactam resistance in gram-negative bacteria.

6.1 *Escherichia coli*

Esherichia coli possesses at least 12 PBPs, seven LmPBPs (AmpH, PBP4, PBP6, PBP6b, PBP4b, PBP5, and PBP7) and five HmPBPs (PBP1a, 1b, and 1c, PBP2, and PBP3 (Fraipont *et al*., 2011; Mohammadi *et al*., 2009). While some beta-lactams target PBP1a, PBP1b and PBP2, PBP3 encoded by the ftsI gene is the most selective for most beta lactams including penicillins, carbapenems and cephalosporins (Ranjitkar *et al*., 2019) and hence the most relevance to beta-lactam resistance (Periasamy *et al*., 2020; Cho *et al*., 2014). Periasamy *et al*. (2020), showed that the localization of other HmPBPs, such as PBP1b at the cleavage site depends on the presence of PBP3. Thus, it was suggested that PBP3 acts together with other HmPBPs during cell wall biosynthesis (Fraipont *et al*., 2011; Mohammadi *et al*., 2009). Although resistance to beta-lactams via the production of beta-lactamases is the most predominant in *E. coli*, recent studies have detected mutations on PBP3 that led to an increase in MICs value (Periasamy *et al*., 2020). The PBP3 of *E. coli* is a 588 amino acids protein with a catalytic residue Ser307. An insertion of YRIN or YRIK at position 333 of the active site was shown to raise MICs of PBP3-targeting antibiotics by 32-fold (Sethuvel *et al*., 2023). The insertion which is near the active site of PBP3 do not interact with beta-lactam, but rather cause structural modifications that prevent beta-lactams interaction with the catalytic residues most especially, beta-lactams with long side chains. Thus, PBP3 of *E. coli* with such modification maintains their transpeptidase activity even at the presence of beta-lactams (Freire *et al*., 2024; Sethuvel *et al*., 2023). This type of insertion-based mutation against beta-lactam has only been documented in *E. coli*, owing to the lower contribution of other resistance base factors such as efflux pump and impermeability; nonetheless, it is critical to properly monitor such mutations since transmission to other species is feasible. Among the LmPBPs, the PBP5, expressed by the dacA gene, is the most common and participates in cell morphology *in vivo* (Nelson *et al*., 2001). PBP5 upregulation causes rod-like *E. coli* to become spherical, whereas PBP5 deletion

during growth causes branching and topological abnormalities (Sujoy *et al.*, 2010; Nelson *et al.*, 2001). Hence, designing novel therapeutic beta-lactams that target PBP5 represents a good alternative mechanism to decrease beta-lactam susceptibility.

6.2 *Pseudomonas aeruginosa*

There are eight PBPs in *P. aeruginosa*, which are numbered 1a, 1b, 2, 3, 3a, 4, 5, and 7 in decreasing order of molecular mass (Glen and Lamont, 2021). Thus, PBP 4, 5, and 7 are the LmPBPs, while PBP 1a, 1b, 2, 3, and 3x are HmPBPs of P. *aeruginosa* (Chen *et al*., 2017). Among Gram negative bacteria, beta-lactam resistance due to PBP-modification has been more prominent in *P. aeruginosa* of which mutation in PBP3 has the highest incidence due to the protein essential involvement in the bacterial growth. Studies have shown the impact of conditional PBP3 mutations in *P. aeruginosa* resulted in cell division errors and increased venerability to beta-lactams (Sethuvel *et al.*, 2023; Chen *et al*., 2017). Another study by Glen and Lamont (2021) demostrated that most beta-lactams utilised in clinical settings that has a low minimum inhibitory concentration (MIC) has a strong affinity for PBP3 (Table 2), the sole PBP that *P. aeruginosa* requires (Glen and Lamont, 2021). The observation from these studies coupled with the findings that the deletion of PBP3 in *P. aeruginosa* significantly reduce MIC of most beta-lactams for *P. aeruginosa* further lent credence to the importance of PBP3 in *P. aeruginosa*. Generally, it can be concluded that PBP3 is the most essential PBPs for drug development against *P. aeruginosa*. Mutations around the PBP3 active site may have varied effects on various beta-lactams due to their modest differences in binding. The analysis of two clinical isolates which possess variations (V465G or A244T) in their PBP3 showed that both variants had resistance to aztreonam and cefsulodin, however, resistance to piperacillin and ceftazidime was only observed in V465G variant (Diaz e*t al*., 2015). In another investigation, R504C variant of PBP3 had low affinity for cefsulodin and ceftazidime, while the P527S variant of the PBP had low affinity for ceftazidime, aztreonam, cefsulodin and cefepime (Clark

et al., 2019; Diaz *et al.*, 2015). The current understanding of the involvement of PBP3 in beta-lactam resistance of *P. aeruginosa* is based on several research works that generate *P. aeruginosa* variant that are resistant to beta-lactam from susceptible strains and then performing genome sequencing analysis to locate alteration in whole genome that are responsible for resistance (Wardell *et al.*, 2019; Yen and Papin 2017). Their findings revealed that altered genes during resistance formation *in vitro* also receive modifications that are predicted to translate to resistance *in vivo* as evidenced by the complete genome sequencing of isolates from people with chronic infections. Such comprehensive whole genome sequencing can be extended to other organisms, perhaps new modification could be identified which might help in the rational development of potent drugs.

Table 2: Binding affinity of selected beta-lactams to PBPs of *P. aeruginosa*

Beta-lactam	Binding affinity ($1C_{50}$ µg/ml)						MIC (µg/ml)
	PBP1a	PBP1b	PBP2	PBP3	PBP4	PBP5	
Ceftazidime	0.2	3	>32	0.1	2	>32	0.5
Aztreonam	2	2	16	0.03	16	>16	4
Doripenem	0.5	0.6	0.06	0.07	0.008	8	0.25
Cefsulodin	19	2	>250	0.3	ND	ND	0.03
cephalexin	35	0.7	ND	41	ND	ND	16

(Adapted from Glen and Lamont, 2021)

Keywords: IC_{50}: concentration needed to inhibit PBPs by 50%, MIC: minimum inhibitory concentration, ND: Not determined

7.0 Interaction of PBPs with beta-lactams

The beta-lactams has bactericidal effect against a variety of bacteria through their ability to inhibit PBPs' transpeptidase and DD-carboxypeptidase activities (Clark *et al*., 2019). PBPs catalyze peptidoglycan pentapeptide precursors by binding to their terminal D-alanine-D-alanyl residues, which are structurally similar to beta-lactams (Glen and Lamont, 2021). The beta-lactam irreversibly inactivates PBP by covalently binding to the catalytic serine in the Ser-XX-Lys motif. Inhibiting PBPs may instigate cell elongation and reduce the structural integrity

of the cell wall, causing bacteria to cell lyse (Glen and Lamont, 2021). To a certain degree, PBPs with no mutation are sensitive to beta-lactams, with which they form a stable acyl-enzyme complex. The rate of acylation of benzylpenicillin with PBPs have been shown to range from 20 $M^{-1}S^{-1}$ in resistant strains of PBPs to about to about 300.000 $M^{-1}S^{-1}$ in susceptible strains PBPs (Hujer *et al*., 2005; Stefanova, *et al*., 2003). Studies have successfully captured the acyl-enzymes complexes of several PBPs and beta-lactam antibiotics and have deduce that beta-lactams covalently linked to the active site serine of PBPs adopt a common and standard positioning that shares some characteristics with PBP4a-α- -aminopimelyl- Ɛ- D-alanyl (Kishida *et al*., 2006; Sauvage *et al*., 2005). This standard positioning shows that the amide group of the beta-lactam is inserted between the asparagine of the second motif and the backbone of beta-3 strand; the carboxylate found in beta-lactams is link by a hydrogen bond to both hydroxyl groups of the third motif of the active site and lastly the carbonyl oxygen lies in the oxyanion hole. Except for the last feature of the standard positioning, the acyl-enzyme complex of PBP2a of *S. aureus* and benzylpenicillin possess all the standard positioning features (Figure 2) (Sauvage *et al*., 2005). Variation in the standard positioning of PBPs-beta-lactam complex which might be due to mutation of the active site might drastically reduce the sensitivity of PBPs to beta-lactams thus increasing MIC concentration.

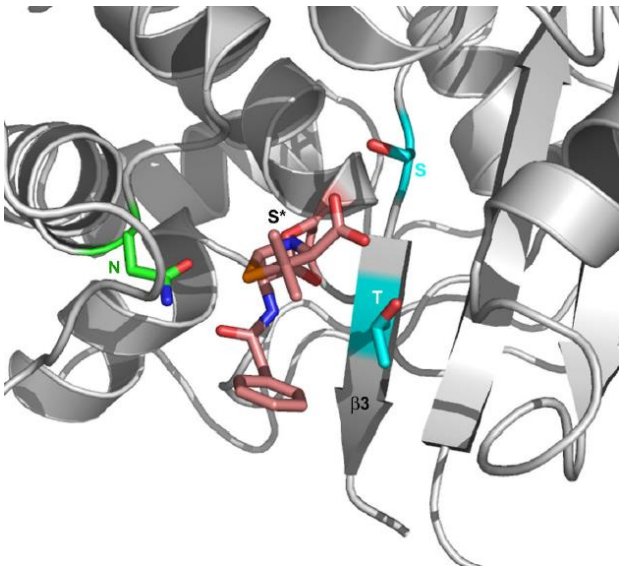


Figure 2: Benzylpenicillin (Pink) interaction at the active site of PBP2a of *S. aureus* adopting two of the standard positioning of PBP4a-α- -aminopimelyl- Ɛ- D-alanyl. The amide group of the Benzylpenicillin is inserted between the asparagine of the second motif (green) and the backbone of beta-3 strand, while the carboxylate of benzylpenicillin is link by a hydrogen bond to both hydroxyl groups of the third motif (cyan) ((Sauvage *et al*., 2005)

8.0 Approaches in tackling PBP modification-based resistance mechanisms

8.1 Extensive molecular characteristics of bacterial whole genome and PBP variants of bacteria

It has been shown that antibiotic exposure at inhibitory doses causes mutational processes, resulting in the evolutionary diversity of PBPs (Glen and Lamont, 2021). This mutation allows bacteria to thrive even in the presence of beta-lactams by relying on resistant strains of PBPs that are less susceptible to beta-lactams. Nonetheless, PBP point mutations may not fully explain the PBPs reduced sensitivity to beta-lactams. A recent study by Lau *et al*. (2020), using a three-dimensional structure-guided mutagenesis approach in screening a library of $PBP^{TET\ A6}$ (likely to be a class A PBP), demonstrate that the variant PBPs carrying randomly introduced point mutations revealed other residue changes that instigate resistance suggesting that co-occurring genomic alterations may contribute to resistance phenotype. Thus, to develop a more potent PBP-targeting treatments that are less prone to resistance development, it is critical to determine the nature of any associated bacterial host genome modifications and characterize the resistance-enabling molecular properties of such PBP variations

8.2 Allosteric cooperation in beta-lactams binding

Current antibiotic research focuses on the identification and development of novel compounds that can inhibit PBP activity by targeting either the catalytic or allosteric regions of the protein. While targeting the active site might require the use of molecules with beta-lactam moieties, allosteric modulation on the other hand can be accomplished using a wholly distinct novel

structures for which bacteria are yet develop resistance to. Allosteric modulation has traditionally been employed to treat eukaryotic illnesses and rarely use in prokaryotic infections (Meisel *et al*., 2017). Nevertheless, recent developments in the biochemical and computational screening techniques, as well as protein structure characterization, suggest that allosteric regulating may be a viable option for addressing PBP modification-based resistance mechanisms (Alhadrami *et al*., 2020; Otero *et al*., 2013; Dundas *et al*., 2006). Specifically, via the allosteric regulation of Methicillin-resistant *Staphylococcus aureus* PBP2a, effective molecules with capability to demonstrate direct antibacterial action while also operating in synergy with current conventional antibiotics due to their ability to bind to PBP2a allosteric site have been identified (Alhadrami *et al*., 2020). Similarly, Ahmad *et al*. (2022) demonstrate that two beta-lactam drugs bound synergistically to the active and allosteric sites of a non-classical transpeptidase protein of *Mycobacterium tuberculosis*, with one non-covalently at the S-pocket (allosteric site) and one covalently at the catalytic site. The binding at the S-pocket was observed to positively influence binding at the catalytic site. This simultaneous beta-lactam-binding events had been unknown in *M. tuberculosis* and if explored and extended to other organisms may offer a novel mean to the structure-based design of new drugs that may help in tackling PBP modification-based resistance mechanisms.

8.3 Identification of anti-PBPs broad spectrum agents

Mutations in more than one PBP have been demonstrated to contribute to the severity of resistance to beta-lactams. Although PBP2x, PBP2b, and PBP1a are the primary PBPs responsible for *S. pneumoniae* resistance, other investigations have suggested that other PBPs may also be involved. In the laboratory, André *et al*. (2008) found that a point mutation in PBP3 of *S. pneumoniae* contributes to resistance to cefotaxime. Another study by Sethuvel *et al*. (2023) demonstrated that mutations in PBP5 of *E. coli* and PBP4 of *P. aeruginosa* contributed to the severity of resistance to beta-lactams. Similarly, the upregulation of PBP5

transforms a rod-like *E. coli* into a spherical-like organism, while the deletion of PBP5 causes morphological distortions in the organism during growth (Sujoy *et al*., 2010; Nelson *et al*., 2001). These findings suggest that agents with multiple PBP binding capabilities and the use of combinations of agents with affinities for several intrinsic PBPs that harbor resistance influencing the potency of beta-lactams relative to narrow-spectrum PBP binding agents might aid in the alleviation of PBP modification-based resistance mechanisms.

9.0 Conclusion and future perspective

Beta-lactams are and will continue to be a key agent in the treatment of common and clinically important Gram-positive and Gram-negative bacterial infections. Nevertheless, the emergence of resistant isolates due to mutations and other important resistance mechanisms complicating the treatment process of many infections is of great concern. The relevance of beta-lactams in treating bacterial infections, along with the prevalence of antibiotic-resistant bacteria, has prompted several studies into the mechanism of beta-lactam action and resistance. As a result, there is a strong grasp of how beta-lactams work and resistance mechanisms, such as bacterial modification that lessen or initiate resistance to beta-lactams. However, significant information gaps remain. Sequence variations in PBPs play a key role in resistance, the effects of different variants of PBPs on antibiotic affinity and efficacy are yet to be fully known. Understanding the influence of PBP polymorphisms on beta-lactam affinity will be crucial to develop novel beta-lactams and will also help to understand cross-resistance between currently used antibiotics. Specifically, while the basic causes of beta-lactam resistance are very well established, the link between genome sequence and phenotype has yet to be entirely known. How do different combinations of resistance mechanisms impact beta-lactam susceptibility? What role does intrinsic resistance play, and how does it change amongst bacterial isolates? Complete knowledge of the link between genotype and phenotype could facilitate advancement of genome-based techniques for quick assessment of antibiotic

susceptibility. Additional approaches to minimise the emergence of resistant bacteria are through allosterism where combinations of antibiotics are used in the treatment of infections, with one binding to the active site and another at the allosteric site for effective synergistic effect. This approach will not only prevent prolonged exposure to antibiotics but also help resuscitate the use of currently known antibiotics which bacteria have develop resistance against. An alternative approach in addressing resistance to beta-lactams is developing novel beta-lactams with different scaffolds that are resistant to beta-lactamases and/or have a wide range effect on several PBPs. In conclusion, the knowledge of the mechanisms of action and resistance to, existing beta-lactams could greatly enhance the rational development of new anti-PBPs antibiotics; thus, future research on the modes of action of beta-lactams, as well as how to overcome the risk posed by antimicrobial resistance, will be critical in the development of new antibiotics while maximizing the use of existing ones.

References

Ahmad, N.; Dugad, S.; Chauhan, V.; Ahmed, S.; Sharma, K.; Kachhap, S.; Zaidi, R.; Bishai, W.R.; Lamichhane, G.; Kumar, P. Allosteric cooperation in β-lactam binding to a non-classical transpeptidase. Elife. **2022**, 11, e73055. https://doi.org/10.7554/eLife.73055

Alhadrami, H.A.; Hamed, A.A.; Hassan, H.M.; Belbahri, L.; Rateb, M.R.; Sayed, A.M. Flavonoids as potential anti-MRSA agents through modulation of PBP2a: a computational and experimental study. Antibiotics. **2020**, 9, 562. https://doi.org/10.3390/antibiotics9090562

André, Z.; Carlos, C.; Thierry, V. Penicillin-binding proteins and beta-lactam resistance. FEMS Microbiol. Rev. **2008**, 32, 361– 385. https://doi.org/10.1111/j.1574-6976.2007.00095.x

Banerjee, R.; Gretes, M.; Harlem, C.; Basuino, L.; Chambers, H.F. A mecA negative strain of methicillin-resistant *Staphylococcus aureus* with high-level beta-lactam resistance contains

mutations in three genes. Antimicrob Agents Chemother. **2010**, 54, 4900–4902. https://doi.org/10.1128/AAC.00594-10.

Beilharz, K.; Novakova, L.; Fadda, D.; Branny, P.; Massidda, O.; Veening, J.W. Control of cell division in *Streptococcus pneumoniae* by the conserved Ser/Thr protein kinase StkP. PNAS. **2012**, 109, 905-913. https://doi.org/10.1073/pnas.1119172109.

Bernardo-Garca, N.; Mahasenan, K.V.; Batuecas, M.T.; Lee, M.; Hesek, D.; Petráčková, D. *et al*. Allostery, recognition of nascent peptidoglycan, and cross-linking of the cell wall by the essential Penicillin-Binding Protein 2x of *Streptococcus pneumoniae*. ACS Chem Bio. **2018**, 13, 694-702. https://doi.org/10.1021/acschembio.7b00817

Born, P.; Breukink, E.; Vollmer, W. In vitro synthesis of cross-linked murein and its attachment to sacculi by PBP1A from *Escherichia coli*. J Biol Chem. **2006**, 281, 26985-26993. https://doi.org/10.1074/jbc.M604083200.

Bush, K. Past and present perspectives on beta-lactamases. Antimicrob Agents Chemother. **2018**, 62, e01076-e1118. https://doi.org/10. 1128/AAC.01076-18.

Chen, W.; Zhang, Y.M.; Davies, C. Penicillin-binding protein 3 is essential for growth of *Pseudomonas aeruginosa*. Antimicrob Agents Chemother. **2017**, 61, e01651-e1716. https://doi.org/10.1128/ AAC.01651-16.

Cho, H.; Uehara, T.; Bernhardt, T.G. Beta-lactam antibiotics induce a lethal malfunctioning of the bacterial cell wall synthesis machinery. Cell. **2014,** 159, 1300 – 1311. https://doi.org/10.1016/j. cell.2014.11.017.

Clark, S.T.; Sinha, U.; Zhang, Y.; Wang, P.W.; Donaldson, S.L.; Coburn, B.; Waters, V.J.; Yau, Y.C.W.; Tullis, D.E.; Guttman, D.S.; *et al.* Penicillin-binding protein 3 is a common

adaptive target among *Pseudomonas aeruginosa* isolates from adult cystic fibrosis patients treated with β-lactams. *Int J Antimicrob. Agents.* **2019**, *53*, 620 – 628. https://doi.org/10.1016/j.ijantimicag.2019.01.009.

Di Guilmi, A.M.; Dessen, A.; Dideberg, O.; Vernet, T. Functional characterization of penicillin-binding protein 1b from *Streptococcus pneumoniae*. J Bacteriol. **2003**, 185, 1650 – 1658. https://doi.org/10.1128/JB.185.5.1650-1658.2003.

Diaz Caballero, J.; Clark, S.T.; Coburn, B.; Zhang, Y.; Wang, P.W.; Donaldson, S.L.; Tullis, D.E.; Yau, Y.C.; Waters, V.J.; Hwang, D.M.; *et al.* Selective sweeps and parallel pathoadaptation drive *Pseudomonas aeruginosa* evolution in the cystic fibrosis lung. mBio. **2015**, 6, e00981-15. https://doi.org/10.1128/mBio.00981-15.

Dundas, J.; Ouyang, Z.; Tseng, J.; Binkowski, A.; Turpaz, Y.; Liang, J. CASTp: computed atlas of surface topography of proteins with structural and topographical mapping of functionally annotated residues. Nucleic Acids Res. **2006**, 34, 116–118. https://doi.org/10.1093/nar/gkl282.

Fisher, J.F.; Mobashery, S. beta-lactam resistance mechanisms: Gram-positive bacteria and *Mycobacterium tuberculosis*. Cold Spring Harb Perspect Med. **2016**, 6, a025221. https://doi.org/10.1101/ cshperspect.a025221.

Fraipont, C.; Alexeeva, S.; Wolf, B.; van der, P.R.; Schloesser, M.; den Blaauwen, T.; Nguyen-Distèche, M. The integral membrane FtsW protein and peptidoglycan synthase PBP3 form a subcomplex in *Escherichia coli*. Microbiology. **2011**, 157, 251 - 259. https://doi.org/10.1099/mic.0.040071-0.

Freire, S.; Findlay, J.; Gruner, E.; Bruderer, V.; Nordmann, P.; Poirel, L. Modification of the penicillin-binding-protein 3 as a source of resistance to broad-spectrum cephalosporins in

Escherichia coli. J Antimicrob Chemother. **2024**, 79, 930 - 932. https:/doi.org/10.1093/jac/dkae020

Ghuysen, J.M. Serine beta-lactamases and penicillin-binding proteins. Annu Rev Microbiol. **1991**, 45: 37 - 67. https://doi.org/10.1371/journal.pone.0117874

Glen, K.A.; Lamont, I.L. β-lactam resistance in *Pseudomonas aeruginosa*: current status, future prospects. Pathogens. **2021**, *10*, 1638. https://doi.org/10.3390/pathogens10121638

Goffin, C.; Ghuysen, J.M. Multimodular penicillin-binding proteins: an enigmatic family of orthologs and paralogs. Microbiol Mol Biol Rev. **1998**, 62, 1079 - 1093. https://doi.org/10.1128/MMBR.62.4.1079-1093.1998.

Hackbarth, C.J.; Kocagoz, T.; Kocagoz, S.; Chambers, H.F. Point mutations in Staphylococcus aureus PBP 2 gene affect penicillin-binding kinetics and are associated with resistance. Antimicrob Agents Chemother. 1995, 39, 103 - 106. https://doi.org/10.1128/aac.39.1.103

Hujer, A.M.; Kania, M.; Gerken, T.; Anderson, V.E.; Buynak, J.D.; Ge, X.; Caspers, P.; Page, M.G.; Rice, L.B.; Bonomo, R.A. Structure-activity relationships of different beta-lactam antibiotics against a soluble form of *Enterococcus faecium* PBP5, a type II bacterial transpeptidase. Antimicrob Agents Chemother. **2005**, 49, 612 - 618. https://doi.org/10.1128/AAC.49.2.612-618.2005

Josephine, H.R.; Charlier, P.; Davies, C.; Nicholas, R.A.; Pratt. R.F. Reactivity of penicillin-binding proteins with peptidoglycan-mimetic beta-lactams: What's wrong with these enzymes?. BioChem. **2006**, 45, 15873 – 15883. https://doi.org/10.1021/cb7001347

Kishida, H.; Unzai, S.; Roper, D.I.; Lloyd, A.; Park, S.Y.; Tame, J.R. Crystal structure of penicillin binding protein 4 (dacB) from *Escherichia coli*, both in the native form and covalently linked to various antibiotics. Biochemistry. **2006**, 45, 783 - 792. https://doi.org/10.1021/bi051533t.

Land, A.D.; Tsui, H.C.; Kocaoglu, O.; Vella, S.A.; Shaw, S.L.; Keen, S.K. *et al*. Requirement of essential Pbp2x and GpsB for septal ring closure in *Streptococcus pneumoniae* D39. Mol Microbiol. **2013,** 90, 939 - 955. https://doi.org/10.1111/mmi.12408

Lau, C.H.; DeJong, E.N.; Dussault, F.; Carrillo, C.; Stogios, P.J.; Savchenko, A.; Topp, E.A Penicillin-binding protein that can promote advanced-generation cephalosporin resistance and genome adaptation in the opportunistic pathogen *Pseudomonas aeruginosa*. Int J Antimicrob Agents. **2020,** 55, 105896. https://doi.org/10.1016/j.ijantimicag.2020.105896

Lovering, A.L.; De Castro, L.; Lim, D.; Strynadka, N.C. Structural analysis of an "open" form of PBP1B from Streptococcus pneumoniae. Protein Sci. **2006**, 15, 1701 - 1709. https:/doi.org/10.1110/ps.062112106.

Macheboeuf, P.; Contreras-Martel, C.; Job, V.; Dideberg, O.; Dessen, A. Penicillin binding proteins: key players in bacterial cell cycle and drug resistance processes. FEMS Microbiol Rev. **2006**, 30, 673 - 691. https:/doi.org/10.1111/j.1574-6976.2006.00024.x.

Meisel, J.E.; Fisher, J.F.; Chang, M.; Mobashery, S. (2017). Allosteric inhibition of bacterial targets: an opportunity for discovery of novel antibacterial classes. In: Fisher, J.F., Mobashery, S., Miller, M.J. (eds) Antibacterials. Top. Med. Chem. **2017,** 25, 119 - 147. https://doi.org/10.1007/7355_2017_21

Mohammadi, T.; Ploeger, G.E.; Verheul J, Comvalius, A.D.; Martos, A.; Alfonso, C.; vanMarle, J.; Rivas, G.; den Blaauwen, T. The GTPase activity of *Escherichia coli* FtsZ

determines the magnitude of the FtsZ polymer bundling by ZapA *in vitro*. Biochemistry. **2009**, 48, 11056 - 11066. https://doi.org/10.1021/bi901461p.

Mouz, N.; Di Guilmi, A.M.; Gordon, E.; Hakenbeck, R.; Dideberg, O.; Vernet, T. Mutations in the active site of penicillin-binding protein PBP2x from *Streptococcus pneumoniae*. role in the specificity for beta-lactam antibiotics. J Biol Chem. **1999**, 274, 19175 - 19180. https://doi.org/10.1074/jbc.274.27.19175.

Nelson, D.E.; Young, K.D. Contributions of PBP 5 and DDcarboxypeptidase penicillin−binding proteins to maintenance of cell shape in *Escherichia coli*. J Bacteriol. **2001**, 183, 3055 – 3064. https://doi.org/10.1128/JB.183.10.3055-3064.2001

Otero, L. H.; Rojas-Altuve, A.; Llarrull, L. I.; Carrasco-Lopez, C.; Kumarasiri, M.; *et al.* How allosteric control of Staphylococcus aureus penicillin binding protein 2a enables methicillin resistance and physiological function. Proc. Natl. Acad. Sci. **2013**, 110, 16808 – 16813. https://doi.org/10.1073/pnas.1300118110

Periasamy, H.; Joshi, P.; Palwe, S.; Shrivastava, R.; Bhagwat, S.; Patel, M. High prevalence of *Escherichia coli* clinical isolates in India harbouring four amino acid inserts in PBP3 adversely impacting activity of aztreonam/avibactam. J Antimicrob Chemother. **2020**, 75, 1650 - 1651. https:/doi.org/10.1093/jac/dkaa021.

Ranjitkar, S.; Reck, F.; Ke, X.; Zhu, Q.; McEnroe, G.; Lopez, S.L.; Dean, C.R. Identification of Mutations in the *mrdA* Gene Encoding PBP2 That Reduce carbapenem and diazabicyclooctane susceptibility of *Escherichia coli* clinical isolates with mutations in *ftsI* (PBP3) and which carry $bla_{\text{NDM-1}}$. mSphere. **2019**, 4, e00074-19. https://doi,org/10.1128/mSphere.00074-19.

Sauvage, E.; Herman, R.; Petrella, S.; Duez, C.; Bouillenne, F.; Frère, J.M.; Charlier, P. Crystal structure of the *Actinomadura* R39 DD-peptidase reveals new domains in penicillin-binding proteins. J Biol Chem. **2005**, 280, 31249 - 31256. https://doi.org/10.1074/jbc.M503271200.

Sauvage, E.; Kerff, F.; Terrak, M.; Ayala, J.A.; Charlier, P. The penicillin-binding proteins: structure and role in peptidoglycan biosynthesis. FEMS Microbiol Rev. **2008**, 32, 234 - 258. https://doi.org/10.1111/j.1574-6976.2008.00105.x.

Scheffers, D. J.; Pinho, M. G. Bacterial cell wall synthesis: new insights from localization studies. Microbiol. Mol. Biol. 2005, 69, 585 – 607. https://doi,org/10.1128/MMBR.69.4.585-607.2005

Schwartz, B.; Markwalder, J.A.; Wang, Y. Lipid II: total synthesis of the bacterial cell wall precursor and utilization as a substrate for glycosyltransferase and transpeptidation by penicillin binding protein (PBP) 1b of *Escherichia coli*. J Am Chem Soc. **2001**, 123, 11638 - 11643. https://doi.org/10.1021/ja0166848

Sethuvel, D.P.M.; Bakthavatchalam, Y.D.; Karthik, Irulappan, M.; Shrivastava, R.; Periasamy, H.; Veeraraghavan, B. Beta-Lactam resistance in ESKAPE pathogens mediated through modifications in penicillin-binding proteins: an overview. Infect Dis Ther. **2023**, 12, 829 – 841. https://doi.org/10.1007/s40121-023-00771-8

Sethuvel, D.P.M.; Bakthavatchalam, Y.D.; Karthik, M.; Irulappan, M.; Shrivastava, R.; Periasamy H.; Veeraraghavan, B. Beta-lactam resistance in ESKAPE pathogens mediated through modifications in penicillin-binding proteins: an overview. Infect Dis Ther. **2023,** 12, 829 - 841. https:/doi.org/10.1007/s40121-023-00771-8.

Stefanova, M.E.; Tomberg, J.; Olesky, M.; Holtje, J.V.; Gutheil, W.G.; Nicholas, R.A. *Neisseria gonorrhoeae* penicillin-binding protein 3 exhibits exceptionally high

carboxypeptidase and beta-lactam binding activities. Biochemistry. **2003**, 42, 14614 -14625. https://doi.org/10.1021/bi0350607.

Sujoy, K.S.; Chiranjit, C.; Anindya, S.G. Deletion of penicillin−binding protein 5 (PBP5) sensitises *Escherichia coli* cells to beta−lactam agents. Int. J Antimicrob Agents. **2010,** 35, 244 – 249. doi: 10.1016/j.ijantimicag.2009.11.004.

Tooke, C.L.; Hinchliffe, P.; Bragginton, E.C.; Colenso, C.K.; Hirvonen, V.H.A.; Takebayashi, Y.; Spencer, J. Beta-lactamases and beta-lactamase inhibitors in the 21st Century. J Mol Biol. **2019**, 431, 3472 - 3500. https://doi.org/10.1016/j.jmb.2019.04.002.

Wardell, S.J.T.; Rehman, A.; Martin, L.W.; Winstanley, C.; Patrick, W.M.; Lamont, I.L. A large-scale whole-genome comparison shows that experimental evolution in response to antibiotics predicts changes in naturally evolved clinical *Pseudomonas aeruginosa*. *Antimicrob. Agents Chemother.* **2019**, 63, e01619 - 19. https://doi.org/10.1128/AAC.01619-19.

Xiaoliang, B.; Harrison, E.M.; Edwards, G.F.; Holden, M.T.; Larsen, A.R.; Petersen, A.; Skov, R.L.; Peacock, S.J.; Parkhill, J.; Paterson, G.K.; Holmes, M.A. Novel mutations in penicillin-binding protein genes in clinical *Staphylococcus aureus* isolates that are methicillin resistant on susceptibility testing but lack the *meC* gene. J Antimicrob Chemother. **2014**, 69, 594 - 597. https://doi.org/10.1093/jac/dkt418.

Yen, P.; Papin, J.A. History of antibiotic adaptation influences microbial evolutionary dynamics during subsequent treatment. PLoS Biol. **2017**, 15, e2001586. https://doi.org/10.1371/journal.pbio.2001586. PMID: 28792497

Zapun, A.; Contreras-Martel, C.; Vernet, T. Penicillin-binding proteins and β-lactam resistance. FEMS Microbiol. Rev. **2008**, 32, 361 – 385. https://doi.org/10.1111/j.1574-6976.2007.00095.x

2.3 Progressive approach of phenolic acids towards the advancement of antimicrobial drug

This section has been published as a book chapter (Chapter five) in Advancement of Phenolic Acids in Drug Discovery, Fundamental and Applications and is presented as it is in the chapter

CHAPTER 5

Progressive approach of phenolic acids toward the advancement of antimicrobial drugs

Jamiu Olaseni Aribisala, Christiana Eleojo Aruwa and Saheed Sabiu
Department of Biotechnology and Food Science, Faculty of Applied Sciences, Durban University of Technology, Durban, South Africa

5.1 Background and introduction

Antimicrobials are medicines that treat or prevent infections in crops and plants, animals and humans. Antimicrobial resistance (AMR) occurs over time when microorganisms (bacteria, fungi, viruses, and parasites) fail to respond to medicines or antibiotics making diseases more difficult to treat, thus increasing their risk of spread, severe morbidities, and mortality [1]. In 2013 about 2 million AMR-associated infections resulted in thousands of deaths in America and the case is not any better in other parts of the world [2]. More recently, AMR caused close to 2 million deaths in 2020 and could prove to be more life threatening than COVID-19 if no suitable solution is provided in the nearest future [3]. Its impact on health-care costs can also not be ignored, as close to €2 billion has been spent on resistant infection therapy in 2022 alone [3,4].

The foregoing worrisome trends led scientists to shift focus to plant secondary metabolites such as phenolics as a readily available source of new and potent chemical entities with antimicrobial properties. Thousands of phenolic compounds are known to date with their characteristic aromatic benzene ring with attached hydroxyl (-OH) groups. The number of -OH groups further contribute to increase or decrease the antimicrobial efficacy of various phenols and phenolic acids (PAs) [5–7]. Base materials to produce phenols in plants include tyrosine and/or phenylalanine which enters the shikimate pathway and the addition of -OH groups is integral in their biosynthesis [8,9]. Phenols may be simple or complex molecules, but PAs or phenol carboxylic acids (PCA) are majorly simple, low-molecular weight compounds. Examples of simple PA are

Advancement of Phenolic Acids in Drug Discovery
DOI: https://doi.org/10.1016/B978-0-443-18538-0.00004-4
© 2024 Elsevier Inc. All rights are reserved, including those for text and data mining, AI training, and similar technologies.

benzoic and cinnamic (the simplest aromatic carboxylic acid), syringic, sinapic (4-hydroxy-3,5-dimethoxy-cinnamic acid), gallic or 3,4,5-trihydroxybenzoic acid, caffeic and ferulic acids [10], hydroxybenzoic, coumaric, protocatechuic, vanillic, veratric, and chlorogenic acids [9]. In addition, 3-hydroxybenzoic acid [11], gallic [12], vanillic also known as 4-hydroxy-3-methoxybenzoic acid [13]; and digallic acid (3,4-dihydroxy-5-(3,4,5-trihydroxybenzoyl)-oxy] benzoic acid, a viral reverse transcriptase inhibitor [14], all show good antimicrobial properties. Rosmarinic acid is also a good antiviral agent [15], with significant antibacterial action against *Micrococcus luteus*, *Bacillus subtilis*, and *Escherichia coli* [16]. Also, salicylic (2-hydroxybenzoic acid) has shown promising antifungal activities against skin infections like psoriasis, seborrheic dermatitis, dandruff, acne, and ichthyosis [17].

PAs contain a carboxylic group attached to the benzene ring and have one or more -OH or methoxy(-OCH_3) groups attached to it [18]. Syringic acid possesses two -OCH_3 in metapositions and one -OH group in a para position, gallic has three -OH at the meta and para positions [19], caffeic has two -OH groups and ferulic has one -OCH_3 and -OH group each [9]. PCAs are distributed in many plant parts including the roots, leaves, stems, fruits, seed coat, and bran, but with plant leaves and stems containing higher levels of PAs [20,21]. In other words, PAs make up a major part of our diets and are found in all foods; fruits, herbs, vegetables, among others [22]. The bioavailability of PAs is, however, dependent on their existence as conjugated or free compounds in foods, and PA levels can be impacted by food processing. Within the host, they are then metabolized by the host gut microflora resulting in chemical and structural changes and conjugations, but host responses vary and are affected by genetic variations, metabolism, and absorption [23].

Research on phenolic compounds over time has associated them with two major antimicrobial mechanisms. One is interruption of chemical biosynthetic pathways or disruption of key component functions in the target bacterial organism, and second is the bypassing of conventional AMR mechanisms in resistant microorganisms [24]. Still, the efficacy of an antimicrobial compound must be viewed in relation to its absorption, distribution, metabolism, excretion, availability, stability, route of administration, target specificity, and ability to control relevant pathways linked to antimicrobial activity [25]. Studies continue to report highly variable antimicrobial efficacy results for pure PAs and PA-containing extracts. Nonetheless, it has been demonstrated that many soluble and insoluble

esterified PCAs are readily taken up in the small intestine and colon, respectively [26,27], and through para-cellular diffusion or monocarboxylic acid transporters (MCT) [28]. Meanwhile, PAs excretion is mainly via the urine and about 1% are excreted through the bile [29].

Considering the foregoing, this chapter targets the increased awareness of all relevant stakeholders to the promise that natural PAs hold for novel antimicrobial drugs development and utilization in infections treatment and prevention, as well as in combating rising AMR trends and improving global public health indices. It updates on scientific efforts and strategies that give credence to the focus on PAs as key metabolites for novel antimicrobials development. Challenges facing the attainment of this venture are also itemized, alongside PAs mechanisms of action, use in various industries, strategies to enhance their antimicrobial activity, and for novel antimicrobials discovery and development. Literature sources utilized in the collation of this chapter were derived from libraries/databases and platforms such as the Nation Centre for Biotechnology Information (NCBI), PubMed, Google Scholar and ScienceDirect, and specialized agency reports (World Health Organization, European Academies' Science Advisory Council [EASAC]), among others. Records cover from inception till August 2022 to help fine-tune results for thorough appraisal of the topic. Contents of this chapter would be of benefit to the science research community, medical and health industries, specialized agencies, and other invested relevant stakeholders.

5.2 Mechanism of antimicrobial action of phenolic acids

Antimicrobial drugs or agents act on one or more microbial targets; protein, membrane and cell wall biosynthesis, metabolic pathways inhibition, RNA and/or DNA repair or replication [30]. Also, innate resistance mechanisms aid bacteria in circumventing antimicrobial drugs. AMR can be developed over time and through microbial generations, such that previously sensitive populations become resistant to antimicrobial drugs [31]. Hence, to reduce development of antibiotic-resistant, one must also be well acquainted with microbial innate mechanisms of antibiotic resistance [32]. Some of these mechanisms include antibiotic drug modification by modifying enzymes, efflux pump activation, and the use of enzymes to destroy antimicrobials (Figs. 5.1 and 5.2) and reducing agent-target affinity by changing target structures in the bacterium (Fig. 5.2) [33]. Each case of drug resistance may also be attributed to one or more of these mechanisms. AMR is also majorly

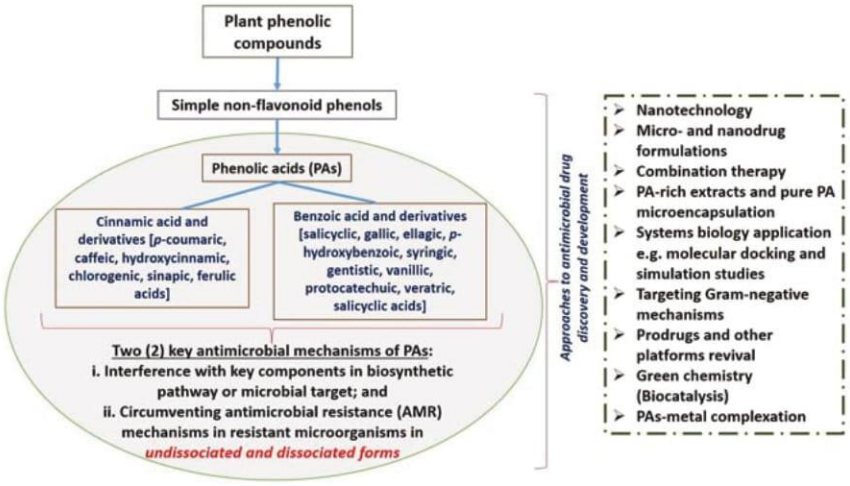


Figure 5.1 Schematic representation of various antimicrobial approaches of phenolic acids.

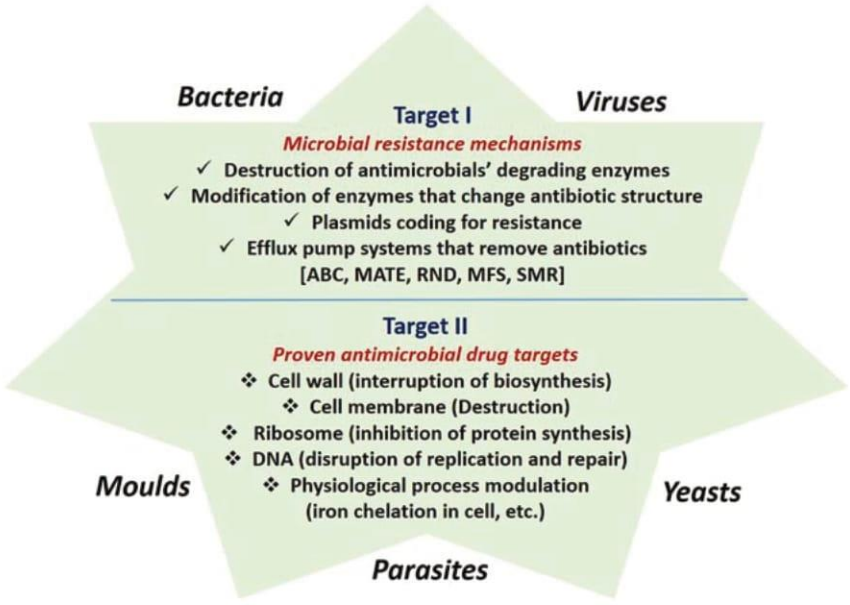


Figure 5.2 Different antimicrobial targets of phenolic acids.

spread through plasmids, that is, genetic materials that can replicate independently of the host microorganism and be transferred through respective bacterial species or strain populations [24].

The antimicrobial efficacy of PAs also depends on the specific attributes of the microorganism or strain (nature of cell membrane or cell wall), the PA chemical nature and concentration, as well as the microbial pathogen's susceptibility and concentration [34]. Likewise, the microbial pathogens mechanism for evading antimicrobial agents must be well understood, and in relation to particular environmental biotic (presence or absence of other microbes and/or pathogens) and abiotic (temperature, pH, composition of media, etc.) factors [35]. Like many antimicrobials, PAs may evince their antimicrobial action by interaction with cellular structures, interfering in cell biosynthetic pathways, and attenuation of energy mechanism and multisite activity [36]. PAs may also participate in complex formation with extracellular soluble proteins to achieve disruption of microbial cell wall, and decrease break down of peroxide (H_2O_2) that enhance oxidative damage via induction of oxidative stress in microbial pathogens [37].

Furthermore, PAs are reported to interfere with substrate adhesion capacity. They bind to adhesion membrane proteins and interrupt the ability of the bacterial pathogen to attach to mucous membranes, thus altering the infectious process through competitive exclusion and attachment. PAs may also cause a reduction in adenosine triphosphate (ATP) levels and breakdown of proton motive force across microbial membranes when they act as proton exchangers, thus resulting in microbial cell death [34]. The disabling of relevant amino acids (AA) biosynthesis through interruption of erythrose-4-phosphate, shikimic acid, and phosphoenolpyruvate stepwise reactions by PAs is another possible mechanism of antimicrobial action, as is the case for polyphenol compounds [38]. PAs may also act by changing the polarity of cellular membrane lipid molecule heads by electron delocalization which achieves the modification of microbial cell membrane integrity [34].

Hydroxyl (-OH) groups in the PA chemical structure can also inactivate microbial enzymes like amylase, ATPase, protease, and histidine decarboxylase. As would be expected, ATPase inhibition is a precursor of cell respiration disruption that can invariably result in microbial cell death [34]. A study by Borges et al. showed that ferulic and gallic acids caused irreversible damage to cell membrane of the test Gram-negative and Gram-positive bacteria: *Listeria monocytogenes*, *E. coli*, *Staphylococcus aureus*, and *Pseudomonas aeruginosa* [39]. There were observable changes in cell permeability, polarity/charge (reduced cell surface negative charge), and physicochemical characteristics (hydrophobicity cell surface changes). Also,

formation of pore breaks and which caused leakage of cellular constituents (potassium).

PAs possess the same basal structure, but the type of substituents, position, and numbers of -OH groups on the benzene ring led to variations in their properties [40]. The number and location of -OH groups are related to antioxidant and antimicrobial activities. Presence of a high number of -OH groups would equate with higher cytotoxic effects. Also, highly oxidized phenols may have improved antimicrobial effect [41]. Gallic, protocatechuic, and salicylic acid are -OH derivatives, while veratric and *p*-anisic acids are methoxy (-OCH_3) derivatives of benzoic acid. The presence of methoxy or hydroxyl functional groups in PAs may influence antimicrobial activity [42]. Except for 2-hydroxybenzoic, it was demonstrated that addition of -OH and -OCH_3 substituents reduced inhibition of *E. coli*. The ortho-positioned -OH group (at the second carbon atom in the benzoic ring) reduced kill time of cells, while -OCH_3 substituents in PAs significantly reduced *E. coli* ability to form biofilms compared to benzoic acid -OH derivatives [43]. PAs modify the nonpolar, polar, and electron acceptor components of microbial cells like *Oenococcus oeni* and *Lactobacillus hilgardii* [39,44], with Gram-positive bacteria being more susceptible to antimicrobial agents than Gram-negative bacteria [45]. Gram-negative bacteria possess a lipopolysaccharide (LPS) cell wall and passage through the membrane depends on the nature of the antibiotic agent and modulated by hydrophilic porin networks that usually do not allow hydrophobic compounds entry. Entry of antimicrobials in this case is facilitated by use of permeabilizers to weaken LPS layer [46]. Carboxyl and phosphate anionic groups on bacterial cell surfaces make them negative charged under physiological conditions. Yet, these charges vary from strain to strain and are affected by pH, ionic strength, and culture age [47,48].

The concentration of the undissociated phenolic acid also affects their antimicrobial action. Since PAs are partially lipophilic, it is assumed that they cross the cell membrane by passive diffusion in their whole form, and in so doing cause cell membrane disruption and acidify the internal cellular environment leading to denaturation of proteins [30]. Hyperacidification can modify cell surface potential, increasing membrane permeability [39]. So, the lipophilicity and pKa (acid dissociation constant) are key determinants of PAs solubility across microbial membranes [30]. Antimicrobial action of PAs has to do with the ability of the hydroxyl group to bind integral enzymes active centers to modify microbial cell

metabolic pathways [49]. Other mechanisms of PA action may include enzymes inactivation, binding to adhesins, substrate deprivation, complex formation with metal ions and cell wall [50,51]. In a study to assess the individual mechanism of action of PAs, it was shown that antimicrobial activity was largely associated with effect of PAs in their undissociated forms, for example, caffeic, vanillic, protocatechuic, and *p*-hydroxybenzoic acids. Ferulic and *p*-coumaric acids showed notably inhibition of *L. monocytogenes* in both dissociated and undissociated forms, except for gallic and chlorogenic acids that acted by reducing pH of the extracellular environment [52]. Chlorogenic acid was also shown to be potent at 8−16 μg/mL concentrations against biofilm formed by *Stenotrophomonas maltophilia*, an emerging nosocomial pathogen. The microbe's ability to adhere to polystyrene plate was greatly reduced by the PA [53,54].

In addition, although antimicrobial activity of PAs is associated with reactive species (ROS) generation, normal body cells are expected to maintain homeostatic balance in ROS levels, and the antioxidant-antimicrobial activity link is poorly understood. Antimicrobials induce oxidative stress by upregulating ROS levels beyond microorganism antioxidant defense systems [55]. The oxidatively stressed microbial cells are then inhibited (-static) or killed (-cidal) when the highly reactive free radicals generated induce cell, tissue, RNA or DNA damage by breakage or cross-linking of ribo-nucleoproteins or reactions with cell membrane proteins, nucleotides, and lipids [56]. Reactive free radical species also result in alkali labile sites, breaks in DNA single strand, and damage pyrimidine and purine bases [57]. Therefore increasing levels of ROS through PA utilization in antimicrobial therapy levels could be a viable option to control infectious cells growth, survival, and antimicrobial resistance.

On the other hand, antiviral activity of PAs is associated with protein and enzymes (reverse transcriptase, polymerase needed in viral replication) inactivation, thus disease onset is stalled by impeding multiplication and spread of the virus in the host. Phenolic acids also inhibit viral adhesins by binding competitively to membrane proteins and preventing membrane and viral envelop fusion [58,59]. Mechanism of antiviral action in phenols is reported to depend on the viral structure and type, but still require further elucidation and research. Likewise, each phenol compound needs to be tested against the wide array of viral families, followed by studies on their synergism with other compounds [60]. An antimicrobial drug design approach involving metal complexation may also be used to enhance phenolic acids antiviral capacities [61]. Novel processing and biotechnological

techniques could suffice to enhance solubility of antiviral agents in vivo for better treatment outcomes [62]. Thus PAs have great prospects as natural and sustainable sources for novel antimicrobial drugs development.

5.3 Phenolic acids toward the advancement of antimicrobial drugs

Pathogenic or opportunistic microorganisms bring about diseases in humans. Unfortunately, over time microbes have also evolved to become resistant to treatment regimens and approaches. Given the limited pool of antimicrobial agents in the face of multidrug resistance (MDR) trends, humans must also evolve new approaches. One of such strategies include research into promising phenol compounds and phenolic acids that abound in nature as potential antimicrobials for drug development [63]. A host of plants and herbs are traditionally used for their medicinal and antimicrobial properties [64,65]. It has been often reported and suggested that antioxidant-rich diets decrease susceptibility to diseases like diabetes, cancer, induced by oxidative stress [66,67]. Medicinal plants are rich in bioactive metabolites and their antioxidant attributes are linked to phenolic acids and flavonoid phenol compounds [68]. Plants also utilize PAs for flavor, color, and odor (smell) development, as well as defense against insects, viruses, and ultraviolet (UV) protection [69].

5.3.1 Toward antibacterial and antifungal drugs development

As a subclass of plant phenols with a carboxyl (-COOH) group, PAs are considered hydroxycinnamic and hydroxybenzoic acids derivatives (Fig. 5.2) [70,71]. They have a phenol component and stable resonant structure that is closely linked to their antioxidative and antimicrobial capacities. Compared to their butyl or methyl ester derivatives, PAs show good antimicrobial potential [66]. An earlier study using caffeic, vanillic, gallic, and protocatechuic acids reported that of all the PAs tested, caffeic acids showed the most significant affect against *L. monocytogenes* [72].

The PA derivatives, protocatechuic and 2,4-dihydroxybenzoic acids, showed significant activity against Gram-positive and Gram-negative bacteria [73]. Inhibition of methicillin sensitive *S. aureus* (MSSA) was observed at 1 mg/mL minimum concentration for *p*-coumaric acids, and 0.5 mg/mL for vanillic, 2,4-dihydroxybenzoic and syringic. Derivatives of cinnamic acid showed better antimicrobial potency against coccoid-shaped Gram-negative and Gram-positive bacteria. Following elaboration

of structure–activity relationship (SAR), it was shown that the presence of two (2) hydroxyl (-OH) groups in para(*p*) and ortho(*o*) positions, as well as carboxylic acid (-COOH) on the benzene ring, and metapositioned methoxy (-OCH3) group seemed relevant to their antimicrobial activity against methicillin-resistant *S. aureus* (MRSA). Hence, PAs could be exploited as antimicrobial agents, namely against MDR-microorganisms [73]. In a more recent study, the components of a biologically active fraction of *Cylicodiscus gabunensis* legume were elucidated using chromatographic and spectrometric techniques. The bioactive compounds included gallic acid, its derivatives, and its chemo-synthesized analogs (alkyl gallates). Longer alkyl-chained gallates showed improved antibacterial activities. The presence of double bond with structure having a confined C-5 side chain had less impact on antibacterial potency. The gallate analogs acted by disrupting the integrity of *S. aureus* bacterial cell wall. Thus, gallic acid and its gallate-based derivatives hold great potential to serve as antimicrobial agents for infection therapy [74]. Another PA, *p*-coumaric acid, was also demonstrated to actively damage the cell membrane of *S. aureus* and other food pathogens at a concentration between 2.5 and 10 mg/mL [75].

Furthermore, at minimum inhibitory concentrations range of 500–2000 mg/mL for gallic acid and 100–1250 mg/mL for ferulic acid, both PAs showed significant antibacterial capacity against *P. aeruginosa*, *E. coli*, *S. aureus*, and *L. monocytogenes* and caused irreversible damage to the cells [39]. The assortment of caffeic, gallic, quinic, and chlorogenic acids were also effective in vitro against fungal (*Candida parapsilosis*, *C. albicans*) and bacterial (*S. aureus*, *Proteus mirabilis*, *E. coli*, *Klebsiella pneumoniae*, *P. aeruginosa*, *B. subtilis*, *Acinetobacter baumannii*, *Enterococcus faecalis*) cells [76]. Also, *p*-hydroxybenzoic and cinnamic acid in honey showed better inhibitory activity against *S. aureus* growth compared to *E. coli*, *B. subtilis*, *K. pneumoniae*, and *S. lentus*. Natural honey also contains ferulic, *p*-coumaric, ellagic, and caffeic acids [77].

Earlier in 1950, Barbour and Vincent utilized the mass inoculum approach to study the bacteriostatic effect of benzoic acid, its derivatives, and phenols over a brief exposure time without disrupting the logarithmic phase of growth in *Enterobacter aerogenes* and *Aspergillus niger* [78]. An inverse association was found between compounds' solubility in water and inhibition potency. Ortho-positioned -COOH and -OH groups increased compounds potency, while para- and metasubstituted groups decreased bacteriostatic potency. In terms of ability to attain up to 50% growth

inhibition and potency, the compounds tested followed the order, benzoic acid and 2 di-hydroxybenzoic acid derivatives > mono-hydroxybenzoic acids. Increased inhibitions were reported as the ability of the compounds to be adsorbed on and appreciably saturate the microbial cell surface. Some slight agreement existed between compound biological adsorbability and inhibition percentage. Still intrinsic differences in terms of biological surface areas affected and efficacy per compound or both were observed and expected [78].

The PA-rich (caffeic and vanillin acid, and other phenols) extract of the olive tree (*Olea europaea*) favorably inhibited *Bacillus cereus*, *Salmonella enterica*, *E. coli*, and *S. aureus* [79,80]. Olive oil rich in cinnamic and ferulic acids also showed notable inhibition of *Helicobacter pylori*, *L. monocytogenes*, *S. enterica*, and *E. coli* [81]. Grapefruit wines rich in vanillic, caffeic, gallic acids, and other phenols, were also active against an array of pathogenic Gram-positive and negative bacteria that included *E. faecalis*, *Moraxella catarrhalis*, *Streptococcus pneumoniae*, and *Streptococcus agalactiae* [72,82]. The crude extracts of *Carduus acanthoides* herb containing caffeic, *p*-coumaric, chlorogenic, *p*-hydroxybenzoic, protocatechuic, gallic, gentisic, vanillic, ferulic, and syringic acids were effective against molds, yeasts, Gram-positive and negative bacteria [83]. Sugarcane phenol extract containing PAs in the order of gallic > ferulic > coumaric > chlorogenic acids significantly inhibited *S. aureus* at 0.625 mg/mL minimum concentration [84]. Common yarrow and chamomile extracts with high concentrations of rosmarinic and caffeic acids were also notably active against *S. aureus*, *L. monocytogenes*, *B. cereus*, *Salmonella infantis*, *E. coli*, and *Campylobacter coli* food pathogens [85].

5.3.2 Toward antiparasitic drugs development

Parasitic infection likewise constitutes a major public health concern for their ability to cause infections and death, especially in developing regions of the world. The symptoms of parasitic infections include bloody stool (dysentery), diarrhea, liver abscesses, abdominal tenderness, and pain, as is associated with amebiasis caused by *Entamoeba histolytica* and other parasitic or protozoan infections [86]. Amebiasis caused by *E. histolytica* affects about a 10th of the global population [86], causing hundreds of thousands of deaths annually [87,88], and if left untreated results in the destruction of intestine tissues and liver amebiasis, both constituting significant complications [89]. In treatment of amebiasis, regular administration of

amebicides through the vein, muscle, or orally, are required. Invasive amebiasis is treated with metronidazole (a nitroimidazole) [90], but few amebicidal drugs are currently administered due to their adverse side effects and narrow spectrum of activity [91].

Likewise, trypanosomiasis (sleeping sickness) is another deadly parasitic infection that is difficult to eradicate because drugs to control it are limited and toxic, and the implicated parasites, *Trypanosoma* species, show drug resistance [92]. *Trypanosoma brucei rhodesiense* and *T. brucei gambiense* cause trypanosomiasis in East, West, Southern, and Central African territories, putting millions of individuals at risk of being infected [93]. The diseases, leishmaniasis, is another prevalent parasitic infection caused by *Leishmania* species. It is prevalent in more than 80 nations of the world and responsible for millions of new cases in over four continents, annually. *Leishmania* species cause thousands to millions of cutaneous or muco-cutaneous and visceral leishmaniasis cases globally [94]. Also, Chagas disease caused by *Trypanosoma cruzi* which affects millions of individuals in America is another parasitic disease of global concern [94,95]. The go-to drug for leishmaniasis therapy are pentavalent antimonials (Sb^{5+}) [96], and medications like miltefosine, paromomycin, pentamidine provide new treatment options but are still faced with the challenges of high cost and toxic side effects [97]. Also, parasites like the *Trypanosoma* exhibit antigenic variation allowing it to evade and resist current therapeutic drug regimens. Also, vaccines are currently not available for many parasitic infections. Hence, studies evaluating natural products as alternative treatments remain relevant for the development of new, efficacious, and safe antiparasitic therapies [98].

In certain research efforts, the extract of *Peucedanum longibracteolatum* plant at minimum concentration of 4 mg/mL have demonstrated a dose- and time-dependent amebicidal activity on *E. histolytica* trophozoites after 3 days of treatment exposure. The extracts were found to contain a rich content of phenolic acids; *o*-coumaric, *p*-hydroxybenzoic, and gallic acids at 14.442, 17.646, and 11.144 mg/g of extract, respectively, alongside other amebicidal phenols. Thus *P. longibracteolatum* plant and its phenolic compound could be further studied and explored as potential drug therapies for amebiasis. Nonetheless, other species of the *P.* genus, that is, *P. caucasicum*, *P. chryseum*, and *P. palimbioides* were also efficacious in decreasing the parasite burden to varied degrees over the course of extract treatment exposures. Again, since a direct correlation was not established

between the PAs and antiparasitic activity, research aimed at evaluating and establishing the existence of such relationship are still needed [99].

In addition, the trypanocidal efficacy of some PAs on *Trypanosom abrucei* was assessed using in vitro assays. Rosmarinic and gallic acids showed notable trypanocidal activities with IC_{50} values of 17.31 and 14.2 μM, respectively. The PAs and deferoxamine (the positive control) showed dose-dependent efficacy on *Trypanosoma* mitochondrion membrane integrity and cell viability. Gallic acid resulted in a 22% loss in kinetoplast of trypanosomes and a 0.6-fold reduction in expression of cyclin 2 genes, ribonucleotide reductase and transferrin receptor. Also, compared to current drugs used and the study control, the phenolic acid was moderately toxic to cell lines in vitro. Gallic acid's trypanocidal mechanism of action was attributed to its iron chelating attribute on *T. brucei* that lead cell cycle arrest, as well as changes in morphology and structure [92].

Iron chelation therapy has been demonstrated to be a possible therapy option for parasitic infections, including malaria [100]. This is closely linked to parasites' need for iron via the degradation of host red blood cells as the cells do not take up iron themselves, thus making the parasites susceptible targets for iron chelators used in chemotherapies [101]. Iron (Fe) is used in energy metabolism, electron transport, and DNA synthesis and Fe chelators act by chelating Fe from sources like extracellular and intracellular Fe and transferrin Fe [102]. Iron chelators' antiparasitic activities depend on the ability of the chelator to enter and exit the cell after treatment, and the chelator's Fe-binding capacity [101]. Phenolic compounds like PAs have chelator potential and therefore can modulate physiological processes requiring transitional metals and Fe in parasites [103,104]. Phenolic acids antimalarial activity may also be associated with their antioxidant activity and potential Fe chelating effect [105].

In another study utilizing conventional in vitro drug assays, a wide array of benzoic and cinnamic acids derivatives were evaluated for their potential antimalarial efficacy [106]. Protocatechuic and gallic acids, as well as ferulic, *o*-coumaric, chlorogenic, rosmarinic, and caffeic acids were tested against *Plasmodium falciparum* 3D7 clones. The most effective antimalarial PAs were protocatechuic, gallic, and caffeic acids with respective IC_{50} values of 30.08, 26.59, and 17.73 μg/mL, while other PAs with higher IC_{50} values demonstrated moderate antimalarial action. Results indicated that natural phenolic compounds like PAs have significant antimalarial activity and could be further explored through structural manipulations and other new and emerging technologies to enhance their antimalarial or antiplasmodial effects [106].

Furthermore, notable antiparasitic activity has been reported for *Guazuma ulmifolia* Lam. (Malvaceae) ethanol leave extract against *Leishmania infantum*, *Leishmania brasiliensis*, and *Trypanosoma cruzi* with 95.23%, 92.20%, and 63.86% growth inhibition, respectively, at 500 lg/mL concentration. Rosmarinic, caffeic, chlorogenic, and gallic acids were identified in the extract, alongside some bioactive flavonoid compounds. The presence of these polyphenolic compounds explained the significant inhibition and leishmanicidal activity of the extract. Nevertheless, a high cytotoxic effect (> 50%) was reported at the highest concentration used (1000 lg/mL) and thus called for further tests prior to conducting in vivo trials [107].

5.3.3 Toward antiviral drugs development

Types 1 and 2 of the herpes simplex virus (HSV) cause disease in humans and constitute risk factors for contracting human immunodeficiency virus (HIV) infection [108]. Unfortunately, AMR to herpes medications have also been reported, and require novel, natural, and safe treatment alternatives. The aqueous extract of *Plantago major* used in Chinese trado-medicine for viral hepatitis therapy had demonstrated notable anti-HSV activity. The extract's rich content of phenol compounds, and in particular, caffeic acid, were responsible for the antiviral activity detected [109]. Anti-HSV 1 and 2 activities were again reported for aqueous extract of *Pelargonium sidoides* containing simple phenolic acids, coumarin, and other phenols [110]. In addition, the array of caffeic, gallic, quinic, and chlorogenic PAs have been shown to possess good antimicrobial activities in vitro. They were efficacious and toxic to the viruses; herpes simplex type 1 DNA and para influenza RNA viruses. Gallic acid specifically showed potent antiviral activity at 0.8−0.05 μg/mL concentrations, while the other phenolic acids showed varied and reduced antiviral efficacies [76].

Chicoric acid (a hydroxycinnamic acid derivative) found in *Cichorium intybus* (chicory leaves), basil, fern, seagrass, and lettuce, is a tartaric acid ester made up of two caffeic acid molecules. Chicoric acid was reportedly involved in HIV reverse transcriptase polymerase and HIV integrase inhibition, both at the IC_{50} value of 17 μM [111,112]. The hydro-alcoholic extract of *Achyrocline satureioides* (Lam.) containing significantly higher content of chlorogenic acid compared to caffeic acid also inhibited the intracellular replication of Western Equine Encephalitis virus (WEEV) at 5 g/mL concentration. The extract also showed no mutagenic or toxic effect in vivo [113]. High levels of gallic acid in extracts and acorns have

further been shown to inhibit severe acute respiratory syndrome coronavirus (SARS-CoV-2) replication [114]. Gallic (18.3% inhibition), chlorogenic (25.5% inhibition), and rosmarinic (22.5% inhibition) acids have also been shown to slightly bind and control the SAR-CoV-2 receptor-binding domain (RBD), inhibiting virion particle attachment, and entry [115].

Salicylic and benzoic acids have also been identified in eucalyptus extracts that inhibited tobacco mosaic virus (TMV) at a concentration of 100 μg/mL [116]. The *Morus alba* (mullberry) juice contains gallic, chlorogenic, caffeic, and *p*-coumaric acids and other phenols, and its extracts were active against the H1N1 influenza virus, influenza A virus (IAV), and infectious bursal disease virus (IBV) families, and probably carried out their antiviral activity through interference with virion attachment and entry into cells [117]. Also, *Arachis hypogaea* (L.) skin extract with rich content of phenolic acids alongside other bioactive phenols at IC_{50} of 1−1.5 μg/mL were also effective against IBV and IAV by disrupting various virion replication stages [118].

Chlorogenic acid [119], like other phenolic acids, shows a different mechanism against various viral families [120], but interferes with DNA synthesis when it binds to HepG2. A64 and HepG2.2.15 receptor proteins to evince its antiviral action on HBV [60]. Gallic acid is reported to adversely impact viral replication cycle by interacting with the amino acid, Arg152, of the neuraminidase protein, and is also efficacious against HIV, hepatitis C virus, HSV-2, enterovirus (EV-71) [121], and human rhinoviruses (HRV). Its antiviral activity has been linked to its viral absorption inhibition and antioxidative properties [122]. Likewise, fungus-derived phenolic acids (mycophenolic acids), gallic, caffeic, and chlorogenic acids have demonstrated sustained antiviral capacity against the human CoVs (HCoVs) [65,123]. Gallic, vanillic, *p*-coumaric, caffeic, syringic, ferulic acids have also been identified as potent alternative drug targets for COVID-19 treatment and its related pneumonia infections [65,124−129].

5.4 Enhancing phenolic acids use in antimicrobial drug development

5.4.1 Combination therapy (phenolic acids and other compounds)

Regarding combination therapy (CT) exploration (Fig. 5.1), more research is required in evaluating the impact of phenolic acids and other

natural and/or synthetic compounds' synergism in comparison with their separate use. The use of CT could enhance efficacy of antimicrobial drug formulations, and reduce the amount and use of drug adjuvants [130]. A study showed partial synergism with combination of carvacrol and thymol or gallic acid for inhibition of resistant *E. faecalis* strains. Gallic acid plus octyl gallate was most effective in reducing minimum inhibitory concentrations by more than 60% when compared with respective concentrations for each compound. Octyl gallate, the more hydrophobic compound, disrupted the microbial cell membrane, thereby providing access for gallic acid to gain entry into the intracellular environment to carry out its own antimicrobial activity [130]. Antimicrobial synergism has also been reported for phenolic acids and quercetin combination against fish bacterial pathogens [131]. Thus synergism of compounds with different mechanisms and site of action on the target cells through combination of PAs with other bioactive compounds is a workable strategy to inhibit the growth and survival of resistant microbial species and pathogens, and reduce AMR trends [132].

5.4.2 Phenolic acids in synergism with antibiotics

Studies have shown that inclusion of caffeic acid at subinhibitory concentration to Mueller Hinton (MH) agar enhanced antimicrobial action of the antibiotics, cefoxitin, clindamycin, and erythromycin against MRSA and MSSA, than when caffeic acid and the antibiotics were used alone [133–135]. Caffeic acid further improved membrane interaction; polarization, permeability, and inhibition of resistant *S. aureus* strain respiratory activity [136]. Caffeic acid's strong nucleophilic properties enable it to donate electron pairs to electrophilic functional groups on cell membrane lipids and/or proteins, resulting in membrane disruption [137]. It is also able to inhibit α-hemolysin secretion in *S. aureus* [136]. Ferulic and gallic acids, and some PAs also show significant activity against Gram-positive microbes, and could demonstrate synergism with antibiotics [138].

5.4.3 Phenolic acids for prevention of antimicrobial resistance

Microbes acquire resistance via mutagenesis and horizontal gene transfer mechanisms, and natural selection of prior resistant strains within a microbial population [139,140]. Subinhibitory levels of antibiotics induce resistance and strengthen pathogens virulence factors leading to more cases of

morbidity and mortality [141]. More than half of all *S. aureus* strains isolated are resistant to methicillin [142]. MRSA is a well-known nosocomial and community-associated pathogen with multidrug resistance to over a dozen antibiotics [143]. Fortunately, interesting findings continue to emerge on the potential of PAs to reduce or stop the development of AMR in pathogenic microbial cells like MRSA. It is reported that following in vitro exposure to PAs, bacterial resistance is either lost or attenuated. The pathogens, MRSA and MSSA, were exposed to the PAs, 2-hydroxycinnamic and vanillic acids at initial subinhibitory concentrations of 1.6 and 2.5 mg/mL, respectively, for both bacterial species, and using vancomycin antibiotic as the positive control at 0.01 mg/mL. Bacterial exposure time continued with increasing inhibitory concentrations. While vancomycin resulted in immediate AMR development, the PAs did not induce resistance. The results gave a strong indication of the potential of PAs as key candidates to be explored in antimicrobial drugs development [144]. Similar effect of PAs in diminishing *S. aureus* resistance was reported by Miklasińska-Majdanik and colleagues [145].

5.5 New technologies for antimicrobial agents' development

5.5.1 Nanotechnology

The use of nano-carriers functionalized with antimicrobial drugs has been suggested, for example, gold nanoparticles [146]. This approach enhances the drug targeting (selective disruption of microbial membranes) and pharmacokinetic attributes. Delivery of nanoparticle encapsulated vanillic, benzoic, gentisic acids showed enhanced inhibition of *L. monocytogenes*, *Salmonella typhimurium*, and *E. coli* O157:H7 food pathogens [147]. Another strategy is the detection of low levels of microbial cells and screening their response to antimicrobial drugs using atomic force microscope cantilevers. Nano-fluidics could also facilitate other nanotechnology platforms like their high-throughput use in identifying antibiotic producing strains and compounds and combination therapy chemistry [148].

5.5.2 Computational and systems biology approach

The discovery of new antimicrobial agents and evaluation of novel antimicrobial mechanisms of action can be daunting tasks and is an uncommon venture in evaluating plant phenolics. However, with the advancements in phenolic compounds' databases and availability of robust

computational softwares, such assessments are becoming easier. Systems biology approaches (Fig. 5.1) remove the bias of target-directed bioassays to facilitate discovery of new mechanism(s) of action against MDR microbes [149]. The use of molecular docking methods has shown the ability of caffeoyl quinic acids to bind in a way that blocks the microbial efflux pump [150]. In another study, Singh et al. [151] identified sinapic acid (−9.0 kcal/mol) and p-coumaric acid (−6.3 kcal/mol) among 22 PAs that were evaluated as promising NorA inhibitors relative to ciprofloxacin using computational tools. Further thermodynamic compatibility analysis using molecular dynamic simulations showed that both PAs were thermodynamically stable with NorA while establishing significant interactions with TYR 76, a critical residue involved in NorA efflux pump inhibition. Similarly, using molecular docking studies and molecular dynamic simulations, Aribisala et al. identified chlorogenic acid as a lead compound against two (DNA gyrase A and topoisomerase ParC) of the four topoisomerase IIA from *Crescentia cujete* [152]. Furthermore, through computational structure–activity relationship studies, studies have lent credence to phenolics, and they are becoming increasingly identified as potent chemical entities that could be repurposed as novel therapeutics targeting key druggable structures in bacteria to offer superior modulatory roles relative to conventional antibiotics [153,154]. These findings highlight the critical importance of computational approaches in the identification of novel antimicrobial drugs. Computational models improved on the traditional way of drug development, which is mostly dependent on discovering drug candidates through the traditional trial and error screening procedure, which is typically time-consuming and expensive with a high failure rate [155].

5.5.3 Prodrugs revival and targeting Gram-negative bacteria mechanisms

A third approach would be to develop physicochemical protocols that allow easier drug assess across Gram-negative microorganisms' cell wall. In addition, the prodrug libraries and databases could also be revived to enhance antimicrobials research, discovery and development based on new insights into microbial intracellular mechanisms. Prodrug candidates are capable of being delivered in their inactive state but with conversion to the pharmacologically active state in vivo or once inside the target cell. Prodrugs can now also be intentionally engineered for specific purposes [156].

5.5.4 Phenolic acid-metal complexing and green chemistry

It has been suggested that for antimicrobial drug development, a shift could be made to generate phenol-metal complexes that demonstrate enhanced antimicrobial capacities [157]. The metaphenolic network (MPN) is a highly ordered inorganic–organic hybrid network created by the interaction of various metal ions with phenolic molecules [158]. Metal ions often utilized in MPNs (Cu^{2+}, Eu^{3+}, Zn^{2+}, Mg^{2+}, and Ag^{+}) have significant antibacterial properties but with high toxicity capabilities [159]. Nonetheless, in complex with phenolic ligands, a synergistic effect is produced, with the phenolic ligands chelating the metal ions to form a stable chemical network, reducing metal ion cytotoxicity, and lowering the level of reactive oxygen species (ROS) induced by metal ions [158,159]. In general, the network generated by phenol-metal complexes extends the length of antibacterial action through photothermal antibacterial effects. As a result, many scientists consider MPNs to be a potent class of novel therapeutics [160,161]. In a recent study, Liang et al., while attempting to design and develop a bio-adhesive gel sealant with self-healing and enhanced antibacterial activity, designed an MPN (cross-linking among ferric iron [Fe], protocatechualdehyde [PA] containing catechol and aldehyde groups, and quaternized chitosan [QCS]) to enable the closure of skin incisions [158]. Findings show that the MPN equipped the hydrogel with significant antibacterial properties against methicillin-resistant *S. aureus* while also allowing for great autonomous healing. For improved MPN performance, phenolic ligands with more hydroxyl groups outperform ligands with fewer hydroxyl groups [158,159]. Now, the majority of MPNs are used based on their application scenarios. For example, Fe^{3+} may be used to give MPNs photothermal characteristics, Zn^{2+} can be used to stimulate bone regeneration, and Ca^{2+} can be utilized to speed up the blood clotting [158,159]. However, it is expected that as more systematic studies on MPNs are conducted, the designing principles and modification methodologies of MPNs will gradually become clearer.

Likewise, the use of green organic synthesis (Fig. 5.1) utilizing natural pant compounds as raw materials could derive novel antimicrobial molecules for future health applications [6,7]. This approach is much needed as PAs being plant-based antimicrobial have weaker antimicrobial characteristics relative to their microbial-derived counterpart. Balakrishna et al. synthesized new phenoylated phosphatidylcholines by combining

1,2-dipalmitoyl phosphatidylcholine/egg 1,2-diacyl phosphatidylcholine with phenolic acids such as ferulic, sinapic, vanillic, and syringic acids [162]. Of the active derivatives, compound 1-(4-hydroxy-3-methoxy) cinnamoyl-2-palmitoyl-sn-glycero-3-phosphocholine demonstrated excellent antibacterial properties against *Klebsiella planticola* with an MIC of 15.6 μg/mL, and compound 1-(4-hydroxy-3-methoxy) benzoyl-2-acyl-sn-glycero-3-phosphocholine showed excellent antifungal activity against *Candida albican* (MIC of 15.6 μg/ mL) relative to the parent starting materials.

5.5.5 Phenolic acid-biomaterials conjugates

The simple nature of Pas allows addition of biomaterial scaffolds for improved therapeutic outcomes. Increased number of -OH and -OCH_3 groups on Pas increase antioxidant activities. A range of Pas tested showed some antimicrobial activity against the *Staphylococcus epidermidis*, *S. aureus*, and *E. coli* strains, at concentrations that could be incorporated into polymeric biomaterials. The study also showed that modification of the phenolic acids' carboxylic acid (-COOH) group does not lead to loss of functionality. Thus manipulation of the basic skeleton of PAs for therapeutics development, either singly or in combination with biomaterial scaffolds, may hold great promise [163]. Phenol-protein conjugates linked by covalent bonds are derived using alkaline and chemical techniques, enzyme-catalyzed and free radical-mediated grafting. Changes to biological, physico-chemical, and structural properties result from such linkages. The most common proteins used include gelatin, whey, and egg proteins. Phenol-protein conjugates also enhanced antimicrobial properties when compared to the original protein, and some have been developed as nanoparticles for controlled metabolites delivery and release, hydrogels, antioxidant emulsions for the delivery of nutraceuticals, metal nanoparticles stabilizers, and edible films for food packaging [164]. One study utilized N-hydroxysuccinimide (NHS) and 1-ethyl-3-(3-dimethylaminopropyl) carbodiimide hydrochloride (EDC) to couple carboxyl groups of chlorogenic acid with the amino groups of gelatin. The conjugate inhibited the activity of *S. aureus*, *E. coli*, *P. aeruginosa*, and *L. monocytogenes* [165]. Likewise, caffeic acid-*b*-lactoglobulin conjugates were prepared using EDC/NHS coupling reagent with coupling efficiency impacted by pH [166]. Rosmarinic acid and whey protein linked using the alkaline and enzyme-catalyzed grafting techniques showed improved antibacterial activity [167]. However, the antimicrobial mechanisms of action of the

conjugates remain unclear. As an added benefit, it is reported that PA-protein conjugates can be transformed into hypoallergenic foods, but more research is required to assess the in vivo allergenicity of such food conjugates to reduce allergenic reactions to proteins [168,169].

5.6 Antimicrobial use of phenolic acids and phenolic acid-rich extracts in other industries

Ferulic acid finds use as a raw material in the cosmetics and food due to its low toxicity. It is also used as an ingredient in the production of sporting foods, vanillin and other preservatives, skin protective products, and in food films and gels production due to its cross-linking capabilities [170]. In the agro-allied industry, spoilage and deterioration of agro-allied products are caused by bacterial and fungal pathogens. Pathogens adversely impact on nutrient composition and product quality, market value, and shelf life [171]. Considering this, plant-derived antimicrobials are being researched as natural alternatives for effective management of postharvest diseases as against the utilization of synthetic chemicals [36]. Several scientific reports have shown that phenol-rich plant extracts possess broad-spectrum antimicrobial capability against foodborne and other pathogens. The phenol-rich *Magnolia schiedean* flower ethanol extract suppressed the growth of *Pseudomonas carotovorum*, a phyto-pathogenic bacterium [172]. *Fusarium* sp. and *Alternaria alternata* phyto-pathogenic fungi have also been inhibited by natural phenol-rich plant fractions. *Annona reticulate* and *Carica papaya* L. extracts inhibited *Rhizopus stolonifer* growth during *Mangifera indica* L. (mango) fruit storage [173]. Likewise, growth of *Penicillium digitatum*, *A. niger*, *A. parasiticus*, *Fusarium oxysporummelonis*, and *A. alternata* were inhibited by the fungistatic effect of bee propolis [174]. A constituent of bee propolis, caffeic acid phenethyl ester was shown to be more effective in *A. alternata* control on tomatoes than commercial fungicides, and had no adverse impact on fruit quality [174]. Cinnamon extracts have also shown efficacy within doses of 330−539 ppm against *Fusarium* species (*F. culmorum*), while doses above 2000 ppm were efficacious against other species [175]. Bambara extracts also inhibited the growth of *E. coli* pathogen due to its phenolic-rich constituent [176]. Phenolic compounds also serve as antifungal agents used in extending shelf life of fruits in storage [177]. Although reports are highly varied with

regard to compound and extract concentrations and minimum inhibitory capacities, PAs and PA-rich extracts continue to be mined for application in other industries.

5.7 Major challenges to the use of phenolic acids in antimicrobial drug development

5.7.1 Potential side effects

Phenolic acids, like other phenol compound groups, may also have adverse impacts on health aside its many health benefits. The side effects may be linked to poor permeability of PAs that may exist as free acids, and ability to cause systemic toxicity when administered in excess. Phenolic acids with the catechol group have been found to behave as pro-oxidants in systems containing redox-active metals. In the presence of oxygen, transition metals such as copper and iron stimulate the redox cycling of PA, resulting in the generation of ROS and phenoxyl radicals that may result in adverse impacts on lipids, proteins, RNA, and DNA of the host [178]. For instance, despite having similar structures and redox potentials, treatment with dihydrocaffeic acid in the presence of copper triggered more DNA single- and double-strand breaks than exposure to caffeic acid, but chlorogenic acid, on the other hand, caused relatively minor damage [179]. Ajiboye et al. implicated the involvement of oxidative stress in the bactericidal activity of PAs (protocatechuic acid, gallic acid, and caffeic acid) via their ability to decrease glutathione level, increase glutathione disulfide and malondialdehyde, and damage of DNA following treatment of bacterial cells with PAs relative to the negative control (dimethyl sulfoxide [DMSO]-treated cell) [180]. Hussain et al. implicated allyl pyrocatechol (AP), the main component of *Piper betle*, in the oxidative killing of *S. aureus* via the ability to induce increased production of superoxide ($O_2^{\bullet -}$) internally [181]. All the findings indicate the generation of ROS ($O_2^{\bullet -}$ and $^{\bullet}OH$) in the bactericidal activity of PAs. Hence, intake of significant quantities of PAs in the form of concentrated supplement may not be deemed safe until after appropriate in vitro and in vivo evaluation of their potential oxidative stress capabilities. In addition, excess doses of PAs could harm healthy body cells and induce formation of blisters. Hence, dose to time response must be appropriately researched and calculated prior to PAs administration [182]. Adverse effects may be ameliorated with the development of micro- and nano-based therapeutic PA formulations.

5.7.2 Bioavailability concerns

Bioavailability of a drug is the extent to which the drug can reach its target or systemic circulation and carry out its activity, following administration [183]. Despite reported in vitro bioactivities of phenols, similar activities are often not recorded in vivo, and is linked to their poor bioavailability in vivo. Poor bioavailability and efficacy may be caused by a poor choice of administration route, inability to cross gut membranes, rapid metabolism by gut flora and hepato-enzymes (gut flora break down flavonoids to PAs that are taken up and processed in the liver), poor gut stability, low aqueous solubility, and difficulty crossing membranes. In another scenario, gut biotransformation of phenols may occur to yield metabolites that are more active than the original phenol molecules. Phenols metabolism and bioavailability impacts are noticed during the in vivo studies on their pharmacological activities [184].

Still, it must be stated that although some metabolites are hydrolyzed during passage in gut, several polyphenols do reach the gut in wholesome forms. This led to the suggestion that the gut microflora reactions may be the key factors associated with stabilizing and modifying administered substances [185]. While many phenols undergo structural changes prior to absorption in the gut, an ex vivo research using rats demonstrated that PAs (chlorogenic acid) absorption can take place in the jejunum, ileum, and colon or at the gastric level [186]. Another challenge is the dearth of research data determining the therapeutic index values (TIVs) of PAs [187]. Thus studies on phenolic metabolites of major interest like phenolic acids need to be increased to enhance industrial applications. Also, application of technological innovations to develop drug formulations with controlled absorption, reduced toxicity and degradation processes, and improved taste and solubility, would enhance bioavailability and drug efficacy in vivo and constitute a major advantage to boosting PAs utilization in antimicrobial drugs development [188].

5.7.3 Promising metabolites assessment methods

An added challenge is the method used in assessing phenolic phytometabolites as antimicrobial agents. These methods include use of selective solvents and extraction technologies, agar disk and well diffusion tests, the poisoned food and spore germination techniques, broth micro- and macro-dilution assays (for antifungal activity), bio-autography methods (agar diffusion or contact, immersion or agar-overlay, and direct

bio-autography), among others. Each method comes with its attendant advantage(s) and disadvantage(s). In other words, evaluation techniques for antimicrobial agents need to be updated with subsequent advancements in technologies and should evolve to achieve uniformity in research reports and facilitate results interpretation. It would further make the search for novel antimicrobials more systematic to better suit pressing needs [189].

Finally, other means of bypassing these and other challenges to PAs use in antimicrobial drug developments would be to increase support for basic, applied, and interdisciplinary research to underpin diverse scientific approaches to combating pathogens; implement new reimbursement systems; improve platforms for compound identification, lead optimization and characterization; remove bureaucratic bottlenecks for preclinical and early clinical trials drug development and create clinical trial networks; create special regulations for drugs active against resistant microorganisms; increasing political and public awareness on the threat of AMR at local, regional, and global levels, and optimizing current global [European Union (EU), World Health Organization (WHO), African Union (AU), etc.] partnerships and diplomatic campaigns that build on AMR strategic frameworks [190].

5.8 Future perspectives and concluding remarks

A plethora of studies report on plant-based phenols and incorporate more in vitro than in vivo assessments. Still, scientific data are required to address study treatment variations. Research to assess the antimicrobial therapeutic efficacy of PAs in pure, extract, PA-metal complexes, micro- and nano-based or conjugated forms, and mechanisms of antimicrobial action are also relevant. Likewise, approaches that decrease dose and toxicity cannot be overemphasized to increase the utilization of PAs in future antimicrobial therapies. Besides the transition from in vitro to in vivo experimentation, acquiring ethical clearance and conducting human clinical trials remain major challenges to novel antimicrobials development. Revising the drug approval protocols, evaluation techniques and increasing governmental and industrial research support for promising phytometabolites like phenolic acids would constitute a significant push in the right direction and facilitate antimicrobial drug discoveries. Nonetheless, currently available scientific evidence shows tremendous promise for use of phenolic acids in future antimicrobial drugs development.

References

[1] World Health Organization (WHO), Antimicrobial resistance <https://www.who.int/news-room/fact-sheets/detail/antimicrobial-resistance>, 2021 (accessed 03.06.22).

[2] S. Maria-Neto, K.C. de Almeida, M.L.R. Macedo, O.L. Franco, Understanding bacterial resistance to antimicrobial peptides: from the surface to deep inside, Biochim. Biophys. Acta 1848 (2015) 3078–3088.

[3] H. Swingler, J. May, Satellite centres to fast-track new antibiotics discovery as drug resistance rises <http://www.news.uct.ac.za/article/-2022-04-28>, 2022 (accessed 29.04.22).

[4] C.A. Pasberg-Gauhl, The need for new generation antibiotics against MRSA resistant bacteria, Drug Discov. Today 11 (2014) 109–116.

[5] W. Russell, G. Duthie, Plant secondary metabolites and gut health: the case for phenolic acids, Proc. Nutr. Soc. 70 (3) (2011) 389–396.

[6] C.E. Aruwa, S.O. Amoo, N. Koorbanally, T. Kudanga, Enzymatic dimerization of luteolin enhances antioxidant and antimicrobial activities, Biocatal. Agric. Biotechnol. 35 (2021) 1–10.

[7] C.E. Aruwa, S.O. Amoo, N. Koorbanally, T. Kudanga, Laccase-mediated modification of isorhamnetin improves antioxidant and antibacterial activities, Process. Biochem. 112 (2022) 53–61.

[8] V. Tzin, G. Galili, The biosynthetic pathways for shikimate and aromatic amino acids in *Arabidopsis thaliana*, The Arabidopsis Book, 8, American Society of Plant Biologists, 2010, p. e0132.

[9] P.G. Anantharaju, P.C. Gowda, M.G. Vimalambike, S.V. Madhunapantula, An overview on the role of dietary phenolics for the treatment of cancers, Nutr. J. 15 (1) (2016) 1–16.

[10] R.G.M. de Lourdes, Food phenolic compounds: main classes, sources and their antioxidant power, in: J.A. Morales-Gonzalez (Ed.), Oxidative Stress and Chronic Degenerative Diseases - A Role for Antioxidants, InTech Open, 2013, pp. 87–112.

[11] D. Sircar, A. Mitra, Accumulation of p-hydroxybenzoic acid in hairy roots of *Daucus carota* 2: confirming biosynthetic steps through feeding of inhibitors and precursors, J. Plant Physiol. 166 (13) (2009) 1370–1380.

[12] H.F. Wang, G.J. Provan, K. Helliwell, Determination of hamamelitannin, catechins and gallic acid in witch hazel bark, twig and leaf by HPLC, J. Pharm. Biomed. Anal. 33 (2003) 539.

[13] A. Itoh, K. Isoda, M. Kondoh, M. Kawase, M. Kobayashi, M. Tamesada, et al., Hepatoprotective effect of syringic acid and vanillic acid on concanavalin A-induced liver injury, Biol. Pharm. Bull. 32 (2009) 1215.

[14] O.V. Njoku, C. Obi, Phytochemical constituents of some selected medicinal plants, Afr. J. Pure Appl. Chem. 3 (2009) 228.

[15] A.R. Hraš, M. Hadolin, Ž. Knez, D. Bauman, Comparison of antioxidative and synergistic effects of rosemary extract with α-tocopherol, ascorbyl palmitate and citric acid in sunflower oil, Food Chem. 71 (2000) 229–233.

[16] C. Sanbongi, H. Takano, N. Osakabe, N. Sasa, M. Natsume, R. Yanagisawa, et al., Rosmarinic acid in perilla extract inhibits allergic inflammation induced by mite allergen, in a mouse model, Clin. Exp. Allergy 34 (6) (2004) 971–977.

[17] A.E. Stuart, C.J.W. Brooks, R.J. Prescott, A. Blackwell, Repellent and antifeedant activity of salicylic acid and related compounds against the biting midge, *Culicoidesimpunctatus* (Diptera: Ceratopogonidae), J. Med. Entomol. 37 (2) (2000) 222–227.

[18] C.S. Yang, J.M. Landau, M.T. Huang, H.L. Newmark, Inhibition of carcinogenesis by dietary polyphenolic compounds, Ann. Rev. Nutr. 21 (2001) 381–406.
[19] N.S. Khan, S.M. Hadi, Structural features of tannic acid important for DNA degradation in the presence of Cu (II), Mutagenesis 13 (3) (1998) 271–274.
[20] A.K.K. Achakzai, P. Achakzai, A. Masood, S.A. Kayani, R.B. Tareen, Response of plant parts and age on the distribution of secondary metabolites on plants found in Quetta,, Pak. J. Bot. 41 (2009) 2129–2135.
[21] J. Dai, R.J. Mumper, Plant phenolics: extraction, analysis and their antioxidant and anticancer properties, Molecules 15 (2010) 7313–7352.
[22] J.P. Spencer, M.M. Abd El Mohsen, A.M. Minihane, J.C. Mathers, Biomarkers of the intake of dietary polyphenols: strengths, limitations and application in nutrition research, Br. J. Nutr. 99 (1) (2008) 12–22.
[23] A. Bento-Silva, V.M. Koistinen, P. Mena, M.R. Bronze, K. Hanhineva, S. Sahlstrøm, et al., Factors affecting intake, metabolism and health benefits of phenolic acids: do we understand individual variability? Eur. J. Nutr. 59 (2020) 1275–1293.
[24] B. Khameneh, M. Iranshahy, V. Soheili, B.S.F. Bazzaz, Review on plant antimicrobials: a mechanistic viewpoint,, Antim. Resist. Infec. Control. 8 (1) (2019) 1–28.
[25] P.V. Turner, T. Brabb, C. Pekow, M.A. Vasbinder, Administration of substances to laboratory animals: routes of administration and factors to consider, J. Am. Assoc. Lab. Anim. Sci. 50 (5) (2011) 600–613.
[26] Y. Konishi, Y. Hitomi, E. Yoshioka, Intestinal absorption of *p*-coumaric and gallic acids in rats after oral administration, J. Agric. Food Chem. 52 (9) (2004) 2527–2532.
[27] S.M. Kern, R.N. Bennett, F.A. Mellon, P.A. Kroon, M.T. Garcia-Conesa, Absorption of hydroxycinnamates in humans after high-bran cereal consumption, J. Agric. Food Chem. 51 (20) (2003) 6050–6055.
[28] Y. Konishi, S. Kobayashi, M. Shimizu, Transepithelial transport of *p*-coumaric acid and gallic acid in Caco-2 cell monolayers, Biosci. Biotechnol. Biochem. 67 (2003) 2317–2324.
[29] A. Adam, V. Crespy, M.A. Levrat-Verny, F. Leenhardt, M. Leuillet, C. Demigné, et al., The bioavailability of ferulic acid is governed primarily by the food matrix rather than its metabolism in intestine and liver in rats, J. Nutr 132 (2002) 1962–1968.
[30] F.M. Campos, J.A. Couto, A.R. Figueiredo, I.V. Tóth, A.O. Rangel, T.A. Hogg, Cell membrane damage induced by phenolic acids on wine lactic acid bacteria, Int. J. Food Microbiol. 135 (2009) 144–151.
[31] F.C. Tenover, Mechanisms of antimicrobial resistance in bacteria, Am. J. Med. 119 (6) (2006) S3–S10.
[32] C. Walsh, Molecular mechanisms that confer antibacterial drug resistance, Nature 406 (6797) (2000) 775–781.
[33] B. Khameneh, R. Diab, K. Ghazvini, B.S.F. Bazzaz, Breakthroughs in bacterial resistance mechanisms and the potential ways to combat them, Microb. Pathogen. 95 (2016) 32–42.
[34] J. Rao, B. Chen, D.J. McClement, Improving the efficacy of essential oils as antimicrobials in food: mechanism of action, Ann. Rev. Food 10 (2019) 3.1–3.23.
[35] R. Barkai-Golan, Attack mechanism of the pathogen, Postharvest Diseases of Fruit and Vegetable: Development and Control, Elsevier Science, Amsterdam, 2001, pp. 418–419.
[36] L.M. Aguilar-Veloz, M. Calderón-Santoyo, Y. Vazquez Gonzalez, J.A. Ragazzo-Sánchez, Application of essential oils and polyphenols as natural antimicrobial agents in postharvest treatments: advances and challenges, Food Sci. Nutr. 8 (2020) 2555–2568.

[37] A. Rodríguez-Maturino, R. Troncoso-Rojas, A. Sánchez-Estrada, D. González-Mendoza, E. Ruiz-Sánchez, R. Zamora-Bustillos, et al., Efectoantifúngico de extractosfenólicos y de carotenoides de chiltepín (*Capsicum annum* var. *glabriusculum*) en*Alternaria alternata* y *Fusarium oxysporum*, Rev. Argent. Microbiol. 47 (2015) 72–77.
[38] F.A. Pagnussatt, L. Kupski, F.T. Darley, P.F. Filoda, É.M.D. Ponte, J. Garda-Buffon, et al., *Fusarium graminearum* growth inhibition mechanism using phenolic compounds from *Spirulina* sp, Ciênc. Tecnol. Aliment. 33 (2013) 75–80.
[39] A. Borges, C. Ferreira, M.J. Saavedra, M. Simões, Antibacterial activity and mode of action of ferulic and gallic acids against pathogenic bacteria, Microb. Drug Resist. 19 (4) (2013) 256–265.
[40] R.J. Robbins, Phenolic acids in foods: an overview of analytical methodology, J. Agric. Food Chem. 51 (2003) 2866–2887.
[41] R.P. Samy, P. Gopalakrishnakone, Therapeutic potential of plants as antimicrobials for drug discovery, Evid. Based Compl. Alter. Med. 7 (3) (2010) 283–294.
[42] L. Sanhueza, R. Melo, R. Montero, K. Maisey, L. Mendoza, M. Wilkens, Synergistic interactions between phenolic compounds identified in grape pomace extract with antibiotics of different classes against *Staphylococcus aureus* and *Escherichia coli*, PLoS ONE 12 (2) (2017) 1–15.
[43] A. Synowiec, K. Żyła, M. Gniewosz, M. Kieliszek, An effect of positional isomerism of benzoic acid derivatives on antibacterial activity against *Escherichia coli*, Open. Life Sci. 16 (1) (2021) 594–601.
[44] F.M. Campos, J.A. Couto, T.A. Hogg, Influence of phenolic acids on growth and inactivation of *Oenococcusoeni* and *Lactobacillus hilgardii*, J. Appl. Microbiol. 94 (2003) 167–174.
[45] H. Hayrapetyan, W.C. Hazeleger, R.R. Beumer, Inhibition of *Listeria monocytogenes* by pomegranate (*Punica granatum*) peel extract in meat pate at different temperatures, Food Control. 23 (2012) 66–72.
[46] L.J. Nohynek, H.L. Alakomi, M.P. Kähkönen, M. Heinonen, I.M. Helander, K.M. Oksman-Caldentey, et al., Berry phenolics: antimicrobial properties and mechanisms of action against severe human pathogens, Nutr. Cancer 54 (1) (2006) 18–32.
[47] F. Ahimou, F.A. Denis, A. Touhami, Y.F. Dufrêne, Probing microbial cell surface charges by atomic force microscopy, Langmuir 18 (2002) 9937–9941.
[48] J. Palmer, S. Flint, J. Brooks, Bacterial cell attachment, the beginning of a biofilm, J. Ind. Microbiol. Biotechnol. 34 (2007) 577–588.
[49] D.J. Bhuyan, A. Basu, Phenolic compounds potential health benefits and toxicity, Utilisation of Bioactive Compounds from Agricultural and Food Production Waste, Taylor and Francis, 2017, pp. 27–59.
[50] M.M. Cowan, Plant products as antimicrobial agents, Clin. Microbiol. Rev. 12 (1999) 564–582.
[51] R. Gyawali, S.A. Ibrahim, Natural products as antimicrobial agents, Food Control. 46 (2014) 412–429.
[52] A. Pernin, L. Guillier, F. Dubois-Brissonnet, Inhibitory activity of phenolic acids against *Listeria monocytogenes*: deciphering the mechanisms of action using three different models, Food Microbiol. 80 (2019) 18–24.
[53] A. Karunanidhi, R. Thomas, A. Van Belkum, V. Neela, *In vitro* antibacterial and antibiofilm activities of chlorogenic acid against clinical isolates of *Stenotrophomonas maltophilia* including the trimethoprim/sulfamethoxazole resistant strain, BioMed. Res. Int. (392058)(2013) 7.
[54] V. Saibabu, Z. Fatima, L.A. Khan, S. Hameed, Therapeutic potential of dietary phenolic acids, Adv. Pharmacol. Sci. 2015 (823539) (2015) 10.

[55] S.S. Gill, N. Tuteja, Reactive oxygen species and antioxidant machinery in abiotic stress tolerance in crop plants, Plant Physiol. Biochem. 48 (2010) 909–930.
[56] Y. Nakabeppu, D. Tsuchimoto, A. Ichinoe, M. Ohno, Y. Ide, S. Hirano, et al., Biological significance of the defence mechanisms against oxidative damage in nucleic acids caused by reactive oxygen species, Mitochondrial Pathogenesis, 1011, Springer, Berlin, Heidelberg, 2004, pp. 101–111.
[57] Z. Nikitaki, C.E. Hellweg, A.G. Georgakilas, J.L. Ravanat, Stress-induced DNA damage biomarkers: applications and limitations, Front. Chem. 3 (2015) 35.
[58] S.A. Jassim, M.A. Naji, Novel antiviral agents: a medicinal plant perspective, J. Appl. Microbiol. 95 (2003) 412–427.
[59] T.T. Cushnie, A.J. Lamb, Antimicrobial activity of flavonoids, Int. J. Antimicrob. Agents 26 (5) (2005) 343–356.
[60] K. Chojnacka, D. Skrzypczak, G. Izydorczyk, K. Mikula, D. Szopa, A. Witek-Krowiak, Antiviral properties of polyphenols from plants, Foods 10 (10) (2021) 2277.
[61] M. Kowalczyk, A. Golonko, R. Świsłocka, M. Kalinowska, M. Parcheta, A. Swiergiel, et al., Drug design strategies for the treatment of viral disease - plant phenolic compounds and their derivatives, Front. Pharmacol. (2021) 1936.
[62] M.F. Montenegro-Landívar, P. Tapia-Quirós, X. Vecino, M. Reig, C. Valderrama, M. Granados, et al., Polyphenols and their potential role to fight viral diseases: an overview, Sci. Total Environ. 801 (2021)149719.
[63] H. Akgul, A. Aslan, I. Akata, S. Gunal, C. Bal, H. Baba, Phenolic content and biological activities of *Trameteshirsuta*, Fresenius Environ. Bull. 30 (4A) (2021) 4130–4135.
[64] S. Sabiu, C.E. Aruwa, V. Mohanlall, H. Baijnath, *Momordica balsamina* L.: an appraisal on morphology, ecological diversity, phytochemistry, pharmacological and biotechnological applications,, Curr. Trad. Med. 6 (2020) 1–11.
[65] A.T. Jamiu, C.E. Aruwa, I.A. Abdulakeem, A.A.-n Ajao, S. Sabiu, Phytotherapeutic evidence against coronaviruses and prospects for COVID-19, Pharmacogn. J. 12 (2020) 1252–1267.
[66] N. Kumar, N. Goelb, Phenolic acids: natural versatile molecules with promising therapeutic applications, Biotech Rep. 24 (2019) e00370.
[67] T. Kudanga, C.E. Aruwa, Industrial applications of *Opuntia* spp. (nopal, fruit and peel powders), in: M.F. Ramadan, T.E.M. Ayoub, S. Rohn (Eds.), *Opuntia* spp.: Chemistry, Bioactivity and Industrial Applications, Springer Nature, Cham, 2020, pp. 841–875.
[68] R. Tsao, Z. Deng, Separation procedures for naturally occurring antioxidant phytochemicals, J. Chrom. B 812 (1–2) (2004) 85–99.
[69] S.A. Heleno, A. Martins, M.J.R. Queiroz, I.C. Ferreira, Bioactivity of phenolic acids: metabolites versus parent compounds: a review, Food Chem. 173 (2015) 501–513.
[70] D.M. Pereira, P. Valentão, J.A. Pereira, P.B. Andrade, Phenolics: from chemistry to biology, Molecules 14 (6) (2009) 2202–2211.
[71] E.A. Akanbong, A. Senol, A.K. Devrim, Phenolic compounds for drug discovery: potent candidates for anti-cancer, anti-diabetes, anti-inflammatory and anti-microbial, Int. J. Vet. Anim. Res. 4 (2021) 115–121.
[72] M.J.R. Vaquero, M.R. Alberto, M.C.M. de Nadra, Influence of phenolic compounds from wines on the growth of *Listeria monocytogenes*, Food Control. 18 (5) (2007) 587–593.
[73] M.J. Alves, I.C. Ferreira, H.J. Froufe, R.M.V. Abreu, A. Martins, M. Pintado, Antimicrobial activity of phenolic compounds identified in wild mushrooms, SAR analysis and docking studies, J. Appl. Microbiol. 115 (2) (2013) 346–357.

[74] O. Aldulaimi, F. Drijfhout, F.I. Uche, P. Horrocks, W.W. Li, Discovery, synthesis and antibacterial evaluation of phenolic compounds from *Cylicodiscusgabunensis*, BMC Complement. Alternat. Med. 19 (1) (2019) 1–11.
[75] Y. Wu, J. Bai, K. Zhong, Y. Huang, H. Qi, Y. Jiang, et al., Antibacterial activity and membrane-disruptive mechanism of 3-p-trans-coumaroyl-2-hydroxyquinic acid, a novel phenolic compound from pine needles of *Cedrus deodara*, against *Staphylococcus aureus*, Molecules 21 (8) (2016) 1084.
[76] B. Özçelik, M. Kartal, I. Orhan, Cytotoxicity, antiviral and antimicrobial activities of alkaloids, flavonoids, and phenolic acids, Pharm. Biol. 49 (4) (2011) 396–402.
[77] L. Estevinho, A.P. Pereira, L. Moreira, L.G. Dias, E. Pereira, Antioxidant and antimicrobial effects of phenolic compounds extracts of Northeast Portugal honey, Food Chem. Toxicol. 46 (2008) 3774–3779.
[78] R.G.H. Barbour, J.M. Vincent, The bacteriostatic action of phenol, benzoic acid and related compounds on *Bacterium aerogenes*, Microbiology 4 (1950) 110–121.
[79] O.H. Lee, B.Y. Lee, Antioxidant and antimicrobial activities of individual and combined phenolics in *Olea europaea* leaf extract, Biores. Technol. 101 (10) (2010) 3751–3754.
[80] W. Laaboudi, J. Ghanam, M. Merzouki, M. Benlemlih, Ecoextraction of phenolic compounds from Moroccan olive fruits and leaves and their potential use as antimicrobial agents, Eur. J. Sci. Res. 132 (2015) 255–265.
[81] S.R.S.J. Cicerale, L.J. Lucas, R.S.J. Keast, Antimicrobial, antioxidant and anti-inflammatory phenolic activities in extra virgin olive oil, Curr. Opin. Biotechnol. 23 (2) (2012) 129–135.
[82] P. Laganà, G. Anastasi, F. Marano, S. Piccione, R.K. Singla, A.K. Dubey, et al., Phenolic substances in foods: health effects as anti-inflammatory and antimicrobial agents, J. AOAC Int. 102 (5) (2019) 1378–1387.
[83] M. Kozyra, A. Biernasiuk, A. Malm, Analysis of phenolic acids and antibacterial activity of extracts obtained from the flowering herbs of *Carduus acanthoides* L, Acta Pol. Pharm. Drug Res. 74 (2017) 161–172.
[84] Y. Zhao, M. Chen, Z. Zhao, S. Yu, The antibiotic activity and mechanisms of sugarcane (*Saccharum officinarum* L.) bagasse extract against food-borne pathogens, Food Chem. 185 (2015) 112–118.
[85] I.G. Mekinić, D. Skroza, I. Ljubenkov, L. Krstulović, S.S. Možina, V. Katalinić, Phenolic acids profile, antioxidant and antibacterial activity of chamomile, common yarrow and immortelle (Asteraceae), Nat. Prod. Commun. 9 (12) (2014). 1934578X1400901222.
[86] S.L. Stanley, Amoebiasis, Lancet 361 (9362) (2003) 1025–1034.
[87] J.P. Ackers, D. Mirelman, Progress in research on *Entamoeba histolytica* pathogenesis, Curr. Opin. Microbiol. 9 (2006) 367–373.
[88] S.L. Stanley, Pathophysiology of amoebiasis, Trends Parasitol. 17 (6) (2001) 280–285.
[89] S. Marion, N. Guillén, Genomic and proteomic approaches highlight phagocytosis of living and apoptotic human cells by the parasite *Entamoeba histolytica*, Int. J. Parasitol. 36 (2) (2006) 131–139.
[90] W.A. Petri, Therapy of intestinal protozoa, Trends Parasitol. 19 (11) (2003) 523–526.
[91] S.C. Swetman, Martindale, The Complete Drug Reference, thirty-third ed., Pharmaceutical Press, London, 2002, p. 594.
[92] C.M. Amisigo, C.A. Antwi, J.P. Adjimani, T.M. Gwira, *In vitro* anti-trypanosomal effects of selected phenolic acids on *Trypanosoma brucei*, PLoS ONE 14 (5) (2019) e0216078.

[93] R. Brun, J. Blum, F. Chappuis, C. Burri, Human African trypanosomiasis, Lancet 375 (2010) 148–159.
[94] World Health Organization (WHO), Working to overcome the global impact of neglected tropical diseases: first WHO report on neglected tropical diseases <http://www.who.int/neglected-diseases/2010report/NTD-2010report-embargoed.pdf>, 2010 (accessed 28.06.2022).
[95] F.G. Figueredo, S.R. Tintino, D.I.V. de Brito, M.F.B.M. Braga, N.F. Leite, B.F.F. Lucena, et al., Evaluation of the potential trypanocidal and antileishmanial activities of the extract of leaves of *Piper arboreum* (Piperaceae) and its fractions, J. Basic Appl. Pharma. Sci. 35 (1) (2014) 149–154.
[96] R.J.S. Bezerra, L. Leon, M. Genestra, Recentesavanços da quimioterapia das leishmanioses: moléculas intracelulares como alvo de fármacos, Rev. Bras. Ciênc. Farm. 40 (2004) 141–148.
[97] I.O. Pereira, L.V.S. Sacramento, M.J. Marques, Leishmanioses: Estado da Arte, Rev. Univ. Val. Rio Verde 9 (1) (2011) 220–238.
[98] S.J. Black, J.M. Mansfield, Prospects for vaccination against pathogenic African trypanosomes, Parasite Immunol. 38 (2016) 735–743.
[99] S. Degerli, T.E.P.E. Bektas, Phenolic acid composition and anti-parasitic effects of four peucedanum species on *Entamoeba histolytica* trophozoites, Iran. J. Parasitol. 10 (3) (2015) 420.
[100] B. Pradines, Iron chelators as antimalarial agents: *in vitro* activity of dicatecholate against *Plasmodium falciparum*, J. Antim. Chemother. 50 (2) (2002) 177–187.
[101] Z.I. Cabantchik, Iron chelators as antimalarials: the biochemical basis of selective cytotoxicity, Parasitol. Today 11 (1995) 74–78.
[102] D.G. Heppner, P.E. Hallaway, G.J. Kontoghiorghes, J.W. Eaton, Antimalarial properties of orally active iron chelators, Blood 72 (1988) 357–361.
[103] D. Blache, P. Durand, M. Prost, N. Loreau, (+)-Catechin inhibits platelet hyperactivity induced by an acute iron load *in vivo*, Free Radic. Biol. Med. 33 (2002) 1670–1680.
[104] M. Elhabiri, C. Carrër, F. Marmolle, H. Traboulsi, Complexation of iron (III) by catecholate-type polyphenols, Inorg. Chim. Acta 360 (2007) 353–359.
[105] Z. Sroka, W. Cisowski, Hydrogen peroxide scavenging, antioxidant and anti-radical activity of some phenolic acids, Food Chem. Toxicol. 41 (2003) 753–758.
[106] P.A. Fordjour, J.P. Adjimani, B. Asare, N.O. Duah-Quashie, N.B. Quashie, Antimalarial activity of phenolic acids is structurally related, Res. Sq. (2020). Available from: https://doi.org/10.21203/rs.3.rs-21702/v1,.
[107] J.T.C. Júnior, S.M. de Morais, C.V. Gomez, C.C. Molas, M. Rolon, A.A. Boligon, et al., Phenolic composition and antiparasitic activity of plants from the Brazilian Northeast "Cerrado,", Saudi J. Biol. Sci. 23 (3) (2016) 434–440.
[108] M.T. Khan, A. Ather, K.D. Thompson, R. Gambari, Extracts and molecules from medicinal plants against herpes simplex viruses, Antivir. Res. 67 (2005) 107–119.
[109] L.C. Chiang, W. Chiang, M.Y. Chang, L.T. Ng, C.C. Lin, Antiviral activity of *Plantago major* extracts and related compounds *in vitro*, Antivir. Res. 55 (2002) 53–62.
[110] P. Schnitzler, S. Schneider, F.C. Stintzing, R. Carle, J. Reichling, Efficacy of an aqueous *Pelargonium sidoides* extract against herpes virus, Phytomedicine 15 (2008) 1108–1116.
[111] B. McDougall, P.J. King, B.W. Wu, Z. Hostomsky, M.G. Reinecke, W.E. Robinson, Dicaffeoylquinic and dicaffeoyltartaric acids are selective inhibitors of human immunodeficiency virus type 1 integrase, Antim. Agents Chemother. 42 (1998) 140–146.

[112] J. Lee, C.F. Scagel, Chicoric acid: chemistry, distribution and production, Font. Chem 1 (2013) 40.
[113] M.C. Sabini, L.N. Cariddi, F.M. Escobar, F. Mañas, L. Comini, D. Iglesias, et al., Potent inhibition of Western Equine Encephalitis virus by a fraction rich in flavonoids and phenolic acids obtained from *Achyroclinesatureioides*, Rev. Bras. Farmacogn. 26 (2016) 571–578.
[114] K. Chojnacka, A. Witek-Krowiak, D. Skrzypczak, K. Mikula, P. Młynarz, Phytochemicals containing biologically active polyphenols as an effective agent against Covid-19-inducing coronavirus, J. Funct. Foods 73 (2020) 104146.
[115] A. Goc, W. Sumera, M. Rath, A. Niedzwiecki, Phenolic compounds disrupt spike-mediated receptor-binding and entry of SARS-CoV-2 pseudo-virions, PLoS ONE 16 (6) (2021) e0253489.
[116] M. Zhou, C. Liu, J. Yang, D. Niu, M. Dong, G. Yang, et al., Alatains A and B, unique hetero-dimeric polyphenols from *Cassia alata* and their anti-tobacco mosaic virus activity, Fitoterapia 147 (2020) 104763.
[117] H. Kim, M.S. Chung, Antiviral activities of mulberry (*Morus alba*) juice and seed against influenza viruses, Evid. Based Compl. Altern. Med. 2018 (2018) 2606583.
[118] E. Nagai, M. Iwai, R. Koketsu, R. Sogabe, R. Morimoto, Y. Suzuki, et al., Inhibition of influenza virus replication by adlay tea, J. Sci. Food Agric. 98 (2018) 1899–1905.
[119] Y. Li, D. Yang, Y. Jia, L. He, J. Li, C. Yu, et al., Research note: anti-inflammatory effects and antiviral activities of baicalein and chlorogenic acid against infectious bursal disease virus in embryonic eggs, Poult. Sci. 100 (2021) 100987.
[120] Y.H. Wu, B.Y. Zhang, L.P. Qiu, R.F. Guan, Z.H. Ye, X.P. Yu, Structure properties and mechanisms of action of naturally originated phenolic acids and their derivatives against human viral infections, Curr. Med. Chem. 24 (38) (2017) 4279–4302.
[121] H.J. Choi, J.H. Song, K.S. Park, S.H. Baek, *In vitro* anti-enterovirus 71 activity of gallic acid from *Woodfordia fruticosa* flowers, Lett. Appl. Microbiol. 50 (2010) 438–440.
[122] H.J. Choi, J.H. Song, L.R. Bhatt, S.H. Baek, Anti-human rhinovirus activity of gallic acid possessing antioxidant capacity, Phytother. Res. 24 (2010) 1292–1296.
[123] J.-R. Weng, C.-S. Lin, H.-C. Lai, Y.-P. Lin, C.-Y. Wang, Y.-C. Tsai, et al., Antiviral activity of *Sambucus formosana* Nakai ethanol extract and related phenolic acid constituents against human coronavirus NL63, Virus Res. 273 (2019) 197767.
[124] A. Khalil, D. Tazeddinova, The upshot of polyphenolic compounds on immunity amid COVID-19 pandemic and other emerging communicable diseases: an appraisal, Nat. Prod. Bioprosp. 10 (6) (2020) 411–429.
[125] S. Kiokias, V. Oreopoulou, A review of the health protective effects of phenolic acids against a range of severe pathologic conditions (including coronavirus-based infections), Molecules 26 (17) (2021) 5405.
[126] J.O. Uhomoibhi, K.A. Idowu, F.O. Shode, S. Sabiu, Molecular modelling identification of potential drug candidates from selected African plants against SARS-CoV-2 key druggable proteins,, Sci. Afr. (2022)e01279.
[127] J.O. Uhomoibhi, F.O. Shode, K.A. Idowu, S. Sabiu, Molecular modelling identification of phytocompounds from selected African botanicals as promising therapeutics against druggable human host cell targets of SARS-CoV-2, J. Mol. Graph. Model. (2022). Available from: https://doi.org/10.1016/j.jmgm.2022.108185.
[128] A.T. Jamiu, C.H. Pohl, S. Bello, T. Adedoja, S. Sabiu, A review on molecular docking analysis of phytocompounds against SARS-CoV-2 druggable targets, All Life 14 (2021) 1100–1128.

[129] F.O. Shode, A.S.K. Idowu, O.J. Uhomoibhi, S. Sabiu, Repurposing drugs and identification of inhibitors of integral proteins (spike protein and main protease) of SARS-CoV-2, J. Biomol. Struc. Dynam. (2021). Available from: https://doi.org/10.1080/07391102.2021.1886993.

[130] J. Gutiérrez-Fernández, M.R. García-Armesto, R. Álvarez-Alonso, P. del Valle, D. de Arriaga, J. Rúa, Antimicrobial activity of binary combinations of natural and synthetic phenolic antioxidants against *Enterococcus faecalis*, J. Dairy Sci. 96 (2013) 4912–4920.

[131] V.G.N.V. Prasad, P.L. Swamy, T.S. Rao, G.S. Rao, Antibacterial synergy between quercetin and polyphenolic acids against bacterial pathogens of fish, Asian Pac. J. Trop. Dis. 4 (2014) S326–S329.

[132] S.P. Denyer, W.B. Hugo, V.D. Hardling, Synergy in preservative combinations, Int. J. Pharm. 25 (1985) 245–253.

[133] M. Kępa, M. Miklasińska-Majdanik, R.D. Wojtyczka, D. Idzik, K. Korzeniowski, J. Smoleń-Dzirba, et al., Antimicrobial potential of caffeic acid against *Staphylococcus aureus* clinical strains, BioMed. Res. Int. (2018)7413504. Available from: https://doi.org/10.1155/2018/7413504.

[134] E. Pinho, I.C. Ferreira, L. Barros, A.M. Carvalho, G. Soares, M. Henriques, Antibacterial potential of North-Eastern Portugal wild plant extracts and respective phenolic compounds, BioMed. Res. Int. 2014 (2014)814590. Available from: https://doi.org/10.1155/2014/814590.

[135] B.M. Kyaw, C.S. Lim, Bactericidal antibiotic-phytochemical combinations against methicillin resistant *Staphylococcus aureus*, Braz. J. Microbiol. 43 (2012) 938–945.

[136] Â. Luís, F. Silva, S. Sousa, A.P. Duarte, F. Domingues, Antistaphylococcal and biofilm inhibitory activities of gallic, caffeic, and chlorogenic acids, Biofouling 30 (2014) 69–79.

[137] J. Nguefack, B.B. Budde, M. Jakobsen, Five essential oils from aromatic plants of Cameroon: their antibacterial activity and ability to permeabilize the cytoplasmic membrane of *Listeria innocua*examined by flow cytometry, Lett. Appl. Microbiol. 39 (5) (2004) 395–400.

[138] O.A. Aldulaimi, General overview of phenolics from plant to laboratory, good antibacterials or not, Pharmacogn. Rev. 11 (22) (2017) 123–127.

[139] L. Laureti, I. Matic, A. Gutierrez, Bacterial responses and genome instability induced by subinhibitory concentrations of antibiotics, Antibiotics 2 (2013) 100–114.

[140] M.A. Kohanski, M.A. DePristo, J.J. Collins, Sublethal antibiotic treatment leads to multidrug resistance via radical-induced mutagenesis, Mol. Cell 37 (2010) 311–320.

[141] M.P. Otto, E. Martin, C. Badiou, S. Lebrun, M. Bes, F. Vandenesch, et al., Effects of subinhibitory concentrations of antibiotics on virulence factor expression by community-acquired methicillin-resistant *Staphylococcus aureus*, J. Antim. Chemo. 68 (7) (2013) 1524–1532.

[142] E.M. Redwan, N.Abd El-Baky, A.M. Al-Hejin, M.N. Baeshen, H.A. Almehdar, A. Elsaway, et al., Significant antibacterial activity and synergistic effects of camel lactoferrin with antibiotics against methicillin-resistant *Staphylococcus aureus* (MRSA), Res. Microbiol. 167 (6) (2016) 480–491.

[143] D. Wang, L. Yu, H. Xiang, J. Fan, L. He, N. Guo, et al., Global transcriptional profiles of *Staphylococcus aureus* treated with berberine chloride, FEMS Microbiol. Lett. 279 (2) (2008) 217–225.

[144] D. Keman, F. Soyer, Antibiotic-resistant *Staphylococcus aureus* does not develop resistance to vanillic acid and 2-hydroxycinnamic acid after continuous exposure *in vitro*, ACS Omega 4 (13) (2019) 15393–15400.

[145] M. Miklasińska-Majdanik, M. Kępa, R.D. Wojtyczka, D. Idzik, T.J. Wąsik, Phenolic compounds diminish antibiotic resistance of *Staphylococcus aureus* clinical strains, Int. J. Environ. Res. Public Health 15 (10) (2018) 2321.
[146] W. Gao, D. Vecchio, J. Li, J. Zhu, Q. Zhang, V. Fu, et al., Hydrogel containing nanoparticles-stabilised liposomes for topical antimicrobial delivery, ACS Nano 8 (3) (2014) 2900–2907.
[147] M. Ravichandran, Enhancement of antimicrobial activity of naturally occurring phenolic compounds by nano-particle mediated delivery against *Listeria monocytogenes*, *Escherichia coli* O157:H7, and *Salmonella typhimurium*, Graduate Theses and Dissertations, <https://scholarworks.uark.edu/etd/2085>, 2014 (accessed 14.05.22).
[148] G. Longo, L. Alonso-Sarduy, L.M. Rio, A. Bizzini, A. Trampuz, J. Notz, et al., Rapid detection of bacterial resistance to antibiotics using AFM cantilevers as nanomechanical sensors, Nat. Nano 8 (7) (2013) 522–526.
[149] C.S. Rempe, K.P. Burris, S.C. Lenaghan, C.N. Stewart Jr, The potential of systems biology to discover antibacterial mechanisms of plant phenolics, Front. Microbiol. 8 (2017) 422.
[150] C. Fiamegos, P.L. Kastritis, V. Exarchou, H. Han, A.M.J.J. Bonvin, J. Vervoort, et al., Antimicrobial and efflux pump inhibitory activity of caffeoylquinic acids from *Artemisia absinthium* against Gram-positive pathogenic bacteria, PLoS ONE 6 (2011) e18127.
[151] K. Singh, R.M. Coopoosamy, N.J. Gumede, S. Sabiu, Computational insights and in vitro validation of antibacterial potential of shikimate pathway-derived phenolic acids as NorA efflux pump inhibitors, Molecules 27 (2022) 2601.
[152] J.O. Aribisala, R.A. Abdulsalam, Y. Dweba, K. Madonsela, S. Sabiu, Identification of secondary metabolites from *Crescentia cujete* as promising antibacterial therapeutics targeting type 2A topoisomerases through molecular dynamics simulation, Comput. Biol. Med. 145 (2022) e105432. H.
[153] J.O. Aribisala, S. Sabiu, Chemoinformatic identification of phenolics as modulators of penicillin-binding protein 2a of *Staphylococcus aureus*: a structure-activity relationship-based study, Pharmaceutics 14 (2022). Available from: https://doi.org/10.3390/xxxxx.
[154] K. Madonsela, K.A. Alayande, S. Sabiu, Enhancement of colistin-mediated bacterial lethality by orientin through redox imbalance, Evid. Based Complement. Altern. Med. 3809232 (2022) 9.
[155] Q. Yuan, L. Ma, G. Ye Piao, The traditional medicine and modern medicine from natural products, Molecules 21 (2016) 559.
[156] K. Lewis, Platforms for drug discovery, Nat. Rev. Drug Discov. 12 (2013) 371–387.
[157] A. Shakeri, Y. Panahi, T.P. Johnston, A. Sahebkar, Biological properties of metal complexes of curcumin, BioFactors 45 (3) (2019) 304–317.
[158] Y. Liang, Z. Li, Y. Huang, R. Yu, B. Guo, Dual-dynamic-bond cross-linked antibacterial adhesive hydrogel sealants with on-demand removability for post-wound-closure and infected wound healing, ACS Nano 15 (2021) 7078.
[159] Y. Li, Y. Miao, L. Yang, Y. Zhao, K. Wu, Z. Lu, et al., Recent advances in the development and antimicrobial applications of metal–phenolic networks, Adv. Sci. (2022). Available from: https://doi.org/10.1002/advs.202202684.
[160] B. Kaczmarek, M. Wekwejt, K. Nadolna, A. Owczarek, O. Mazur, A. Pałubicka, The mechanical properties and bactericidal degradation effectiveness of tannic acid-based thin films for wound care, J. Mech. Behav. Biomed. Mater. 110 (2020) 103916.

[161] Z. Li, X. Huang, L. Lin, Y. Jiao, C. Zhou, Z. Liu, Polyphenol and Cu2 + surface-modified chitin sponge synergizes with antibacterial, antioxidant and pro-vascularization activities for effective scarless regeneration of burned skin, Chem. Eng. J. 419 (2021) 129488.
[162] M. Balakrishna, S.S. Kaki, S.L. Mallampalli,Karuna, S. Sarada, C.G. Kumar, R.B.N. Prasad, Synthesis and in vitro antioxidant and antimicrobial studies of novel structured phosphatidylcholines with phenolic acids, Food Chem. 221 (2017) 664–672.
[163] J. Liu, C. Du, H.T. Beaman, M.B.B. Monroe, Characterization of phenolic acid antimicrobial and antioxidant structure-property relationships, Pharmaceutics 12 (5) (2020) 419.
[164] J. Liu, H. Yong, X. Yao, H. Hu, D. Yun, L. Xiao, Recent advances in phenolic–-protein conjugates: synthesis, characterization, biological activities and potential applications, RSC Adv. 9 (61) (2019) 35825–35840.
[165] Y.S. Fu, C. Wu, T. Wu, H. Yu, S. Yang, Y. Hu, Preparation and characterisation of chlorogenic acid-gelatin: a type of biologically active film for coating preservation, Food Chem. 221 (2017) 657–663.
[166] A.A.A. El-Maksoud, I.H. Abd El-Ghany, H.S. El-Beltagi, S. Anankanbil, C. Banerjee, S.V. Petersen, et al., Adding functionality to milk-based protein: preparation, and physico-chemical characterization of β-lactoglobulin-phenolic conjugates, Food Chem. 241 (2018) 281–289.
[167] M. Ali, J.K. Keppler, T. Coenye, K. Schwarz, Covalent whey protein–rosmarinic acid interactions: a comparison of alkaline and enzymatic modifications on physico-chemical, antioxidative, and antibacterial properties, J. Food Sci. 83 (8) (2018) 2092–2100.
[168] H. Xu, T. Zhang, Y. Lu, X. Lin, X. Hu, L. Liu, et al., Effect of chlorogenic acid covalent conjugation on the allergenicity, digestibility and functional properties of whey protein, Food Chem. 298 (2019) 125024.
[169] X. Wu, Y. Lu, H. Xu, D. Lin, Z. He, H. Wu, et al., Reducing the allergenic capacity of β-lactoglobulin by covalent conjugation with dietary polyphenols, Food Chem. 256 (2018) 427–434.
[170] M. Goleniowski, M. Bonfill, R. Cusido, J. Palazon, Phenolic acids, in: K.G. Ramawat, J.M. Mérillon (Eds.), Natural Products, Springer-Verlag, Heidelberg, 2013, pp.1951–1973. https://doi.org/10.1007/978-3-642-22144-6-64.
[171] C.J. Arias, J. Toledo, Manual de Manejo Postcosecha de Frutas Tropicales. Organización de las Naciones Unidas para la Agricultura y la Alimentación (FAO), n.d. <http://www.fao.org/inpho/content/documents/vlibrary/ac304s/ac304s00.htm> 2018 (accessed 26.04.22).
[172] T. Ramírez-Reyes, N. Flores-Estévez, M. Luna-Rodríguez, J.C. Noa- Carrazana, L.R. Sánchez-Velásquez, A. Trigos-Landa, Extractos crudos de Magnolia schiedeanaSchltdl. para el control de bacterias fitopatógenas, Madera Bosques 21 (2015) 159–164.
[173] S. Bautista-Baños, M. Hernández-López, E. Bósquez-Molina, C.L. Wilson, Effects of chitosan and plant extracts on growth of *Colletotrichum gloeosporioides*: anthracnose levels and quality of papaya fruit, Crop Prot. 22 (2003) 1087–1092.
[174] A.J. Ojeda-Contreras, J. Hernández-Martínez, Z. Domínguez, J. Mercado, Utilization of caffeic acid phenethyl ester to control *Alternaria alternata* rot in tomato (*Lycopersicon esculentum* Mill.) fruit, J. Phytopathol. 156 (2008) 164–173.
[175] Y.M. Ochoa-Fuentes, E. Cerna-Chávez, J. Landeros-Flores, S. Hernández-Camacho, J.C.y Delgado-Ortiz, Evaluación *in vitro* de la actividad antifúngica de cuatro extractos vegetales metanólicos para el control de tres especies de *Fusarium* spp, Rev. Int. Bot. Exp. 81 (1) (2012) 69–73.

[176] S.A. Oyeyinka, A.O. Abdulsalam, A.M.A. El-Imam, A.T. Oyeyinka, O.F. Olagunju, F.L. Kolawole, et al., Total phenolic content, antioxidant, anti-inflammatory and anti-microbial potentials of Bambara groundnut (*Vigna subterranea* L.) seed extract, Br. Food J. 123 (11) (2021) 3421–3425.
[177] A. Hernández, S. Ruiz-Moyano, A.I. Galván, A.V. Merchán, F.P. Nevado, E. Aranda, et al., Anti-fungal activity of phenolic sweet orange peel extract for controlling fungi responsible for post-harvest fruit decay, Fungal Biol. 125 (2021) 143–152.
[178] Z. Kyselova, Toxicological aspects of the use of phenolic compounds in disease prevention, Interdiscip. Toxicol. 4 (4) (2011) 173–183.
[179] Y. Sakihama, M.F. Cohen, S.C. Grace, H. Yamasaki, Plant phenolic antioxidant and pro-oxidant activities: phenolics-induced oxidative damage mediated by metals in plants, Toxicology 177 (2002) 67–80.
[180] T.O. Ajiboye, E. Skiebe, G. Wilharm, Phenolic acids potentiate colistin-mediated killing of *Acinetobacter baumannii* by inducing redox imbalance, Biomed. Pharmacother. 101 (2018) 737–744.
[181] R.M. Hussain, N.F. Abdullah, Z. Amom, Killing of *Staphylococcus aureus* by allylpyrocatechol is potentiated by induction of intracellular oxidative stress and inhibition of catalase activity, J. Integr. Med. 14 (2016) 456–464.
[182] W. Vermerris, R. Nicholson, Phenolic compounds and their effects on human health, in: W. Vermerris, R. Nicholson (Eds.), Phenolic Compound Biochemistry, Springer Science, 2006, pp. 235–255.
[183] G.R. Velderrain-Rodríguez, H. Palafoxcarlos, A. Wall-Medrano, J.F. Ayalazavala, C.-Y.O. Chen, M. Robles-SAnchez, et al., Phenolic compounds: their journey after intake, Food Funct. 5 (2014) 189–197.
[184] J.E.D. De Souza, L.M. Casanova, S.S. Costa, Bioavailability of phenolic compounds: a major challenge for drug development? RevistaFitos 9 (2015) 1–72.
[185] J. Correa-Betanzo, E. Allen-Vercoe, J. Mcdonald, K. Schroeter, M. Corredig, G. Paliyath, Stability and biological activity of wild blueberry (*Vaccinium angustifolium*) polyphenols during simulated *in vitro* gastrointestinal digestion, Food Chem. 165 (2014) 522–531.
[186] S. Lafay, A. Gil-Izquierdo, C. Manach, C. Morand, C. Besson, A. Scalbert, Chlorogenic acid is absorbed in its intact form in the stomach of rats, J. Nutr. 136 (2006) 1192–1197.
[187] I. Peluso, M. Palmery, Flavonoids at the pharma-nutrition interface: is a therapeutic index in demand? Biomed. Pharm. 71 (2015) 102–107.
[188] B.V. Bonifácio, P.B.D. Silva, M.A.D.S. Ramos, K.M.S. Negri, T.M. Bauab, M. Chorilli, Nanotechnology-based drug delivery systems and herbal medicines: a review, Int. J. Nanomed. 9 (2014) 1–15.
[189] K. Das, R.K.S. Tiwari, D.K. Shrivastava, Techniques for evaluation of medicinal plant products as antimicrobial agents: current methods and future trends, J. Med. Plants Res. 4 (2010) 104–111.
[190] European Academies' Science Advisory Council (EASAC), Antimicrobial drug discovery: greater steps ahead. Available at <http://www.easac.eu.>, 2014 (accessed 06.03.22).

2.4 Redox Impact on bacterial macromolecule: A promising avenue for discovery and development of novel antibacterials

This section has been published as a review article in Biomolecules and is presented as it is in the article

biomolecules

MDPI

Review

Redox Impact on Bacterial Macromolecule: A Promising Avenue for Discovery and Development of Novel Antibacterials

Jamiu Olaseni Aribisala and Saheed Sabiu *

Department of Biotechnology and Food Science, Faculty of Applied Sciences, Durban University of Technology, P.O. Box 1334, Durban 4000, South Africa
* Correspondence: sabius@dut.ac.za; Tel.: +27-31-373-5330

Abstract: Antibiotic resistance in bacteria has remained a serious public health concern, resulting in substantial deaths and morbidity each year. Factors such as mutation and abuse of currently available antibiotics have contributed to the bulk of the menace. Hence, the introduction and implementation of new therapeutic strategies are imperative. Of these strategies, data supporting the role of reactive oxygen species (ROS) in bacterial lethality are intriguing, with several antimicrobials, including antibiotics such as fluoroquinolones, β-lactams, and aminoglycosides, as well as natural plant compounds, being remarkably implicated. Following treatment with ROS-inducing antimicrobials, ROS such as $O_2^{\bullet-}$, $^{\bullet}OH$, and H_2O_2 generated in bacteria, which the organism is unable to detoxify, damage cellular macromolecules such as proteins, lipids, and nucleic acids and results in cell death. Despite the unique mechanism of action of ROS-inducing antibacterials and significant studies on ROS-mediated means of bacterial killing, the field remains a topical one, with contradicting viewpoints that require frequent review. Here, we appraised the antibacterial agents (antibiotics, natural and synthetic compounds) implicated in ROS generation and the safety concerns associated with their usage. Further, background information on the sources and types of ROS in bacteria, the mechanism of bacterial lethality via oxidative stress, as well as viewpoints on the ROS hypothesis undermining and solidifying this concept are discussed.

Keywords: antibiotic resistance; antioxidants; bacterial lethality; oxidative stress; reactive oxygen species

Citation: Aribisala, J.O.; Sabiu, S. Redox Impact on Bacterial Macromolecule: A Promising Avenue for Discovery and Development of Novel Antibacterials. *Biomolecules* **2022**, *12*, 1545. https://doi.org/10.3390/biom12111545

Academic Editor: Andrey Zamyatnin

Received: 20 September 2022
Accepted: 20 October 2022
Published: 22 October 2022

Publisher's Note: MDPI stays neutral with regard to jurisdictional claims in published maps and institutional affiliations.

Copyright: © 2022 by the authors. Licensee MDPI, Basel, Switzerland. This article is an open access article distributed under the terms and conditions of the Creative Commons Attribution (CC BY) license (https://creativecommons.org/licenses/by/4.0/).

1. Introduction

Antimicrobial resistance has evolved as one of the most severe public health challenges of the 21st century, threatening efficient prevention and treatment of microbial infections that are no longer sensitive to most conventional antibiotics [1,2]. Over the years, multidrug-resistant microorganisms (MRM) have developed a varying degree of resistance to each new antibiotic released into the market, with various accompanying dire consequences [3,4]. Yearly, about 700,000 deaths occur worldwide due to infections caused by MRM, and this number could increase to 10 million by the year 2050, depending on resistance evolution patterns and, more importantly, the status of available, effective therapeutic alternatives [5–7]. The estimated associated cost of infections caused by MRM is an annual global GDP of 3.8%, culminating in 28.3 million people being subjected to extreme poverty globally [6,7]. Unfortunately, the misuse and abuse of antibiotics, which are majorly implicated in the increased emergence of antibiotic resistance, are still on the rise [1,3,6,7]. Moreover, the inadequate measures for effective prevention and control of microbial infections in developing countries, as well as the increased failure rate in the discovery and development of new therapeutics, have further aggravated the problem of antimicrobial resistance [1,3,6]. Hence, more success in the discovery of new and more

potent therapeutics would significantly and undoubtedly help in the fight against antimicrobial resistance [8]. Of the viable strategies in the discovery and development of therapeutics, the contributions of reactive oxygen species (ROS) to the antimicrobial arsenal of antibiotics or antibacterial agents have been proficiently demonstrated and continue to attract research interests [9–12].

Generally, living organisms depend on oxygen for cellular aerobic respiration and metabolism [13]. However, the existence of oxygen in the form of free radicals may trigger cellular oxidative stress, with possible dire consequences in many organisms [10,14]. During aerobic respiration, ROS are generated in small concentrations, but cell defense mechanisms generally detoxify them without causing damage to cells [11,15]. However, excessive levels of ROS generated via redox reaction or as a result of antibiotic treatment may overcome the cellular defense mechanisms, resulting in oxidative stress. During oxidative stress, small quantities of ROS that cells have limited appropriate defenses against may quickly become lethal, particularly to bacteria [9,10,13]. This concept has long been employed in antiseptics and disinfectants but has not found extensive usage as therapeutics due to ROS' perceived toxicity and unacceptable damage to the host tissue [8,15]. However, evidence supporting their role in therapeutic lethality has been strengthened in recent times, and novel means of producing ROS have been identified, allowing their therapeutic use to be investigated for topical and systemic infections [8,10,11,16]. The revelation that bactericidal antimicrobials such as fluoroquinolones, β-lactam, and aminoglycoside kill bacteria through the induction of oxidative stress [17–19], combined with the knowledge of how generated ROS are utilized by host defense cells (e.g., neutrophils) in pathogen elimination, has sparked renewed interest in the appreciation of ROS and oxidative stress as a novel antibacterial therapeutic strategy.

ROS-inducing agents are finding practical usage as therapeutics. For instance, Surgihoney (produced in the UK by Healing Honey International), a genetically modified kind of honey with wound-healing properties, owes its potent antibacterial actions to high levels of cellular ROS (in the form of H_2O_2) as its primary means of antibacterial action [8]. However, future implementation and widespread usage of more novel ROS-inducing antimicrobials (whose primary means of antibacterial action is based on ROS generation) would require insight into the nature of the ROS involved in antimicrobial activity and safety concerns associated with their use [8]. This is necessary, as ROS differ in their toxicity, and host cells have limited defense against ROS such as $^{\bullet}OH$ [8,16]. Moreover, though several studies have implicated the involvement of ROS in the lethality of antibiotics and some natural therapeutic agents [8,16–19], various other studies citing limitations to this hypothesis have surfaced over the years [20–22]. This controversial nature of the field has caught the attention of more current studies and continues to culminate in novel findings. Thus, this study forms part of the ongoing efforts to provide a more balanced insight into the purview of oxidative stress in bacterial lethality.

Previous studies attempting to review ROS-induced antibacterial agents have focused mostly on ROS-inducing antibiotics, with only a few studies on ROS-inducing plant-derived natural and synthetic compounds. Moreover, in recent times, new studies implicating ROS in the antibacterial activity of several novel plant-derived natural and synthetic compounds have surfaced, and this necessitates an up-to-date appraisal. Hence, this study presents information on ROS-induced plant-derived natural (most especially phenolics) and synthetic compounds. Further, as previous reviews have focused on studies implicating ROS in the killing of all microorganisms, this study gathered only information reported on bacteria in an attempt to understand the unique mechanism and type of ROS associated with the killing of bacteria. Equally, information on non-toxicity issues of some ROS-inducing antibacterial agents on human tissues and cells was reviewed and presented for the first time in this study. Background information on the sources and types of ROS generated and antioxidant defense mechanisms in bacteria, the mechanism of bacterial lethality via oxidative stress induction, as well as viewpoints on hypotheses undermining and solidifying the antibacterial potential of ROS, are also discussed in the study.

Although this was undertaken with the view to having a better understanding of divergent perspectives on the concept of ROS-mediated bacterial lethality, it is hoped that opinions from this study will guide future studies seeking to understand the role of oxidative stress in the antibacterial potential of synthetic and natural plant-derived therapeutics.

2. Materials and Methods

The Preferred Reporting Items for Systematic Reviews and Meta-Analyses (PRISMA) protocol [23] was followed for the search. Information was gathered between the years 2015 and 2022 from major scientific databases (Google Scholar, Scopus, Science Direct, Web of Science, PubMed, Springer, and BioMed Central) using journals as well as books and/or chapters. Reactive oxygen species and/or oxidative stress were searched and cross-referenced with terminologies such as bacterial and plant interaction, natural plant-derived compounds, phenolics, synthetic compounds, and safety concerns. Following the removal of duplicates, eighteen research articles not within the scope of the study (e.g., studies implicating ROS in the killing of other microorganisms different from bacteria and studies not written in English) were excluded from the studies examined. Ninety-one scientific papers that provided relevant information within the scope of the review were used in the review, and Figure 1 depicts the PRISMA flowchart for this investigation.

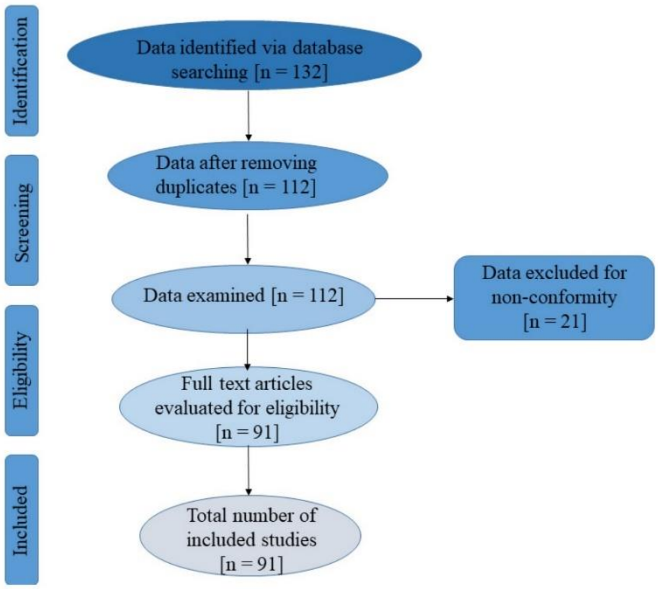


Figure 1. PRISMA flowchart of the literature screened, included, and evaluated for this study.

2.1. Background Information on ROS Sources, Types, Generation, and Impact on Bacterial Macromolecules

2.1.1. Sources and Types of ROS in Bacteria

Aerobic respiration remains the major endogenous source of ROS in bacteria. Respiration in bacteria occurs mostly in the cytoplasm, during which molecular oxygen (O_2) is transformed into water, carbon dioxide, and energy (in the form of adenosine triphosphate (ATP)) [24]. However, during this process, partial reductions of oxygen species often occur, resulting in superoxide anion ($O_2^{\bullet -}$) being released from electron transport chains, which are catalyzed into hydrogen peroxide (H_2O_2) [15,25,26]. During subsequent

reactions, hydroxyl radicals (•OH) and singlet oxygen ($^1O_2$) are frequently formed (Table 1) [25,26]. Another endogenous source of ROS in bacteria includes antimicrobial treatment [24]. Endogenous ROS accumulation in bacteria via antibiotic treatment is drug-specific [27]. Antibiotics such as fluoroquinolones, β-lactams, and aminoglycosides, as well as several natural agents, have been demonstrated to increase the rate of respiration in bacteria following treatment, leading to subsequent high endogenous ROS generation [17–19]. In addition, some studies have suggested that the primary antibiotics target damage following treatment with antimicrobials, which may trigger mechanisms such as the envelope stress response and programmed cell death, resulting in ROS buildup in bacteria [24,27,28]. Furthermore, the redox cycling potential of some antibacterials (such as nitroaromatic and phenolics) in the bacterial cell have been shown to increase endogenous superoxide anions. These agents in the presence of oxygen in bacterial cells deplete NADH to derive their toxicity.

Exogenous sources of ROS in bacteria occur as a result of host–pathogen interaction, which results in bacteria being attacked by ROS of the host cell [29]. Due to ROS' ability to act as a signaling molecule in the host, ROS are capable of inciting host defense (e.g., phagosomes) against several bacteria [30] during infection. In this case, specialized phagocytes such as neutrophils and macrophages engulf pathogens into a membrane-derived vesicle called a phagosome, where they bombard bacteria pathogens with a complex mixture of reactive oxygen (ROS), nitrogen (RNS), and chlorine species [29]. This process is known as "oxidative burst," and it is triggered by the NADPH oxidase complex (NOX2), which is critical for successful pathogen killing [31]. The phagosomal membrane helps in NOX2 assembling [31]. NOX2 is responsible for catalyzing the partial reduction of oxygen through the addition of one electron from NADPH to molecular oxygen, which results in the generation of superoxide anion ($O_2^{\bullet-}$) [30]. The subsequent generation of H_2O_2 from $O_2^{\bullet-}$ is catalyzed by the enzyme myeloperoxidase (MPO), which also helps convert H_2O_2 to hypochlorous acid (HOCL), a very powerful oxidant in vivo [29]. Bacteria, particularly the pathogenic ones, have developed excellent counterstrategies to survive the "oxidative burst" of the host [27]. Some bacteria control phagocytic cells to reduce their antibacterial activity. For example, neutrophils infected with *Francisella tularensis* do not generate ROS effectively because the bacteria hinder NOX2 assembly in the host [27,29].

The four major types of ROS in bacteria include $O_2^{\bullet-}$, H_2O_2, •OH, and singlet oxygen ($^1O_2$) [32] (Table 1). These ROS have varying kinetics and degrees of activity [25,26], and due to the low reactivity and ability to be detoxified by natural antioxidants (enzymatic and nonenzymatic), $O_2^{\bullet-}$ and H_2O_2 pose fewer risks than •OH and $^1O_2$ [32–35]. Because no enzyme can detoxify $^1O_2$ and •OH, these radicals are very poisonous and can be fatal [32–34]. Thus, oxygen plays a dual role in the aerobic metabolism of bacteria: it generates energy for bacteria, and its reduction via the electron transport system creates species ($O_2^{\bullet-}$, •OH, and H_2O_2) that are lethal to bacteria (Table 1). In host cells, together with unstable intermediates from lipid peroxidation, ROS have a significant impact on human health [32–35]. For instance, illnesses such as atherosclerosis, Alzheimer's, and autoimmune disorders, among others, are caused by oxidative stress that occurs when the radical-scavenging systems of the body are overwhelmed [33–35].

Table 1. Stepwise reduction of ROS byproducts via electron transfer in bacterial cells.

ROS Species	Generation Steps and Characteristics of ROS	Stepwise Reduction Equation	References
hydroperoxyl radical ($HO_2^{\bullet}$)	During a series of events during respiration, molecular oxygen is reduced to hydroperoxyl radical ($HO_2^{\bullet}$).	$O_2 + e^- + H^+ \rightarrow HO_2^{\bullet}$	[15,25,36]
superoxide ($O_2^{\bullet -}$)	The hydroperoxyl radical ($HO_2^{\bullet}$) dissociates to form superoxide ($O_2^{\bullet -}$). The reduction potential of this species is based on the environmental conditions of the solution. It can act as a mild oxidizing agent in an aqueous solution and, under other environmental conditions, it can act as a reducing agent.	$HO_2^{\bullet} \rightarrow H^+ + O_2^{\bullet -}$ $Fe^{2+} + O_2 \leftrightarrow Fe(II)O2 \leftrightarrow Fe(III)O_2^- \leftrightarrow Fe^{3+} + O_2^{\bullet -}$	[15,25,26,36]
Hydrogen peroxide (H_2O_2)	Superoxide ($O_2^{\bullet -}$) undergoes additional transformations as a result of a well-known dismutation reaction. This process is hastened by the superoxide dismutase (SOD) enzyme, which has a copper-zinc core to generate hydrogen peroxide (H_2O_2). However, other enzymes (e.g., urate oxidase and glucose oxidase) have been shown to catalyze this reaction. It is critical that the cells "neutralize" H_2O_2 since the species can be reduced through Fenton chemistry to $^{\bullet}OH$, which is lethal.	$O_2^{\bullet -} + 2H^+ + e^- \rightarrow H_2O_2$ $2H+ + O_2^{\bullet -} + O_2^{\bullet -} \rightarrow H_2O_2 + O_2$	[26,32,36,37]
Hydroxyl radical ($^{\bullet}OH$)	A hydroxyl radical ($^{\bullet}OH$) is generated through the Fenton reaction. Of note, in live organisms and at physiological pH, the ferrous ion (Fe^{2+}) that accelerates the Fenton reaction has a short lifespan and can quickly auto-oxidize to ferric (Fe^{3+}). The hydroxyl radical is a highly aggressive radical that can impede the correct functioning of a variety of biological molecules.	$H_2O_2 + e^- \rightarrow HO^- + {}^{\bullet}OH$ $H_2O \rightarrow {}^{\bullet}OH + H^{\bullet} + e^-_{aq} \rightarrow H_2O_2$ $Fe^{2+} + H_2O_2 \rightarrow Fe^{3+} + {}^-OH + {}^{\bullet}OH$	[25,26,36]
Singlet oxygen ($^1O_2$)	Singlet oxygen is considered one of the most dangerous species of ROS generated through the natural process, with huge biological significance.	(a) Energy transfer to photosynthetic cells from light-sensitive molecule (b) Coexisting of oxygen and light in cells containing molecules such as flavins, quinones, porphyrins, etc. (c) Production through aromatic chemicals such as naphthalene, methylene blue, and several antimicrobial agents (d) Macrophage respiratory bursts (e) Lipid peroxidation activities	[33,36]

2.1.2. Defense against ROS Generation in Bacteria

In *Escherichia coli*, the regulatory response to ROS (H_2O_2 and $O_2^{\bullet-}$) generation is through the activation of superoxide dismutase (SOD) and catalase [15,38] (Figure 2). Unlike human cells with only two SOD isoforms, *E. coli* utilizes three distinct kinds of SOD with various metal cationic locations: CuZnSOD (sodC), FeSOD (sodB), and MnSOD (sodA) [10,38]. These enzymes catalyze the conversion of superoxide anion ($O_2^{\bullet-}$) to hydrogen peroxide (H_2O_2), thereby limiting the accumulation of superoxide radicals in bacteria cells [10,15]. Catalases, on the other hand, catalyze H_2O_2 into H_2O and O_2, and *E. coli* possesses two types of catalases (hydroperoxidase I (HPI) and hydroperoxidase II (HPII)), which are also present in several other bacteria [39–41]. Alkyl hydroperoxidase in the bacterial cell has also been demonstrated to be important in limiting ROS generation by making use of two peroxidases (AhpD and AhpC) in its catalytic action [15,42]. The AhpC acts as the catalytic component, and AhpD works as an essential protein adaptor during metabolism [15]. Further, some small proteins that are referred to as thiols (e.g, glutathione, thioredoxin, and peroxiredoxin) in bacteria stimulate the breakdown of ROS, reactive nitrogen species (RNS), and their intermediates to repair oxidatively and nitrosatively damaged proteins [8,42]. Thiol's lower cellular level of disulfide and glutathione, which is the most abundant, not only serves as a cofactor to glutathione peroxidase but also helps reversion of other non-enzymatic antioxidants, such as α-tocopherol and ascorbic acid, to their active form [8,42]. In addition to the general stress regulon (RpoS), SOD and catalase are controlled by OxyR and SoxRS regulons [43]. These have been studied extensively using *E. coli* as a model, and their impacts as SOD and catalase regulators on a wide range of bacterial phyla ranging from Actinobacteria to Proteobacteria have been reported [15,42]. In anaerobic bacteria that do not have catalase for H_2O_2 elimination, OxyR has been demonstrated to be important in their tolerance to H_2O_2. In addition, OxyR is involved in the defense against singlet oxygen and cellular damage caused by lipid peroxidation in bacteria [8,15,43]. Mutations in OxyR in *E. coli* have been shown to reduce cellular sensitivity to H_2O_2, resulting in an increase in one of the three enzymes (catalase hydroperoxidase I, catalase hydroperoxidase II, and alkyl hydroperoxide reductase) implicated in the elimination of organic ROS and H_2O_2 [8,16,44]. These three enzymes are controlled by the katG gene product, katEF, and Ahp genes, respectively [16,43]. SoxS, on the other hand, is critical to activating gene transcription to minimize superoxide and nitric oxide stress in bacterial cells, as well as regulating membrane permeability through efflux pump and outer membrane porin production [8,44]. Generally, defense against ROS in bacteria protects pathogenic bacteria against both the host immune response and antimicrobial therapy, which enable bacteria to cause chronic infections in the host.

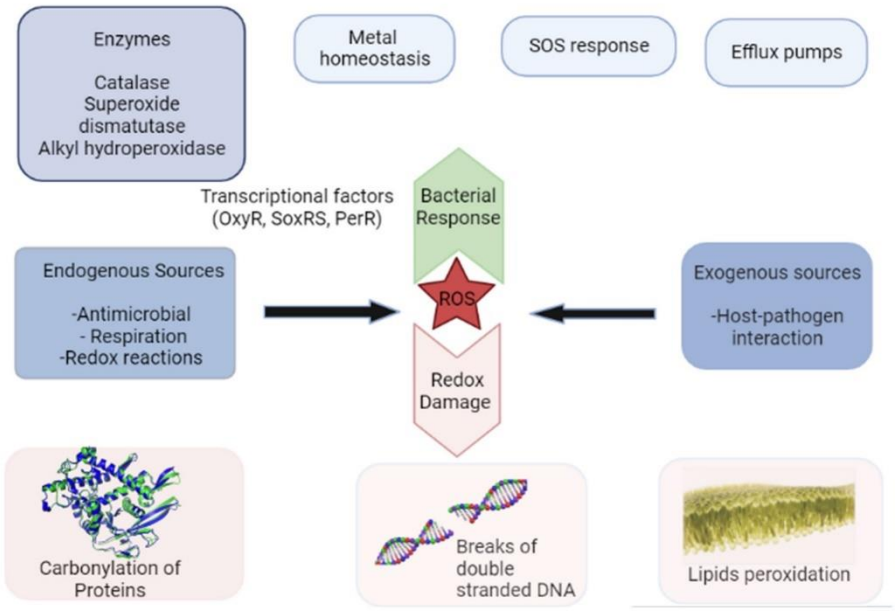


Figure 2. Antioxidant defense against ROS generation in bacteria that could originate from both exogenous and endogenous sources. Repair mechanisms as a means of bacterial response involving both enzymatic and non-enzymatic ways help ensure normal redox potential in bacteria, which are often controlled by transcriptional factors such as OxyR, PerR, and SoxRS. In the case of the repair mechanisms being overwhelmed, the oxidative stress (redox impact) is set such that it could damage bacteria macromolecules such as proteins, lipids, and deoxyribonucleic acid (DNA).

2.1.3. Mechanism of Bacterial Lethality via Oxidative Stress

The term ROS refers to a group of highly reactive compounds that include molecular oxygen (O_2) [8,25]. Electron reduction of oxygen during metabolism in the cell generates superoxide anion (O_2^-). Superoxide anion is a major ROS that can be further converted to H_2O_2 by SOD [15,43] (Figure 3). Hydroxyl radical ($^{\bullet}OH$) is produced through the Fenton reaction, which involves the reduction of H_2O_2. The Fenton reaction is normally activated through the disruption of iron homeostasis that results in an elevated amount of independent cellular Fe^{2+} [42] (Figure 3). Normal cells have a finely regulated and well-balanced redox state due to the continuous generation and detoxification of cellular ROS. However, exogenous stressors such as antibiotics can speed up the natural process of respiration or microbial metabolism of food, leading to a high generation of endogenous ROS that weakens the ROS defense mechanisms [8,16,44]. The subsequent degeneration of the defense systems due to overwhelming ROS production can lead to oxidative stress, which is lethal to cells, since ROS such as hydroxyl radicals' accumulation can stimulate autoxidation of cellular macromolecules such as nucleic acids, lipids, and proteins, thereby altering their biological activity [10,11] (Figure 3). Autoxidation of cellular macromolecules (e.g., lipid peroxidation) is a process in which ROS remove electrons from macromolecules and subsequently generate reactive intermediates that can undergo further reactions. Bacterial cell membranes, or organelle membranes, are particularly susceptible to ROS damage, due to their high levels of polyunsaturated fatty acids. Lipid peroxidation damages bacterial phospholipids directly and can also act as a cell death signal-inducing programmed cell death. Thus, since no protein-based mechanism can detoxify the hydroxyl radicals, ROS induce their key antibacterial activity when stress becomes severe, leading to the self-destruction of bacteria cells [12,45,46].

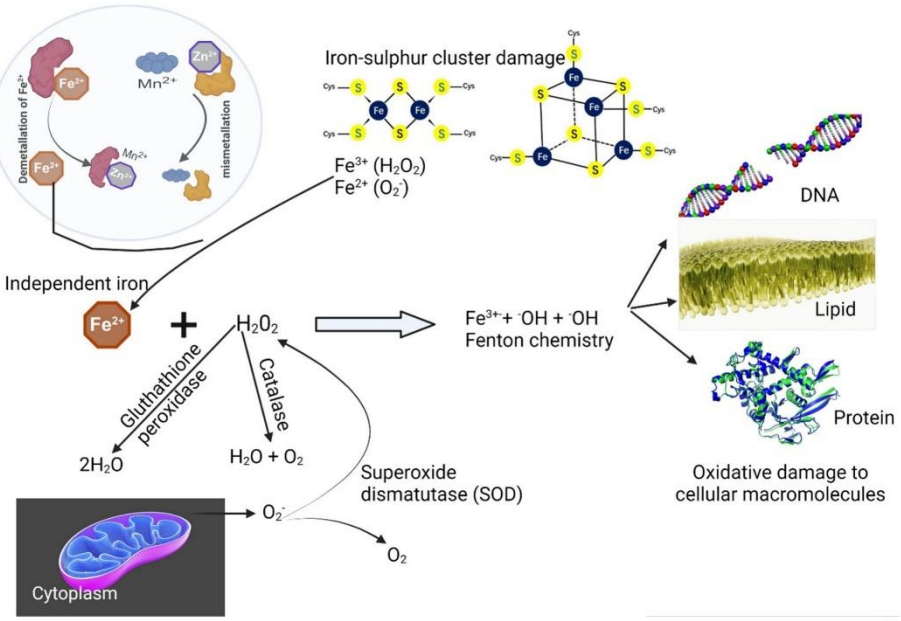


Figure 3. A multiscale explanation of the metabolism and a macromolecular example of how ROS causes macromolecule damage. ROS demetallize mononuclear Fe^{2+} proteins, which are then mismetallized with alternative divalent metal ions. Further, through damage to the iron-sulfur cluster, independent Fe^{2+} are generated. Independent Fe^{2n+} spontaneously interacts with H_2O_2 (produced via dismutase of superoxide (O_2^-)) via the Fenton reaction, releasing hydroxyl radicals that can damage bacterial macromolecules.

Generally, oxidative stress can either be endogenous or exogenous [11]. Exogenous oxidative stress occurs as a result of host–pathogen interactions in bacteria, whereas antibiotics treatment, respiration, and intracellular redox reactions contribute to endogenous oxidative stress [10,11] (Figure 2). Enzymes such as catalase, SODs, alkyl hydroperoxide reductase, and glutathione peroxidase can detoxify ROS in bacteria and are controlled by regulons such as SoxRS, OxyRS, SOS, and PerR, which help counteract the damaging effect of ROS [8,16,44]. For instance, *E. coli* defends itself against oxidative stress by increasing the activity of SOD and catalase, which catalyze the dismutation of O_2 and H_2O_2, respectively. Furthermore, the OxyR and SoxRS regulons in *E. coli* govern the oxidation response by transcriptionally regulating catalase and SOD in reaction to H_2O_2 and O_2, respectively [44].

2.1.4. Antibiotic-Mediated ROS Lethality

Antibiotics' principal mechanisms of action in bacteria are an attack to cell wall (β-lactam antibiotics), protein synthesis (aminoglycosides), and DNA replication (fluoroquinolones) [47,48]. However, some investigations have found that antibiotics cause ROS generation by the overexcitation of electrons through the Krebs cycle and the release of iron, which activates Fenton chemistry [17,19,47,48]. Hence, antibiotics with dissimilar primary mechanisms of action were discovered to share a common secondary mechanism in the form of ROS generation [47,48]. Arriaga-Alba et al. [49] were the first to establish that oxidative stress generation by quinolones contributed to the antibiotic's mechanism of action in *Salmonella typhimurium* killing. Thereafter, antibiotics such as aminoglycosides, β-lactams, rifampicin, and chloramphenicol have been demonstrated to induce ROS

generation, resulting in bacteria lethality [17,50,51]. However, nitrofurantoin and polymyxin B are the two of the most commonly implicated antibiotics in ROS-mediated bacterial lethality [16]. Regardless of their unique targets, ROS-inducing antibiotics cause oxidative damage through the increase in bacteria respiration, which results in NADH depletion, iron-sulfur cluster instability, and iron misregulation [19]. For instance, using aminoglycoside antibiotics, Kohanski et al. [50] found that the formation of •OH caused mistranslation and abnormal folding of membrane-associated proteins, resulting in a stress response. Further, topoisomerase inhibitors have their primary mechanisms of bacterial killing via DNA poisoning, lesion repair inhibition, and interfering with DNA replication [52]. Dwyer et al. [18] implicated the involvement of oxidative damage (mediated by $O_2^{\bullet-}$ and •OH) in the lethality of topoisomerase inhibitors. In another study by Foti et al. [53], bactericidal antibiotics caused cell death by oxidizing the guanine nucleotide pool. Dorsey-Oresto et al. [54] published the first proof of post-stress programmed cell death mediated by ROS in bacteria. They implicated the YihE protein kinase in *E. coli* as an essential protein responsible for the bacteria's self-destructive response to fatal stress. YihE protein kinase is controlled by the Cpx envelope (a response system to stress), which, together with MazF toxin and superoxide, helps assist bacteria in deciding whether to live or die in response to stress. Although it has been proven that oxidative stress induced by some bactericidal antibiotics plays a vital role in bacterial cell death, a study by Kohanski et al. [50] has also shown that at sub-lethal levels, ROS play a key role in bactericidal antibiotic-induced mutagenesis. In addition, studies by Imlay [20], Keren et al. [21], and Liu and Imlay [22] have argued that the formation of ROS contributed to antibiotic lethality because antibiotics appear to act under anaerobic circumstances. Hence, studies associating ROS generation with antibiotics have been largely controversial, with various viewpoints undermining and solidifying the hypothesis presented in Table 2. Despite these contradictions, the metabolism in bacteria influences antibiotic potency (for example, metal homeostasis and iron-sulfur proteins) [28,47,55].

Two Commonly Implicated Antibiotics in ROS-Mediated Bacterial Lethality

Nitrofurantoin

Nitrofurantoin is a medication whose mechanism of action has been poorly understood since its discovery in the 1940s [56]. However, recent studies have implicated ROS generation as one of its major mechanisms of action [16]. The mechanism is based on cellular NADH depletion to create nitroaromatic anion radicals, which, in the presence of molecular oxygen (O_2), often auto-oxidize to produce superoxide (O_2^-) [10,16] (Figure 4). The continued redox cycling of nitrofurantoin in bacteria cells results in the accumulation of O_2^-, which is often frequently converted to more lethal ROS (e.g., •OH) that can damage bacteria cell macromolecules. The drug is employed in clinical practice to treat lower urinary tract infections (UTI) [10]. Because of nitrofurantoin's quick infiltration into the lower urinary tract, the drug is only suitable for infections that affect the lower part of the urinary tract and would not work for other types of infections, as they would not achieve therapeutic concentrations [56]. This indicates that the basis for the adoption of the drug in clinical practice is seemingly based on its discriminating accessibility to the urinary tract [16]. The drug was approved by FDA in the 1950s and was widely used for the treatment of UTI infection until the 1970s, when other drugs such as β-lactams and trimethoprim-sulfamethoxazole became available [56]. However, recently, several procedures have declared nitrofurantoin to be the first-line treatment for UTI infections due to resistance to newer drugs [16]. Several researchers believe that the continued effectiveness and minimal resistance to the drug could be due to its minimal effects on bowel flora and its mechanism of action, which is based on ROS generation [56]. Hence, one advantage of ROS-inducing antimicrobial agents compared to other antibacterial polymeric materials could be their lower susceptibility to resistance.

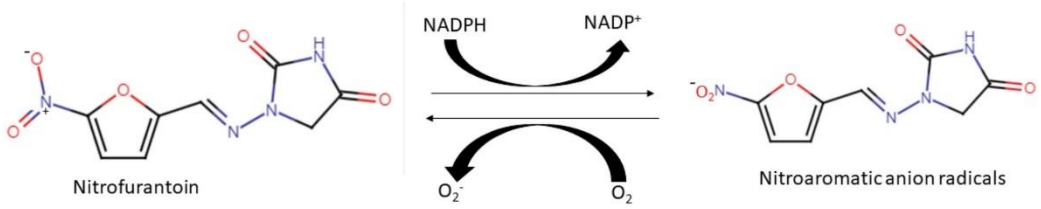


Figure 4. Redox cycling potential of nitrofurantoin, which demonstrates nitroaromatic anion formation through depletion of NADPH. In the presence of molecular oxygen, nitroaromatic anion generates superoxide anion.

Polymyxin B

Polymyxin B is a peptide-based antibacterial agent [57]. It is often employed in the treatment of infections caused by Gram-negative bacteria such as *Pseudomonas aeruginosa* [16]. However, as a result of some toxicity issues (neurotoxicity and nephrotoxicity) implicated in its usage, the drug is often reserved as a last resort for treatment [57,58]. The drug derives its potency via the accumulation of hydroxyl radicals, which consequently facilitate the disruption and loss of integrity of the cell membrane in Gram-negative bacteria. More crucially, PMB was found to be lethal to Gram-negative bacteria even at lower concentrations [58]. The ROS-mediated antibacterial action of PMB was brought to light through the revelation that PMB toxicity increases under aerobic conditions, as well as through deletion of the katA gene essential for H_2O_2 resistance in *P. aeruginosa* [57].

2.2. Natural and Synthetic Agents Contributing to ROS-Mediated Bacterial Lethality

Some natural agents such as phenolic compounds, honey, peptides, siderophores, and carotenoids, as well synthetic agents, have been linked to microbial mortality via ROS production. The mechanisms of action of these natural and synthetic antibacterial agents are presented in Table 3.

Table 2. Viewpoints undermining and solidifying the involvement of antibiotics in ROS-mediated bacterial lethality hypotheses.

Basis of Opinion	Views Undermining the Opinion	Studies Solidifying the Opinion
Involvement of ROS in antibiotics bacterial lethality	Iron/iron-sulfur clusters' effect on bacterial killing by antibiotics is largely dependent on how antibiotics are taken up; ROS play no role [59]. Further, ROS accumulation and cell death in an antibiotic-treated cell are discordant [21]. Hydroxyl radical (•OH) accumulation did not often correspond to antimicrobial death [21].	Belenky et al. [60] demonstrated the involvement of ROS in antibiotic lethality by showing that cells exposed to antibiotics had cytotoxic changes including malondialdehyde adducts, protein carbonylation, double-strand DNA breaks, and nucleotide oxidation. which are indicative of ROS involvement. Further, the findings of Luan et al. [61] also laid justice to the involvement of ROS by demonstrating that katG mutants produce more ROS, which subsequently resulted in their high rate of death relative to the wild type after antibiotic treatment.
Type (antibiotics) and conditions that influence ROS generation	The ROS-mediated mechanism of killing is shared by all antibiotics, and anaerobiosis inhibits the lethality of norfloxacin (quinolone) at a low concentration. Furthermore, Iron chelator (dipyridyl) and hydroxyl radical scavenger (thiourea) prevented cells from being killed by antimicrobials under both aerobic and anaerobic conditions [21].	In 2014, Dwyer et al. [17] demonstrated that antibiotics belonging to fluoroquinolones, β-lactams, and aminoglycosides generate ROS while interacting with their target sites, though information on ROS generation of other classes of antibiotics is unconvincing. Further, findings from the study showed that ampicillin, gentamicin, and norfloxacin have only attenuated lethality under highly anaerobic conditions. Furthermore, Malik et al. [62,63] showed that the choice of norfloxacin by Keren et al. [21] was not a good candidate for ROS experiments due to the intermediate reactions to anaerobic cell death caused by quinolones.
Quantity of ROS generated	ROS produced during antibiotic treatment are too minute to truly kill bacterial cells [22].	The findings of Luan et al. [61] and Hong et al. [64], have, to a degree, debunked the claim on the quantity of ROS generation by demonstrating that stress can increase the number of sites available for ROS assault and that a high ROS concentration may not be required. Moreover, the findings of Luan et al. [61] and Dwyer et al. [17], through demonstration of stressors that created lesions that were

		hypersensitive to ROS attack, could also reduce the credibility of the argument. The actual evidence on the quantity of ROS generation relative to cell death came from Hong et al. [46] and Dorsey-Oresto et al. [54], who postulated that intracellular levels of ROS were capable of killing cells once the initial triggering stressor had been removed.
Detection of ROS	The low specificity of dyes for ROS detection and antibiotic therapy did not increase ROS [22].	The claim about low specificity of dyes for ROS was addressed by Dwyer et al. [17] in a ROS quantification experiment conducted in 2014, in which they used a wide range of fluorescent dyes to identify several kinds of ROS in bacteria, including H_2O_2, which could not be detected with the previously utilized HPF dye (3′-(p-hydroxyphenyl) fluorescein). In their findings, bactericidal agents including ampicillin, gentamicin, and norfloxacin increased H_2O_2 generation in bacteria after treatment.
Effectiveness of exogenous antioxidant	The possibility of chemical agents such as thiourea and dipyridyl causing off-target effects cannot be fully ruled out [20,22].	This causative argument about off-target effects of ROS scavenger could be countered by the findings of Luan et al. [61], who demonstrated that katG mutants produce more ROS, which subsequently resulted in their high rate of death relative to the wild type after antibiotic treatment.

2.2.1. Phenolic Compounds

Because of their low redox potential, catechol-containing phenolic compounds could be excellent pro-oxidants that generate a considerable quantity of ROS through autoxidation in the presence of transition metals [45,65] (Figure 5). The ROS ($O_2^{\bullet-}$ and H_2O_2) produced through this autoxidation are not highly reactive, and are hence less toxic to bacterial macromolecules [45,66]. However, the reaction of these ROS with independent ferrous ions in the cell via the Fenton reaction (Fe^{2+} + •OH + •OH) can produce a highly reactive hydroxyl radical (•OH) that causes damage to bacteria's macromolecules and subsequent lethality [66] (Figure 3).

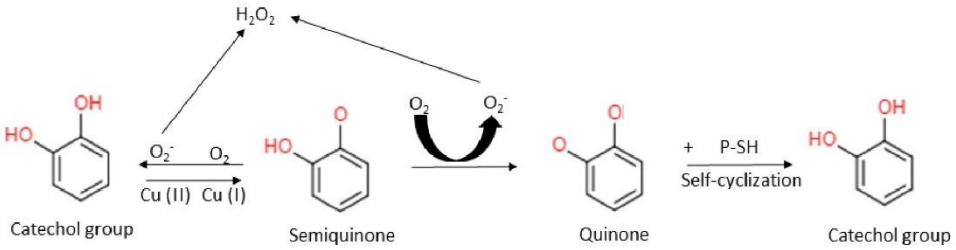


Figure 5. Redox cycling potential of catechol-bearing phenolic compounds, which demonstrates ROS and quinone formation in the presence of transition metal ions and oxygen and the subsequent reversion to catechol moieties through reaction with protein thiols (P-SH) or self-cyclization.

Specifically, Singh et al. [67] established the capacity of hydroxychavicol isolated from *Piper betle* to kill *E. coli* via ROS induction and damage of DNA in *E. coli* cells. The study demonstrated that treatment of *E. coli* with hydroxychavicol in the presence of copper cleaves DNA and instigates DNA damage repair genes. Treatment in the presence of antioxidants protected cells against hydroxychavicol-induced ROS lethality, and damage to iron-sulfur proteins significantly amplifies oxidative stress instigated by hydroxychavicol. The *E. coli* wild type was less susceptible to hydroxychavicol treatment relative to the *E. coli gshA* mutant, which indicates the significant involvement of oxidative stress in the lethality of hydroxychavicol. Hydroxychavicol was found to be potent against other Gram-negative organisms isolated from persons with clinical symptoms and diverse resistance patterns. Later in 2021, Singh et al. [68], while working with the same compound, postulated the exact kinetics and series of events that occurred in the killing of *E. coli*. The study implicated the potential of hydroxychavicol to damage the *E. coli* cell membrane via oxidative stress as one of the earlier mechanisms involved in hydroxychavicol lethality. These findings showed that oxidative stress set in immediately after 10 min of treatment with hydroxychavicol and resulted in membrane damage at 30 min, followed by DNA breakage before 60 min (Figure 6). Genes involved in repairing DNA damage were not activated until after 60 min of treatment. Abnormal growth and cell breakage of *E. coli* were noted after 1 h of hydroxychavicol treatment at 125 μg/mL and 750 μg/mL, respectively. Cell porosity was observed to increase in the presence of magnesium ion (Mg^{2+}), but this was halted in the presence of ethylenediaminetetraacetic acid (EDTA). The study concluded that hydroxychavicol pretreatment of Gram-negative organisms, which are most impervious to antibiotic treatment due to their outer membrane, could help in the treatment of infections caused by Gram-negative bacteria due to the damaging effects that hydroxychavicol had on the cell membrane.

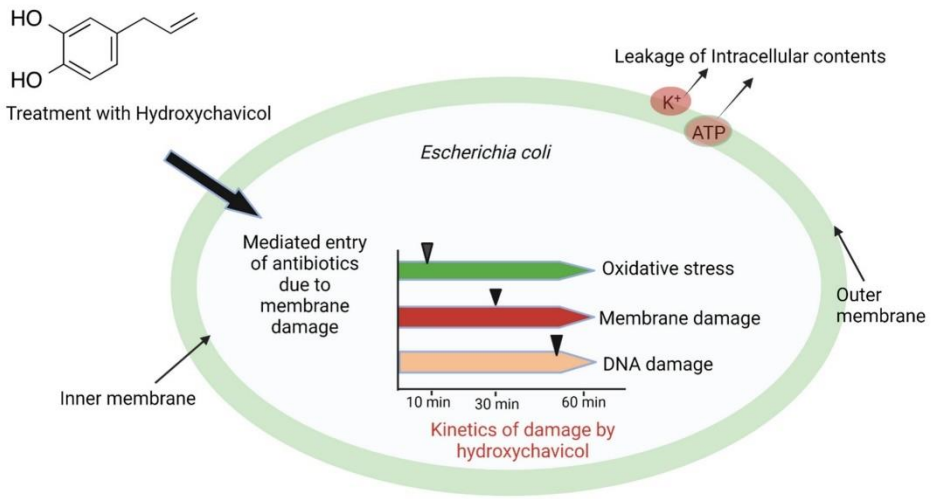


Figure 6. Antibacterial mechanisms of action of hydroxychavicol against *E. coli.*

Sinsinwar and Vadivel [69] worked on the antibacterial activity of catechin obtained from the shell nut of cashew against *Staphylococcus aureus* (both methicillin-sensitive and methicillin-resistant). The study revealed the minimum inhibitory concentration (MIC) of catechin against both methicillin-resistant and methicillin-sensitive *S. aureus* to be between 78.1 to 156.2 µg/mL. Following treatment with catechin, about 1.5-fold and 1.9-fold increases in ROS generation were noted in methicillin-sensitive and methicillin-resistant *S. aureus*, respectively, relative to the control (methicillin). Moreover, catechin treatment resulted in toxicity to the cell membrane and an increase in the leakage of nucleic acids (× 18) and proteins (× 16) relative to cells treated with methicillin. The specific activity of SOD and catalase drastically decreased from 9.63 to 5.31 U/mg and 3930 to 1573 U/mg, respectively, relative to the control. The study ascribed the effects of treatment with catechin to the involvement of oxidative stress in the killing of both methicillin-sensitive and methicillin-resistant *S. aureus*.

Ajiboye et al. [66] demonstrated the contribution of oxidative stress in the bactericidal activity of protocatechuic acid. Protocatechuic acid has an MBC value of 700, 800, and 800 µg/mL and a MIC value of 600 µg/mL each against *E. coli*, *P. aeruginosa,* and *S. aureus,* respectively. The protocatechuic acid-killing rate of bacterial cells was time-dependent, and the amount of ROS (superoxide anion) generated following treatment at 4× MIC increased significantly relative to the negative control (dimethyl sulfoxide (DMSO)-treated cells). Following treatment of bacterial cells with protocatechuic acid, SOD, NAD^+/NADH, and catalase increased considerably relative to the negative control. Equally, there was a decrease in glutathione levels and an increase in glutathione disulfide, malondialdehyde, and damage of DNA following treatment of bacterial cells with protocatechuic acid relative to the negative control. All findings from the study indicate the generation of ROS ($O_2^{\bullet-}$and $^{\bullet}OH$) in the bactericidal activity of protocatechuic acid against *E. coli*, *P. aeruginosa,* and *S. aureus.* The study concludes that protocatechuic acid instigates ROS generation possibly through Fenton chemistry, autoxidation, and hampering of the electron transport chain, consequently resulting in the peroxidation of lipids, the breakage of DNA, and the ultimate cell death of the bacterial cell. In another study by Ajiboye et al. [70], the authors reported that phenolic acids (protocatechuic acid, gallic acid, and caffeic acid) increased colistin-mediated bacterial killing via the disruption of redox homeostasis. Making use of the wild and mutant strains, the antibacterial activity of all the phenolics

showed that the wild type had higher MIC values relative to the sodB and katG mutant strains of *Acinetobacter* baumannii AB5075. Protocatechuic acid had the highest antibacterial activity among the phenolics, with a MIC of 32 g/mL against the sodB mutant strain and 64 g/mL against the katG mutant strain. The checkerboard analysis further showed that the phenolics could potentiate colistin antibacterial activity. Treatment with the phenolics revealed the generation of superoxide anion and an increase in the pair NAD+/NADH and ADP/ATP, which all pointed to the contribution of oxidative stress in the lethality to bacteria induced by the study phenolics. Similarly, a reduced level of glutathione was also noted, which further confirmed the involvement of oxidative stress in the killing of *A. baumannii*. The study concluded that via oxidative stress, the studied phenolic compounds enhanced the potency of colistin against *A. baumannii* AB5075.

Xiong et al. [71] studied the antibacterial properties of epigallocatechin gallate (EGCG) isolated from green tea against *E. coli*. Findings from the study demonstrated that the antibacterial activity of EGCG is not directly due to H_2O_2 generated by the compound but is rather a result of the increase in endogenous ROS and a reduced adaptive response to ROS in *E. coli*. It was also observed that EGCG acted synergistically with paraquat (a well-known pro-oxidant) in eliciting its effect. These observations substantiated the mechanism of antibacterial action of EGCG, which was previously unclear. However, the antibacterial effect of EGCG was impeded under anaerobic conditions, but it was concluded that EGCG increased intracellular oxidative stress in the inhibition of *E. coli* growth.

Hussain et al. [72] studied the effects of allyl pyrocatechol (AP), the main component in *Piper betle* ethanolic extract, on essential oxidative stress enzymes required for the survival of *S. aureus*, a significant pathogen in the human host. The nitroblue tetrazolium (NBT) reduction assay was used in the study to detect ROS by the chromogenic production of reduced formazan. This method makes it easier to distinguish between the quantities of ROS produced intracellularly and extracellularly. The absorbance values (A575nm) for the NBT reduction test were 0.709 and 0.695 for untreated and AP-treated cells, respectively, at a concentration of 2 mg/mL MIC, indicating the existence of ROS. However, AP-treated *S. aureus* cells displayed decreased ROS levels both extracellularly and intracellularly relative to the untreated cells, but larger amounts of ROS stayed intracellularly at an absorbance of 0.457 relative to extracellular levels at an absorbance of 0.137 at $P<0.05$. This observation is unlike previous studies in which catechol-containing phenolic compounds caused increased ROS relative to untreated cells [66,70]. However, this observation could have been due to the method employed in the study, as NBT is only reduced by $O_2^{\bullet-}$, denoting that other ROS formed through the Fenton reaction were not considered [73]. This opinion was reinforced, as AP-treated *S. aureus* cells had higher *sodA* (1.5-fold) and *sodM* (0.7-fold) expression, with an equivalent increase in total SOD activity (12.24 U/mL) relative to the untreated cells (10.85 U/mL). Likewise, the transcription of ahpC was greatest in AP-treated cells with 5.5-fold upregulation compared to untreated cells at $P<0.05$. Accordingly, ahpC activity was greater in AP-treated cells at 0.672 (A310nm) compared to untreated cells, which were 0.394 (A310nm). The findings revealed that AP's pro-oxidant activity caused sufficient internal oxidative stress in *S. aureus*. As a result, *S. aureus* raised SOD expression and activity (*SodA, SodM*) to deal with the increased oxidative stress. The higher expression of *sodA* compared to *sodM* shows that the stress was induced internally by increasing $O_2^{\bullet-}$.

2.2.2. Honey

Surgihoney is a kind of honey for wound healing that has an antibacterial action that is based on high amounts of ROS in the form of H_2O_2. This honey is produced in the UK by Healing Honey International. Cooke et al. [74] investigated the antibacterial effects of Surgihoney and modified honey 1 and 2 (produced from *Apis mellifera*) against *S. aureus* and reported that the modified honeys had significantly higher antibacterial activity relative to Surgihoney. Surgihoney had a phenol activity of 31.5% relative to 63% and > 63%

observed in modified honey 1 and 2, respectively. Furthermore, higher H_2O_2 was generated by the modified honey relative to surgihoney over 24 h. The modified honey 1 and 2 produced 1 and 1.5 mM H_2O_2, respectively, versus 0.2 mM H_2O_2 produced by surgihoney over the same period. This observation demonstrates the correlation between the increase in phenol activity and the production of H_2O_2 which was correlated with the antibacterial activity noted in the study. The study concluded that the modified honey would afford a simple-to-apply, effective, and non-toxic wound-dressing agent.

2.2.3. Carotenoid

Aribisala et al. [75] used in silico and in vitro approaches to examine the role of oxidative stress in astaxanthin-mediated bacterial mortality. It was observed that astaxanthin had a MIC of 8 μg/mL, which was lower than the 16 μg/mL observed for novobiocin against *S. aureus*. However, against *E. coli* and *P. aeruginosa*, novobiocin showed lower MICs of 0.25 and 0.125 μg/mL, respectively, compared to astaxanthin's MIC of 16 g/mL against both species. Following further examination into the role of ROS in the antibacterial activity of astaxanthin, it was observed that treatment with astaxanthin stimulated increased superoxide anion production compared to DMSO-treated cells. The observed increase in ROS competed well with those elicited by the reference standards (novobiocin and ciprofloxacin) and was accompanied by both glutathione (GSH) depletion and a considerable increase in ADP/ATP ratio. Furthermore, a time-dependent inhibition of hydroxyl radicals in the presence of 2,2'dipyridyl drastically reduced the rate of killing of the tested organisms. These findings indicate the contribution of oxidative stress in astaxanthin bactericidal activity. The in vitro findings were also consistent with the in silico evaluations on topoisomerase 2As, a target implicated in facilitating ROS generation when interacting with fluoroquinolones. The study concluded that astaxanthin could be developed as a novel natural topo2A inhibitor that has antibacterial activity based on ROS production.

2.2.4. Antimicrobial Peptide

Using the *Mo*-CBP_3 (MC) amino acid sequence isolated from the seeds of *Moringa oleifera* as the starting peptide, Oliveira et al. [76] designed three peptides (MC-PepI, MC-PepII, and MC-PepIII) and evaluated their antibacterial activities against two Gram-positive (*Bacillus subtilis* and *S. aureus*) and two Gram-negative bacteria (*E. coli* and *Klebsiella pneumoniae*). Findings from the study showed PepIII to be the most potent among the three peptides, and it had the highest potency against *S. aureus,* with an MIC_{50} value of 4.4 μM. Using *C. parapsilosis* as a model, it was demonstrated that the mechanism of action of PepIII (the most active peptide) functioned via an elevated accumulation of ROS and the incorporation of propidium iodide following treatment. The scanning electron microscopy analysis demonstrated damage to the cell membrane, consequently leading to cytoplasm content leakage and cell death. Furthermore, the three peptides demonstrated against human red blood cells did not cause hemolysis, and PepIII (the most potent peptide), when demonstrated against Vero cells even at a higher concentration (57 × MIC_{50} of S. *aureus*), did not result in cytotoxicity. The study concluded that the observations, however, demonstrated PepIII as a prospective antimicrobial candidate for bacterial and fungal infections.

2.2.5. Siderophore

Ong et al. [77] worked on the antibacterial activity of pyochelin, a siderophore isolated from *Burkholderia paludis*. The antibacterial activity was carried out against *S. aureus* and *E. faecalis*. Findings from the study showed *Enterococcus faecalis* (MIC of 3.13 μg/mL) to be more susceptible relative to *S. aureus* (MIC of 6.26 μg/mL). Following 24 h treatment with 1, 2, and 4 × MIC of pyochelin, an elevated increase in ROS in *E. faecalis* was noted and caused an increase in malondialdehyde levels, suggesting lipid peroxidation relative

to the control (Figure 7). Furthermore, cell membrane disruption and cytoplasmic content leakage resulted in the cell death of the organism. When *E. faecalis* was treated for 24 h with 2 and 4 × MIC of the siderophore, the survival rate of the organisms was drastically reduced by roughly 80% relative to the negative control. The study concluded that pyochelin could be developed as therapeutics for infections caused by *E. faecalis* and *S. aureus* due to pyochelin's capability to generate endogenous ROS in bacterial cells.

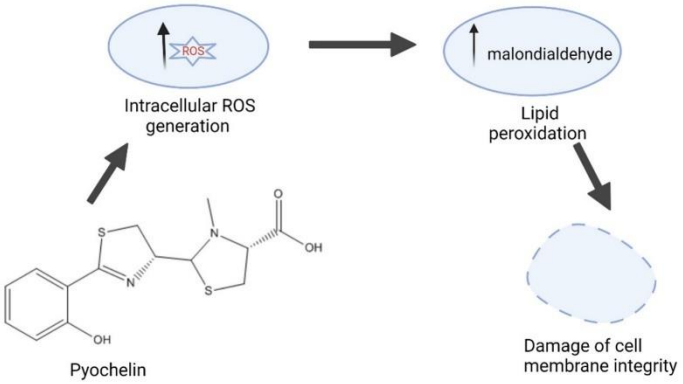


Figure 7. Pyochelin antibacterial mechanism of action.

2.2.6. Synthetic Agents in ROS-Mediated Bacterial Lethality

Wang et al. [78] worked on the photobiological activities of six derivatized cationic complexes ((i), phenanthroline, (ii), 3,8dipyrenylphenanthroline, (iii) 3,8dipyrenylphenanthroline, (iv) 3-phenylphenanthroline, (v) 3-pyrenylphenanthroline, and (vi) 3,8diphenylethynylphenanthroline) containing heteroleptic (III) with tris-diimine moiety in vitro. Findings from their study revealed that complexes 3 and 5 at 81 and 72%, respectively, had the highest quantum yield of singlet oxygen among all studied derivatives. The derivatives had long-lived triplet excited states, which allowed for intramolecular contact with ground-state oxygen and significant ROS generation. Following photoactivation and after treatment with derivatives 3 and 5, elevated production of ROS in SK-MEL-28 (human malignant cells) was observed relative to the dark control and tert-butyl hydrogen peroxide (positive control). Furthermore, after photoactivation, derivatized 3 and 5 demonstrated significantly enhanced antibacterial activity against the studied strains *S. aureus* (EC_{50} of 0.17 μM) and *S. mutans* (0.18 μM) relative to the dark condition, with a mean EC_{50} of 11.2 μM and 5.59 μM for *S. mutans* and *S. aureus* respectively. They concluded that the derivatives could be promising photoactivation agents against pathogenic bacteria through their capability of eliciting ROS.

Wang et al. [79] developed a light-responsive T-TCP micelle and determined its antibacterial activity against bacterial biofilms. The T-TCP micelle is a self-assembling amphiphilic copolymer comprising thymol, toluidine blue O (TBO), grafted chitosan, and propylene sulfide (PPS). When the T-TCP micelle was irradiated with a 670 nm light source, about a four-fold higher fluorescence intensity of singlet oxygen sensor green was observed relative to the non-irradiated T-TCP, whose fluorescence intensity of singlet oxygen sensor green remain the same. A dramatic increase from 5 to 57% in transmittance was observed with the T-TCP micelle that was irradiated. The ROS generation under irradiation of T-TCP micelles by light activation of TBO was evidenced by the oxidation of thioether (hydrophobic) to sulfoxide (hydrophilic). Treatment of *S. aureus* and *Listeria monocytogenes* biofilms with irradiated T-TCP significantly reduced the formation of biofilms and killed almost all bacterial cells relative to the non-irradiated T-TCP, and it was

observed that the reduction in biofilm formation and killing of cells was due to the drug release and ROS generated due to light activation of TBO. Cell wall damage was observed in cells treated with both T-TCP and T-TCP with thymol relative to the control (thymol), which did not result in cell wall damage of *S. aureus* after treatment. They concluded that the developed micelles could be employed as an antibacterial agent for disinfection.

Song et al. [80] worked on the antibacterial activity of the synthesized bis-quaternary ammonium salt (SBQA), a high molecular weight, long-chain organic compound. The antibacterial activity was carried out on two pathogenic bacteria (*S. aureus* and *E. coli*), and findings from their study showed that *S. aureus* (MIC value range 8- 32 μg/mL) was more susceptible to SBQA than *E. coli* (16–64 μg/mL). Further, the rate of cell death was concentration-dependent, with a death rate increase from 40% to 99% as the concentration increased from 12.5 μg/mL to 200 μg/mL. At the same concentration of 25 μg/mL, SBQA had higher inhibitory effects on both *S. aureus* (95%) and *E. coli* (74%) than the positive control (CTAB) (55% and 50% killing rate for *E. coli* and *S. aureus*, respectively). SEM and TEM examination of bacterial cells treated with 200 μg/mL of SBQA revealed damage to the bacterial cell wall and a subsequent leakage of protein. The observed leakage of cytoplasm content was due to the ability of SBQA to induce ROS production, which causes damage to the cell membrane. The increase in ROS generation correlates with an increase in the concentration of SBQA administered, as revealed by the increased intensity of green fluorescence. Relative to the control group, a greater-than five- and four-fold increase in ROS generation was observed against *S. aureus* and *E. coli*, respectively, with no signs of cytotoxicity on the growth of mouse breast cancer cells (4T1) at a concentration lesser than 50 μg/mL. The authors concluded that SBQA could serve as a promising therapeutic drug candidate for bacterial infections.

Hu et al. [81] derivatized two derivatives from HL, HL1 and HL2 (Figure 8) and examined their antibacterial potency against *E. coli* and *B. subtilis*. Their findings showed that the two derivatives had potent antibacterial activity relative to the parent compound HL due to the attached Sn atom (Figure 8). Among the derivatives, HL1 had the highest antibacterial activity against both organisms, and it was observed that HL1 alky chain flexibility and the compound lipophilicity enable its easy absorption through the cell membrane and, in so doing, cause damage. Relative to kanamycin (MIC 8 μg/mL), which serves as the positive control, HL1 showed a higher antibacterial effect with a MIC of 2 μg/mL. Against HELF, a human lung fibroblast, HL1 had a negligible cytotoxic effect even when the concentration was raised to 10 μg/mL and evaluated over a 24 h period. SEM evaluation of the treated cells (2 h) revealed that HL1 was able to pass through the *E. coli* cell membrane and enter the cell, causing cell membrane damage and leakage of cytoplasm content. In *B. subtilis* and *E. coli* treated with HL1, a significant amount of fluorescence was observed as a result of ROS generation, which could lead to oxidative stress and cause damage to the cell membrane and ultimately cell death. The authors concluded that ROS generation and subsequent damage caused by the release of ROS could be the key mechanisms employed by HL1 in bacterial killing and that the compound could be further developed and used for the treatment of infections caused by bacteria.

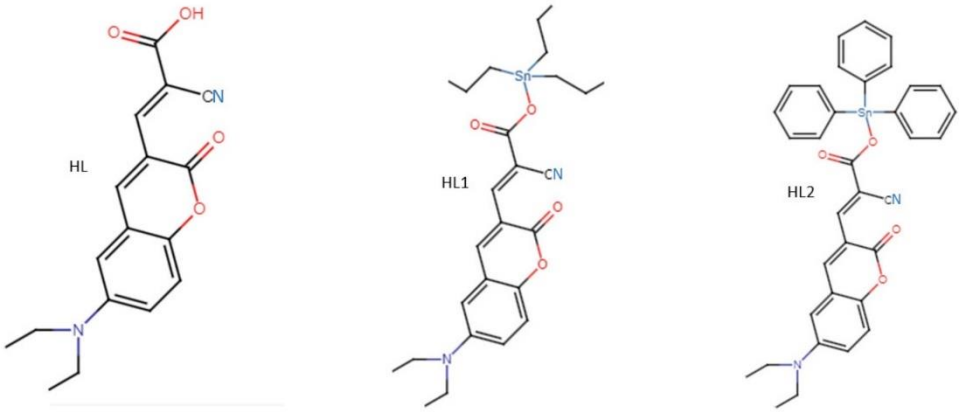


Figure 8. 2D structure of HL, HL1, and HL2.

Liu et al. [82] designed a catechol-modified chitosan film (similar to melanin capsules produced by the immune system of insects in response to infection) and determined its in vitro antibacterial activity against *S. aureus* and *E. coli* and its in vivo wound-healing efficiency. Findings revealed that the catechol-chitosan film could accelerate electron transfer from redundant ascorbate to molecular oxygen to ensure continuous ROS production. After treatment with 1 and 10 mM of ascorbate, non-modified chitosan, oxidized catechol-chitosan film, and the reduced catechol-chitosan film had no sign of cytotoxicity on human keratinocyte cells. However, when the concentration of ascorbate used for treatment was increased to 300 mM, a 15% reduction in cell viability was observed. In the in vivo assay (exploring the subcutaneous administration model in rats), relative to the non-modified chitosan, a two-log average reduction in *S. aureus* viable count was noted in rats treated with catechol-chitosan film (reduced with 300 mM ascorbate) after three days. Moreover, the wounds of rats treated with catechol-chitosan film reduced with 10 mM ascorbate showed remarkable closure, with more evenly distributed collagen and the development of more epithelium and blood vessels after 14 days relative to wounds treated with chitosan alone or with oxidized catechol-chitosan film, which shows increased inflammation. A higher reduction in the bacterial count was also noted in rats treated with reduced catechol-chitosan film relative to other studied groups, correlating with the in vitro assay findings. The authors concluded that the reduced catechol-chitosan film had the potential for wound healing through ROS generation, which prevents bacteria invasion.

Table 3. Recent studies on natural and synthetic compounds supporting ROS-mediated bacterial killing.

Agent Commpound Classes	Agents	Bacteria	Implicated ROS and Mechanisms of Involvement in Antibacterial Activity	References
		Natural agents		
Phenolics	(1) hydroxychavicol	*E. coli*	Time-dependent destruction of cellular macromolecules by oxidative stress caused by hydroxyl radical (•OH). Destruction of the cell membrane occurs 30 min after treatment, and DNA damage onset occurs after 30 min.	[67,68]
	(2) Catechin	*S. aureus* (both methicillin-sensitive and methicillin-resistant)	Increased generation of ROS ($O_2^{\bullet-}$ and H_2O_2) resulted in the onset of oxidative stress and subsequent damage to the cell membrane, nucleic acid, and protein by hydroxyl radical (•OH).	[69]
	(3) Epigallocatechin gallate	*E. coli*	Increased endogenous hydrogen peroxide (H_2O_2), leading to inhibition of *E. coli* growth	[71]
	(4) protocatechuic acid, gallic acid, and caffeic acid	*A. baumannii* (wild, sodB, and katG mutants)	Elevated superoxide anion ($O_2^{\bullet-}$) production by the phenolic acids resulted in increased colistin-mediated bacterial killing via the destruction of redox homeostasis.	[70]
	(5) protocatechuic acid	*E. coli*, *P. aeruginosa*, and *S. aureus*	Protocatechuic acid instigates ROS ($O_2^{\bullet-}$, H_2O_2, •OH) generation through Fenton chemistry, autoxidation, and hampering of electron transport chain, consequently resulting in peroxidation of lipid, breakage of DNA, and ultimate cell death of bacterial cells.	[66]

	(6) Allyl pyrocatechol	*S. aureus*	Allyl pyrocatechol provoked internal oxidative stress in *S. aureus* ($O_2^{\bullet-}$), thereby amplifying the transcription and activities of SODs (*SodA, SodM*) in *S. aureus* to adapt to the increased oxidative stress.	[72]
Honey	(1) Surgihoney	*S. aureus*	Hydrogen peroxide (H_2O_2)	
	(2) Modified honey 1	*S. aureus*	The elevated quantity of hydrogen peroxide (H_2O_2) resulted in higher antibacterial activity.	[74]
	(3) Modified honey 2	*S. aureus*	The elevated quantity of hydrogen peroxide (H_2O_2) resulted in higher antibacterial activity.	
Carotenoid	Astaxanthin	*S. aureus* *E. coli* *P. aeruginosa*	ROS accumulation of superoxide anion ($O_2^{\bullet-}$) and hydroxyl radical ($^{\bullet}OH$) causes a reduction in cellular glutathione level and increases the rate of bacterial death.	[75]
Antimicrobial peptide	(1) Mo-CBP3-PepI, II and III	Bacteria (*K. pneumoniae, B. subtilis, S. aureus, and E. coli*) and fungi (*C. tropicalis and C. albicans*)	Elevated accumulation of ROS (H_2O_2, $O_2^{\bullet-}$, $^{\bullet}OH$) causes loss of cell membrane integrity and ultimate cell death.	[76]
Siderophore	pyochelin	*E. faecalis* *S. aureus*	Elevated ROS production ($O_2^{\bullet-}$, H_2O_2, $^{\bullet}OH$) causes lipid peroxidation and cell death.	[77]
			Synthetic agents	
Organic cationic salts	Bis-quaternary ammonium salt	*S. aureus* *E. coli*	Induced ROS ($O_2^{\bullet-}$, H_2O_2, $^{\bullet}OH$) cause cytoplasm content leakage and cell membrane damage.	[80]
Synthetic organic cationic complexes	Derivatives of cationic heteroleptic (III) complexes with tris-diimine ligands moiety. (i) phenanthroline (ii) 3,8-diphenylphenanthroline (iii) 3,8dipyrenylphenanthroline (iv) 3-phenylphenanthroline (v) 3-pyrenylphenanthroline (vi) 3,8diphenylethynylphenanthroline	*S. aureus* *S. mutans*	Photoactivation of singlet oxygen ($^1O_2$) against pathogenic bacterial cells	[78]

Amphiphilic copolymer	T-TCP micelles (comprising of propylene sulfide and toluidine blue O (TBO) grafted chitosan)	*S. aureus* *L. monocytogenes*	Potent antibacterial activity due to ROS (H_2O_2, $O_2^{\bullet-}$, $^{\bullet}OH$) produced by TBO activation	[79]
Organotin complexes	Organotin complexes (1) HL1 (2) HL2	*E. coli* *B. subtilis*	An increase in the amount of accumulated ROS (H_2O_2, $O_2^{\bullet-}$, $^{\bullet}OH$) caused membrane damage and leakage of cytoplasm content in the organism.	[81]
Modified chitosan	Catechol-modified chitosan with melanin capsule	Methicillin-resistant *S. aureus* (MRSA) *S. aureus* *E. coli*	Electron transfer catalyzed by Catechol-modified film from ascorbate to molecular oxygen instigated continued ROS generation (H_2O_2, $O_2^{\bullet}$) and triggered improved antibacterial activities in vitro and in vivo.	[82]

2.3. Safety Concerns Associated with ROS as a Contributory Antimicrobial Agent

The concept of ROS-mediated microbial killing has long been exploited in disinfectants and antiseptics but has only recently been identified in therapeutic applications, hence the safety and toxicity concern related to its usage is of great relevance. Studies on ROS-induced antibacterial agents have demonstrated an increase in potency at higher concentrations of ROS [39,74,83]. However, the potential risk of toxicity to host cells and tissues at such a high concentration is anticipated and hence should be prudently considered. ROS have been linked to mutagenesis. A study by Kohanski et al. [50] directly linked ROS with mutagenesis at sub-lethal levels, and through the blockage of ROS generation, mutagenesis was avoided. Furthermore, no protein-based mechanism can detoxify the hydroxyl radical (•OH), which can cause oxidative damage to several cells and tissues of the body made up of lipids, proteins, DNA, and carbohydrates [8,84]. The skin, which is made up of polyunsaturated fatty acids, is one of the most susceptible targets of ROS, where it can initiate lipid peroxidation [15]. For instance, cellular ROS generation has been shown to correlate with cytotoxicity in HFF-1 (human skin cells) [82] and HaCaT (human keratinocyte cells) [42,85]. Further, following treatment with particulate matter, findings show stress to the endoplasmic reticulum, mitochondrial damage, autophagy, and apoptosis in human keratinocytes, and mice with hairless skin tissues were reported to be due to ROS production [86]. Furthermore, in human keratinocytes and mouse skin, Jin et al. [87] noticed that particulate matter produced inflammation via ROS-mediated activation of inflammatory cytokines IL-8 and matrix metalloproteinase1 (MMP-1). However, using ROS with a lower redox potential (such as H_2O_2), as previously used in Surgihoney by Healing Honey International, could be the way to go for the treatment of infections topically [74]. Relative to hydroxyl radicals (•OH), hydrogen peroxide is less reactive and can be more easily scavenged by competent cells in the body.

Interestingly, studies showing non-toxicity issues due to treatment with ROS on human tissues and cells have also been reported over the years. Hu et al. [81] reported on two derivatives (HL1 and HL2) from HL (Figure 8) and demonstrated the ability of HL1 (the most effective among the derivatives) against HELF (human lung fibroblast). Findings from the study showed negligible cytotoxic effects even when the concentration was raised to 10 μg/mL (5 × MIC) over a 24 h period. Similarly, Song et al. [80] worked on the antibacterial activity of SBQA (synthesized bis-quaternary ammonium), a high-molecular weight, long-chain organic compound, and noticed no signs of cytotoxicity on the growth of mouse breast cancer cells (4T1) at concentrations lesser than 50 μg/mL. Using the *Mo*-CBP_3 (MC) amino acid sequence isolated from the seeds of *Moringa oleifera* as the starting peptide, Oliveira et al. [76] designed three peptides (*M*C-PepI, *M*C-PepII, and *M*C-PepIII) and evaluated their toxicity against human red blood cells. Findings from the study showed no sign of hemolysis, and when PepIII (the most potent peptide) was demonstrated against Vero cells even at a higher concentration of 57 × MIC of *S. aureus* and 64 x MIC of *Candida* spp., no sign of cytotoxicity issues was observed.

Hence, in the use of ROS as an effective therapeutic strategy in humans for the treatment of microbial infections, considerable effort must be put into the appropriate quantification of ROS generated by antimicrobials and the determination of the minimum concentration that can elicit toxicity in host cells and tissues. However, the determination of such concentrations might be problematic, as the ROS-scavenging capability of patients differs and is controlled by factors relating to age, pregnancy, immune system, and underlying ailments such as diabetes.

3. Conclusions and Perspectives

The use of ROS-inducing antimicrobial agents to treat pathogenic infections is a promising and emerging field that provides an alternative viable strategy for antibacterial medication development and enhancement. This approach will not only broaden the

scope of the antibiotic arsenal but also help fight against the menace of antibiotic resistance that has become a major public health concern. For the successful use of this approach, some of the limitations, such as toxicity issues associated with ROS (most especially the hydroxyl radical) and the quantification of ROS for the appropriate determination of ROS generated by each agent, need to be swiftly addressed. ROS cannot discriminate between bacterial and mammalian cells and, like microorganisms, most human cells have limited defense against hydroxyl radicals. Hence, the mechanism through which ROS contribute to antimicrobial lethality, which is based on hydroxyl radical generation during oxidative stress that often causes damage to critical bacterial macromolecules (lipids, proteins, and DNA), and subsequent death may also cause damage to the host cell. In humans, oxidative stress is treated with antioxidants such as vitamin E, ascorbic acid, selenium, carotenoids, and lycopene, among others. However, clinical trials on the scavenging capability of hydroxyl radicals with such antioxidants have failed to produce the desired results over the years [88]. Hence, future research on more potent antioxidants against hydroxyl radicals will be a boost to the full implementation and usage of novel antibacterials employing the involvement of ROS against human pathogenic infections. However, recent findings on nanoenzymes, specifically silver-palladium bimetallic alloys, showed their ability to generate surface-bound ROS that selectively kills bacterial cells over mammalian cells [89]. Interestingly, the nanoenzyme was potent against antibiotic-resistant bacteria while also delaying the development of antibiotic resistance in bacteria. This, however, suggests another viable approach for the utilization of ROS for the treatment of infections.

The issue of resistance in bacteria due to the ability of ROS to cause mutagenesis is another limitation. However, since combination therapy of ROS-inducing novel antibacterials with conventional antibiotics (such as isoquercitrin in combination with AmB and FLC [90] and kanamycin in combination with alanine [91]) has been shown to show promise to achieve enhanced antibacterial efficacy, such resistance in bacteria could be managed. Similarly, more research on the capability of ROS-inducing agents to act simultaneously on more than one target in bacteria could also help in the management of resistance. Overall, ROS-inducing antimicrobial agents have demonstrated increased potency at higher ROS concentrations, but the potential toxicity risk to host cells and tissues is anticipated. Hence, the prudent use of this approach for treatment should be carefully considered to reduce cytotoxicity issues and other adverse effects in patients. In doing this and to reduce resistance in bacteria, combination therapy of conventional antibiotics and ROS-inducing agents could be employed. Furthermore, the use of less reactive ROS such as H_2O_2 (as previously employed in Sugihoney) could also be employed for the treatment of infections topically, as H_2O_2 can be more easily scavenged by competent cells in the body.

Author Contributions: Conceptualization, S.S..; methodology and collection of data, J.O.A.; writing—review and editing, J.O.A. and S.S.; supervision, S.S.; funding acquisition, S.S. All authors have read and agreed to the published version of the manuscript.

Funding: The authors specially acknowledge the financial assistance from the Directorate of Research and Postgraduate Support, Durban University of Technology, and the South African Medical Research Council (SA MRC) under a Self-Initiated Research Grant, as well as the National Research Foundation (NRF) Research Development Grant for rated researchers (grant number 120433) to S. Sabiu. The views and opinions expressed are those of the authors and do not necessarily represent the official views of the funders.

Data Availability Statement: The data are contained within the article.

Acknowledgments: The NRF- TWAS Doctoral Scholarship (grant number 129950) to J.O.A. is duly acknowledged.

Conflicts of Interest: The authors declare no conflicts of interest.

References

1. Larsson, G.D.G.J.; Flach, C.F. Antibiotic resistance in the environment. *Nat. Rev. Microbiol.* **2022**, *20*, 257–269.
2. Kohler, V.; Vaishampayan, A.; Grohmann, E. Problematic Groups of Multidrug-Resistant Bacteria and Their Resistance Mechanisms. In *Antibacterial Drug Discovery to Combat*; MDR; Ahmad, I., Ahmad, S., Rumbaugh, K., Eds.; Springer: Singapore, 2019.
3. Malik, B.; Bhattacharyya, S. Antibiotic drug-resistance as a complex system driven by socio-economic growth and antibiotic misuse. *Sci. Rep.* **2019**, *9*, 9788.
4. Nelson, R.E.; Slayton, R.B.; Stevens, V.W.; Jones, M.M.; Khader, K.; Rubin, M.A.; Jernigan, J.A.; Samore, M.H. Attributable mortality of healthcare-associated infections due to multidrug-resistant gram-negative bacteria and methicillin-resistant Staphylococcus aureus. *Infect. Control Hosp. Epidemiol.* **2017**, *38*, 848–856.
5. World Health Organization. Stop Using Antibiotics in Healthy Animals to Prevent 666 the Spread of Antibiotic Resistance. Available online: https://www.who.int/news-room/detail/07-11-2017-stop-using-antibiotics-in-healthy-animals-to-prevent-the-spread-of-antibiotic-resistance (accessed on 10 September 2019).
6. Rather, I.A.; Kim, B.C.; Bajpai, V.K.; Park, Y.H. Self-medication and antibiotic resistance: Crisis, current challenges, and prevention. *Saudi J. Biol. Sci.* **2017**, *24*, 808–812.
7. Ventola, C.L. The antibiotic resistance crisis: Part 1: Causes and threats. *Phys. Ther.* **2015**, *40*, 277–283.
8. Lam, P.L.; Wong, R.S.M.; Lam, K.H.; Hung, L.K.; Wong, M.; Yung, L.H.; Ho, Y.W.; Wong, W.Y.; Hau, D.K.P.; Gambari, R.; et al. The Role of Reactive Oxygen Species in the Biological 1 Activity of Antimicrobial Agents: An Updated Mini Review. *Chem.-Biol. Interact.* **2020**, *320*, 109023.
9. Mourenza, A.; Gil, J.A.; Mateos, L.M.; Letek, M. Oxidative stress-generating antimicrobials, a novel strategy to overcome antibacterial resistance. *Antioxidants* **2020**, *9*, 361.
10. Kim, S.Y.; Park, C.; Jang, H.J.; Kim, B.O.; Bae, H.W.; Chung, I.Y.; Kim, E.S.; Cho, Y.H. Antibacterial strategies inspired by the oxidative stress and response networks. *J. Microbiol.* **2019**, *57*, 203–212.
11. Dryden, M. Reactive oxygen species: A novel antimicrobial. *Int. J. Antimicrob. Agents* **2018**, *51*, 299–303.
12. Wang, X.; Zhao, X. Contribution of oxidative damage to antimicrobial lethality. *Antimicrob. Agents Chemother.* **2009**, *53*, 1395–1402.
13. Alvarado, A.; Arce, I. Antioxidants in respiratory diseases: Basic science research and therapeutic alternatives. *Clin. Res. Trials* **2016**, *3*, 1–11.
14. Fanjul-Moles, M.L.; López-Riquelme. M.L. Relationship between oxidative stress, circadian rhythms, and AMD. *Oxidative Med. Cell. Longev.* **2016**, *2016*, 7420637.
15. Vatansever, F.; De Melo, W.C.; Avci, P.; Vecchio, D.; Sadasivam, M.; Gupta, A.; Chandran, R.; Karimi, M.; Parizotto, N.A.; Yin, R. et al. Antimicrobial strategies centered around reactive oxygen species—Bactericidal antibiotics, photodynamic therapy, and beyond. *FEMS Microbiol. Rev.* **2013**, *37*, 955–989.
16. Vaishampayan, A.; Grohmann, E. Antimicrobials Functioning through ROS-Mediated Mechanisms: Current Insights. *microrganisms* **2022**, *10*, 61.
17. Dwyer, D.J.; Belenky, P.A.; Yang, J.H.; MacDonald, I.C.; Martell, J.D.; Takahashi, N.; Chan, C.T.Y.; Michael, A.L.; Braff, D.; Schwarz, E.G.; et al. Antibiotics induce redox-related physiological alterations as part of their lethality. *Proc. Natl. Acad. Sci. USA* **2014**, *5*, 100–109.
18. Dwyer, D.J.; Kohanski, M.A.; Hayete, B.; Collins, J.J. Gyrase inhibitors induce an oxidative damage cellular death pathway in *Escherichia coli*. *Mol. Syst. Biol.* **2007**, *3*, 91.
19. Kohanski, M.A.; Dwyer, D.J.; Hayete, B.; Lawrence, C.A.; Collins, J.J. A common mechanism of cellular death induced by bactericidal antibiotics. *Cell* **2007**, *130*, 797–810.
20. Imlay, J.A. Diagnosing oxidative stress in bacteria: Not as easy as you might think. *Curr. Opin. Microbiol.* **2015**, *24*, 124–131.
21. Keren, I.; Wu, Y.; Inocencio, J.; Mulchay, L.R.; Lewis, K. Killing by bactericidal antibiotics does not depend on reactive oxygen species. *Science* **2014**, *339*, 1213–1216.
22. Liu, Y.; Imlay, J.A. Cell death from antibiotics without the involvement of reactive oxygen species. *Science* **2013**, *339*, 1210–1213.
23. Moher, D.; Liberati, A.; Tetzlaff, J.; Altman, D.G. Preferred reporting items for systematic reviews and meta-analyses: The PRISMA statement. *PLoS Med.* **2009**, *6*, e1000097.
24. Lobritz, M.A.; Belenky, P.; Porter, C.B.; Gutierrez, A.; Yang, J.H.; Schwarz, E.G.; Dwyer, D.J.; Khalil, A.S.; Collins, J.J. Antibiotic efficacy is linked to bacterial cellular respiration. *Proc. Natl. Acad. Sci. USA* **2017**, *112*, 8173–8180.
25. Finnegan, M.; Linley, E.; Denyer, S.P.; McDonnell, G.; Simons, C.; Maillard, J.Y. Mode of action of hydrogen peroxide and other oxidizing agents: Differences between liquid and gas forms. *J. Antimicrob. Chemother.* **2010**, *65*, 2108–2115.
26. Forman, H.J.; Torres, M. Signaling by the respiratory burst in macrophages. *IUBMB Life* **2001**, *51*, 365–371.
27. Van Acker, H.; Coenye, T. The role of reactive oxygen species in the antibiotic-mediated killing of bacteria. *Trends Microbiol.* **2017**, *25*, 456–466.
28. Stokes, J.M.; Lopatkin, A.J.; Lobritz, M.A.; Collins, J.J. Bacterial Metabolism and Antibiotic Efficacy. *Cell Metab.* **2019**, *30*, 251–259.
29. Winterbourn, C.C.; Kettle, A.J.; Hampton, M.B. Reactive oxygen species and neutrophil function. *Annu. Rev. Biochem.* **2016**, *85*, 765–792.
30. Mortaz, E.; Alipoor, S.D.; Adcock, I.M.; Mumby, S.; Koenderman, L. Update on neutrophil function in severe inflammation. *Front. Immunol.* **2018**, *9*, 2171.

31. Müller, A.; Langklotz, S.; Lupilova, N.; Kuhlmann, K.; Bandow, J.E.; Leichert, L.I.O. Activation of RidA chaperone function by N-chlorination. *Nat. Commun.* **2014**, *5*, 5804.
32. Chen, P.R.; Brugarolas, P.; He, C. Redox signaling in human pathogens. *Antioxid. Redox Signal.* **2011**, *14*, 1107–1118.
33. Glaeser, J.; Nuss, A.M.; Berghoff, B.A.; Klug, G. Singlet oxygen stress in microorganisms. *Adv. Microb. Physiol.* **2011**, *58*, 141–173.
34. Altman, N. *The Oxygen Prescription: The Miracle of Oxidative Therapies*; Healing Arts Press: Rochester, VT, USA, 2007.
35. Droge, W. Free radicals in the physiological control of cell function. *Physiol. Rev.* **2002**, *82*, 47–95.
36. Buettner, G.R. The pecking order of free radicals and antioxidants: Lipid peroxidation, alpha-tocopherol, and ascorbate. *Arch. Biochem. Biophys.* **1993**, *300*, 535–543.
37. Authen, R.L.; Davis, J.M. Oxygen toxicity and reactive oxygen species: The devil is in the Details. *Pediatr. Res.* **2009**, *66*, 121–127.
38. Kim, S.Y.; Kim, E.J.; Park, J.W. Control of singlet oxygen-induced oxidative damage in *Escherichia coli*. *J. Biochem. Mol. Biol.* **2002**, *35*, 353–357.
39. Drlica, K.; Zhao, X. Bacterial death from treatment with fluoroquinolones and other lethal stressors. *Expert Rev. Anti-Infect. Ther.* **2021**, *19*, 601–618.
40. Memar, M.Y.; Ghotaslou, R.; Samiei, M.; Adibkia, K. Antimicrobial use of reactive oxygen therapy: Current insights. *Infect. Drug Resist.* **2018**, *11*, 567–576.
41. Szczepaniak, P.; Laskowska, E. Antibiotics promoting oxidative stress inhibit formation of Escherichia coli biofilm via indole signaling. *Res. Microbiol.* **2010**, *161*, 847–853.
42. Li, H.; Zhao, X.; Huang, Y.; Liao, B.; Cheng, L.; Ren, B, Reactive Oxygen Species in Pathogen Clearance: The Killing Mechanisms, the Adaption Response, and the Side Effects. *Front. Microbiol.* **2021**, *11*, 3610.
43. Akhova, A.V., Tkachenko, A.G. Role of Secondary Oxidative Stress in the Bactericidal Action of Antibiotics. Moscow Univ. Biol.Sci. Bull. 2020, 75, 218–223.
44. Yoon, S.J.; Park, J.E.; Yang, J.H.; Park, J.W. OxyR regulon controls lipid peroxidation-mediated oxidative stress in *Escherichia coli*. *J. Biochem. Mol. Biol.* **2002**, *35*, 297–301.
45. Yang, L.; Mih, N.; Anand, A.; Park, J.-O.; Tan, J.; Yurkovich, I.T.; Monk, J.M.; Lloyd, C.T.; Sandberg, T.E.; Seo, S.W.; et al. Cellular responses to reactive oxygen species are predicted from molecular mechanisms. *Proc. Natl. Acad. Sci. USA* **2019**, *116*, 14368–14373.
46. Hong, Y.; Zeng, J.; Wang, X.; Drlica, K.; Zhao, X. Post-stress bacterial cell death mediated by reactive oxygen species. *Proc. Natl. Acad. Sci. USA* **2019**, *116*, 10064–10071.
47. Paulander, W.; Wang, Y.; Folkesson, A.; Charbon, G.; Løbner-Olesen, A.; Ingmer, H. Bactericidal antibiotics increase hydroxyphenyl fluorescein signal by altering cell morphology. *PLoS ONE* **2014**, *9*, e92231.
48. Yeom, J.; Imlay, J.A.; Park, W. Iron homeostasis affects antibiotic-mediated cell death in *Pseudomonas* species. *J. Biol. Chem.* **2010**, *285*, 22689–22695.
49. Arriaga-Alba, M.; Rivera-Sánchez, R.; Parra-Cervantes, G.; Barro-Moreno, F.; Flores-Paz, R.; García-Jeménez, E. Antimutagenesis of beta-carotene to mutations induced by quinolone on *Salmonella typhimurium*. *Arch. Med. Res.* **2000**, *31*, 156–161.
50. Kohanski, M.A.; Dwyer, D.J.; Wierzbowski, J.; Cottarel, G.; Collins, J.J. Mistranslation of membrane proteins and two-component system activation trigger antibiotic-mediated cell death. *Cell* **2008**, *135*, 679–690.
51. Kolodkin-Gal, I.; Sat, B.; Keshet, A.; Engelberg-Kulka, H. The communication factor EDF and the toxin-antitoxin module mazEF determine the mode of action of antibiotics. *PLoS Biol.* **2008**, *6*, e319.
52. Couturier, M.; Bahassi, M.; Van Melderen, L. Bacterial death by DNA gyrase poisoning. *Trends Microbiol.* **1998**, *6*, 269–275.
53. Foti, J.J.; Devadoss, B.; Winkler, J.A.; Collins, J.J.; Walker, G.C. Oxidation of the guanine nucleotide pool underlies cell death by bactericidal antibiotics. *Science* **2012**, *336*, 315–319.
54. Dorsey-Oresto, A.; Lu, T.; Mosel, M.; Wang, X.; Salz, T.; Drlica, K.; Zhao, X. YihE kinase is a central regulator of programmed cell death in bacteria. *Cell Rep.* **2013**, *3*, 528–537.
55. Ezraty, B.; Vergnes, A.; Banzhaf, M.; Duverger, Y.; Huguenot, A.; Brochado, A.R.; Su, S.-Y.; Espinosa, L.; Loiseau, L.; Py, B. et al. Fe-S cluster biosynthesis controls uptake of aminoglycosides in a ROS-less death pathway. *Science* **2013**, *340*, 1583–1587.
56. Barber, A.E.; Norton, J.P.; Spivak, A.M.; Mulvey, M.A. Urinary tract infections: Current and emerging management strategies. *Clin. Infect. Dis.* **2013**, *57*, 719–724.
57. Chua, N.G.; Zhou, Y.P.; Tan, T.T.; Lingegowda, P.B.; Lee, W.; Lim, T.P.; Teo, J.; Cai, Y.; Kwa, A.L. Polymyxin B with dual carbapenem combination therapy against carbapnemase-producing *Klebsiella pneumonia*. *J. Infect.* **2015**, *70*, 309–311.
58. Sampson, T.R.; Liu, X.; Schroeder, M.R.; Kraft, C.S.; Burd, E.M.; Weiss, D.S. Rapid killing of Acinetobacter baumannii by polymyxins is mediated by a hydroxyl radical death pathway. *Antimicrob. Agents Chemother.* **2012**, *56*, 5642–5649.
59. Walling, C. The Nature of the Primary Oxidants in Oxidations Mediated by Metal Ions. In *Oxidases and Related Redox Systems: Proceedings of the Third International Symposium*; King, T.E., Mason, H.S., Morrison, M., Eds.; Pergamon Press: New York, NY, USA, 1982; pp. 85–97.
60. Belenky, P.; Ye, J.D.; Porter, C.B.; Cohen, N.R.; Lobritz, M.A.; Ferrante, T.; Jain, S.; Korry, B.J.; Schwarz, E.G.; Walker, G.C.; et al. Bactericidal Antibiotics Induce Toxic Metabolic Perturbations that Lead to Cellular Damage. *Cell Rep.* **2015**, *13*, 968–980.
61. Luan, G.; Hong, Y.; Drlica, K.; Zhao, X. Suppression of Reactive Oxygen Species Accumulation Accounts for Paradoxical Bacterial Survival at High Quinolone Concentration. *Antimicrob. Agents Chemother.* **2018**, *62*, e01622-17.
62. Malik, M.; Hussain, S.; Drlica, K. Effect of anaerobic growth on quinolone lethality with *Escherichia coli*. *Antimicrob. Agents Chemother.* **2007**, *51*, 28–34.

63. Malik, M.; Hoatam, G.; Chavda, K.; Kerns, R.J.; Drlica, K. Novel approach for comparing abilities of quinolones to restrict the emergence of resistant mutants during quinolone exposure. *Antimicrob. Agents Chemother.* **2010**, *54*, 149–156.
64. Hong, Y.; Li, L.; Luan, G.; Drlica, K.; Zhao, X.; Contribution of reactive oxygen species to thymineless death in *Escherichia coli*. *Nat. Microbiol.* **2017**, *2*, 1667–1675.
65. Eghbaliferiz, S.; Iranshahi, M. Prooxidant activity of polyphenols, flavonoids, anthocyanins and carotenoids: Updated review of mechanisms and catalyzing metals. *Pharmacol. Res.* **2016**, *30*, 1379–1391.
66. Ajiboye, T.O.; Habibu, R.S.; Saidu, K.; Haliru, F.Z.; Ajiboye, H.O.; Aliyu, N.O.; Ibitoye, O.B.; Uwazie, J.N.; Muritala, H.F.; Bello, S.A.; et al. Involvement of oxidative stress in protocatechuic acid-mediated bacterial lethality. *Microbiologyopen* **2017**, *6*, e00472.
67. Singh, D.; Narayanamoorthy, S.; Gamre, S.; Majumdar, A.G.; Goswami, M.; Gami, U.; Cherian, S.; Subramanian, M. Hydroxychavicol, a key ingredient of *Piper betle* induces bacterial cell death by DNA damage and inhibition of cell division. *Free. Radic. Biol. Med.* **2018**, *120*, 62–71.
68. Singh, D.; Majumdar, A.G.; Gamre, S. Mahesh Subramanian Membrane damage precedes DNA damage in hydroxychavicol treated *E. coli* cells and facilitates cooperativity with hydrophobic antibiotics. *Biochimie* **2021**, *180*, 158–168.
69. Sinsinwar, S.; Vadivel, V. Catechin isolated from cashew nut shell exhibits antibacterial activity against clinical isolates of MRSA through ROS-mediated oxidative stress. *Appl. Microbiol. Biotechnol.* **2020**, *104*, 8279–8297.
70. Ajiboye, T.O.; Skiebe, E.; Wilharm, G. Phenolic acids potentiate colistin-mediated killing of *Acinetobacter baumannii* by inducing redox imbalance. *Biomed. Pharmacother.* **2018**, *101*, 737–744.
71. Xiong, L.G.; Chen, Y.J.; Tong, J.W.; Huang, J.A.; Li, J.; Gong, Y.S.; Liu, Z.H. Tea polyphenol epigallocatechin gallate inhibits *Escherichia coli* by increasing endogenous oxidative stress. *Food Chem.* **2017**, *217*, 196–204.
72. Hussain, R.M.; Abdullah, N.F.; Amom, Z. Killing of *Staphylococcus aureus* by allylpyrocatechol is potentiated by induction of intracellular oxidative stress and inhibition of catalase activity. *J. Integr. Med.* **2016**, *14*, 456–464.
73. Volk, A.P.D.; Moreland, J.G. ROS-Containing Endosomal Compartments: Implications for Signaling. *Methods Enzymol.* **2014**, *535*, 201–224.
74. Cooke, J.; Dryden, M.; Patton, T.; Brennan, J.; Barrett, J. The antimicrobial activity of prototype modified honeys that generate reactive oxygen species (ROS) hydrogen peroxide. *BMC Res. Notes* **2015**, *8*, 20.
75. Aribisala, J.O.; Nkosi, S.; Idowu, K.; Nurain, I.O.; Makolomakwa, G.M.; Shode, F.O.; Sabiu, S. Astaxanthin-Mediated Bacterial Lethality: Evidence from Oxidative Stress Contribution and Molecular Dynamics Simulation. *Oxidative Med. Cell. Longev.* **2021**, *2021*, 7159652.
76. Oliveira, J.T.A.; Souza, P.F.N.; IVasconcelos, M.; Dias, L.P.; Martins, T.F.; Van Tilburg, M.F.; Guedes, M.I.F.; Sousa, D.O.B. Mo-CBP3-PepI, Mo-CBP3-PepII, and Mo-CBP3-PepIII are synthetic antimicrobial peptides active against human pathogens by stimulating ROS generation and increasing plasma membrane permeability. *Biochimie* **2019**, *157*, 10–21.
77. Ong, K.S.; Cheow, Y.L.; Lee, S.M. The role of reactive oxygen species in the antimicrobial activity of pyochelin. *J. Adv. Res.* **2017**, *8*, 393–398.
78. Wang, L.; Monro, S.; Cui, P.; Yin, H.; Liu, B.; Cameron, C.G.; Xu, W.; Hetu, M.; Fuller, A.; Kilina, S.V.; et al. Heteroleptic Ir(III)N6 complexes with long-lived triplet excited states and in vitro photobiological activities. *ACS Appl. Mater. Interfaces* **2019**, *11*, 3629–3644.
79. Wang, Z.; Bai, H.; Lu, C.; Hou, C.; Qiu, Y.; Zhang, P.; Duan, J.; Mu, H. Light controllable chitosan micelles with ROS generation and essential oil release for the treatment of bacterial biofilm. *Carbohydr. Polym.* **2019**, *205*, 533–539.
80. Song, H.; Wang, Y.; Wu, J.; Gu, S.; Li, H. Fabrication of Bis-Quaternary Ammonium Salt as an Efficient Bactericidal Weapon Against *Escherichia coli* and *Staphylococcus aureus*. *ACS Omega* **2018**, *3*, 14517–14525.
81. Hu, L.; Wang, H.; Xia, T.; Fang, B.; Shen, Y.; Zhang, Q.; Tian, X.; Zhou, H.; Wu, J.; Tian, Y. Two-Photon-Active Organotin(IV) Complexes for Antibacterial Function and Superresolution Bacteria Imaging. *Inorg. Chem.* **2018**, *57*, 6340–6348.
82. Liu, H.; Qu, X.; Kim, E.; Lei, M.; Dai, K.; Tan, X.; Xu, M.; Li, J.; Liu, Y.; Shi, X.; et al. Bio inspired redox-cycling antimicrobial film for sustained generation of reactive oxygen species. *Biomaterials* **2018**, *162*, 109–122.
83. Lee, W.; Woo, E.R.; Lee, D.G. Effect of apigenin isolated from *Aster yomena* against *Candida albicans*: Apigenin-triggered apoptotic pathway regulated by mitochondrial calcium signaling. *J. Ethnopharmacol.* **2019**, *231*, 19–28.
84. Abadi, P.G.; Shirazi, F.H.; Joshaghani, M.; Moghimi, H.R. Influence of formulation of ZnO nanoblokes containing metallic ions dopants on their cytotoxicity and protective factors: An in vitro study on human skin cells exposed to UVA radiation. *Toxicol. Rep.* **2018**, *5*, 468–479.
85. Ali, D.; Tripathi, A.; Al Ali, H.; Shahi, Y.; Mishra, K.K.; Alarifi, S.; Alkahtane, A.A.; Manohardas, S. ROS dependent Bax/Bcl2 and caspase 3 pathway-mediated apoptosis induced by zineb in human keratinocyte cells. *OncoTargets Ther.* **2018**, *11*, 489–497.
86. Piao, M.J.; Ahn, M.J.; Kang, K.A.; Ryu, Y.S.; Hyun, Y.J.; Shilnikova, K.; Zhen, A.X.; Jeong, J.W.; Choi, Y.H.; Kang, H.K.; et al. Particulate matter 2.5 damages skin cells by inducing oxidative stress, subcellular organelle dysfunction, and apoptosis. *Arch. Toxicol.* **2018**, *92*, 2077–2091.
87. Jin, S.P.; Li, Z.; Choi, E.K.; Lee, S.; Kim, Y.K.; Seo, E.Y.; Chung, J.H.; Cho, S.Urban particulate 859 matter in air pollution penetrates the barrier-disrupted skin and produces ROS-dependent cutaneous inflammatory response in vivo. *J. Dermatol. Sci.* **2018**, *91*, 175–183.
88. Lipinski, B. Hydroxyl radical and its scavengers in health and disease. *Oxidative Med. Cell. Longev.* **2011**, *2011*, 809696.
89. Gao, F.; Shao, T.; Yu, Y.; Xiong, Y.; Yang, L. Surface-bound reactive oxygen species generating nanozymes for selective antibacterial action. *Nat. Commun.* **2021**, *12*, 745.

90. Kim, S.; Woo, E.R.; Lee, D.G. Synergistic Antifungal Activity of Isoquercitrin: Apoptosis and Membrane Permeabilization Related to Reactive Oxygen Species in *Candida albicans*. *IUBMB Life* **2019**, *71*, 283–292.
91. Ye, J.Z.; Su, Y.B.; Lin, X.M.; Lai, S.S.; Li, W.X.; Ali, F.; Zheng, J.; Peng, B. Alanine Enhances Aminoglycosides- Induced ROS Production as Revealed by Proteomic Analysis. *Front. Microbiol.* **2018**, *9*, 29.

View publication stats

References for section 2.1

Ajiboye, T.O., Habibu, R.S., Saidu, K., Haliru, F.Z., Ajiboye, H.O., Aliyu, N.O., *et al*. Involvement of oxidative stress in protocatechuic acid-mediated bacterial lethality. *Microbiol open*, 2017, 6, e00472.

Ajiboye, T.O., Skiebe, E., Wilharm, G. Phenolic acids potentiate colistin-mediated killing of *Acinetobacter baumannii* by inducing redox imbalance. *Biomed Pharmacother*. 2018, 101, 737 – 744.

Aldulaimi, O.A. General overview of phenolics from plant to laboratory, good antibacterials or not. *Pharmacogn.* 2017, 11, 123 – 127.

Alhadrami, H. A., Hamed, A. A. , Hassan, H. M., Belbahri, L., Rateb, M. R., Sayed. A. M. Flavonoids as potential anti-MRSA agents through modulation of PBP2a: A computational and experimental study. *Antibiotics.* 2020, 9, 562

Al-Orphaly, M., Hadi, H. A., Eltayeb, F. K., Al-Hail, H., Samuel, B. G., Sultan, A. A., Skariah, S. Epidemiology of multidrug-resistant *Pseudomonas aeruginosa* in the middle east and north Africa region. *Msphere.* 2021, 6, 202 - 221.

Araya-Cloutier, C., Vuncken, J.P., Ederen, R., den Besten, H.M.W., Gruppen H. Rapid membrane permeabilization of *Listeria monocytogenes* and *Escherichia coli* induced by antibacterial prenylated phenolic compounds from legumes. *Food Chem*. 2018, 240, 147 - 155.

Bouarab-Chibane, L., Degraeve, P., Ferhout, H., Bouajila, J., Oulahal, N. Plant antimicrobial polyphenols as potential natural food preservatives. *J Sci Food Agric.* 2019, 2019, 99, 1457 - 1474

Dwyer, D.J., Belenky, P.A., Yang, J.H.,, MacDonald, I. C. Martell, J.D., Takahashi, N. Chan, C.T.Y., Michael, A. Lobritz. *et al*. Antibiotics induce redox-related physiological alterations as part of their lethality. *PNAS*. 2014, 5, 100 - 109

Eghbaliferiz, S., Iranshahi, M. Prooxidant activity of polyphenols, flavonoids, anthocyanins and carotenoids: updated review of mechanisms and catalyzing metals. *Phytother Res*. 2016, 30, 1379 - 1391.

Eiamphungporn, W., Schaduangrat, N., Malik, A. A., Nantasenamat, C. Tackling the antibiotic resistance caused by class A β-lactamases through the use of β-lactamase inhibitory protein. *Int J Mol Sci.* 2018, 19, 2222.

Galati, G., Sabzevari, O., Wilson, J.X., O'Brien, P.J. Prooxidant activity and cellular effects of the phenoxyl radicals of dietary flavonoids and other polyphenolics. *Toxicology*. 2002, 177, 91 – 104.

Gulumbe, B. H., Faggo, A. A. Epidemiology of multidrug-resistant organisms in Africa. *J. Infect Microb Antimicrob*. 2019, 8, 25

Klein, A.R., Sarri. E., Kelch, S.E. Basinska, J.J., Vaidya, S., Alristilde, L. Probing the fate of different structures of beta-lactam antibiotics: hydrolysis, mineral capture, and influence of organic matter. *ACS Earth Space Chem.* 2021, 5, 1511 - 1551

Palacios, A.R., Rossi, M.A., Mahler, G.S., Vila, A.J. Metallo-β-lactamase inhibitors inspired on snapshots from the catalytic mechanism. *Biomolecule.* 2020, 10, 854

Thakuria, B., Lahon, K. The beta-lactam antibiotics as an empirical therapy in a developing country: An update on their current status and recommendations to counter the resistance against them. *J Clin Diagn Res.* 2013, 6, 1207 - 1214

Wang, X., Zhao, X., Malik, M., Drlica, K. Contribution of reactive oxygen species to pathways of quinolone-mediated bacterial cell death. *J Antimicrob Chemother*. 2010, 65, 495 - 520.

WHO, World health statistics 2019: monitoring health for the SDGs, sustainable development goals World Health Organization; 2018(https://www.who.int/publications/i/item/9789241565707

CHAPTER THREE

3.0 Identification of lead phenolic compounds against PBPs druggable targets of common and clinically significant pathogenic bacteria using computational methods and determination of their pharmacokinetics and ADMET properties

3.1 Cheminformatics identification of phenolics as modulators of key penicillin−binding proteins of *Escherichia coli* towards interventive antibacterial therapy (***Published in Molecular Simulation***) …….**129**

3.2 Cheminformatics identification of phenolics as modulators of penicillin-binding protein-3 of *Pseudomonas aeruginosa* towards interventive antibacterial therapy (**Published in *Journal of Biomolecular Structure and Dynamics***) …….**.....147**

3.3 *In silico* exploration of phenolics as modulators of penicillin binding protein (PBP) 2x of *Streptococcus pneumoniae* (***Published in Scientific Reports***) ……**164**

3.4 Cheminformatics identification of phenolics as modulators of penicillin-binding protein 2a of *Staphylococcus aureus*: A structure–activity-relationship-based study (***Published in Pharmaceutics***) **186**

This chapter was published as four separate manuscripts in four different DHET/ISI accredited journals (Pharmaceutic, Journal of Biomolecular Structure and Dynamics, Molecular Simulation and Scientific Reports). Each of the publications focused on the identification of lead phenolics against each of the key penicillin-binding proteins of bacteria (*Escherichia coli, Pseudomonas aeruginosa, Streptococcus pneumoniae* and *Staphylococcus aureus*) investigated in this study

3.1 Cheminformatics identification of phenolics as modulators of key penicillin−binding proteins of *Escherichia coli* towards interventive antibacterial therapy

This section has been published in Molecular Simulation and is presented as it is in the article

MOLECULAR SIMULATION
https://doi.org/10.1080/08927022.2023.2228423

Taylor & Francis
Taylor & Francis Group

Check for updates

Cheminformatics identification of phenolics as modulators of key penicillin–binding proteins of *Escherichia coli* towards interventive antibacterial therapy

Jamiu Olaseni Aribisala[a], Kehinde Idowu[a], Talent Raymond Makhanya[b] and Saheed Sabiu[a]

[a]Department of Biotechnology and Food Science, Faculty of Applied Sciences, Durban University of Technology, Durban, South Africa; [b]Department of Chemistry, Faculty of Applied Sciences, Durban University of Technology, Durban, South Africa

ABSTRACT

Data implicating the mutation in penicillin-binding protein (PBP) 3 and occasionally PBP5 in the resistance of *Escherichia coli* to beta–lactams is intriguing. Thus, the identification of an improved class of inhibitors of PBP3 and PBP5 is imperative, and in this study, phenolics due to their promising antibacterial activities were screened using structure–based pharmacophore and molecular docking approaches against PBP3, and the ability of the lead phenolics to modulate PBP3 and PBP5 was studied using molecular dynamics simulation. The results demonstrated various inhibitory capacities of the lead phenolics, with lysidicichin (−41.66 kcal/mol) and silicristin (−31.11 kcal/mol) being the most potent against PBP3, while epicatechin 3-O-(3-O-methylgallate) (−38.97 kcal/mol) and epigallocatechin-4-benzyl thioether (−37.01 kcal/mol) had higher affinities towards PBP5. Overall, epicatechin gallate had the best broad-spectrum of activity, as the compound was able to bind favourably to both targets. Additionally, the thermodynamic information confirmed the stability of the lead phenolics with both targets. Conclusively, while these observations are suggestive of the modulatory role of the lead phenolics on the growth of *E. coli*, further *in vitro* and *in vivo* validation of the activity elicited by the phenolics in this study is imperative, and efforts are underway in this direction.

ARTICLE HISTORY
Received 20 March 2023
Accepted 16 June 2023

KEYWORDS
Resistance; penicillin –binding proteins; phenolics; molecular dynamics simulation; molecular docking

1. Introduction

Escherichia coli is a Gram-negative bacterium implicated in diseases that are becoming increasingly difficult to treat due to antibiotic resistance and therefore pose a major public health problem [1,2]. Pathogenic *E. coli* are the leading cause of cholecystitis, bacteremia, cholangitis, urinary tract infections, neonatal meningitis, and bacterial gastroenteritis in developing and developed countries, resulting in severe morbidity and mortality [1,3]. These infections have been widely reported in communities, hospitals, and long-term care facilities around the world, putting a significant strain on medical and economic resources [4,5]. The most commonly used antibiotics for *E. coli* infections are the beta–lactams, and recent evidence has shown reduced sensitivity or outright resistance to this class of antibiotics [amoxicillin (85%), cefuroxime (65%), and cefatriaxone (60%)] [1] due to drug overprescription/overuse. Consequently, resistance to beta-lactam antibiotics is a growing concern in the treatment of infections caused by *E. coli* and thus necessitates the need for development of new alternatives with unique modes of action.

The penicillin-binding proteins (PBPs) are the target site of beta-lactams in bacteria [6]. These essential proteins are involved in the construction of peptidoglycan, the main component of bacterial cell walls [7]. Penicillin-binding proteins catalyze the glycan strand (transglycosylation) and the cross-linking between glycan chains (transpeptidation), while beta-lactams mimic the d-Ala-d-Ala dipeptide in the peptidoglycan in the process of inactivating the enzyme, forming a very stable acyl-enzyme complex that inhibits the function of the protein [6,7]. Some PBP classes such as the low molecular weight (LMM) PBPs, lack transglycosylation activity, and as such are not critical for microorganism survival [8,9]. *Escherichia coli* possesses seven LMM-PBPs (PBP4, PBP5, PBP6, PBP6b, PBP7, PBP4b, and AmpH) and five high molecular mass (HMM) PBPs ((PBP1a, PBP1b, PBP1c, PBP2, and PBP3) [8,9]. Of the HMM-PBPs, PBP3 is the most selective for β–lactams, and the localisation at the cleavage site of some of the other HMM-PBPs, such as PBP1b, depends on the presence of PBP3 [10]. Therefore, studies have suggested that PBP3 acts in concert with other HMM–PBPs during cell wall biosynthesis and is therefore very crucial for cell division, growth, and resistance to β-lactams in *E. coli* [10]. Moreover, of the LMM-PBPs, PBP5, encoded by the *dacA* gene, is the most abundant and plays a prominent role in maintaining the diameter, contour, and morphology of *E. coli in vivo* [11]. Overexpression of PBP5 transforms rod–shaped *E. coli* into an osmotically stable spherical shape, while the loss of PBP5 promotes branching and topological distortions during growth [11,12]. Hence, PBP5 could also serve as a good therapeutic target for drug candidates with capabilities to modulate *E. coli* growth. Therefore, in this study, both PBP3 and PBP5 were exploited as therapeutic targets in identifying active inhibitors that could modulate the growth of *E. coli* in the treatment of infections caused by the organism.

There are accumulating data on the antibacterial effects of phenolics against both Gram-positive and Gram-negative

CONTACT Saheed Sabiu sabius@dut.ac.za
Supplemental data for this article can be accessed online at https://doi.org/10.1080/08927022.2023.2228423.
© 2023 Informa UK Limited, trading as Taylor & Francis Group

bacteria with their mechanism of action being implicated in membrane damage, inhibition of virulence factors such as enzymes, and suppression of bacterial biofilm formation [13,14]. The presence of hydroxyl groups in phenolics has been implicated to enhance strong protein binding while increasing affinity for cytoplasmic membranes, hence increasing antibacterial action [15]. In addition to the direct antibacterial effect, some natural phenolic compounds have synergistic effects when coupled with conventional chemotherapeutic agents, a strategy that has been potentiated for the therapeutic treatment of infections caused by drug −resistant bacteria [16,17]. Thus, as several phenolics have been isolated and reported in databases (e.g. ZINCPharmer) over the years [18], we used for the first time in this study, structure−activity relationship−based pharmacophore and molecular docking techniques to screen for phenolics with the ability to modulate PBP3 of *E. coli.* These approaches could serve as a less expensive method to rank and gain an understanding on phenolic interactions with PBP3. However, as molecular docking method lack the ability to refine and access the binding pose stability of a ligand at the active site of a protein [19], the most promising phenolics were further investigated for their thermodynamic compatibility with PBP3 and their ability to inhibit PBP5 using molecular mechanics/GB surface area approaches and a 120 ns molecular dynamic simulation. This was done to identify potentially active antibacterial candidates that could modulate the growth of *E. coli*.

2. Methodology

2.1 Acquisition, optimisation, and binding site identification of druggable targets

The X-ray crystal structures of PBP3 (PDB ID: 6I1I) [20] and PBP5 (PDB: 1Z6F) [21] of *E. coli* were obtained from the protein data bank (PDB) (https://www.rcsb.org). The structures were optimised for molecular docking by removing water molecules and nonstandard amino acids using the UCSF Chimera v1.15 software [22] as earlier reported [23]. The x-y-z coordinates and amino acid residues at the active of PBP3 [(centre (X: 24.14; Y: 12.99; Z: −14.20); size (X: 21.25; Y:23.39; Z: 19.96)] and PBP5 [(centre (X: 43.26; Y: 11.89; Z: 30.41); size (X: 22.19; Y: 22.48; Z: 21.42)] of *E. coli* were defined as previously reported [24] using Discovery Studio version 21.1.0 [25] and thereafter validated from literature [20,21].

2.2. Screening of phenolic compounds using pharmacophore–based and docking techniques and validation of the docking techniques

A preliminary computational screening was carried out using the ZINCPharmer database (http://zincpharmer.csb.pitt.edu), where a library of phenolics against PBP3 was compiled [26]. This approach is necessary as there are presently over 10,000 phenolic compounds available in the literature and manual identification and compiling will be ineffective and time-consuming [18]. Succinctly, the *E. coli* PBP3 3D structure and a consensus phenolic pharmacophore from PharmaGist (https://bioinfo3d.cs.tau.ac.il/PharmaGist/php.php) (made from 40 phenolics) were utilised for the screening. A total of 1649 phenolics (Figure S1) that interacted with the active site of PBP3 in *E. coli* were identified using features such as aromatic ring, hydrogen acceptors and donors, and hydrophobic interaction between the ligand and the receptor atoms (Table S1). Interestingly, all 40 known phenolics that were utilised for pharmacophore building were present in the 1649 library of generated phenolics which serve as a validation step for the pharmacophore search.

Using Python Prescription (PyRx) v 0.9.5 [27] the docking technique was utilised to filter down the built phenolics library at the active site of PBP3 (Figure 1). Prior to docking, the phenolics and reference beta−lactam antibiotic (amoxicillin, cefotaxime, aztreonam, and doripenem) were optimised by adding Gasteiger charges using the Open Babel programme present on PyRx [27]. The optimised protein (PBP3) and ligands (made up of the library of phenolics and reference beta−lactam antibiotics) were then docked using the AutoDock programme plug-in on PyRx [27,28]. By choosing amino acid residues in the PBP3 active site whose grid box coordinates match the established x-y-z coordinates, docking at the active site was executed. Following the sorting of the top 20 compounds with higher affinity and interactions with PBP3 relative to the reference beta-lactam antibiotics, the phenolics' fingerprinting similarities, pharmacokinetic friendliness, and synthetic feasibility evaluation were used to select the top five leads. Subsequently, the top five phenolics were docked at the active site of PBP5 (Figure 2), by separately obtaining the top five compounds from PubChem [29] optimised using the UCSF Chimera v 1.15 software [22], and then docked (grid box coordinate of the active site corresponding with established x-y-z coordinates) using the AutoDock tool available on PyRx. The top five phenolic docked complexes with PBP3 and PBP5 that had the highest energy−minimized conformation (highest binding interactions and affinity) were obtained in PDB format. Following the separation of the complexes, the protonation state of both the ligands and the protein were adjusted using the UCSF Chimera v 1.15 software for further thermodynamic evaluation.

However, confirmation of docking studies is frequently needed since molecular docking techniques frequently produce pseudo-positive binding conformation as the best energy-minimized posture. Measuring the Root Mean Square Deviation (RMSD) of the ligand from its reference location in the response complex after optimum superimposition is one of the most used methods for assessing the accuracy of a docking geometry [30]. The same binding orientation is suggested by a low RMSD value of <1 **Å** between the docked ligand and its reference location in the response complex, which provides validity for the docking method used [31]. Through the superimposition method, the experimental co −crystal structures of PBP3 (PDB ID: 6I1I) and PBP5 (PDB: 1Z6F) from *E. coli* were used in this investigation to validate the docking pose. The superimposition demonstrated that the top five phenolic compounds and cefotaxime achieved the same orientation as the native inhibitor of both targets with a low RMSD value of <1 **Å** (Figures 1 and 2), validating the docking techniques used in the study.

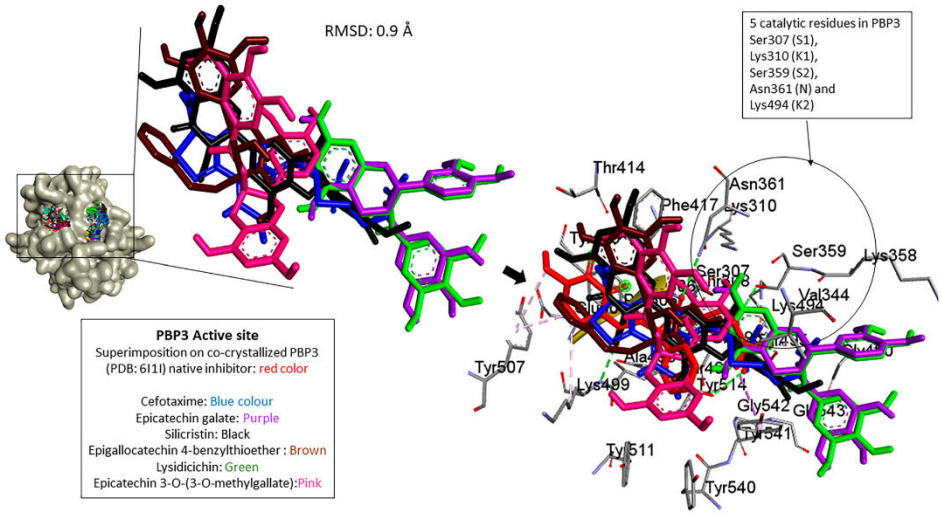


Figure 1. Validation of docking via the redocking approach against the co–crystal structure of PBP3 (6I1I) of *E. coli*. The superimpositions of the docked top–ranked phenolics had an RMSD value of 0.9 Å from the native inhibitor. The docked phenolics interacted with the five catalytic residues (Ser307, Lys310, Ser359, Asn361, and Lys494) of PBP3.

2.3. Top twenty phenolics pharmacokinetic properties prediction and molecular fingerprinting

The toolkits SwissADME web (http://swissadme.ch/index.php) and Molinspiration (https://www.molinspiration.com/cgi-bin/properties) were used for the robust prediction of the physicochemical properties, pharmacokinetics, drug similarity, and medicinal chemistry friendliness of the identified top 20 phenolics in this study. On the other hand, the toxicological profiles were assessed using the Protox II web server (https://tox–new.charite.de/protox_II/). Together with the binding affinity of the top 20 phenolic compounds, the pharmacokinetics and toxicity properties were used to narrow down to five compounds. Furthermore, Galaxy Europe (https://usegalaxy.eu./#) was used to create a molecular fingerprint of the top 20 compounds to establish that the top five phenolics are not conformers. In short, Galaxy Europe's molecular–to–fingerprint tool was used to convert the ligands smile format into Open Babel FP2 fingerprints. The Open Babel FP2 fingerprints were then clustered using the Taylor–Butina fingerprinting algorithms and NxN clustering with thresholds of 0.8 and 0.0, respectively [32].

2.4. Molecular dynamic (MD) simulation analysis of top five hit phenolics

The MD simulation was performed as previously described [28]. To summarise, the AMBER 18 package was utilised, and the simulation was run for 120 ns using the FF18SB variation of the AMBER force field to characterise the operating systems. Similarly, the ANTECHAMBER was employed to generate the atomic partial charges of the ligands by applying General Amber Force Field (GAFF) and Restrained Electrostatic Potential (RESP) techniques. The Leap module's hydrogen atoms, Na^+, and Cl^- counter ions were used to neutralise the systems. The amino acid residues in each case (PBP3: 1 – 430; PBP5: 1 – 325) were suitably numbered, and the systems were suspended inside an orthorhombic box of TIP3P water molecules in such a way that all atoms were within 8 Å of any box edge. For each simulation, an initial minimisation of 2000 steps was performed using a restriction potential of 500 kcal/mol. They were performed for 990 steps using the steepest descent technique, followed by 990 steps using conjugate degrees. The conjugate gradient approach was used to perform an additional 990 steps of full (unlimited) minimisation. Heating MD simulations from 0 K to 300 K (gradual) were run for 50 ps with the systems maintaining a constant number of atoms and volume. The solutes in the systems have a potential harmonic restraint of 10 kcal/mol and a collision frequency of 1.0 ps. Subsequently, each system was equilibrated for about 500 ps while the operating temperature was kept constant at 300 K. The SHAKE method was used to limit the hydrogen atom bonds in each simulated system. Each simulation had a step size of 2 fs, which corresponded to the isobaric–isothermal ensemble (NPT) with randomised seeding, a temperature of 300 K, a constant pressure of 1 bar, and a Langevin thermostat with a collision frequency of 1.0 ps and a pressure–coupling constant of 2 ps. Following that, the 120 ns MD simulation findings were reviewed and classified as post–dynamic data.

2.5. Post–dynamic analysis

The post-dynamic analysis was performed by saving the systems' coordinates and trajectories throughout the simulation period and then evaluating them post–simulation using the

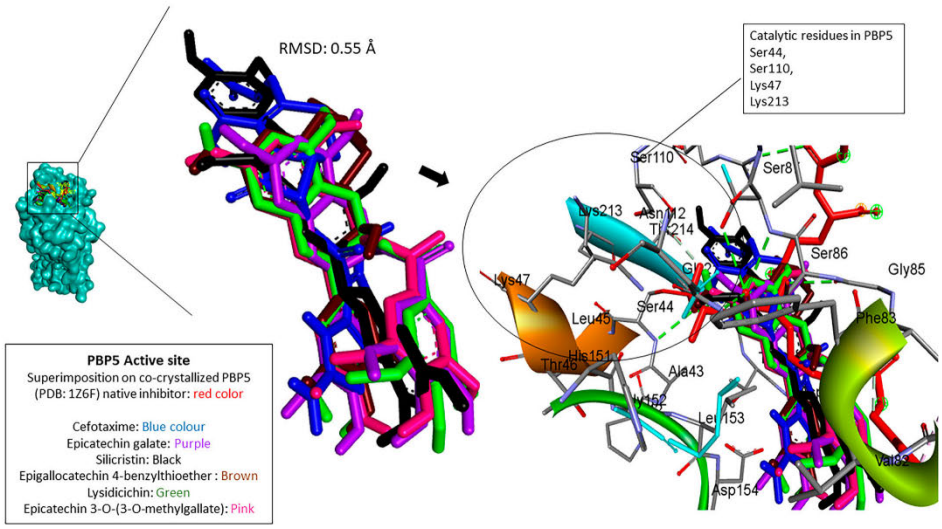


Figure 2. Superimposition of the top−ranked phenolics against the co−crystal structure of PBP5 (1Z6F) of *E. coli*. The superimpositions showed that the top−ranked phenolics had an RMSD value of 0.9 Å from the native inhibitor of PBP5. The docked phenolics interacted with the catalytic residues (Ser44, Ser110, Lys47, and Lys213) of PBP5.

PTRAJ module of the AMBER 18 package [33]. Exploiting the CPPTRAJ module of the same package, the analysis of root means square deviation (RMSD), root means square fluctuation (RMSF), the radius of gyration (ROG), and solvent−accessible surface area (SASA) were carried out and their plots were generated using Origin v 6.0 [33]. Likewise,

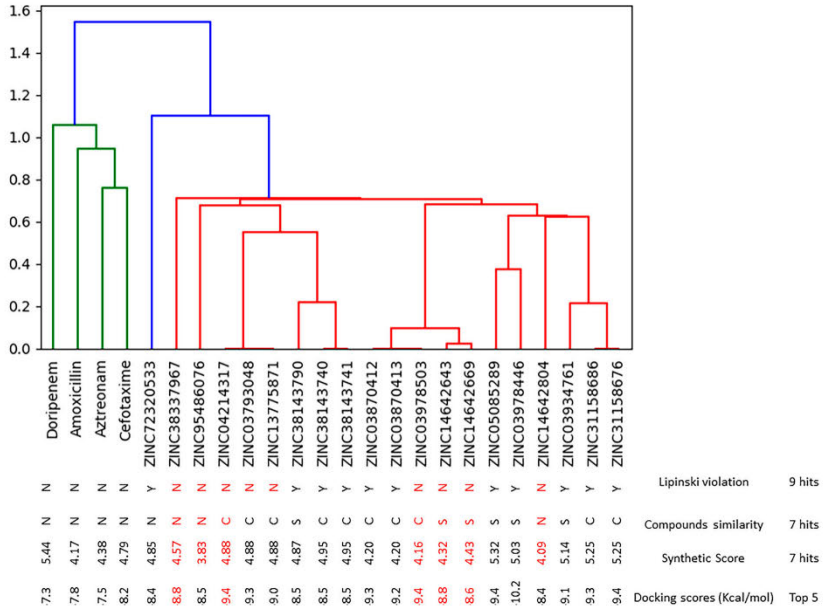


Figure 3. Screening of phenolics using cheminformatics and molecular docking score. More similarities existed between compounds with the same colour and cluster. The top 20 phenolics differ structurally from antibiotics (Green). Conformer (Phenolics that are member of the same cluster with similarity scores of zeros), that do not violate the Lipinski rule with the highest negative docking score was selected among the top five phenolics (red) (Figure 3). While avoiding top five phenolics that are conformers of one another, the resorcinol structure, is a common moiety similar to the top five phenolics.

using the Molecular Mechanics/GB Surface Area (MMGBSA) approach, the binding free energy was estimated using an average among 120,000 snapshots taken from a 120 ns MD simulation trajectory [34]. The equations below represent the method for the calculation of the free binding energy (ΔG) for each molecular species (complex, ligand, and receptor):

$$\Delta G_{bind} = G_{complex} - G_{receptor} - G_{ligand} \quad (1)$$

$$\Delta G_{bind} = E_{gas} + G_{sol} - TS \quad (2)$$

$$E_{gas} = E_{int} + E_{vdw} + E_{ele} \quad (3)$$

$$G_{sol} = G_{GB} + G_{SA} \quad (4)$$

$$G_{SA} = \gamma SASA \quad (5)$$

E_{gas} indicates the gas–phase energy, which consists of the internal energy E_{int}, Coulomb energy E_{ele} and the van der Waals energies E_{vdw}. The E_{gas} was directly estimated from the FF14SB force field terms. Solvation–free energy, G_{sol}, was calculated from the energy contribution from the polar states, G_{GB}, and non–polar states, G. The non–polar solvation energy, SA. The G_{SA} was defined from the solvent–accessible surface area (SASA), using a water probe radius of 1.4Å. In distinction, the polar solvation, G_{GB}, the contribution was calculated by solving the GB equation. S and T represent the total entropy of the solute and temperature, respectively.

The PBPs–ligand plots, which indicate molecular interactions between ligands and amino acid residues at the PBP3 and PBP5 active site, were identified from the final complexes obtained and visualised with Discovery Studio v21.1.0 [25]

3. Results and discussion

3.1 Pharmacophore and molecular docking screening of phenolics with affinity for PBP3 of E. coli.

The structure–based pharmacophore used in this study allows for hit searching using distinct features specific to phenolic and PBP3 of *E. coli* [26]. Using this method, all the currently known phenolics to date were screened down to 1649 that can interact with the active site of *E. coli* PBP3 (Figure S1). Following molecular docking, the top 20 phenolics were identified from the library of 1649 phenolics. Molecular docking is a structure–based virtual screening method that ranks ligands based on their orientations and affinity at the active site of a protein, and a higher negative value suggests better ligand affinity and interactions with a protein [35]. In this study, the top 20 phenolics had higher negative docking scores between −8.4 and −10.2 Kcal/mol than all the conventional beta–lactams [amoxicillin (−7.5 Kcal/mol), cefotaxime (−8.2 Kcal/mol), aztreonam (−7.5 Kcal/mol), and doripenem (−7.3 Kcal/mol)] with ZINC03978446 (Isotheaflavin) having the highest negative docking score (Figure 3). The higher negative docking score observed for the top 20 phenolics compared to the conventional beta–lactams suggests that the phenolics potentially have better affinities for the active site of PBP3, which also reflects the efficiency of the method used in the study. This observation is consistent with the study by Koes and Camacho [26] demonstrating the accuracy and effectiveness of structure–based pharmacophore in identifying hits to a target.

For a better chance of the lead phenolics passing the preclinical and clinical phases of drug development, several cheminformatic properties of the top 20 phenolics such as the pharmacokinetics, drug-likeness, synthetic feasibility, and compound similarities characteristic were evaluated in ranking the top five phenolics (Figure 3). Remarkably, all the top five phenolics [silicristin, epicatechin gallate, epigallocatechin 4 –benzylthioether, epicatechin 3-O-(3-O–methylgallate), and lysidicichin] passed the Lipinski's rule of five (Figure 3). According to Lipinski *et al.* [36], molecules with fewer than two violations of the rule of five, which restrict the molecular weight to 500 g/mol, the hydrogen acceptor to 10, the hydrogen bond donor to 5, and the octanol coefficient to 5, would be orally accessible. The top five compounds fulfilling these criteria demonstrates their capacity to be orally bioavailable, suggesting their potential to reach target cells/tissues/organs and exhibit their pharmacological impact. The top–ranked compounds were water–soluble, with bioavailability scores higher than cefotaxime at 0.55 each. Similar to cefotaxime, the top–ranked phenolics showed minimal gastrointestinal tract absorption characteristics (Table 1). All these observations suggest that the top five phenolics are potential drug candidates for therapeutic purposes. Cytochrome P450 (CYP), an essential isoenzyme in drug metabolism, is important for assessment of toxicity profile of drugs [37]. In this study, only epicatechin gallate and cefotaxime are not inhibitors of all CYPP450 isoenzymes, which means that they are unlikely to cause drug –drug interactions when co–administered with other drugs that are normally metabolised by CYPP450 isoenzymes [37]. Silicristin, epigallocatechin 4-benzylthioether, Epicatechin 3-O-(3-O- methylgallate), and lysidicichin inhibited CYP3A4, suggesting that they may interact with other medicines processed by the enzyme. Except for silicristin, epicatechin 3-O-(3-O-methylgallate), and lysidicichin, all of the top–ranked phenolics and cefotaxime were inactive for all the toxicity endpoints (Table 1). Additionally, the top–ranked phenolics belonged to drug toxicity classes (classes five and four) that are suitable for drug development [38] and had synthetic feasibility scores of less than five, which is a limit for compounds that will be less difficult to synthesise [39]. These observations are suggestive of possibility of structural modifications that could be done on the top–ranked compounds to enhance their druggability. Generally, the top five phenolics could be adjudged to be medicinally and pharmacokinetically friendly, have drug–like qualities, and maybe derivatized for increased druggability and decreased toxicity.

The top five phenolics against PBP3 were docked against PBP5 of *E. coli*, due to the high relevance of PBP5 in maintaining the optimal morphology of *E. coli* [11,12]. Remarkably, three of the top–ranked compounds, epicatechin gallate (−8.0 Kcal/mol), silicristin (−8.6 Kcal/mol), and epigallocatechin 4–benzylthioether (−7.9 kcal/mol), had higher negative docking scores and interactions for PBP5 than cefotaxime (−7.8 Kcal/mol) (Table 2). This observation is suggestive of the better affinity of epicatechin gallate, silicristin, and epigallocatechin 4–benzylthioether for PBP5 and hence might have modulatory role on the optimal growth of *E. coli*.

Table 1. Pharmacokinetics and toxicity properties of top-ranked phenolics.

										Inhibitor of CYP 450s										
Popular Name	MW <500 (g/mol)	HB−A ≤ 10	HB−D≤ 5	Log $P_{o/w}$ ≤ 5	RT−B ≤ 9	WS	GI − A	BS	pgp	CYP 1A2	CYP 2C19	CYP 2C9	CYP 2D6	CYP 3A4	H	C	IM	M	CY	TC
Cefotaxime	455.4	12	3	−0.27	9	VS	L	0.11	N	N	N	N	N	N	I	I	I	I	I	6
(−)−Epicatechin gallate	442.3	10	7	1.3	4	S	L	0.55	N	N	N	N	N	N	I	I	I	I	I	4
Silicristin	482.4	10	6	1.47	4	S	L	0.55	N	N	N	N	N	Y	I	I	A	I	I	4
Epicatechin 3−O−(3−O−methylgallate)	456.4	10	6	1.77	5	S	L	0.55	N	N	N	N	N	Y	I	I	A	I	I	4
Epigallocatechin 4−benzylthioether	428.4	7	6	2.22	4	MS	L	0.55	N	N	N	N	N	Y	I	I	I	I	I	5
Lysidicichin	470.4	10	5	1.94	6	MS	L	0.55	N	N	N	N	N	Y	I	I	A	I	I	4

Keywords: HB−A: Hydrogen bond acceptor; MW: Molecular weight; Log $P_{o/w}$: Partition coefficient; RT−B: rotatable bond; WS: HB−D: Hydrogen bond donor; GI− A: Gastrointestinal absorption; Pgp: Permeability glycoprotein substrate; Water solubility; VS: very soluble; MS: Moderately soluble; CYP: Cytochrome; S: Soluble; Y: Yes, L: low; N: No; A: Active, LV: Lipinski violations, I: Inactive; BS: H: Hepatotoxicity, Bioavailability score, IM: Immunotoxicity, M: Mutagenicity, C: Carcinogenicity, LD: Lethal dose, CY: Cytotoxicity, TC: Toxicity class.

3.2 Energy components of top–ranked phenolics after 120 ns simulation against PBP3 and 5 of E. coli.

Using the Molecular Mechanics/GB Surface Area approaches, the docking study was refined by estimating the free energies of binding of the high-ranking phenolics for PBP3 and PBP5 through 120 ns molecular dynamic simulations [19]. Several energy components such as the $\Delta E_{elec,}$ $E_{gas,}$ $E_{vdw\ and}$ G_{sol} contributes to the total free energy of binding of a ligand to a receptor. In this study, the G_{sol} which estimate the sum of three contributions originating from the cavitation of the solute by the solvent, the solute-solvent repulsion and dispersion interactions, and the electrostatic solvation of the solute [38], contributed most to the total binding free energy observed for all the complexes studied (Table 3). The higher the negative free energy of binding, the higher the probability of a compound binding to a macromolecular receptor [39]. In this study, while lysidicichin (−15.43 kcal/mol) against PBP5 had binding free energy that compares to cefotaxime (−15.39 kcal/mol), the other top−ranked phenolics had higher binding free energy against both PBP3 and PBP5 than cefotaxime. This observation is consistent with the docking results and thus confirms the better affinity of the top−ranked phenolics for PBP3 and PBP5 of *E. coli* (Table 3). Among the phenolics, lysidicichin (−41.66 kcal/mol) followed by silicristin (−31.11 kcal/mol) had the highest binding free energy with PBP3 whereas, against PBP5, these compounds had the least values. Similarly, epicatechin 3-O-(3-O-methylgallate) (−38.97 kcal/mol) and epigallocatechin 4−benzylthioether (−37.01 kcal/mol) with the highest binding free energy to PBP5 had the least scores against PBP3. Epicatechin gallate on the other hand had slightly comparable free energy of binding to both targets (Table 3). These observations denote the different capabilities of the high−ranked phenolics towards exerting inhibitory effect against *E. coli*. Lysidicichin and silicristin being the most potent through their ability to inactivate PBP3 and epicatechin 3-O-(3-O-methylgallate) and epigallocatechin 4−benzylthioether having the capability to modulate *E. coli* growth through binding to PBP5. Epicatechin gallate, however, had the best broad-spectrum of activity through its ability to bind favourably to both targets. This observation agrees with the study of Verma *et al.* [39] where phenolics had diverse capability in inhibiting *Staphylococcus aureus* by inactivating PBP2a. Overall, the binding free energy analysis had demonstrated the advantage of the top-ranked phenolics over cefotaxime in the treatment of infections caused by *E. coli*. Current evidence has suggested reduced susceptibility or outright resistance of *E. coli* infections to most beta-lactams [amoxicillin (85%), cefuroxime (65%) and cefatriaxone (60%)] [1] due to drug overprescribing/ or drug overuse. Thus, the development of the top ranked phenolics after further *in vitro* and *in vivo* evaluations of their activities as possible beta-lactams will strengthen our antibiotic arsenal by increasing the number of effective antibiotics for treatment of infections caused by the organism.

Table 2. Docking scores of top ranked phenolics against PBP5 (kcal/mol).

Ligands zinc code	Popular name	PBP5
Cefotaxime	Cefotaxime	−7.8
ZINC03978503	(-)-Epicatechin gallate	−8.0
ZINC04214317	Silicristin	−8.6
ZINC14642643	Epicatechin 3-O-(3-O-methylgallate)	−7.7
ZINC38337967	Epigallocatechin 4-benzylthioether	−7.9
ZINC14642669	Lysidicichin	−7.6

3.3 Thermodynamics stability, flexibility and compactness of top–ranked phenolics after 120 ns simulation at the binding domain of PBP3 and PBP5 of E. coli.

Thermodynamic stability is a function of the structural deviation of a complex from its original structure during simulation, with indicators such as RMSD [29,40] and sometimes ROG and SASA being helpful in this regard [41]. A lower average RMSD value means better stability of a protein−ligand complex during simulation and an advantage for the ligand to modulate the protein [38]. In this study, after equilibration of the ligand−protein complexes in each case of the target before 10 ns (Figures 4 and 5(a)), each of the complex had different routes and distinct fluctuation patterns, which had consequences on the average RMSD values. Against PBP3, silicristin and the apo−PBP3 had the highest fluctuation at 15 ns (3 and 4.8 Å) and 45 ns (2.5 and 4 Å), respectively and this was maintained throughout the simulation period. This fluctuation pattern must have contributed to the relatively higher mean RMSD values observed with silicristin−PBP3 (3.97 Å) and the apo−PBP3 (3.5 Å) (Table 4), which are higher than the 3 Å limit as earlier reported [35] and thus could suggest possible reduced stability of silicristin-PBP3 complex after 15 ns and the apo−PBP5 after 45 ns. Other ligands against PBP3 had a considerable stable fluctuation pattern during the simulation period, and this contributed to the observed lower mean RMSD values (Table 4), which are lower than the value observed for apo-PBP3 which signifies possible thermodynamic stability This observation agrees with the results of Sainsbury et al. [42] who experimentally showed that binding of beta−lactam antibiotics (carbenicillin and ceftazidime) to purified PBP3 increases the thermostability of PBP3 through local conformational changes at the active site. In this study, epicatechin 3-O-(3-O−methylgallate) (1.89 Å) had the lowest RMSD value, followed by epicatechin gallate (2.39 Å) and epigallocatechin 4-benzylthioether (2.58 Å) all of which are lower to 2.86 Å observed for cefotaxime against PBP3 (Table 4). These observations suggest epicatechin 3-O-(3-O−methylgallate) as the most stable phenolic against PBP3 and hence its better advantage as a potential PBP3 inhibitor. These findings partially agree with the observed binding free energy values in this study where epicatechin-3-O-(3-O-methylgallate), epicatechin gallate and epigallocatechin−4−benzylthioether occurred has better PBP3 inhibitors than cefotaxime. Lysidicichin against PBP3, being the phenolics with the highest binding free energy value, had an RMSD value (2.88 Å) that is comparable to cefotaxime and less than 3.0 Å limit, thus, suggesting the thermodynamic compatibility and advantage of lysidicichin for PBP3 as an inhibitor. However, the silicristin−PBP3 complex had the highest RMSD with a value higher than the limit for good deviation and thus denotes that further structural adjustment of the compound for stability is

Table 3. Energy components (kcal/mol) of top-ranked phenolics against PBP3 and PBP5 of *E. coli* after 120 ns MD simulations.

Systems	Δ E_{vdW}	ΔE_{elec}	ΔG_{gas}	ΔG_{solv}	ΔEsur	ΔG_{bind}
PBP3						
Cefotaxime	−28.24 ± 7.06	−23.82 ± 13.08	−52.06 ± 18.02	35.20 ± 13.14	−3.69 ± 1.02	−16.85 ± 6.24
(-)-Epicatechin gallate	−27.75 ± 5.93	−55.41 ± 15.80	−83.16 ± 16.58	52.27 ± 9.33	−4.64 ± 0.62	−30.88 ± 8.02
Silicristin	−39.77 ± 3.85	−23.81 ± 6.80	−63.60 ± 7.90	32.49 ± 5.21	−4.87 ± 0.53	−31.11 ± 4.30
Epicatechin 3-O-(3-O-methylgallate)	−31.09 ± 3.76	−27.11 ± 9.19	−58.21 ± 9.73	34.45 ± 6.11	−4.43 ± 0.44	−23.75 ± 4.86
Epigallocatechin 4-benzylthioether	−26.09 ± 3.16	−31.23 ± 7.98	−57.33 ± 8.10	31.19 ± 4.77	−3.63 ± 0.33	−26.13 ± 4.75
Lysidicichin	−35.79 ± 5.06	−55.98 ± 19.93	−91.78 ± 22.46	50.12 ± 11.46	−5.41 ± 0.32	−41.66 ± 11.66
PBP5						
Cefotaxime	−26.78 ± 5.56	−5.14 ± 11.87	−31.93 ± 12.87	16.53 ± 11.80	−2.94 ± 0.64	−15.39 ± 4.53
(-)-Epicatechin gallate	−17.83 ± 4.99	−58.51 ± 16.07	−76.35 ± 15.09	47.02 ± 10.98	−3.53 ± 0.38	−29.32 ± 5.52
Silicristin	−26.61 ± 9.69	−19.66 ± 10.49	−46.30 ± 16.51	24.13 ± 10.29	−3.38 ± 1.18	−22.16 ± 9.40
Epicatechin 3-O-(3-O-methylgallate)	−32.95 ± 5.31	−60.83 ± 18.60	−93.79 ± 18.99	54.82 ± 12.29	−4.91 ± 0.59	−38.97 ± 8.58
Epigallocatechin 4-benzylthioether	−23.42 ± 6.01	−62.69 ± 13.93	−86.12 ± 12.10	49.10 ± 9.32	−3.83 ± 0.38	−37.01 ± 5.74
Lysidicichin	−20.35 ± 4.38	−14.40 ± 9.04	−34.75 ± 10.62	19.31 ± 7.14	− 2.58 ± 0.60	−15.43 ± 5.17

ΔG_{solv} = solvation free energy, ΔE_{gas} = gas phase free energy; ΔE_{elec} = electrostatic energy; ΔG_{bind} = total binding free energy; and ΔE_{vdW} = van der Waals energy.

necessary, which could be of great benefit to further increase the compound potency for PBP3. Unlike PBP3, a more stable fluctuation in PBP5 for all the systems was observed throughout the 120 ns simulation (Figure 5(a)). Averagely, the cefotaxime−PBP5 complex (2.12 Å) had the lowest RMSD value and the value was comparable to that observed for the apo−PBP5 (Table 4). However, the binding of the top−ranked phenolics caused an increase in the RMSD value (Table 4). These observations signify an advantage for cefotaxime in the inhibition of PBP5 relative to the investigated phenolics. Even though epicatechin 3-O-(3-O-methylgallate) (2.63 Å) and lysidicichin (2.91) had RMSD values that were less than 3 Å, the better thermodynamic stability of the other top−ranked phenolics with RMSD values that were higher than the 3 Å limit would generally further enhanced their potency in the inhibition of PBP5. Epicatechin 3-O-(3-O-methylgallate) being the phenolic with the least RMSD value correlates with its binding free energy and hence pinpoints its benefits over other phenolics as an inhibitor of PBP5. Generally, the RMSD finding of the study has demonstrated the different thermodynamic stability of the top−ranked phenolics for the targets.

Another metrics known as the ROG, estimate the extent of compactness and folding of a complex during a simulation. High compactness and folding suggest better degree of thermodynamic orderliness and sometimes stability in a complex, an occurrence which have been linked to the several parameters relating to the protein (e.g. protein topology, size, and length), ligand (e. g molecular weight) and point of contact on the target [41,43]. In this study, against PBP3, a gradual decrease with minimal swaying in ROG pattern was observed throughout the simulation period for all the systems and was more obvious in the silicristin−PBP3 complex (Figure 4(b)). In the silicristin−PBP3 complex, a gradual decrease from 23.6 Å (at 0 ns) to 22.6 Å (100 ns) was observed during the

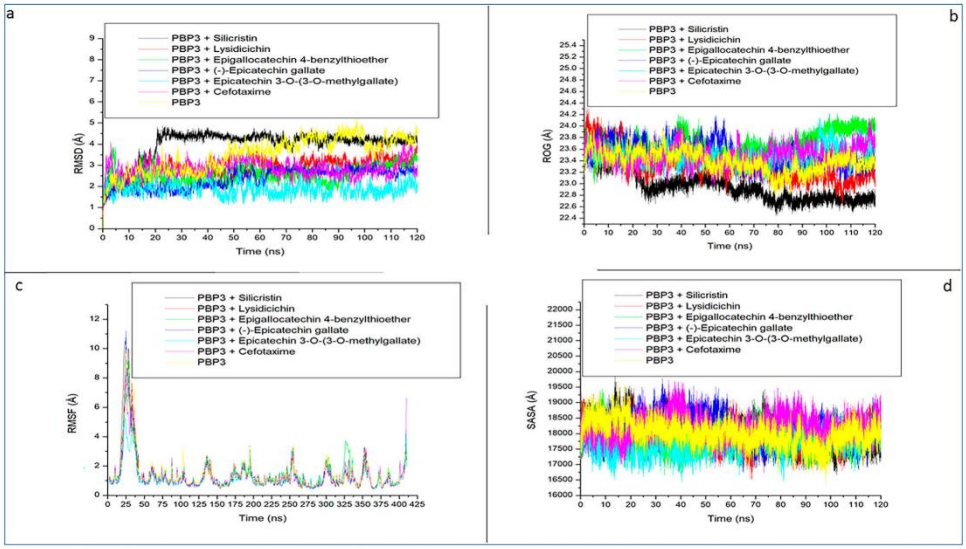


Figure 4. Comparative RMSD (a), ROG (b), RMSF (c) and SASA (d) plots of alpha−carbon, cefotaxime and top 5 lead phenolics against PBP3 of *E. coli* over a 120 ns simulation period.

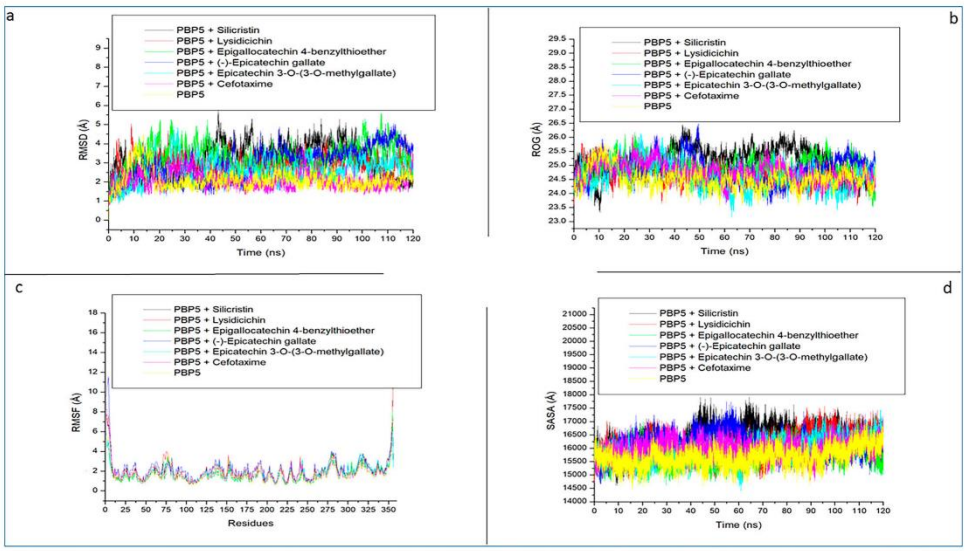


Figure 5. Comparative RMSD (a), ROG (b), RMSF (c) and SASA (d) plots of alpha−carbon, cefotaxime and top 5 lead phenolics against PBP5 of *E. coli* over a 120 ns simulation period.

simulation. Consequently, of all the system, the silicristin −PBP3 complex had the lowest average ROG value (22.95 Å), which suggest better compactness of the complex relative to other studied systems (Table 4). This observation could be due to the high molecular weight of silicristin (484.4 g/mol) relative to the other top−ranked compounds and cefotaxime (Table 1). The high molecular weight of silicristin might have given the compound a better surface area for interactions compared to the other studied compounds. This observation agrees with the report of Lobanov et al. [41], who demonstrated the importance of the molecular weight of a ligand in the mean ROG value of a complex. Consequently, the ROG findings were partially in contrast with the RMSD results of this study where the silicristin−PBP3 complex had the highest RMSD value and hence suggest the little impact of silicristin−PBP3 complex folding on the stability of the complex. This observation is in agreement with a previous study where the binding of phenolics to PBP2a of *Staphylococcus aureus* cause stability that was dissociated from compactness [29]. Remarkably, the little variance in the molecular weight (42 g/mol) (Table 1) of the other top−ranked compounds and cefotaxime could have contributed to the relatively similar mean ROG values observed for them against PBP3 which ranges between 23.31 and 23.49 Å (Table 4). The apo-PBP3 also had ROG value (23.39 Å) that falls within this range which suggests the little impact of ligand binding on PBP3 folding and hence pinpoints the negligible influence of complex folding on the high stability observed with the phenolics and cefotaxime complexes with PBP3. Generally, inference from the ROG findings of PBP3 suggests that silicristin cause the folding of PBP3 following binding due to its high molecular weight relative to the other investigated compounds, while other studied compound had no effect on folding, which signifies lack of entropy following binding of PBP3. These observations partially correlate with the RMSD results of this study, which indicate that binding of the highest−rank compounds does not disrupt the thermodynamic orderliness in the protein. Unlike PBP3, a more stable swaying in the ROG plots of PBP5 with minimal fluctuation was observe throughout the simulation period for all the system (Figure 5(b)). Consequently, except for silicristin-PBP5 complex, all other systems had a negligible variance of 0.28 Å ROG (between 24.62 and 24.90 Å) (Table 4). This observation is similar to that observed with PBP3, where binding of all the studied compounds with the exception of silicristin had negligible effect on the ROG values relative to the apo−PBP5 which could be due to the smaller variance in their molecular weight. Compared to the apo−PBP5 (24.54 Å), ligand binding slightly caused increased ROG value which was more obvious in the silicristin−PBP5 complex (25.23 Å) (Table 4). The reason for this is not far−fetched, as the active site (point of contact) on PBP5 is not centralised, thus ligand binding generally causes an increase in the length or weight of the complexes rather than a complex fold. This observation agrees with Lobanov et al. [43], who define ROG as the mass−weighted root mean square distance of a collection of atoms from their common centre of mass, and therefore specifying the position of the binding of the ligand relative to the centre of mass can have implications for ROG values. Therefore, in this study, the highest molecular weight silicristin had the highest ROG against PBP5, which is in contrast to its complex with PBP3. However, unlike PBP5, PBP3 has an active site (contact point) that is centralised. Hence, the lack of compactness of silicristin-PBP5 complex and the marginally increased ROG values observed with the

Table 4. Average RMSD, ROG, RMSF, SASA, and intramolecular hydrogen bonds number and distance and angle values of top five phenolics and cefotaxime following 120 ns MD simulation at the active site of PBP3 and PBP5 of *E. coli*.

Ligands	RMSD (Å)	RMSF(Å)	ROG (Å)	SASA (Å)	No of total H-bonds	Distance of H-bonds (Å)	Angle (°) of H-bonds	No of intermolecular H-bonds
PBP3								
Unliganded	3.50 ± 0.79	1.51 ± 1.38	23.39 ± 0.17	17996.66 ± 383	204,67 ± 8.5	2.86 ± 0.06	151,57 ± 7.3	
Cefotaxime	2.86 ± 0.36	1.38 ± 1.15	23.48 ± 0.17	18220.40 ± 355	204,97 ± 9.2	2.86 ± 0.06	151,56 ± 7.4	2.7 ± 0.01
(-)-Epicatechin gallate	2.39 ± 0.44	1.33 ± 1.29	23.49 ± 0.21	18124.00 ± 407	204,80 ± 9.4	2.86 ± 0.06	151,63 ± 7.2	3.0 ± 0.01
Silicristin	3.97 ± 0.70	1.44 ± 1.47	22.95 ± 0.25	17051.17 ± 380	206,94 ± 8.6	2.86 ± 0.05	151,71 ± 7.3	2.9 ± 0.02
Epicatechin 3-O-(3-O-methylgallate)	1.89 ± 0.31	1.24 ± 0.78	23.49 ± 0.14	17743.30 ± 310	205,99 ± 8.9	2.86 ± 0.05	151,67 ± 7.5	3.0 ± 0.02
Epigallocatechin 4-benzylthioether	2.58 ± 0.40	1.43 ± 1.17	23.67 ± 0.19	17918.14 ± 325	205,40 ± 9.5	2.86 ± 0.06	151,71 ± 7.3	2.8 ± 0.01
Lysidicichin	2.88 ± 0.42	1.38 ± 1.19	23.31 ± 0.26	18005.19 ± 354	206,03 ± 9.6	2.86 ± 0.06	151,62 ± 7.2	3.1 ± 0.02
PBP5								
Unliganded	2.15 ± 0.48	1.64 ± 0.82	24.54 ± 0.34	15727.36 ± 392	172,77 ± 6.9	2.85 ± 0.06	152.05 ± 7.4	
Cefotaxime	2.12 ± 0.44	1.72 ± 0.97	24.73 ± 0.34	16008.63 ± 323	174,47 ± 5.8	2.85 ± 0.05	151.94 ± 6.4	3.2 ± 0.01
(-)-Epicatechin gallate	3.22 ± 0.94	2.19 ± 1.22	24.90 ± 0.42	16169.08 ± 356	174,97 ± 6.7	2.85 ± 0.05	151.79 ± 7.2	3.5 ± 0.02
Silicristin	3.07 ± 0.82	1.92 ± 1.30	25.23 ± 0.54	16306.53 ± 419	174,65 ± 7.8	2.85 ± 0.06	152.02 ± 7.3	3.4 ± 0.02
Epicatechin 3-O-(3-O-methylgallate)	2.63 ± 0.59	1.80 ± 0.82	24.62 ± 0.43	15954.78 ± 424	180,13 ± 8.3	2.85 ± 0.04	151.92 ± 7.4	3.5 ± 0.01
Epigallocatechin 4-benzylthioether	3.28 ± 0.65	1.64 ± 0.83	24.66 ± 0.35	15865.42 ± 307	176,85 ± 8.0	2.85 ± 0.04	152.43 ± 7.3	3.3 ± 0.02
Lysidicichin	2.91 ± 0.48	2.06 ± 1.14	24.90 ± 0.32	16176.18 ± 413	175,91 ± 8.1	2.85 ± 0.04	151.40 ± 7.5	3.2 ± 0.02

other investigated compounds relative to the apo−PBP5 does not necessarily suggest less stability but rather could mean lack of thermodynamic disorderliness in PBP5.

The mobility of residues upon binding of ligands to PBP3 and 5 was examined by analyzing the RMSF. The RMSF value takes into account the average volatility of atoms and residues in a protein structure over a simulation time, which can be linked to their capacity to form intra and intermolecular stable bonds [22,44]. The lower the volatility, particularly at the active site where ligand binding and catalysis occurs, the stronger the binding and affinity of the ligand for the protein. In this study, a higher fluctuation in residues between 10 and 50 in PBP3 and residues at the terminal end of PBP5 was observed during the simulation (Figures 4 and 5(c)). These observations point to the lesser capability of these residues in forming stable bonds. Interestingly none of the catalytic residues in PBP3 and PBP5 falls within this region of high fluctuation which could be the reason why the average RMSF values observed in the whole PBP3 and PBP5 (Table 4) were higher than those observed at the catalytic sites of both targets (Table 5). This observation denotes stronger intra and Intermolecular bonding in PBP3 and PBP5 active site during the simulation. Among the studied compounds, lysidicichin had the lowest catalytic residue fluctuation which correlates with the highest binding free energy obtained with the compound for PBP3, however in the whole protein, epicatechin 3-O-(3-O-methylgallate) had the lowest RMSF value. Generally, ligand binding caused reduced catalytic residues fluctuation and fluctuation within the whole protein which suggests better intra and intermolecular bond stability and compactness. These observations are consistent with the binding free energy, RMSD and ROG finding of this study and hence suggest the potential of the studied compounds and most especially lysidicichin, as PPB3 inhibitor. Of the catalytic residues in PBP3, Asn361 had the least fluctuation which signify the important of the residues in forming stable bond with the investigated compounds during the simulation. Against PBP5, epigallocatechin 4-benzylthioether had the lowest catalytic residue fluctuation and fluctuation within the protein which correlates it high binding free energy obtained during the simulation. Except for epigallocatechin 4-benzylthioether, binding of PBP5 generally caused increase RMSF value when compared with the apo-PBP5 (Table 4), however, this fluctuation is generally within the good deviation limit of <3 Å, which shows that the residues fluctuations were good for stability. Among the catalytic residues of PBP5, Lys213, had the least fluctuation and hence its importance in the stability obtained with the investigated ligand (Table 5). In general, epicatechin 3-O-(3-O-methylgallate) against PBP3 and epigallocatechin 4−benzyl thioether against PBP5 had the lowest RMSF among the top phenolics investigated, pinpointing their advantage as potential inhibitors of the respective targets.

Another important thermodynamic metric that analyzes protein folding and surface area changes during a simulation

Table 5. Catalytic residues fluctuations (Å) in PBP3 and PBP5 during simulation.

System	Catalytic residues in PBP3 active site					Catalytic residues in PBP5 active site				
	Ser307	Lys310	Lys359	Asn361	Total RMSF	Ser44	Ser110	Lys47	Lys213	Total RMSF
Cefotaxime	0.79	1.36	1.42	0.75	1.08	0.80	0.92	1.05	1.00	0.93
(-)-Epicatechin gallate	0.81	1.10	1.37	0.93	1.05	1.25	1.14	1.51	1.22	1.28
Silicristin	1.38	1.37	1.30	0.77	1.20	1.00	1.01	1.20	0.94	1.04
Epicatechin 3-O-(3-O-methylgallate)	1.23	1.18	1.35	0.77	1.13	0.97	1.02	1.16	0.87	1.00
Epigallocatechin 4-benzylthioether	1.29	1.26	1.46	0.86	1.21	0.80	0.80	0.98	0.88	0.87
Lysidicichin	0.86	1.07	1.43	0.89	1.06	1.18	1.16	1.37	0.99	1.18
Apo-proteins	0.99	1.45	1.56	0.95	1.23	1.05	0.88	1.14	0.85	0.98
Total RMSF	1.05	1.25	1.35	0.84		1.00	0.99	1.19	0.96	

is the SASA, with higher SASA values indicating an increase in protein volume [28]. Similar to the ROG results, a gradual decrease with minimal swaying in SASA systems against PBP3 was observe throughout the simulation period for all the systems and was more prominent in the silicristin-PBP3 complex (Figure 4(d)). Thus, of all the system, silicristin −PBP3 complex had the lowest average SASA value (17051.17 Å) (Table 4) which suggest a decreased in the surface area of the complex. Similar to the ROG findings of this study, the higher molecular weight of silicristin (484.4 g/mol) relative to the other studied compounds could have afford the compound a higher surface area for interactions with PBP3 interestingly as the active site of the protein is centrally located. This observation could be responsible for why silicristin−PBP3 complex folding had little impact on its RMSD value. However, the small variance in molecular weight (42 g/mol) of the other high−ranking compounds and cefotaxime may have contributed to the relatively similar SASA values observed for their complexes against PBP3, ranging between 17743.30 and 18220.40 Å (Table 4). The apo−PBP3 also had a SASA value (7996.66 Å) within this range, pinpointing the minor influence of ligand binding on PBP3 folding and thus establishing the negligible influence of complex folding on the high stability observed with the investigated compounds against PBP3. Unlike PBP3, a more stable movement in SASA plots with minimal fluctuation was observe throughout the simulation period for all the system against PBP5 (Figure 5(d)). Compared to the apo−PBP5 (15727.36 Å), ligand binding caused increase in mean SASA value with silicristin-PBP5 having the highest value. These observations are consistent with the ROG findings of this study where ligand binding of PBP3 and most especially silicristin caused increase surface area of the resulting complexes. As noted with the ROG analysis, the non−centrality (point of contact) of the active site of PBP5 could have contribute to the increased complex length and surface area which insinuate that the increase SASA value following binding of the investigated phenolic compounds does not necessarily mean less stability of the complexes. Although, when compared with the apo−PBP5, the increase SASA value correlated with the RMSD findings of the study. Generally among the studied phenolics, silicristin against PBP3 and epigallocatechin 4−benzylthioether against PBP5 had the least SASA value and might suggest their advantage as a potential inhibitor of the respective target.

Hydrogen bonds formed and their corresponding distance and angle are essential for the stability of a complex and can be evaluated during simulation to understand the impact of ligand binding on protein stability [45,46]. In this study, against PBP3 (Figure 6(a)) and PBP5 (Figure 7(a)), a stable fluctuation in the pattern of the number of hydrogen bonds formed in all the systems was observed during the simulation. Averagely, except for the cefotaxime−PBP3 complex, ligand binding instigated an increase in intramolecular hydrogen bonds in PBP3 and PBP5 during the 120 ns simulation period (Table 4). The rise in intramolecular hydrogen bonds in both targets shows that the ligands occupied some intramolecular space of the proteins, and the increased hydrogen bonds might indicate hydrogen bond interactions mediated by intermolecular bindings of ligands to the protein. Interestingly, top −ranked phenolics with better affinities for *E. coli* PBP3 and 5 than cefotaxime initiated more intramolecular hydrogen bonding than cefotaxime in PBP3 and 5, suggesting the relativeness of hydrogen bonding to binding free energy. Similarly, among the investigated phenolics, silicristin, and lysidicichin had the highest intramolecular hydrogen bonding with PBP3 while against PBP5, epicatechin 3−O−(3−O−methylgallate) had the highest. This observation while being consistent with the binding free energy finding of this study where lysidicichin against PBP3 and epicatechin 3-O-(3-O-methylgallate) against PBP5 demonstrated the highest affinity for the targets, is coherent with previous findings where the best phenolics instigated the highest number of total hydrogen bonds in PBP2a of *S. aureus* [29]. Assessments of the intramolecular hydrogen bond distance during the simulation showed a continued reduction (Figures 6 and 7(b)) in both PBP3 and 5 following ligand binding. The average hydrogen bond distance is 2.86 and 2.85 Å in all the systems with PBP3 and PBP5 respectively (Table 4). Intramolecular hydrogen bond distance has been shown to be <3.5 Å [45,46] and the lesser the value the stronger the hydrogen bonding. Therefore, in this study, having a hydrogen bond distance that was less than 3.5 Å scores mean good hydrogen bonding during the simulation. The observation of having the same scores for the apo-proteins and the bonding systems in both targets suggests thermodynamic orderliness in both PBP3 and PBP5 following ligand binding which further corroborates other thermodynamic metric assessed in his study. Another parameter for the assessment of the quality of hydrogen bonding is the bonding angle with values closer to 180° suggesting a stronger hydrogen bond [47]. In this study, a stable fluctuation of hydrogen bond angle in PBP3 and PBP5 was observed as the simulation progresses (Figures 6 and 7(c)). At the beginning of the simulation, a wide range of swaying between 137° and 168° in all the systems was observed in both target plots. However, as the simulation continued, the swaying reduces drastically toward 180° in all the system for both targets. The lesser fluctuation towards 180° as the simulation progresses indicates the better strength of the bonding, which correlates with the findings of the hydrogen bond distance of this study. Averagely, the hydrogen bond angles values vary between 151.56° and 151.71° and 151.40° and 152.02° respectively for PBP3 and PBP5 (Table 4). The closely related values observed for all the systems point to the lack of disorder in PBP3 and PBP5 following ligand binding and thus agree with other thermodynamic metrics assessed in this study for stability, compactness, and flexibility. Generally, the closely related values for hydrogen distance and angle observed for all the system in both targets points to their negligible influence on the binding free energy obtained in this study.

The intermolecular hydrogen bonds are the hydrogen bonds that exit between the ligand and the protein during the 120 ns MD simulation. Generally, the plots (Figure 8(a and b) for PBP3 and PBP5, respectively) presented stable fluctuations of intermolecular hydrogen bonds between the ligands (top-ranked phenolics and amoxicillin) and the targets, with average values ranging between 2.7 and 3.1 and 3.2 and 3.5, respectively, for PBP3 and PBP5, with cefotaxime having the lowest values against both targets (Table 4). The

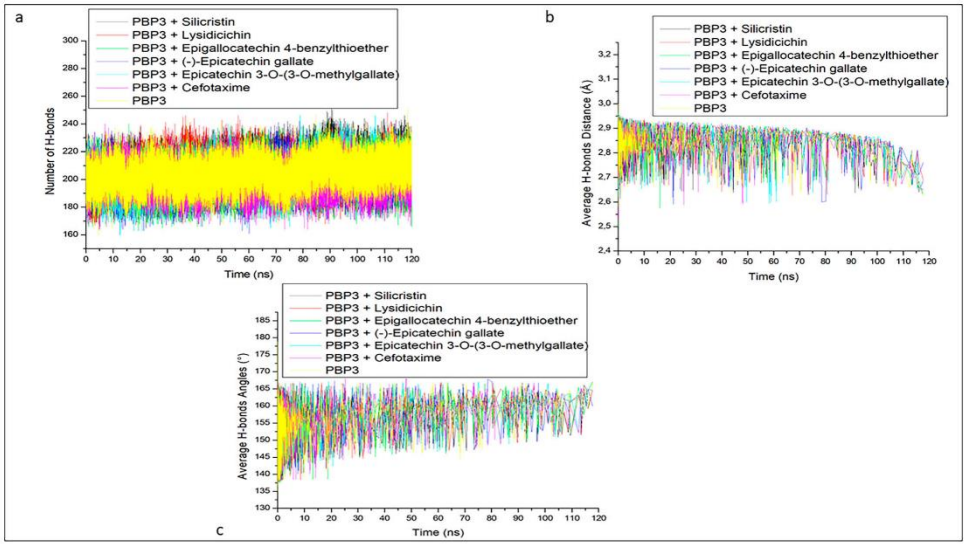


Figure 6. Time evolution of the number of intramolecular hydrogen bonds (a) and distance (b) and angle (c) formed in PBP3 of *E. coli* following binding of cefotaxime and the top five phenolics during the 120 ns simulation period.

lower average number of intermolecular hydrogen bonds of cefotaxime against both PBP3 and PBP5 might have contributed to the reduced binding free energy observed with the compound relative to the top-ranked phenolics. Similarly, among the top-five phenolics, lysidicichin (3.1) and epicatechin 3-O-(3-O-methylgallate) (3.5), with the highest binding free energy against PBP3 and PBP5, also had a slightly higher number of average intermolecular hydrogen bonds compared to other investigated compounds. These observations are indicative of the relevance of the number of intermolecular hydrogen bonds in the binding free energy noted in this study.

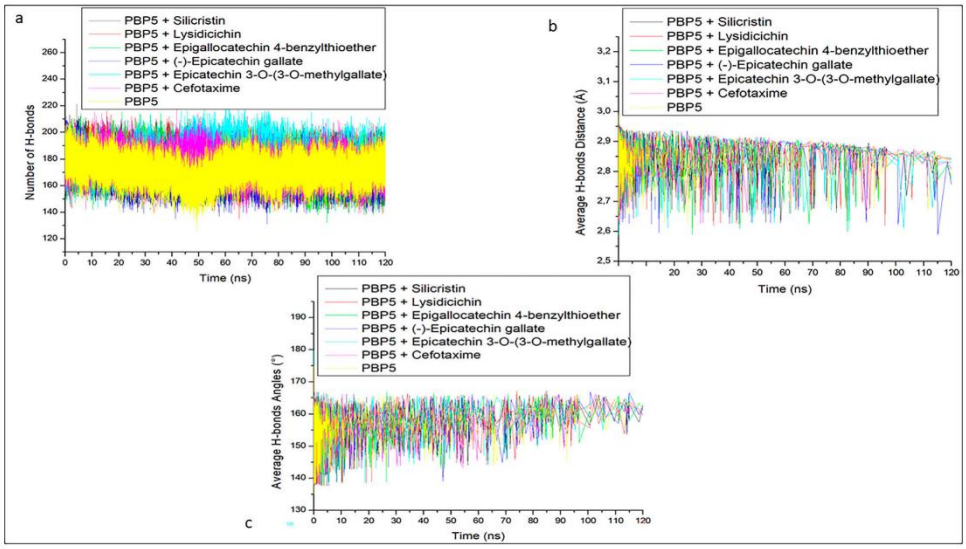


Figure 7. Time evolution of the number of intramolecular hydrogen bonds (a) and distance (b) and angle (c) formed in PBP5 of *E. coli* following binding of cefotaxime and the top five phenolics during the 120 ns MD simulation period.

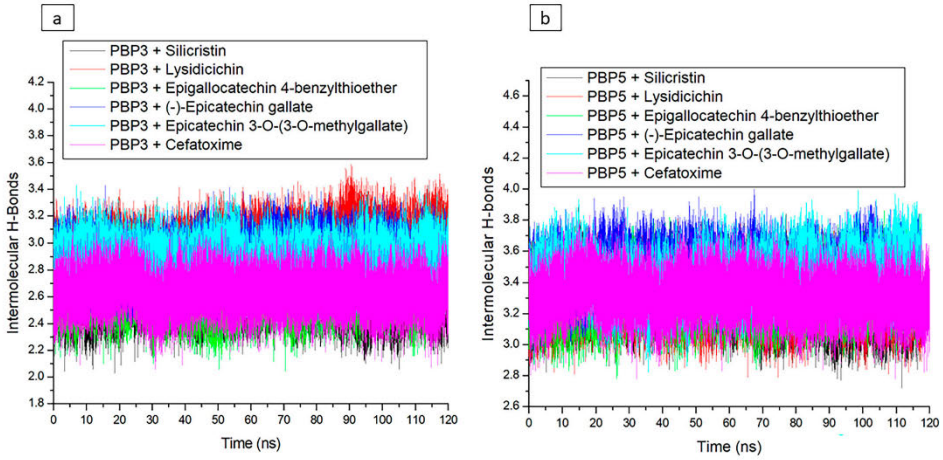


Figure 8. Time evolution of the number of intermolecular hydrogen bonds formed by the ligands (top-ranked phenolics and cefotaxime) against both PBPs [(a)PBP3 (b) PBP5 (b)] during the 120 ns MD simulation period.

3.4. Bond analysis of top–ranked compounds with PBP3 and 5 of E. coli *after 120 ns MD simulation*

The affinity of a compound for a protein and the stability of the resulting complex is related to the nature of interactions, bond lengths, and number of interactions within the complex [45,46,48,49]. Thus, in this study, these characteristics were assessed in the binding of the top−ranked phenolics with PBP3 and PBP5 of *Escherichia coli* after the 120 ns simulation period. The plot of interactions for cefotaxime and phenolics with the highest binding free energy with PBP3 and PBP5 are presented in Figures 9 and 10 respectively while that of the other top five phenolics are shown in Table S2. In this study, interactions such as hydrogen bonds, Van der Waals, amide π-stacked, π-anion, π-sigma, π-cation, π-π t-cation, π-π t-shaped, π-π t-stacked, π-alkyl, alky, π-Sulphur as well as some unfavourable donor−donor interactions exist between the top−ranked phenolics and the investigated PBPs. In this study, lysidicichin with the highest binding free energy with PBP3 had the highest number of interactions (19) and the shortest average bond length (4.23 Å) including six hydrogen bonds contacts with Phe266, Ser156, Asn210, Glu153 (2) and Thr346 of PBP3 (Table 6, Figure 9(a)). These observations linked the higher affinity observed in the Lysidicichin-PBP3 complex to the number, nature, and distance of interactions that exist in the complex. Similar observations were observed with the other investigated ligands against PBP3 (Table 6) as all the top-ranked phenolics with significantly higher binding free energy than cefotaxime against PBP3, all had higher number of interactions, including hydrogen bond contacts, with significantly shorter bond lengths than the interactions in the cefotaxime−PBP3 complex. Epicatechin gallate, epicatechin 3-O-(3-O-methylgallate), silicristin, and epigallocatechin 4−benzylthioether had 16, 18, 13, and 12 interactions respectively with PBP3 which were all higher than the 3 interactions formed in cefotaxime−PBP3 complex (Figure 9(b), Figure S2 and Table 6). Moreover, the 3 interactions in cefotaxime-PBP3 (Figure 9(b)) were all Van der Waals interactions as against the interactions between PBP3 and the top-ranked phenolics which include at least one hydrogen bond contact and 2 other important interactions (Table 6). Hydrogen bonds have emerged as one of the most important non −covalent bonds in drug discovery because of their unusually strong intermolecular interactions [46,50]. Thus, the presence of at least one hydrogen bond in the interactions of the investigated phenolics with PBP3 coupled with the significantly shorter bond lengths which have been demonstrated as relevant for increased binding free energy [45] could have contributed to the better affinity observed for the top−ranked phenolics relative to cefotaxime against PBP3. Similar to the investigated compounds' interactions with PBP3, epicatechin 3-O-(3-O-methylgallate) with the highest binding free energy against PBP5 had the highest number of interactions (18) (Figure 10(a), Table 6), majority of which were hydrogen bond contacts with Asp216, His214 (2), Lys 217, Asp39 (2), Leu151, Gly83 and Ala41 after 120 ns simulation period. Also, other top−ranked phenolics with higher binding free energy than cefotaxime also had higher number of interactions and hydrogen bond contacts than cefotaxime (Figure 10(b), Table 6) against PBP5. All these observations are suggestive of the importance of the number and nature of interactions in binding free energy estimation as earlier observed in the interactions against PBP3 in this study. The catalytic residues in PBP3 and PBP5 which includes Ser307, Lys310, Lys359, Asn361 in PBP3 and Ser44, Ser110, Lys47, Lys213 in PBP5 which were present in the molecular docking interactions were not observed in the interactions of the investigated ligands complexes with PBP3 and PBP5 after 120 ns simulation. This observation might be due to the dynamic nature of simulation which enables protein and the ligand flexibility and the observation is consistent with the findings of Al-

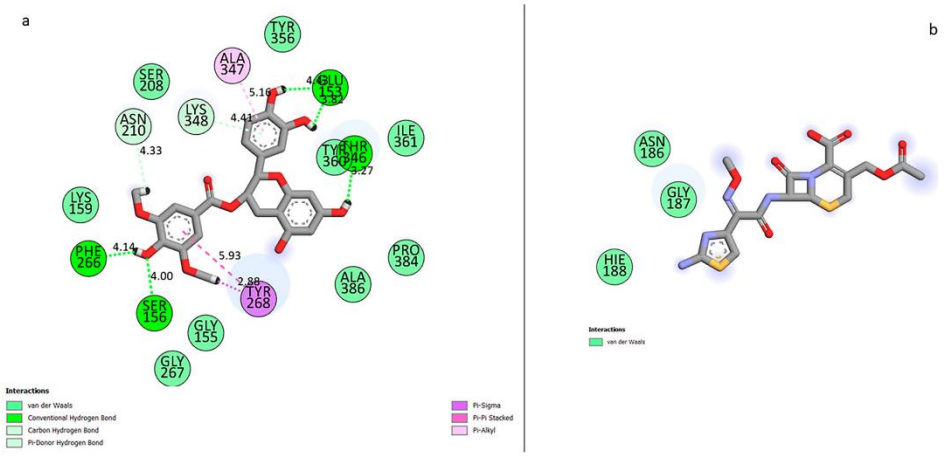


Figure 9. Plot of interactions of lysidicichin (a) and cefotaxime (b) against the active site of PBP3 of *E. coli*.

Karmalawy et al. [51], where alacepril had significant shift away from hACE2 catalytic region during a 70 ns simulation period. However, the lower fluctuation of the catalytic residues relative to the fluctuation within the protein as revealed by the RMSF analysis of this study suggest that the investigated compounds occupy the active region of the protein most during the simulation as intermolecular ligand binding have been correlated with lesser residues fluctuation [44]. Of the residues observed after 120 ns simulation, Asn210, which forms hydrogen bonds with epicatechin 3-O-(3-O-methylgallate), epigallocatechin 4-benzylthioether, and Lysidicichin and Glu153 which forms hydrogen bonds with silicristin and lysidicichin are important amino acids in the interactions of the top−ranked phenolics with PBP3 which are absent in cefotaxime-PBP3. Similarly, Asp39 and Ala41 of PBP5 which formed hydrogen bonds with epicatechin gallate, epicatechin 3-O-(3-O-methylgallate), and epigallocatechin 4 −benzylthioether are important amino acids in the interactions of the top−ranked phenolics with PBP5 which are absent in cefotaxime−PBP5.

4. Conclusions

The results of this study have revealed the different capabilities of the top-ranked phenolics as potential inhibitors of crucial PBPs in *E. coli*, with lysidicichin and silicristin being the most potent due to their ability to inactivate PBP3 and epicatechin 3-O-(3-O-methylgallate) and epigallocatechin−4 −benzyl thioether with the ability to modulate the growth of *E. coli* by binding to PBP5. However, epicatechin gallate had the best broad-spectrum of activity due to its ability to bind favourably to both PBP3 and PBP5. Moreover, except

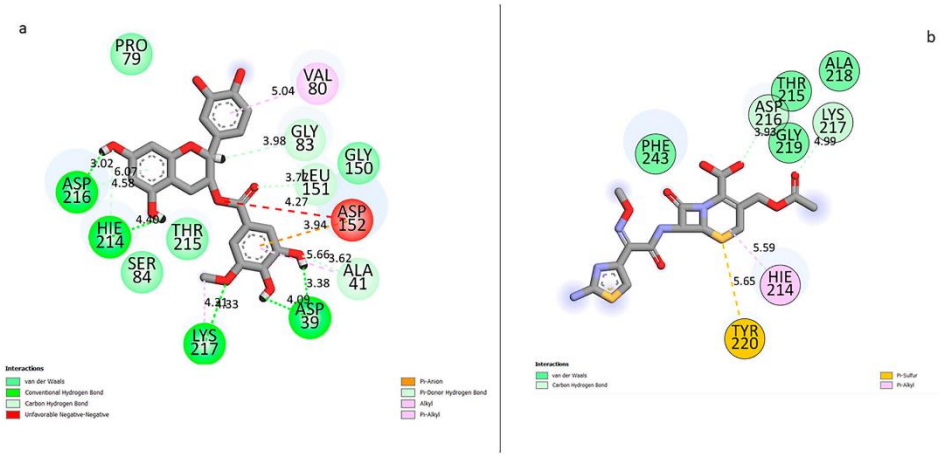


Figure 10. Plot of interactions of epicatechin 3−O−(3−O−methylgallate) (a) and cefotaxime (b) against the active site of PBP5 of *E. coli*.

Table 6. Bond interactions against the active site of PBP3 and PBP5 of *E. coli* by the top five phenolics and cefotaxime.

Top-ranked compounds	Total number of interactions (average distance in Å)	Number of hydrogen bonds (average distance in Å) and interaction residues	Other important interactions (average distance in Å) and residues	Unfavorable bonds
PBP3				
Cefotaxime	3(—)	None	None	None
(-)-Epicatechin gallate	16 (4.71)	8(4.70)[Lys348,Glu189,His188,Asn210, Phe266,Lys159, Glu156(2)]	1 (7.62) [Phe266]	None
Silicristin	13 (4.48)	1 (4.29) [Glu153]	5 (4.52) [Leu249,Pro251,Gly269,Glu260, Tyr356]	None
Epicatechin 3-O-(3-O-methylgallate)	18 (4.89)	6 (4.4) [Ser208,Asp102 (2), Asn210,Lys191 Val193]	3 (5.38) [yr268, Asn210,Val193]	1 (6.44) Lys159
Epigallocatechin 4-benzylthioether	12 (5.13)	5 (4.83) [Asp192 (2), Lys207, Asn210, Lys191]	2 (5.88) [Tyr268, Val193]	None
Lysidicichin	19 (4.23)	6 (4.05) [Phe266, Ser156, Asn210, Glu153 (2), Thr346]	3 (4.65) [Ala349, Tyr268(2)]	None
PBP5				
Cefotaxime	8 (5.04)	2 (4.46) [Lys217, Asp216]	2 (5.62) [Tyr220, His214]	None
(-)-Epicatechin gallate	10 (4.17)	4(3.62) [Asp39 (2), Asp152, Ala41]	2 (5.09) [Asp216, Lys217]	2 (4.33) [Thr215 (2)]
Silicristin	14 (3.03)	3 (2.13) [Asn78, Ser84, Thr76]	2 (4.39) [Phe88, Arg196]	None
Epicatechin 3-O-(3-O-methylgallate)	18 (4.29)	9 (4.12) [Asp216, His214 (2), Lys 217, Asp39 (2), Leu151, Gly83, Ala41)	4 (4.73) [Lys217, Ala41, Asp152, Val80]	1 (4.27) [Asp152]
Epigallocatechin 4-benzylthioether	12 (4.33)	7 (3.97) [Asp39 (2), Gly150, Asp216, His214, Asp152 (2)]	1 (6.70 [Ala41)	None
Lysidicichin	13 (4.28)	8 (4.41) [Gln94, Asn189,Gly92 (2), Gly190, Gln99,Pro96 Leu66]	1 [Met93]	None

for silicristin which might require further structural modification for better stability against PBP3, the thermodynamic information through 120 ns simulation confirmed the stability, flexibility, and compactness of the top—ranked phenolics with PBP3 and PBP5 which are attributable to the number and nature of interactions in the resulting complex in each case. These observations are suggestive of the lead phenolics and most especially lysidicichin against PBP3 and epicatechin 3-O-(3-O-methylgallate) against PBP5 as a possible inhibitor of PBP3 and PBP5 of *E. coli* and might have an advantage in the treatment of infections caused by the organism. Additionally, the lead phenolics displayed favourable pharmacokinetics and a viable synthetic score, indicating their susceptibility to possible structural changes for improved druggability and reduced toxicity. Nevertheless, further *in vitro* and *in vivo* confirmation of the activity observed in this study is strongly encouraged and efforts are underway in this direction.

Acknowledgments

The assistance of the National Research Foundation (NRF— TWAS Doctoral Scholarship, grant number 129950), South Africa, to Mr. J. O. Aribisala is duly and thankfully acknowledged. The Centre for High —Performance Computing (CHPC), South Africa is equally acknowledged for granting access to the computing systems used in this study.

Funding

The authors specially acknowledge the financial assistance of the Directorate of Research and Postgraduate Support, Durban University of Technology (DUT), and the South African Medical Research Council (SAMRC) under a Self-Initiated Research Grant as well as the National Research Foundation (NRF) Research Development Grant for Rated Researchers (Grant number 120433) and the Competitive Programme for Rated Researchers Support (SRUG2204193723) to S. Sabiu. The views and opinions expressed are those of the authors and do not necessarily represent the official views of the funders.

Author's contribution

SS conceptualised, mobilised funds and managed the study. SS and TRM supervised the study. JOA generated and analyzed the data. JOA wrote the manuscript, while KI revised the first draft. All authors read and contributed to the critical review of the manuscript for intellectual content and approved the submission for publication

Disclosure statement

No potential conflict of interest was reported by the author(s).

Funding

The authors specially acknowledge the financial assistance of the Directorate of Research and Postgraduate Support, Durban University of Technology (DUT), and the South African Medical Research Council (SAMRC) under a Self-Initiated Research Grant as well as the National Research Foundation (NRF) Research Development Grant for Rated Researchers (Grant number 120433) and the Competitive Programme for Rated Researchers Support (SRUG2204193723) to S. Sabiu. The views and opinions expressed are those of the authors and do not necessarily represent the official views of the funders.

Supplementary description

Additional data on the pharmacophore classes of the phenolics and the 2D and 3D interactions of the top—ranked phenolics against PBP3 and PBP5 are presented in the supplementary file (Supplementary Tables S1 and S2, Figure S1).

References

[1] Wu D, Ding Y, Yao K, et al. Antimicrobial resistance analysis of clinical *Escherichia coli* isolates in neonatal ward. Front Pediatr. 2021;9:670470. DOI:10.3389/fped.2021.670470

[2] Baker KS. Demystifying *Escherichia coli* pathovars. Nat Rev Microbiol. 2015;13:5. DOI:10.1038/nrmicro3411

[3] Croxen MA, Law RJ, Scholz R, et al. Recent advances in understanding enteric pathogenic *Escherichia coli*. Clin Microbiol Rev. 2013;26:822–880. DOI:10.1128/CMR.00022–13
[4] Poolman JT, Wacker M. Extra intestinal pathogenic *Escherichia coli*, a common human pathogen: challenges for vaccine development and progress in the field. J Infect Dis. 2016;213:6–13. DOI:10.1093/infdis/jiv429
[5] Majowicz SE, Scallan E, Jones–Bitton A, et al. Global incidence of human shigatoxin–producing *Escherichia coli* infections and deaths: asystematic review and knowledge synthesis. Foodborne Pathog Dis. 2014;11:447–455. DOI:10.1089/fpd.2013.1704
[6] Kocaoglu O, Carlson EE. Profiling of beta–lactam selectivity for penicillin–binding proteins in *Escherichia coli* strain DC2. Antimicrob Agents Chemother. 2015;59:2785–2790. DOI:10.1128/AAC.04552-14
[7] Sauvage E, Kerff F, Terrak M, et al. The penicillin–binding proteins: structure and role in peptidoglycan biosynthesis. FEMS Microbiol Rev. 2008;32:234–258.
[8] Muller P, Ewers C, Bertsche U, et al. The essential cell division protein FtsN interacts with the murein (peptidoglycan) synthase PBP1B in *Escherichia coli*. J Biol Chem. 2007;282:36394–36402.
[9] Mohammadi T, Ploeger GE, Verheul J, et al. The GTPase activity of *Escherichia coli* FtsZ determines the magnitude of the FtsZ polymer bundling by ZapA in vitro. Biochem. 2009;48:11056–11066.
[10] Fraipont C, Alexeeva S, Wolf B, et al. The integral membrane FtsW protein and peptidoglycan synthase PBP3 form a subcomplex in *Escherichia coli*. Microbiology. 2011;157:251–259. DOI:10.1099/mic.0.040071–0
[11] Nelson DE, Young KD. Contributions of PBP 5 and DD carboxypeptidase penicillin–binding proteins to maintenance of cell shape in *Escherichia coli*. J Bacteriol. 2001;183:3055–3064.
[12] Sujoy KS, Chiranjit C, Anindya SG. Deletion of penicillin–binding protein 5 (PBP5) sensitises *Escherichia coli* cells to beta–lactam agents. Int J Antimicrob Agents. 2010;35:244–249.
[13] Alhadrami HA, Hamed AA, Hassan HM, et al. Flavonoids as potential anti–MRSA agents through modulation of PBP2a: a computational and experimental study. Antibiotics. 2020;9:562. DOI:10.3390/antibiotics9090562
[14] Cuschnie TP, Lamb AJ. Recent advances in understanding the antibacterial properties of flavonoids. Int J Antimicrob Agents. 2011;38:99–107. DOI:10.1016/j.ijantimicag.2011.02.014
[15] Avila HP, Smânia FA, Monache FD, et al. Structure–activity relationship of antibacterial chalcones. Bioorg Med Chem. 2008;16:9790–9794. DOI:10.1016/j.bmc.2008.09.064
[16] Aldulaimi OA. General overview of phenolics from plant to laboratory, good antibacterials or not? Pharmacogn. 2017;11:123–127. DOI:10.4103/phrev.phrev_43_16
[17] Qin R, Xiao K, Li B, et al. The combination of catechin and epicatechin gallate from fructus crataegi potentiates beta–lactam antibiotics against methicillin–resistant *staphylococcus aureus* (MRSA) in vitro and in vivo. Int J Mol Sci. 2013;14:1802–1821. DOI:10.3390/ijms14011802
[18] Chiorcea–Paquim AM, Enache TA, De Souza GE, et al. Natural phenolic antioxidants electrochemistry: towards a new food science methodology. Compr Rev Food Sci. 2020;19(4):1680–1726. DOI:10.1111/1541-4337.12566
[19] Cerón–Carrasco JP. When virtual screening yields inactive drugs: dealing with false theoretical friends. Chem Med Chem. 2022;17:e202200278. DOI:10.1002/cmdc.202200278
[20] Dom B, Lizbé K, Hector N, et al. Novel and improved crystal structures of H. influenzae, *E. Coli* and P. aeruginosa Penicillin–Binding Protein 3 (PBP3) and N. gonorrhoeae PBP2: toward a better understanding of β–lactam target–mediated resistance. J Mol Biol. 2019;431:3501–3519. DOI:10.1016/j.jmb.2019.07.010
[21] Nicola G, Peddi S, Stefanova M, et al. Crystal structure of *Escherichia coli* penicillin–binding protein 5 bound to a tripeptide boronic acid inhibitor: a role for Ser–110 in deacylation†. Biochem. 2005;44:8207–8217. DOI:10.1021/bi0473004
[22] Pettersen EF, Goddard TD, Huang CC, et al. UCSF chimera – a visualization system for exploratory research and analysis. J Comput Chem. 2004;25(13):1605–1612.
[23] MubarakAli D, MohamedSaalis J, Sathya R, et al. An evidence of microalgal peptides to target spike protein of COVID–19: in silico approach. Microb Pathog. 2021;160:105189. DOI:10.1016/j.micpath.2021.105189
[24] Aribisala JO, Abdulsalam RA, Dweba Y, et al. Identification of secondary metabolites from crescentia cujete as promising antibacterial therapeutics targeting type 2A topoisomerases through molecular dynamics simulation. Comput Biol Med. 2022;145:105432. DOI:10.1016/j.compbiomed.2022.105432
[25] BIOVIA, Dassault Systèmes, BIOVIA Workbook, Release. BIOVIA pipeline pilot, release 2021. San Diego: Dassault Systèmes; 2021.
[26] Koes DR, Camacho CJ. ZINCPharmer: pharmacophore search of the ZINC database. Nucleic Acids Res. 2012;40:409–414. DOI:10.1093/nar/gks378
[27] Dallakyan S, Olson AJ. Small–molecule library screening by docking with PyRx. Methods Mol Biol. 2015;1263:243–250. DOI:10.1007/978-1-4939-2269-7_19
[28] Uhomoibhi JO, Shode FO, Idowu KA, et al. Molecular modelling identification of phytocompounds from selected African botanicals as promising therapeutics against druggable human host cell targets of SARS–CoV–2. J Mol Graph Model. 2022;114:108185. DOI:10.1016/j.jmgm.2022.108185
[29] Aribisala JO, Sabiu S. Cheminformatics identification of phenolics as modulators of penicillin–binding protein 2a of *staphylococcus aureus*: a structure–activity–relationship–based study. Pharmaceutics. 2022;14:1818. DOI:10.3390/pharmaceutics14091818
[30] Fahad M, Al–Khodairy M, Kalim A, et al. In silico prediction of mechanism of erysolin–induced apoptosis in human breast cancer cell lines, American. J Bioinform. 2013;3:62–71. DOI:10.5923/j.bioinformatics.20130303.03
[31] Kufareva I, Abagyan R. Methods of protein structure comparison. Methods Mol Biol. 2012;857:231–257. DOI:10.1007/978–1–61779–588–6_10
[32] Bajorath J. Selected concepts and investigations in compound classification, molecular descriptor analysis, and virtual screening. J Chem Inf Comput Sci. 2001;41:233–245. DOI:10.1021/ci0001482
[33] Sabiu S, Balogun FO, Amoo SO. Phenolics profiling of *carpobrotus edulis* (L.) NE Br. and insights into molecular dynamics of their significance in type 2 diabetes therapy and its retinopathy complication. Molecules. 2021;26:4867. DOI:10.3390/molecules26164867
[34] Ylilauri M, Pentikäinen OT. MMGBSA as a tool to understand the binding affinities of filamin–peptide interactions. J Chem Inf Model. 2013;53:2626–2633. DOI:10.1021/ci4002475
[35] Ramirex D, Caballero J. Is it reliable to use common molecular docking methods for comparing the binding affinities of enantiomer pairs for their protein target. Int J Mol Sci. 2016;17:525–545. DOI:10.1016/j.biotechadv.2018.11.013
[36] Lipinski CA, Lombardo F, Dominy BW. Experimental and computational approaches to estimate solubility and permeability in drug discovery and development settings. Adv Drug Deliv Rev. 2001;46:3–26. DOI:10.1016/S0169–409X(00)00129–0
[37] Khumbulani M, Alayande KA, Sabiu S. Orientin enhances colistin–mediated bacterial lethality through oxidative stress involvement. Evidence–Based Complement Altern Med. 2022;3809232. DOI:10.1155/2022/3809232
[38] Gonçalves PF, Stassen H. Free energy of solvation from molecular dynamics simulations for low dielectric solvents. J Comput Chem. 2003;24:1758–1765. DOI:10.1002/jcc.10294
[39] Verma AK, Ahmed SF, Hossain MS. Molecular docking and simulation studies of flavonoid compounds against PBP–2a of methicillin-resistant staphylococcus aureus. J Biomol Struct Dyn. 2020;1:1–17. DOI:10.1080/07391102.2021.1944911
[40] Ertl P, Schuffenhauer A. Estimation of synthetic accessibility score of drug–like molecules based on molecular complexity and fragment contributions. J Cheminform. 2009;1:8. DOI:10.1186/1758–2946–1–8

[41] Stella L, Melchionna S. Equilibration and sampling in molecular dynamics simulations of biomolecules. J Chem Phys. 1998;109:10115–10117. DOI:10.1063/1.477703
[42] Sainsbury S, Bird L, Rao V, et al. Crystal Structures of Penicillin-Binding Protein 3 from Pseudomonas aeruginosa: Comparison of Native and Antibiotic-Bound Forms. *J Mol Biol*. 2011;405:173–184.
[43] Lobanov MY, Bogatyreva NS, Galzitskaya OV. Radius of gyration as an indicator of protein structure compactness. Mol Biol. 2008;42:623–628. DOI:10.1134/S0026893308040195
[44] Baig MH, Sudhakar DR, Kalaiarasan P, et al. Insight into the effect of inhibitor resistant S130G mutant on physico–chemical properties of SHV type BetaLactamase: A molecular dynamics study. PLoS One. 2014;9:e112456. DOI:10.1371/journal.pone.0112456
[45] Mousavi SS, Karami A, Haghighi TM, et al. In silico evaluation of Iranian medicinal plant phytoconstituents as inhibitors against main protease and the receptor–binding domain of SARS–CoV –2. Molecules. 2021;26:5724. DOI:10.3390/molecules26185724
[46] Du X, Li Y, Xia YL, et al. Insights into protein–ligand interactions: mechanisms, models, and methods. Int J Mol Sci. 2016;17:144. DOI:10.3390/ijms17020144
[47] Izadi H, Stewart KME, Penlidis A. Role of contact electrification and electrostatic interactions in gecko adhesion. J R Soc Interface. 2014;11:371–398. DOI:10.1098/rsif.2014.0371
[48] Kretschmer R, Kinzel D, Gonza´ Lez L. The role of hydrogen bonds in protein-ligand interactions. DFT calculations in 1,3 –Dihydrobenzimidazole–2 thione derivatives with glycinamide as model HIV RT inhibitors. Int J Quantum Chem. 2010;112:1787–1795. DOI:10.1002/qua
[49] Nasution F, Toepak MA, Alkaff EP, et al. Flexible docking–based molecular dynamics simulation of natural product compounds and ebola virus nucleocapsid (EBOV NP): a computational approach to discover new drug for combating ebola. BMC Bioinform. 2018;19:419–436. DOI:10.1186/s12859–018–2387–8
[50] Bissantz C, Kuhn B, Stahl MA. Medicinal chemist's guide to molecular interactions. J Med Chem. 2010;14:5061–5084. DOI:10.1021/jm100112j
[51] Al–Karmalawy AA, Dahab MA, Metwaly AM, et al. Molecular docking and dynamics simulation revealed the potential inhibitory activity of ACEIs against SARS–CoV–2 targeting the hACE2 receptor. Front Chem. 2021;9:661230. DOI:10.3389/fchem.2021.661230

3.2 Cheminformatics identification of phenolics as modulators of penicillin-binding protein-3 of *Pseudomonas aeruginosa* towards interventive antibacterial therapy

This section has been published in Journal of Biomolecular Structure and Dynamics and is presented as it is in the article

JOURNAL OF BIOMOLECULAR STRUCTURE AND DYNAMICS
https://doi.org/10.1080/07391102.2023.2192808

Taylor & Francis
Taylor & Francis Group

Check for updates

Cheminformatics identification of phenolics as modulators of penicillin-binding protein-3 of *Pseudomonas aeruginosa* towards interventive antibacterial therapy

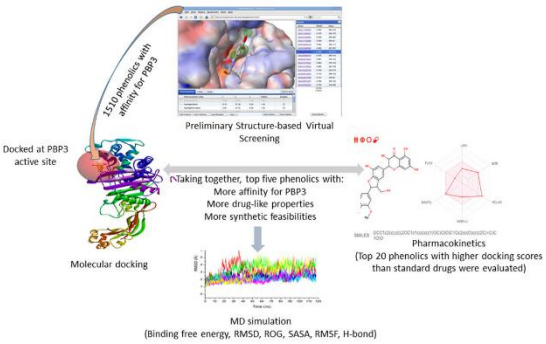
Jamiu Olaseni Aribisala and Saheed Sabiu

Department of Biotechnology and Food Science, Faculty of Applied Sciences, Durban University of Technology, Durban, South Africa

Communicated by Ramaswamy H. Sarma

ABSTRACT

Antibacterial resistance to β-lactams in microorganisms has been attributed majorly to alterations in penicillin-binding proteins (PBPs) coupled with β-lactams' inactivation by β-lactamase. Consequently, the identification of a novel class of therapeutics with improved modulatory action on the PBPs is imperative and plant secondary metabolites, including phenolics, have found relevance in this regard. For the first time in this study, the over 10,000 phenolics currently known were computationally evaluated against PBP3 of *Pseudomonas aeruginosa*, a superbug implicated in several nosocomial infections. In doing this, a library of phenolics with an affinity for PBP3 of *P. aeruginosa* was screened using structure-activity relationship-based pharmacophore and molecular docking approaches. Subsequent thermodynamic screening of the top five phenolics with higher docking scores, more drug-likeness attributes, and feasible synthetic accessibility was achieved through a 120 ns molecular dynamic (MD) simulation. Four of the top five hits had higher binding free energy than cefotaxime (−18.72 kcal/mol), with catechin-3-rhamside having the highest affinity (−28.99 kcal/mol). All the hits were stable at the active site of the PBP3, with catechin-3-rhamside being the most stable (2.14 Å), and established important interactions with Ser294, implicated in the catalytic activity of PBP3. Also, PBP3 became more compact with less fluctuation of the active site amino acid residues following the binding of the hits. These observations are indicative of the potential of the test compounds as PBP3 inhibitors, with catechin-3-rhamside being the most prominent of the compounds that could be further improved for enhanced druggability against PBP3 *in vitro and in vivo*.



ARTICLE HISTORY
Received 29 November 2022
Accepted 11 March 2023

KEYWORDS
Phenolics; β-lactam antibiotics; structure-based pharmacophores; molecular docking; molecular dynamic simulation

1. Introduction

Yearly, about 700,000 deaths occur worldwide due to infections caused by multi-drug resistant microorganisms, and this number could increase to 10 million by the year 2050 depending on resistance evolution patterns and, more importantly, if no effective therapeutic alternatives are available (World Health Organisation, 2019). Of great significance is the risk of infections posed by *Pseudomonas aeruginosa* to hospitalized and immunocompromised patients, which are usually very difficult to treat and, as such, have drastically reduced treatment strategies (Al-Orphaly et al., 2021). *P. aeruginosa* is implicated in more than 50% of nosocomial infections (Al-Orphaly et al., 2021). Of the classes of

CONTACT Saheed Sabiu sabius@dut.ac.za Department of Biotechnology and Food Science, Faculty of Applied Sciences, Durban University of Technology, P.O. Box 1334, Durban 4000, South Africa

Supplemental data for this article can be accessed online at https://doi.org/10.1080/07391102.2023.2192808.

© 2023 Informa UK Limited, trading as Taylor & Francis Group

antibiotics used in treating nosocomial infections, resistance to β-lactams, the most frequently administered antibiotics because of their minimal side effects relative to other classes of antibiotics, remains a growing challenge (Klein et al., 2021; Pang et al., 2019). Hence, the development of novel therapeutic strategies against such resistance is imperative.

Penicillin-binding proteins (PBPs) are enzymes involved in the synthesis and remodeling of peptidoglycan, a unique and vital structural element of the bacterial cell wall (Kumar et al., 2020). Bacteria possess diverse PBPs (PBP1a, PBP2a, PBP2x, PBP3, PBP4, PBP5, PBP6, and PBP7) with molecular weights ranging from 40,000 to 120,000 daltons (Thakuria & Lahon, 2013). The low molecular weight PBPs (PBP4, PBP5, PBP6, and PBP7) act as carboxypeptidases and endopeptidases, which are believed to facilitate the restructuring and remodeling of peptidoglycan during the bacterial life cycle and, as such, can be genetically deleted without exerting any significant effect on cell viability or growth (Josephine et al., 2006; Zapun et al., 2008). However, the high molecular weight PBPs (PBP1a, PBP1b, PBP2a, PBP2b, PBP2x, and PBP3) act as transpeptidases and are essential for the final stage of peptidoglycan formation in bacteria (Kumar et al., 2020; Ren et al., 2016). Among the high molecular weight PBPs, PBP3 remains the most important and particularly essential for the survival of *P. aeruginosa* (Chen et al., 2017). Hence, PBP3 represents a viable therapeutic target for identifying and developing potent drug candidates against infections caused by multi-drug-resistant *P. aeruginosa*.

In both Gram-positive and Gram-negative bacteria, the efficiency of β-lactam antibiotics has been attributed to their ability to penetrate the outer cell membrane, resist inactivation by plasmid or chromosomal encoded β-lactamase, and bind efficiently with mutated PBPs that are of therapeutic importance (Frere & Loris, 1985; Pang et al., 2019). These characteristics have been reported in phytonutrients including phenolics (Zhao et al., 2002). Phenolics occur most frequently in plants, and their diverse health and therapeutic benefits against degenerative diseases such as cancers, Parkinson's and Alzheimer's diseases, and microbial infections have been reported (Dai et al., 2006; Panat et al., 2016; Weinreb et al., 2004; Zhao et al., 2002). Also, their ability to effectively bind and modulate bacterial druggable targets such as β-lactamase (Zhao et al., 2002) and consequently inhibit various multi-drug resistant Gram-negative and Gram-positive bacteria have been reported (Aldulaimi, 2017; Alhadrami et al., 2020), while also increasing cell membrane permeability for antimicrobial absorption (Araya-Cloutier et al., 2018). Hence, for the first time in this study, phenolic compounds with affinity for PBP3 of *Pseudomonas aeruginosa* were screened from the over 10,000 phenolics currently known (Chiorcea-Paquim et al., 2020) using structure-activity relationship-based pharmacophore and molecular docking approaches. Molecular docking and molecular dynamic simulation have been employed in several studies involving the computational investigation of protein-ligand interactions including ligand-PBPs studies (Aribisala & Sabiu, 2022, Tonmoy et al., 2022; Verma et al., 2020, 2022) and thus could serve as a less expensive approach to ranked and gain an understanding of phenolic interactions with PBP3 of *pseudomonas aeruginosa*. However, virtual screening limitations relating to lack of subsequent refinement (rescoring) and assessment of binding pose stability coupled with evaluations with a few randomly selected molecules have been shown to contribute to the increased rate of inactive molecules that are certain to fail the next phase of drug development (Acharya, 2020; Cerón-Carrasco, 2022; Verma et al., 2022). Hence, in this study, in addition to screening a considerable number of phenolics (over 10,000 phenolics ever known), the Autodock vina scoring function was refined using molecular mechanics/GB surface area approaches while studying essential biomolecular processes relating to stability, flexibility, and compactness of the protein following binding of phenolics using molecular dynamics simulations (Figure 1). Identifying lead compounds using these approaches against PBP3, which is of great structural element in the cell wall of *pseudomonas aeruginosa* could help identify promising antimicrobial candidates from phenolics that could be developed as therapeutics against infections caused by *Pseudomonas aeruginosa*.

2. Methodology

2.1. Acquisition, preparation, and identification of PBP3 active site

The X-ray crystal structure of PBP3 of *P. aeruginosa* (6VJE) bound to an inhibitor, was retrieved from the protein data bank (PDB) (https://www.rcsb.org). In preparation for molecular docking, the structure was optimized (removal of water molecules and nonstandard amino acids) using the UCSF Chimera v1.15 software package (Sabiu et al., 2021). The x-y-z coordinates [center (X: 2.13; Y: 6.40; Z: 24.84); radius (9.87)] of the PBP3 active site were defined using Discovery Studio version 21.1.0 (MubarakAli et al., 2021).

2.2. Hierarchical screening, acquisition, and preparation of phenolics

With over 10,000 phenolic compounds currently known (Chiorcea-Paquim et al., 2020), a preliminary computational screening was performed where a library of phenolic compounds against PBP3 was built using the ZINCPharmer database (http://zincpharmer.csb.pitt.edu). A structure-based pharmacophore was employed in which the 3D structure of PBP3 of *P. aeruginosa* and a consensus phenolic pharmacophore (derived from 32 phenolics) developed from PharmaGist (https://bioinfo3d.cs.tau.ac.il/PharmaGist/php.php) were used (Table S1) (Dror et al., 2009). Characteristics such as the presence of an aromatic ring, hydrogen-bond formation, charge, and hydrophobic contact between ligand and receptor atoms (Table S1) were employed in screening out 1510 phenolics that established interactions with the PBP3 druggable target of *P. aeruginosa*. As a validation step for the pharmacophore features, the known 32 phenolics used in generating a consensus phenolics pharmacophore were expected in the list of the

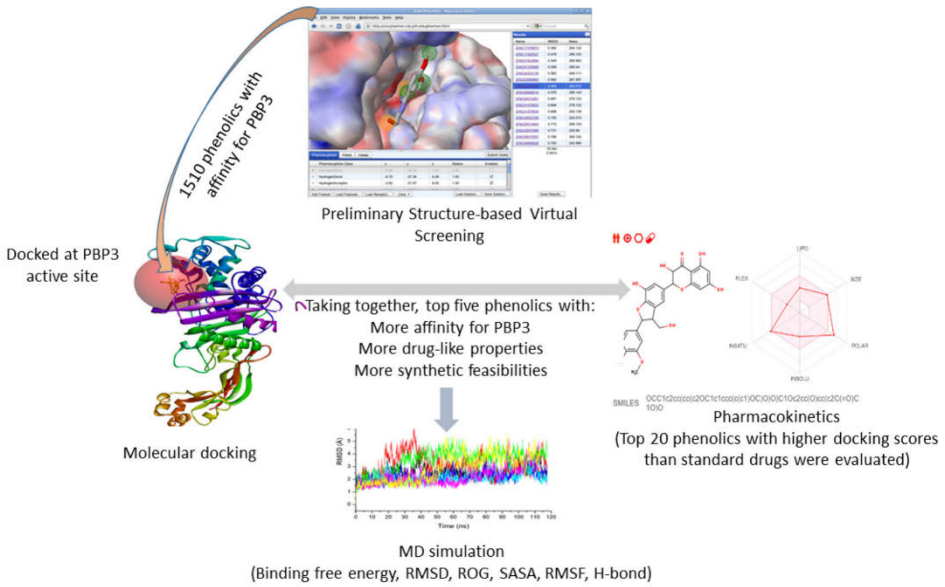


Figure 1. Workflow of the strategy adopted

generated 1510 libraries of phenolics. Interestingly, all 32 known compounds were included in the generated library.

Screening down of the 1510 library of phenolics was carried out via the docking approach at the active site of PBP3 using the Python Prescription v 0.9.5 (PyRx). The phenolics and the reference β-lactam antibiotics (amoxicillin, cefotaxime, aztreonam, and doripenem) were optimized through the addition of Gasteiger charges using the UCSF Chimera v 1.15 software program (MubarakAli et al., 2021). Docking at the active site of PBP3 was ensured through selections of amino acid residues at the active site of PBP3 whose grid box coordinates coincide with the established x-y-z coordinates [center {X: 2.13; Y: 6.40; Z: 24.84); radius (9.87)]. Afterward, docking of the cleaned 3D protein (PBP3) and the ligands [phenolics library and reference β-lactam antibiotics (amoxicillin, cefotaxime, aztreonam, and doripenem)] was carried out using the AutoDock vina of the Python Prescription v 0.9.5 (Parakkal et al., 2022). The resulting docked complexes with the best poses were ranked in order of affinity for the protein and the pose with the best affinity in each case was saved in PDB format. The top 20 phenolics with the best affinity for PBP3 were sorted using the binding affinity of the highest-ranked β-lactam antibiotic (cefotaxime) as the benchmark.

2.3. Validation of docking method

The docking technique and parameters utilized were further validated via the redocking approach (Fahad et al., 2013). This was necessary to verify that the orientation of the top five phenolics acquired from docking studies was likely to reflect true and plausible possible binding patterns of the native inhibitor (inhibitor bound to PDB: 6VJE). Docked ligand [cefotaxime (β-lactam antibiotic with the highest affinity) and the top five ranked phenolics] and native inhibitor (Ceftobiprole) were superimposed into the native protein with experimental native inhibitor (6VJE) to test the ability of the AutoDock vina of the Python Prescription program to duplicate the inhibitor's orientation and location as seen in the crystal structure of 6VJE. The RMSD between the docked location of the ligand and the experimentally obtained position for the inhibitor was used to rank the top conformational clusters from the dock. Following optimal superimposition, cefotaxime, and the top five ranked phenolics achieved the same binding orientation with the docked native inhibitor. However, the experimental native inhibitor had a slight deviation at the tail end relative to the docked compounds (native inhibitor and investigated ligands) with an RMSD of 0.95 Å. Thus, the validation protocol demonstrated the same binding orientation for the investigated ligands and the docked native inhibitor, while having a partial binding site with the experimental native inhibitor. These observations encouraged the docking technique used in this study. The superimposition of the 6VJE native inhibitor (docked and experimental) with silicristin (phenolic with the highest docking score) and cefotaxime are presented in Figures 2 and 3, respectively, while the superimposition with other top five phenolics is presented in Figure S2. Furthermore, a set of non-β-lactam conventional antibiotics was used as decoy compounds against PBP3 of *P. aeruginosa* and interestingly, all of the decoy compounds had a docking score that was less the −3 kcal/mol, suggesting their inability to bind to PBP3.

Table 1. Binding affinity and ADMET properties of top five phenolics against PBP3 of *P. aeruginosa*.

Ligands zinc code	Popular name	B A (kcal/mol)	MW <500 (g/mol)	HB-A ≤ 10	HB-D ≤ 5	Log $P_{o/w}$ ≤ 5	RT-B ≤ 9	LV < 2	WS	GI - A	BS	pgp	Inhibitor of CYP 450s									
													CYP 1A2	CYP 2C19	CYP 2C9	CYP 2D6	CYP 3A4	H	C	IM	M	CY	TC	SA
Cefotaxime	Cefotaxime	−9.0	455.47	9	3	−0.27	9	N	VS	L	0.11	N	N	N	N	N	N	I	I	I	I	I	6	4.79
ZINC04214317	Silicristin	−10.4	482.44	10	6	1.47	4	N	S	L	0.55	N	N	N	N	N	Y	I	I	A	I	I	4	4.88
ZINC95486076	Chroman-4-one	−9.8	356.37	6	3	3.42	3	N	MS	H	0.55	N	Y	N	Y	N	Y	I	I	A	I	I	4	3.83
ZINC03978503	Epicatechin gallate	−9.3	442.37	10	7	1.04	4	N	S	L	0.55	N	N	N	N	N	N	I	I	I	I	I	4	4.16
ZINC14642804	Catechin-3-rhamside	−9.2	258.31	3	0	3.02	2	N	S	H	0.55	Y	N	N	N	Y	N	I	I	A	I	I	6	4.09
ZINC71621503	Propan-2-one	−9.2	458.46	7	6	3.84	6	N	MS	L	0.55	N	N	N	Y	N	Y	I	I	I	I	I	4	3.67

ADMET: absorption, distribution, metabolism, excretion, and toxicity, BA: Binding affinity; MW: Molecular weight; HB-D: Hydrogen bond donor; HB-A: Hydrogen bond acceptor; RT-B: rotatable bond; Log $P_{o/w}$: Partition coefficient; GI- A: Gastrointestinal absorption; Pgp: Permeability glycoprotein substrate WS: Water solubility; CYP: Cytochrome; S: Soluble; VS: very soluble; MS: Moderately soluble; Y: Yes; N: No; BS: Bioavailability score; I: A: Active; Inactive; L: low; LV: Lipinski violations; H: Hepatotoxicity; IM: Immunotoxicity; M: Mutagenicity; C: Carcinogenicity CY: Cytotoxicity; TC: Toxicity class; LD: Lethal dose; SA: Synthetic accessibility; Chroman-4-one (2S)-5,7-dihydroxy-2-[3-hydroxy-4-methoxy-5-(2-methylprop-1-enyl)phenyl]chroman-4-one; Propan-2-one: (1 R,3S)-1,3-diphenyl-1,3-bis(2,4,6-trihydroxyphenyl)propan-2-one.

2.4. Pharmacokinetic properties prediction of hit phenolics

In this study, the SwissADME web (http://swissadme.ch/index.php) and Molinspiration (https://www.molinspiration.com/cgi-bin/properties) toolkits were used for robust prediction of the physicochemical properties, pharmacokinetics, drug-likeness, and medicinal chemistry friendliness of hit phenolics, while the toxicological profiles were evaluated using the Protox II webserver (https://tox-new.charite.de/protox_II/). Taken together, the findings from these analyses were used to further screen the identified top 20 phenolics down to five.

2.5. Molecular dynamic (MD) simulations of top five hit phenolics

The MD simulation was done as earlier reported (Aribisala et al., 2022). Briefly, the AMBER 18 package was used, and the simulation was performed over a 120 ns period. The operating systems were described using the FF18SB variant of the AMBER 18 package. Likewise, the ligands' atomic partial charges were created using the ANTECHAMBER by exploiting the GAFF (general amber force field) measures and RESP (restrained electrostatic potential). The Leap Module's Na^+, hydrogen atoms, and Cl^- counter ions were utilized in neutralizing the systems. In each case of the simulation, the numbering of the amino acid residues was done appropriately, and the systems were suspended inside a TIP3P orthorhombic box of water molecules to ensure that all atoms were inside an 8 Å of box edge. For each simulation, an initial minimization of 2000 steps was performed using a restriction potential of 500 kcal/mol. They were performed for 990 steps using the steepest descent technique, followed by 990 steps using conjugate degrees. The conjugate gradient approach was used to perform an additional 990 steps of full (unlimited) minimization. Heating MD simulations from 0 to 300 K (gradual) were run for 50 ps with the systems maintaining a constant number of atoms and volume. The solutes in the systems have a potential harmonic restraint of 10 kcal/mol and a collision frequency of 1.0 ps. Subsequently, each system was equilibrated for about 500 ps while the operating temperature was kept constant at 300 K. Using the SHAKE algorithm, the hydrogen bonds atom in each simulation were restrained. The simulation in each case had a 2 fs step size, which matched with the NPT (isobaric–isothermal ensemble) with randomized seeding, the temperature of 300 K, constant pressure of 1 bar, and pressure-coupling constant of 2 ps (Langevin thermostat). Subsequently, the results of the 120 ns MD simulation were used as post-dynamic data.

2.6. Post-dynamic analysis

The post-dynamic analysis was carried out by saving the systems' coordinates and trajectories during the simulation period and later analyzing them post-simulation using the PTRAJ module of the AMBER 18 package. Exploiting the CPPTRAJ module of the same package, the analysis of root mean square fluctuation (RMSF), the radius of gyration (ROG), root means square deviation (RMSD), and solvent-accessible surface area (SASA) were carried out and their plots were

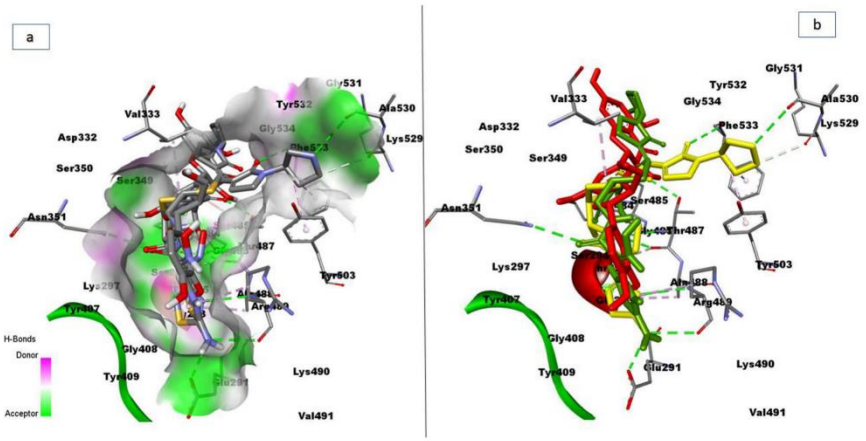


Figure 2. Superimposition of 6VJE experimental native inhibitor (Ceftobiprole) with docked native inhibitor and silicristin using AutoDock vina of the Python Prescription program, which demonstrates the same binding orientation for the docked native inhibitor and silicristin and a partial binding site for the docked compounds (native inhibitor and silicristin) and experimental native inhibitor. (a) Showed different atoms of the ligands with the green portions of the proteins being hydrogen donor regions while the purple portions are acceptors of hydrogen bonds. (b) Showed the various amino acid residues of PBP3 interacting with silicristin (red), docked native inhibitor (green), and experimental native inhibitor (yellow) following optimal superimposition.

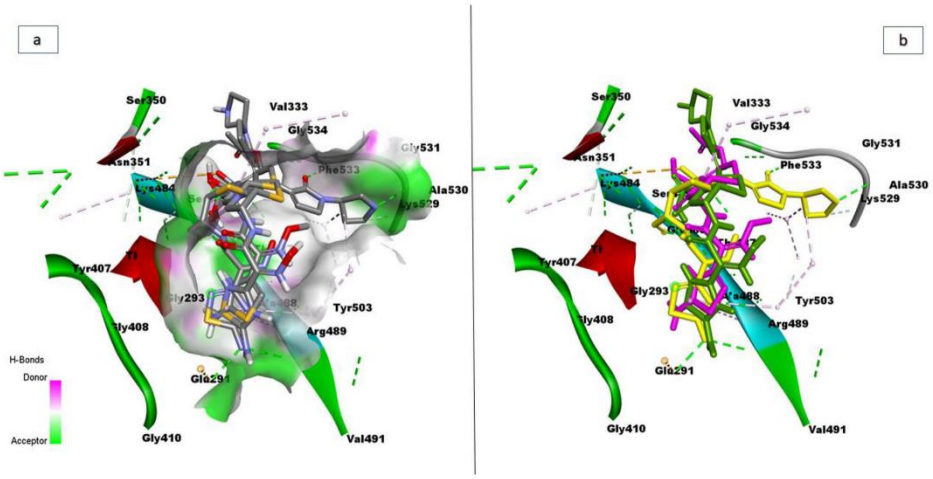


Figure 3. Superimposition of 6VJE experimental native inhibitor (Ceftobiprole) with docked native inhibitor and cefotaxime using AutoDock vina of the Python Prescription program, which demonstrate the same binding orientation for the docked native inhibitor and silicristin and a partial binding site for the docked compounds (native inhibitor and cefotaxime) and experimental native inhibitor. (a) Showed different atoms of the ligands with the green portions of the proteins being hydrogen donor regions while the purple portions are acceptors of hydrogen bonds. (b) Showed the various amino acid residues of PBP3 interacting with cefotaxime (purple), docked native inhibitor (green), and experimental native inhibitor (yellow) following optimal superimposition.

generated using Origin v 6.0 (Aribisala et al., 2021). Likewise, using the Molecular Mechanics/GB Surface Area (MMGBSA) approach, the binding free energy was estimated using an average among 100,000 snapshots taken from a 120 ns MD simulation trajectory using the equation $\Delta G_{bind} = G_{complex} - (G_{Receptor} + G_{ligand})$. The PBP3-ligand plots, which indicate molecular interactions between ligands and amino acid residues at the PBP3 active site, were identified from the final complexes obtained and visualized with Discovery Studio v21.1.0 which have adopted a MdmDiscoveryScript to provide functions, properties, constants, and data structures.

3. Results and discussion

3.1. Hierarchical screening of phenolics against PBP3 of Pseudomonas aeruginosa

Due to the large number of phenolics currently known, a preliminary structure-based virtual screening was carried out in which a consensus phenolics pharmacophore and the PBP3 druggable target of *P. aeruginosa* was employed in identifying phenolics that established prominent affinity for PBP3 of *P. aeruginosa*. Structure-based screening for hits enables the use of a well-defined pharmacophore to describe

the spatial arrangements of specific features for screening (Koes & Camacho, 2012). Using this technique, promising lead candidates for drug discovery have been identified, and in this study, a total of 1510 phenolics that showed an affinity for PBP3 of *P. aeruginosa* were observed (Figure S1). Further screening of these compounds for leads with a better affinity for PBP3 of *P. aeruginosa* was done using the molecular docking method. Molecular docking enables the measurement of the pose and affinity of a compound at the active site of a protein, and the higher the negative score, the better the pose and interaction of the compound with the protein (Kitchen et al., 2004). In this study, following sorting of the docked 1510 compounds based on their binding affinity for PBP3 of *P. aeruginosa*, the top 20 hits had negative binding scores ranging from −9.2 to −10.4 kcal/mol (Table S2), which were higher than those of the control β-lactams (amoxicillin, cefotaxime, aztreonam, and doripenem), which ranged from −8.2 to − 9.0 kcal/mol (Table S2) with cefotaxime having the highest negative binding score among the controls and hence was selected as the reference standard for subsequent analyses. The observation that the top 20 hit phenolics had higher docking scores than the reference β-lactams used in this study could be a pointer to their prospective affinity for PBP3 of *P. aeruginosa* and an indication of the effectiveness of the structure-based pharmacophore used. This observation is consistent with the view of Koes and Camacho (2012), who reported on the advantage of structure-based pharmacophores over ligand-based pharmacophores in hits-target specificity and applicability screening.

The top 20 phenolics were further screened for their pharmacokinetics, drug-likeness, toxicity profile, and feasibility to be synthesized for enhanced druggability against PBP3 of *P. aeruginosa*. Only nine of the 20 compounds [ZINC04214317, ZINC13775871, ZINC03793048, ZINC34953149, ZINC34953150, ZINC95486076, ZINC03978503, ZINC14642804, and ZINC71621503] (Table S2) passed the Lipinski rule of 5, which states that the limit of a hydrogen donor, hydrogen acceptor, molecular weight, and octanol coefficient to be $\leq$5, $\leq$10, $<$500 g/mol, and $<$5, respectively (Lipinski et al., 2001). These limits are important to ensure that the screened phenolics will be bioavailable to reach druggable targets in the body in a sufficient concentration for pharmacological effects to take place. Of these nine compounds, five were conformers of silicristin (Table S2), and as such, the best conformer of silicristin (ZINC04214317) with the highest affinity for PBP3 of *P. aeruginosa* was selected with the remaining four hits to constitute the top five hit phenolics. The cytochrome P450 (CYP) isoenzymes are important determinants of drug toxicity because they play an important role in drug metabolism (Verma et al., 2020). In this study, of the five compounds, only epicatechin gallate (ZINC71621503) (Table 1) was observed to be a non-inhibitor of all the CYP isoenzymes, with others as inhibitors of one or two of the isoenzymes (Table 1). This observation shows that epicatechin gallate will not result in drug-drug interaction when co-administered with other drugs being metabolized by these isoenzymes. Interestingly, all five compounds were predicted as non-hypertoxic, non-carcinogenic, non-mutagenic, and non-cytotoxic, with only epicatechin gallate being non-immunogenic (Table 1). However, since the synthetic scores of all the compounds were less than the synthetic limit of 5 (Table 1) (Ertl & Schuffenhauer, 2009), it indicates that they can be easily structurally modified for enhanced druggability with lesser toxicity profiles. Furthermore, based on the lethal dose 50 (LD_{50}) and the toxicity class, the compounds stand the chance of being considered drugs as they all belong to toxicity class 4 and above (Table 1), which are ideal for drug development (Verma et al., 2020). Generally, the characteristics employed in this study for screening have been shown to be important in drug development to drastically reduce the fraction of toxicological and pharmacokinetics-related failures in the preclinical and clinical phases (Lipinski et al., 2001; Verma et al., 2020). Also, as further optimization of the lead is necessary for improved druggability, having a top five leads with a feasible synthetic score will enable drug optimization in the latter phase of drug development.

3.2. MD Simulation of top five hit phenolics at PBP3 active site

One of the key characteristics of potent antimicrobial drugs is their ability to bind efficiently with therapeutically important targets in bacterial cells, and the β-lactams are not an exception (Pang et al., 2019). The binding efficiency, flexibility, and stability of the five phenolics with the *P. aeruginosa* PBP3 active site were further investigated in this study using MD simulation. This was important to complement the molecular docking, which does not permit protein flexibility during ligand binding and hence only returns scores for surface interaction with the protein active site using a simple scoring function (Nasution et al., 2018; Ramirex & Caballero, 2016). On the other hand, MD simulation allows for the measurement of negative free binding energy, RMSD, ROG, and RMSF as metrics for binding affinity, complex stability, protein compactness, and flexibility, respectively, over a specific evaluation period (Verma et al., 2020). Similar to the docking score, the higher the free binding energy, the better the interactions,

Table 2. Binding free energy scores of top five phenolics against PBP3 of *P. aeruginosa*.

Components of energy (kcal/mol)						
Target	Ligands	Δ E_{vdW}	ΔE_{elec}	ΔG_{gas}	ΔG_{solv}	ΔG_{bind}
P. aeruginosa PBP3 +	Cefotaxime	−30.79 ± 4.39	−15.76 ± 7.35	−46.55 ± 9.24	27.82 ± 6.36	−18.72 ± 4.45
	Silicristin	−34.63 ± 4.72	−16.57 ± 8.68	−51.22 ± 9.57	27.55 ± 5.72	−23.66 ± 5.32
	Chroman-4-one	−31.94 ± 4.00	−15.90 ± 6.64	−47.85 ± 8.29	23.95 ± 4.90	−23.89 ± 4.78
	Epicatechin gallate	−26.60 ± 6.42	−16.42 ± 11.06	−43.02 ± 12.65	25.50 ± 7.96	−17.52 ± 5.55
	Catechin 3-rhamside	−40.79 ± 3.79	−20.90 ± 8.04	−61.70 ± 8.82	32.71 ± 5.71	−28.99 ± 5.09
	Propan-2-one	−31.57 ± 5.87	−19.84 ± 10.81	−51.42 ± 12.21	30.26 ± 7.57	−21.15 ± 6.56

ΔE_{vdW}: van der Waals energy; ΔG_{bind}: total binding free energy; ΔE_{gas}: gas phase free energy; ΔE_{elec}: electrostatic energy; ΔG_{sol}: solvation free energy.

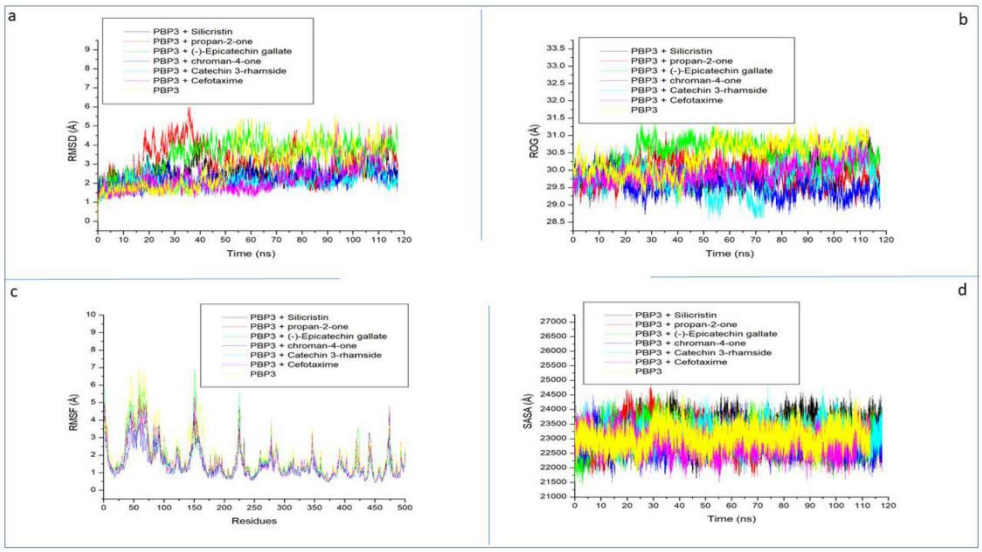


Figure 4. Comparative (a) root mean squared deviation (RMSD), (b) radius of gyration (ROG), (c) root mean squared fluctuation (RMSF), and (d) solvent-accessible surface area (SASA) plots of alpha-carbon, top five phenolics, and cefotaxime against PBP3 of *P. aeruginosa* over a 120 ns MD simulation period.

Table 3. RMSD, ROG, RMSF, and SASA values of top five phenolics against PBB3 of *P. aeruginosa*.

Target	Ligands	RMSD (Å)	RMSF(Å)	ROG (Å)	SASA (Å)
P. aeruginosa	Unbound	2.88 ± 1.10	1.23 ± 0.05	30.39 ± 0.44	23371.92 ± 354.72
PBP3 +	Cefotaxime	2.24 ± 0.70	0.97 ± 0.04	29.95 ± 0.29	22857.68 ± 330.34
	Silicrhistin	2.56 ± 0.50	0.89 ± 0.04	29.89 ± 0.34	23277.40 ± 405.85
	Chroman-4-one	2.24 ± 0.42	0.77 ± 0.03	29.56 ± 0.28	22899.97 ± 325.78
	Epicatechin gallate	3.46 ± 0.82	1.13 ± 0.05	30.33 ± 0.36	23072.11 ± 398.59
	Catechin-3-rhamside	2.14 ± 0.43	0.96 ± 0.04	29.80 ± 0.42	23124.46 ± 336.57
	Propan-2-one	3.04 ± 0.86	0.98 ± 0.04	29.98 ± 0.35	23052.20 ± 428.21

and in this study, the five phenolics, except for epicatechin gallate (−17.52 kcal/mol), had a negative free binding energy higher than cefotaxime (−18.72 kcal/mol), with catechin-3-rhamside (−28.99 kcal/mol) having the highest affinity (Table 2). This observation agrees with the results of the docking score, which shows the hit phenolics had a potential affinity for PBP3 of *P. aeruginosa* but, as expected, differed in their ranking of affinity for the target. While molecular docking ranked silicristin (−10.4 kcal/mol) as the compound with the best affinity for PBP3, catechin-3-rhamside was observed with the best affinity and probable better stability with PBP3 after the 120 ns simulation period. This observation further underscores the importance of MD simulation and the duration of simulation in identifying potential drug candidates for drug development, as earlier noted by Verma et al. (2020). Further insight into complex stability, protein compactness, and amino acid residue flexibility was carried out. This was important due to the flexible nature of MD simulation, which allows for protein conformational changes following ligand binding, which in turn has been demonstrated to either enhance or inhibit protein biological functions. To examine these characteristics, parameters such as the RMSD, ROG, and RMSF measured over a 120 ns simulation period are presented in Figure 4 for unbound PBP3 and bond complexes (PBP3 + top five phenolics and cefotaxime).

The RMSD is a measure of the extent of stability of a complex, and the lower the RMSD value, the better the stability (Aribisala et al., 2021). In this study, the top five phenolics had an average RMSD value within a deviation limit of <3.0 Å (Aribisala et al., 2021; Ramirex & Caballero, 2016) with values ranging from 2.14 to 3.46 Å (Table 3), indicating the potential and general stability of the compounds with PBP3 of *P. aeruginosa*. Three of the compounds [catechin-3-rhamside (2.14 Å), silicristin (2.56 Å), and chroman-4-one (2.24 Å)] and the standard [cefotaxime (2.24 Å)] had lower RMSD value than the unbound PBP3 (2.88 Å) (Table 3), indicating their capability to promote increased structural stability of PBP3. This observation is in correlation with the findings of Sainsbury et al. (2011), who demonstrated experimentally that the binding of β-lactam antibiotics (carbenicillin and ceftazidime) to purified PBP3 increases the thermostability of PBP3 through local conformational changes at the active site. The fact that catechin-3-rhamside had a marginally lower RMSD value than cefotaxime indicates its relative superiority over cefotaxime as a PBP3 inhibitor. Interestingly, this observation is in agreement with the energy component profile where catechin-3-rhamside had the best binding affinity for PBP3, which is tantamount to better structural stability and compactness of the resulting complex. A similar pattern was also observed with epicatechin

gallate (3.46 Å) whose significantly higher RMSD value was proportional to the significantly lower affinity for PBP3 observed in this study. Also, in the RMSD plot (Figure 4a), as expected, the system was observed to equilibrate during the first 20 ns of the simulation, during which there was slight fluctuation instability. However, between 20 and 35 ns, a high fluctuation instability was observed, especially for propan-2-one, catechin-3-rhamside, and silicristin. After 35 ns, the system then maintains a stable fluctuation throughout the simulation period for all the compounds, cefotaxime, and the unbound PBP3, which further corroborates the reason for the lower RMSD value observed in this study for all tested compounds, which was the good deviation limit of <3.0 Å (Ramirex & Caballero, 2016). This observation is in agreement with the work of Alhadrami et al. (2020), where flavonoids were able to achieve stability at the active site of *Staphylococcus aureus* PBP2a. The ROG is another metric that measures the total compactness of a complex, and the higher the ROG value, the lesser the complex folding with conformational entropy (Sabiu et al., 2021). Unlike the RMSD results, all the phenolics had ROG values that were marginally lower than the unbound PBP3 (30.39 Å) (Table 3 and Figure 4b). The average ROG value for the phenolics was 29.90 Å with values ranging from 29.80 Å to 30.33 Å (Table 3 and Figure 4b), which indicates that PBP3 became generally more compact in the bound state with the five phenolics than when in the unbound state. Among the compounds, catechin-3-rhamside (29.80 Å) had the lowest ROG value, which was marginally lower than 29.95 Å for cefotaxime (Table 3 and Figure 4b), further suggesting its advantage as a potential lead and novel inhibitor of PBP3 of *P. aeruginosa*, as this was also consistent with the observations with RMSD, and the energy component profile observed in this study. Generally, while a little variance (0.53 Å) in ROG exists between the top five leads and cefotaxime following binding of PBP3, which could mean ligand binding had no differential effect in ranking the hit, findings from the binding affinity and stability in this current study have showcased the potential affinity of the top five phenolics for PBP3 of *P. aeruginosa,* with catechin-3-rhamside having a slightly better advantage as the lead compound.

The structural flexibility of amino acid residues at the active site of PBP3 of *P. aeruginosa,* measured as RMSF, was further evaluated and as expected, the RMSF values of the active site amino acid residues (Table 4) were higher than the average RMSF values observed for the whole protein (Table 3, Figure 4c). The unbound PBP3, cefotaxime, silicristin, chroman-4-one, epicatechin gallate, catechin-3-rhamside, and propan-2-one had RMSF values of 1.39 and 1.23 Å, 1.07 and 0.97 Å, 1.04 and 0.89 Å, 0.95 and 0.77 Å, 1.11 and 1.13 Å, 1.05 and 0.96 Å, and 1.12 and 0.98 Å, respectively, at the active site and in the whole protein (Tables 3 and 4). This observation indicates more fluctuations of amino acid residue at the active site when compared to other parts of the protein. High fluctuations of residues indicate more flexibility and unstable bonds, while low fluctuations, on the other hand, mean less flexibility and more structural stability (Mousavi et al., 2021). Residues Tyr329, Ser349, and Tyr498 contributed the most to the high fluctuation at the protein's active site during the 120 ns simulation period (Table 4). However, compared to the RMSF of unbound PBP3, the observed lower RMSF value observed at the active site and in the whole PBP3 when bound with the five phenolics and cefotaxime indicates the potential affinity of these compounds for PBP3 as this suggests their capability to reduce flexibility and form stable bonds with PBP3 amino acid residues. The lowest RMSF values at both the active site and in the whole protein were observed with chroman-4-one at 0.95 and 0.77 Å, respectively, (Tables 3 and 4), while the highest RMSF values at the active site and in the whole protein were observed with propan-2-one and epicatechin gallate, respectively. Chroman-4-one having the lowest RMSF value, suggestive of its better capability to form stable bonds with the PBP3 active site, though significant, is not entirely in agreement with the energy component profile, RMSD, and ROG findings of this study, which show catechin-3-rhamside to be the best in terms of potential affinity for PBP3. However, catechin-3-rhamside's ability to stabilize the amino acid flexibility at both the active site and in the whole protein is much better than the effect shown by cefotaxime, and the remaining phenolics follow this pattern. In addition, in accordance with the energy component profile, RMSD, and ROG findings, epicatechin gallate had the highest RMSF value in this study, indicating its lesser potential affinity for PBP3 of *P. aeruginosa* when compared to the other phenolics studied.

The solvent-accessible surface area (SASA) is another significant index that examines protein folding and the changes

Table 4. PBP3 active site average RMSF (Å) when bonded with top five phenolics.

	Top five phenolics						
PBP3 active site amino acid residue	Unbound PBP3	Cefotaxime	Silicrhistin	Chroman-4-one	Epicatechin gallate	Catechin 3-rhamside	Propan-2-one
Ser294	1.26	0.96	0.94	0.91	1.05	0.90	1.02
Lys297	1.22	0.92	0.85	0.78	1.15	0.85	1.13
Tryr329	1.55	1.74	1.24	1.42	1.31	1.30	1.29
Ser349	2.12	1.55	1.54	1.27	1.61	1.75	1.80
Asn351	1.88	1.33	1.37	1.10	1.45	1.55	1.72
Tyr407	1.29	0.96	0.97	0.89	0.98	0.95	0.92
Tyr409	0.95	0.73	0.71	0.65	0.72	0.71	0.72
Lys484	0.84	0.64	0.71	0.66	0.78	0.67	0.76
Ser485	1.18	0.86	0.95	0.86	0.96	0.92	0.95
Tyr487	1.11	0.81	0.86	0.74	0.89	0.81	0.87
Arg489	1.33	0.95	1.02	0.82	0.96	0.92	1.00
Tyr498	1.90	1.32	1.34	1.27	1.45	1.31	1.30
Active site average RMSF	1.39	1.07	1.04	0.95	1.11	1.05	1.12

in a protein's surface area during simulation, with higher SASA values indicating an increase in surface area and lower SASA values indicating a decrease in protein volumes (Mousavi et al., 2021). In this study, the binding of the five phenolics and cefotaxime marginally reduced the SASA value when compared to the unbound PBP3, with a SASA value of 23371.92 Å (Table 3 and Figure 4d). Cefotaxime, silicristin, chroman-4-one, epicatechin gallate, catechin-3-rhamside, and propan-2-one had SASA values of 22857.68, 23277.40, 22899.97, 23072.11, 23124.46, and 23052.20 Å (Table 3 and Figure 4d), respectively. This observation suggests that more of the residues in the unbound state are sticking out to the solvent, indicating protein compactness. This agrees with the findings observed with other simulation metrics (RMSD, ROG, and RMSF) studied in this work and also corroborates the findings of Mousavi et al. (2021), who reported that the interactions of ligands with proteins can have a significant impact on SASA value. Chroman-4-one had the lowest SASA value (22899.97 Å) among the five compounds when bound with PBP3, indicating fewer available PBP3 residues for solvent interaction, which supports the RMSF findings that chroman-4-one demonstrated less residue fluctuation at both the active site and throughout the protein. Contrary to this trend and the findings of RMSD, ROG, and free binding energy is the marginally lower SASA value observed with cefotaxime (22857.68 Å) in this study when compared to catechin-3-rhamside (23124.46 Å), suggesting cefotaxime's better ability to prevent PBP3 molecules from interacting with the solvent. However, with a negligible variance of 420 Å of SASA between the top five lead phenolics and cefotaxime following the binding of PBP3, it could be inferred that the compounds binding of PBP3 had little or no effect on the SASA value of PBP3 and thus had no differential effect in ranking the best hit and observation that was also true for the ROG result of this study.

The potential of a ligand for a receptor has been demonstrated to depend on the type of interaction existing between them (Izadi et al., 2014; Kataria et al., 2021; Uhomoibhi et al., 2022). Hence, in this study, the interactions plot of the top five phenolics as well as cefotaxime with the active site amino acid residues of PBP3 were further analyzed and are presented in Figures 5 to 10. The interactions between the compounds and the active site amino acid residues of PBP3 after 120 ns of the simulation were hydrogen bonds (conventional, π-donor, and carbon), Van der Waals, π-π t-cation, π-π t-shaped, π-π t-stacked, π-alkyl, alky, π-Sulphur as well as few unfavorable acceptor-acceptor and donor-donor interactions (Figures 5 to 10). The type, bond length, and a number of interactions differed from one compound to the other and were observed to have significant effects on the stability and free binding energy obtained in this study. Cefotaxime had the highest number of interactions with PBP3 but with a significantly higher bond length when compared to those formed with the five investigated compounds, except for epicatechin gallate and propan-2-one. Cefotaxime formed 20 interactions with an average bond length of 4.91 Å with the active site amino acid of PBP3 (Table 5), of which 8 interactions were Van der Waals [Tyr498, Ala488, Tyr503, Ile347, Lys348, Val471, Gly535, and Lys484], 8 were hydrogen bonds [Arg489, Thr487, Asn351, Ser294, Gly486, Ser349, and Ser485(2)], 1 was π-π stacked [Tyr409], 1 was π-alkyl [Val33], 1 was alky bond [Phe533] and 1 π-Sulphur [Tyr407] (Figure 5). The observation that cefotaxime had the highest number of interactions with PBP3 does not directly correlate with the free binding energy observed with the compound when complexed with PBP3. However, the observed longer bond length of interactions between cefotaxime and PBP3 could have significantly reduced the effect of the interactions formed. This observation is in agreement with the findings of Du et al. (2016), who

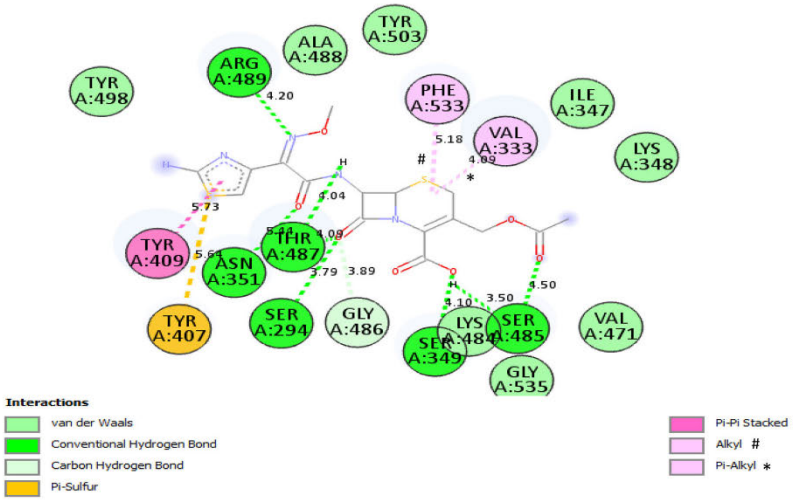


Figure 5. 2D interaction types and plots between cefotaxime and active site of PBP3 of *P. aeruginosa*.

Table 5. Average bond length, nature, and number of interactions between the active site amino acid residues of PBP3 and top five phenolic compounds after 120 ns.

Top-ranked compounds	Total number of interactions (average distance)	Number of hydrogen bonds (average distance) and interaction residues	Other important interactions and residues	Unfavorable bonds
PBP3				
Cefotaxime	20 (4.91)	9 (4.20) [Arg489, Asn351 (2), Thr487, Ser294, Ser349, Ser485 (2), Gly486]	4 (5.32) [Tyr409, Tyr407, Phe533, Val333]	None
Epicatechin gallate	18 (4.97)	6 (4.8) [Ser349, Arg489, Arg331, Thr329 (2), Tyr407]	5 (5.48) [Tyr498, Tyr409, Val333, Arg331, Arg489]	None
Catechin-3-rhamside	17 (3.62)	3 (3) [Thr329, Asn351, Tyr409]	4 (4.81) [Val333 (2), Arg331, Tyr407]	1(Thr487)
Silicristin	17 (3.90)	5 (2.56) [Thr487(2), Arg489, Arg331, Asn351]	2 (4.83) [Val33(2)]	None
Chroman-4-one	19 (3.48)	5 (2.55) [Ser485(2), Lys484, Ser349, Asn351]	4 (4.89) [Phe533, Val333 (2), Arg289]	1 (Tyr409)
Propan-2-one	18 (5.63)	3 (5.73) [Tyr407, Tyr409, Arg489]	5 (5.56) [Tyr498,Tyr409, Val333, Arg331 (2)]	None

reported that binding affinity could be attributed to the difference in interaction bond length. A shorter bond length indicates a more stable bond and a stronger pull between two entities where their atoms are held together more tightly. A similar trend was also observed with the interactions formed between epicatechin gallate and PBP3. Epicatechin gallate formed 18 interactions with an average distance of 4.97 Å with the active site amino acid residues of PBP3 (Table 5), of which 7 interactions were Van der Waals [Ala488, Asn351, Ser294 Lys297, Phe533, Ile330, and Thr404], 6 interactions were hydrogen bonds [Tyr407, Tyr329 (2), Arg331, Arg489, and Ser349], 2 were π-π t-shaped [Try498 and Tyr409], 1 was π-π stacked [489] 1 π-alkyl [Arg489] and a π-π t-cation [Arg331] (Figure 6). This number of interactions observed between epicatechin gallate and PBP3 was marginally higher than those observed with catechin-3-rhamside [17 interactions with an average distance of 3.62 Å with the active site of PBP3 (Table 5) out of which 9 interactions were Van der Waals (Gly486, Tyr503, Asp332, Arg489, Ile330, Ser349, Lys297, Gly293, and Ser294), 3 were hydrogen bonds (Thr329, Asn351 and Tyr 409), 1 was π-π t-shaped (Tyr407), 2 were π-alkyl (Arg331 and Val333), 1 was alky interaction (Val333) and 1 was unfavorable donor-donor interaction (Thy 487)] (Figure 7) and silicristin [17 interactions with an average distance of 3.90 Å with the active site of PBP3 (Table 5) out of which 9 interactions were Van der Waals [Tyr532, Tyr503, Phe533, Tyr407, Asn351, Ser294, Ser349, Ser485, and Lys484], 5 were hydrogen bonds [Thr487 (2), Arg489, Arg331, and Thr487] while 2 were π-alkyl [Val33(2)] (Figure 8) and thus does not directly correlate with the free binding energy obtained in this study. However, similar to what was observed with the cefotaxime-PBP3 complex, the higher bond length between epicatechin gallate and PBP3 could have significantly lowered its binding affinity when compared to catechin-3-rhamside and silicristin, with lesser interaction but with significant binding affinity. Further corroborating the importance of bond length on free binding energy observed in this study is the higher bond length of interaction observed with epicatechin gallate relative to cefotaxime, which explains why epicatechin gallate was the only compound with lesser free binding energy relative to cefotaxime in this study. The observation that chroman-4-one had a marginally lesser interaction than cefotaxime and interactions that are similar to epicatechin gallate does not entirely justify its significantly higher free-binding energy relative to these two compounds. However, chroman-4-one's significantly lower bond length of interactions relative to these two compounds could have contributed to its stable bond interaction and a stronger pull with PBP3, hence resulting in its higher free binding energy against PBP3. Chroman-4-one formed 19 interactions with an average bond length of 3.48 Å with the active site of PBP3 (Table 5) out of which 9 interactions were Van der Waals [Val471, Gly535, Gly486, Tyr532, Ser294, Tyr503, Ser334, Tyr409, and Tyr407], 5 were hydrogen bonds [Ser485 (2), Lys484, Tyr487, and Asn351], 2 were π-alkyl [Arg489 and Val33], 2 were alkyl [Val33 and Phe533] and 1 was an unfavorable donor-donor interaction [Asn351] (Figure 9). Similarly, propan-2-one had a higher number of interactions than catechin-3-rhamside and silicristin but with a significantly higher bond length. Propan-2-one formed 18 interactions with an average distance of 5.63 Å with the active site of PBP3 (Table 5) out of which 10 interactions were Van der Waals [Phe533, Tyr532, Tyr503, Thr487, Lys297, Ser349, Ala 488, Ser294, Ile330, Thr404], 3 were hydrogen bonds [Tyr409, Tyr407Arg489], 2 were π-π t-shaped [Tyr498 and Tyr409], 1 was π-π stacked [Arg489] while 2 were π-alkyl [Val33 and Arg331] (Figure 10).

In this study, except for the π-π t-shaped bond observed in the interaction plot of catechin-3-rhamside and silicristin (Figures 7 and 8), other important interactions such as hydrogen bonds (conventional, π-donor, and carbon), Van der Waals, π-π t-stacked, π-alkyl and alky interactions observed in the cefotaxime plot (Figure 5) were also observed in study compounds that have significantly higher free binding affinity than cefotaxime. However, the presence of these important bonds in cefotaxime, despite their higher bond lengths, may have contributed to cefotaxime's higher stability for PBP3 relative to silicristin, propan-3-one, and epicatechin gallate observed in this study. While the presence of π-π t-shaped bond in the interaction plot of epicatechin gallate (Figure 6) which has a significantly lower free binding energy relative to catechin-3-rhamside and silicristin indicates the

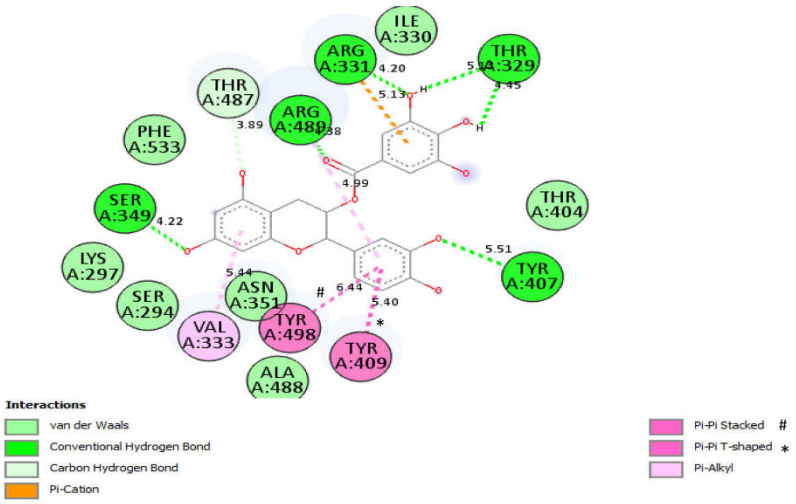


Figure 6. 2D interaction types and plots between epicatechin gallate and active site of PBP3 of *P. aeruginosa*.

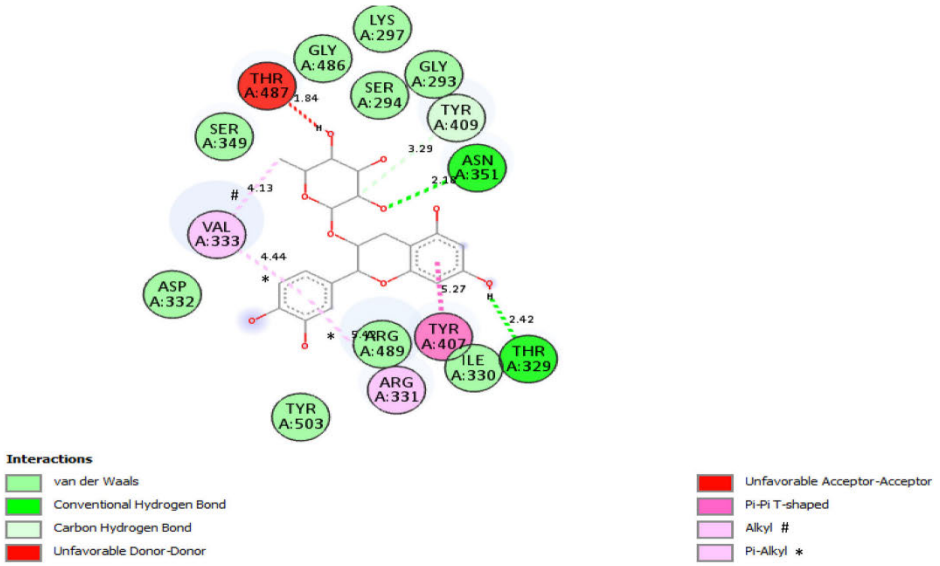


Figure 7. 2D interaction types and plots between catechin-3-rhamside and active site PBP3 of *P. aeruginosa*.

negligible effect of the presence of the bond in contributing to the higher affinity observed with catechin-3-rhamside and silicristin for PBP3 relative to cefotaxime observed in this study. Also, the presence of some unfavorable donor-donor and acceptor-acceptor interactions in the interaction plot of chroman-4-one and catechin-3-rhamside, respectively, were observed to have a minor effect on the affinity and stability of these compounds for PBP3, if their higher free binding energy, lower RMSD, RMSF, and SASA values observed in this study are taken into consideration. This, however, provides a clue to some strategic portion of the ligand that could be further modified for better affinity and stability for the protein. In PBP3 of *P. aeruginosa*, the C-terminal transpeptidase cross-linking domain harbored the conserved catalytic residue Ser294 residue, which has been demonstrated to facilitate the binding of peptidoglycan precursor (D-alanyl-D-alanine) and β-lactams (Kumar et al., 2020). In this study, this important catalytic residue established Van der Waals's interaction with all five investigated phenolics (Figures 6 to 10). This observation is coherent with the experimental study of Sainsbury et al. (2011) where different β-lactam antibiotics such as carbenicillin, and ceftazidime were co-crystalized

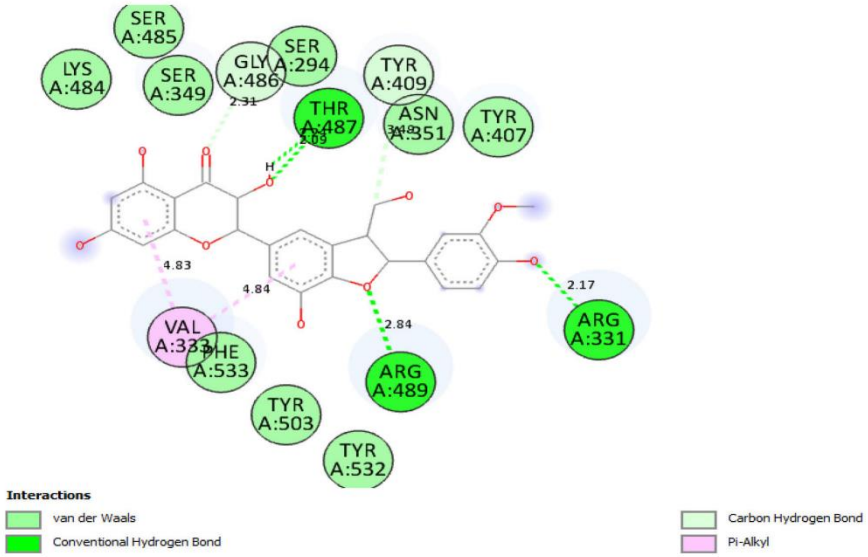


Figure 8. 2D interaction types and plots between silicristin and active site of PBP3 of *P. aeruginosa*.

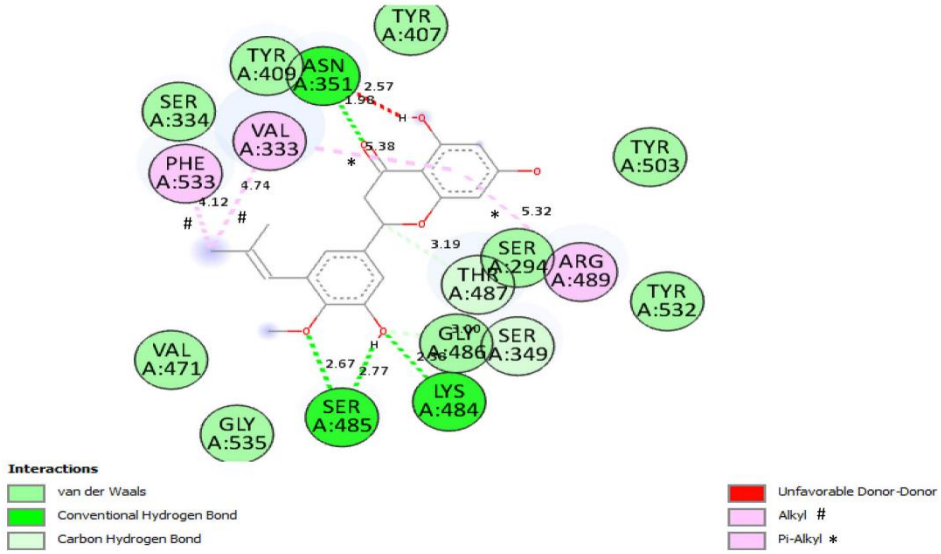


Figure 9. 2D interaction types and plots between chroman-4-one and active site of PBP3 of *P. aeruginosa*.

with PBP3 of *P. aeruginosa* and interacted with Ser294, suggestive of a similar binding pattern of the top five phenolics to the conserved binding mode of β-lactam antibiotics. Ser294 had a relatively lower fluctuation when compared to the average fluctuation of all the amino acids at the active site of PBP3 during the simulation and had the least fluctuation with catechin-3-rhamside (0.90 Å) and the highest fluctuation with epicatechin gallate (1.05 Å) (Table 4). This observation further corroborates the observed stability and affinity of the five phenolics, especially catechin-3-rhamside for PBP3, as lower fluctuations imply more stability. On the other hand, only cefotaxime interacted with Ser294 via a hydrogen bond (Figure 5), with a fluctuation of 0.96 Å, which was slightly higher than that observed with catechin-3-rhamside (0.90 Å). Hydrogen bonds are stronger bonds relative to Van der Waals force Izadi et al., 2014. The fact that only cefotaxime interacted via hydrogen bond with Ser294 of PBP3 could have contributed to its observed higher stability relative to epicatechin gallate,

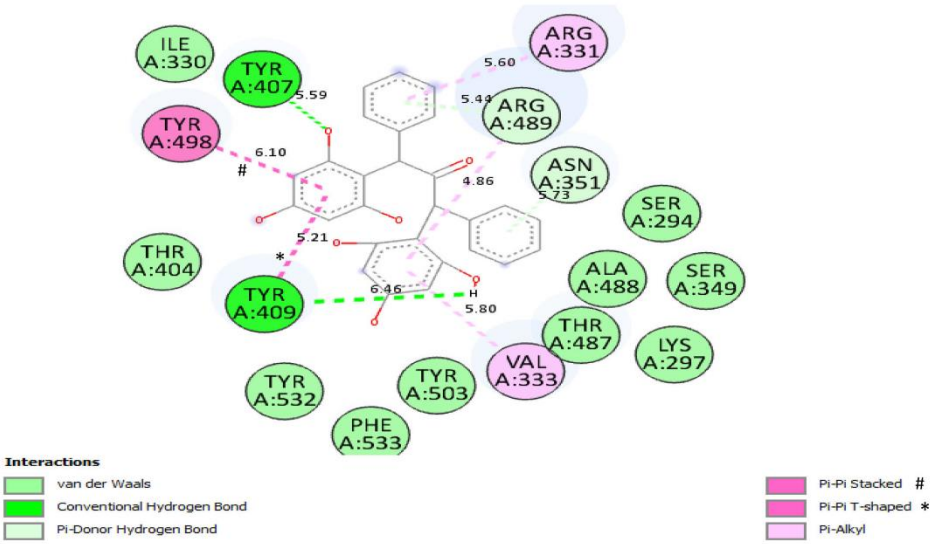


Figure 10. 2D interaction types and plots between propan-2-one and active site of PBP3 of *P. aeruginosa*.

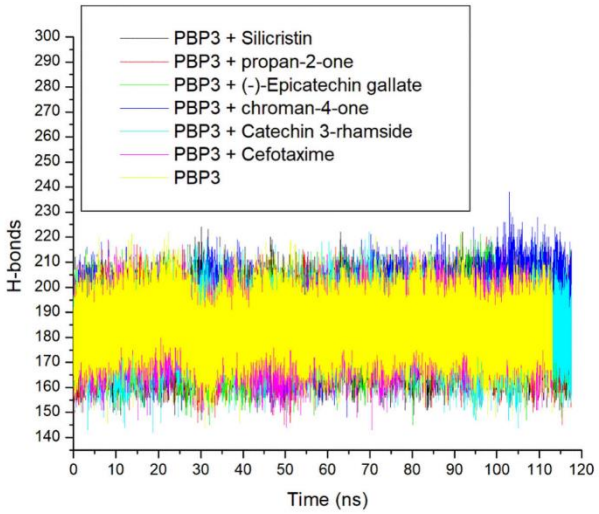


Figure 11. Time evolution of intramolecular hydrogen bond formed in PBP3 following binding of cefotaxime and the top five phenolics during the 120 ns md simulation.

propan-2-one, and silicristin noted in this study. Other important residues contributing to stability at the active site of PBP3 were Val333 forming π-alkyl interaction with all the five compounds and cefotaxime (Figures 5–10), Asn351 forming a hydrogen bond with catechin 3-rhamside, cefotaxime, and chroman-4-one (Figures 5, 7, and 9), Ser485 forming a hydrogen bond with chroman-4-one and cefotaxime (Figures 5 and 9) as well as Thr329, Lys484, Tyr407, Tyr409, Arg331, Arg489, Thr487, Ser485, Ser349 forming hydrogen bonds and/or other important interaction with one or more of the compounds and cefotaxime (Figures 5–9). This is in accordance with the studies of Kumar et al. (2020) and Sainsbury et al. (2011) who also confirmed the importance of these amino acid residues alongside Ser294 in the stability and C-terminal transpeptidase activity of PBP3 of *P. aeruginosa*.

Hydrogen bonds (H-bonds) are determinants and crucial for the conformational stability and compactness of a protein structure (Du et al., 2016; Izadi et al., 2014; Kataria et al., 2021). As a result, H-bonding analysis can be used to assess the stability of protein and protein–ligand complexes (Du

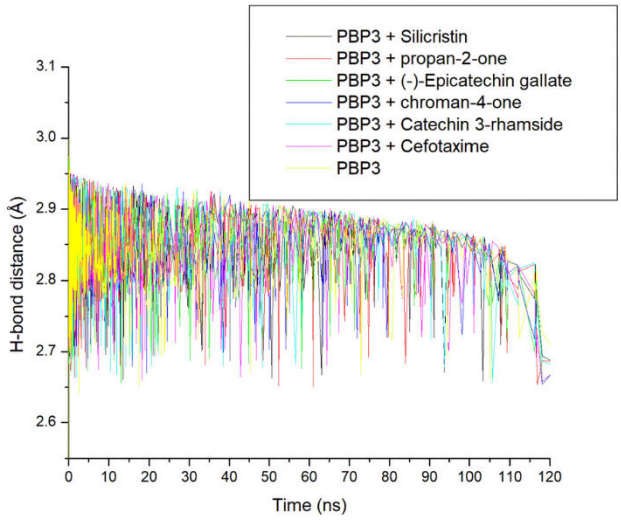


Figure 12. Time evolution of the distance of the intramolecular hydrogen bond formed in PBP3 following binding of cefotaxime and the top five phenolics during the 120 ns md simulation.

Table 6. PBP3 average intramolecular hydrogen bonds and distance during the 120 ns md simulation.

Top five phenolics	Number of intramolecular H-bonds	Intramolecular H-bond distance (Å)
Unbound	181.36 ± 8.85	2.88 ± 0.05
Cefotaxime	182.38 ± 8.92	2.86 ± 0.05
Silicristin	184.36 ± 8.82	2.84 ± 0.05
Chroman-4-one	184.40 ± 9.48	2.84 ± 0.05
Epicatechin gallate	183.21 ± 9.16	2.86 ± 0.05
Catechin-3-rhamside	185.42 ± 9.10	2.84 ± 0.05
Propan-2-one	182.35 ± 8.84	2.86 ± 0.05

et al., 2016). To further investigate the stability of the structures of PBP3 and its complex with the top five phenolics during the simulation, the formation of intramolecular H-bonds and the distance of the H-bonds during the 120 ns simulation period were studied and presented in Figures 11 and 12. Figure 11 shows a fair overlapping and consistency in H-bonding formed within PBP3 before and after the top five phenolic and cefotaxime binds of PBP3. These results demonstrate that the formation of H-bonds in PBP3 is constant, retaining the protein geometry even after ligand binding. Similar observations were observed in the RMSD and ROG findings of this study where the stability of PBP3 following the binding of the top five phenolics and cefotaxime was observed. Specifically, the average intramolecular bonds in PBP3 following the binding of silicristin (184), chroman-4-one (184), epicatechin gallate (183), cefotaxime (183), and catechin-3-rhamside (185), were higher than those observed within the unbound PBP3 (181), with the interaction of PBP3 with catechin-3-rhamside resulting in the highest intramolecular H-bonds (Table 6). Although with a negligible variance of 4 hydrogen bonds between the intramolecular bonds of PBP3 following binding of the top five phenolics and cefotaxime, it can be inferred that none of the ligand bindings, disrupted the thermodynamic properties of PBP3. Figure 12 shows a continuous reduction in the distance of H-bonds formed within PBP3 following the binding of the top five phenolics and cefotaxime during the 120 ns simulation. This observation indicates stronger pull and compactness within PBP3 after binding of the top five phenolics and cefotaxime. This observation is in agreement with the ROG findings of this study and the report of Du et al. (2016), who demonstrated shorter bond lengths to indicate a more stable bond and a stronger pull between two entities where their atoms are held together more tightly. This observation also indicates the occupancy of some intramolecular space by the ligands. The average distance of intramolecular H-bonds formed within PBP3 following the binding of the top 5 phenolics and cefotaxime are presented in Table 6. All of the top five phenolics and cefotaxime had slightly lower average intramolecular H-bond distances relative to the unbound PBP3 with a negligible variance of 0.04 Å in distance among the systems which points to the thermodynamic orderliness of PBP3 following binding of the top five phenolics and cefotaxime. This agrees with the ROG findings of this study that PBP3 becomes slightly more compact following cefotaxime and the top five phenolics binding.

4. Conclusion

Findings from this study have demonstrated the importance and effectiveness of structure-based pharmacophores in identifying hits for PBP3 of *P. aeruginosa* as four out of five-hit phenolics identified in this study demonstrated significantly higher binding affinity than cefotaxime after *MD simulation*. The top five hit phenolics established Van der Waals interactions with the conserved catalytic residue Ser294 of *P. aeruginosa* PBP3 implicated most in the binding of β-lactams and the transpeptidases activity of the protein. This observation

indicates a similar binding pattern of the top five phenolics to the conserved binding mode of β-lactam antibiotics. Of the five compounds, catechin-3-rhamside had the best affinity for PBP3 and facilitated its enhanced stability, indicating its superior advantage as a lead for *P. aeruginosa*. Furthermore, the five compounds passed the pharmacokinetics, synthetic, and toxicity characteristics employed in this study for screening, which further increases their chances of being used as drugs or being improved through further *in vitro and in vivo* confirmatory studies for the treatment of infections caused by *P. aeruginosa* and work in this direction is currently underway.

Acknowledgments

The assistance of the National Research Foundation (NRF- TWAS Doctoral Scholarship, grant number 129950), South Africa, to Mr. J. O. Aribisala is duly and thankfully acknowledged. The Centre for High-Performance Computing (CHPC), South Africa is equally acknowledged for granting access to the computing systems used in this study.

Disclosure statement

No potential conflict of interest was reported by the authors.

Supplementary description

Additional data on the validation of molecular docking of other top-ranked compounds, pharmacokinetics and molecular docking scores for the top 20 hit phenolics and that of the antibiotics used as controls are presented in the supplementary file (Supplementary Tables S1 and S2, Figure S1).

Funding

This work is based on the research supported in part by the National Research Foundation of South Africa (Ref Numbers 120433, and SRUG2204193723). Also, the financial assistance of the Directorate of Research and Postgraduate Support, Durban University of Technology, and the South African Medical Research Council (SA MRC) under a Self-Initiated Research Grant is especially acknowledged.

Author's contribution

SS conceptualized and supervised the study. JOA generated and analyzed the data. JOA wrote the manuscript. All authors read and contributed to the critical review of the manuscript for intellectual content and approved the submission for publication.

Data availability statement

The data is contained within the article or supplementary material.

References

Acharya, A., Agarwal, R., Baker, M. B., Baudry, J., Bhowmik, D., Boehm, S., Byler, K. G., Chen, S. Y., Coates, L., Cooper, C. J., Demerdash, O., Daidone, I., Eblen, J. D., Ellingson, S., Forli, S., Glaser, J., Gumbart, J. C., Gunnels, J., Hernandez, O., … Zanetti-Polzi, L. (2020). Supercomputer-based ensemble docking drug discovery pipeline with application to Covid-19. *Journal of Chemical Information and Modeling*, *60*(12), 5832–5852. https://doi.org/10.1021/acs.jcim.0c01010

Aldulaimi, O. A. (2017). General overview of phenolics from plant to laboratory, good antibacterials or not? *Pharmacognosy Reviews*, *11*(22), 123–127. https://doi.org/10.4103/phrev.phrev_43_16

Alhadrami, H. A., Hamed, A. A., Hassan, H. M., Belbahri, L., Rateb, M. R., & Sayed, A. M. (2020). Flavonoids as potential anti-MRSA agents through modulation of PBP2a: A computational and experimental study. *Antibiotics*, *9*, *562* https://doi.org/10.3390/antibiotics9090562

Al-Orphaly, M., Hadi, H. A., Eltayeb, F. K., Al-Hail, H., Samuel, B. G., Sultan, A. A., & Skariah, S. (2021). Epidemiology of multidrug-resistant Pseudomonas aeruginosa in the Middle East and North Africa region. *Msphere*, *6*, 202–221. https://doi.org/10.1128/mSphere.00202-21

Araya-Cloutier, C., Vincken, J. P., van Ederen, R., den Besten, H. M. W., & Gruppen, H. (2018). Rapid membrane permeabilization of Listeria monocytogenes and Escherichia coli induced by antibacterial prenylated phenolic compounds from legumes. *Food Chemistry*, *240*, 147–155. https://doi.org/10.1016/j.foodchem.2017.07.074

Aribisala, J. O., & Sabiu, S. (2022). Cheminformatics identification of phenolics as modulators of penicillin-binding protein 2a of *Staphylococcus aureus*: A structure–activity-relationship-based study. *Pharmaceutics*, *14*, 1818. https://doi.org/10.3390/pharmaceutics14091818

Aribisala, J. O., Abdulsalam, R. A., Dweba, Y., Madonsela, K., & Sabiu, S. (2022). Identification of secondary metabolites from Crescentia cujete as promising antibacterial therapeutics targeting type 2A topoisomerases through molecular dynamics simulation. *Computers in Biology and Medicine*, *145*, 105432. https://doi.org/10.1016/j.compbiomed.2022.105432

Aribisala, J. O., Nkosi, S., Idowu, K., Nurain, I. O., Makolomakwa, G. M., Shode, F. O., & Sabiu, S. (2021). Astaxanthin-mediated bacterial lethality: Evidence from oxidative stress contribution and molecular dynamics simulation. *Oxidative Medicine and Cellular Longevity*, *2021*, e7159652. https://doi.org/10.1155/2021/7159652

Cerón-Carrasco, J. P. (2022). When virtual screening yields inactive drugs: Dealing with false theoretical friends. *Chem Med Chem*. *17*(16), e202200278. https://doi.org/10.1002/cmdc.202200278

Chen, W., Zhang, Y. M., & Davies, C. (2017). Penicillin-binding protein 3 is essential for growth of *Pseudomonas aeruginosa*. *Antimicrob, Agents Chemother*, *61*(2017), e01651-16. https://doi.org/10.1128/AAC.01651-16

Chiorcea-Paquim, A. M., Enache, T. A., De Souza, G. E., & Oliveira-Brett, A. M. (2020). Natural phenolic antioxidants electrochemistry: Towards a new food science methodology. *Comprehensive Reviews in Food Science and Food Safety*, *2020*, 1680–1726. https://doi.org/10.1111/1541-4337.12566

Dai, Q., Borenstein, A. R., Wu, Y., Jackson, J. C., & Larson, E. B. (2006). Fruit and vegetable juices and Alzheimer's disease: The Kame project. *The American Journal of Medicine*, *119*(9), 751–759. https://doi.org/10.1016/j.amjmed.2006.03.045

Dror, O., Schneidman-Duhovny, D., Inbar, Y., Nussinov, R., & Wolfson, H. J. (2009). Novel approach for efficient pharmacophore-based virtual screening: method and applications. *Journal of Chemical Information and Modeling*, *49*(10), 2333–2343. https://doi.org/10.1021/ci900263d

Du, X., Li, Y., Xia, Y. L., Ai, S. M., Liang, J., Sang, P., Ji, X. L., & Liu, S. Q. (2016). Insights into Protein-Ligand Interactions: Mechanisms, Models, and Methods. *International Journal of Molecular Sciences*. *17*, 144. https://doi.org/10.3390/ijms17020144

Ertl, P., & Schuffenhauer, A. (2009). Estimation of synthetic accessibility score of drug-like molecules based on molecular complexity and fragment contributions. *Journal of Cheminformatics*, *1*, 8. https://doi.org/10.1186/1758-2946-1-8

Fahad, M., Al-Khodairy, M., Kalim, A., Khan, M., Kunhi, M., Pulicat, M. S., Akhtar, S., & Arif, J. M. (2013). In silico prediction of mechanism of erysolin-induced apoptosis in human breast cancer cell lines American. *Journal of Bioinformatics*, *3*, 62–71. https://doi.org/10.5923/j.bioinformatics.20130303.03

Frere, J. M., & Loris, B. (1985). Penicillin-sensitive enzymes in peptidoglycan biosynthesis. *Critical Reviews in Microbiology*. *11*, 299–239. https://doi.org/10.3109/10408418409105906

Izadi, H., Stewart, K. M. E., & Penlidis, A. (2014). Role of contact electrification and electrostatic interactions in gecko adhesion. *Journal of the Royal Society, Interface*. *11*, 371–398. https://doi.org/10.1098/rsif.2014.0371

Josephine, H. R., Charlier, P., Davies, C., Nicholas, R. A., & Pratt, R. F. (2006). Reactivity of penicillin-binding proteins with peptidoglycan-mimetic β-lactams: What's wrong with these enzymes? *Biochemistry*, *45*, 15873–15883. https://doi.org/10.1021/cb7001347

Kataria, J., Rani, P., & Devi, P. (2021). Evaluation of molecular interactions in binary mixtures comprising ethylene and di-ethylene glycol with ethyl lactate through thermophysical and spectroscopic studies. *Journal of Molecular Liquids*. *343*, 117626. https://doi.org/10.1016/j.molliq.2021.117626

Kitchen, D. B., Decornez, H., Furr, J. R., & Bajorath, J. (2004). Docking and scoring in virtual screening for drug discovery: methods and applications. *Nature Reviews. Drug Discovery*, *3*(11), 935–949. 2004. https://doi.org/10.1038/nrd1549

Klein, A. R., Sarri, E., Kelch, S. E., Basinska, J. J., Vaidya, S., & Alristilde, L. (2021). Probing the fate of different structures of β-lactam antibiotics: Hydrolysis, mineral capture, and influence of organic matter. *ACS Earth and Space Chemistry*. *5*, 1511–1551. https://doi.org/10.1021/acsearthspacechem.1c00064

Koes, D. R., & Camacho, C. J. (2012). ZINCPharmer: pharmacophore search of the ZINC database. *Nucleic Acids Research*. *40*, 409–414. https://doi.org/10.1093/nar/gks378

Kumar, V., Tang, C., Bethel, C. R., Papp-Wallace, K. M., Wyatt, J., Desarbre, E., Bonomo, R. A., & Akker, F. V. (2020). Structural Insights into ceftobiprole inhibition of *Pseudomonas aeruginosa* penicillin-binding protein 3. *Antimicrobial Agents and Chemotherapy*, *64*, e00106-20. https://doi.org/10.1128/AAC.00106-20

Lipinski, C. A., Lombardo, F., Dominy, B. W., & Feeney, P. J. (2001). Experimental and computational approaches to estimate solubility and permeability in drug discovery and development settings. *Advanced Drug Delivery Reviews*, *46*(1-3), 3–26. https://doi.org/10.1016/S0169-409X(00)00129-0

Mousavi, S. S., Karami, A., Haghighi, T. M., Tumilaar, S. G., Fatimawali, I. R., Mahmud, S., Celik, I. A., Gagündüz, D., & Tallei, T. E. (2021). In silico evaluation of Iranian medicinal plant phytoconstituents as inhibitors against main protease and the receptor-binding domain of SARS-CoV-2. *Molecules*, *26*, 5724. https://doi.org/10.3390/molecules26185724

MubarakAli, D., MohamedSaalis, J., Sathya, R., Irfan, N., & Kim, J.-W. (2021). An evidence of microalgal peptides to target spike protein of COVID-19: In silico approach. *Microbial Pathogenesis*, *160*, 105189. https://doi.org/10.1016/j.micpath.2021.105189

Nasution, F., Toepak, M. A., Alkaff, E. P., & Tambunan, U. S. F. (2018). Flexible docking-based molecular dynamics simulation of natural product compounds and Ebola virus Nucleocapsid (EBOV NP): A computational approach to discover new drug for combating Ebola. *BMC Bioinformatics*, *19*, 419–436. https://doi.org/10.1186/s12859-018-2387-8

Panat, N. A., Singh, B. G., Maurya, D. K., Sandur, S. K., & Ghaskadbi, S. S. (2016). Troxerutin, a natural flavonoid binds to DNA minor groove and enhances cancer cell killing in response to radiation. *Chemico-Biological Interactions*. *5*, 34–44. https://doi.org/10.1016/j.cbi.2016.03.024

Pang, Z., Raudonis, R., Glick, B. R., Lin, T. J., & Cheng, Z. (2019). Antibiotic resistance in Pseudomonas aeruginosa: mechanisms and alternative therapeutic strategies. *Biotechnology Advances*, *37*(1), 177–192. https://doi.org/10.1016/j.biotechadv.2018.11.013

Parakkal, S. C., Datta, R., Muthu, S., Irfan, A., & Jeelani, A. (2022). Computational investigation into structural, topological, electronic properties, and biological evaluation of spiro[1H-indole-3,2′-3H-1,3-enzothiazole]-2-one. *Journal of Molecular Liquids*. *359*, 119234. https://doi.org/10.1016/j.molliq.2022.119234

Ramirex, D., & Caballero, J. (2016). Is it reliable to use common molecular docking methods for comparing the binding affinities of Enantiomer pairs for their protein target. *International Journal of Molecular Sciences*. *17*, 525–545. https://doi.org/10.1016/j.biotechadv.2018.11.013

Ren, J., Nettleship, J. E., Males, A., Stuart, D. I., & Owens, R. J. (2016). Crystal structures of penicillin-binding protein 3 in complexes with azlocillin and cefoperazone in both acylated and deacylated forms. *FEBS Letters*, *590*(2), 288–297. https://doi.org/10.1002/1873-3468.12054

Sabiu, S., Balogun, F. O., & Amoo, S. O. (2021). Phenolics profiling of Carpobrotus edulis (L.) N.E.Br. and insights into molecular dynamics of their significance in type 2 diabetes therapy and its retinopathy complication. *Molecules*, *26*, 4867. https://doi.org/10.3390/molecules26164867

Sainsbury, S., Bird, L., Rao, V., Shepherd, S. M., Stuart, D. I., Hunter, W. N., Owens, R. J., & Ren, J. (2011). Crystal structures of penicillin-binding protein 3 from pseudomonas aeruginosa: Comparison of native and antibiotic-bound forms. *Journal of Molecular Biology*, *405*(1), 173–184. https://doi.org/10.1016/j.jmb.2010.10.024

Thakuria, B., & Lahon, K. (2013). The β-lactam antibiotics as an empirical therapy in a developing country: An update on their current status and recommendations to counter the resistance against them. *Journal of Clinical and Diagnostic Research: JCDR*, *7*(6), 1207–1214. https://doi.org/10.7860/JCDR/2013/5239.3052

Tonmoy, M. I. Q., Ahmed, S. F., Hami, I., Shakil, M. S. K., Verma, A. K., Hasan, M., Reza, H. A., Bahadur, N. M., Rahaman, M. M., & Hossain, M. S. (2022). Identification of novel inhibitors of high affinity iron permease (FTR1) through implementing pharmacokinetics index to fight against black fungus: An in silico approach. *Infection, Genetics and Evolution: Journal of Molecular Epidemiology and Evolutionary Genetics in Infectious Diseases*, *106*, 105385. https://doi.org/10.1016/j.meegid.2022.105385

Uhomoibhi, J. O., Shode, F. O., Idowu, K. A., & Sabiu, S. (2022). Molecular modelling identification of phytocompounds from selected African botanicals as promising therapeutics against druggable human host cell targets of SARS-CoV-2. *Journal of Molecular Graphics & Modelling*, *114*, 108185. https://doi.org/10.1016/j.jmgm.2022.108185

Verma, A. K., Aarfah, A., Shahadat, H. M., Faisal, A. S., Mohammad, A., Asger, B. A., Upadhyay, S. K., Kumar, V. N., & Mudassir, A. (2022). Identification of 1, 2, 4-triazine and its derivatives against lanosterol 14-demethylase (CYP51) property of Candida albicans: Influence on the development of new antifungal therapeutic strategies. *Frontiers in Medical Technology*, *4*, 845322. DOI =https://doi.org/10.3389/fmedt.2022.845322

Verma, A. K., Ahmed, S. F., Hossain, M. S., Bhojiya, A. A., Mathur, A. A., Upadhyay, S. K., Srivastava, A. K., Vishvakarma, N. K., Barik, M., Rahaman, M. M., & Bahadur, N. M. (2020). Molecular docking and simulation studies of flavonoid compounds against PBP-2a of methicillin-resistant Staphylococcus aureus. *Journal of Biomolecular Structure and Dynamics*, *1*, 1–17. https://doi.org/10.1080/07391102.2021.1944911

Verma, A. K., Hossain, M. S., Ahmed, S. F., Hussain, N., Ashid, M., Upadhyay, S. K., Vishvakarma, N. K., Bhojiya, A. A., & Srivastava, S. K. (2022). *In silico* identification of ethoxy phthalimide pyrazole derivatives as IL-17A and IL-18 targeted gouty arthritis agents. *Journal of Biomolecular Structure and Dynamics*. https://doi.org/10.1080/07391102.2022.2071338

Weinreb, O., Mandel, S., Amit, T., Moussa, B., & Youdim, H. (2004). Neurological mechanisms of green tea polyphenols in Alzheimer's and Parkinson's diseases. *The Journal of Nutritional Biochemistry*, *15*(9), 506–516. https://doi.org/10.1016/j.jnutbio.2004.05.002

World Health Organisation. (2019). International organizations unite on critical recommendations to combat drug-resistant infections and prevent a staggering number of deaths each year. https://www.who.int/news/item/29-04-2019-new-report-calls-for-urgent-action-to-avert-antimicrobial-resistance-crisis, (accessed 5 January 2022).

Zapun, A., Contreras-Martel, C., & Vernet, T. (2008). Penicillin-binding proteins and β-lactam resistance. *FEMS Microbiology Reviews*, *32*(2), 361–385. https://doi.org/10.1111/j.1574-6976.2007.00095.x

Zhao, W. H., Hu, Z. Q., Hara, Y., & Shimamura, T. (2002). Inhibition of penicillinase by epigallocatechin- gallate resulting in restoration of antibacterial activity of penicillin against penicillinase- producing Staphylococcus aureus, Antimicrob. *Antimicrobial Agents and Chemotherapy*, *46*(7), 2266–2268. https://doi.org/10.1128/AAC.46.7.2266-2268.2002

3.3 *In silico* exploration of phenolics as modulators of penicillin binding protein (PBP) 2x of *Streptococcus pneumoniae*

This section has been published in Scientific Reports and is presented as it is in the article

scientific reports

Check for updates

OPEN

In silico exploration of phenolics as modulators of penicillin binding protein (PBP) 2× of *Streptococcus pneumoniae*

Jamiu Olaseni Aribisala, Nosipho Wendy S'thebe & Saheed Sabiu✉

Infections caused by multidrug-resistant *Streptococcus pneumoniae* remain the leading cause of pneumonia-related deaths in children < 5 years globally, and mutations in penicillin-binding protein (PBP) 2 × have been identified as the major cause of resistance in the organism to beta-lactams. Thus, the development of new modulators with enhanced binding of PBP2x is highly encouraged. In this study, phenolics, due to their reported antibacterial activities, were screened against the active site of PBP2x using structure-based pharmacophore and molecular docking techniques, and the ability of the top-hit phenolics to inhibit the active and allosteric sites of PBP2x was refined through 120 ns molecular dynamic simulation. Except for gallocatechin gallate and lysidicichin, respectively, at the active and allosteric sites of PBP2x, the top-hit phenolics had higher negative binding free energy (ΔG_{bind}) than amoxicillin [active site (− 19.23 kcal/mol), allosteric site (− 33.75 kcal/mol)]. Although silicristin had the best broad-spectrum effects at the active (− 38.41 kcal/mol) and allosteric (− 50.54 kcal/mol) sites of PBP2x, the high thermodynamic entropy (4.90 Å) of the resulting complex might suggest the need for its possible structural refinement for enhanced potency. Interestingly, silicristin had a predicted synthetic feasibility score of < 5 and quantum calculations using the DFT B3LYP/6-31G+ (dp) revealed that silicristin is less stable and more reactive than amoxicillin. These findings point to the possible benefits of the top-hit phenolics, and most especially silicristin, in the direct and synergistic treatment of infections caused by *S. pneumoniae*. Accordingly, silicristin is currently the subject of further confirmatory in vitro research.

Keywords Penicillin binding protein, Phenolics, Molecular dynamic simulation, Antibacterial, *Streptococcus pneumoniae*

The incidence of antibiotic-resistant *Streptococcus pneumoniae* has been on the increase since its first report in the 1960s[1]. Globally, *S. pneumoniae* is the leading cause of community-acquired pneumonia, bacteremia, meningitis, and otitis media[2] and in children < 5 years of age, the pathogen remains the leading cause of pneumonia-related deaths[3–5]. With more than half of *S. pneumoniae* isolates frequently showing reduced susceptibility to beta-lactam antibiotics[6,7], the most frequently administered antibiotics for pneumococcal infections, treatment of the diseases has become problematic, necessitating the need for the discovery and development of novel drug candidates with an alternative mode of binding of key therapeutic target of the organism[6]. Penicillin-binding proteins (PBPs) are the typical target enzymes for beta-lactams and are engaged in the late phases of peptidoglycan biosynthesis, where their essential function involve transpeptidation of two muropeptides[8]. Mutation of important PBPs is a resistance mechanism which has been described in various bacteria species[9,10]. The mutation entails modifying key PBPs such that interaction with beta-lactams occurs at considerably higher antibiotic doses than with PBPs from susceptible strains, and therefore the biological activity of the antibiotics is significantly diminished[8]. Thus, identifying improved modulators against critical PBPs of *S. pneumoniae* may aid in the battle against infections caused by multidrug resistant *S. pneumoniae*.

Streptococcus pneumoniae possesses six PBPs, including PBP1a, PBP1b, and PB2a, which are Class A high-molecular-mass PBPs (hmm-PBPs), PBP2x and PBP2b (Class B hmm-PBPs), and PBP3, a D,D-carboxypeptidase low-molecular-mass PBP (lmm-PBP)[11]. Antibiotic resistance in *S. pneumoniae* has been linked to all six PBPs[9]. However, only the class B hmm-PBPs (PBP2x and PBP2b) are key beta-lactam targets, and thus far, only PBP2x

Department of Biotechnology and Food Science, Faculty of Applied Sciences, Durban University of Technology, P.O. Box 1334, Durban 4000, South Africa. ✉email: sabius@dut.ac.za

has been characterized as a major PBP target in clinical isolates since PBP2x genes that express low-affinity variants of *S. pneumoniae* can transfer beta-lactam resistance to susceptible strains[12]. Also, resistance due to mutations in PBP 2b and 1a of *S. pneumoniae* has been shown to occur in strains that already have a low affinity PBP2x, suggesting PBP2x as the most essential PBP in *S. pneumoniae* that is responsible for resistance[12]. Beta-lactams interact with PBP2x by acylating the active site serine residue located in the first of three conserved motifs (S*XXK, SXN, and KS/TG) of PBP2x, and mutations in this region have been attributed to resistance, which is the primary resistance mechanism for beta-lactam antibiotics in *S. pneumoniae* (Tsui et al. 2014). Interestingly, a PASTA domain located adjacent to the active site (27 Å), whose function has been well-deciphered over the years, has in recent times been demonstrated to be active as an allosteric site in the generation of promising peptidoglycan and thus, when appropriately bound, could aid beta-lactam entry into the active site[12,13]. Bernardo-Garca et al.[12] showed that the complexation of a pentapeptide strain at the PASTA domains prompts another pentapeptide strand in the same nascent peptidoglycan strand to enter the active site for the turnover events. Thus, the PASTA domain of PBP2x could serve as a good therapeutic target for identifying drug candidates that could be active in synergy with beta-lactams[14], and in this study, both the active site and the allosteric site of PBP2x were employed in the identification of drug candidates against infections caused by *S. pneumoniae*.

Plant and plant-derived metabolites have long been used in the treatment of human diseases. Interestingly, the increased interest in plant-based antimicrobials in recent years, particularly phenolic compounds, has resulted in the identification of numerous phenolic candidates demonstrating promising pharmacological properties[15,16]. Phenolics ability to cause membrane damage, bind to virulence factors such as PBPs, and cause the suppression of bacteria biofilm formation, among other properties, has been implicated in its ability to inhibit both Gram-positive and Gram-negative microorganisms[17,18]. The characteristic hydroxyl groups attached to the benzene rings of phenolics have been shown to enhance strong protein binding while increasing affinity for cytoplasmic membranes[16]. Alongside their direct antibacterial activity against microorganisms, several phenolics have been shown to work in synergy with conventional antibiotics, an approach that is encouraged in the treatment of infections caused by multi-drug-resistant bacteria[19]. Several phenolics have been identified from various plant parts, with repositories in several databases[20]. Repurposing phenolics could have the potential to reduce the time and costs to identify potent antimicrobials against PBP2x of *S. pneumoniae*[20]. Thus, in this study, all the currently known phenolics were repurposed against PBP2x by compiling phenolics that could interact with the protein from the ZINCPharmer database using structural-based pharmacophore and molecular docking techniques (Fig. 1). The limitations of docking techniques relating to lack of energy refinement and assessment of stability were addressed using molecular dynamic (MD) simulation and mechanics/GB surface area

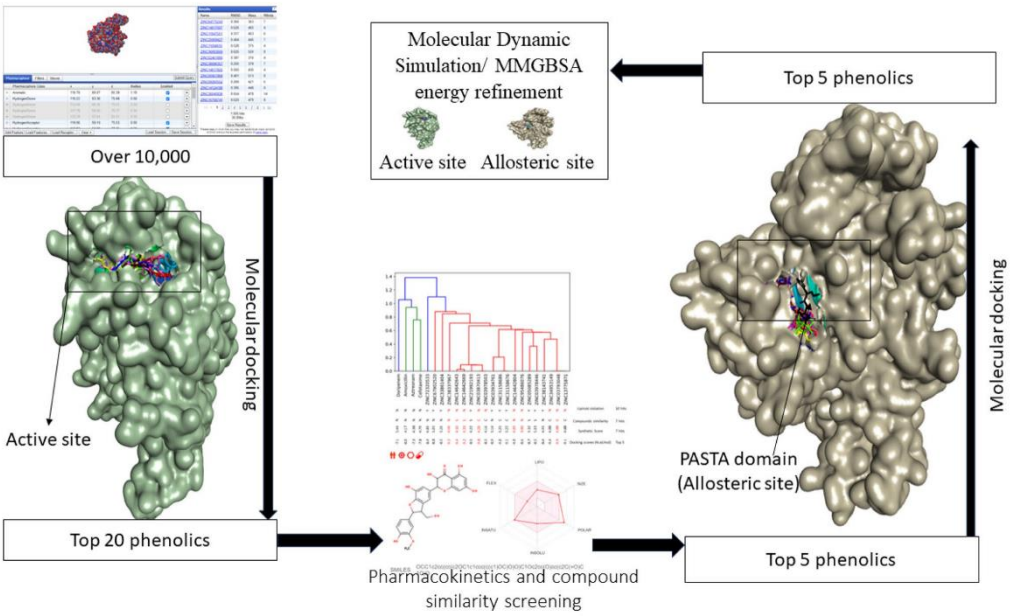


Figure 1. Workflow of the strategy adopted. Over 10,000 currently known phenolics were screened against the active site of PBP2x using structural-based pharmacophore, molecular docking techniques and pharmacokinetics properties. The top-ranked phenolics were subsequently evaluated for their binding free energy, stability, flexibility, and compactness at the active and allosteric site of PBP2x using MMGBSA approach and MD simulation.

(MMGBSA) approaches. Due to the effectiveness of these techniques in the identification of leads from a library of compounds, coupled with the precision of density functional theory in studying the geometries and molecular properties of drug molecules[21], these computational techniques have become an important tool in drug discovery and development. Thus, in this study, they have been employed in the identification of potentially active antibacterial candidates that can treat or act in synergy with conventional antibiotics in the treatment of infections caused by *S. pneumoniae*.

Materials and methods

PBP2x acquisition, optimization, and identification of active and allosteric sites

The experimental crystal structures of PBP2x from *S. pneumoniae* (1QMF for the active site evaluation and 5OIZ for the allosteric site) were obtained from the protein data bank (PDB) (https://www.rcsb.org)[10,12]. The crystal structures were optimized by eliminating water molecules and nonstandard amino acids using the UCSF Chimera v1.15 software tool[22]. Afterward, the x–y–z coordinates and amino acid residues at the active {center [x (116.22), y (60.78), z (71.98], dimension [x (22.75), y (22.06), z (24.82)]} and allosteric site {center [x (99.33), y (67.22), z (52.41], dimension [x (21.94), y (27.41), z (20.75)]} of the protein were defined as previously reported using Discovery Studio version 21.1.0[23] and thereafter validated from literature[10,12].

Screening of phenolics using structure-based pharmacophore

Using the structure-based pharmacophore strategy specific for a ligand and a receptor[24], more than 10,000 phenolics currently known were screened against PBP2x. Briefly, a generalized pharmacophore for phenolics (Table S1) was generated from PharmaGist (https://bioinfo3d.cs.tau.ac.il/PharmaGist/php.php) using 32 phenolics. Afterwards, the generated pharmacophore was used as a query search on the ZINCPharmer database (http://zincpharmer.csb.pitt.edu) using optimized PBP2x as a receptor to aid the search. A total of 1555 phenolics (Fig. S1) were obtained from the search, and the presence of the 32 phenolics used for the pharmacophore building in the total phenolics obtained served as a validation step for the analysis (Table S1).

Ligand acquisition, preparation, and molecular docking at the active and allosteric sites of PBP2x

The library of phenolics built from the ZINCPharmer database was filtered using molecular docking techniques. Four conventional beta-lactams (cefotaxime, amoxicillin, doripenem, and aztreonam) were used as standards for the screening. Prior to molecular docking, the Open Babel tool present on Python Prescription (PyRx) v.0.9.5[25] was employed for the optimization of the ligands (phenolics and standards) via the addition of Gasteiger charges[25]. Subsequently, the molecular docking of the ligands was done at the active site of PBP2x using the AutoDock Vina tool plug-in on PyRx v.0.9.5. Docking at the active site was guaranteed via the selection of the critical residues at the active site of PBP2x, with the grid box coordinates of the selection matching the established x–y–z coordinates (Sect. "PBP2x acquisition, optimization, and identification of active and allosteric sites"). After sorting the top 20 phenolics using the docking score of the reference beta-lactam antibiotics as a benchmark, the similarity of the compounds, pharmacokinetic assessment, and synthetic feasibility evaluation were used to rank the top 5 phenolics. After the top-hit phenolics acquisition from PubChem (https://pubchem.ncbi.nlm.nih.gov/) and preparation via charge addition using the UCSF Chimera v. 1.15 software program[22] the top-hit phenolics were then docked at the allosteric site of PBP2x using the AutoDock tool present on PyRx. The docking at the allosteric site was ensured by selecting the residues at the site with the coordinates of the grid box corresponding with the established x–y–z coordinates for allosteric site in Sect. "PBP2x acquisition, optimization, and identification of active and allosteric sites". For each of the top five phenolics, the docking conformation with the highest negative docking score at both the active and allosteric sites of PBP2x were saved in PDB format for further molecular dynamic (MD) simulation.

To validate the docking conformation, the superimposition techniques was employed[26] where appropriate root mean square deviation (RMSD) of a docked phenolics from its reference point (points of native inhibitors) in PBP2x was calculated[25]. A relative smaller RMSD (usually < 2 Å) between the docked ligand and the native inhibitor in the response complex means comparable binding conformation[26]. The superimposition demonstrated that the top-hit phenolics, amoxicillin, and the docked native inhibitors of 1QMF (active) and 5OIZ (allosteric) had relative binding orientation at both sites of the protein with RMSD values of 1.5 Å (active site) and 1.4 Å (allosteric site). Furthermore, all the ligands interacted with the key amino acid residue[10] in the active (Ser337) (Fig. 2a) and allosteric (Arg426)[12] sites of PBP2x (Fig. 2b). These findings supported the validity of the docking scores obtained in the study.

Pharmacokinetic and physicochemical prediction of phenolics

Using the simplified molecular input line entry system (SMILES) of each structure, the pharmacokinetics, physicochemical, and drug-like properties of the top twenty phenolics were predicted using the SwissADME web tools (http://swissadme.ch/index.php) and afterwards validated using the Molinspiration toolkit (https://www.molinspiration.com/cgi-bin/properties). On the other hand, the Protox II webserver (https://tox-new.charite.de/protox_II/) was employed in the prediction of the toxicity properties of the compounds. Coupled with the docking scores, the cheminformatics information obtained from these analyses were used in ranking the top hit phenolics.

Chemical fingerprinting of phenolics

To understand how each of the top 20 compounds is chemically similar to each other, molecular fingerprinting was carried out using Galaxy Europe (https://usegalaxy.eu./#)[27]. The information obtained from this study enables the selection of the top hit phenolics that are more diverse from each other[27]. In a nutshell, Galaxy Europe's "molecule to fingerprint" tool was used to convert the compounds' smile format into "Open Babel FP2 fingerprints."

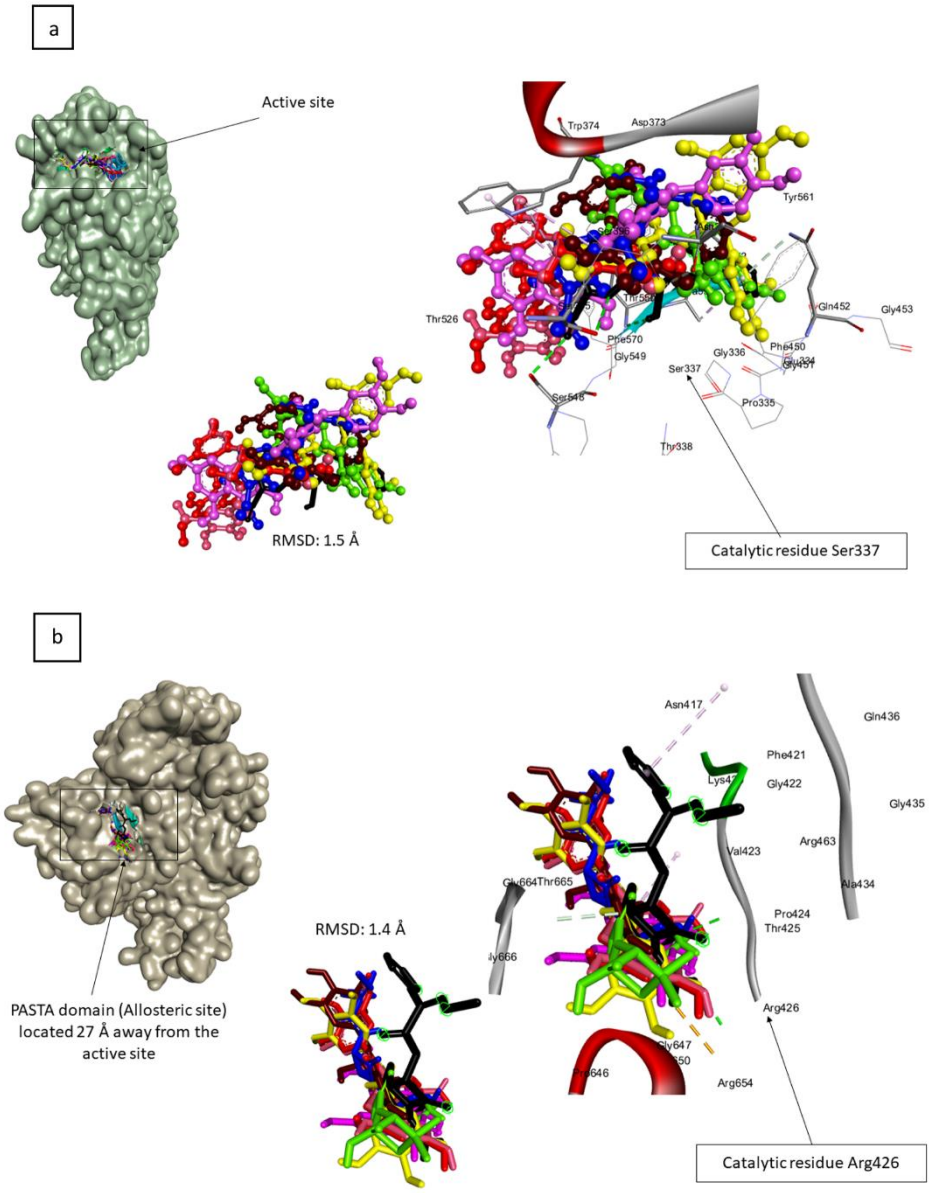


Figure 2. Docking protocol validation via superimposition of the docked top-hit phenolics with the experimental native inhibitor at the active (**a**) and allosteric (**b**) sites of 1QMF and 5OIZ respectively. The docked experimental inhibitor (blue), reference standard (green) and top-hit phenolics [silicristin (magneta), ECBE (cyan), lysidicichin (red), ECMG (orange) and GCG (yellow)] all had an RMSD of 1.5 Å and 1.4 Å from the experimental native inhibitor at the active and allosteric site of 1QMF and 5OIZ, respectively, suggesting partial binding orientation of the docked compounds and the experimental native inhibitors.

The "Open Babel FP2 fingerprints" were then clustered using the fingerprinting algorithms "Taylor-Butina" and "NxN clustering," with thresholds of 0.8 and 0.0, respectively.

Molecular dynamic (MD) simulations and post simulation analysis of phenolics

The AMBER 18 package of the CHPC (Centre for High Performance Computing) was used to perform a 120 ns MD simulation of each of the top hit phenolics, amoxicillin and apo-PBP2x, utilizing the AMBER force field's FF18SB variant to describe the operating systems[28]. Using the General Amber Force Field (GAFF) and Restrained Electrostatic Potential (RESP) approaches, the ANTECHAMBER was used to create the atomic partial charges of the ligands. The protonation states were assigned using the AMBER LEaP module, which by default helps investigate and assign the correct protonation states for each amino acid residue using Na^+, hydrogen atoms, and Cl^- counter ions. The numbering of residues from 1 to 650 was done and dipping of the systems in a manner that allows each of the atoms to be within 8 Å of any box edge was done in an orthorhombic box of TIP3P water molecules. For each of the top hit phenolics, amoxicillin and apo-PBP2x simulation, an initial equilibrium configuration (2000 steps) was achieved by a means of 500 kcal/mol restriction potential. Afterward, two 990 steps by means of steepest descent technique and conjugate degrees were carried out respectively, followed by a 990 steps unlimited minimization using the conjugate gradient approach[28]. For 50 ps, heating simulation was done gradually from 0 to 300 K and ensuring that a constant number of atoms and volume was maintained. The potential harmonic constraint of the solutes in the systems is 10 kcal/mol, and the collision frequency is 1.0 ps. Following that, each system was equilibrated for approximately 500 ps while the operating temperature remained constant at 300 K. Restriction of hydrogen bonds using the SHAKE method was done for each simulation and each system had a randomized seeding and a 2 fs step size (corresponding to the isobaric–isothermal ensemble (NPT)). Also, a specific temperature (300 K) and constant pressure (1 bar) were maintained during each of the simulations. A Langevin thermostat was used to keep the collision frequency at 1.0 ps and the pressure-coupling constant at 2 ps[28]. Following that, the findings of the 120 ns MD simulation were analyzed and categorized as post-dynamic data. The post simulation analysis was carried out by gathering the systems' coordinates and trajectories using the PTRAJ module. The study of RMSD, root means square fluctuation (RMSF), radius of gyration (ROG), and solvent accessible surface area (SASA) was carried out using the CPPTRAJ module, and their plots were made using Origin v 6.0. Similarly, the binding free energy (ΔGbind) was determined using 120,000 snapshots (at 1.0 ps interval) collected from a 120 ns MD simulation trajectory using the equations below, utilizing the MMGBSA technique[29]

$$\Delta \mathrm{Gbind} = \mathrm{G_{complex}} - (\mathrm{G_{receptor}} + \mathrm{G_{ligand}}) \tag{1}$$

$$\Delta \mathrm{Gbind} = -\mathrm{TS} + (\mathrm{G_{sol}} + \mathrm{E_{gas}}) \tag{2}$$

$$\mathrm{E_{ele}} + \mathrm{E_{int}} + \mathrm{E_{vdw}} = \mathrm{E_{gas}} \tag{3}$$

$$-(\mathrm{G_{GB}} - \mathrm{G_{SA}}) = \mathrm{G_{sol}} \tag{4}$$

$$\gamma \mathrm{SASA} = \mathrm{G_{SA}} \tag{5}$$

where Egas = the gas-phase energy, E_{int} = the internal energy, E_{ele} = coulomb energy E_{vdw} = the van der Waals energy, Gsol = solvation-free energy from polar state, G_{GB} = solvation – free energy from polar state non – polar states, S = total entropy and T = temperature.

The interaction plots of the top hit phenolics and amoxicillin against PBP2x at both active and allosteric sites of the protein were visualized and analyzed with (LigPlot v2.2.8[30].

Quantum chemical calculations

The purpose of this investigation was to predict the molecular characteristics of the best phenolics at the active and allosteric sites of PBP2x. The most generally used DFT/B3LYP/631G/+ (d, p) basis set[31,32] was utilized. The Centre for High Performance Computing's Gaussian 16 program package was employed for the analysis and the results were evaluated with GaussView 6 software V. 6.0.16. The conceptual density functional theory (CDFT) descriptors such as softness, hardness, electrophilicity index, energy gap, ionization energy, and chemical potential were subsequently estimated from the energies of frontier lowest unoccupied molecular orbital (LUMO) and highest occupied molecular orbital (HOMO) consideration the Parr and Pearson interpretation[33,34] of DFT and Koopmans theorem[34] on the correlation of ionization potential (I) and electron affinities (E) with HOMO and LUMO energy. The following equations were used for the calculations:

$$[\mathrm{E_LUMO} - \mathrm{E_HOMO}]\,(\mathrm{eV}) = \text{Energy gap } (\Delta E) \tag{6}$$

$$[I = -\mathrm{E_HOMO}]\,(\mathrm{eV}) = \text{Ionization energy } (I) \tag{7}$$

$$[A = -\mathrm{E_LUMO}) = \text{Electron affinity } (A) \tag{8}$$

$$[\eta = (I - A)/2](\mathrm{eV}) = \mathrm{Hardness}(\eta) \tag{9}$$

$$[S = 1/\eta](\text{eV}) = \text{Softness}(S) \tag{10}$$

$$[\chi = (I + A)/2](\text{eV}) = \text{Electronegativity}(\chi) \tag{11}$$

$$[\mu = -\chi = -(I + A)/2](\text{eV}) = \text{Chemicalpotential}(\mu) \tag{12}$$

$$[\omega = \mu^2/2\eta]\,(\text{eV}) = \text{Electrophilicity index}\ (\omega) \tag{13}$$

Declaration of preprint sharing

We declare that the manuscript was shared as a preprint on the preprint server for biology "bioRxiv".

Results and discussion

Screening of phenolics at the active site of PBP2x using structure-based pharmacophore and molecular docking

Following the evaluation of the binding positioning and interaction of the 1555 phenolics obtained via structure-based pharmacophore at the active site of PBP2x using the molecular docking approach, the top 20 phenolics had higher docking scores than all the beta-lactam antibiotics used as standards. The top 20 phenolics had docking scores ranging between − 8.4 and − 9.9 kcal/mol, with ZINC03793048 having the highest docking score, while the beta-lactams had docking scores between − 7.1 and − 8.0 kcal/mol, with amoxicillin having the highest docking score (Fig. 3), and hence it was selected as a standard for further analysis. The docking scores observed for the top 20 phenolics in this study fall within the scores observed by Singh et al.[35] whose exploration of antibacterial molecules from Asinex antibacterial library revealed some promising antibacterial molecules against pneumonia infections. Thus, the better interactions and orientation of the top 20 phenolics at the active site of PBP2x relative to the standards in this study might suggest their better potential as anti-PBP2x. However, as virtual screening often produces inactive molecules in the preclinical and clinical stages of drug development[36], the identified top 20 compounds were further screened cheminformatically to identify the top hit phenolics that will be pharmacokinetically friendly, have drug-like properties, and have a synthetic score that can enable structural

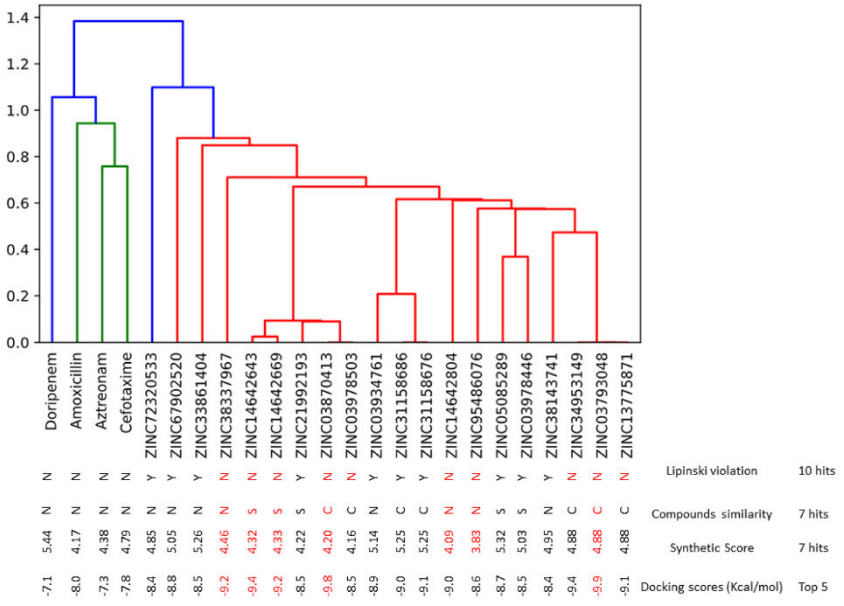


Figure 3. Cheminformatics and docking scores ranking of the top-hit phenolics. The same colour and cluster signifies more similarity. Except for ZINC72320533, all top twenty phenolics had the same colour meaning they are more similar than the beta-lactams with different colour. Compounds of the same clusters with zero similarity scores are conformers and in ranking the top-hit, only one (compounds that fulfilled the Lo5 and has the highest docking score) from a set of conformers are chosen. The top-hit phenolics all had a synthetic sore of < 5 and possess the resorcinol structure as a common moiety.

alterations for enhanced druggability (Fig. 3). Using these approaches, the top hit phenolics obtained and the standards passed the Lipinski rule of 5 (LRo5), which serves as a pioneering physicochemical filter, relating the physicochemical parameters of compounds to their pharmacokinetic properties and oral bioavailability[37]. The LRo5 limits the molecular weight, hydrogen donor, hydrogen acceptor, and octanol coefficient of a bioactive drug to 500 g/mol, 5, 10, and 5, respectively (Fig. 3). Also, the top-hit phenolics and the standards had a synthetic score of < 5 (Fig. 3) that would encourage structural alteration to improve potency[38]. GCG (ZINC03870413) had the lowest synthetic score (4.20) among the top-hit phenolics, with a value that compares well with amoxicillin (4.17), suggesting that the compound will be the most susceptible to structural modification for enhanced druggability. Other predicted pharmacokinetic properties (Table 1), such as the bioavailability scores, solubility, and gastrointestinal tract absorption of the top-hit phenolics, all point to the drug-like properties of the compounds[39], as they all have characteristics that compare well with amoxicillin. The top-hit phenolics toxicity profiles suggest that they are non-inhibitors of most of the cytochrome P450 (CYP), an important isoenzyme in drug metabolism[40]. GCG and amoxicillin are non-inhibitors of all the isoenzymes, suggesting that they would not result in drug-drug interactions (DDI) when co-administered with phase I- and phase II-dependent drugs. However, other top hit phenolics inhibit CYP3A4, suggesting their potential ability to cause DDI with drugs that are metabolized by the isoenzyme. This observation pinpoints to the need for further structural alteration to improve the toxicity profile of the compounds, more so as some of the compounds [silicristin, lysidicichin, and ECMG] were also predicted to be active for immunotoxicity (Table 1). However, ECBE, GCG, and amoxicillin are predicted to be non-active for all the toxicity endpoints. Remarkably, all the top-hit phenolics belong to either toxicity class 4 or 5 and can be deployed as medications[37,39]. Generally, the top-hit phenolics in this study have pharmacokinetic, synthetic, and drug-like properties that suggest them as potential drug candidates that can be structurally modified for enhanced potency.

Energy components refinement of the top-hit phenolics against the active site of PBP2x

The molecular docking study has been shown to be a poor predictor of binding affinity and the identification of active inhibitors due to its scoring functions inability to account for the dynamics of the atoms of the ligand and the protein involved[36]. Thus, in this study, energy refinement of the docking score was done using the MMGBSA approach[29]. Using this approach, the ΔGbind, which gives the sum of all the intermolecular interactions that are present between a ligand and a target during a simulation, was calculated. Several energy components, such as the ΔE_{elec}, ΔE_{gas}, ΔE_{vdw} and ΔG_{sol} contributed to the total ΔGbind of a ligand to a receptor. In this study, the ΔG_{sol}, which estimates the the electrostatic solvation of the solute[40,41], had the highest contribution to the total ΔGbind observed for all the investigated complexes (Table 2). Three of the top-hit phenolics [ECMG (− 42.18 kcal/mol), silicristin (− 38.41 kcal/mol), and lysidicichin (− 29.85 kcal/mol)] had higher ΔGbind than amoxicillin, with ECMG having the highest negative value (Table 2). This observation, is not only consistent with previous studies on the antibacterial properties of phenolics and drugs against PBPs of common and clinically important Gram-positive organisms[17,39,42], but also indicative of the enhanced potential of the three phenolics as modulators of PPBP2x, with ECMG being the most promising compound. ECBE (− 19.72 kcal/mol) had ΔGbind scores that compared with amoxicillin (− 19.23 kcal/mol), while the value observed for GCG (− 14.93 kcal/mol) was significantly lower relative to amoxicillin (Table 2). This observation is suggestive of the lesser ability of ECBE and most especially GCG to modulate PBP2x of *S. pneumoniae*, thus contradicting the observed docking scores, where the two compounds had higher scores than amoxicillin. This finding substantiates the report of Cerón-Carrasco[36] that virtual screening required further energy refinement in the selection of active molecules. Overall, the findings from the thermodynamic ΔGbind of this study demonstrated the benefit of ECMG, silicristin, and lysidicichin over amoxicillin in the management/treatment of infections caused by multidrug resistant *S. pneumoniae*.

Thermodynamic information of PBP2x following binding at the active site

To understand the structural stability of PBP2x and its complexes after ligand binding, the RMSD was assessed. The RMSD is a function of the time-dependent deviation of a complex structure from its apo structure, with lower RMSD values indicating better complex stability[42]. In this study, the RMSD seems to equilibrate before 10 ns for all the investigated systems, while each system subsequently took a more diverse route, which appears to converge at 85 ns of simulation, thus impacting the different average RMSD values observed for each system (Fig. 4). The bound systems with average values ranging between 3.31 and 4.90 Å, generally had a reduced RMSD value compared to the apo-PBP2x (6.32 Å) with lysidicichin and ECMG having the lowest values, which compared well with amoxicillin (Table 3). The reduced RMSD value of PBP2x following binding of ligands generally denotes enhanced thermodynamic stability of the complexes[43]. This observation agrees with the report of Sainsbury et al.[44], where experimental beta-lactam binding of PBP3 increases the thermodynamic stability of PBP3 through local conformational changes at the active site. The fact that lysidicichin and ECMG had RMSD values that compared well with amoxicillin following binding of PBP2x indicates their advantage as inhibitors of PBP2x over the other top-hit phenolics. This observation partially agrees with the ΔGbind findings of this study, where ECMG had the highest negative ΔGbind. However, silicristin, which also had higher ΔGbind against PBP2x, had the highest RMSD value at 4.90 Å (Table 3) and thus denotes that further structural adjustment of the compound for stability might improve potency. Overall, the RMSD finding of the study showed that ligand binding of PBP2x increases stability when compared to the apo-PBP2x and that while lysidicichin and ECMG are the most structurally compactible with PBP2x, silicristin and probably GCG might require further structural adjustment to increase their potency.

The ROG estimates the degree of folding with great folding meaning better thermodynamic organization and sometimes also stability in a complex, a phenomenon related to protein (topology, size, and length) and ligand (molecular weight) parameters and their point of contact[44,45]. Like the RMSD, following ligand binding of

Ligands zinc code	Popular name	Code	MW <500 (g/mol)	HB-A≤10	HB-D≤5	Log Po/w≤5	RT-B≤9	WS	GI—A	BS	pgp	Inhibitor of CYP 450s				H	C	IM	M	CY	TC
												CYP 1A2	CYP 2C19	CYP 2C9	CYP 2D6	CYP 3A4					
Amoxicillin	Amoxicillin	–	365.4	6	4	-0.39	5	VS	L	0.55	N	N	N	N	N	N	I	I	I	I	6
ZINC03793048	Silicristin	–	482.44	10	6	1.42	4	S	L	0.55	N	N	N	N	N	Y	I	I	A	I	4
ZINC38337967	Epigallocatechin 4-benzylthioether	ECBE	428.46	7	6	2.22	4	MS	L	0.55	N	N	N	N	N	Y	I	I	I	I	5
ZINC14642669	Lysidicichin	–	470.43	10	5	1.94	6	MS	L	0.55	N	N	N	N	N	Y	I	I	A	I	4
ZINC14642643	Epicatechin 3-O-(3-O-methyl-gallate)	ECMG	456.4	10	6	1.77	5	S	L	0.55	N	N	N	N	N	Y	I	I	A	I	4
ZINC03870413	(−)-Gallocatechin gallate	GCG	458.37	10	8	1.01	4	S	L	0.17	N	N	N	N	N	N	I	I	I	I	4

Table 1. Physicochemical, pharmacokinetics and toxicity profile of the top-hit phenolics. Molecular weight = MW; Hydrogen bond acceptor = HB-A; Active = A; Permeability glycoprotein substrate = Pgp; Hydrogen bond donor = HB-D; Partition coefficient = Log Po/w; Very soluble = VS; Rotatable bond = RT-B; Water solubility = WS; Cytotoxicity = CY; Gastrointestinal absorption = GI- A; Cytochrome = CYP; Moderately soluble = MS; Soluble = S; No = N; Toxicity class = TC; Yes = Y; Low = L; Inactive = I; Bioavallability score = BS; Hepatotoxicity = H; Carcinogenicity = C; Immunotoxicity = IM; Mutagenicity = M.

Systems	Δ E_{vdW}	ΔE_{elec}	ΔG_{gas}	ΔG_{solv}	ΔGbind
Amoxicillin	− 29.65 ± 4.89	− 290.87 ± 33.31	− 320.52 ± 34.44	301.29 ± 27.75	− 19.23 ± 7.96
Silicristin	− 46.96 ± 4.46	− 41.91 ± 9.87	− 88.90 ± 9.57	50.48 ± 7.77	− 38.41 ± 6.07
ECBE	− 23.59 ± 8.08	− 22.28 ± 14.23	− 45.88 ± 18.96	26.15 ± 12.22	− 19.72 ± 8.15
Lysidicichin	− 37.47 ± 7.64	− 32.83 ± 10.17	− 70.30 ± 13.40	40.45 ± 7.24	− 29.85 ± 8.56
ECMG	− 49.42 ± 3.96	− 45.24 ± 8.76	− 94.66 ± 8.28	52.48 ± 5.19	− 42.18 ± 4.53
GCG	− 16.35 ± 13.69	− 27.02 ± 22.28	− 43.37 ± 29.16	28.43 ± 19.81	− 14.93 ± 10.27

Table 2. Thermodynamic energy (kcal/mol) of the top-five phenolics against the active site of PBP2x of *S. pneumoniae*. Keyword: ΔE_{vdW} means van der Waals energy, ΔGbind means total binding free energy, ΔE_{gas} means gas phase free energy, ΔE_{elec} means electrostatic energy, while ΔG_{solv} means solvation free energy.

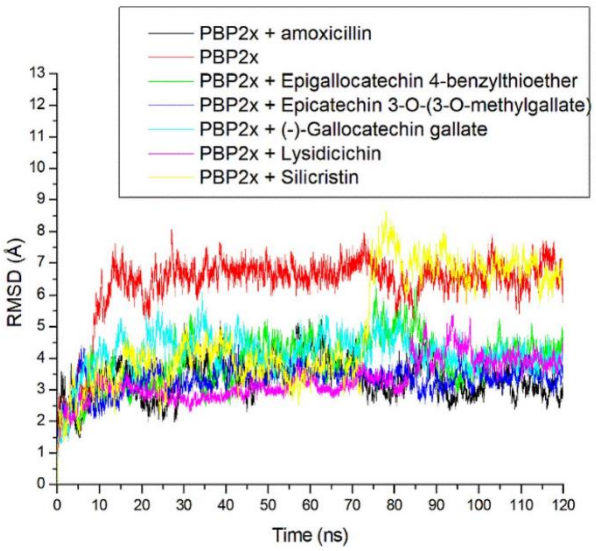


Figure 4. Relative root means square deviation plots of alpha-carbon, amoxicillin, and top-hit phenolics at the active site of PBP2x of *S. pneumoniae* over a 120 ns simulation period.

Systems	RMSD (Å)	RMSF (Å)	ROG (Å)	SASA (Å)	Number of H-bonds	Average distance of H-bonds
Apo-PBP2x	6.32 ± 1.08	1.76 ± 1.02	30.04 ± 0.17	27,812.69 ± 465.30	328.68 ± 1.02	2.85 ± 0.04
Amoxicillin	3.33 ± 0.61	2.16 ± 1.35	29.37 ± 0.50	28,553.79 ± 520.35	329.78 ± 1.12	2.85 ± 0.05
Silicristin	4.90 ± 1.72	2.62 ± 2.18	29.63 ± 0.41	28,080.16 ± 436.40	333.65 ± 1.05	2.85 ± 0.04
ECBE	3.88 ± 0.78	1.83 ± 1.15	29.51 ± 0.23	28,586.34 ± 465.61	331.34 ± 0.99	2.85 ± 0.02
Lysidicichin	3.31 ± 0.61	1.76 ± 1.00	29.15 ± 0.19	28,065.41 ± 565.10	331.32 ± 0.98	2.85 ± 0.04
ECMG	3.32 ± 0.39	1.64 ± 1.01	29.61 ± 0.22	28,612.65 ± 434.72	333.98 ± 1.13	2.85 ± 0.03
GCG	4.14 ± 0.62	1.85 ± 2.08	30.01 ± 0.25	28,378.68 ± 453.43	330.02 ± 1.08	2.85 ± 0.06

Table 3. Thermodynamics data of the top-five phenolics after 120 ns MD simulation at the active site of PBP2x of *S. pneumoniae*.

PBP2x, a marginal reduction in the ROG values was observed with the bound systems relative to the apo-PBP2x (Table 3, Fig. 5). The reduced ROG value following ligand binding of PBP2x could be suggestive of the increased structural compactness in the bound systems due to folding[45]. The bound system had average ROG values ranging between 29.15 and 30.01 Å with lysidicichin having the lowest value (Table 3). Lysidicichin having the lowest ROG value agrees with the RMSD findings of this study, where the compound also had the lowest RMSD value,

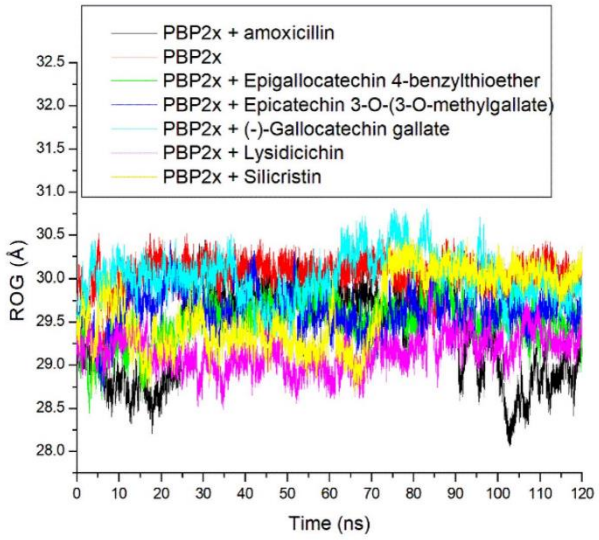


Figure 5. Relative radius of gyration plots of alpha – carbon, amoxicillin and top-hit phenolics at the active site of PBP2x of *S. pneumoniae* over a 120 ns simulation period.

and thus suggests the advantage of the compound as a potential PBP2x inhibitor. However, with a variance of 0.86 Å (Table 3) among the bound systems regarding the average ROG, it can be inferred that the compactness of PBP2x following ligand binding had little impact on ranking the top-hit phenolics.

Root mean square fluctuation evaluates the mobility of residues following ligand binding of PBP2x[46]. In this study, higher swaying in amino acid residues between 25 and 175 and a lesser fluctuation between residues 250 and 425, and 550 and 625 were noted in all the systems, with the degree of swaying varying among systems (Fig. 6a), thus affecting the average RMSF. Interestingly, Ser337, which is the catalytic residue in PBP2x[10], occurred where the fluctuation was minimal (Fig. 6b). Ser337 had fluctuations ranging between 0.87 and 1.29 Å in all the system with the apo-PBP2x having the highest fluctuation of Ser337 (Table 4). This observation suggests

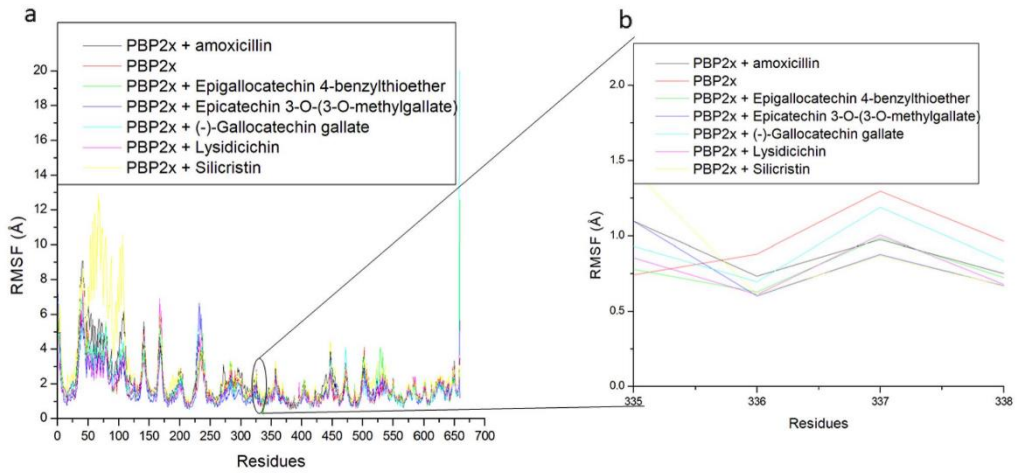


Figure 6. Relative root means square fluctuation plots of alpha – carbon, amoxicillin and top-hit phenolics at the active site of PBP2x (**a**) and the critical residue of PBP2x (**b**) of *S. pneumoniae* over a 120 ns simulation period.

that ligand binding generally reduced the fluctuation of Ser337, indicating an active involvement of Ser337 in the intramolecular binding of other residues of PBP2x or the intermolecular binding of the ligands. The reduced effect of ligand binding on the Ser337 of PBP2x is in agreement with our previous report, where the gatekeeper residue (Tyr446) of PBP2a had reduced fluctuation following binding of phenolics[47]. Silicristin (0.87 Å) and ECMG (0.88 Å) with the highest negative ΔGbind against PBP2x also had the lowest fluctuation of Ser337, pinpointing the importance of reduced fluctuation of the catalytic residue in the observed ΔGbind in the study. However, except for the ECMG-PBP2x complex (1.64 Å), the fluctuation of residues in the whole protein was greatly enhanced following the top-hit phenolics and amoxicillin binding of PBP2x (Table 3). The apo-PBP2x had an RMSF of 1.76 Å, while the bound systems had average RMSF values ranging between 1.64 and 2.62 Å with only ECMG-PBP2x having a lesser value than the apo-PBP2x. The lesser RMSF value of ECMG-PBP2x suggests enhanced structural organization with the binding domain of PBP2x due to strong intra and intermolecular binding and could have contributed to the higher negative ΔGbind observed in ECMG-PBP2x relative to other investigated complexes in this study. Like the findings on the RMSD, the silicritin-PBP2x complex had the highest fluctuation of residues in the whole protein, suggesting the need for structural adjustment of the compound for stability. Other top-hit phenolic complexes with PBP2x, such as ECBE-PBP2x (1.83 Å), lysidicichin-PBP2x (1.76 Å), GCG-PBP2x (1.85 Å) had relatively lower RMSF values than amoxicillin-PBP2x (2.16 Å) (Table 3), suggesting the advantage of ECBE, lysidicichin, and GCG as potential inhibitors of PBP2x. Overall, the RMSF findings of this study have demonstrated the importance of reduced fluctuation of Ser337 in the observed ΔGbind noted in this study and that ECMG among the investigated ligands caused enhanced structural organization in PBP2x, which could have contributed to its higher negative ΔGbind. Silicristin, on the other hand, despite having a high ΔGbind, might require further structural adjustment to increase its potency due to its high RMSF value, and this observation is also noted by the RMSD finding of this study.

Like the ROG, the SASA also analyzes protein folding and surface area changes during a simulation, with higher SASA values indicating a rise in volume[48]. The SASA plot had a more stable fluctuation throughout the simulation for all the systems (Fig. 7). Averagely, the bound system had slightly higher SASA values ranging between 28,065.41 Å and 28,612.65 Å compared to the apo-PBP2x, with lysidicichin having the lowest value (Table 3). This observation highlighted the slightly higher surface area of PBP2x following ligand binding, which

PBP2x active site critical residue	Top hit phenolics						
	Apo-PBP2x	Amoxicillin	Silicristin	ECBE	Lysidicichin	ECMG	GCG
Ser337	1.29	0.97	0.87	0.99	1.00	0.88	1.19

Table 4. PBP2x active site Ser337 fluctuation (Å) after 120 ns simulation of the top-hit phenolics at the active site.

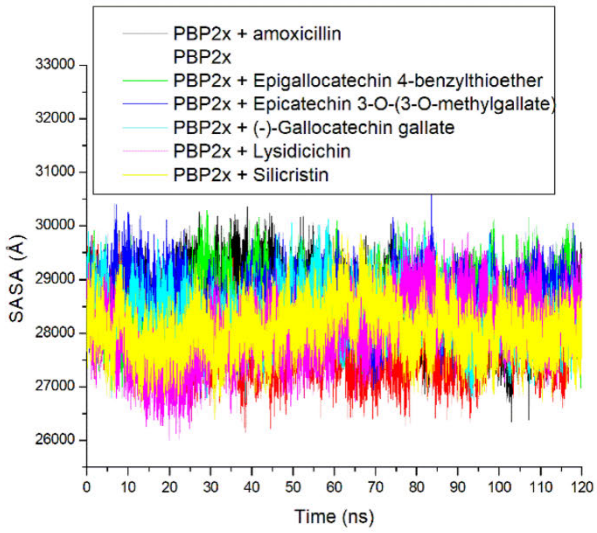


Figure 7. Relative solvent – accessible surface area plots of alpha – carbon, amoxicillin and top-hit phenolics at the active site of PBP2x of *S. pneumoniae* over a 120 ns simulation period.

is in contrast with the findings of Mousavi et al.[47], who reported that the interactions of ligands with proteins can cause protein folding. The increase in surface area following ligand binding also did not agree with the ROG findings of this study. This observation might not necessarily mean less stability of the complexes, as a smaller SASA variance of 800 Å exists between the bound system and the apo-PBP2x (Table 3). However, lysidicichin, among the investigated compounds, has the lowest SASA value, which agrees with the ROG and RMSD findings of this study and thus further corroborates the advantage of the compound as PBP2x inhibitor. Overall, with a smaller SASA variance of 547 Å among the bound systems, it can be concluded that the surface area folding of PBP2x following ligand binding had little impact on ranking the top-hit phenolics.

Hydrogen bonds and distances are important for the structural stability of proteins and can hence be evaluated during simulation to understand the influence of ligand binding on protein stability[49]. A stable fluctuation in the number of intramolecular hydrogen bonds was observed with bonded and apo-PBP2x during the simulation (Fig. 8a). This observation, while being consistent with other thermodynamic metrics of this study, further indicates the thermodynamic orderliness of the systems[50]. Following ligand binding of PBP2x, a higher number of hydrogen bonds in PBP2x was observed with the bound system (ranging between 329.78 and 333.98) relative to the apo-PBP2x (Table 3), with ECMG having the highest number of hydrogen bonds. The increase in the hydrogen bond of the bound system relative to the apo-PBP2x is indicative of some intermolecular hydrogen bonds contributed by ligand binding of the protein, with ECMG having the highest intermolecular contribution of hydrogen bonds during the simulation. This observation could have contributed to ECMG having the highest negative ΔGbind against PBP2x and the higher negative ΔGbind observed with silicristin, ECBE, lysidicichin, and ECMG relative to amoxicillin. The relatively similar pattern of fluctuations in the distance of hydrogen bonds of PBP2x [with an average of 2.85 Å for each of the systems (Table 3)] following the top-hit phenolics binding of PBP2x, which continues to shorten as the simulation progresses (Fig. 8b) also further emphasized the orderliness in the protein following the compounds binding at the active site, an observation that agrees with other thermodynamic metrics of this study.

Molecular docking of top hit phenolics at the allosteric site of PBP2x of S. pneumoniae

The PASTA domain of PBP2x has been demonstrated to act as an allosteric site, which, when properly occupied, could facilitate entering the active site of PBP2x and thus prompt the acylation of Ser337 of the active site[12]. To investigate the ability of the top-ranking phenolics binding the allosteric site of PBP2x, molecular docking was carried out to assess the fitness of the phenolics at the site. The top-hit phenolics had higher negative docking scores at the allosteric site, ranging between −9.1 and −9.9 kcal/mol, than amoxicillin (−8.8 kcal/mol), with silicristin having the highest negative docking scores (Table 5). This observation might be indicative of the better fitness of the top-hit phenolics relative to amoxicillin at the allosteric site of PBP2x, with silicristin showing the better fitness. The docking scores observed at the allosteric site are comparable with those observed at the active site, which also range between −9.2 and −9.9 kcal/mol, with silicristin having the highest negative docking scores at both sites. However, as molecular docking approach only serves as a screening process for obtaining the pose, orientation, and interactions of a ligand at the binding pocket of a protein, MMGBSA and molecular dynamic studies were further carried out to assess the ΔGbind, thermodynamic stability, and fluctuation of the active site Ser337 following binding of the PBP2x allosteric site by the top-hit phenolics.

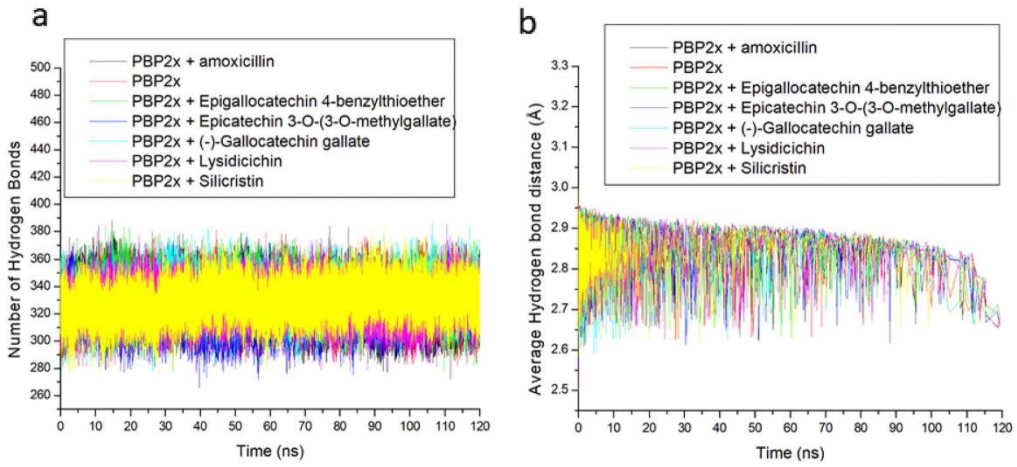


Figure 8. Time progression of (**a**) number of H-bonds, and (**b**) distance formed in PBP2x following ligand binding at the active site during the simulation.

Systems	Docking score (kcal/mol)	ΔGbind (kcal/mol)	RMSF (Å)	RMSF of Ser337 (Å)
Apo-PBP2x			13.05 ± 0.79	11.44 ± 0.12
Amoxicillin	− 8.8	− 33.75 ± 9.87	10.56 ± 0.77	14.97 ± 0.30
Silicristin	− 9.9	− 50.54 ± 4.88	7.86 ± 0.79	18.75 ± 0.22
ECBE	− 9.3	− 45.82 ± 9.74	10.78 ± 0.64	16.59 ± 0.23
Lysidicichin	− 9.2	− 33.53 ± 5.84	8.43 ± 0.79	15.48 ± 0.24
ECMG	− 9.1	− 35.06 ± 6.12	15.79 ± 0.74	14.03 ± 0.12
GCG	− 9.4	− 44.21 ± 5.74	9.61 ± 0.64	16.60 ± 0.23

Table 5. Molecular docking, thermodynamics ΔGbind, whole RMSF and RMSF values of Ser337 following binding of top hit phenolics at the allosteric site of PBP2x of *S. pneumoniae*.

Thermodynamic ΔGbind, stability and compactness following simulation of the top-ranked phenolics at the allosteric site of PBP2x of *S. pneumoniae*

Following energy refinement of the top-hit phenolics at the allosteric site of PBP2x, silicristin (− 50.54 kcal/mol), ECBE (− 45 kcal/mol), ECMG (− 35.06 kcal/mol), and GCG (− 44.21 kcal/mol) had higher negative ΔGbind at the allosteric site of PBP2x than amoxicillin (− 33.75 kcal/mol), with silicristin having the highest negative score (Table 5, Table S2). This observation is suggestive of the better affinity of the top-hit phenolics for the allosteric site of PBP2x, with silicristin being the most promising as a probable inhibitor at the site, and interestingly, this finding agrees with the docking findings of this study. The observed high affinity of silicristin at both the active and allosteric sites of PBP2x points to the probable broad-spectrum activity of the compound as an inhibitor that can treat or act in synergy with conventional antibiotics in the treatment of infections caused by *S. pneumoniae*. This observation is consistent with previous studies where phenolics show good synergistic properties with conventional antibiotics[14,19]. ECBE and GCG also had good ΔGbinds at the allosteric site of PBP2x, indicating their probable capability to act in synergy with conventional beta-lactams (Table 5). ECMG and lysidicichin, on the other hand, had moderately higher negative ΔGbinds than amoxicillin (Table 5). Analysis of the thermodynamic stability suggests stable trajectories of the top-hit phenolics at the allosteric site of PBP2x with RMSD values that are less than 3 Å limit[51] (ranging between 1.74 and 2.19 Å) and negligible ROG and SASA variances of 0.23 Å and 1042 Å respectively, between the bonded systems and the apo-PBP2x (Fig. S2, Table S3). These observations are revealing of the thermodynamic compatibility of the top-hit phenolics at the allosteric site of PBP2x. While two different experimental structures of PBP2x were used for the active and allosteric site evaluations, the low RMSD values and smaller ROG variance following binding at the allosteric site relative to the active site could be pinpointing the higher thermodynamic stability of the top-hit phenolics at the allosteric site.

Thermodynamic fluctuation of the active site Ser337 following simulation of the top-ranked phenolics at the allosteric site of PBP2x of *S. pneumoniae*

The RMSF fluctuation of PBP2x following the top-hit phenolics and amoxicillin binding of PBP2x ranges between 9.61 and 15.79 Å with silicristin having the lowest value (Table 5, Fig. 9a). Unlike the active site, this observation implies a significantly higher fluctuation of the residues of PBP2x following the top-hit phenolics and amoxicillin binding at the allosteric site. However, it is worth acknowledging that the different experimental crystal structures of PBP2x used in this study for the active and allosteric sites might have played a major role in the differences observed. Substantiating this observation is the fact that except for ECMG (15 Å), the top-hit phenolics and amoxicillin binding of PBP2x all resulted in a reduced fluctuation of residues relative to the apo-PBP2x (Table 5, Fig. 9a). This observation implies that the residues were able to form stable intra- and intermolecular bonds[49,52] during the MD simulation of the investigated compounds at the allosteric site of PBP2x. Silicristin having the lowest RMSF value at 7.86 Å (Table 5) suggests the advantage of the compound as a probable inhibitor of the site, an observation that is consistent with the thermodynamic ΔGbind findings of this study. However, it is surprising that while silicristin had the lowest RMSF value in the whole protein, the compound instigated the highest fluctuation of Ser337 (Table 5, Fig. 9b), a critical residue at the active site PBP2x[10]. The highest fluctuation of Ser337, in silicristin-PBP2x complex is coherent with the highest negative ΔGbind of silicristin (− 50.54 kcal/mol) at the allosteric site of PBP2x. Similarly, ECBE (− 45.82 kcal/mol) and GCG (− 44.21 kcal/mol), with the second and third highest negative ΔGbind at the allosteric site, had higher fluctuations of Ser337 than other investigated compounds at 16.59 Å and 16.60 Å respectively (Table 5, Fig. 8b). While other investigated compounds with moderately high negative ΔGbind at the allosteric site also have a higher fluctuation of Ser337 than apo-PBP2x (Table 5, Fig. 9b). All these observations are suggestive of the high instability of Ser337 of the active site following ligand binding of the allosteric site, with the ΔGbind of the ligands at the allosteric site partially correlating the fluctuation of the critical amino acid. Another conclusion from this is that there is less involvement of the critical amino acid in the intramolecular binding of other important residues at the active site, which might mean less obstruction and thus encourage the entry of beta-lactam. This observation is consistent with the earlier report of Bernardo-Garca et al.[12], who demonstrated that the complexation of a pentapeptide strain at the PASTA domains, prompts another pentapeptide strand in the same nascent peptidoglycan strand to enter the active site of PBP2x. Another study by Mahasenan et al.[53] also showed experimentally that the displacement of adjacent residues that can enter intramolecular interactions with Tyr446 (the critical amino acid in PBP2a) after allosteric binding of PBP2a with cefepime, which has also been demonstrated computationally by Aribisala

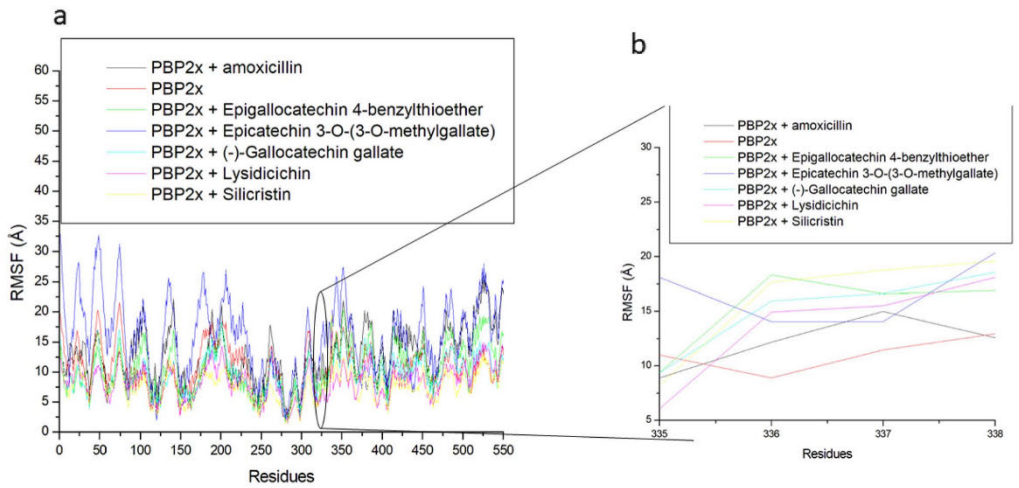


Figure 9. Relative root means square fluctuation plots of alpha – carbon, amoxicillin, and top-hit phenolics at the allosteric site of PBP2x (**a**) and the critical residue at the active site of PBP2x following binding at the allosteric site (**b**) of *S. pneumoniae* over a 120 ns simulation period.

and Sabiu[46], that appropriate occupancy of the allosteric site of PBP2a by phenolics caused high fluctuation of Tyr446. Thus, the high fluctuation of Ser337 following ligand binding to the allosteric site of PBP2x is consistent with previous report. This can be further substantiated when the fluctuation of the critical amino acid is compared to the fluctuations when the top-hit phenolic and amoxicillin bind at the active site. Binding of the top-hit phenolics at the active site caused significant lesser fluctuation of Ser337 (between 0.87 and 1.19 Å) relative to the apo-PBP2x (1.27 Å) (Table 4, Fig. 6b) while binding at the allosteric site caused significant higher fluctuation (between 14.03 and 18.75 Å) relative to the apo-PBP2x (11.44 Å) (Table 5, Fig. 9b). This observation is revealing of the inter- or intramolecular involvement of Ser337 following ligand binding at the active site, while binding at the allosteric site, on the other hand, causes lesser involvement of the residue in the intramolecular binding or obstruction of the active site.

Interactions plots analysis of the top-hit phenolics at the active and allosteric site of PBP2x of *S. pneumoniae* after 120 ns MD simulation

To understand how the nature of interactions impacted the ΔGbind and stability of the top-hit phenolics against PBP2x, the plots of interactions for each system after the 120 ns simulation were analyzed. The binding of drugs to biological targets has been demonstrated to rely on specific non-covalent interactions between partner molecules, including electrostatic interactions such as hydrogen bonds, van der Waals interactions, and hydrophobic effects[54]. In this study, the number, nature, and lengths of interactions between partner molecules (ligands and PBP2x) were noted to have an impact on the ΔGbind and stability observed in this study. The plots of interactions of the reference standards and phenolics with the highest ΔGbind at both the active and allosteric sites of PBP2x are presented in Figs. 9, 10, 11 and 12, while those of the other top-hit phenolics are shown in Figs. S3 and S4 for the active and allosteric sites, respectively. At the active site, except for silicristin, epicatechin 3-O-(3-O-methylgallate), which had the highest negative ΔGbind against PBP2x interacted with the highest number of interactions at 15, three of which are hydrogen bond contacts with the lowest average distance at 2.84 Å with residues Glu295, Asn294, and Asp472 (Table 6, Fig. 10). The high number of interactions and the significantly lower length of the hydrogen bond contacts could have drastically contributed to the observed high negative ΔGbind of ECMG against PBP2x. Silicristin, which has the second highest negative ΔGbind against PBP2x, had the highest number of interactions at 16, five of which are hydrogen bond contacts with an average length of 3.16 Å with residues Ser465, Tyr503, Glu295, Asn294 and Ser254 (Table 6, Fig. S3). Compared to ECMG-PBP2x, even though silicristin-PBP2x had the highest number of interactions, including hydrogen bond contacts, the observed higher average distance of hydrogen bond contact in the silicristin-PBP2x complex could have contributed to its lower negative ΔGbind and stability relative to ECMG-PBP2x complex. The importance of hydrogen bond length observed in this study is consistent with the findings of Du et al.[50], who showed the relevance of reduced interaction length in the higher pull between two intramolecular or intermolecular molecules. Reduced bond length will facilitate the atoms of two molecules being held together more tightly, resulting in greater affinity and stability[50]. Similarly, lysidicichin, with a moderately higher negative ΔGbind relative to amoxicillin (Table 6, Fig. 11), and other top hit phenolics had 10 interactions, 4 of which were hydrogen bond contacts with an average distance of 2.98 Å with Ser504 (2), Gln499, and Thr443 (Table 6, Fig. S3). The higher number and reduced average distance of hydrogen bond contacts of lysidicichin against PBP2x could have impacted the higher negative ΔGbind relative to amoxicillin-PBP2x, ECBE-PBP2x, and GCG-PBP2x, thus further highlighting the

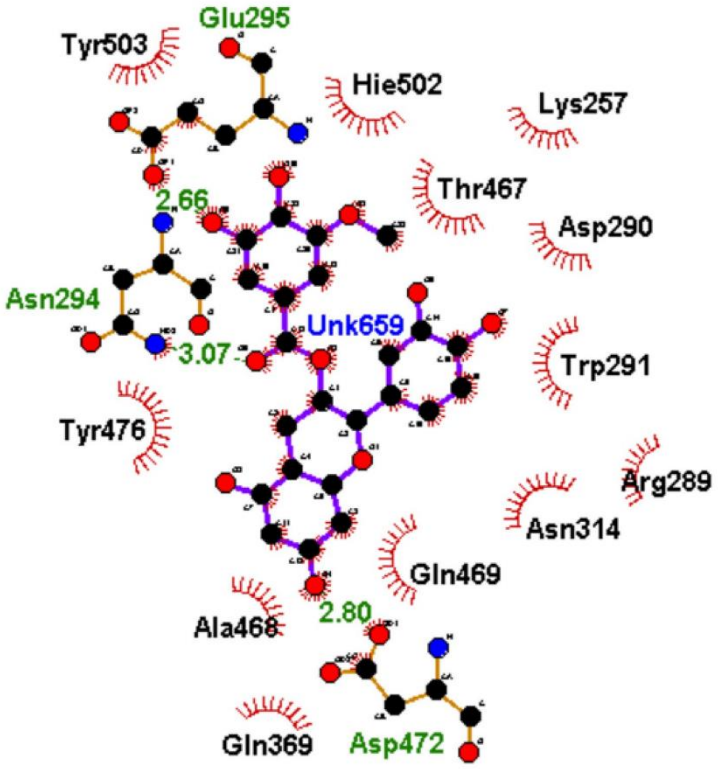


Figure 10. 2D plot of interactions of ECMG at the active site of PBP2x.

importance of the number and bond length in ΔGbind determination. ECBE and GCG against PBP2x only had 3 and 4 total interactions with PBP2x with no hydrogen bond contacts (Table 6, Fig. S3). This observation could have immensely contributed to the significantly lower ΔGbind observed with the ECBE-PBP2x and GCG-PBP2x relative to other studied complexes in this study. At the allosteric site, a considerable similar number of interactions, ranging from 13 to 16 total interactions, were observed between the investigated compounds and the allosteric site of PBP2x, with GCG having the highest interaction (Table 6). Silicristin (Fig. 12), ECBE (Fig. S4), and amoxicillin (Fig. 12) had the same number of interactions at 15. The high number of interactions in the silicristin, GCG, and ECBE complex with PBP2x could have impacted the higher negative ΔGbind of the compounds at the allosteric site of PBP2x. Despite having a similar number of total interactions with silicristin and ECBE, amoxicillin has a considerably lower negative ΔGbind, which could be partly attributable to the reduced number of hydrogen bond contacts in the amoxicillin-PBP2x complex (Fig. 13) relative to silicristin (Fig. 12) and ECBE (Table 6, Fig. S4). The catalytic residues (such as Ser337, Tyr568, Pro335, Ser396, Trp374 and Ser395 at the active site and Arg426, Gly422, Phe421, Asn417, and Val423 at the allosteric site) present in the molecular docking interactions of the investigated compounds with PBP2x were not observed in the interaction plots of both sites after the 120 ns MD simulation. Similar observation was noted by Al-Karmalawy et al.[55], following simulation of alacepril with hACE2 and might have been due to the dynamic nature of simulation employed. Nevertheless, the lesser fluctuation of Ser337 (the catalytic residue in PBP2x) compared to the RMSF of the whole protein means that the top-ranked phenolics and amoxicillin during the simulation reside most at the active region of the protein, as lesser fluctuation is tantamount to strong intermolecular bonding[56]. Furthermore, snapshots of protein–ligand complexes of the lead phenolic and amoxicillin at different time intervals of the 120 ns MD simulation (0 ns, 40 ns, 80 ns and 120 ns) (Fig. S4) revealed that the catalytic residues (such as Ser337, Tyr568, Pro335, Ser396, Trp374 and Ser395) were present in the early interaction plots of the complexes suggesting suitable occupancy of this region during the period of the simulation. This observation corroborates the RMSF findings of this study on the lesser fluctuation of the catalytic residues of PBP2x relative to other residues in the protein. However, the absence of the active site residue after 80 ns could indicate a displacement of the ligand from the binding pocket of PBP2x, possibly due to a local conformational change in the protein which triggers the unbinding of the ligand from the binding pocket.

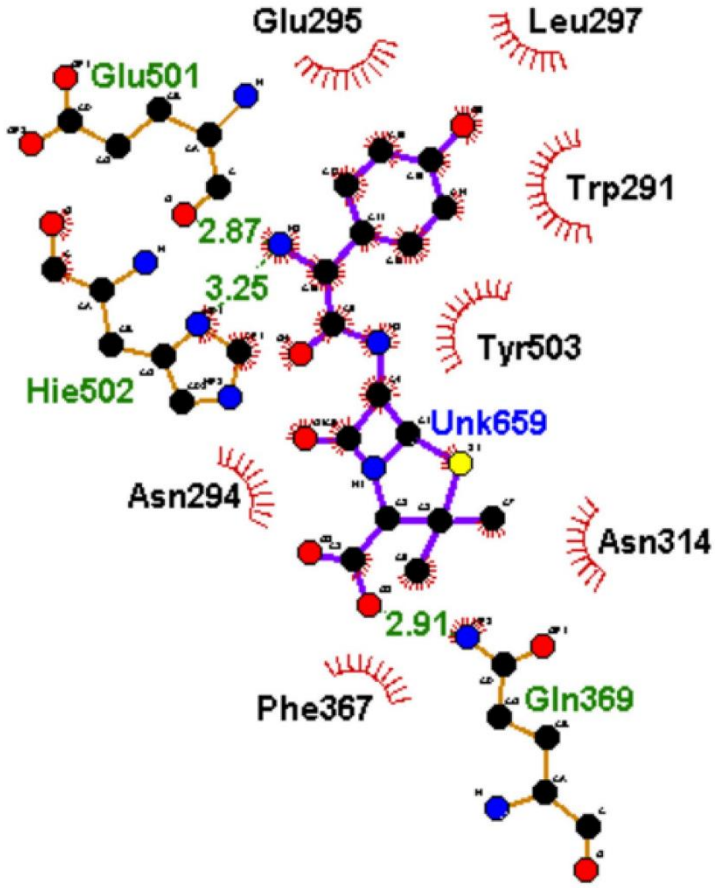


Figure 11. 2D plot of interactions of amoxicillin at the active site of PBP2x.

Molecular orbital properties of best performing phenolics at the active and allosteric sites of PBP2x

Understanding the HOMO and LUMO characteristics of a compound could provide crucial chemical insights relevant to the actual use of the compound as a medicinal molecule[32,33]. The energy gap (LUMO–HOMO) of a compound provides information about its stability; A larger energy gap means high stability, which can prevent ligand binding to a protein[34,35]. In this study, silicristin (4.0510 eV) and ECMG (4.5388 eV) had lower energy gaps than amoxicillin (5.3234 eV) (Table 7 Fig. 14). This observation points to the high instability of silicristin and ECMG relative to amoxicillin. The higher softness and lower hardness of silicristin and ECMG relative to amoxicillin (Table 7), might suggest better reactivity of silicristin and ECMG compounds compared to amoxicillin. According to Pearson[33], higher chemical softness and lower chemical hardness signify higher compound reactivity. The high instability and better reactivity of silicristin and ECMG relative to amoxicillin could have positively impacted their better interactions at the active and allosteric sites of PBP2x. Furthermore, the ability of an atom or a functional group of a compound to attract electrons could be assessed by evaluating the electronegativity and chemical potential. In this study, the higher electronegativity and higher negative chemical potential of silicristin and ECMG relative to amoxicillin (Table 7) means better capability of the atoms and functional groups of silicristin and ECMG to attracts electron at the binding pockets of PBP2x and hence their better affinity for PBP2x than amoxicillin in this study. This observation is also further supported by the higher electrophilicity index of silicristin and ECMG compared to amoxicillin (Table 7), which indicates the better tendency of these compound to acquire electron density relative to amoxicillin[35].

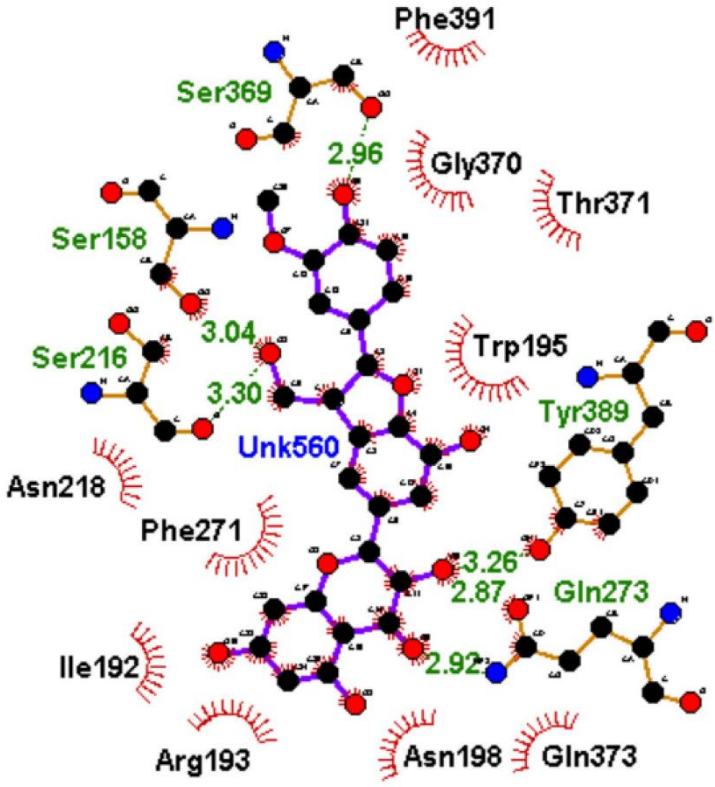


Figure 12. 2D plot of interactions of silicristin at the allosteric site of PBP2x.

Top-ranked phenolics and standard	Total number of interactions	Number of hydrogen bonds, average distance and interaction residues
Active site		
Amoxicillin	10	3 (3.01 Å) [Glue501, Hie502, Asp472]
Silicristin	16	5 (3.16 Å) [Ser465, Tyr503, Glu295, Asn294, Ser254]
ECBE	3	None
Lysidicichin	10	4 (2.98 Å) [Ser504 (2), Gln499, Thr443]
ECMG	15	3 (2.84 Å) [Glu295, Asn294, Asp472]
GCG	4	None
Allosteric site		
Amoxicillin	15	5 (2.82 Å) [Glu377, Gly381, Arg193, Gln273
Silicristin	15	6 (3.05 Å) [Gln273 (2), Tyr389, Ser216, Ser158, Ser369]
ECBE	15	8 (2.94 Å) [Asn198, Tyr382, Ser216, Gln373, Lys161, Gln273, Phe271, Asn218]
Lysidicichin	13	6 (2.89 Å) [Asp189, Thr191 (2), Asn262, Val264, Asp376]
ECMG	13	6 (2.94 Å) [Asn218, Asp194 (2),Tyr381, Gly274, Glu155]
GCG	16	3 (2.85 Å) [Leu383, Phe271, Ser158]

Table 6. Interactions plots analysis of the top-hit phenolics at the active and allosteric site of PBP2x of *S. pneumoniae* after 120 ns MD simulation.

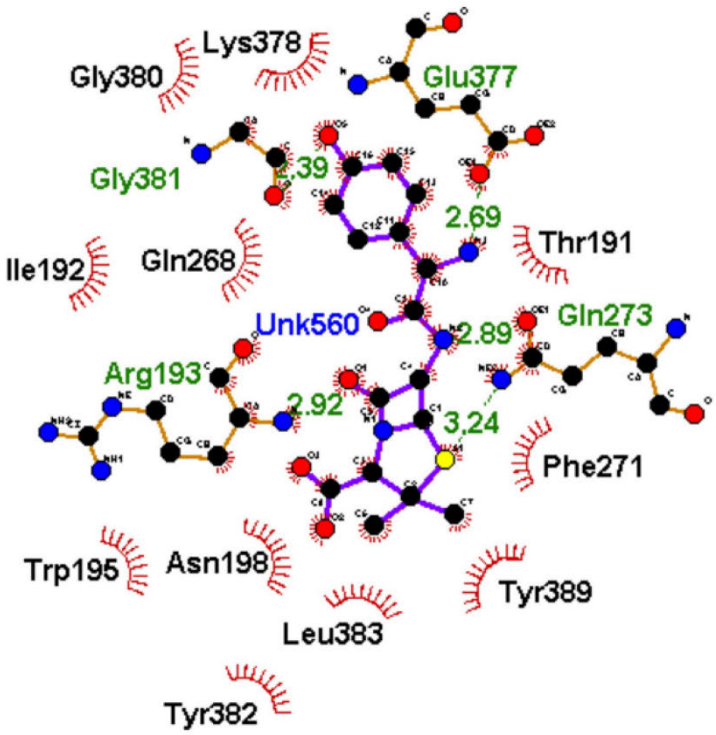


Figure 13. 2D plot of interactions of amoxicillin at the allosteric site of PBP2x.

CDFT descriptors (eV)	Amoxicillin	Silicristin	ECMG
E_LUMO	−1.0116	−1.8273	−1.4335
E_HOMO	−6.3350	−5.8784	−5.9723
Energy gap (ΔE)	5.3234	4.0510	4.5388
Ionization energy (I)	6.3350	5.8784	5.9723
Electron affinity (A)	1.0115	1.8273	1.4335
Hardness (η)	2.6617	2.0255	2.2694
Softness (S)	0.3756	0.4937	0.4406
Electronegativity (χ)	3.6733	3.8528	3.7029
Chemical potential (μ)	−3.6733	−3.8529	−3.7029
Electrophilicity index	2.5346	3.6644	3.0210

Table 7. The CDFT of the best performing phenolics at the active and allosteric site of PBP2x using DFT calculated by B3LYP/6-31G + (dp).

Conclusion

The findings from this study revealed the diverse capability of phenolics in the binding of the active and allosteric sites of PBP2x, with ECMG having advantages in the binding of the PBP2x active site. On the other hand, silicristin had better affinity at the allosteric site. Compared to other top-ranked phenolics, the high affinity of silicristin at both the active and allosteric sites of PBP2x showed that the compound had the best broad-spectrum effects and thus had an advantage over other top hit phenolics and amoxicillin as inhibitors of PBP2x. However, relative to other top hit phenolics, silicristin elicited higher thermodynamic entropy following binding at the active site. This discovery might point to the necessity for further structural modifications to the molecule for stability, which could greatly boost its affinity for PBP2x. Protein ligand interaction analysis revealed the involvement of the active site residue such as Ser337 at the early stage of the MD simulation in the stability of

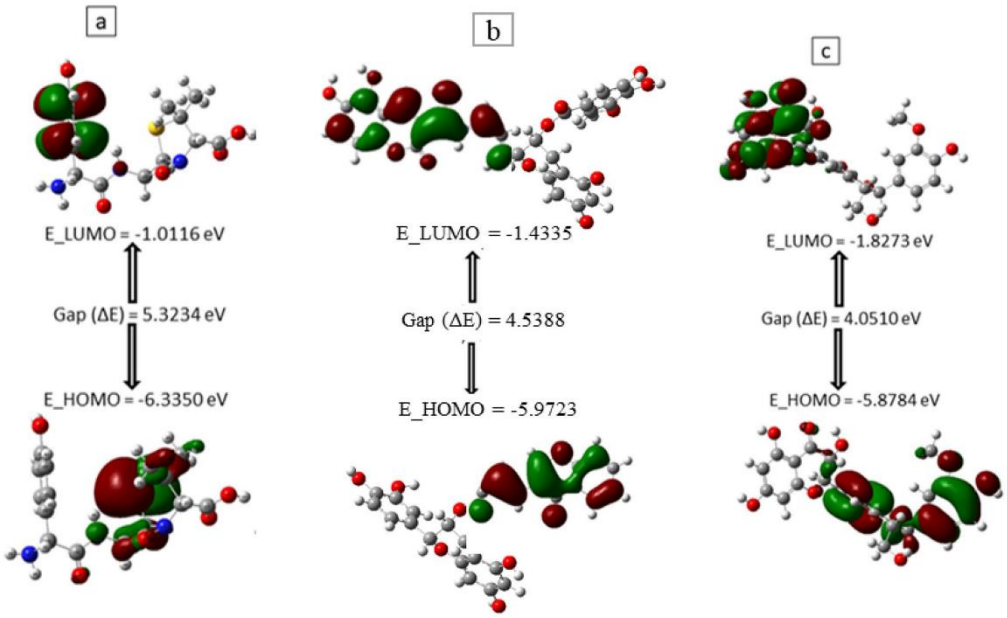


Figure 14. Frontier molecular orbitals for (**a**) amoxicillin, (**b**) ECMG, and (**c**) silicristin,

ECMG and amoxicillin against PBP2x. Allosteric modulation of Ser337, the critical amino acid at the active site of PBP2x, was noted as ECBE, GCG, and silicristin with higher negative ΔGbind at the allosteric site instigated more fluctuation of Ser337 than amoxicillin, lysidicichin, and ECMG with moderately high affinity. This observation could imply that higher affinity of the top-hits at the allosteric site of PBP2x causes less obstruction of the active site due to the lesser involvement of Ser337 in intramolecular binding of adjacent residues. Comparably, binding of the top hit phenolics and amoxicillin at the active site of PBP2x causes less fluctuation of Ser337, suggesting that the residue could be involved in inter- and intra-molecular interaction. These findings hint to the potential advantages of top-hit phenolics, particularly silicristin, in the direct and synergistic treatment of *S. pneumoniae* infections with conventional beta-lactam medicines. More importantly, the top-hits phenolics had drug-like pharmacokinetics and toxicity profile that potentiate them as probable drug candidates. However, further in vitro and in vivo validation of the activities of the top-hits phenolics is highly suggested, and work is ongoing in this regard.

Data availability

All data generated or analysed during this study are included in this published article and its supplementary information files.

Received: 3 February 2024; Accepted: 11 April 2024
Published online: 16 April 2024

References

1. Evans, W. & Hansman, D. Tetracycline-resistant pneumococcus. *Lancet* **281**, 451. https://doi.org/10.1016/S0140-6736(63)92350-X (1963).
2. Sader, H. S. *et al.* Antimicrobial susceptibility of *Streptococcus pneumoniae* from North America, Europe, Latin America, and the Asia-Pacific region: results from 20 years of the SENTRY antimicrobial surveillance program (1997–2016). *Open Forum Infect. Dis.* **6**, S14-23. https://doi.org/10.1093/ofid/ofy263 (2019).
3. Lewnard, J. A., Lo, N. C., Arinaminpathy, N., Frost, I. & Laxminarayan, R. Childhood vaccines and antibiotic use in low- and middle-income countries. *Nature* **581**, 94–99. https://doi.org/10.1038/s41586-020-2238-4 (2020).
4. Buckley, B. S. *et al.* Impact of vaccination on antibiotic usage: A systematic review and meta-analysis. *Clin. Microbiol. Infection* **25**, 1213–1225. https://doi.org/10.1016/j.cmi.2019.06.030 (2019).
5. Walker, C. L. F. *et al.* Global burden of childhood pneumonia and diarrhoea. *Lancet* **381**(9875), 1405–1416. https://doi.org/10.1016/S0140-6736(13)60222-6 (2013).
6. Cherazard, R. *et al.* Antimicrobial resistant *Streptococcus pneumoniae*: Prevalence, mechanisms, and clinical implications. *Am. J. Therap.* **24**, e361–e369. https://doi.org/10.1097/MJT.0000000000000551 (2017).
7. Cornick, J. E. & Bently, S. D. *Streptococcus pneumoniae*: The evolution of antimicrobial resistance to beta-lactams, fluoroquinolones and macrolides. *Microbes Infection* **14**, 573–583. https://doi.org/10.1016/j.micinf.2012.01.012 (2012).

8. Typas, A., Banzhaf, M., Gross, C. A. & Vollmer, W. From the regulation of peptidoglycan synthesis to bacteria growth and morphology. *Nat. Rev. Microbiol.* **10**, 123–136. https://doi.org/10.1038/nrmicro2677 (2011).
9. Beilharz, K. *et al.* Control of cell division in *Streptococcus pneumoniae* by the conserved Ser/Thr protein kinase StkP. *Proc. Natl. Acad. Sci. USA* **109**, E905-913. https://doi.org/10.1073/pnas.1119172109 (2012).
10. Gordon, E., Mouz, N., Duee, E. & Dideberg, O. The crystal structure of the penicillin-binding protein 2x from *Streptococcus pneumoniae* and its acyl-enzyme form: implication in drug resistance. *J. Mol. Biol.* **299**, 477–485. https://doi.org/10.1006/jmbi.2000.3740 (2000).
11. Land, A. D. *et al.* Requirement of essential Pbp2x and GpsB for septal ring closure in *Streptococcus pneumoniae* D39. *Mol. Microbiol.* **90**, 939–955. https://doi.org/10.1111/mmi.12408 (2013).
12. Bernardo-García, N. *et al.* Allostery, recognition of nascent peptidoglycan, and cross-linking of the cell wall by the essential penicillin-binding protein 2x of *Streptococcus pneumoniae*. *ACS Chem. Biol.* **13**, 694–702. https://doi.org/10.1021/acschembio.7b00817 (2018).
13. Peters, K. *et al. Streptococcus pneumoniae* PBP2x mid-cell localization requires the C-terminal PASTA domains and is essential for cell shape maintenance. *Mol. Microbiol.* **92**, 733–755. https://doi.org/10.1111/mmi.12588 (2014).
14. Meisel, J. E., Fisher, J. F., Chang, M. & Mobashery, S. Allosteric inhibition of bacteria targets: an opportunity for discovery of novel antibacterial classes. In *Topics in Medicinal Chemistry* (eds Fisher, J. F. *et al.*) 83–117 (Springer, 2018).
15. Cuschnie, T. P. & Lamb, A. J. Recent advances in understanding the antibacterial properties of flavonoids. *Int. J. Antimicrobial Agents* **38**, 99–107. https://doi.org/10.1016/j.ijantimicag.2011.02.014 (2011).
16. Aldulaimi, O. A. General overview of phenolics from plant to laboratory, good antibacterials or not?. *Pharmacogn.* **11**, 123–127. https://doi.org/10.4103/phrev.phrev_43_16 (2017).
17. Alhadrami, H. A. *et al.* Flavonoids as potential anti-MRSA agents through modulation of PBP2a: A computational and experimental study. *Antibiotics* **9**, 562. https://doi.org/10.3390/antibiotics9090562 (2020).
18. Araya-Cloutier, C., Vincken, J. P., van Ederen, R., den Besten, H. M. W. & Gruppen, H. Rapid membrane permeabilization of Listeria monocytogenes and *Escherichia coli* induced by antibacterial prenylated phenolic compounds from legumes. *Food Chem.* **240**, 147–155. https://doi.org/10.1016/j.foodchem.2017.07.074 (2018).
19. Qin, R. *et al.* The combination of catechin and epicatechin callate from Fructus Crataegi potentiates beta-lactam antibiotics against methicillin-resistant *staphylococcus aureus* (MRSA) in vitro and in vivo. *Int. J. Mol. Sci.* **14**, 1802–1821. https://doi.org/10.3390/ijms14011802 (2013).
20. Rudrapal MJ, Khairnar SG, Jadhav A (2020) Drug Repurposing (DR): An Emerging Approach in Drug Discovery [Internet]. Drug Repurposing - Hypothesis, Molecular Aspects and Therapeutic Applications. IntechOpen 12. https://doi.org/10.5772/intechopen.93193
21. Tandon, H., Chakraborty, T. & Suhag, V. A brief review on importance of DFT in drug design. *Res. Med. Eng. Sci.* https://doi.org/10.31031/RMES.2019.07.00068 (2019).
22. Pettersen, E. F. *et al.* UCSF Chimera—A visualization system for exploratory research and analysis. *J. Comput. Chem.* **25**(13), 1605–1612. https://doi.org/10.1002/jcc.20084 (2004).
23. BIOVIA, Dassault Systèmes, BIOVIA Workbook, Release 2021; BIOVIA Pipeline Pilot, Release 2021, San Diego: Dassault Systèmes, [2021].
24. Koes, D. R. & Camacho, C. J. ZINCPharmer: Pharmacophore search of the ZINC database. *Nucleic Acids Res.* **40**, 409–414. https://doi.org/10.1093/nar/gks378 (2012).
25. Dallakyan, S. & Olson, A. J. Small-molecule library screening by docking with PyRx. *Methods Mol. Biol.* **1263**, 243–250. https://doi.org/10.1007/978-1-4939-2269-7_19 (2015).
26. Fahad, M. A., Kalim, M., Pulicat, M. S., Akhtar, S. & Arif, J. M. In silico prediction of mechanism of erysolin-induced apoptosis in human breast cancer cell lines. *Am. J. Bioinform. Res.* **3**(3), 62–71. https://doi.org/10.5923/j.bioinformatics.20130303.03 (2013).
27. Bajorath, J. Selected concepts and investigations in compound classification, molecular descriptor analysis, and virtual screening. *J. Chem. Inform. Comput. Sci.* **41**, 233–245. https://doi.org/10.1021/ci0001482 (2001).
28. Hospital, A., Goñi, J. R., Orozco, M. & Gelpí, J. L. Molecular dynamics simulations: Advances and applications. *Adv. Appl. Bioinform. Chem.* **8**, 37–47. https://doi.org/10.2147/AABC.S70333 (2015).
29. Ylilauri, M. & Pentikäinen, O. T. MMGBSA as a tool to understand the binding affinities of filamin–peptide interactions. *J. Chem. Inform. Model.* **53**, 2626–2633. https://doi.org/10.1021/ci4002475 (2013).
30. Wallace, A. C., Laskowski, R. A. & Thornton, J. M. LIGPLOT: A program to generate schematic diagrams of protein-ligand interactions. *Protein Eng.* **8**, 127–134. https://doi.org/10.1093/protein/8.2.127 (1995).
31. Aihara, J. Reduced HOMO-LUMO Gap as an index of kinetic stability for polycyclic aromatic hydrocarbons. *J. Phys. Chem. A* **103**, 7487–7495. https://doi.org/10.1021/jp990092i (1999).
32. Ayers, P. W., Parr, R. G. & Pearson, R. G. Elucidating the hard/soft acid/ base principle: A perspective based on half-reactiveions. *J. Chem. Phys.* **124**, 194107. https://doi.org/10.1063/1.2196882 (2006).
33. Pearson, R. G. Absolute electronegativity and hardness correlated with molecular orbital theory. *Proc. Natl. Acad. Sci.* **83**, 8440–8441. https://doi.org/10.1073/pnas.83.22.8440 (1986).
34. Pearson, R. G. (1995) The HSAB Principle-more quantitative aspects. *Inorganica Chimica Activea.* **240**(1–2), 93–98. https://doi.org/10.1016/0020-1693(95)04648-8ssssss (1995).
35. Singh, V., Dhankhar, P., Dalal, V., Tomar, S. & Kumar, P. In-silico functional and structural annotation of hypothetical protein from Klebsiella pneumonia: A potential drug target. *J. Mol. Graph. Model.* **116**, 108262. https://doi.org/10.1016/j.jmgm.2022.108262 (2022).
36. Cerón-Carrasco, J. P. When virtual screening yields inactive drugs: Dealing with false theoretical friends. *ChemMedChem* **17**, e202200278. https://doi.org/10.1002/cmdc.202200278 (2022).
37. Lipinski, C. A., Lombardo, F., Dominy, B. W. & Feeney, P. J. Experimental and computational approaches to estimate solubility and permeability in drug discovery and development settings. *Adv. Drug Deliv. Rev.* **46**, 3–26. https://doi.org/10.1016/S0169-409X(00)00129-0 (2001).
38. Ertl, P. & Schuffenhauer, A. Estimation of synthetic accessibility score of drug-like molecules based on molecular complexity and fragment contributions. *J. Cheminform.* **1**, 8. https://doi.org/10.1186/1758-2946-1-8 (2009).
39. Aribisala, J. O. & Sabiu, S. Cheminformatics identification of phenolics as modulators of penicillin–binding protein 2a of Staphylococcus aureus: A structure–activity–relationship–based study. *Pharmaceutics* **14**, 1818. https://doi.org/10.3390/pharmaceutics14091818 (2022).
40. Khumbulani, M., Alayande, K. A. & Sabiu, S. Orientin enhances colistin-mediated bacteria lethality through oxidative stress involvement. *Evidence-Based Complement. Alternative.* https://doi.org/10.1155/2022/3809232 (2022).
41. Gonçalves, P. F. & Stassen, H. Free energy of solvation from molecular dynamics simulations for low dielectric solvents. *J. Comput. Chem.* **24**, 1758–1765. https://doi.org/10.1002/jcc.10294 (2003).
42. Dalal, V. *et al.* Structure-based identification of potential drugs against FmtA of Staphylococcus aureus: Virtual screening, molecular dynamics, MM-GBSA, and QM/MM. *Protein J.* **40**, 148–165. https://doi.org/10.1007/s10930-020-09953-6 (2011).
43. Stella, L. & Melchionna, S. Equilibration and sampling in molecular dynamics simulations of biomolecules. *J. Chem. Phys.* **109**, 10115–10117. https://doi.org/10.1063/1.477703 (1998).
44. Sainsbury, S. *et al.* Crystal structures of penicillin-binding protein 3 from Pseudomonas aeruginosa: Comparison of native and antibiotic-bound forms. *J. Mol. Biol.* **405**, 173–184. https://doi.org/10.1016/j.jmb.2010.10.024 (2011).

45. Lobanov, M. Y., Bogatyreva, N. S. & Galzitskaya, O. V. Radius of gyration as an indicator of protein structure compactness. *Mol. Biol.* **42**, 623–628. https://doi.org/10.1134/S0026893308040195 (2008).
46. Aribisala, J. O. *et al.* Astaxanthin-mediated bacteria lethality: Evidence from oxidative stress contribution and molecular dynamics simulation. *Oxidative Med. Cell. Longevity.* https://doi.org/10.1155/2021/7159652 (2021).
47. Mousavi, S. S. *et al.* In silico evaluation of Iranian medicinal plant phytoconstituents as inhibitors against main protease and the receptor-binding domain of SARS-CoV-2. *Molecules* **26**, 5724. https://doi.org/10.3390/molecules26185724 (2021).
48. Aribisala, J. O. & Sabiu, S. Cheminformatics identification of phenolics as modulators of penicillin-binding protein-3 of Pseudomonas aeruginosa towards interventive antibacterial therapY. *J. Biomol. Struct. Dynam.* **42**, 298–313. https://doi.org/10.1080/07391102.2023.2192808 (2024).
49. Uhomoibhi, J. O., Shode, F. O. & Sabiu, I. K. A. Molecular modelling identification of phytocompounds from selected African botanicals as promising therapeutics against druggable human host cell targets of SARS-CoV-2. *J. Mol. Graph. Model.* **114**, 108185. https://doi.org/10.1016/j.jmgm.2022.108185 (2022).
50. Du, X. *et al.* Insights into protein-ligand interactions: Mechanisms, models, and methods. *Int. J. Mol. Sci.* **17**, 144. https://doi.org/10.3390/ijms17020144 (2016).
51. Bissantz, C., Kuhn, B. & Stahl, M. A. Medicinal chemist's guide to molecular interactions. *J. Med. Chem.* **14**, 5061–5084. https://doi.org/10.1021/jm100112j (2010).
52. Ramirex, D. & Caballero, J. Is it reliable to use common molecular docking methods for comparing the binding affinities of Enantiomer pairs for their protein target. *Int. J. Mol. Sci.* **17**, 525–545. https://doi.org/10.1016/j.biotechadv.2018.11.013 (2016).
53. Mahasenan, K. V. *et al.* Conformational dynamics in penicillin-binding protein 2a of methicillin-resistant Staphylococcus aureus, allosteric communication network and enablement of catalysis. *J. Am. Chem. Soc.* **139**, 2102–2110. https://doi.org/10.1021/jacs.6b12565 (2017).
54. Liang, Z. & Li, Q. X. π-Cation interactions in molecular recognition: Perspectives on pharmaceuticals and pesticides. *J. Agric. Food Chem.* **66**, 3315–3323. https://doi.org/10.1021/acs.jafc.8b00758 (2018).
55. Al-Karmalawy, A. A. *et al.* Molecular docking and dynamics simulation revealed the potential inhibitory activity of ACEIs against SARS-CoV-2 targeting the hACE2 receptor. *Front. Chem.* **9**, 661230. https://doi.org/10.3389/fchem.2021.661230 (2021).
56. Baig, M. H. *et al.* Insight into the effect of inhibitor resistant S130G mutant on physico–chemical properties of SHV type Beta-Lactiveamase: A molecular dynamics study. *PLoS ONE* **9**, e112456. https://doi.org/10.1371/journal.pone.0112456 (2014).

Acknowledgements

The assistance of the National Research Foundation (NRF-TWAS Doctoral Scholarship, Grant number 129950), South Africa, to Mr. J. O. Aribisala is duly and thankfully acknowledged. The Centre for High-Performance Computing (CHPC), South Africa is equally acknowledged for granting access to the computing systems used in this study.

Author contributions

SS conceptualized, mobilized funds, and managed the study. SS supervised the study. JOA generated and analyzed the data. JOA and NWS wrote the manuscript. All authors read and contributed to the critical review of the manuscript for intellectual content and approved the submission for publication.

Funding

The authors specially acknowledge the financial assistance of the Directorate of Research and Postgraduate Support, Durban University of Technology (DUT), and the South African Medical Research Council (SAMRC) under a Self-Initiated Research Grant as well as the National Research Foundation (NRF) Research Development Grant for Rated Researchers (Grant number 120433) and the Competitive Programme for Rated Researchers Support (SRUG2204193723) to S. Sabiu. The views and opinions expressed are those of the authors and do not necessarily represent the official views of the funders.

Competing interests

The authors declare no competing interests.

Additional information

Supplementary Information The online version contains supplementary material available at https://doi.org/10.1038/s41598-024-59489-3.

Correspondence and requests for materials should be addressed to S.S.

Reprints and permissions information is available at www.nature.com/reprints.

Publisher's note Springer Nature remains neutral with regard to jurisdictional claims in published maps and institutional affiliations.

Open Access This article is licensed under a Creative Commons Attribution 4.0 International License, which permits use, sharing, adaptation, distribution and reproduction in any medium or format, as long as you give appropriate credit to the original author(s) and the source, provide a link to the Creative Commons licence, and indicate if changes were made. The images or other third party material in this article are included in the article's Creative Commons licence, unless indicated otherwise in a credit line to the material. If material is not included in the article's Creative Commons licence and your intended use is not permitted by statutory regulation or exceeds the permitted use, you will need to obtain permission directly from the copyright holder. To view a copy of this licence, visit http://creativecommons.org/licenses/by/4.0/.

© The Author(s) 2024

3.4 Cheminformatics identification of phenolics as modulators of penicillin-binding protein 2a of *Staphylococcus aureus*: A structure–activity-relationship-based study

This section has been published in Pharmaceutics and is presented as it is in the article

pharmaceutics

MDPI

Article

Cheminformatics Identification of Phenolics as Modulators of Penicillin-Binding Protein 2a of *Staphylococcus aureus*: A Structure–Activity-Relationship-Based Study

Jamiu Olaseni Aribisala and Saheed Sabiu *

Department of Biotechnology and Food Science, Faculty of Applied Sciences, Durban University of Technology, P.O. Box 1334, Durban 4000, South Africa
* Correspondence: sabius@dut.ac.za; Tel.: +27-31-373-5330

Abstract: The acquisition of penicillin-binding protein (PBP) 2a in resistant strains of *Staphylococcus aureus* allows for the continuous production of cell walls even after the inactivation of intrinsic PBPs. Thus, the discovery of novel therapeutics with enhanced modulatory activity on PBP2a is crucial, and plant secondary metabolites, such as phenolics, have found relevance in this regard. In this study, using computational techniques, phenolics were screened against the active site of PBP2a, and the ability of the lead phenolics to modulate PBP2a's active and allosteric sites was studied. The top-five phenolics (leads) identified through structure–activity-based screening, pharmacokinetics and synthetic feasibility evaluations were subjected to molecular dynamics simulations. Except for propan-2-one at the active site, the leads had a higher binding free energy at both the active and allosteric sites of PBP2a than amoxicillin. The leads, while promoting the thermodynamic stability of PBP2a, showed a more promising affinity at the allosteric site than the active site, with silicristin (−25.61 kcal/mol) and epicatechin gallate (−47.65 kcal/mol) having the best affinity at the active and allosteric sites, respectively. Interestingly, the modulation of Tyr446, the active site gatekeeper residue in PBP2a, was noted to correlate with the affinity of the leads at the allosteric site. Overall, these observations point to the leads' ability to inhibit PBP2a, either directly or through allosteric modulation with conventional drugs. Further confirmatory in vitro studies on the leads are underway.

Keywords: phenolics; penicillin-binding protein; structure–activity-based virtual screening; allosteric; molecular dynamic simulation

check for updates

Citation: Aribisala, J.O.; Sabiu, S. Cheminformatics Identification of Phenolics as Modulators of Penicillin-Binding Protein 2a of *Staphylococcus aureus*: A Structure–Activity-Relationship-Based Study. *Pharmaceutics* **2022**, *14*, 1818. https://doi.org/10.3390/pharmaceutics14091818

Academic Editor: Marios Spanakis

Received: 28 July 2022
Accepted: 26 August 2022
Published: 29 August 2022

Publisher's Note: MDPI stays neutral with regard to jurisdictional claims in published maps and institutional affiliations.

Copyright: © 2022 by the authors. Licensee MDPI, Basel, Switzerland. This article is an open access article distributed under the terms and conditions of the Creative Commons Attribution (CC BY) license (https://creativecommons.org/licenses/by/4.0/).

1. Introduction

Staphylococcus aureus is a Gram-positive bacterium that has remained a major public health concern over the years, due to its resistance to major antibacterial therapies [1]. For instance, Methicillin-resistant *S. aureus* (MRSA) is currently one of the most common global causes of infective endocarditis, as well as skin and respiratory system infections [2,3]. In many countries, strict policies are in place regarding the use of antibiotics, to keep the organism vulnerable due to the limited treatment options that are available [1,4]. However, even with limited usage, the number of strains of MRSA with reduced sensitivity or outright resistance to currently available antibiotics, such as daptomycin, ceftaroline, vancomycin, amoxicillin, linezolid, and cefotaxime have risen in recent times [2,4–7]. Thus, in addition to raising public awareness about safe antibiotic usage, developing new therapeutics with novel modes of action to circumvent and keep up with the increased rate of antibiotic resistance remains a top priority for many antimicrobial drug development research groups.

The survival of bacteria is dependent on the integrity of their cell walls, which are made up of peptidoglycan as the primary building unit [8,9]. Peptidoglycan consists of a repeating unit of a disaccharide (N-acetyl glucosamine (NAG)–N-acetylmuramic acid (NAM)) with the peptide stems on the NAM unit, and through crosslinking of peptide stems of nearby peptidoglycan, a mature cell wall is formed [10,11]. The peptide stem

differs in various organisms and in *S. aureus*, it is a five-chain peptide L-Ala-γ-D-Glu-L-Lys$(Gly)_5$-D-Ala-D-Ala with the lysine side chain being linked to pentaglycyl during cell wall crosslinking [10]. The transglycosylase (synthesis of peptidoglycan backbone) and transpeptidase (crosslinking of peptidoglycan) activities during cell wall production are carried out by the penicillin-binding proteins (PBPs) [9]. Due to the essential role of PBPs in cell wall synthesis, which is critical for bacterial survival, they act as an excellent target for antibiotics, particularly the β-lactams [6,10].

Staphylococcus aureus possesses four inherent PBPs (PBP1, PBP2, PBP3, and PBP4) [11]. However, due to the acquisition of the *mecA* gene, a fifth PBP known as PBP2a is frequently found in MRSA, conferring antibiotic resistance in the organism [12]. As a result, MRSA can continue cell wall synthesis while other PBPs are inhibited by β-lactam antibiotics [12,13]. Penicillin-binding protein 2a from *S. aureus* is a high-molecular-weight class B PBP identified solely in antibiotic-resistant strains of *S. aureus*. Penicillin-binding protein 2a's transpeptidase active site, like that of other PBPs, contains the active site serine (S403) at the N-terminus of the SXXK sequence motif [12,14,15]. Interestingly, the activity of this protein is controlled by allosterism at a position, 60 Å away from the active site, where cell wall crosslinking occurs [12,16]. As a result, previously inert β-lactam antibiotics may now reach and inactivate this crucial protein, thereby inhibiting the organism [12,16]. Allosteric modulation is mostly used to treat eukaryotic disorders rather than prokaryotic infections [12]. However, recent advances in the infectiveness of biochemical and computational screening approaches, alongside protein structure characterization, point to the prospects of allosteric activity regulation as a novel concept for antibiotic discovery [12–14,16]. Specifically, by exploiting allosteric modulation of PBP2a of MRSA, promising compounds with the capacity to exhibit direct antibacterial activity while also working in synergism with existing conventional antibiotics have been identified [1,16]. Hence, in this study, the active site of PBP2a was employed in screening compounds against MRSA, while the modulation of the active site was studied via the binding of compounds to the PBP2a allosteric site.

Most currently accessible antibiotics were produced from microbial sources, while plant-based antibiotics have been largely ignored, owing to their weaker activity relative to their microbial-derived counterparts [16]. However, with the increased interest in plant-based antimicrobials in recent years, most especially the phenolic compounds, numerous candidates demonstrating promising pharmacological properties have been identified which can be further developed into therapeutics [16,17]. In bacteria, the efficiency of β-lactam antibiotics has been attributed to their ability to penetrate the outer cell membrane, resist inactivation by plasmid- or chromosomal-encoded β-lactamase, and bind efficiently with mutated penicillin-binding proteins (e.g., PBP2a, a target that has been implicated in the resistant strain of *S. aureus*) [9]. These characteristics have been reported in phytonutrients, including phenolics [16,17]. Phenolics' ability to effectively bind and modulate bacterial druggable targets, such as β-lactamase, and consequently inhibit various multidrug-resistant Gram-negative and Gram-positive bacteria has been reported [16,17], while also enhancing cell membrane permeability for antimicrobial absorption [18]. In addition, being the most frequently occurring metabolite in plants, phenolics offer other health and therapeutic benefits as antioxidants and against degenerative diseases, such as cancer and diabetes [16,17,19–21]. These characteristics of phenolics point to their prospective antibacterial capabilities for treatment or synergistic effects with conventional antibiotics in the treatment of infections caused by multidrug-resistant *S. aureus*. Thus, with over 10,000 phenolics isolated over the years and reported in the literature with different pharmacological characteristics [22], we employed for the first time in this study, structure–activity-relationship-based pharmacophore and molecular docking approaches to screen phenolics with capabilities to inhibit the activities of PBP2a of *S. aureus*. The most promising phenolics were further studied for their thermodynamic compatibility with PBP2a and their ability to modulate the active site of PBP2a following binding at the allosteric site (Figure 1). This was undertaken to identify prospective antibacterial

candidates that can treat or act in synergy with conventional antibiotics in the treatment of infections caused by MRSA.

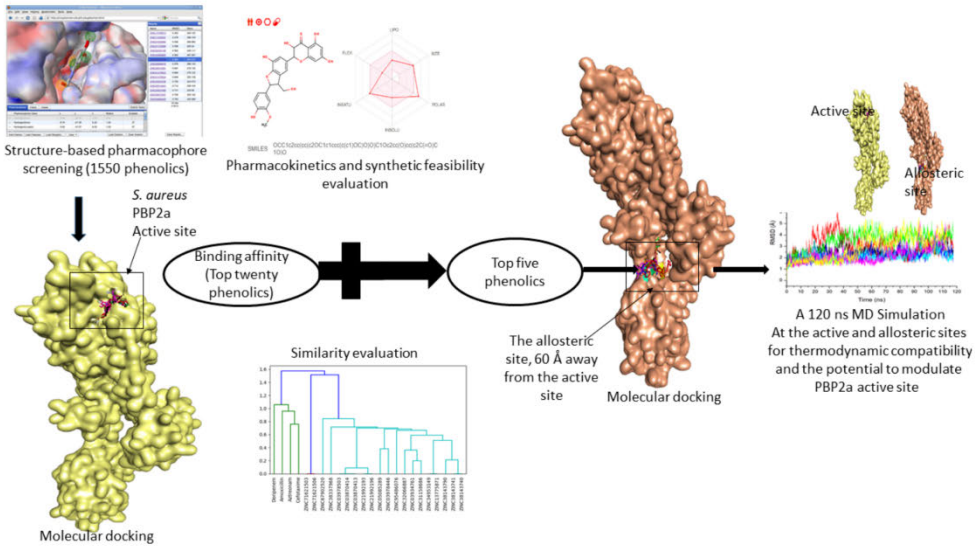


Figure 1. Workflow of the strategy adopted.

2. Materials and Methods

2.1. Druggable Target Acquisition, Preparation, and Identification of Binding Sites

The X-ray crystal structure of PBP2a of *S. aureus* (3ZFZ) was obtained from the protein data bank (PDB) (https://www.rcsb.org, accessed on 21 August 2021). The structure was prepared via removal of water molecules and nonstandard amino acids in preparation for molecular docking using the UCSF Chimera v1.15 software tool [23]. The x-y-z coordinates and amino acid residues at the active (centre (X: 28.9; Y: 29.43; Z: 87.60); radius (14.9)] and allosteric sites (centre (X: 11.34; Y: 33.75; Z: 22.74); radius (13.5)] of PBP2a were defined as previously reported using Discovery Studio version 21.1.0 [24] and afterwards validated by literature [16].

2.2. Structure-Based Pharmacophore Screening of Phenolic Compounds

With over 10,000 phenolic compounds currently accessible in the literature [22], a preliminary computational screening was performed, where a library of phenolics against PBP2a was built by utilizing the ZINCPharmer database (http://zincpharmer.csb.pitt.edu, accessed on 21 August 2021). For the screening, the 3D structure of PBP2a from *S. aureus* and a consensus phenolic pharmacophore (derived from 32 phenolics) produced from PharmaGist (https://bioinfo3d.cs.tau.ac.il/PharmaGist/php.php, accessed on 17 August 2021) were used [25]. Characteristics, such as the presence of an aromatic ring, the creation of hydrogen bonds, the charge of the ligand, and the hydrophobic contact between the ligand and the receptor atoms, were utilised to identify 1550 phenolics that interacted with the active site of PBP2a in *S. aureus* (Table S1).

2.3. Ligand Retrieval, Optimization, and Molecular Docking at the Active and Allosteric Site of PBP2a

The docking strategy was used to screen down the constructed phenolics library at the active site of PBP2a using Python Prescription (PyRx) v 0.9.5. (Figure 2). Before docking, the library of phenolics and reference β-lactam antibiotics (amoxicillin, cefotaxime, aztreonam,

and doripenem) [16] were optimised through the addition of Gasteiger charges using the Open Babel program plug-in on PyRx [24]. Following that, docking of the prepared protein (PBP2a) and optimised ligands (made up of the built library of phenolics and reference β-lactam antibiotics) was performed using the AutoDock tool present on PyRx [22]. Docking at the active site of PBP2a was assured by selecting amino acid residues at the active site whose grid box coordinates match the established x-y-z coordinates. Following the selection of the top-twenty phenolics with the highest binding affinity at the active sites of PBP2a using the reference β-lactam antibiotics as the benchmark, compound similarity, pharmacokinetics friendliness, and synthetic feasibility evaluation were employed in selecting the top five from the top-twenty phenolics. Afterward, the docking of the top-five phenolics was done at the allosteric site of PBP2a (Figure 3). Here, the top-five phenolics were individually retrieved from PubChem, prepared via charge addition using the UCSF Chimera v 1.15 software program, and then docked at the allosteric site of PBP2a via amino acid selections at the allosteric site (grid box coordinate coinciding with established x-y-z coordinates) using the AutoDock tool present on PyRx. The docked complexes of the top-five phenolics with the most-energy-minimised conformation (maximum binding affinity) at both the active and allosteric sites were afterward retrieved in PDB format for further molecular dynamic (MD) simulation.

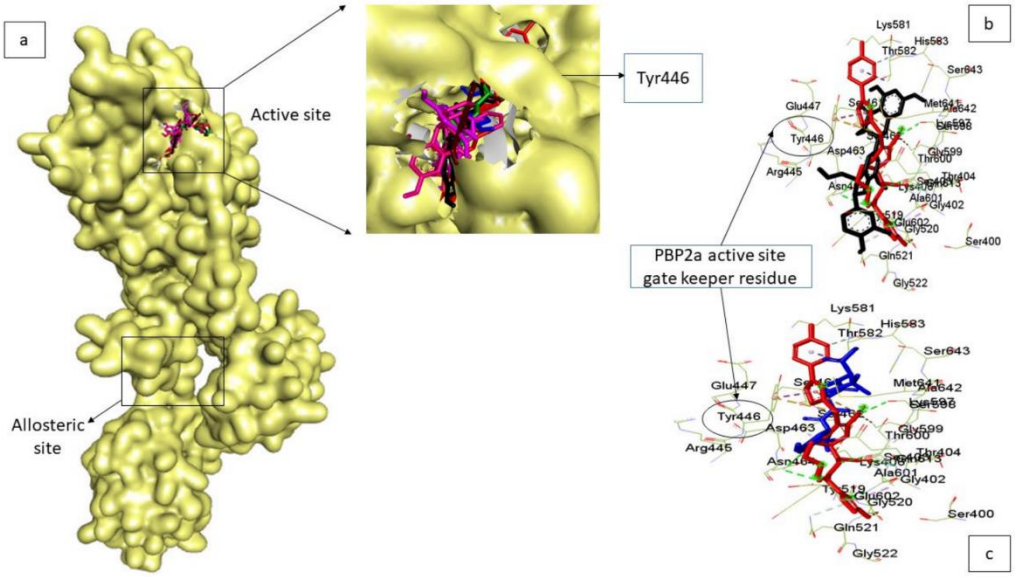


Figure 2. Validation of docking technique and parameters via the redocking approach against the co-crystal structure of PBP2a from *S. aureus* (3ZFZ). (**a**) the superimposition showed that the top-five phenolics (chroman-4-one (green), epicatechin gallate (purple), epigallocatechin 4-benzylthioether (brown), propan-2-one (pink), silicristin (black) and amoxicillin (blue)) could achieve the same orientation with the native inhibitor (red) of 3ZFZ with a low RMSD value of <1. (**b**,**c**) showed the superimposition of silicristin (phenolic with the highest docking score) and amoxicillin (antibiotic with the highest docking score) with the native inhibitor of 3ZFZ, displaying the amino acid at the active site (located 60 Å away from the allosteric site) and the active site gatekeeper residue (Tyr 446) [16].

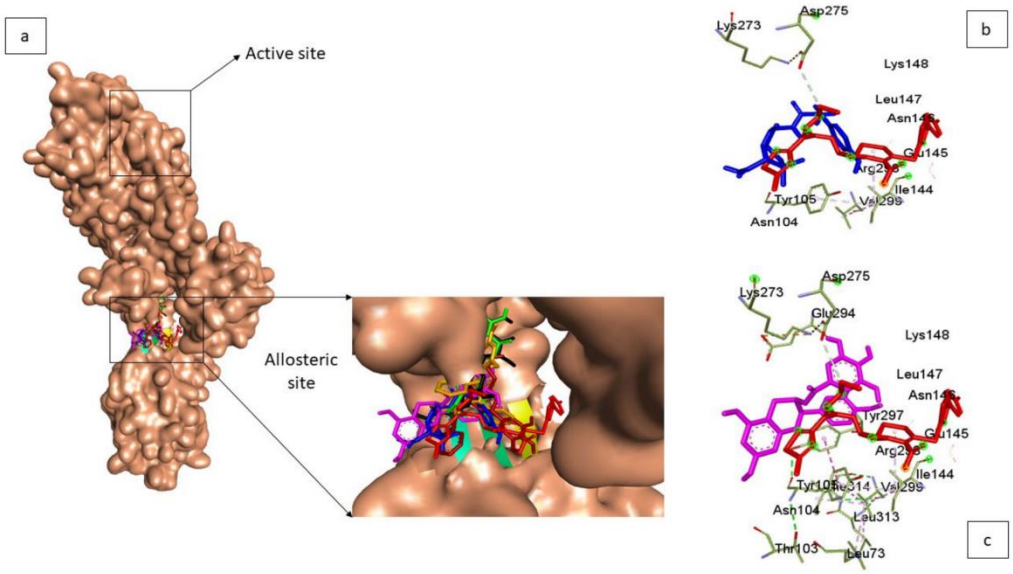


Figure 3. (**a**) Superimposition at the allosteric site of the co-crystal structure of PBP2a from *S. aureus* (3ZFZ), demonstrating the capability of the top-five phenolics (chroman-4-one (green), epicatechin gallate (purple), epigallocatechin 4-benzylthioether (brown), propan-2-one (pink), silicristin (black) and amoxicillin (blue)) to achieve the same orientation with the native inhibitor of 3ZFZ (red) with a low RMSD value of <1. (**b**,**c**) showed the superimposition of epicatechin gallate (phenolic with the highest docking score) and amoxicillin (antibiotic with the highest docking score) with the native inhibitor of 3ZFZ, displaying the amino acid at the allosteric site of PBP2a of *S. aureus* (located 60 Å away from the active site) [16].

However, as molecular docking methods often produce pseudo-positive binding conformations as the most-energy-minimised pose, validation of docking studies is often required. One of the most common ways to evaluate the correctness of docking geometry is to measure the root-mean-square deviation (RMSD) of the ligand from its reference position in the answer complex after optimal superimposition [26]. A low RMSD value of <1 between the docked ligand from its reference position in the answer complex suggests the same binding orientation, which encouraged docking technique validation [27]. In this study, validation of the docking pose was performed via the superimposition approach against the experimental co-crystal structure of PBP2a from *S. aureus* (3ZFZ). The superimposition showed that the top-five phenolics and amoxicillin achieved the same orientation with the native inhibitor of 3ZFZ with a low RMSD value of <1, which validated the docking scores observed in the study; these are presented in Figures 2 and 3 for the PBP2a active and allosteric sites, respectively.

2.4. Top-Twenty Phenolics Pharmacokinetic Properties Prediction

The SwissADME web (http://swissadme.ch/index.php, accessed on 15 October 2021) and Molinspiration (https://www.molinspiration.com/cgi-bin/properties, accessed on 15 October 2021) toolkits were used in this study for a robust prediction of hit phenolics' physicochemical properties, pharmacokinetics, drug-likeness, and medicinal chemistry friendliness, while the toxicological profiles were evaluated using the Protox II webserver (https://tox-new.charite.de/protox_II/, accessed on 15 October 2021). Taken together with the binding affinity of the top-twenty phenolic compounds, the results of these investigations were utilised to narrow down the list to five compounds.

2.5. Molecular Fingerprinting of the Top-Twenty Phenolics

Galaxy Europe (https://usegalaxy.eu./#, accessed on 15 July 2022) was used to molecularly fingerprint the top-twenty compounds. In a nutshell, Galaxy Europe's "molecule to fingerprint" tool was used to convert the compounds' smile format into "Open Babel FP2 fingerprints." The "Open Babel FP2 fingerprints" were then clustered using the fingerprinting algorithms "Taylor-Butina" and "NxN clustering", with thresholds of 0.8 and 0.0, respectively [22].

2.6. Molecular Dynamic (MD) Simulations of Top-Five Hit Phenolics

The MD simulation was performed as previously described [28]. To summarise, the AMBER 18 package was utilised, and the simulation was run for 120 ns using the FF18SB variation of the AMBER force field to characterise the operating systems. Similarly, the ANTECHAMBER was employed to generate the atomic partial charges of the ligands by applying general amber force field (GAFF) measurements and constrained electrostatic potential (RESP). The Leap module's hydrogen atoms, Na+ and Cl− counter ions were used to neutralise the systems. The amino acid residues in each case were suitably numbered, and the systems were suspended inside an orthorhombic box of TIP3P water molecules in such a way that all atoms were within 8 Å of any box edge. The SHAKE method was used to limit the hydrogen atom bonds in each simulated system. Each simulation had a step-size of 2 fs, which corresponded to the isobaric–isothermal ensemble (NPT) with randomised seeding, a temperature of 300 K, a constant pressure of 1 bar, and a Langevin thermostat with a collision frequency of 1.0 ps and a pressure-coupling constant of 2 ps. Following that, the 120 ns MDS findings were reviewed and classified as post-dynamic data.

2.7. Post-Dynamic Analysis

The post-dynamic analysis was performed by saving the systems' coordinates and trajectories throughout the simulation period and then evaluating them post-simulation using the PTRAJ module of the AMBER 18 package. Exploiting the CPPTRAJ module of the same package, the analysis of root-mean-square deviation (RMSD), root-mean-square fluctuation (RMSF), the radius of gyration (ROG), and solvent-accessible surface area (SASA) were carried out and their plots were generated using Origin v 6.0 [29]. Likewise, using the Molecular Mechanics/GB Surface Area (MMGBSA) approach, the binding free energy was estimated using an average among 100,000 snapshots taken from a 120 ns MD simulation trajectory using the equation $\Delta G_{bind} = G_{complex} - (G_{Receptor} + G_{ligand})$. The PBP2a-ligand plots, which indicate molecular interactions between ligands and amino acid residues at the PBP2a active site or allosteric site, were identified from the final complexes obtained and visualised with Discovery Studio v 21.1.0 (Dassault Systemes BIOVIA, San Diego, CA, USA) [30].

3. Results and Discussion

3.1. Ranking of Phenolics against the Active Site of PBP2a of S. aureus

Screening using the structure-based pharmacophore as employed in this study allowed for hit-searching using distinct characteristics specific for phenolics and PBP2a [25]. Using this method, over 10,000 phenolics currently accessible from the literature were narrowed down to 1550 phenolics with capabilities to interact with the active site of PBP2a of *S. aureus* (Figure S1). Following molecular docking, the top-twenty phenolics were identified from the 1550 phenolics. Molecular docking is a structure–activity-based virtual screening technique that enables compounds to be ranked based on their orientations and interactions at the binding site of a protein, and the higher the negative value, the better the affinity of the compound for the protein [28]. In this study, the top-twenty phenolics had higher negative docking scores (−6.8 to −8.5) than all the conventional antibiotics (amoxicillin (−6.2), cefotaxime (−6.0), aztreonam (−5.5), and doripenem (−5.8)) with ZINC03978446 (Isotheaflavin) having the highest negative docking score (Figure 4). This finding regarding the top-twenty compounds could be an indication of their better potential affinity for the

PBP2a active site relative to the standards, which also lent credence to the effectiveness of the structure–activity-based pharmacophore strategy employed in this study. This observation agrees with the report of Koes and Camacho [25], who demonstrated the specificity and efficiency of structure–activity-based pharmacophores in screening hits for a target.

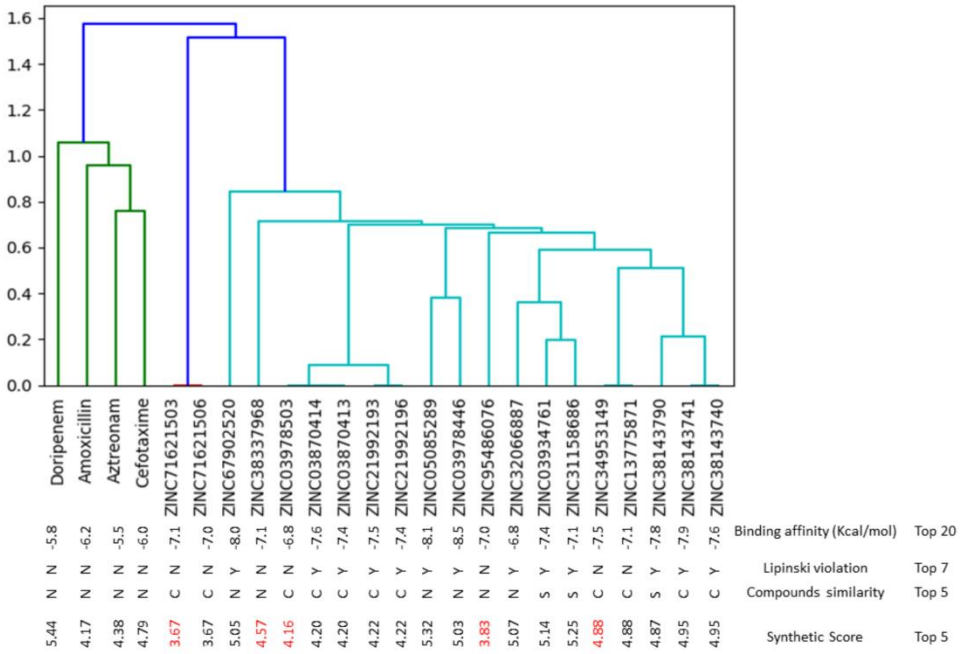


Figure 4. Molecular fingerprinting of the top-twenty phenolics. Compounds of the same colour and cluster were more similar than compounds of different colours and clusters. The top-twenty compounds were structurally different from the antibiotics which had the same colour (Green). Phenolics with similarity scores of zero and belonging to the same clusters were conformers, and in selecting the top five (highlighted in red colour), the conformer with the highest binding affinity that did not violate the Lipinski violation was selected among the top five. While avoiding the top-five phenolics that were conformers of each another, one common moiety that the top-five-ranked compounds had was resorcinol. Two (ZINC38337968 and ZINC03978503) of the top-five phenolics had a pyrogallol structure and from the cluster chart, these two compounds appeared to be the most similar among the top-five compounds. Only one (ZINC03978503) of the top-five phenolics had the catechol group. The top-five compounds all had a synthetic score of less than five.

Due to the high failure rate at the preclinical and clinical phases of drug development, the pharmacokinetics, drug-likeness, synthetic feasibility, and toxicity characteristics of the top-twenty phenolics were evaluated in ranking the top-five phenolics. Since the evaluation of the pharmacokinetics and medicinal chemistry of compounds via the in silico tools used in this study can sometimes produce pseudo-positive results, different online tools [SwissADME web and Molinspiration toolkits] equipped with models for robust prediction were employed in the study to enable a comparison and validation of the pharmacokinetics and medicinal chemistry information of the phenolics. This was performed in order to have a high confidence level against false-positive results prior to further in vitro and in vivo validations. Interestingly, all the top-five phenolics (ZINC34953149 (silicristin), ZINC71621503 (propan-2-one), ZINC38337968 (epigallocatechin 4-benzylthioether),

ZINC95486076 (Chroman-4-one), and ZINC03978503 (epicatechin gallate)) passed the Lipinski rule of five (Figure 4 and Table 1). Lipinski et al. [31] predicted that compounds with less than two violations of the rule of five, which limit the molecular weight to <500 g/mol, the hydrogen acceptor to $\leq$10, the hydrogen bond donor to $\leq$5, and the octanol coefficient to <5, will be orally bioavailable. The top-five compounds fulfilling this rule show their ability to be orally bioavailable to reach target sites and exert their pharmacological effects. The top-five phenolics were soluble in water, with a bioavailability score of 0.55 each, similar to that of amoxicillin. Except for ZINC95486076 (Chroman-4-one), with a higher gastrointestinal tract absorption rate, the other top-rated phenolics had similar gastrointestinal tract absorption traits similar to amoxicillin (Table 1 and Figure 4). All these observations are a pointer to the drug-likeness properties of the top-five phenolics. Cytochrome P450 (CYP), being an important isoenzyme in drug metabolism, plays a key role in drug toxicity [32]. Only ZINC03978503 (epicatechin gallate) and amoxicillin were observed to be non-inhibitors of all the CYPP450 isoenzymes (CYP1A2, CYP2C19, CYP2C9, CYP2D6, and CYP3A4), which predict their low capability to cause drug–drug interactions when used with other drugs, as CYPP450 isoenzymes are responsible for metabolizing about 80% of all medications used [32]. ZINC34953149 (silicristin), ZINC38337968 (epigallocatechin 4-benzylthioether), ZINC71621503 (propan-2-one), and ZINC95486076 (Chroman-4-one) all inhibit CYP3A4, which proposes their likely capability to cause drug interaction with other drugs being metabolised by this enzyme. Except for ZINC34953149 (silicristin) and ZINC95486076 (Chroman-4-one), which were predicted to be active for immunotoxicity, the other top-ranked phenolics and amoxicillin were predicted to be inactive for carcinogenicity, hepatotoxicity, mutagenicity, cytotoxicity, and immunotoxicity (Table 1). Moreover, the top-five phenolics belonged to drug toxicity classes (five and four) that are suitable for drug development [6] with less than five synthetic feasibility scores, a limit for compounds that will be less complex to synthesise [33], which hints that structural alterations can be made on them for druggability improvement. Findings from this aspect of the study suggest the medicinal and pharmacokinetics friendliness as well as the drug-likeness properties of the top-five phenolics with their capability to be derivatised and synthesised for improved druggability and reduced toxicity.

3.2. Thermodynamic Binding Free Energy of Top-Five Phenolics at the Active Site of PBP2a of S. aureus

The binding free energy measures the difference in energy between a complex (ligand and receptor) and its unbound receptor component and the higher the negative value, the better the ligand's affinity for the protein [34]. In this study, except for propan-2-one, the top-ranked phenolics had higher binding free energy for the active site of PBP2a of *S. aureus* than amoxicillin. Silicristin, epigallocatechin 4-benzylthioether, chroman-4-one, and epicatechin gallate, when complexed with PBP2a at the active site had −25.61 kcal/mol, −24.75 kcal/mol, −22.34 kcal/mol, and −23.11 kcal/mol, respectively, which were all higher than the −21.54 kcal/mol observed with amoxicillin, with silicristin having the highest binding free energy score (Table 2). This observation is suggestive of the better potential of silicristin, epigallocatechin 4-benzylthioether, chroman-4-one, and epicatechin gallate as inhibitors of PBP2a, with silicristin being the most promising among the top-five phenolics. The top-five phenolics, particularly silicristin, showing better potential for the PBP2a active site than amoxicillin after the 120 ns MD simulation corroborated the molecular docking findings of this study, in which the top-five phenolics all had higher docking scores than amoxicillin, with silicristin having the highest value as well. Generally, findings from the thermodynamic binding free energy investigations of this study revealed the advantage of the top-five phenolics over amoxicillin in the management/treatment of infections caused by MRSA.

Table 1. Binding affinity of the top-five phenolics against the active site of PBP2a and their ADMET properties.

Ligands Zinc Code	Popular Name	B A (kcal/mol)	MW < 500 (g/mol)	HB-A ≤ 10	HB-D ≤ 5	Log $P_{o/w}$ ≤ 5	RT-B ≤ 9	LV < 2	WS	GI -A	BS	PgP	Inhibitor of CYP 450s					H	C	IM	M	CY	TC	SA
													CYP 1A2	CYP 2C19	CYP 2C9	CYP 2D6	CYP 3A4							
Amoxicillin	Amoxicillin	−6.2	365.40	6	4	−0.39	5	N	VS	L	0.55	N	N	N	N	N	N	I	I	I	I	I	6	4.17
ZINC34953149	Silicristin	−7.5	482.44	10	6	1.49	4	N	S	L	0.55	N	N	N	N	N	Y	I	I	A	I	I	4	4.88
ZINC71621503	Propan-2-one	−7.1	458.46	7	6	3.3	6	N	MS	L	0.55	N	N	N	Y	N	Y	I	I	I	I	I	4	3.67
ZINC38337968	Epigallocatechin 4-benzylthioether	−7.1	428.46	7	6	2.23	4	N	MS	L	0.55	N	N	N	N	N	Y	I	I	I	I	I	5	4.57
ZINC95486076	Chroman-4-one	−7.0	356.37	6	3	3.09	3	N	MS	H	0.55	N	Y	N	Y	N	Y	I	I	A	I	I	4	3.83
ZINC03978503	Epicatechin gallate	−6.8	442.37	10	7	1.3	4	N	S	L	0.55	N	N	N	N	N	N	I	I	I	I	I	4	4.16

Keywords: BA: Binding affinity; MW: Molecular weight; HB-A: Hydrogen bond acceptor; HB-D: Hydrogen bond donor; Log $P_{o/w}$: Partition coefficient; RT-B: rotatable bond; WS: Water solubility; GI- A: Gastrointestinal absorption; Pgp: Permeability glycoprotein substrate; CYP: Cytochrome; VS: very soluble; MS: Moderately soluble; S: Soluble; N: No; Y: Yes; L: low; I: Inactive; A: Active; LV: Lipinski violations; BS: Bioavailability score; H: Hepatotoxicity; C: Carcinogenicity; IM: Immunotoxicity; M: Mutagenicity; CY: Cytotoxicity; LD: Lethal dose; TC: Toxicity class; SA: Synthetic accessibility; and BA: binding affinity.

Table 2. Energy components (kcal/mol) of the top-five phenolics against the active site of PBP2a of *S. aureus*.

Systems	ΔE_{vdW}	ΔE_{elec}	ΔG_{gas}	ΔG_{solv}	ΔG_{bind}
PBP2a + amoxicillin	−22.30 ± 7.99	−74.82 ± 26.08	−97.12 ± 28.39	75.58 ± 23.67	−21.54 ± 6.59
PBP2a + silicristin	−35.15 ± 8.08	−32.24 ± 12.41	−67.42 ± 15.90	41.80 ± 10.24	−25.61 ± 7.08
PBP2a + propan-2-one	−23.27 ± 5.46	−35.71 ± 16.25	−58.99 ± 18.62	39.92 ± 12.55	−19.06 ± 7.26
PBP2a + epigallocatechin 4-benzylthioether	−19.36 ± 4.64	−49.56 ± 13.09	−68.93 ± 11.38	44.18 ± 7.98	−24.75 ± 4.72
PBP2a + chroman-4-one	−22.23 ± 4.56	−47.43 ± 10.23	−65.56 ± 12.34	−42.78 ± 23.34	−22.34 ± 5.23
PBP2a + epicatechin gallate	−20.61 ± 4.45	−43.07 ± 16.16	−63.69 ± 16.86	40.58 ± 10.45	−23.11 ± 7.45

ΔE_{vdW} = van der Waals energy; ΔG_{bind} = total binding free energy; ΔE_{gas} = gas phase free energy; ΔE_{elec} = electrostatic energy; and ΔG_{solv} = solvation free energy.

3.3. Thermodynamic Stability, Compactness and Flexibility of the Top-Five Phenolics at the Active Site of PBP2a of S. aureus

The thermodynamic stability of the top-five phenolics at the active site of PBP2a of *S. aureus* was studied by evaluating the RMSD, ROG, SASA and intramolecular numbers of hydrogen bonds and distances over a 120 ns simulation time. The RMSD trajectory depicts the time-dependent departure of a complex's structure from its unbound structure and the lower the RMSD value, the closer the complex structure to the unbound structure which depicts stability [34]. According to Ramirex and Caballero [35], an RMSD value of less than 3 Å is generally acceptable and considered good. In this study, during the first 10 ns of the simulation, all the systems (unbound PBP2a and complexed PBP2a) were observed to be equilibrating, a situation in which atoms of the macromolecules (PBP2a) and the surrounding solvent relaxed before the system reached a stationary state [36]. After equilibration, each of the systems was observed to take a more diverse trajectory, an observation which impacted the average RMSD observed after the 120 ns simulation period (Figure 5 and Table 3). More specifically, at the active site, the unbound PBP2a and PBP2a + propan-2-one complex deviated by 4.5 Å and 2.5 Å, respectively, immediately after equilibrating and maintained such deviation with little swaying throughout the simulation (Figure 5). This observation impacted the high average RMSD observed for unbound PBP2a and PBP2a + propan-2-one complex throughout the remaining simulation periods, at 6.86 Å and 5.78 Å, respectively (Table 3). These values are not within the good deviation limit of less than 3 Å and hence suggest that the systems may not enjoy reasonable degrees of stability. On the other hand, the PBP2a + silicristin complex maintained a more stable deviation within the 2 Å and 3 Å range before 60 ns, however after this period, the PBP2a + silicristin complex showed a greater deviation to 10 Å from 3 Å and maintained such deviation throughout the simulation, which also contributed to the high average RMSD at 5.65 Å which may also indicate less stability (Figure 5 and Table 3). Other systems, such as PBP2a + amoxicillin, PBP2a + epigallocatechin 4-benzylthioether, PBP2a + chroman-4-one, and PBP2a + epicatechin gallate all fluctuated within a more stable deviation between 2 and 5 Å during the entire simulation time and had lower average RMSD values of 4.07 Å, 3.49 Å, 3.26 Å, and 3.42 Å, respectively, with PBP2a + chroman-4-one having the lowest RMSD (Figure 5 and Table 3). Although, the RMSD values of the simulated compounds were greater than 3 Å, when compared to the unbound PBP2a system with an RMSD value of 6.86 Å, it could be generally inferred that the binding of PBP2a with the top-five phenolics as well as amoxicillin caused an improved thermodynamic structural stability, and hence indicated their possible prospects as a PBP2a inhibitor. Relative to amoxicillin + PBP2a complex; PBP2a + epigallocatechin 4-benzylthioether, PBP2a + chroman-4-one, and PBP2a + epicatechin gallate all had lower RMSD values which insinuated their advantage over amoxicillin as PBP2a inhibitors and this observation agreed with the results of the thermodynamic binding free energy investigations in this study, where epigallocatechin 4-benzylthioether, chroman-4-one, and epicatechin gallate all had a higher binding free energy than amoxicillin. This finding is consistent with the work of Alhadrami et al. [16], where flavonoids

enhanced the stability of *S. aureus* PBP2a when bound at its active site relative to the reference β-lactams investigated. Notably, silicristin having a higher RMSD value than amoxicillin when complexed with PBP2a, suggestive of silicristin's lesser thermodynamic stability with PBP2a did not support the higher binding free energy observed for silicristin relative to amoxicillin in this study, however, this observation could be attributed to the sudden drop in stability (the increase in RMSD) after 60ns as observed from the RMSD plot (Figure 5) and hence highlights the importance of a longer duration of simulation in drug discovery.

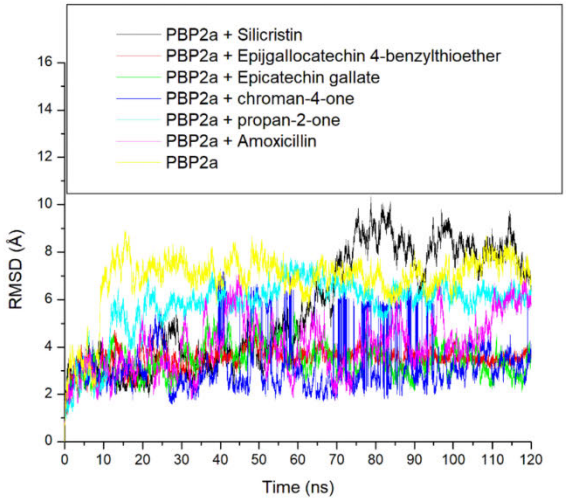


Figure 5. Comparative root-mean-squared deviation (RMSD) plots of alpha-carbon, the top-five phenolics, and amoxicillin against the active site of PBP2a of *S. aureus* over a 120 ns MD simulation period.

Table 3. Average RMSD, ROG, RMSF, SASA, and intramolecular-hydrogen-bond number and distance values of the top-five phenolics following a 120 ns simulation at the active site of PBP2a of *S. aureus*.

Systems	RMSD (Å)	RMSF(Å)	ROG (Å)	SASA (Å)	Number of Intramolecular H-Bond	Intramolecular H-Bond Distance (Å)
Unbound PBP2a	6.86 ± 1.18	2.71 ± 0.91	35.37 ± 0.45	26786.05 ± 473.91	339.24 ± 12.45	2.85 ± 0.06
PBP2a + Amoxicillin	4.07 ± 1.15	2.85 ± 1.24	37.57 ± 0.29	27484.50 ± 458.31	341.44 ± 13.23	2.85 ± 0.06
PBP2a + Silicristin	5.65 ± 2.34	2.26 ± 2.09	36.47 ± 1.15	27160.02 ± 545.40	346.00 ± 12.15	2.85 ± 0.05
PBP2a + Propan-2-one	5.78 ± 1.21	2.45 ± 1.13	35.34 ± 0.55	26303.34 ± 464.78	342.94 ± 12.13	2.85 ± 0.06
PBP2a + Epigallocatechin 4-benzylthioether	3.49 ± 0.42	2.27 ± 1.14	36.92 ± 0.32	27060.31 ± 531.98	344.00 ± 12.22	2.85 ± 0.06
PBP2a + Chroman-4-one	3.26 ± 1.16	2.49 ± 3.22	37.84 ± 0.46	27311.74 ± 408.97	345.47 ± 12.13	2.85 ± 0.05
PBP2a + Epicatechin gallate	3.42 ± 0.67	2.38 ± 1.14	37.19 ± 0.29	27187.53 ± 411.42	343.16 ± 12.12	2.85 ± 0.06

The ROG is another thermodynamic stability metric which measures the time-dependent compactness of a complex during an MD simulation and the lesser the value the more compact and stable the complex [16,29]. In this study, lesser fluctuations in compactness were observed in PBP2a + amoxicillin, PBP2a + epigallocatechin 4-benzylthioether, PBP2a + chroman-4-one, and PBP2a + epicatechin gallate complexes throughout the 120 ns simulation period (Figure 6). This observation could mean that the binding of PBP2a with amoxicillin, epigallocatechin 4-benzylthioether, chroman-4-one, and epicatechin gallate had little impact in causing the folding of PBP2a and this observation was evidenced by their respective average ROG values (37.57 Å, 36.92 Å, 37.84 Å, and 37.19) which were higher than 35.37 Å and 35.34 Å observed for the unbound PBP2a and PBP2a + propan-2-one that enhanced PBP2a folding just after

10 ns of the simulation (Table 3). The binding of silicristin to PBP2a, on the other hand, caused no folding of PBP2a until after 60 ns (Figure 6). Generally, the observations from the ROG findings in this study were inversely proportional to that observed in the RMSD study, which indicated that the higher thermodynamic stability observed in the binding of PBP2a following binding of the top-five phenolics as well as amoxicillin relative to unbound PBP2a is not directly due to the ability of the top-five phenolics and amoxicillin to cause PBP2a folding. This observation is not in accordance with the study by Aribisala et al. [29] where ROG findings of type 2A topoisomerases following binding with metabolites from *C. cujete* correlated with the RMSD findings. However, a previous study by Baig et al. [37] reported that ROG is the mass-weighted root-mean-square distance of a collection of atoms from their common centre of mass, which indicates that the position of binding of ligands relative to the centre of the mass may have impacts on ROG values. In this study, the point of interaction (active site) of PBP2a is far from the centre of the mass and hence may have resulted in the little impact noted in the folding of PBP2a following binding with the top-five phenolics relative to the unbound PBP2a. Furthermore, characteristics, such as protein topology, size, length, point of interactions, and amino-acid packing have also been shown to have impacts on protein folding [38], and could be the likely reasons for the observations with ROG patterns in this study.

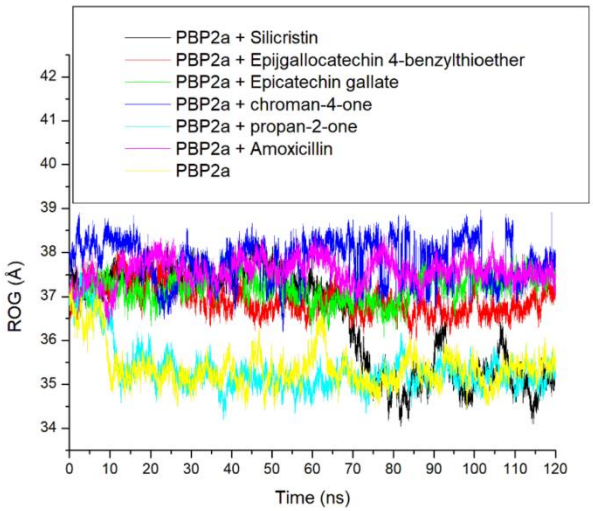


Figure 6. Comparative radius of gyration (ROG) plots of alpha-carbon, the top-five phenolics, and amoxicillin against the active site of PBP2a of *S. aureus* over a 120 ns MD simulation period.

Another important thermodynamic stability metric that analyses protein folding and changes in surface area during a simulation is the SASA, with higher SASA values suggesting an increase in protein volume [39]. Similar to the ROG findings, a lesser fluctuation in SASA in PBP2a + amoxicillin, PBP2a + epigallocatechin 4-benzylthioether, PBP2a + chroman-4-one, and PBP2a + epicatechin gallate complexes plots was observed throughout the 120 ns simulation period which points to the lesser impact of amoxicillin, epigallocatechin 4-benzylthioether, chroman-4-one, and epicatechin gallate in reducing the surface area of PBP2a (Figure 7 and Table 3). However, unbound PBP2a and PBP2a + propan-2-one displayed a slight reduction in SASA value, which suggests a reduction in protein volume just after 10 ns and maintained such reduction with minor swaying throughout the simulation period. These observations impacted their overall average SASA values, as the unbound PBP2a (26786.05 Å) and PBP2a + propan-2-one

(26,303.34 Å) both had lesser SASA values than the other investigated systems (Table 3 and Figure 7). On the other hand, the binding of silicristin on PBP2a revealed a more stable complex till 60 ns before instigating a reduction in SASA value, which specifies protein folding. This observation further corroborates the RMSD and ROG findings of this study on the importance of a longer duration of simulations in determining the compatibility of a ligand–protein complex. Generally, the observations from the SASA findings of this study were in agreement with the ROG findings that the higher stability observed in the binding of PBP2a with the top-five phenolics as well as amoxicillin relative to unbound PBP2a may not be due to their ability to cause PBP2a folding.

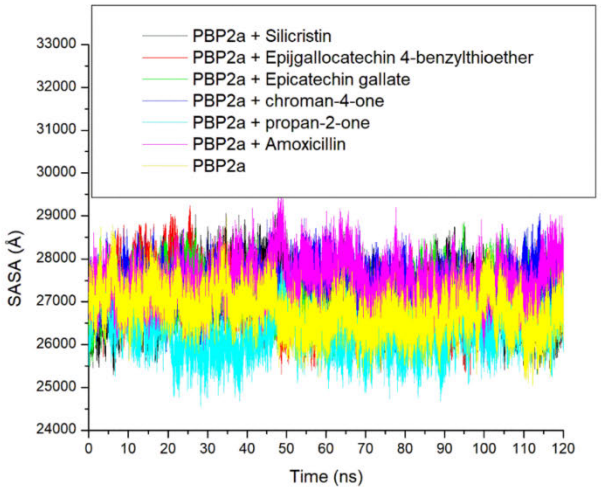


Figure 7. Comparative solvent-accessible surface area (SASA) plots of alpha-carbon, the top-five phenolics, and amoxicillin against the active site of PBP2a of *S. aureus* over a 120 ns MD simulation period.

Intramolecular hydrogen bonds and distance are important in the stability of a protein structure and hence can be assessed to understand the impact of ligand binding on the stability of a protein during simulation [34,40]. Figure 8a displayed a stable fluctuation in the pattern of the number of hydrogen bonds formed in PBP2a generally between 300 and 380 before and following bindings of the top-five phenolics and amoxicillin. This observation signifies the non-disruption of the thermodynamic entropy of PBP2a following bindings with the top-five phenolics and amoxicillin. Averagely, the top-five phenolics and amoxicillin, when complexed with PBP2a, resulted in more intramolecular hydrogen bonds (between 341 and 346) than unbound PBP2a at 339 (Table 3 and Figure 8a). This observation suggests the occupancy of some intramolecular space by the ligands and the increase in the intramolecular hydrogen bonds suggests the hydrogen bond interactions between the top-five phenolics as well as amoxicillin with PBP2a. This observation correlates with the RMSD findings of this study, which suggest the thermodynamic compatibility of the top-five phenolics and amoxicillin with PBP2a. The top-five phenolics binding to PBP2a resulted in more intramolecular hydrogen bonds than PBP2a + amoxicillin (341), with PBP2a + silicristin (346) having the highest intramolecular hydrogen bonds. This observation signifies that the complexes formed by the top-five phenolics and most especially by silicristin, formed more hydrogen bonds with PBP2a during the 120 ns simulation time which could have contributed to the higher binding free energy observed with epigallocatechin 4-benzylthioether, chroman-4-one, epicatechin gallate, and silicristin towards PBP2a relative to amoxicillin. Figure 8b displayed a continued reduction in intramolecular-hydrogen-bond distance as the simulation progressed, which was similar

in all the systems (unbound-PBP2a- and phenolics-PBP2a-complexed systems). All the systems had an average intramolecular-hydrogen-bond distance of 2.85 Å (Table 3), which suggests that the binding of PBP2a with the top-five phenolics and amoxicillin did not disrupt the arrangement and the original geometry of PBP2a but rather caused more internal pull between the atoms and residues of PBP2a as the simulation progressed. This further corroborates the thermodynamic compatibility of the top-five phenolics and amoxicillin with PBP2a observed in this study as established by the RMSD findings.

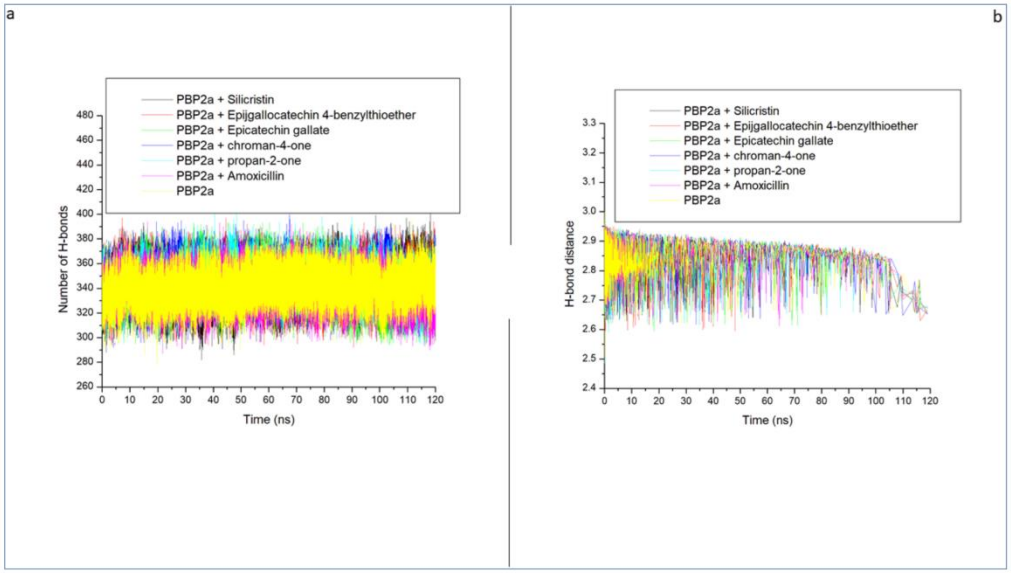


Figure 8. Time evolution of the number of intramolecular hydrogen bonds (**a**) and distance (**b**) formed in PBP2a following the binding of amoxicillin and the top-five phenolics at the active site of PBP2a of *S. aureus* during the 120 ns MD simulation period.

The thermodynamic flexibility of amino acid residues following the binding of the top-five phenolics at the active site of PBP2a of *S. aureus* was studied through the measurement of the RMSF value. The RMSF value takes into consideration the average fluctuation of atoms and residues of a protein structure over a simulation time which can be related to their ability to form intra- and intermolecular stable bonds and the lesser the fluctuation, especially at the active site where ligand binding and catalysis takes place, the stronger the bonds and the affinity of the ligand for the protein [39]. In this study, higher fluctuation in residues between 1 and 100, 125 and 300, and 575 and 590, as well as a lesser fluctuation between residues 300 and 575, and 590 and 645 were observed in all the systems with the level of fluctuation varying from one system to the other, which consequently impacted the average RMSF observed (Figure 9a and Table 3). Generally, binding of the top-five phenolics (epigallocatechin 4-benzylthioether (2.27 Å), chroman-4-one (2.49 Å), epicatechin gallate (2.38 Å) propan-2-one (2.45 Å), and silicristin (2.26 Å)) with PBP2a resulted in a lesser average RMSF than the unbound PBP2a (2.71 Å) and PBP2a + amoxicillin (2.85 Å). This observation suggests the lesser flexibility of PBP2a amino acid residues following binding of the top-five phenolics, with silicristin binding of PBP2a being the most prominent, revealing their stronger attraction and ability to promote PBP2a amino acid residue stability. These findings are consistent with the observed thermodynamic binding free energy, where silicristin had the most favourable affinity towards PBP2a. Interestingly, when the active site gatekeeper residue (Tyr446), which has been demonstrated to obstruct drug access to

complex. This observation could be suggestive of the greater potential affinity of the compounds for the allosteric site than amoxicillin. When compared with the observations at the main active site, the top-five phenolics showed better affinities for the allosteric site (8.0–8.5 kcal/mol) than the active site (6.8–7.5 kcal/mol) (Tables 1 and 5). However, since molecular docking is only a preliminary indication of how a compound interacts with a protein, further rigorous binding calculation at the allosteric site was carried out using the Molecular Mechanics/GB Surface Area (MMGBSA) approach over a 120 ns simulation period. In addition, in order to understand how simulation at the allosteric site affects the active site, the binding free energies of the top-five phenolics at the allosteric site were correlated with the fluctuation of the active site gatekeeper residue (Tyr446), and studied via RMSF evaluation.

Table 5. Molecular docking, binding free energy and RMSF values of the top-five phenolics at the allosteric site of PBP2a of *S. aureus*.

Systems	Binding Affinity (Kcal/mol)	ΔG_{bind} (Kcal/mol)	RMSF (Å)
Unbound PBP2a			2.71 ± 1.17
PBP2a + Amoxicillin	−7.7	−14.36 ± 6.00	2.56 ± 1.32
PBP2a + Silicristin	−8.4	−33.57 ± 5.38	2.45 ± 1.11
PBP2a + Propan-2-one	−8.3	−28.55 ± 8.07	2.49 ± 1.14
PBP2a + Epigallocatechin 4-benzylthioether	−8.1	−36.83 ± 8.04	3.48 ± 1.84
PBP2a + Chroman-4-one	−8.0	−29.52 ± 4.20	2.55 ± 1.32
PBP2a + Epicatechin gallate	−8.5	−47.65 ± 8.42	2.06 ± 0.95

ΔG_{bind} = total binding free energy.

3.5. Thermodynamic Binding Free Energy Following 120 ns Simulation of the Top-Five Phenolics at the Allosteric Site of PBP2a of S. aureus

The binding of the top-five phenolics (Silicristin (−33.57 kcal/mol), propan-2-one (−28.55 kcal/mol), epigallocatechin 4-benzylthioether (−36.83 kcal/mol), chroman-4-one (−29.52 kcal/mol), and epicatechin gallate (−47.65 kcal/mol)) with PBP2a resulted in a higher binding free energy than the amoxicillin (−14 kcal/mol) complex at the allosteric site. This observation, while corroborating the molecular docking scores at the allosteric site, further demonstrates the potential affinity of the top-five phenolics for the allosteric site, revealing their probable capability to modulate the amino acid residues of PBP2a allosteric site. Interestingly, this finding is in correlation with the observation of Alhadrami et al. [16] where some flavonoids showed a better affinity at the allosteric site of PBP2a of *S. aureus* than conventional β-lactam antibiotics (e.g., ampicillin and ceftaroline). Interestingly, epicatechin gallate and other top-five phenolics which demonstrated their potential affinity for the allosteric site of PBP2a in the order of epigallocatechin 4-benzylthioether > silicristin > chroman-4-one > propan-2-one, all had a higher binding free energy at the allosteric site than at the active site. This observation demonstrates the better potential affinity of the top-five phenolics and most especially epicatechin gallate for the allosteric site, revealing their potential benefit in treating *S. aureus* infections in combination with standard β-lactam antibiotics.

3.6. Allosteric Modulation of PBP2a Active Site Amino Acid Residues Following 120 ns Simulation at the Allosteric Site

The allosteric modulation of the active site gatekeeper residue of PBP2a was studied by evaluating the RMSF of PBP2a through a 120 ns simulation time. Except for epigallocatechin 4-benzylthioether, binding at the allosteric site of PBP2a by the top-five phenolics (silicristin (2.45 Å), propan-2-one (2.49 Å), chroman-4-one (2.55 Å), and epicatechin gallate (2.06 Å)) and amoxicillin (2.56 Å) resulted in a lesser average RMSF than the unbound PBP2a (2.71 Å), with epicatechin gallate having the lowest RMSF value (Table 5). This observation shows the potential of the top-five phenolics and most especially epicatechin gallate in promoting PBP2a internal amino acid stability following binding at the allosteric site. However, further insight into how allosteric binding influences access to the PBP2a active site was achieved by evaluating fluctuations of the gatekeeper residue, Tyr446, which has been demonstrated

PBP2a [12,16], was further evaluated to understand its flexibility during the simulation, findings showed that Tyr446 had a reduced average RMSF compared with the average RMSF of the whole PBP2a in all the systems (Table 4 and Figure 9b). This observation was more prominent in the bound systems than the unbound system, suggestive of the active involvement of Tyr446 in the binding of the top-five phenolics and amoxicillin. Specifically, except for the PBP2a-epigallocatechin 4-benzylthioether complex (1.76 Å), the binding of PBP2a with the top-five phenolics (propan-2-one (1.67 Å), chroman-4-one (1.53 Å), epicatechin gallate (1.50 Å), and silicristin (1.49 Å)) resulted in a lesser Tyr446 fluctuation than PBP2a + amoxicillin (1.72 Å) and unbound PBP2a (1.92 Å), with PBP2a + silicristin having the lowest value (Table 4, Figure 9b). This observation further determines the affinity of the top-five phenolics and most especially silicristin, with the active site gatekeeper residue being suggestive of their advantage over amoxicillin as PBP2a inhibitors.

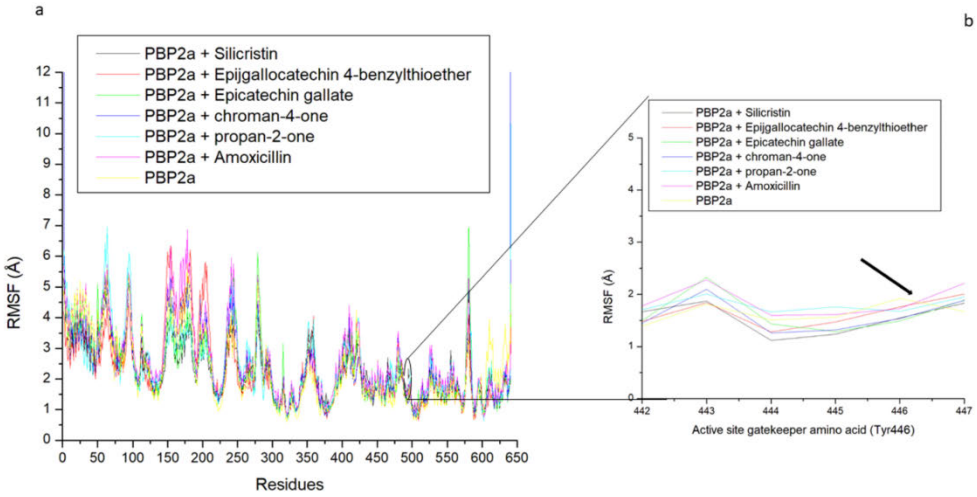


Figure 9. Comparative root-mean-square fluctuation (RMSF) plots of alpha-carbon, the top-five phenolics, and amoxicillin against residues of PBP2a of *S. aureus* (**a**), and gatekeeper residue [Tyr446 (black arrow)] of PBP2a (**b**) when the top-five phenolics and amoxicillin were bound at the active site of PBP2a over a 120 ns MD simulation period.

Table 4. PBP2a active site gatekeeper residue average fluctuation (Å) after 120 ns simulation of the top-five phenolics at the active site.

PBP2a Active Site Gatekeeper Residue	**Top-Five Phenolics**						
	Silicristin	Epigallocatechin 4-benzylthioether	Epicatechin gallate	Chroman-4-one	Propan-2-one	Amoxicillin	Unbound PBP2a
Tyr446	1.55	1.76	1.49	1.53	1.67	1.72	1.92

3.4. Molecular Docking of Top-Five Phenolics at the Allosteric Site of PBP2a of S. aureus

The molecular docking at the allosteric site distal to the active site is based on the fact that when properly occupied, it simultaneously opens the gatekeeper amino acid residue (Tyr446) inside the active site and realigns the conformation of key residues to allow catalysis [41]. Docking at the allosteric site revealed that the top-five phenolics all had higher docking scores than amoxicillin (Table 5). PBP2a + Silicristin, PBP2a + propan-2-one, PBP2a + epigallocatechin 4-benzylthioether, PBP2a + chroman-4-one, and PBP2a + epicatechin gallate had docking scores of −8.4 kcal/mol, −8.3 kcal/mol, −8.1 kcal/mol, −8.0 kcal/mol, and −8.5 kcal/mol, respectively, which were all higher than the −7.7 kcal/mol observed for the PBP2a-amoxicillin

to hinder drugs from entering the PBP2a active site. The average RMSF of Tyr446 is presented in Table 6 while its plots are presented in Figure 10b. Interestingly, PBP2a allosteric binding of epicatechin gallate (3.61 Å), silicristin (2.91 Å), epigallocatechin 4-benzylthioether (3.12 Å), and propan-2-one (2.27 Å) all resulted in the higher RMSF of Tyr446 relative to the unbound PBP2a (1.66 Å) and PBP2a + amoxicillin (1.30 Å). This observation is suggestive of the higher fluctuation of the gatekeeper residue during the 120 ns allosteric binding of PBP2a with epicatechin gallate, silicristin, epigallocatechin 4-benzylthioether, and propan-2-one. Another inference from this observation is the lesser involvement of Tyr446 in the intramolecular interactions of adjacent residues (α9 helix (Q577–Y588) and M641 residues) of PBP2a thereby resulting in its higher instability in bond formation and its reduced obstruction of the PBP2a active site. This inference correlates with the report of Mahasenan et al. [41], who experimentally demonstrated the shifting of adjacent residues that may form intramolecular interactions with Tyr446 following the allosteric binding of PBP2a with cefepime. Remarkably, the higher fluctuation of the gatekeeper residue following allosteric binding of the top-five phenolics relative to amoxicillin was in agreement with the observed binding free energy findings in this study, where the top-five phenolics demonstrated higher binding free energy than amoxicillin (−14.36 kcal/mol). Specifically, the higher fluctuation of Tyr446 was noted to partially correlate with the binding free energy obtained in this study with the top-five phenolics at the allosteric site of PBP2a (epicatechin gallate (ΔG_{bind}: −47.65 kcal/mol; RMSF: 3.61 Å) > epigallocatechin 4-benzylthioether (ΔG_{bind}: −36.83 kcal/mol, RMSF: 3.12 Å), silicristin (ΔG_{bind}: −33.57 kcal/mol; RMSF: 2.91) > propan-2-one (ΔG_{bind}: −28.55 kcal/mol, RMSF: 2.27 Å) > Chroman-4-one (ΔG_{bind}: −29.52 kcal/mol, RMSF: 1.63 Å) > amoxicillin (ΔG_{bind}: −14.36, RMSF:1.30 Å)) and the graft is presented in Figure 11. This observation pinpoints that the higher the affinity of a compound to the allosteric site of PBP2a, the higher the instability of Tyr446. This finding is also in agreement with the report of Mahasenan et al. [41] who demonstrated both experimentally and computationally how appropriate allosteric site binding of PBP2a simultaneously opened the gatekeeper residue of the active site. Furthermore, the top-five phenolics, when bound to the allosteric site, have higher fluctuations of the gatekeeper residue relative to when they are complexed directly at the PBP2a active site. This observation could be investigative of the gatekeeper residue's lesser involvement in intramolecular interactions with other residues of PBP2a when the top-five phenolics were bound at the allosteric site rather than intermolecular interactions with the top-five phenolics when bound at the active site. Interestingly, a lesser fluctuation of the gatekeeper residue was noted in amoxicillin when bound at the allosteric site relative to the active site, suggesting that the gatekeeper residue was more actively involved in intramolecular interactions with other PBP2a residues when amoxicillin was bound at the allosteric site compared with intermolecular interactions with amoxicillin when bound at the active site. This observation may be analytical of the advantages of the top-five phenolics in the allosteric modulation of PBP2a over amoxicillin. Generally, findings from this aspect of the study partially correlates the affinity of the top-five phenolics at the allosteric site of PBP2a with the fluctuation of the active site gatekeeper residue (Tyr446). In addition, the study demonstrated the lesser involvement of Tyr446 in the intramolecular interactions with other PBP2a residues when the top-five phenolics bind at the allosteric site compared with their intermolecular interactions at the active site, suggestive of the reduced obstruction of the active site, an observation that was not observed with amoxicillin. Interestingly, binding of PBP2a at the allosteric site caused the enhanced thermodynamic stability of PBP2a as the bound system (4.06 Å) had a lesser average RMSD value than the unbound PBP2a (6.86 Å), with chroman-4-one having the lowest RMSD value (3.24 Å) (Table S2 and Figure S2). Similarly, the ROG and SASA findings showed the orderliness of PBP2a geometry following binding of the top-five phenolics and amoxicillin at the allosteric site (Table S2 and Figure S2). All of these observations suggest the thermodynamic compatibility of the top-five phenolics and amoxicillin at the allosteric site of PBP2a.

Table 6. PBP2a active site gatekeeper residue average fluctuation (Å) after 120 ns simulation of the top-five phenolics at the allosteric site.

PBP2a Active Site Gatekeeper Residue	Top-Five Phenolics						
	Silicristin	Epigallocatechin 4-benzylthioether	Epicatechin gallate	Chroman-4-one	Propan-2-one	Amoxicillin	Unbound PBP2a
Tyr446	2.91	3.12	3.61	1.63	2.27	1.33	1.93

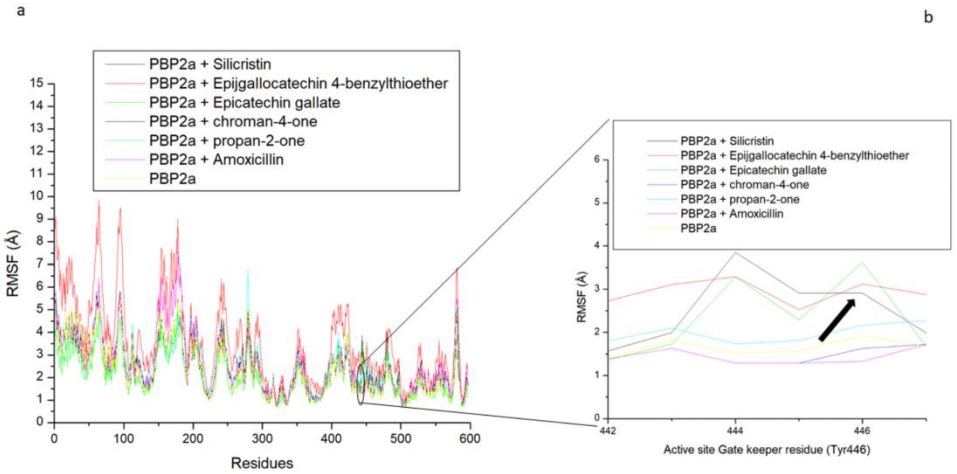


Figure 10. Comparative root-mean-square fluctuation (RMSF) plots of alpha-carbon, the top-five phenolics, and amoxicillin against residues of PBP2a of *S. aureus* (**a**), and gatekeeper residues [Tyr446 (black arrow)] of PBP2a (**b**) when the top-five phenolics and amoxicillin were bound at the allosteric site of PBP2a over a 120 ns MD simulation period.

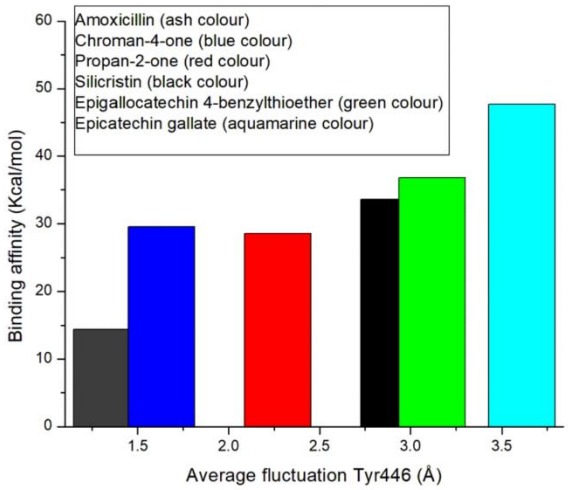


Figure 11. Correlation of the binding free energy of the top-five phenolics at the allosteric site of PBP2a and fluctuation of Tyr446 of PBP2a of *S. aureus*.

3.7. Bonds Analysis of the Interaction Plots of the Top-Five Phenolics against the Active and Allosteric Sites of PBP2a of S. aureus

In general, the ability of a ligand to bind and inactivate a protein is determined by a variety of thermodynamic criteria relating to the flexibility of amino acid residues, protein stability and compactness, and, most importantly, the nature of interactions with the essential amino acids of a protein [42,43]. Thus, in this study, the number, nature, and length of bond interactions formed by the top-five phenolics with PBP2a at both the active and allosteric sites were analysed. The plot of interactions for amoxicillin and phenolics with the highest binding free energy at both the active and allosteric sites are presented in Figure 12a,b, respectively, while the plots for other top-five phenolics are presented in Table S3. The nature, bond lengths, and numbers of interactions of the top-five phenolics as well as amoxicillin at the active site of PBP2a differs from one compound to another and were noted to have impacts on the binding free energy observed in this study. These bond interactions include hydrogen bonds (conventional and carbon), Van der Waals, amide π-stacked, π-anion, π-sigma, π-cation, π-π t-cation, π-π t-shaped, π-π t-stacked, π-alkyl, alky, π- Sulphur, as well as some unfavourable donor–donor interactions. In this study, propan-2-one and amoxicillin (Figure 12a) had the highest number, with 17 interactions each (Table 7 and Table S3). This observation is not directly in accordance with the free binding energy scores of this study where silicristin, epigallocatechin 4-benzylthioether, chroman-4-one, and epicatechin gallate had a higher free binding energy than amoxicillin and propan-2-one. However, when the interactions were further analysed as to the nature and distance of the bonds formed with amoxicillin and propan-2-one, more insight into why they have a low binding free energy relative to the other compounds was revealed. Hydrogen bond interactions have been demonstrated as one of the most important non-covalent bonds in drug discovery as they exhibit unusually strong intermolecular interactions [40]. Propan-2-one had only one hydrogen bond interaction with Tyr447 (Table 7) relative to four hydrogen bonds each formed by silicristin (Tyr446, Thyr600, Asn464, Glu602) (Figure 12b), epigallocatechin 4-benzylthioether (Lys584, Glu460, Thr582, Asp586), and amoxicillin (Ala642, Ser643, Ser461, Ser462) as well as five hydrogen bonds formed by epicatechin gallate (Lys581, Ser461, Glu447 (2), Gly599) against the active site of PBP2a of *S. aureus* (Table 7 and Table S3). Although, chroman-4-one also had one hydrogen bond interaction with Ser642 of PBP2a, however, when the average distance of interactions of PBP2a + chroma-4-one (4.99 Å) was compared with PBP2a + propan-2-one (5.53 Å), the average bond length of the former was considerably lower, which could have contributed to its observed higher binding free energy relative to PBP2a + propan-2-one. The importance of bond length observed in this study agrees with the report of Du et al. [34], who demonstrated the importance of shorter bond length in the stronger pull between two intra- or intermolecular entities, which may lead to their atoms being held together more tightly and hence a greater affinity. Similarly, the lower binding free energy of amoxicillin relative to the other top-four phenolics observed in this study could also be partly attributed to its higher bond length, which is second only to silicristin against PBP2a. Furthermore, relative to the top-five phenolics with no unfavourable bonds (except silicristin), amoxicillin had two unfavourable donor-donor bonds which are relatively shorter in length (2.66 Å) when compared to the average bond interaction distance of PBP2a + amoxicillin (5.14 Å). The formation of the unfavourable bonds which imply the presence of a repelling force in the PBP2a + amoxicillin complex [44], and the short distance of the unfavourable bond which suggests how strong the repulsion was, could have greatly impacted the lower binding free energy observed with the PBP2a-amoxicillin complex relative to the top-five phenolics despite amoxicillin forming 17 interactions (of which four were hydrogen bonds) with PBP2a (Table 7 and Table S3). Although one interaction in the PBP2a-silicristin interaction plot was also unfavourable, with a longer bond length of 6.35 Å relative to the average bond interaction length of PBP2a-silicristin (5.75 Å) (Figure 12b), this implied its lesser impact on the binding free energy observed in silicristin against PBP2a. While the PBP2a-silicristin complex (16) had one interaction greater than the interactions observed with PBP2a-epigallocatechin 4-benzylthioether, PBP2a-epicatechin gallate, and PBP2a-chroman-4-one complexes, having a remarkably higher average bond length did not

entirely justify the PBP2a-silicristin complex having a higher binding free energy against PBP2a than the other three complexes. However, among the top-five phenolics as well as amoxicillin, only silicristin interacted with a hydrogen bond with Tyr446, an important amino acid residue at the active site of PBP2a [16,41] (Figure 12b), a clue of its affinity for the PBP2a active site which could have impacted its higher binding free energy observed in this study. Amoxicillin interacted with a π-cation, propan-2-one interacted with a π-π t-shaped, epigallocatechin 4-benzylthioether interacted with a π-Sulphur, while epicatechin gallate and chroman-4-one both interacted with Van der Waals interactions, all of which are of lesser strength relative to the hydrogen bonds. Generally, none of the top-five phenolics as well as amoxicillin interacted with the catalytic residue Ser403 [16] that was sandwiched between the α2-α3 loop and ß3–ß4 loop of the PBP2a active site, suggesting the partial occupancy of the active site by the top-five phenolics and amoxicillin.

Table 7. Bond interactions against the active and allosteric site of PBP2a of *S. aureus* by the top-five phenolics.

Top-Five Phenolics and Standard	Total Number of Interactions (Average Distances in Å)	Number of Hydrogen Bonds and Interaction Residues	Other Important Interactions and Residues	Unfavourable Bonds (Bond Length in Å)
Active Site				
Amoxicillin	17 (5.14)	4 (Ala642, Ser643, Ser461, Ser462)	3 (Tyr446, Ala642, His583)	2 (Thyr600, Ala642) (2.96)
Silicristin	16 (5.75)	4 (Tyr446, Thyr600, Asn464, Glu602)	3 (Met641, Glu602, Arg445)	1 (Gln521) (6.35)
Propan-2-one	17 (5.53)	1 (Tyr447)	3 (His583, Tyr446, Ala642)	None
Epigallocatechin 4-benzylthioether	15 (4.91)	4 (Lys584, Glu460, Thr582, Asp586)	3 (Ala642, His583, Tyr446)	None
Chroman-4-one	15 (4.99)	1(Ser642)	2 (His583, Ala642)	None
Epicatechin gallate	15 (4.94)	5 (Lys581, Ser461, Glu447 (2), Gly599)	2 (Ala642, His583)	None
Allosteric Site				
Amoxicillin	8 (5.44)	2 (Lys122, Asp294)	2 (Lys122, Glu212)	None
Silicristin	16 (5.37)	5 (Lys273, Lys148, Asn146, Asp295(2))	3 (Asp275, Lys316, Tyr297)	(Tyr297) (6.06)
Propan-2-one	16 (5.23)	4 (Asp275, Lys273, Asn146 (2))	2 (Tyr297, Lys273)	none
Epigallocatechin 4-benzylthioether	23 (4.71)	7 (Asp269, Ser214, Glu213, Glu144, Val251, Ala250, Hie267)	2 (Val251, Pro332)	none
Chroman-4-one	12 (5.0)	4 (Lys148, Lys273, Val277, Ala276)	1 (Tyr297)	none
Epicatechin gallate	11 (3.87)	5 (Asn104, Gly296, Asn146 (2), Asp295)	1 (Tyr297)	Lys273 (4.61)

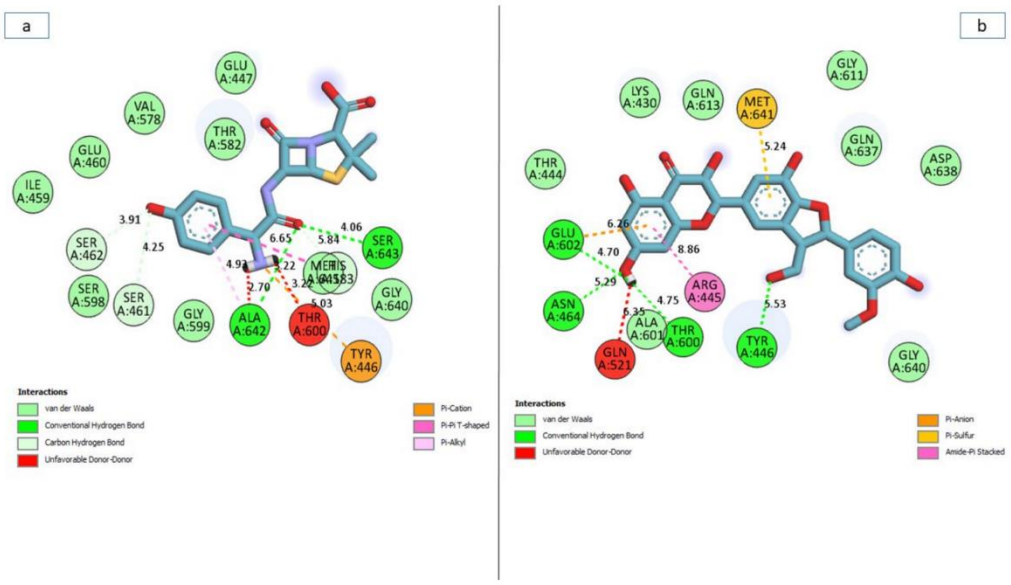


Figure 12. Plot of interactions of amoxicillin (**a**) and silicristin (**b**) against the active site of PBP2a of *S. aureus*.

Similar to the active site, the nature, bond lengths and numbers of interactions of the top-five phenolics as well as amoxicillin at the allosteric site of PBP2a differs from one compound to another and were noted to have impacts on the binding free energy observed in this study. These bond interactions include hydrogen bonds (conventional, carbon, and π-donor), Van der Waals, amide π-stacked, π-anion, π-sigma, π-cation, π-π t-cation, π-π t-shaped, π-π t-stacked, π-alkyl, alky as well as some unfavourable donor–donor interactions (Table S3). The PBP2a + epigallocatechin 4-benzylthioether complex having the highest number of total interactions (23) and hydrogen bond interactions (7 (Asp269, Ser214, Glu213, Glu144, Val251, Ala250, Hie267)) (Table 7 and Table S3) could have contributed to epigallocatechin 4-benzylthioether having a significantly higher binding free energy over amoxicillin (Figure 13a), silicristin, propan-2-one, and chroman-4-one at the allosteric site of PBP2a (Table S3). Nevertheless, this observation did not entirely justify PBP2a + epigallocatechin 4-benzylthioether having a significantly lower binding free energy relative to PBP2a + epicatechin gallate (Figure 13b) observed in this study. However, among the top-five phenolics, only epigallocatechin 4-benzylthioether failed to interact with some of the essential amino acids of the allosteric site (Table 7 and Table S3). According to Alhadrami et al. [16], amino acids, such as Tyr297, Tyr105, Asn146, Ile144, and 296 are important at the allosteric site of PBP2a of *S. aureus*, all of which are absent in the interaction plot of PBP2a + epigallocatechin 4-benzylthioether, which could have impacted epigallocatechin 4-benzylthioether having a lower binding free energy relative to epicatechin gallate at the allosteric site. This observation is suggestive of the partial occupancy of epigallocatechin 4-benzylthioether at the allosteric site of PBP2a and hence its lesser potential to cause a higher fluctuation of Tyr446 (active site gatekeeper residue) relative to epicatechin gallate despite the high number of interactions. Moreover, epicatechin gallate at the allosteric site of PBP2a (11 interactions), interacted with a relatively shorter bond length (3.87 Å) when compared with epigallocatechin 4-benzylthioether and other studied compounds (Figure 13b and Table 7). In addition, despite having the least number of interactions among the top-five phenolics, PBP2a + epicatechin gallate alongside PBP2a + silicristin had the second-highest number of hydrogen bond interactions (five) (Figure 13b and Table 7). All

these observations could have contributed to the significantly higher binding free energy noted in this study by epicatechin gallate at the allosteric site of PBP2a relative to epigallocatechin 4-benzylthioether and other study compounds and hence re-emphasises the impact of bond length and hydrogen bonds in the stability and affinity of a compound for a protein. PBP2a + silicristin, PBP2a + Propan-2-one, and PBP2a + Chroman-4-one all had interactions including hydrogen bonds that justified their respective binding free energy observed in this study (Table 7 and Table S3). PBP2a + silicristin had sixteen interactions at the allosteric site of PBP2a, of which five interactions were hydrogen bond interactions with residues Lys273, Lys148, Asn146, and Asp295(2) and three interactions were other important interactions with Asp275, Lys316, and Tyr297. PBP2a + Propan-2-one had sixteen interactions at the allosteric site of PBP2a, of which four interactions were hydrogen bond interactions with residues Lys148, Lys273, Val277, and Ala276 and two interactions were other important interactions with Tyr297, Lys273. Similarly, PBP2a + Chroman-4-one had twelve interactions at the allosteric site of PBP2a, of which four interactions were hydrogen bond interactions with residues Lys148, Lys273, Val277, and Ala276 and one other important interaction with Tyr297. The extra hydrogen bond interaction and at least one other important interaction had by PBP2a + silicristin over PBP2a + Propan-2-one, and PBP2a + Chroman-4-one could have contributed to silicristin's higher binding free energy over propan-2-one and chroman-4-one at the allosteric site of PBP2a. In this study, all the top-five phenolics interacted with a higher number of interactions, hydrogen bond interactions and other important interactions than amoxicillin (Figure 13a) at the allosteric site of PBP2a, which could have contributed to amoxicillin's significantly lower binding free energy at the allosteric site of PBP2a relative to the top-five phenolics. PBP2a + amoxicillin had eight interactions at the allosteric site of PBP2a, of which two interactions were hydrogen bond interactions with residues Lys122 and Asp294 and two other important interactions with Lys122 and Glu212. Similar to PBP2a + epigallocatechin 4-benzylthioether, none of the interacted amino acid residues in the PBP2a + amoxicillin plot were among the essential amino acid residues at the allosteric site of PBP2a, suggesting the partial occupancy of this site by amoxicillin and could have imparted the lesser fluctuation of gatekeeper residue (Tyr446) observed in this study relative to the top-five phenolics and hence the lesser ability of amoxicillin to modulate the PBP2a active site when bound at the allosteric site.

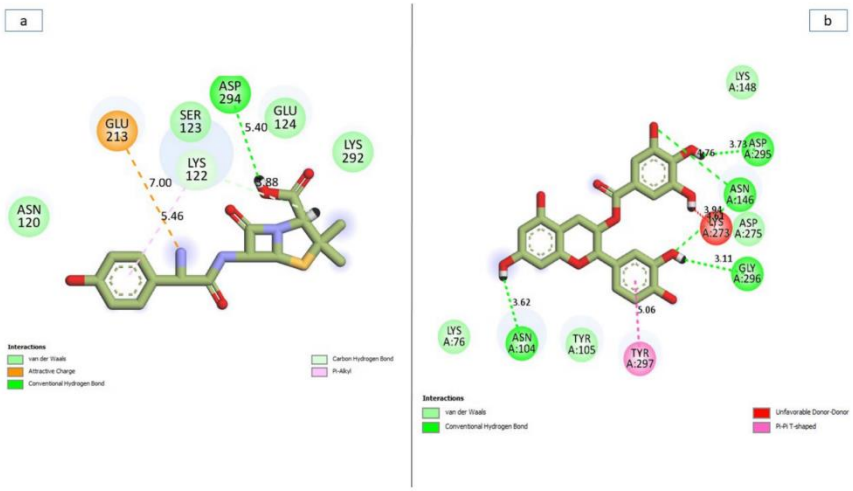


Figure 13. Plot of interactions of amoxicillin (**a**) and epicatechin gallate (**b**) against the allosteric site of PBP2a of *S. aureus*.

4. Conclusions

Findings from this study have identified lead phenolics with the capability to bind to the active and allosteric sites of PBP2a of *S. aureus*. Specifically, the lead phenolics showed more promising affinity at the allosteric site than the active site, with silicristin and epicatechin gallate having the best affinity at the active and allosteric sites of PBP2a, respectively. Interestingly, the modulation of Tyr446, a residue implicated in impeding access of β-lactams to the PBP2a active site, was noted to correlate with the affinity of the lead phenolics with the allosteric site of PBP2a with epicatechin gallate, which has the highest binding free energy, resulting in the highest fluctuation of Tyr446. This observation is indicative of the lesser involvement of Tyr446 in the intramolecular interactions of adjacent residues of PBP2a, thereby creating lesser obstructions of the PBP2a active site. Furthermore, when the lead phenolics bind at the active site of PBP2a, Tyr446 had less fluctuation, implying its active involvement in the binding of the compounds. These observations are suggestive of the possible advantage of the lead phenolics in the direct and synergistic treatment of infections caused by *S. aureus* and, interestingly, as the lead phenolics had favourable pharmacokinetics and a feasible synthetic score, signifying the possibility of structural alterations for improved druggability and toxicity. However, further in vitro and in vivo confirmation of the activities observed in this study is strongly recommended and efforts are underway in this direction.

Supplementary Materials: The following supporting information can be downloaded at: https://www.mdpi.com/article/10.3390/pharmaceutics14091818/s1, Figure S1: Observed 1550 hit compounds; Table S1: Consensus phenolic pharmacophore spatial arrangements; Table S2: Average RMSD, RMSF, ROG, and SASA of the top-five phenolics and amoxicillin following 120 ns simulation at the allosteric site of PBP2a of *S. aureus;* Figure S2: Comparative (a) root-mean-squared deviation (RMSD), (b) radius of gyration (ROG), (c) root-mean-squared fluctuation (RMSF), and (d) solvent-accessible surface area (SASA) plots of alpha-carbon, the top-five phenolics, and amoxicillin against the allosteric site PBP2a of *S. aureus* over a 120 ns MD simulation period; Table S3: 2D plot interactions of the top-five phenolics at the active and allosteric sites after 120 ns simulation.

Author Contributions: Conceptualization, S.S.; methodology, J.O.A. and S.S.; software, J.O.A.; formal analysis, J.O.A.; investigation, J.O.A. and S.S.; writing—original draft preparation, J.O.A.; writing—review and editing, J.O.A. and S.S.; supervision, S.S.; funding acquisition, S.S. All authors have read and agreed to the published version of the manuscript.

Funding: The authors especially acknowledge the financial assistance of the Directorate of Research and Postgraduate Support, Durban University of Technology, and the South African Medical Research Council (SA MRC) under a Self-Initiated Research Grant as well as the National Research Foundation (NRF) Research Development Grant for rated researchers (Grant number 120433) to S. Sabiu. The views and opinions expressed are those of the authors and do not necessarily represent the official views of the funders.

Institutional Review Board Statement: Not applicable.

Informed Consent Statement: Not applicable.

Data Availability Statement: The data are contained within the article or Supplementary Material.

Acknowledgments: The NRF-TWAS Doctoral Scholarship (Grant number 129950) to J.O.A. is duly acknowledged. The Centre for High-Performance Computing (CHPC), South Africa is equally acknowledged for granting access to the computing systems used in this study.

Conflicts of Interest: The authors declare no conflict of interest.

References

1. Kalalo, M.J.; Fatimawali, F.; Kalalo, T.; Imanuel, C.; Rambi, J. Tea bioactive compounds as inhibitor of MRSA penicillin binding protein 2a (PBP2a): A molecular docking study. *Pharm. Med. J.* **2020**, *20*, 70–75. [CrossRef]
2. Rahman, M.M.; Amin, K.B.; Rahman, S.M.M.; Khair, A.; Rahman, M.; Hossain, A.; Rahman, A.K.M.A.; Parvez, M.S.; Miura, N.; Alam, M.M.; et al. Investigation of methicillin-resistant Staphylococcus aureus among clinical isolates from humans and animals by culture methods and multiplex PCR. *BMC Veter. Res.* **2018**, *14*, 300. [CrossRef] [PubMed]

3. Abdel-Moein, K.A.; Zaher, H.M. Occurrence of multidrug-resistant methicillin-resistant *Staphylococcus aureus* among healthy farm animals: A public health concern. *Int. J. Veter. Sci. Med.* **2019**, *7*, 55–60. [CrossRef] [PubMed]
4. Stryjewski, M.; Corey, G.R. Methicillin-Resistant Staphylococcus aureus: An Evolving Pathogen. *Clin. Infect. Dis.* **2013**, *58*, S10–S19. [CrossRef]
5. Malik, B.; Bhattacharyya, S. Antibiotic drug-resistance as a complex system driven by socio-economic growth and antibiotic misuse. *Sci. Rep.* **2019**, *9*, 9788. [CrossRef]
6. Verma, A.K.; Ahmed, S.F.; Hossain, S.; Bhojiya, A.A.; Mathur, A.; Upadhyay, S.K.; Srivastava, A.K.; Vishvakarma, N.K.; Barik, M.; Rahaman, M.; et al. Molecular docking and simulation studies of flavonoid compounds against PBP-2a of methicillin-resistant *Staphylococcus aureus*. *J. Biomol. Struct. Dyn.* **2021**, 1–17. [CrossRef]
7. Larsson, D.G.J.; Flach, C.-F. Antibiotic resistance in the environment. *Nat. Rev. Genet.* **2021**, *20*, 257–269. [CrossRef]
8. Josephine, H.R.; Charlier, P.; Davies, C.; Nicholas, R.A.; Pratt, R.F. Reactivity of penicillin-binding proteins with peptidoglycan-mimetic β-lactams: What's wrong with these enzymes? *ACS Chem. Biol.* **2006**, *45*, 15873–15883. [CrossRef]
9. Zapun, A.; Contreras-Martel, C.; Vernet, T. Penicillin-binding proteins and β-lactam resistance. *FEMS Microbiol. Rev.* **2008**, *32*, 361–385. [CrossRef]
10. Sauvage, E.; Kerff, F.; Terrak, M.; Ayala, J.A.; Charlier, P. The penicillin-binding proteins: Structure and role in peptidoglycan biosynthesis. *FEMS Microbiol. Rev.* **2008**, *32*, 234–258. [CrossRef]
11. Scheffers, D.-J.; Pinho, M.G. Bacterial Cell Wall Synthesis: New Insights from Localization Studies. *Microbiol. Mol. Biol. Rev.* **2005**, *69*, 585–607. [CrossRef] [PubMed]
12. Meisel, J.E.; Fisher, J.F.; Chang, M.; Mobashery, S. Allosteric Inhibition of Bacterial Targets: An Opportunity for Discovery of Novel Antibacterial Classes. In *Antibacterials*; Fisher, J.F., Mobashery, S., Miller, M.J., Eds.; Springer: Cham, Switzerland, 2017; pp. 119–147. [CrossRef]
13. Otero, L.H.; Rojas-Altuve, A.; Llarrull, L.I.; Carrasco-López, C.; Kumarasiri, M.; Lastochkin, E.; Fishovitz, J.; Dawley, M.; Hesek, D.; Lee, M.; et al. How allosteric control of *Staphylococcus aureus* penicillin binding protein 2a enables methicillin resistance and physiological function. *Proc. Natl. Acad. Sci. USA* **2013**, *110*, 16808–16813. [CrossRef] [PubMed]
14. Dundas, J.; Ouyang, Z.; Tseng, J.; Binkowski, A.; Turpaz, Y.; Liang, J. CASTp: Computed atlas of surface topography of proteins with structural and topographical mapping of functionally annotated residues. *Nucleic Acids Res.* **2006**, *34*, W116–W118. [CrossRef]
15. Fisher, J.F.; Mobashery, S. β-lactam resistance mechanisms: Gram-positive bacteria and *Mycobacterium tuberculosis*. *Cold Spring Harb. Perspect Med.* **2020**, *6*, a025221. [CrossRef]
16. Alhadrami, H.A.; Hamed, A.A.; Hassan, H.M.; Belbahri, L.; Rateb, M.E.; Sayed, A.M. Flavonoids as Potential anti-MRSA Agents through Modulation of PBP2a: A Computational and Experimental Study. *Antibiotics* **2020**, *9*, 562. [CrossRef] [PubMed]
17. Aldulaimi, O. General overview of phenolics from plant to laboratory, good antibacterials or not. *Pharmacogn. Rev.* **2017**, *11*, 123–127. [CrossRef]
18. Araya-Cloutier, C.; Vincken, J.-P.; van Ederen, R.; Besten, H.M.D.; Gruppen, H. Rapid membrane permeabilization of Listeria monocytogenes and *Escherichia coli* induced by antibacterial prenylated phenolic compounds from legumes. *Food Chem.* **2018**, *240*, 147–155. [CrossRef]
19. Weinreb, O.; Mandel, S.; Amit, T.; Youdim, M.B. Neurological mechanisms of green tea polyphenols in Alzheimer's and Parkinson's diseases. *J. Nutr. Biochem.* **2004**, *15*, 506–516. [CrossRef]
20. Panat, N.A.; Singh, B.G.; Maurya, D.K.; Sandur, S.K.; Ghaskadbi, S.S. Troxerutin, a natural flavonoid binds to DNA minor groove and enhances cancer cell killing in response to radiation. *Chem. Interact.* **2016**, *251*, 34–44. [CrossRef]
21. Dai, Q.; Borenstein, A.R.; Wu, Y.; Jackson, J.C.; Larson, E.B. Fruit and Vegetable Juices and Alzheimer's Disease: The Kame Project. *Am. J. Med.* **2006**, *119*, 751–759. [CrossRef]
22. Chiorcea-Paquim, A.; Enache, T.A.; De Souza Gil, E.; Oliveira-Brett, A.M. Natural phenolic antioxidants electrochemistry: Towards a new food science methodology. *Compr. Rev. Food Sci. Food Saf.* **2020**, *19*, 1680–1726. [CrossRef] [PubMed]
23. Aribisala, J.O.; Abdulsalam, R.A.; Dweba, Y.; Madonsela, K.; Sabiu, S. Identification of secondary metabolites from Crescentia cujete as promising antibacterial therapeutics targeting type 2A topoisomerases through molecular dynamics simulation. *Comput. Biol. Med.* **2022**, *145*, 105432. [CrossRef] [PubMed]
24. MubarakAli, D.; MohamedSaalis, J.; Sathya, R.; Irfan, N.; Kim, J.-W. An evidence of microalgal peptides to target spike protein of COVID-19: In silico approach. *Microb. Pathog.* **2021**, *160*, 105189. [CrossRef] [PubMed]
25. Koes, D.R.; Camacho, C.J. ZINCPharmer: Pharmacophore search of the ZINC database. *Nucleic Acids Res.* **2012**, *40*, W409–W414. [CrossRef]
26. Fahad, M.; Al-Khodairy, M.; Kalim, A.; Khan, M.K.; Manogaran, S.P.; Salman, A.; Jamal, M.A. In Silico Prediction of Mechanism of Erysolin-induced Apoptosis in Human Breast Cancer Cell Lines, American. *J. Bioinform.* **2013**, *3*, 62–71. [CrossRef]
27. Kufareva, I.; Abagyan, R. Methods of Protein Structure Comparison. *Methods Mol. Biol.* **2012**, *857*, 231–257. [CrossRef]
28. Sabiu, S.; Balogun, F.O.; Amoo, S.O. Phenolics Profiling of *Carpobrotus edulis* (L.) N.E.Br. and Insights into Molecular Dynamics of Their Significance in Type 2 Diabetes Therapy and Its Retinopathy Complication. *Molecules* **2021**, *26*, 4867. [CrossRef]
29. Aribisala, J.O.; Nkosi, S.; Idowu, K.; Nurain, I.O.; Makolomakwa, G.M.; Shode, F.O.; Sabiu, S. Astaxanthin-Mediated Bacterial Lethality: Evidence from Oxidative Stress Contribution and Molecular Dynamics Simulation. *Oxidative Med. Cell. Longev.* **2021**, *2021*, e7159652. [CrossRef]

30. Uhomoibhi, J.O.-O.; Shode, F.O.; Idowu, K.A.; Sabiu, S. Molecular modelling identification of phytocompounds from selected African botanicals as promising therapeutics against druggable human host cell targets of SARS-CoV-2. *J. Mol. Graph. Model.* **2022**, *114*, 108185. [CrossRef]
31. Lipinski, C.A.; Lombardo, F.; Dominy, B.W.; Feeney, P.J. Experimental and computational approaches to estimate solubility and permeability in drug discovery and development settings. *Adv. Drug Deliv. Rev.* **2001**, *46*, 3–26. [CrossRef]
32. Khumbulani, M.; Alayande, K.A.; Sabiu, S. Orientin Enhances Colistin-Mediated Bacterial Lethality through Oxidative Stress Involvement. *Evid. -Based Complement. Altern. Med.* **2022**, *2022*, 3809232. [CrossRef] [PubMed]
33. Ertl, P.; Schuffenhauer, A. Estimation of synthetic accessibility score of drug-like molecules based on molecular complexity and fragment contributions. *J. Cheminform.* **2009**, *1*, 8–11. [CrossRef] [PubMed]
34. Du, X.; Li, Y.; Xia, Y.-L.; Ai, S.-M.; Liang, J.; Sang, P.; Ji, X.-L.; Liu, S.-Q. Insights into Protein–Ligand Interactions: Mechanisms, Models, and Methods. *Int. J. Mol. Sci.* **2016**, *17*, 144. [CrossRef] [PubMed]
35. Ramirex, D.; Caballero, J. Is it reliable to use common molecular docking methods for comparing the binding affinities of Enantiomer pairs for their protein target. *Int. J. Mol. Sci.* **2016**, *17*, 525. [CrossRef] [PubMed]
36. Stella, L.; Melchionna, S. Equilibration and sampling in molecular dynamics simulations of biomolecules. *J. Chem. Phys.* **1998**, *109*, 10115–10117. [CrossRef]
37. Baig, M.H.; Sudhakar, D.R.; Kalaiarasan, P.; Subbarao, N.; Wadhawa, G.; Lohani, M.; Khan, M.K.A.; Khan, A.U. Insight into the Effect of Inhibitor Resistant S130G Mutant on Physico-Chemical Properties of SHV Type BetaLactamase: A Molecular Dynamics Study. *PLoS ONE* **2014**, *9*, e112456. [CrossRef]
38. Lobanov, M.Y.; Bogatyreva, N.S.; Galzitskaya, O.V. Radius of gyration as an indicator of protein structure compactness. *Mol. Biol.* **2008**, *42*, 623–628. [CrossRef]
39. Mousavi, S.S.; Karami, A.; Haghighi, T.M.; Tumilaar, S.G.; Idroes, R.; Mahmud, S.; Celik, I.; Ağagündüz, D.; Tallei, T.E.; Fatimawali; et al. In Silico Evaluation of Iranian Medicinal Plant Phytoconstituents as Inhibitors against Main Protease and the Receptor-Binding Domain of SARS-CoV-2. *Molecules* **2021**, *26*, 5724. [CrossRef]
40. Izadi, H.; Stewart, K.M.E.; Penlidis, A. Role of contact electrification and electrostatic interactions in gecko adhesion. *J. R. Soc. Interface* **2014**, *11*, 20140371. [CrossRef]
41. Mahasenan, K.V.; Molina, R.; Bouley, R.; Batuecas, M.T.; Fisher, J.F.; Hermoso, J.A.; Chang, M.; Mobashery, S. Conformational Dynamics in Penicillin-Binding Protein 2a of Methicillin-Resistant *Staphylococcus aureus*, Allosteric Communication Network and Enablement of Catalysis. *J. Am. Chem. Soc.* **2017**, *139*, 2102–2110. [CrossRef]
42. Kitchen, D.B.; Decornez, H.; Furr, J.R.; Bajorath, J. Docking and scoring in virtual screening for drug discovery: Methods and applications. *Nat. Rev. Drug Discov.* **2004**, *3*, 935–949. [CrossRef] [PubMed]
43. Nasution, M.A.F.; Toepak, E.P.; Alkaff, A.H.; Tambunan, U.S.F. Flexible docking-based molecular dynamics simulation of natural product compounds and Ebola virus Nucleocapsid (EBOV NP): A computational approach to discover new drug for combating Ebola. *BMC Bioinform.* **2018**, *19*, 419–436. [CrossRef] [PubMed]
44. Bissantz, C.; Kuhn, B.; Stahl, M.A. Medicinal chemist's guide to molecular interactions. *J. Med. Chem.* **2010**, *14*, 5061–5084. [CrossRef] [PubMed]

CHAPTER FOUR

4.0 Retrosynthesis and derivatization of identified lead phenolic compounds and evaluation of their enhanced druggability relative to the parent compounds using *in silico* methods

4.1 Structural optimization of silicristin against key penicillin-binding proteins of selected clinically important bacteria yielded putatively potent chalcone bis-coumarin derivatives……**213**

Abstract ……..**213**

1.0 Introduction …… ……**215**

2.0 Methodology ……**218**

3.0 Results and discussion ……**230**

4.0 Conclusion……....**286**

References……..**287**

Supplementary information…….....**300**

This chapter has been formatted for submission to Computers in Biology and Medicine

4.1 Structural optimization of silicristin against key penicillin-binding proteins of selected clinically important bacteria yielded putatively potent chalcone bis-coumarin derivatives

Jamiu Olaseni Aribisala[a], Talent Raymond Makhanya[b] and Saheed Sabiu[a]*

[a]Department of Biotechnology and Food Science, Faculty of Applied Sciences, Durban University of Technology, P.O. Box 1334, Durban 4000, South Africa

[b]Department of Chemistry, Faculty of Applied Sciences, Durban University of Technology, P.O. Box 1334, Durban 4000, South Africa

Correspondence: sabius@dut.ac.za

Abstract

Improved thermodynamic stability has been demonstrated to be critical in affinity/potency of a drug for a target and its subsequent efficacy *in vitro* and *in vivo*. This study employed pharmacophore hybridization and structural simplification techniques to enhance thermodynamic stability of silicristin against the key penicillin-binding proteins (PBP) of four (PBP3 and 5 of *Escherichia coli*, PBP3 of *Pseudomonas aeruginosa*, PBP2a of *Staphylococcus aureus* and PBP2x of *Streptococcus pneumoniae*) clinically important bacteria. The knowledge of the interactions of silicristin with the selected key PBPs was employed in designing 25 novel derivatives of chalcone bis-coumarin from easily synthesizable starting materials of coumarin moieties. Following molecular docking, pharmacokinetic screening, molecular dynamic (MD) simulation and energy refinement of the 25 derivatives, RD2c (PBP3 of *E. coli*: -46.26 kcal/mol), RD1c (PBP3 of *P. aeruginosa*: -39.42 kcal/mol and PBP2x active site: -42.90 kcal/mol), RD1a (PBP2a active site: -37.56 kcal/mol), D1a (PBP5 of *E. coli*: -37.19 kcal/mol), D1h (allosteric site of PBP2a: -53.09 kcal/mol and PBP2x of *S. pneumoniae*:-38.53 kcal/mol), were identified as best derivatives with enhanced binding free energy, stability, and pharmacokinetics properties relative to silicristin. Quantum calculations using DFT B3LYP/6-

31G+ (dp) techniques further showed that the best derivatives are more reactive and with higher ability to form hydrogen bonds due to their higher electrostatic potential compared to silicristin. Except for PBP2x, this observation is consistent with the bond analysis post-MD simulation as the best derivative in each case of the PBP formed higher number of hydrogen bonds compared to silicristin. The exploration of catechol, resorcinol, and hydroquinone either alone or in combination with each other at either end of the derivatives promoted good pharmacological properties, while the presence of a pyrogallol and/or a benzene ring with more than two hydroxy group at one or both ends of the derivatives caused reduced oral bioavailability relative to silicristin. The synthetic accessibility of the best derivatives was exploited in the laboratory through the synthesis of their parent compound using the Knoevenagel condensation, Vilsmeiers Haack and Aldol condensation reactions. The successfully synthesised parent compound was elucidated using nuclear magnetic resonance (NMR) and was further validated with the gauge independent atomic orbital (GIAO) method. The findings from this study showed noticeable improvement in the binding capacity and pharmacokinetic properties of the best derivatives relative to silicristin; an observation that could translate to enhanced potency. Adoptionof the synthetic route of the parent compound for the profiled derivatives for subsequent evaluation of their potency *in vitro* and *in vivo* is highly recommended.

Keywords: Derivatives, Silicristin, Chalcone bis-coumarin, Hybridization, Binding free energy, Thermodynamic stability

1.0 Introduction

Silicristin is one of the bioactive compounds of silymarin, a standardized extract from the dried seeds of milk thistle (*Silybum marianum* L. Gaertn.) (Johannes *et al*., 2016). Other important components of silymarin are silybin, silydianin, isosilybin, isosilychristin and taxifolin, with silybin being the most abundant component of the standardized extract (Kren and Walterova, 2005). Silymarin has long been used as a natural remedy for hepatitis and cirrhosis of the liver (Tyagi *et al*., 2007; Tyagi *et al*., 2004). Studies have demonstrated the exceptionally antibacterial activities of silymarin against both Gram-positives and Gram-negative bacteria (Abdelazim, 2017; Biedermann *et al*., 2016; de Oliveira *et al*., 2015; Lee *et al*., 2003). More specifically, silymarin was demonstrated to have moderate antibacterial effects on multidrug-resistant *Staphylococcus aureus*, *Pseudomonas aeruginosa* and *Escherichia coli* at a minimum inhibitory concentration (MIC) of 512 µg/mL (De Oliver *et al*., 2015). Rapid killing of bacteria has also been reported when silymarin was combined with conventional antibiotics such as ampicillin and oxacillin (Lee *et al*., 2012; Kang *et al*., 2011). Although, the pharmacological properties of silymarin including the antibacterial properties have been attributed majorly to silybin (Wadhwa *et al.*, 2022; De Oliver *et al.*, 2015), recent *in silico* studies of phenolics against key penicillin-binding proteins (PBPs) of *S. aureus*, *P. aeruginosa*, *E. coli* and *Streptococcus pneumoniae* identified silicristin (Figure 1) as potential anti- PBPs drug candidate (Aribisala and Sabiu, 2022; 2023, Aribisala *et al.*, 2023). Prior to the *in silico* studies, little or no information was reported on the antibacterial properties of silicristin. The recommendation from the studies showed that silicristin, had good potentials as a promising PBPs modulator, but can also instigate significant thermodynamic disorderliness in the protein. Thus, optimizing silicristin, using lead optimisation techniques (Barcelos *et al.*, 2022) that can enhance thermodynamic stability while also reducing toxicity might help identify novel derivatives of silicristin with improved druggability effect.

Although, the knowledge of the structural interactions of lead molecules with druggable targets is necessary. Lead optimization often requires identifying a set of acceptable reaction steps from accessible starting materials (Hughes *et al.*, 2011). In this regard, retrosynthesis, a process of "deconstructing" a desired molecule into easily accessible starting materials via imaginary bond breaking and the transformation of one functional group into another, enables medicinal chemists to identify a set of acceptable compound reaction steps (Lim *et al*., 2023; Clara *et al*., 2012). Chemists can create novel molecules tailored to fulfil certain tasks in cells due to the accessibility of synthetic routes for the development of new compound. A phenomenon that is greatly important in medicine for druggability improvement, symptom suppression, and disease treatment (Lim *et al*., 2023; Clara *et al*., 2012). Thus, the capacity to balance chemical dynamics, initiate new reactions, and optimize certain features in molecules might help create active lead molecules that could achieve desirable molecular behaviour in cells (Agamah *et al*., 2020). In medicinal chemistry, the hybridization of pharmacophore/skeleton and structural simplification of complex lead compounds is an effective strategy for obtaining active lead compounds (Pawełczyk *et al.* 2018). These strategies involve shortening unnecessary groups/molecules/ring to improve synthetic accessibility but also enhancing pharmacokinetic profiles (Wang *et al.*, 2019) and thus an appealing source of drug candidate in drug discovery. In this study, taking understanding from the interactions of silicristin with key PBPs of *S. aureus*, *P. aeruginosa*, *E. coli* and *Streptococcus pneumoniae*, novel derivatives of chalcone bis-coumarin were designed from easily synthesizable starting materials.

Previous studies have shown that natural products containing the coumarin moiety and synthesized coumarin derivatives exhibit broad biological properties, including antibacterial activities (Singh *et al.*, 2019; Hu *et al.*, 2018; Gao *et al.*, 2018; Hamdi *et al.*, 2010). For instance, Sahoo *et al.* (2019c), showed that coumarin mannich based derivatives had potent antibacterial effect against *S. aureus* at MIC 12.50 µg/mL. A similar study of curcumin and isatin-linked

coumarin derivatives had an MIC of 6.25 µg/mL against *E. coli* (Singh *et al.*, 2019), while a 3-Aroyl substituted coumarin derivatives had potent antibacterial effects against *S. aureus, E. coli, P. aeruginosa* at MIC value of 30 µg/mL in comparison to the standard drug cefoxitin (Belkhir-Talbi *et al.*, 2019). Aside their reported antibacterial activities, coumarins and their analogues display relatively low cardiotoxicity, cutaneous toxicity, nephrotoxicity, hepatotoxicity, and other adverse effects, making them an attractive contender in drug development (Gao *et al*., 2018; Hamdi *et al*., 2010). Similarly, chalcone, which serves as a precursor to flavonoids and isoflavonoids, has been demonstrated to be an effective antibacterial owing to the presence of the reactive α β-unsaturated system. The modification of the chalcone through hybridization with other substituent groups can increase potency, reduce toxicity, and broaden pharmacological action (Dhaliwal *et al*., 2022). Thus, in the study, the approach of hybridizing coumarin moieties via chalcone to produce novel drug candidates with potentially optimized modes of binding relative to silicristin was carried out. This was done to discover and develop novel drug candidate with enhanced antibacterial efficiency, high selectivity, reduced toxicity and favourable pharmacokinetics relative to silicristin.

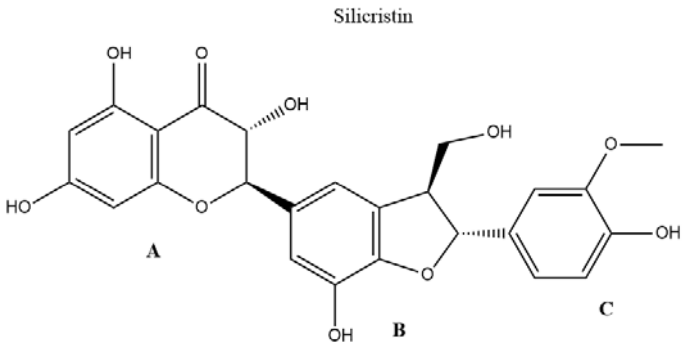
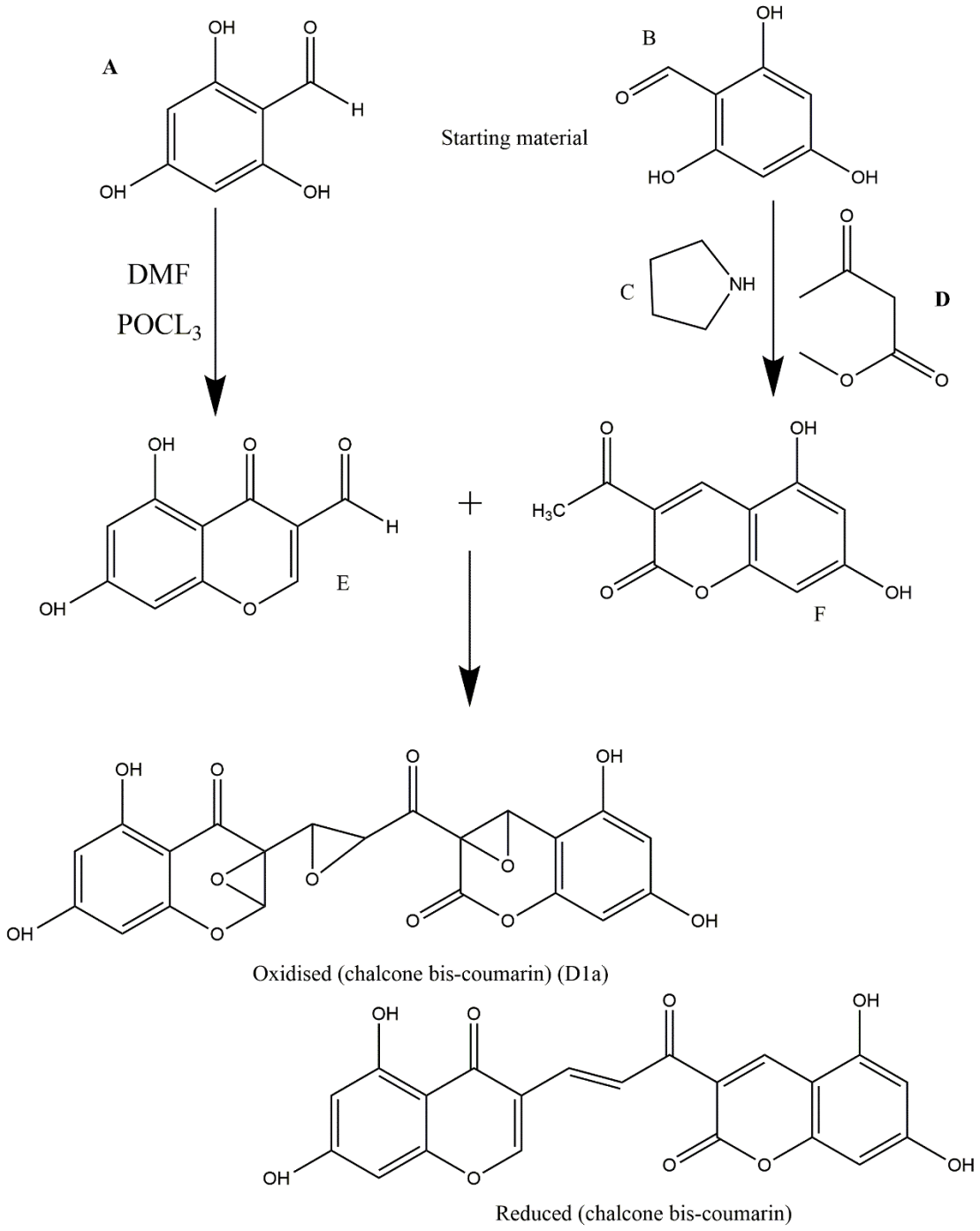


Figure 1: The 2D structure of silicristin showing subunit A, B and C

2.0 Methodology

2.1 Analysis of the interaction of silicristin with key PBPs of selected bacteria and derivatization of novel derivatives of chalcone bis-coumarin

In addition to the seemingly basic technique of detecting and 'tuning' the drug-target binding interactions, the alteration of lead structures to enhance their potency (pharmacodynamics) and delivery (pharmacokinetics) might require a variety of techniques (Wang *et al*., 2019). Structure extension is a typical strategy that involves adding additional functional group to the lead structure to test for extra binding interactions with the target. However, since silicristin appropriately occupy the binding regions available in most of the key PBPs, with only a few unused rings (Supplementary Figure S1), this study exploits the second approach of varying/adjusting the rings of silicristin to come up with new design molecules. Exploiting the interaction of silicristin with key PBPs of *E. coli*, *S. aureus*, *S. pneumoniae* and *P. aeruginosa* (Supplementary Figure S1 and Supplementary Table S1), twenty-five novel derivatives of chalcone bis-coumarin (Supplementary Figure S2) were designed using 12 stating materials. In designing the novel derivatives, the resorcinol phenolic moiety in silicristin was retained at both ends of D1a (Scheme 1). In the other 24 derivatives, different combinations of phenolic moieties such as pyrogallol, catechol and hydroquinone were used. This was important to understand the impact of the positioning of hydroxyl group on the biological activities of the derivatives. The interaction of silicristin with the key PBPs of *E. coli*, *S. aureus*, *S. pneumoniae* and *P. aeruginosa* showed less involvement of subunit B and C of silicristin (Figure 1 and Supplementary Figure S1) with the key PBPs, with most of the interactions formed by these units being majorly van der Waals forces and less hydrogen bonds. Consequently, subunit C of silicristin was altered to coumarin moieties while the B subunit was transformed to a chalcone to hybridize the coumarin moieties.



Scheme 1: Synthetic route of oxidized and reduced derivative of chalcone bis-coumarin (D1a). The 24 other derivatives (D1b-D3e) are presented in Supplementary Figure S2. A: 2,4,6 tryhydroxyacetophenone, B: salicylaldehyde, C: piperidine, D: acetoacetate, E: formyl coumarin, F: acetyl coumarin, DMF: dimethyl fumarate, $POCl_3$: phosphorous oxychloride

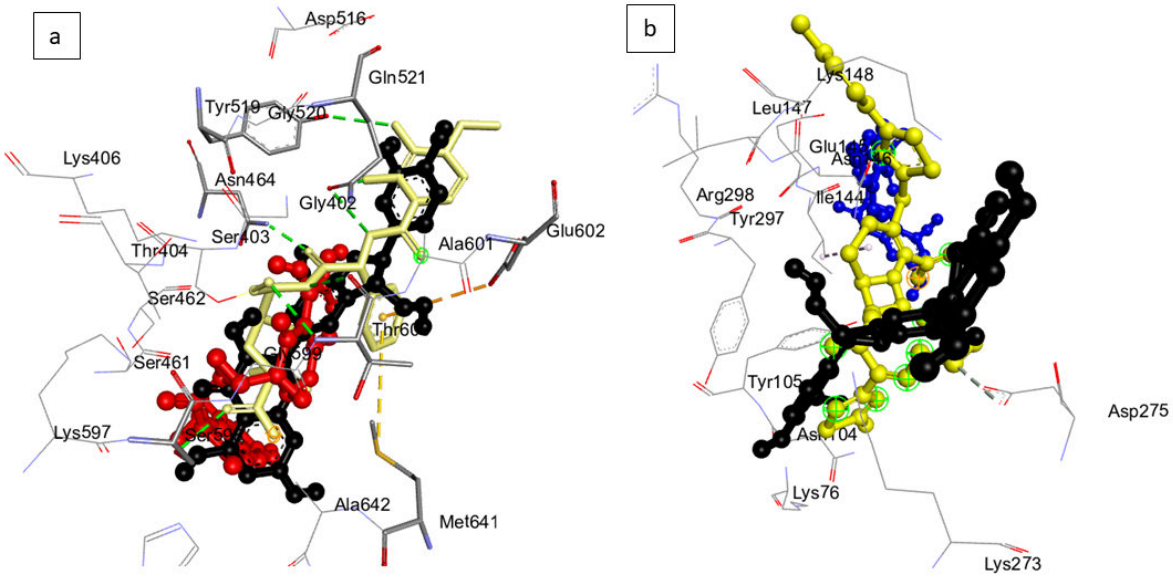
2.2. Evaluation of the novelty of the derivatives

The uniqueness of the derivatives was confirmed using the "Search ChEMBL database" tools present on Galaxy Europe (https://usegalaxy.eu./# accessed 12 Feb, 2022) (Bajorath, 2001) which enables for searching of compounds that are similar to a simplified molecular-input line-entry system (SMILES) input, or which contain the SMILES input as a substructure. Similarity search was done at 40 "Tanimoto cutoff score", the minimum value for similarity search on the tool. Further confirmation was done on ZINCPharmer database (http://zincpharmer.csb.pitt.edu) using the ligand-based pharmacophore techniques which enables for 3D similarity search of an imputed ligand. The similarity search for silicristin, was used as a control.

2.3 Ligand building, protein preparation, molecular docking and validation at the active sites of the key PBPs

The 25 designed derivatives of chalcone bis-coumarin were constructed using the ChemDraw professional v 15.0 (PerkinElmer, Inc, Waltham, Massachusetts, USA) (Mills, 2006) and optimised via addition of Gasteiger charges using the Open Babel program plug-in on Python Prescription (PyRx) v 0.9.5 (Sargis Dallakyan, Scripps Research Institute, San Diego, CA, USA). The key PBPs including PBP2a of *S. aureus* (PDB ID: 3ZFZ) (Otero *et al.*, 2013), PBP2x of *S. pneumoniae* (PBP ID: 1QMF) (Land *et al*., 2013; Gordon *et al*., 2000), PBP 3 of *P. aeruginosa* (PBP ID: 6VJE) (Kumar *et al.*, 2020) and PBP 3 (PDB ID: 6I1I) (Fraipon *et al*., 2011) and 5 (PDB ID: 1Z6F) (Nelson and Young, 2001) of *E. coli* were downloaded from the protein data bank (https://www.rcsb.org) and afterward optimised via removal of water molecules and nonstandard amino acids using the UCSF Chimera v1.15 software (University of California, San Francisco, CA, USA) (Pettersen *et al*., 2004). Docking of the optimized

PBPs and ligands (the 25 derivatives, using silicristin as reference standard) was performed using the AutoDock tool present on PyRx (Dallakyan, 2015). Docking at the active site of the PBPs was assured by selecting amino acid residues at the active site of the key PBPs (Aribisala and Sabiu, 2022, Aribisala and Sabiu, 2023, Aribisala *et al.*, 2023). Ranking of the derivatives against each of the PBPs were done using the docking score of silicristin as benchmark. Docking study validation was done as earlier reported (Fahad *et al.*, 2013) through superimposition and measuring of the root mean square deviation (RMSD) of the best docked derivatives and silicristin from the experimental native inhibitors of the PBPs (Figure 2). The docked complexes of the top ranked derivatives of chalcone bis-coumarin against each of the PBPs relative to silicristin with the most-energy-minimised conformation (maximum binding affinity) were then retrieved in PDB format for further molecular dynamic (MD) simulation.



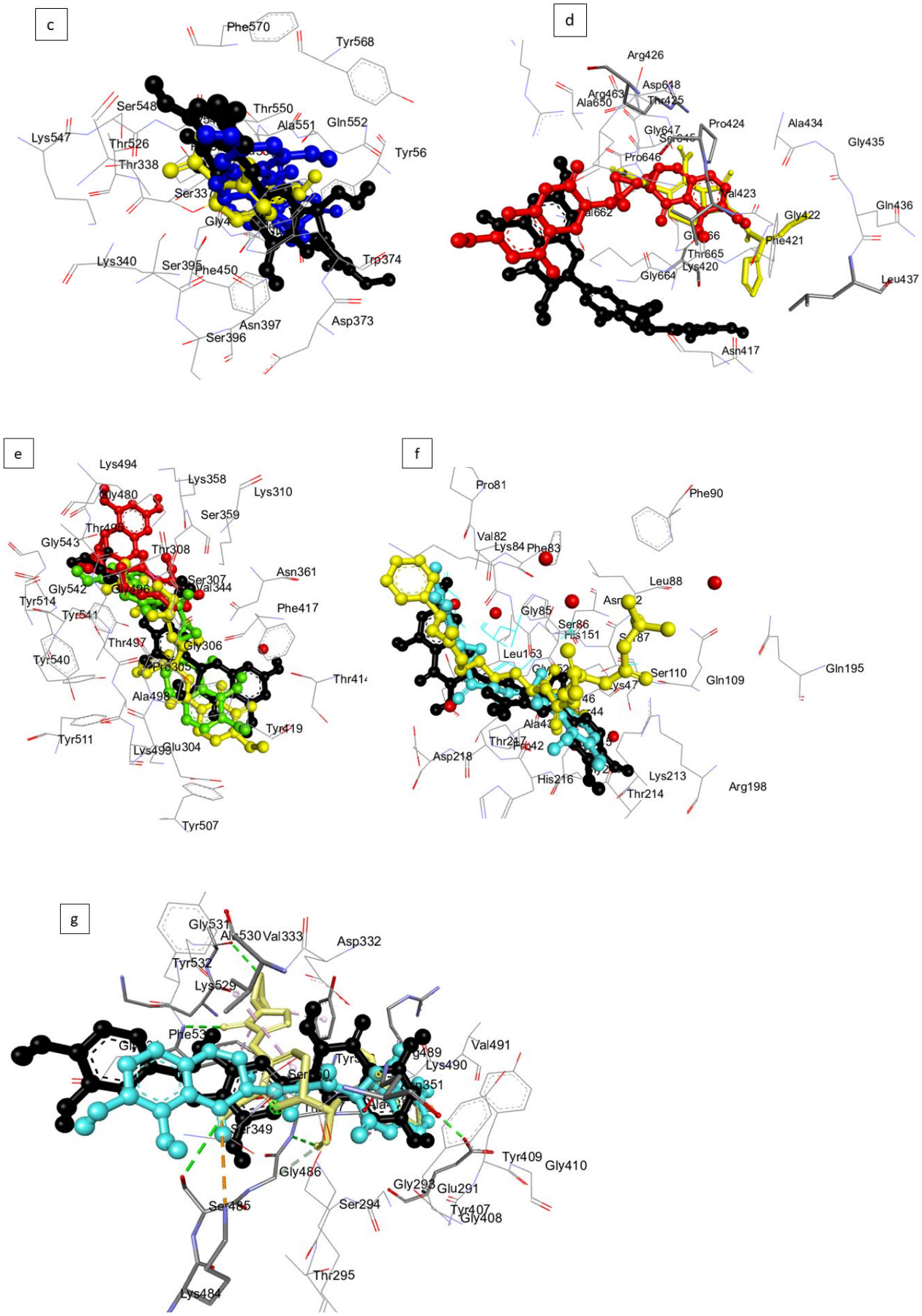

c
Phe570
Tyr568
Ser548
Thr550
Ala551
Gln552
Lys547
Thr526
Tyr56
Thr338
Ser33
Gly4
Lys340
Ser395
Phe450
Trp374
Asn397
Asp373
Ser396
d
Arg426
Asp648
Arg463
Ala650
Thr425
Pro424
Ala434
Gly647
Gly435
Pro646
Val423
Gln436
Gly422
Phe421
Thr665
Lys420
Gly664
Leu437
Asn417
e
Lys494
Lys358
Gly480
Lys310
Ser359
Gly543
Thr308
Asn361
Ser307
Gly542
Val344
Tyr514
Phe417
Tyr541
Thr497
Gly306
Tyr540
Thr414
Ala498
Tyr419
Tyr511
Lys499
Glu304
Tyr507
f
Pro81
Phe90
Val82
Lys84
Phe83
Leu88
Gly85
Ser86
His151
Leu153
Ser110
Gln109
Gln195
Ala43
Thr247
Phe42
Asp218
His216
Lys213
Thr214
Arg198
g
Gly531
Ala530
Val333
Asp332
Tyr532
Lys529
Phe53
Val491
Lys490
Ser349
Gly486
Tyr409
Gly410
Gly293
Glu291
Ser485
Ser294
Tyr407
Gly408
Thr295
Lys484

Figure 2: Docking validation study via the superimposition techniques of the best docked derivatives [(a) D1c against PB2a active site: red; (b) D1a against PBP2a allosteric site: blue; (c) D1a against PBP2x active site: blue; (d) D1c against PBP2x allosteric site: red; (e) D1c (red) and D2c (green) against PBP3 of *E. coli*; (f) D1h against PBP5 of *E. coli*: cyan; (g) D1c against PBP3 of *P. aeruginosa*: [cyan] and silicristin (black) on native inhibitors (yellow) of each PBPs [PBP2a (3ZFZ) of *S. aureus*, PBP2x (1QMF) of *S. pneumoniae*, PBP 3 (6VJE) of *P. aeruginosa* and PBP 3 (6I1I) and 5 (1Z6F) of *E. coli*]

2.4. Pharmacokinetic and toxicity prediction of derivatives

Utilizing the SMILES of the molecules, the SwissADME online resource (http://swissadme.ch/index.php) was used to compute the pharmacological physicochemical, and drug-like properties of the 25 newly designed derivatives. The predictions were then confirmed with the Molinspiration toolbox (https://www.molinspiration.com/cgi-bin/properties) (Filimonov *et al.*, 2014). Conversely, the toxicity features of the derivatives were predicted using the Protox II website (https://tox-new.charite.de/protox_II/). The cheminformatics data from this investigation alongside the docking scores was utilized in screening top-ranked derivatives against each of the essential PBPs.

2.5. Molecular dynamic (MD) simulations and post simulation analysis of top ranked derivatives

A 120-ns MD simulation of each of the top-ranked derivatives, silicristin and apo-PBPs, was carried out using the AMBER 18 program of the in-house module domiciled at CHPC (Centre for High Performance Computing), Cape Town, South Africa. The operating systems were described using the FF18SB variant of the AMBER force field (Hospital *et al*., 2015). The ANTECHAMBER was utilized to generate the atomic partial charges of the ligands utilizing

the General Amber Force Field (GAFF) and Restrained Electrostatic Potential (RESP) techniques. The AMBER LEaP module, which by default assists in determining and assigning the proper protonation states for each amino acid residue using Na^+, hydrogen atoms, and Cl^- counter ions, was used. The numbering of residues for each PBPs (PBP2x of *S. pneumoniae*: 1 – 650, PBP3 of *E. coli*: 1 – 430; PBP5 of *E. coli*: 1 – 325, PBP3 of *P. aeruginosa*: 1 – 500, PBP2a of *S. aureus*: 1 – 600) was carried out, and the systems were dipped in a rhombic box of TIP3P water atoms so that any atom could be approximately 8 Å of any box edge. A 500 kcal/mol constraint force was used to achieve the first optimum configuration (2000 steps) for each of the top-ranked derivatives, silicristin and apo-PBPs simulation. After that, 990 steps were minimized indefinitely using the conjugate gradient strategy, and another 990 steps were minimized using the steepest descent technique and conjugate degrees respectively (Hospital *et al*., 2015). The heating was carried out step-by-step for 50 ps, with a constant volume and number of atoms being maintained between 0 and 300 K. The collision frequency in the systems is 1.0 ps, and the potential harmonic constraint of the solutes is 10 kcal/mol. After then, each system was allowed to equilibrate for around 500 ps at a constant operating temperature of 300 K. Each simulation featured the restriction of hydrogen bonds using the SHAKE method, with randomized seeding and a 2-fs step size (equivalent to the isobaric−isothermal ensemble (NPT)) in each system). Additionally, for each simulation, a precise temperature of 300 K and a steady pressure of 1 bar were maintained. The pressure-coupling constant was maintained at 2 ps and the collision frequency at 1.0 ps using a Langevin thermostat (Hospital *et al*., 2015). Subsequently, the results of the MD simulation were examined and classified as post-dynamic data. The PTRAJ module was used to collect the systems' coordinates and trajectories to perform the post-simulation analysis. Using the CPPTRAJ modules, the following metrics were studied: intramolecular hydrogen bonds, radius of gyration (ROG), solvent accessible surface area (SASA), RMSD and

root means square fluctuation (RMSF). Plots of these metrics were generated using Origin v 6.0 (Microcal TM Origin R, Northampton, PA, USA). In a similar vein, the binding free energy (ΔGbind) was ascertained by applying the Molecular Mechanics/GB Surface Area (MMGBSA) approach (Ylilauri and Pentikäinen, 2013) to an average of 120,000 snapshots taken from a 120 ns MD simulation trajectory

$\Delta G_{bind} = G_{complex} - (G_{receptor} + G_{ligand)}$ ……. 1

$\Delta G_{bind} = -TS + (G_{sol} + E_{gas})$ …….. 2

$E_{ele +} E_{int} + E_{vdw} = E_{gas}$ …….. 3

$-(G_{GB} - G_{SA}) = G_{sol}$ …… 4

$\gamma SASA = G_{SA}$ ……. 5

solvation-free energy from polar state (G_{sol}), temperature (T), the gas-phase energy (Egas), the internal energy (E_{int}), coulomb energy (E_{ele}), total entropy (S), the van der Waals energy (E_{vdw}), and solvation−free energy from polar state non−polar states (G_{GB})

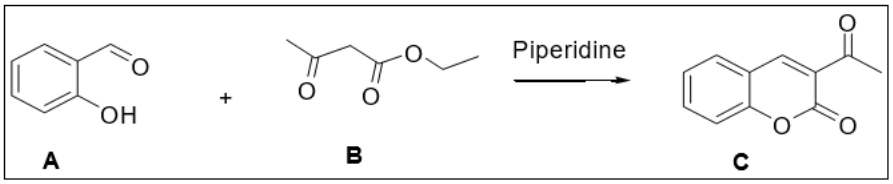
The interaction plots of the top-ranked derivatives and silicristin against each of the PBPs, were visualized and analysed with Discovery Studio v21.1.0 (Dassault Systtemes Biovia Corp, San Diego, CA, USA).

2.6 Optimalization of the parent structures of the best derivatives

Using the variation of the ring size/content approach (Ertl *et al*., 2022), the parent structure of best derivatives was further optimized by evaluating the likelihood of improving the binding of key PBPs following reduction of the oxidized chalcone bis-coumarins. In doing this, the oxygen molecules in the parent structure of the best derivatives were substituted for double bond and further molecular docking and MMGBSA energy refinement were carried out.

2.7 Synthesis of the parent structure of the best chalcone bis-coumarins derivatives

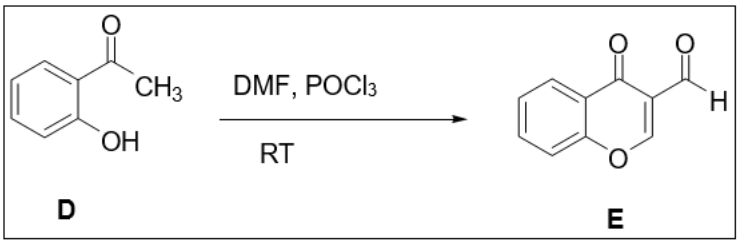
To explore the synthetic route of the derivatives, the parent structure of the best derivatives (the derivative from the top-ranked of each PBPs with the highest negative binding free energy) was synthesized in the laboratory starting from the synthesis of acetyl coumarin (Scheme 2) using the Knoevenagel condensation reaction (Verdía *et al*., 2011). Briefly, in a 125 mL Erlenmeyer flask immersed in an ice bath, 2.0 mL of salicylaldehyde and 3 mL of acetoacetate were added. Afterwards, 5 drops of piperidine were carefully added while swirling for 10-15 minutes. Thereafter the flask was removed from the ice bath and neutralized with 5 drops of 1M HCl. The progress of the reaction was monitored by thin layer chromatography (TLC) using aluminum plates with silica gel (Sigma-Aldrich). The orange / yellow solid was collected using suction filtration and the slightly wet crude product was recrystallized using 95% ethanol. The product was further dissolved in hot ethanol while water dropwise was added to reach the cloud. Following crystallization, the product was filtered and dried.



Scheme 2: Synthesis of acetyl coumarin via Knoevenagel condensation. A: salicylaldehyde, B: acetoacetate, C: acetyl coumarin

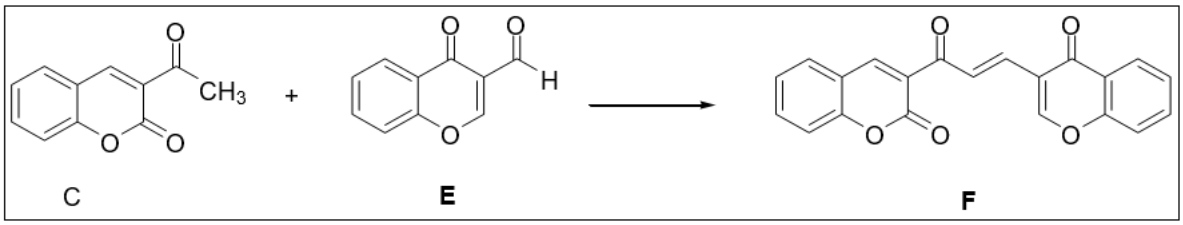
The synthesis of formyl coumarin (Scheme 3) was carried out using the Vilsmeiers Haack reaction (Jing *et al*., 2022). Succinctly, after careful addition of $POCl_3$ (34 mL) into DMF (28 mL) was done drop wisely at interval in an ice bath, 8.42 g of 2- hydroxyacetophenone was added slowly and the mixture was allowed to stir overnight on an oil bath at room temperature. Afterward, a yellowish precipitate was obtained after precipitation in ice. Unprecipitated samples were extracted with chloroform and transferred into a rotary vapour to remove excess

solvent. The existence of the product was monitored by TLC after filtration and drying. The spots on the TLC plates were visualized in the U.V. lamp. The crude product was further purified by column chromatography using silica gel as the stationary phase and an eluting solvent system of petroleum ether and ethyl acetate (8:2).



Scheme 3: Synthesis of formyl coumarin via Vilsmeiers Haack reaction. D: 2-hydroxyacetophenone, E: formyl coumarin

Hybridization of acetyl coumarin (1 mmol) and formyl coumarin (1 mmoL) into chalcone bis-coumarin (Scheme 4) was carried out via the Aldol condensation reaction (Perrin *et al*., 2016). Briefly, 0.188 g of acetyl coumarin and 0.174 g formyl coumarin were measured and transferred into a 50 mL flask. Thereafter, adding of 0.1 g tert butylate potassium and 20 mL of 1,4, Dioxane into the flask was done and the mixture was allowed to reflux for 24 h at 100 ^{o}C and 900 stirs/min. On completion of the reaction, a reddish precipitate was obtained after precipitation in ice containing HCL and the purity of the product was monitored by TLC after filtration and drying. The spots on the TLC plates were visualized in the U.V. lamp. Unprecipitated samples were extracted using ethyl acetate and excess solvent was removed by distillation. The crude product was further purified by column chromatography using silica gel as the stationary phase and an eluting solvent system of hexane and ethyl acetate (8:2).



Scheme 4: Synthesis of chalcone bis-coumarin via Aldol condensation reaction. C : acetyl coumarin, E : formyl coumarin, F : chalcone bis-coumarin. Reaction condition (Catalyst : Tert butylate potassium (0.1 g), solvent : 1,4 dioxane, solvent quantity : 20mL, temperature: 100 ^{o}C, duration: 24 h)

2.8. NMR Characterization techniques

The NMR spectra were recorded with a BRUKER 400 or 600 MHz spectrometer using the internal standard tetramethylsilane (TMS). The chemical shift values were recorded on δ scale, and the coupling constants (J) were reported in Hertz. A Time-of-flight mass spectrometry (TOF-MS) analyzer was used for mass measurement (Al-Majedy *et al*., 2014). Spectra were interpreted by noting that chemical shifts are in their appropriate range for the assigned protons' local magnetic environment, that the peaks exhibit the appropriate multiplicity and appropriate integral value

2.9 Quantum chemical calculations and nuclear magnetic resonance

This analysis was done to predict the molecular properties of silicristin and the best derivatives. Due to the low cost and efficacy of density functional theory (DFT), the methodology is the most preferred and widely used for molecular properties prediction (Ayers *et al*., 2006). In this study, the most common DFT/B3LYP/631G/+ (d,p) basis set (Ayers *et al*., 2006) was used to optimise and performed the frequency and nuclear magnetic resonance of the investigated ligands using the Gaussian 16 program package of the Centre for High Performance Computing and the result was viewed using GaussView 6 software V. 6.0.16 (Gaussian, Inc. Wallingford, CT, USA). The NMR calculation was carried out with the gauge independent atomic orbital (GIAO) method. NMR output gives the chemical shifts for all the represented atoms in the

compounds to enable correlation with experimental results. For every investigated ligand, internal electronic energy, enthalpy, Gibb's free energy and dipole moment were calculated. Following calculation of the frontier molecular orbital using the DFT/B3LYP/631G/+ (d,p) basis set, hardness (η) and softness of all compounds were subsequently calculated from the energies of frontier HOMOs and LUMOs considering Parr and Pearson interpretation (Aihara,1999, Pearson, 1995) of DFT and Koopmans theorem (Luo *et al*., 2006; Pearson, 1986) on the correlation of ionization potential (I) and electron affinities (E) with HOMO and LUMO energy (ε). The following equations are used for the calculation of hardness (η) and softness (S):

Energy gap (ΔE) [E_LUMO − E_HOMO] (eV)

Ionization energy (I) [$I = -$ E_HOMO] (eV)

Electron affinity (A) [$A =-$E_LUMO)

Hardness (η) [$\eta = (I - A)/2$] (eV)

Softness (S) [$S = 1/\eta$] (eV)

Electronegativity (χ) [$\chi = (I + A)/2$] (eV)

Chemical potential (μ) [$\mu = -\chi = -(I + A)/2$] (eV)

Electrophilicity index (ω) [$\omega = \mu^2/2\,\eta$] (eV)

3.0 *Results and discussion*

3.1 Evaluation of novelty of the 25 designed derivatives

The similarity search of the 25 designed derivatives on "Search ChEMBL database" tools present on Galaxy Europe (https://usegalaxy.eu./# accessed 19 Feb, 2022) (Bajorath, 2001) return zero match even at about 40 "Tanimoto cutoff score" which is the minimum value for similarity search on the tools. ChEMBL is a database that contained over 2.3 million distinct compounds (Tanwar *et al.*, 2022). The observation of zero hit following screening of the derivatives through ChEMBL might be suggestive of the uniqueness of the 25 newly designed derivatives of the chalcone bis-coumarin. However, when similarity search was done for silicristin, about 349 hits were found, pointing to the observation that different metabolites like silicristin or with moieties similar to silicristin exist in nature and have been profiled and deposited in appropriate databases. Further confirmation search on ZincPharmer, a database with over 176 million conformers of 18.3 million distinct compounds (Koes and Camacho, 2012) also highlighted the uniqueness of the 25 derivatives, as searching of the derivatives using ligand-based pharmacophore resulted in zero hit of conformers at 50 % and 100 % refining (Supplementary Figure S3). Silicristin on the other hand, had 170 hits at 50% refining (Supplementary Figure S4) suggesting that similar moieties of silicristin are on ZincPharmer, further lending credence to the novelty of the derivatives.

3.2 Molecular docking and pharmacokinetic screening of the derivatives

Molecular docking is a preliminary computational approach that helps to screen compounds based on their fitness, orientation, and interactions at the active site of a receptor (Cerón-Carrasco, 2022). A higher negative docking score indicates better fitness and interaction of the ligand at the binding pocket of the receptor. Following molecular docking at the binding pocket of the PBPs (PBP2a of *S. aureus*, PBP3 and 5 of *E. coli*, PBP3 of *P. aeruginosa* and PBP2x of

S. pneumoniae), the higher negative docking score of some of the derivatives at the binding pocket of each of the essential PBPs relative to silicristin (supplementary Table S2) means their better fitness for the sites and thus highlights the varying capacities of the derivatives. Against PBP2a of *S. aureus* (RMSD: 3 Å), PBP2x of *S. pneumoniae* (2.9 Å) and PBP3 of *P. aeruginosa* (3 Å), docking validation of the best derivatives (derivative with the highest negative docking score) and silicristin showed partial binding orientation as the native inhibitor in each case of the PBPs (Figure 2). However, against PBP3 and 5 of *E. coli* and the allosteric site of PBP2a and PBP2x of *S. aureus* and *S. pneumoniae*, respectively, docking validation showed relatively similar binding orientation as the native inhibitor due to the low RMSD value of < 2.0 Å observed in each case (Figure 2). This observation is consistent with previous study (Ramirex and Caballero, 2016; Fahad *et al*., 2013) where < 2.0 Å and < 3.5 Å RMSD was shown to mean the same binding orientation and partial binding orientation, respectively, and thus lent credence to the docking scores obtained in this study. However, as virtual screening often produces inactive molecules in the preclinical and clinical stages of drug development (Cerón-Carrasco, 2022), the 25 designed derivatives were further subjected to cheminformatics analyses to identify the top-ranked derivatives that will be pharmacokinetically viable and with drug-like properties. Using the Lipinski rule of 5, which serves as a pioneering physicochemical filter, relating the physicochemical parameters of compounds to their pharmacokinetic properties and oral bioavailability (Lipinski *et al*., 2001), the 25 designed derivatives were screened down to nine derivatives (D1a, D1b, D1c, D1f, D1g, D1h, D2a, D2b and D2c) that fulfilled the rule (Supplementary Table S2). The Lipinski rule of 5 limits the molecular weight, hydrogen donor, hydrogen acceptor, and octanol coefficient of a bioactive drug to 500 g/mol, 5, 10, and 5, respectively. As silicristin also fulfilled the Lipinski rule of 5, screening out compounds that do not satisfy the rule is necessary to have compounds that could be use as oral drugs. Interestingly, all the nine identified derivatives are very soluble as

compared to silicristin that is just soluble. Also, the nine derivatives had predicted bioavailability scores and gastrointestinal tract absorption that compared to silicristin. These observations point to the drug-like properties of the derivatives with the identified nine derivatives having a better chance of been transported through the systemic circulation (Verma *et al.*, 2020) compared to silicristin. Except for D1a, the toxicity profiles of the identified nine derivatives suggest that they are non-inhibitors of all the cytochrome P450 (CYP), an important isoenzyme in drug metabolism (supplementary Table S2) (Khumbulani *et al*., 2022). Compared to silicristin, this observation is an improvement on the toxicity profile of the derivatives, thus suggesting their lesser likelihood to result in drug-drug interactions (DDI) when co-administered with phase I- and phase II-dependent drugs. Like silicristin, all the identified nine compounds belong to toxicity class 4 that can be deployed as medications (Lipinski *et al*., 2001; Verma *et al*., 2020). Generally, the designed derivatives shown improvement in solubility and toxicity profile relative to silicristin which might be significant in the later phase of drug development. Derivatives D1a, D1c, D1h, D2a, and D2c among the identified nine derivatives generally had higher broad spectrum docking scores against all the PBPs and thus were selected as the top ranked compounds for further investigation. However, since docking is merely an early reflection of a ligand's suitability in a protein binding pocket (Cerón-Carrasco, 2022), the resulting complexes in each case of the top ranked derivatives against the PBPs with the best fitness were subjected to more rigorous binding energy calculations and MD simulations to assess the effects of the top-ranked derivatives binding to the PBPs relative to silicristin. This was done by monitoring parameters such as the RMSD, RMSF, ROG and SASA over a 120-ns MD simulation evaluation period.

3.3. Binding free energy of the top-ranked derivatives at the binding pocket of the key PBPs of the investigated organisms

Using the molecular mechanics/GB surface area approach, the virtual screening technique was refined by estimating the binding free energy values of the top-ranked derivatives against each of the key PBPs through 120 ns MD simulations (Ylilauri and Pentikäinen, 2013). Of the several energy components contributing to the total binding free energy, the E_{gas} contributed most to the total binding free energy observed for all the complexes studied (Table 1). Against PBP3 of *E. coli,* D1a (-34.10 kcal/mol), D2a (-34.12 kcal/mol), and D2c (-43.26 kcal/mol), had higher negative binding free energy values than silicristin (-31.11 kcal/mol), while against PBP5 of the same organism, only D1a (-37.19 kcal/mol) and D2a (-28.11 kcal/mol) had higher negative binding free energy, with D2c and D1c competing favourably with silicristin (Table 1). Compared to silicristin, the higher binding free energy of D1a, D2a, and D2c as well as D1a and D2a against PBP3 and PBP5 of *E. coli,* respectively, points to the improved optimization of the derivatives as putative inhibitors of PBP3 and PBP5 of *E. coli*. However, against PBP3 of *P. aeruginosa,* only D1c (-37.14 kcal/mol) of the top-ranked derivatives had higher negative binding free energy than silicristin with D2c and D1a having comparable values (Table 1). This observation shows that the structural alteration of silicristin led to optimisation in only D1c and the higher docking scores observed for the other top-ranked derivatives relative to silicristin could be false positive predictions. This observation is in line with prior findings (Aribisala and Sabiu, 2022; Aribisala *et al.*, 2023) and the report of Cerón-Carrasco (2022) where MMGBA energy refinement approach helps in the efficient prediction of active biomolecules. Similar observation is also noted against PBP2x of *S. pneumoniae*, with only D1c (-40.88 kcal/mol) and D1h (-50.09 kcal/mol) having higher negative binding free energy than silicristin at the active (-38.41 kcal/mol) and allosteric site (-50.54 kcal/mol) respectively after energy refinement (Table 1). Against PBP2a of *S. aureus* on the other hand, 3 (D2c, D1h and D1a) and 2(D2a and D1h) of the top-ranked derivatives had higher negative binding free energy than silicristin at the active and allosteric site respectively (Table 1), suggesting their improved

potency as inhibitors of PBP2a relative to silicristin. The observation that at least one of the top-ranked derivatives had higher negative binding free energy than silicristin against each of the investigated PBPs after energy refinement pinpoint the efficiency of the optimization techniques employed in this study. This observation is consistent with the study of Taha *et al*. (2017), where lead optimisation of tertiary amine led to series of novel tetrahydroisoquinoline histone deacetylases (HDAC) inhibitors with at least one of the novel derivatives having higher HDAC inhibitory properties. Among the top-ranked derivatives, D2c against PBP3 of *E. coli* and the active site of PBP2a of *S. aureus*, D2a against PBP5 of *E. coli*, D1c against PBP3 of *P. aeruginosa* and the active site of PBP2x of *S. pneumoniae*, D1h against the allosteric site of PBP2x and PBP2a had the highest negative binding free energy values and were selected as best derivatives in each case of the PBPs. Worth noting however is that D1c (*P. aeruginosa* and *S. pneumoniae)* and D2c (*E. coli* and *S. aureus*) had a good broad-spectrum effect against both Gram-positive and Gram-negative organism. On the other hand, D1h had better effect at the allosteric site of PBP2x and PBP2a and this could be suggestive of its potential as a drug candidate that can find utility in combinatory therapy with other conventional beta-lactam antibiotics.

Table 1: Energy components (kcal/mol) of the top-ranked derivative against each of the PBPs of the investigated bacteria

Targets	Ligands	ΔE_{vdW}	ΔE_{elec}	ΔG_{gas}	ΔG_{solv}	ΔG_{bind}
E. coli +	PBP3					
	D1a	-39.83 ± 4.21	-52.85 ± 12.65	-92.69 ± 14.00	61.58 ± 8.25	-34.10 ± 6.82
	D1c	-29.18 ± 5.23	-30.96 ± 11.57	-60.14 ± 13.88	36.96 ± 8.41	-26.18 ± 7.48
	D1h	-28.61 ± 4.41	-32.03 ± 12.01	-60.65 ± 13.92	37.45 ± 8.05	-26.19 ± 6.66
	D2a	-36.64 ± 3.16	-48.75 ± 9.03	-85.39 ± 8.92	53.37 ± 6.57	-34.12 ± 3.90
	D2c	-35.27 ± 3.93	-71.94 ± 11.00	-107.21 ± 10.27	63.94 ± 7.42	-43.26 ± 5.63
	Silicristin	-39.77 ± 3.85	-23.81 ± 6.80	-63.60 ± 7.90	32.49 ± 5.21	-31.11 ± 4.30
	PBP5					
	D1a	-33.56 ± 3.89	-44.42 ± 8.14	-77.99 ± 7.98	40.80 ± 7.28	-37.19 ± 5.98
	D1c	-29.21 ± 6.39	-18.20 ± 11.00	-47.41 ± 14.45	25.89 ± 9.74	-21.51 ± 7.34
	D1h	-15.56 ± 4.33	-7.94 ± 10.27	-23.51 ± 11.45	14.49 ± 9.53	-9.01 ± 3.46
	D2a	-32.01 ± 3.75	-50.35 ± 10.15	-82.36 ± 9.297	54.25 ± 7.19	-28.11 ± 3.81
	D2c	-28.07 ± 3.45	-34.67 ± 14.34	-62.74 ± 14.93	39.76 ± 12.24	-22.97 ± 4.89
	Silicristin	-26.61 ± 9.69	-19.66 ± 10.49	-46.30 ± 16.51	24.13 ± 10.29	-22.16 ± 9.40
P. aeruginosa PBP3 +	D1a	-36.41 ± 4.29	-25.02 ± 9.69	-61.44 ± 11.89	39.42 ± 9.02	-22.02 ± 4.65
	D1c	-43.83 ± 3.56	-44.46 ± 3.56	56.46 ± 9.59	-88.29 ± 8.78	-37.14 ± 4.04
	D1h	-32.94 ± 5.61	-15.04 ± 10.88	-47.99 ± 13.15	29.64 ± 10.71	-18.34 ± 4.70
	D2a	-38.89 ± 5.58	-15.37 ± 9.53	-54.27 ± 10.71	37.81 ± 7.66	-16.45 ± 5.12
	D2c	-42.01 ± 3.39	-22.37 ± 7.28	-64.38 ± 7.84	41.58 ± 6.95	-22.80 ± 4.70
	Silicristin	-34.63 ± 4.72	-16.57 ± 8.68	-51.22 ± 9.57	27.55 ± 5.72	-23.66 ± 5.32
S. pneumoniae PBP2x +	Active site					
	D1a	-39.84 ± 7.34	-21.15 ± 10.48	-60.99 ± 8.98	35.44 ± 6.84	-30.54 ± 3.80
	D1c	-35.93 ± 3.93	-51.56 ± 25.58	-87.49 ± 24.92	51.61 ± 16.56	-40.88 ± 8.96
	D1h	-44.74 ± 6.70	-19.42 ± 9.99	-64.17 ± 11.56	34.50 ± 7.12	-34.66 ± 6.33
	D2a	-41.84 ± 4.92	-17.00 ± 10.51	-58.84 ± 13.60	29.16 ± 7.64	-34.67 ± 6.85
	D2c	-39.93 ± 3.01	-8.94 ± 9.72	-48.87 ± 10.13	20.14 ± 9.32	-33.72 ± 3.10
	Silicristin	-46.96 ± 4.46	-41.91 ± 9.87	-88.90 ± 9.57	50.48 ± 7.77	-38.41 ± 6.07
	Allosteric site					
	D1a	-49.42 ± 3.82	-27.40 ± 10.82	-76.83 ± 9.23	45.64 ± 7.67	-48.72 ± 4.29
	D1c	-42.02 ± 3.86	-25.15 ± 7.27	-67.18 ± 8.26	46.59 ± 5.95	-38.13 ± 4.60
	D1h	-23.79 ± 5.00	-75.67 ± 19.57	-99.47 ± 17.18	63.92 ± 12.74	-53.09 ± 19.57
	D2a	-40.79 ± 5.54	-28.74 ± 13.56	-69.54 ± 11.80	38.00 ± 8.40	-49.08 ± 5.93

	D2c	-41.89 ± 5.00	-26.47 ± 15.09	-68.36 ± 14.53	40.18 ± 10.09	-45.72 ± 5.75
	Silicristin	-55.40 ± 3.44	-32.14 ± 11.31	-87.55 ± 10.47	37.01 ± 7.39	-50.54 ± 4.88
	Active site					
S. aureus	D1a	-29.23 ± 5.39	-35.80 ± 12.91	-65.03 ± 14.55	43.02 ± 10.18	-33.00 ± 7.26
	D1c	-17.73 ± 5.71	-26.61 ± 16.17	-44.35 ± 17.65	32.01 ± 13.53	-23.23 ± 5.19
PBP2a +	D1h	-26.97 ± 5.46	-44.40 ± 21.24	-71.37 ± 19.30	53.45 ± 7.85	-28.81 ± 7.85
	D2a	-15.98 ± 6.78	-19.73 ± 15.36	-35.72 ± 19.68	23.84 ± 13.86	-22.77 ± 6.55
	D2c	-25.98 ± 6.43	-44.16 ± 10.64	-70.14 ± 10.74	52.25 ± 8.37	-28.79 ± 5.51
	Silicristin	-35.15 ± 8.08	-32.24 ± 12.41	-67.42 ± 15.90	41.80 ± 10.24	-25.61 ± 7.08
	Allosteric site					
	D1a	-40.65 ± 3.64	-69.81 ± 12.49	-110.46 ± 12.43	79.00 ± 9.64	-31.46 ± 4.73
	D1c	-39.40 ± 6.25	-34.69 ± 12.26	-74.10 ± 13.87	41.80 ± 9.00	-32.29 ± 7.21
	D1h	-45.34 ± 3.67	-39.19 ± 9.62	-84.54 ± 9.89	46.00 ± 7.14	-38.53 ± 4.67
	D2a	-35.42 ± 3.79	-71.53 ± 22.02	-106.95 ± 21.67	72.63 ± 11.46	-34.32 ± 11.56
	D2c	-26.26 ± 6.73	-83.44 ± 33.93	-109.71 ± 31.46	77.82 ± 22.44	-31.88 ± 10.47
	Silicristin	-40.15 ± 4.63	-44.11 ± 15.24	-84.28 ± 14.98	50.70 ± 11.36	-33.57 ± 5.38

Abbreviations: ΔG_{solv} = solvation free energy, ΔE_{gas} = gas phase free energy; ΔE_{elec} = electrostatic energy; ΔG_{bind} = total binding free energy; and ΔE_{vdW} = van der Waals energy

3.4. Thermodynamic stability, flexibility, and compactness of the top-ranked derivatives at the binding pocket of the key PBPs of the investigated organisms

The thermodynamic stability, flexibility, and compactness of the top-ranked derivatives at the binding pocket of each of the key PBP of the investigated organisms were analysed by evaluating the RMSD, RMSF and ROG. The RMSD, is a metric of stability derived from the time-dependent deviation of a complex from its apo-protein during a simulation and can help evaluate the stability of complexes formed by the top-ranked derivatives with investigated key PBPs (Uhomoibhi *et al*., 2022). The smaller the RMSD value the better the stability (Ramirex and Caballero, 2016). Root means square fluctuation on the other had helps investigate the mobility of residues of a protein following ligand binding and could aid the evaluation of the strength of inter- and intramolecular bonds following top-ranked derivatives binding of the investigated PBPs (Aribisala and Sabiu, 2022). The compactness of the complex formed by the top-ranked derivatives with key PBPs was estimated by the ROG and SASA. Smaller ROG and SASA values could encourage stability due to the better confinement of the ligand in the protein (Murali *et al.*, 2023).

Against PBP3 of *E. coli,* the equilibration at 10 ns and convergence of the systems at 65 ns during the 120 ns MD simulation denote the efficiency and accuracy of the simulation, suggesting its reproducibility (Matteo *et al.*, 2021). Following equilibration, silicristin+PBP3 and apo-PBP3 had a sudden rise in RMSD at 20 ns and 40 ns respectively (Figure 3a) and was maintained throughout the simulation. This observation denotes lesser structural stability in silicristin+PBP3 and apo-PBP3 systems during the simulations. The top-ranked derivatives on the other hand maintained a stable fluctuation after equilibration and consequently all the top-ranked derivatives had lesser average RMSD compared to silicristin+PBP3 and apo-PBP3 (Supplementary Table S3). This observation suggests the improved structural stability in PBP3

of *E. coli* following the binding of the top ranked. This observation is a plus to D1a, D2a and D2c as a potential PBP3 inhibitor due to their higher binding free energy than silicristin. The ROG on the other hand suggests improved compactness in silicristin+PBP3 and apo-PBP3 systems relative to the top-ranked derivatives complexes with PBP3 (Figure 3b). Like the RMSD, a stable fluctuation in the top-ranked derivatives complexes with PBP3 was observed throughout the simulation and might mean they do not instigate thermodynamic disorderliness. However, the dissociation of compactness from stability in silicristin+PBP3 and apo-PBP3 agrees with our previous study (Aribisala and Sabiu, 2022) and might have been due to the different parameters relating to the protein and the ligands that could influence ROG (Baig *et al*., 2014; Lobanov *et al*, 2008). The RMSF shows that the active site residues such as Asn361, Lys358, Lys310, Glu304, Ser359 were not at the zone of higher residues fluctuations between 1 and 50 (Figure 3c), suggesting their active intra and intermolecular activities. Interestingly, except for D1a, all the top-ranked derivatives had lesser RMSF values than silicristin+PBP3 (1.44 Å) and apo-PBP3 (1.51 Å), an observation which suggest lesser flexibility of the residues of PBP3 following binding of the top-ranked derivatives. This finding is in correlation with the RMSD and binding free energy of this study and thus further attest to the improved binding efficiency of the top-ranked derivative against PBP3 of *E. coli* relative to silicristin. Like the ROG, a stable fluctuation in the SASA plots of the top-ranked derivative with PBP3 was observed throughout the simulation suggesting thermodynamic orderliness in the top-ranked derivative complexes with PBP3 (Figure 3d). Unlike the ROG, silicristin+PBP3 (18051 Å) had higher average SASA value relative to the top-ranked derivatives suggesting the benefits of the derivatives over silicristin as potential inhibitors of PBP3. Overall, the RMSD, RMSF, SASA and binding free energy findings of this study have suggested the enhanced binding efficiency of the top-ranked derivatives and most especially D1a, D2a and D2c against PBP3 of *E. coli* relative to silicristin.

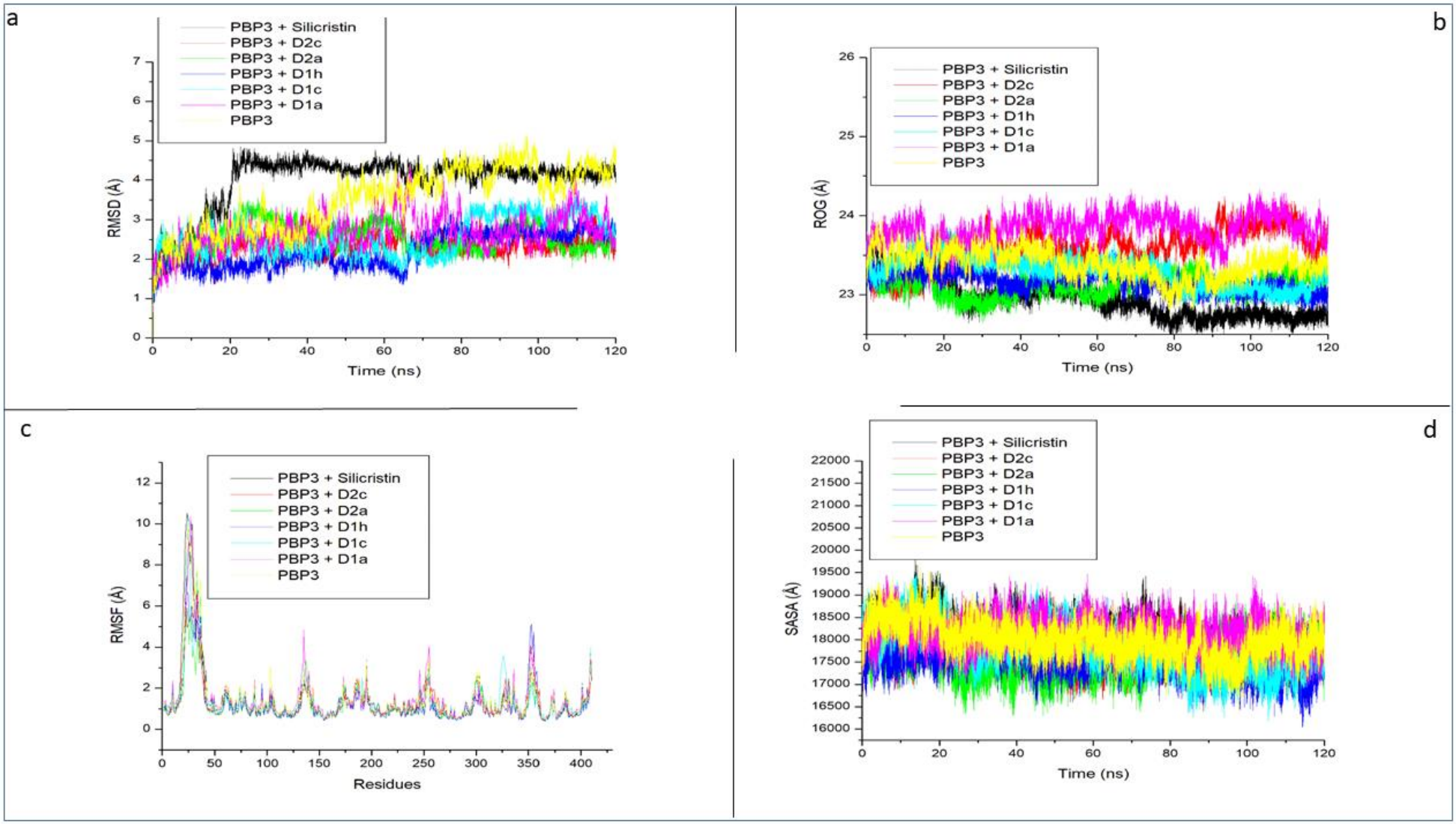


Figure 3: Comparative RMSD (a), ROG (b), RMSF (c) and SASA (d) plots of top-ranked derivatives against PBP3 of *E. coli* after 120 ns of MD simulation

Against PBP5 of *E. coli*, after equilibration at 10 ns and convergence of the RMSD plots at 30 and 60 ns, the systems maintained a stable fluctuation with minor swaying throughout the 120 ns MD simulation (Figure 4a). The equilibration and convergence of the system during the 120 ns MD simulation pinpoint the efficiency of the simulation while the stable fluctuations afterwards suggest structural stability in all the systems investigated. Specifically, except for D1h (3.44 Å) and D2c (3.19 Å), all the top-ranked derivatives had lesser RMSD value compared to silicristin (3.07 Å) against PBP5 of *E. coli* (Supplementary Table S3). This observation means enhance structural stability in the complexes formed with PBP5 by D1a, D1c and D2a and thus their advantage over silicristin as potential inhibitors of PBP5. Moreso, D1a and D2a had higher binding free energy than silicristin hence suggesting the effectiveness of the optimization techniques employed in this study. The ROG plots show varies fluctuations among the systems (Figure 4b). D2a had a sudden drop in ROG after 40 ns and was maintained throughout the simulation. Compared to PBP5+silicristin, lesser ROG values were noted with all the top-ranked derivatives against PBP5 with D2a having the lowest ROG value. This observation suggests increased compactness of PBP5 following binding of the top-ranked derivatives with PBP5+D2a being the most compact. Except for D2c, this observation is consistent with the RMSD findings of this study and thus a further attestation to the improved binding efficiency of PBP5 by the derivatives relative to silicristin. The average RMSF also showed reduce fluctuation of the residues of PBP5 following binding of the derivatives relative to silicristin (Figure 4c) suggesting enhanced intramolecular binding in PBP5. The lesser fluctuations between residues 80 and 200 for all the systems which are the areas that include the active site residues also suggest stronger intermolecular binding. The strong intra and inter-molecular binding in PBP5 following binding of the top-ranked derivatives lent evidence on the improved binding efficiency of the derivatives against PBP5. The SASA plots (Figure 4d) and the average SASA values (Supplementary Table S3) also follow the same trend as the top-

ranked derivatives all had SASA values that were lesser than silicristin against PBP5. In all, the RMSD, RMSF, SASA and binding free energy findings of this study suggest enhanced binding efficiency of the top-ranked derivatives against PBP5 of *E. coli* and most especially D1a, D1h with higher binding free energy compared to silicristin.

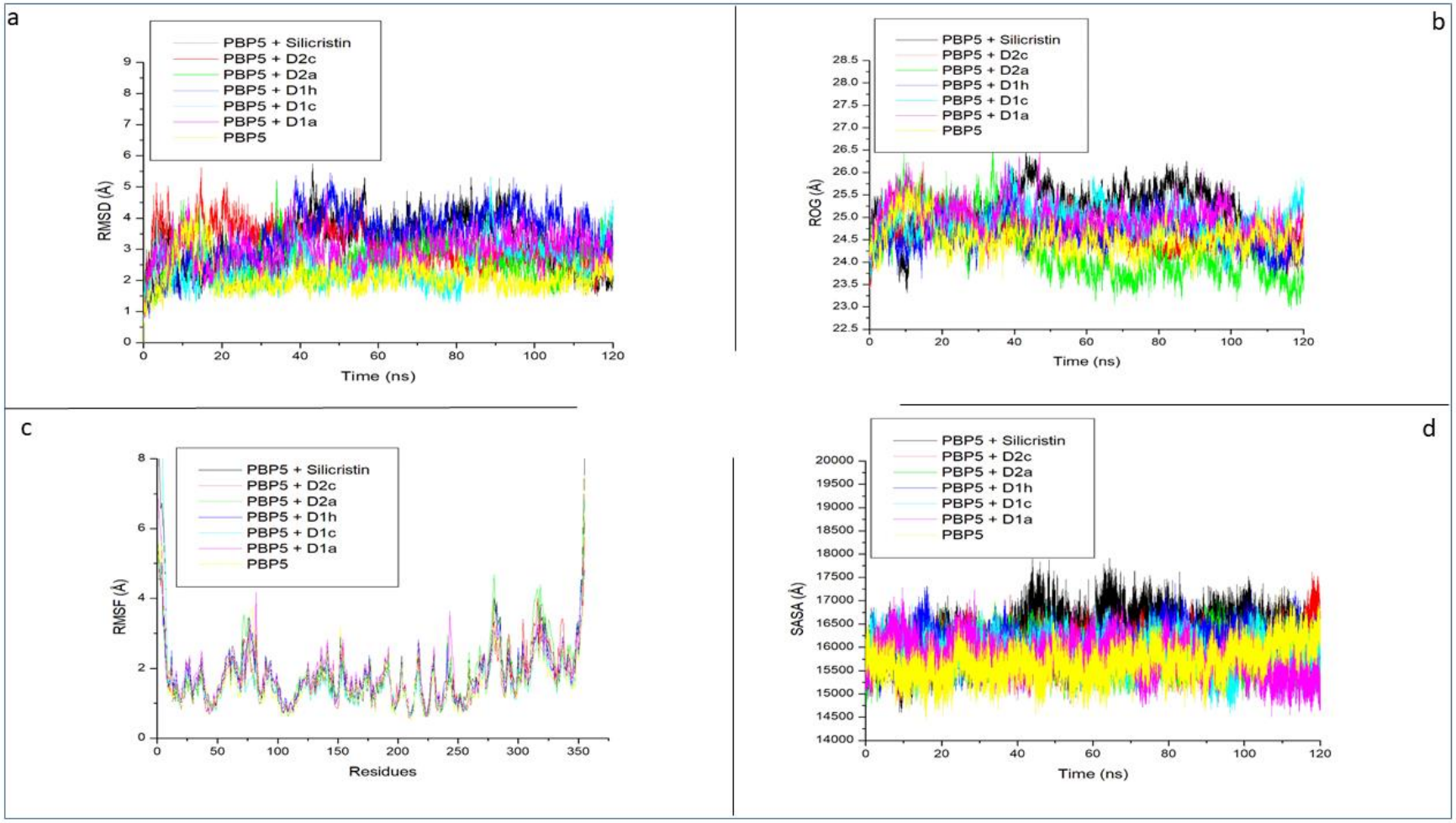


Figure 4: Comparative RMSD (a), ROG (b), RMSF (c) and SASA (d) plot of top-ranked derivatives against PBP5 of *E. coli*

Regarding PBP3 of *P. aeruginosa*, the equilibration of all the system before 10 ns and convergence at 80 ns suggest the suitability of the 120 ns MD simulation employed in this study (Figure 5a). Of the top-ranked derivatives, complexes formed by D1c (2.33 Å) and D2a (2.34 Å) with PBP3 of *P. aeruginosa* had relatively lesser RMSD value than silicristin (2.56 Å) (Supplementary Table S3) suggesting enhanced thermodynamic stability in PBP3 + D1c and PBP3 + D2a complexes. This observation is a plus to the potential of D1c as a promising inhibitor of PBP3 being the only top-ranked derivative with higher binding free energy than silicristin. This observation is consistent with study of Sherif *et al.* (2023) where series of newly designed spirocyclic aminopyrimidines had at least one compound (compound 4) with better stability and affinity against beta-ketoacyl-acp synthase Iii (FabH) of *P. aeruginosa* than the control compound. Other top ranked derivatives and most especially D1h (between 20 ns and 120 ns) caused higher thermodynamic disorderliness in PBP3 relative to silicristin (Figure 5a). The ROG plots show varies fluctuations among the systems (Figure 5b). D1h had a sudden drop in ROG at 80 ns and was maintained throughout the simulation (Figure 5b), thus, compared to PBP3+silicristin (29.89 Å), D1h (29.35 Å) had lesser ROG value. D1a and D2a on the other hand had slightly higher ROG value while D1c and D2c had comparable ROG values as silicristin (Supplementary Table S3). This observation suggests increased structural compactness in PBP3 following binding of D1h relative to silicristin. However, the comparable ROG values of all the bound systems relative to apo-PBP3 means that binding cause no thermodynamic entropy in PBP3 of *P. aeruginosa*. This observation is consistent with previous study where newly designed compound caused no thermodynamic entropy FabH of *P. aeruginosa* (Sherif *et al*., 2023). The RMSF findings of this study on the other had suggest lesser flexibility in PBP3 following binding of all the top ranked derivatives relative to silicristin (1.89 Å) with D1c (1.58 Å) and D2a (1.58 Å) causing the lesser flexibility of the residues (Supplementary Table S3). This observation suggests strong intramolecular binding

in PBP3 following binding of the top-ranked derivative compared to silicristin, with D1c and D2a instigating the stronger intramolecular bond in PBP3. Higher fluctuations were observed in most of the residues between 1 and 290, while in residues between 290 and 500 minor swaying was observed (Figure 5c). Interestingly, the active site residues such as Ser294, Gly486, Ser349, Val491 and Lys490 were all at the region of minor swaying suggesting strong intermolecular binding of the top-ranked derivatives and silicristin during the simulation. The SASA plots (Figure 5d) and the average SASA values (Supplementary Table S3) showed that the top-ranked derivatives all had SASA values that were slightly higher than silicristin against PBP3 of *P. aeruginosa* suggesting minimal increase in surface area following binding of the top-ranked derivatives. This observation is in contrast to other thermodynamic metrics evaluated for PBP3 of *P. aeruginosa*. In all, the RMSD, RMSF and binding free energy findings of this study suggest enhanced binding efficiency of D1c relative to silicristin against PBP3 of *P. aeruginosa*.

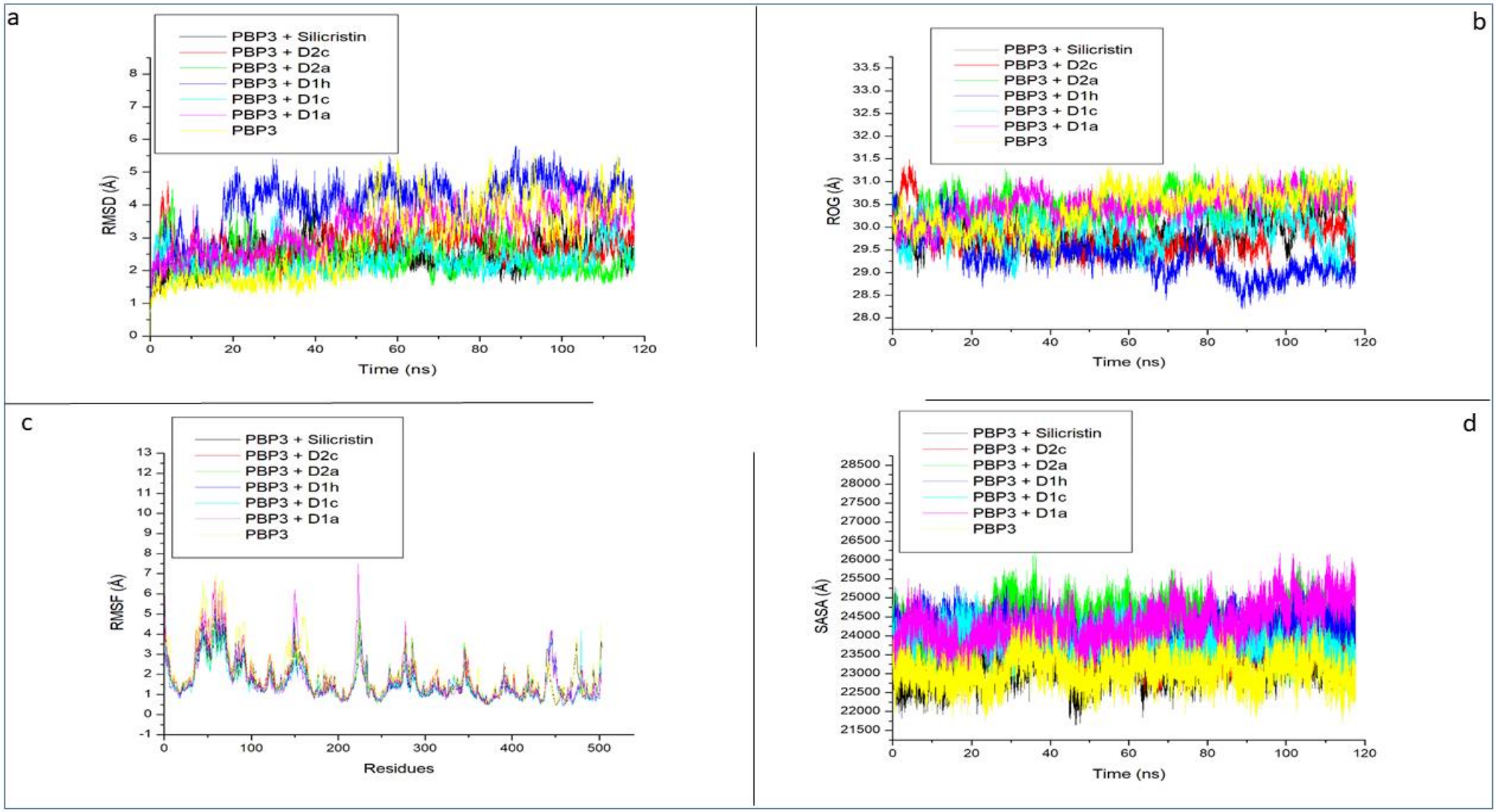


Figure 5: Comparative RMSD (a), ROG (b), RMSF (c) and SASA (d) plot of top-ranked derivatives against PBP3 of *P. aeruginosa*

At the active site of PBP2a of *S. aureus*, like against PBP3 of *E. coli*, had RMSD equilibration at 10 ns and convergences at 60 ns for all the systems specifying efficiency of the 120 ns MD simulation and the possibility of the simulation being reproduce (Matteo *et al*., 2021). The RMSD plots however showed a sudden drop in stability for apo-PBP2a just after equilibration and silicristin+PBP2a after 60 ns (Figure 6a). The complexes formed by PBP2a with the top-ranked derivatives on the other hand enjoyed relatively stable fluctuation with minor swaying throughout the simulation (Figure 6a). Thus, the top-ranked derivatives complexes with PBP2a at the active site had lower average RMSD values relative to silicristin+PBP2a (5.65 Å) and apo-PBP2a (6.86 Å) (Supplementary Table S3) suggesting better structural stability of PBP2a following binding of the derivatives. Relative to silicristin, this observation is an added advantage to D1a, D1h and D2a as a potential inhibitor of PBP2a as they all had higher negative binding free energy than silicristin. The RMSD findings is however distant from the ROG findings of this study where silicristin+PBP2a and apo-PBP2a had sudden drop in ROG stipulating higher compactness at 10 and 60 ns respectively (Figure 6b). Consequently, complexes formed by the top-ranked derivatives all had slightly higher mean ROG values relatives to silicristin+PBP2a (36.47 Å) and apo-PBP2a (35.37 Å) (Supplementary Table S3). This observation is consistent with our earlier report (Aribisala and Sabiu, 2022) where stability of phenolics with PBP2a was withdrawn from complex folding. However, the inconsistency between ROG and RMSD findings has been associated to the different parameters of the protein (protein topology, size, length) and ligand (point of interactions and molecular weight) that affect ROG values (Lobanov *et al*., 2008). The increase in structural stability (lower RMSD) in PBP2a following binding of the top ranked derivatives relative to silicristin is however consistent with the mean RMSF which shows that except for D1c, all the top-ranked derivatives binding of PBP2a caused lower fluctuation of PBP2a amino acid residues compared to silicristin+PBP2a (Figure 6c and Supplementary Table S3). This observation demonstrated strong intramolecular interactions in PBP2a following binding of the top-ranked derivatives

with D2c instigating the strongest intramolecular binding of residues. A look into the fluctuations of the active site's residue such as Ser461, Ala642, Lys406, Tyr446, Asp516, Tyr519 shows that they are all at the region of minimal fluctuation between 300 and 550, suggesting strong intermolecular binding during the simulation. The SASA plots (Figure 6d) shows a stable fluctuation for all the systems during the simulation. Averagely, except for D1a (26364 Å) and D2c (27051 Å) with lesser SASA values relative to silicristin+PBP2a (27160 Å), (Supplementary Table S3) all other top-ranked derivatives caused increased surface area in PBP2a which is also consistent with the ROG result of this study. However, the lesser SASA findings for D1a and D2c relative to silicristin points to their benefits as promising inhibitor of PBP2a and most especially D1a which have the highest negative binding free energy against the active site of the protein. Overall, the RMSD and RMSF findings of this study have points to the enhanced binding efficiency of the top-ranked derivative relative to silicristin. Furthermore, the potential of D1a as a promising inhibitor of PBP2a active site was further highlighted by the SASA findings thus pinpointing D1a as the best derivative for the active site of PBP2a as the derivative also had the highest negative binding free energy. Thus, the identification of derivatives (D1a and D1h and D2c) with enhanced binding efficiency instigating structural stability following binding of PB2a relative to silicristin suggest the efficacy of the optimisation techniques used in this study.

At the allosteric site of PBP2a of *S. aureus,* the RMSD plots equilibrate before 10 ns while full convergences occur at 40 ns and 65 ns (Supplementary Figure S5a). This observation indicates adequacy of the 120 ns MD simulation and the possibility of the simulation being reproduce (Matteo *et al*., 2021). A stable fluctuation with minimal swaying among the systems was noted throughout the simulation. Averagely, D1c (4.52 Å), D2a (5.18 Å), and D2c (4.41 Å) all had higher RMSD values than silicristin (3.48 Å) and the apo-PBP2a (3.66 Å) when bounded at the allosteric site of PBP2a (Supplementary Table S3). This observation may indicate the lower

suitability of D1c, D2a and D2c as a potential inhibitor at the allosteric site of PBP2a compared to silicristin and contrasts with the active site finding, where binding of all derivatives results in increased thermodynamic stability in PBP2a compared to silicristin promotes. However, D1a had comparable RMSD value, while D1h had lesser RMSD value than silicristin at the allosteric site. This observation might mean D1a and D1h encourage improved structural stability when bounded at the allosteric site of PBP2a. More importantly, D1h had higher negative binding free energy than silicristin and thus a plus to the derivative as a promising inhibitor at the allosteric site of PBP2a. Unlike the RMSD, a quick drop in ROG which indicates compactness was noted just before equilibration for D2a at the allosteric site of PBP2a and was retained throughout the simulation (Supplementary Figure S5b). For other systems, a stable fluctuation with minimal swaying was observed all through the simulation. This observation means while D2a encourage folding of PBP2a, other derivatives including silicristin maintained original geometry of PBP2a following binding at the allosteric site. Comparatively, all the top-ranked derivatives had lesser ROG values relative to silicristin and apo-PBP2a following binding at the allosteric site with D2a having the lowest value (Supplementary Table S3). This observation suggests enhanced compactness which might encourage stability following binding of the derivatives and most especially D2a at the allosteric site of PB2a. This observation is unlike the RMSD result where only D1h had better stability than silicristin and might further demonstrate the disagreement that might occur between RMSD and ROG due to the various parameters of the protein and ligand as earlier stated in this study. The RMSF plot at the allosteric site showed a similar pattern to the RMSF plots at the active site as residues before 200 had higher fluctuation while residues just after 200 had minimal swaying. Specifically, the allosteric site residues such as Lys273, Asp275, Tyr297, Arg298 were at the region of minimal swaying while allosteric site residues such as Lys76, Tyr105, Leu147 and Tyr 105 were at the region of higher fluctuation (Supplementary Figure S5c). This observation might suggest loose intermolecular binding of ligands at some

region of the allosteric site while at other part of the allosteric site strong intermolecular binding might have occur. Averagely, except for D2c, all the top-ranked derivatives had lesser RMSF values than silicristin with D2a having the lowest value (Supplementary Table S3). This observation while suggesting improved structural stability in PBP2a following the top-ranked derivative binding of PB2a allosteric site, further highlights the benefit of D2a and D1h as potential allosteric site inhibitor of PBP2a as they were the only derivative with a higher negative binding free energy than silicristin. The SASA plot showed stable fluctuations with minimal swaying for all the systems (Supplementary Figure S5d). This observation could suggest that binding of the derivative and silicristin had little effect on the surface area of PBP2a and thus might mean no disorderliness was caused following binding. More so, as negligible variance of 1239 Å exist between the bounded system and apo-PBP2a (Supplementary Table S3). Specifically, all the top-ranked derivatives had higher SASA values compared to silicristin at the allosteric site of PBP2a suggesting increased in surface area that are available for solvent interaction following binding of PBP2a by the derivatives. Among the derivatives D2a had the least SASA value an observation that is consistent with the RMSF and ROG finding of this study. Overall, D1h seems to be the best inhibitor of PBP2a allosteric site as the derivative had a combined thermodynamic property (higher negative binding free energy, lower RMSD, ROG, and RMSF) that suggest enhanced binding efficiency at the allosteric site of PBP2a relative to silicristin.

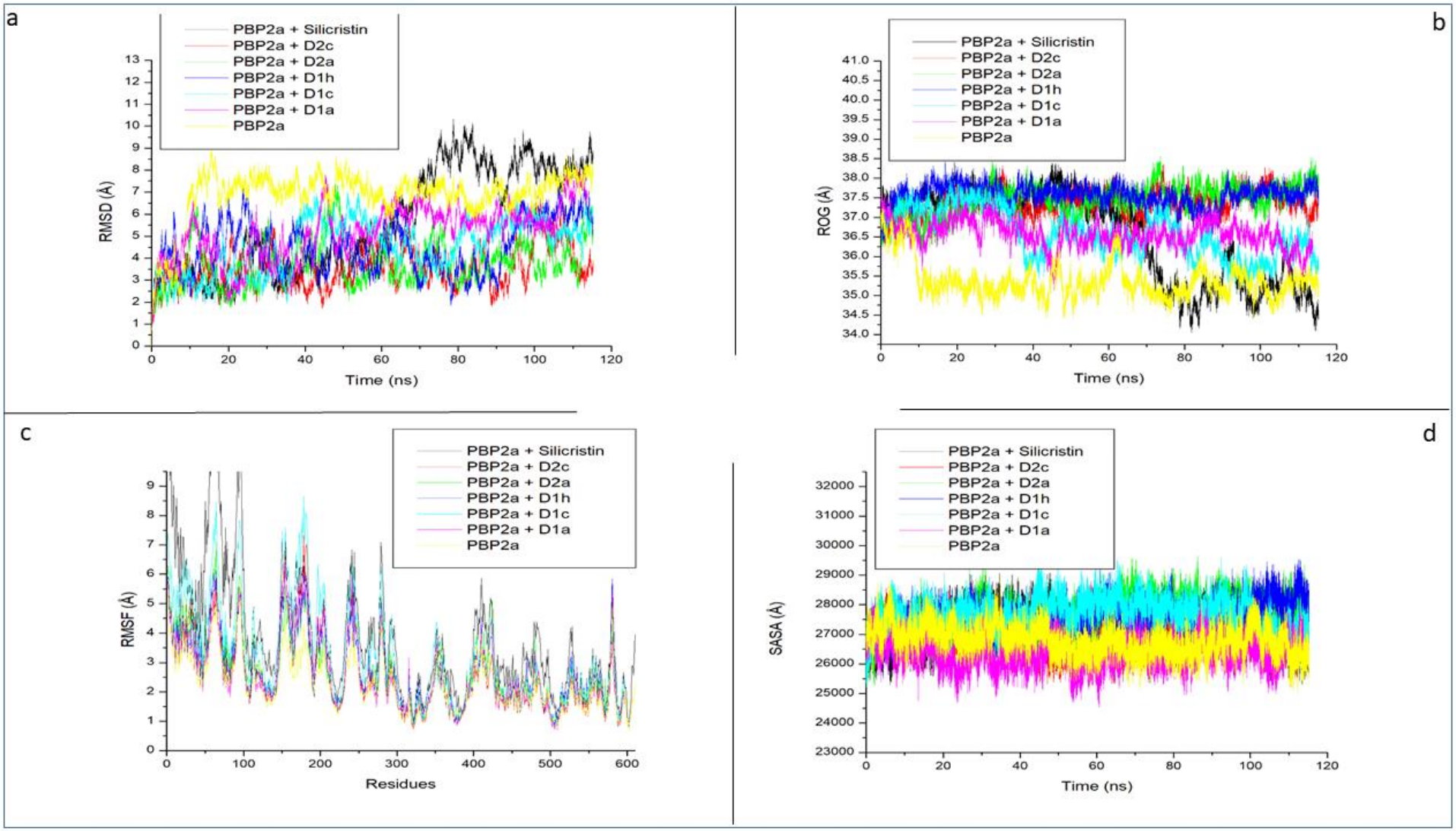


Figure 6: Comparative RMSD (a), ROG (b), RMSF (c) and SASA (d) plot of top-ranked derivatives against the active site of PBP2a of *S. aureus*

At the active site of PBP2x of *S. pneumoniae,* equilibration at 10 ns, partial convergences at 50 ns and 65 ns were observed for all the system (Figure 7a) which specified efficiency and reproducibility of the 120 ns MD simulation. A sudden drop in stability was observed with apo-PBP2x and D1c-PBP2x just after 10 ns and was maintained with minor swaying throughout the simulation (Figure 7a). On the other hand, silicristin-PBP2x and D1h-PBP2x maintained stable fluctuation till 70 ns before a sudden increase in RMSD which was maintained all through the simulation (Figure 7a). This observation means thermodynamic stability at the region of stable fluctuations and means otherwise at the region of sudden increase in RMSD (Lanrewaju *et al*., 2023). Other investigated systems (D1a-PBP2x, D2a-PBP2x and D2c-PBP2x) maintained stable fluctuations throughout the simulation, consequently D1a-PBP2x (3.41 Å), D2a-PBP2x (2.95 Å) and D2c-PBP2x (3.13 Å) all had lesser RMSD value relative apo-PBP2x (6.32 Å) and silicristin-PBP2x (4.90 Å) with D2a-PBP2x having the lowest values (Supplementary Table S3). The lesser RMSD value of D1a-PBP2x, D2a-PBP2x and D2c-PBP2x relative to silicristin-PBP2x in this study suggest improved binding efficiency of D1a, D2a and D2c against PBP2x of *S. pneumoniae*. Similarly, the ROG plots (Figure 7b) suggest increased folding and compactness of PBP2x following binding of all the derivatives relative to apo-PBP2x and silicristin-PBP2x with D2a-PBP2x instigating the highest compactness of PBP2x. The observation that D2a caused the highest compactness in PBP2x is consistent with the RMSD result of this study and thus an indication of its potential as promising PBP2x inhibitor. Following the same pattern is the average RMSF values of all the derivatives (Supplementary Table S3 and Figure 7c) against PBP2x which were lesser than silicristin-PBP2x (2.62 Å) with D2a-PBP2x (1.79 Å) and D1a-PBP2x (1.72 Å) having the lowest values. This observation is an indication of the strong intramolecular interaction in PBP2x following the binding of the derivatives suggesting their better thermodynamic compatibility with PBP2x relative to silicristin. Higher amino acid fluctuations

between residues 1 and 100 during the simulation suggest lesser intramolecular binding at the region of the protein (Figure 7c). Interestingly the active site residues such as Lys547, Lys340, Ser548, Thr526, Thr338, Ser395, Phe 450, Ser396, Asp397 were at the region of lesser fluctuation (Figure 7c) suggesting the possibility of strong intra and intermolecular binding during the simulation. The SASA plots showed stable fluctuations for all the systems during the simulation with minor swaying (Figure 7d). Compared to silicristin, except for D2c (28939 Å), all the derivatives had lesser average SASA values relative to silicristin (28080 Å) against PBP2x. This observation while suggesting enhanced thermodynamic compactness following binding of the derivative, is also consistent with the ROG and RMSF findings of this study. The thermodynamic stability of the derivatives against PBP2x as demonstrated by the RMSD, ROG, RMSF and SASA in this study is consistent with previous work where newly designed drug candidate against NDM-1 an enzyme associated with resistant to a broad range of beta-lactam antibiotic showed enhanced thermodynamic stability (Salih and Ali, 2023). Overall, the ROG, RMSF and SASA findings of this study have highlighted the benefits of the derivatives and most especially D1c (being the only derivative with a higher binding free energy than silicristin) as promising inhibitors of PBP2x.

At the allosteric site of PBP2x, stable fluctuation for all the system was observed throughout the simulation with equilibration of the system occurring at 10 ns and full convergence happening at 40ns (Supplementary Figure S 6a). This observation might suggest the efficiency of the 120 ns MD simulation and the relative stability of all the systems during the simulation. Comparatively, except for D2c-PBP2x (4.72 Å), the top-ranked derivatives had lower RMSD values relative to silicristin-PBP2x (4.36 Å) and apo-PBP2x (4.36) at the allosteric site of PBP2x with D1a-PBP2x having the lowest RMSD values (Supplementary Table S3). This observation might suggest the enhanced binding efficiency of the top-ranked derivatives at the allosteric site of PBP2x relative to silicristin with D1a being the most promising of the

derivatives. This observation is in contrast with the binding free energy findings of this study where only D1h had better affinity than silicristin and thus an added advantage to the potential of D1h as inhibitor of PBP2x allosteric site. Similar observation is also noted with the ROG plots (Supplementary Figure S 6b) as all the derivatives against PBP2x all had enhanced compactness depicted by their lower ROG values relative to silicristin-PBP2x (29.03 Å) and apo-PBP2x (28.74 Å). Although D2a had the lowest ROG values among the derivatives, the lower ROG values observed for D1h (the only derivative with higher binding free energy than silicristin) relative to silicristin also further pinpoint the benefits of the D1h as inhibitor of PBP2x allosteric site. The RMSF plots (Supplementary Figure S6c) depict higher fluctuations in residues between 1 and 150 and in other regions, a relatively lower fluctuation was observed. The relatively lower fluctuation of the active site amino acid residues generally found between residues 416 and 550 suggest strong intermolecular binding of the derivatives and silicristin during the simulation an observation which is consistent with the RMSD and ROG findings of this study. Relatively, all the derivatives had higher average RMSF values compared to silicristin against PBP2x (Supplementary Table S3). This observation might mean that the binding of the derivatives caused higher fluctuations of residues of PBP2x relative to silicristin-PBP2x and thus could suggest lesser intra and intermolecular binding in the complexes of the derivatives with PBP2x. This finding while been consistent with the binding free energy observed in this study where silicristin had higher negative binding free energy than most of the derivative (except D1h), is in contrast with the RMSD and ROG result. However, the observation that the RMSF values were all lesser than the 3Å limit (Ramirex and Caballero, 2016) suggest that the residues fluctuations in PBP2x following the derivatives bindings are suitable for ligand binding and protein inactivation. Among the derivatives D1h caused the least fluctuations of amino acids in PBP2x, further suggesting the potential of the derivatives as inhibitor of the allosteric sites of PBP2x an observation that is consistent with the binding

free energy, RMSD and ROG result of this study. The SASA plots (Supplementary Figure S6d) showed stable fluctuations for all the systems during the simulation with minor swaying. Compared to silicristin, only D1h (28089 Å) had lesser SASA value further suggesting the benefits of D1h as a better inhibitor of PBP2x allosteric site. In summary, the dynamics study of top-ranked derivatives with PBP2x allosteric site pinpointed the potential of D1h as a better inhibitor of PBP2x allosteric site compared to silicristin an observation that is consistent with the binding free energy result of this study.

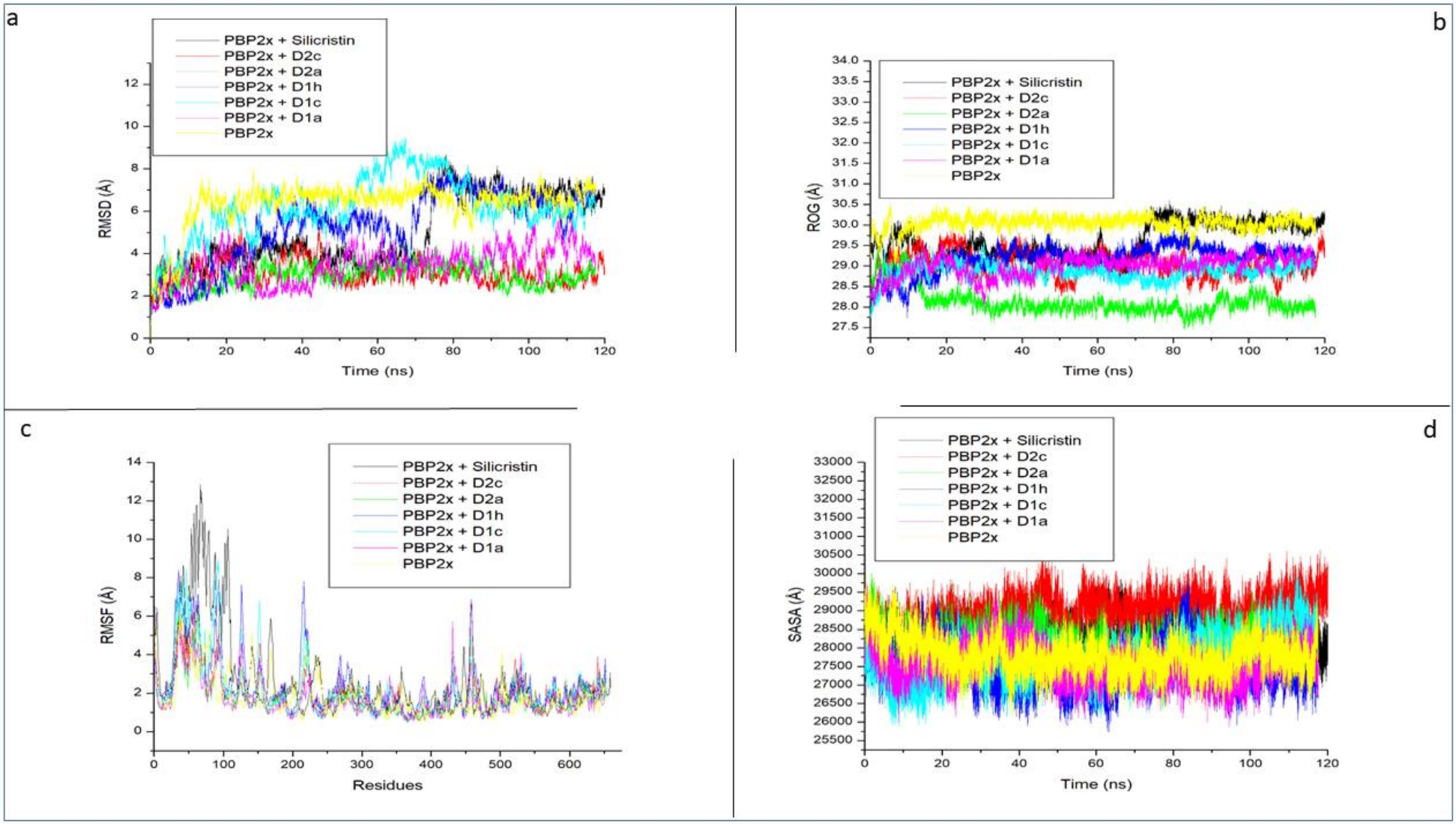


Figure 7: Comparative RMSD (a), ROG (b), RMSF (c) and SASA (d) plot of top-ranked derivatives against the active site of PBP2x of *S. pneumoniae*

3.5. Optimization of the parent compound of the best derivative

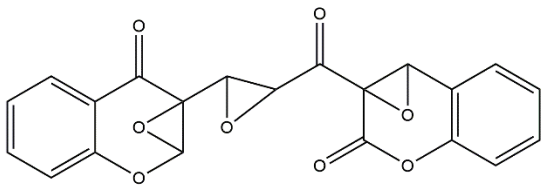
MD simulation and MMGBSA evaluation of the top-ranked derivatives against each of the key PBPs identified the best derivatives as D1a against PBP5 of *E. coli* and active site of PBP2a, D1c against PBP3 of *P. aeruginosa* and active site of PBP2x of *S. pneumoniae*, D1h against the allosteric site of PBP2x and PBP2a, and D2c against PBP3 of *E. coli* relative to silicristin. To further optimize the best derivatives against their respective targets, the parent structure which is similar in each of the best derivatives was further optimized by evaluating the likelihood of improving their binding potential. This was done by altering the oxygen molecules in the parent structure of the best derivatives for double bond. Structural simplification is an effective strategy to improve the efficiency and success rate of drug design by avoiding molecular obesity (Wang *et al.*, 2019). Structural simplification of large or complex lead compounds by shortening unnecessary groups or molecules could not only improve their synthetic accessibility but also improve their pharmacokinetic profiles and reduce side effects (Wang *et al.*, 2019). Compared to the oxidized parent structure, the reduced parent structure had comparable docking scores against each of the investigated PBPs (Figure 8). However, following energy refinement, except for PBP5, the reduced parent structure had higher binding free energy at the active site of the investigated PBPs [PBP3 of *E. coli* (-19.85 kcal/mol), PBP3 of *P. aeruginosa* (-21.74 kcal/mol), PBP2a of *S. aureus* (-11.37 kcal/mol), and PBP2x of *S. pneumoniae* (-25.25 kcal/mol] relative to the oxidized parent structure [PBP3 of *E. coli* (-16.70 kcal/mol), PBP3 of *P. aeruginosa* (-17.41 kcal/mol), PBP2a of *S. aureus* (-9.86 kcal/mol), and PBP2x of *S. pneumoniae* (-23.52 kcal/mol)] (Figure 8). On the other hand, the oxidized parent structure had better binding free energy at the allosteric site (Figure 8). These observations are suggestive of the prospect of the reduced best derivatives as direct inhibitors of the PBPs relative to the oxidized best derivatives and vice versa at the allosteric site. To further probe into this observation, the docking and MMGBSA analysis

of the reduced format of the best derivative [RD2c against PBP3 of *E. coli*, RD1c against PBP3 of *P. aeruginosa*, RD1c against *S. pneumoniae* and RD1a against PBP2a of *S. aureus*] against their respective target were investigated. The reduced format of the best derivative against PBP5 (RD1a) and the allosteric sites of PBP2a (RD1h) and PBP2x (RD1h) were not carried out as the oxidized parent structure had better binding free energy against these targets. Interestingly, following molecular docking, all the reduced form of the best derivatives [RD2c against PBP3 of *E. coli* (-9.8 kcal/mol), RD1c against PBP3 of *P. aeruginosa* (-10.5 kcal/mol), RD1c against *S. pneumoniae* (-10.1 kcal/mol) and RD1a against PBP2a of *S. aureus* (-9.1 kcal/mol)], had comparable negative docking scores with their oxidized derivative [D2c against PBP3 of *E. coli* (-9.7 kcal/mol), D1c against PBP3 of *P. aeruginosa* (-10.6 kcal/mol), RD1c against *S. pneumoniae* (-9.9 kcal/mol) and RD1a against PBP2a of *S. aureus* (-8.9 kcal/mol)] (Table 2). The comparable docking scores of the reduced format of the best derivatives could be suggestive of their potential as inhibitors of the targets. But as molecular docking is deemed too preliminary in the selection of active molecules due to its lack of stability evaluation, further energy refinement involving binding free energy evaluation and dynamic information of the complexes formed by the reduced best derivatives were investigated relative to their oxidized derivative. Remarkably, a noticeable improvement in binding free energy was observed with the reduced best derivative [RD2c against PBP3 of *E. coli* (-46.26 kcal/mol), RD1c against PBP3 of *P. aeruginosa* (-39.42 kcal/mol), RD1c against PBP2x active site of *S. pneumoniae* (-42.90 kcal/mol) and RD1a against PBP2a active site of *S. aureus* (-37.56 kcal/mol)] relative to the oxidized derivative [D2c against PBP3 of *E. coli* (-43.26 kcal/mol), D1c against PBP3 of *P. aeruginosa* (-37.14 kcal/mol), RD1c against *S. pneumoniae* (-40.88 kcal/mol) and RD1a against PBP2a of *S. aureus* (-33.00 kcal/mol)] (Table 2). This observation is indicative of the enhanced potential of the reduced form of the best derivatives as inhibitors of PBP3 of *E. coli*, PBP3 of *P. aeruginosa*, PBP2a of *S. aureus*, and PBP2x of *S. pneumoniae*. Moreso, the reduced form

also does not instigate any thermodynamic entropy compared to the apo-PBPs (Figure 9, supplementary Figure S7 and supplementary Figure S8). Relative to the oxidized format, the reduced best derivatives had comparable RMSD value against PBP3 of *E. coli* [RD2c:2.42 Å], PBP3 of *P. aeruginosa* (RD1c: 2.34 Å), and PBP2a of *S. aureus* (RD1a: 5.22 Å) (Table 2). However, against PBP2x of *S. pneumoniae* the reduced format (RD1c: 2.92 Å) had significant reduction in RMSD value relative to the oxidized format (D1c: 6.19 Å). This observation while in agreement with other thermodynamic metrics is suggestive of the significant stability instigated by RD1c in PBP2x relative to D1c which may transformed to higher potency in the treatment of infections caused by *S. pneumoniae.*

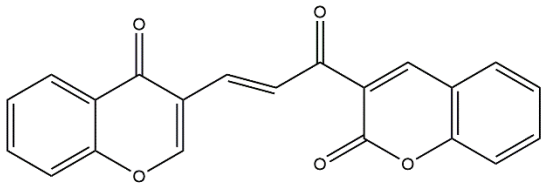
In addition, the evaluation of the pharmacokinetics and toxicity properties of the reduced format of the best derivatives showed that RD1a, RD1c, RD1h and RD2c had zero violations of the LRo5 (supplementary Table S2), whereas the oxidized format each had one violation of the Lipinski rule of 5 (supplementary Table S4). This observation suggests an improvement in the pharmacokinetic properties of the derivatives. The reduced format of the best derivatives all belongs to toxicity class 5 (supplementary Table S4) as against the toxicity class 4 of the oxidized derivatives (supplementary Table S2). This observation is an improvement in the toxicity profile, as compounds belonging to toxicity class 5 are better suited as drug candidate (Verma *et al.*, 2020). However, while an improvement in pharmacokinetics and toxicity properties were noted, a reduction in solubility was observed for the reduced derivatives relative to their oxidized format (supplementary Table S2 and supplementary Table S4). More specifically, RD1a was predicted to be better drug candidate that can be co-administered with phase I- and phase II-dependent drugs as the derivative was noted to be non-inhibitors of all the CYP450s. This observation is a significant improvement as D1a was predicted to be inhibitors of CYP3A4 an important isoenzyme responsible for the metabolism of about 50 % of all drugs used (Khumbulani *et al*., 2022). Other reduced format of the best derivatives (RD1c, RD1h and

RD2c) were also non inhibitors of CYP3A4 (supplementary Table S4), an observation that is comparable to their oxidized format (Supplementary Table S2). Due to the improved binding of the reduced format of the derivative against PBP3 of *E. coli* (RD2c), PBP2x active site *S. pneumoniae* (RD1c), PBP2a active site of *S. aureus* (RD1a) and PBP3 of *P. aeruginosa* (RD1c) coupled with the enhanced pharmacokinetics and toxicity profile, they were identified as best derivatives against in each case of the PBP. Against PBP5 of *E. coli and* the allosteric site of PBP2a of *S. aureus* and PBP2x of *S. pneumoniae,* the oxidized format [PBP3 of *E. coli* (D1a), PBP2a allosteric site (D1h) and PBP2x allosteric site (D1h)] was identified as better inhibitors of the target due better binding capability relative to the reduced format.



Oxidised parent structure of the best derivatives

Key PBPs	Molecular docking score (kcal/mol)	Binding free energy (kcal/mol)
PBP3 of *E. coli*	-9.3	-16.7
PBP5 of *E. coli*	-8.4	-22.95
PBP3 of *P. aeruginosa*	-11.2	-17.41
PBP2a of *S. aureus* (active site)	-8.0	-9.86
PBP2a of S. aureus (allosteric site)	-6.9	-20.38
PBP2x of *S. pneumoniea* (active site)	-10.0	-23.52
PBP2x of *S. pneumoniae* (allosteric site)	-10.2	-33.83



Reduced parent structure of the best derivative

Key PBPs	Molecular docking score (kcal/mol)	Binding free energy (kcal/mol)
PBP3 of *E. coli*	-8.7	-19.85
PBP5 of *E. coli*	-8.7	-14.88
PBP3 of *P. aeruginosa*	-11.7	-21.74
PBP2a of *S. aureus* (active site)	-7.9	-11.37
PBP2a of *S. aureus* (allosteric site)	-7.4	-18.45
PBP2x of *S. pneumoniae* (active site)	-9.9	-25.25
PBP2x of *S. pneumoniae* (allosteric site)	-10.0	-18.32

Figure 8: Comparative docking and binding free energy of the reduced and oxidized format of the parent structure of the best derivatives

Table 2: Comparative docking, binding free energy and RMSD information of oxidized and reduced best derivative of investigated PBP

Complexes	Docking scores (kcal/mol)		Binding free energy (kcal/mol)		RMSD (Å)	
	Oxidized format	Reduced format	Oxidized format	Reduced format	Oxidized format	Reduced format
D2c + PBP3 of *E. coli*	-9.7	-9.8	-43.26 ± 5.63	-46.26 ± 6.15	2.31 ± 0.28	2.42 ± 0.40
D1c + PBP3 of *P. aeruginosa*	-10.6	-10.5	-37.14 ± 4.04	-39.42 ± 5.79	2.34 ± 1.02	2.34 ± 1.02

D1a + PBP2a of *S. aureus*	-8.9	-9.1	-33.00 ± 7.26	-37.56 ± 4.23	5.17 ± 1.53	5.22 ± 1.21
D1c + PBP2x of *S. pneumoniae*	-9.9	-10.1	-40.88 ± 8.96	-42.90 ± 5.20	6.19 ± 1.62	2.92 ± 1.23

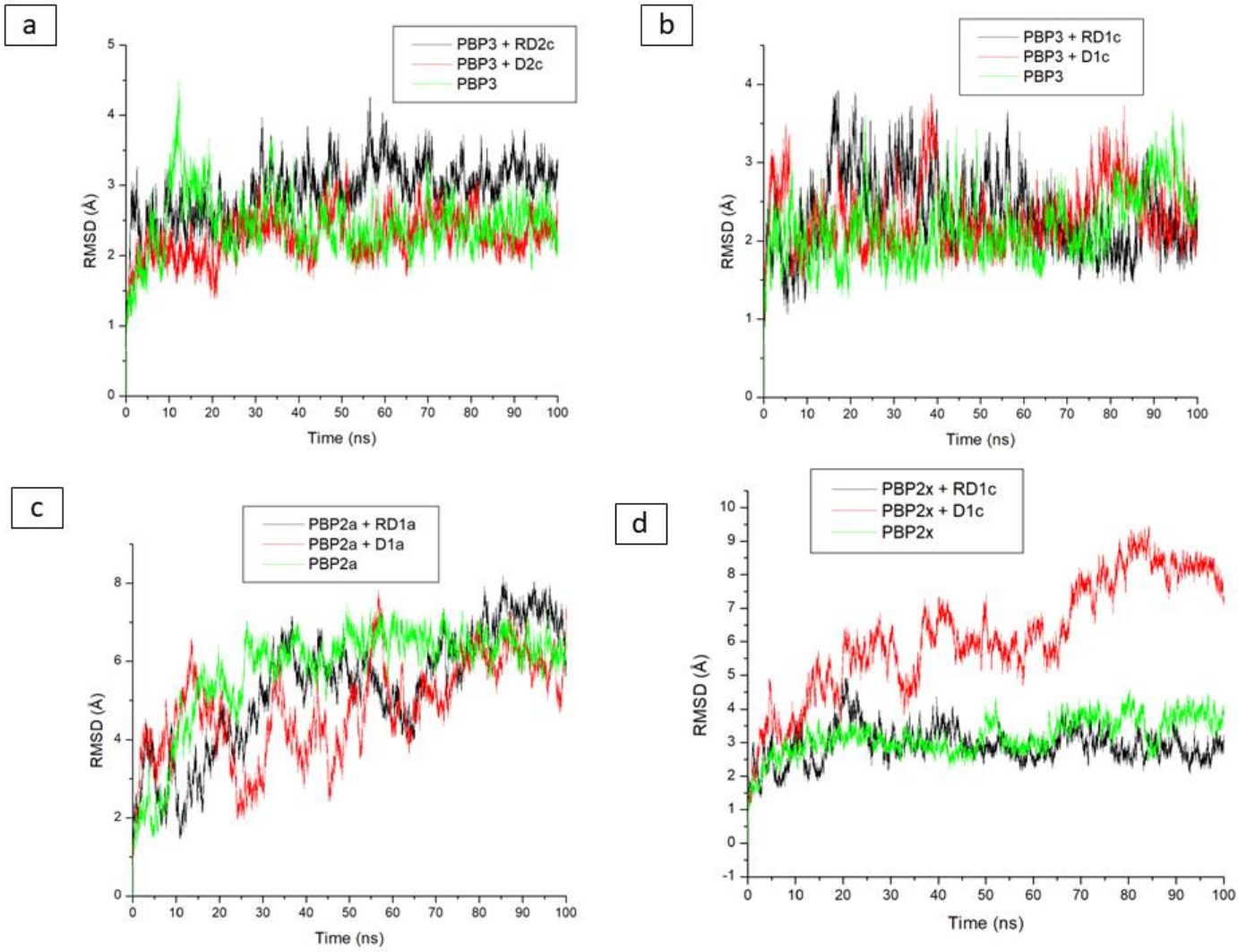


Figure 9: Comparative root means square deviation of reduced and oxidized best derivatives against (a) PBP3 of *E. coli* (b) PBP3 of *P. aeruginosa* (c) PBP2a of *S. aureus* and (d) PBP2x of *S. pneumoniae* over a 100 ns MD simulation

3.6. Comparative interactions analysis of best derivative in each case of the PBPs and silicrsitin after MD simulation

The impact of the number and nature of interactions on the observed improvement of binding free energy and stability of the best derivative in each case of the PBPs [RD2c against PBP3 of *E. coli*, RD1c against PBP3 of *P. aeruginosa*, RD1c against PBP2x active site of *S. pneumoniae*, RD1a against PBP2a active site of *S. aureus*, D1a against PBP5 of *E. coli*, D1h against the allosteric site of PBP2a of *S. aureus* and PBP2x of *S. pneumoniae*] relative to silicristin were analyzed after MD simulation. The binding of drugs to biological targets has been shown to rely on specific noncovalent interactions between partner molecules, including electrostatic interactions such as hydrogen bonds, van der Waals interactions and hydrophobic effects (Liang and Li, 2018). In this study, the number and nature of interactions between partner molecules (best derivatives and PBPs) were noted to have an impact on the improved binding free energy and stability of the best derivative relative to silicristin in each case of the investigated PBPs. Against PBP5 of *E. coli*, silicristin had a total interaction of 14, three and two of which are hydrogen bonds contact and other important interaction respectively (Table 3 and Supplementary Figure S9a). The best derivative (D1a) against PBP5 on the other hand had an enhanced interaction relative to silicristin with a total interaction of 20 (Table 3), including nine and two hydrogen bond contact and other important interactions respectively (Supplementary Figure S9b). The increased total interactions and most especially hydrogen bonds contact of the best derivatives (D1a) against PBP5 relative to silicristin might have contributed to D1a higher binding free energy. The importance of hydrogen bonds has been demonstrated in drug discovery, owing to its unusually strong intermolecular contacts (Du *et al.*, 2016 and Bissantz *et al*., 2010). Interestingly, the best derivatives also interacted with more of the catalytic residues in PBP5 such Ser44, Ser110, Lys47, Ser86, Ser87 (Nelson and Young, 2001) relative to silicristin (Table 3 and Supplementary Figure S9). The ability of a ligand to

interact with essential amino acids of a protein has been shown to be crucial in the inactivation of a protein (Bissantz *et al*., 2010). Hence, the capability of D1a to interacted with more of the catalytic residues in PBP5 relative to silicristin might have contributed to its better binding capability. Similar observations were noted with PBP3 of *E. coli*, with the best derivative against the target, RD2c, having higher total interactions, hydrogen bond contacts and more interactions with the catalytic residues of PBP3 of *E. coli* such as Ser307 and Lys310 (Fraipont *et al*., 2011) relative to silicristin (Table 3 and Supplementary Figure S10). This observation while been consistent with the binding free energy, also demonstrated the improved binding capability due to higher hydrogen bonds and ability to interact with essential amino acid of PBP3 of *E. coli* of RD2c compared to silicristin. Against PBP3 of *P. aeruginosa* on the other hand, the enhanced binding capability of the best derivative (RD1c) (Supplementary Figure S 11a) against the target was mainly due to the ability of the best derivative to form more hydrogen bonds than silicristin (Supplementary Figure S11b) as both compounds interacted with the catalytic residues in PBP3 of *P. aeruginosa* (Ser294) (Kumar *et al*., 2020) (Table 3). Regarding the active site of PBP2a of *S. aureus*, the best derivative (RD1a) against the target had comparable total number of interactions, hydrogen bond contact and other important interactions as silicristin (Supplementary Figure S12). Unlike silicristin-PBP2a, the best derivative (RD1a) (Supplementary Figure S12a) against the active site of PBP2a of *S. aureus*, despite the dynamic nature of MD simulation interacted with the gatekeeper residues (Tyr446) (Otero *et al*., 2013) after MD simulation, suggesting the affinity of RD1a for PBP2a active site. At the allosteric site of PBP2a on the other hand (Supplementary Figure S13), the best derivative against the target (D1h), had higher total interaction, hydrogen bond contact and other important interactions compared to silicristin. This observation is suggestive of the optimised capability of D1h as inhibitors of PBP2a allosteric site relative to silicristin, an observation that is consistent with the binding free energy result of this study. Against the

active (Supplementary Figure S14) and allosteric (Supplementary Figure S15) sites of PBP2x of *S. pneumoniae*, silicristin was observed to have higher total interaction, hydrogen bond contact and other important interactions than the best derivative of the targets (RD1c against the active site and D1h against the allosteric site). This observation does not support the enhanced binding free energy of the best derivative against both target relative to silicristin. However, the ability of the best derivative in each case of the target to interact with essential amino acids such as Asn377 and Trp374 at the active site (Gordon *et al*., 200) and Gly422 at the allosteric site (Land *et al*., 2013) of PBP2x of *S. pneumoniae*, an observation which was lacking in the interaction with silicristin might have contributed to the enhanced binding of the best derivative against the active and allosteric sites of PBP2x of *S. pneumoniae.* Overall, in this study, the enhanced binding capability of the best derivative in each case of the investigated PBPs was owed to either higher total interactions, better hydrogen bond contact or enhanced ability to interacts with essential amino acid of the investigated PBPs.

Table 3: *Comparative interactions analysis of best derivative of each PBPs and silicrsitin after MD simulation*

Investigated PBPs		Total number of interactions	Total number of hydrogen bonds	Total number of other important interaction	Catalytic residues interacted with
PBP5 of *E. coli*	D1a	20	9	2	Ser44, Ser110, Lys47, Ser86, Ser87
	silicristin	14	3	2	Ser85
PBP3 of *E. coli*	RD2c	17	5	2	Ser307, Lys310
	silicristin	13	1	5	None
PBP3 of *P. aeruginosa*	RD1c	20	7	2	Ser294
	silicristin	20	4	3	Ser294
PBP2a active site of *S. aureus*	RD1a	14	4	2	Tyr443 (gate keeper residues)
	silicristin	15	4	2	None
PBP2a allosteric site of *S. aureu*s	D1h	19	5	6	None
	Silicristin	18	3	5	None
	RD1c	15	4	2	Asn377, Trp374

PBP2x active site of *S. pneumoniae*	Silicristin	21	7	4	None
PBP2x allosteric site of *S. pneumoniae*	D1h	17	5	None	Gly422
	silicristin	19	10	3	None

3.7. The Conceptual Density Functional Theory (CDFT) parameter of best derivatives

The quantitative chemical parameters of the best derivative in each case of the investigated PBPs (RD2c against PBP3 of *E. coli*, RD1c against PBP3 of *P. aeruginosa*, RD1c against PBP2x active site of *S. pneumoniae*, RD1a against PBP2a active site of *S. aureus*, D1a against PBP5 of *E. coli*, D1h against the allosteric site of PBP2a of *S. aureus* and PBP2x of *S. pneumoniae*) and silicristin were analyzed to understand the importance of molecular properties on the observed enhanced pharmacodynamics and pharmacokinetics of the best derivatives relative to silicristin. The HOMO and LUMO parameters are crucial to understanding the molecular parameter of a compound (Aihara, 1999), thus, evaluating them could afford necessary information needed to investigate the probable mechanism of action (Ayers *et al*., 2006). The energy gap (LUMO-HOMO) parameters provide information on the stability of the compound, with a smaller energy gap specifying lesser stability and better capability to bind a protein (Aihara, 1999). Compared to silicristin (4.0510 eV), the lower energy gap observed for all the best derivatives [RD1a (3.4878 eV) RD1c (3.3830 eV), D1h (3.1077 eV), RD2c (3.0063 eV) and D1a (3.4878)] suggests their lesser stability (Table 4 and Figure 10). This observation could have positively influenced the capability of the best derivative to bind to protein as observed by their higher docking scores and subsequent higher binding free energy against the key PBPs. The association of reduced energy gaps with higher negative docking score and binding free energy reported in this work is in tandem with the findings of Ma *et al.* (2022), who found that amentoflavone and hinokiflavone with smaller energy gaps had higher negative docking scores and binding free energy against SARS-CoV-2's major protease. Although lesser than the best derivatives, the parent structure of the best

derivatives also had lesser energy gap relative to silicristin suggesting the alteration of the subunit B of silicristin to a chalcone had enhanced effect on the molecular characteristics of the derivatives. Also deducible is that the characteristic hydroxy group (most especially the combination of resorcinol+resorcinol, resorcinol+catechol and catechol+ catechol) of the best derivative further improved the molecular properties of the derivatives as the best derivatives all had lesser energy gap relatives to the parent structure. To gain insight into the molecular information relevant for practical applications of the derivatives as therapeutic molecules, other molecular parameters such ionization potential, electron affinity, electronegativity, chemical potential, chemical hardness, chemical softness, and electrophilicity of the derivative were evaluated (Table 4). According to Pearson's HSAB principle (Pearson, 1995), chemical hardness and softness could provide information on chemical reactive of a compound with higher softness and lesser hardness stipulating higher reactivity of a molecule. In this study, the best derivative in each case of the investigated PBPs had higher softness [RD1a (0.5734 eV), RD1c (0.5911eV), D1h (0.6435eV), RD2c (0.6652 eV), D1a (0.5834 eV)] and lower hardness [RD1a (1.7439 eV), RD1c (1.6915 eV), D1h (1.5538 eV), RD2c (1.5031eV), and D1a (1.6939 eV)] relative to silicristin [softness (0.4937 eV), hardness (2.0255 eV)] (Table 4). This observation might be suggestive of the better reactivity of the best derivatives relative to silicristin, an observation that might have positively influenced their better anti-PBPs activities. The parent structure of the best derivative had lower softness and higher hardness value that the best derivatives suggesting that the characteristic hydroxy group of the best derivative contribute to their better reactivity. Similarly, the parent structure of the best derivative had better reactivity than silicristin pinpointing the benefit of the structural alteration made by the substitution of subunit C of silicristin to coumarin moieties and the transformation of subunit B of silicristin to a chalcone. The electronegativity and electron affinity parameters which measure the ability of an atom and/or a functional group to attract electrons (Pearson, 1986),

also suggest the higher tendency of the derivatives {electronegativity [(RD1a: 4.6176 eV), (RD1c: 4.7186 eV), (D1h: 4.6042 eV), (RD2c), D1a (4.5976 eV)]; electron affinity [(RD1a: 2.8736 eV), (RD1c: 3.0271 eV), (D1h: 3.0503), (RD2c: 3.0170) (D1a (2.9736 eV)]} acquiring and/or donating electrons at the binding pocket of the key PBPs relative to silicristin [electronegativity (3.8528 eV); electron affinity (1.8273 eV)] (Table 4). This observation could have contributed to the higher docking scores of the derivatives relative to silicristin and an at least one derivative having higher binding free energy than silicristin after energy refinement against all the key PBPs. Similar observation was noted with the electrophilicity index as all the best derivatives had higher electrophilicity index [(RD1a: 6.1132 eV), (RD1c: 6.1132 eV), (D1h: 6.8213), (RD2c: 6.7963), (D1a: 6.1932 eV)] values than silicristin (Table 4), suggesting their lesser ability to resist electron exchange at the binding pocket of a protein (Luo *et al*., 2006). Compared to the parent structure on the other hand, the best derivatives had lesser electron affinity, electronegativity and electrophilicity index suggesting that the characteristic hydroxy groups of the best derivatives slightly reduced the tendency of the derivative to attract nor donate electron. Overall, it can be concluded that the structural optimization of silicristin as carried out in this study yielded chalcone bis-coumarin derivatives that are more reactive but with a lesser capability to donate nor acquire electron at the binding pocket of a protein compared to silicristin.

Table 4: The Conceptual Density Functional Theory (CDFT) of best derivatives using DFT calculated at B3LYP/6-31G + (dp)

CDFT descriptors (eV)	Silicristin	Reduced parent structure of best derivatives	Best derivatives against each of the investigated PBPs ()				
			RD1a	RD1c	RD2c	D1h	D1a
E_LUMO	-1.8273	-3.0304	-2.8736	-3.0271	-3.0170	-3.0503	-2.9736
E_HOMO	-5.8784	-6.6024	-6.3615	-6.4101	-6.0234	-6.1580	-6.2615
Energy gap (ΔE)	4.0510	3.5720	3.4878	3.3830	3.0063	3.1077	3.4878
Ionization energy (I)	5.8784	6.6024	6.3615	6.4101	6.0234	6.1580	6.1615
Electron affinity (A)	1.8273	3.0604	2.8736	3.0271	3.0170	3.0503	2.9736
Hardness (η)	2.0255	1.7860	1.7439	1.6915	1.5031	1.5538	1.6939
Softness (S)	0.4937	0.5599	0.5734	0.5911	0.6652	0.6435	0.5834
Electronegativity (χ)	3.8528	4.8164	4.6176	4.7186	4.52024	4.6042	4.5976
Chemical potential (μ)	-3.8529	-4.8164	-4.6176	-4.7186	-4.5202	-4.6042	-4.5676
Electrophilicity index	3.6644	6.4943	6.1132	6.5816	6.7963	6.8213	6.1932

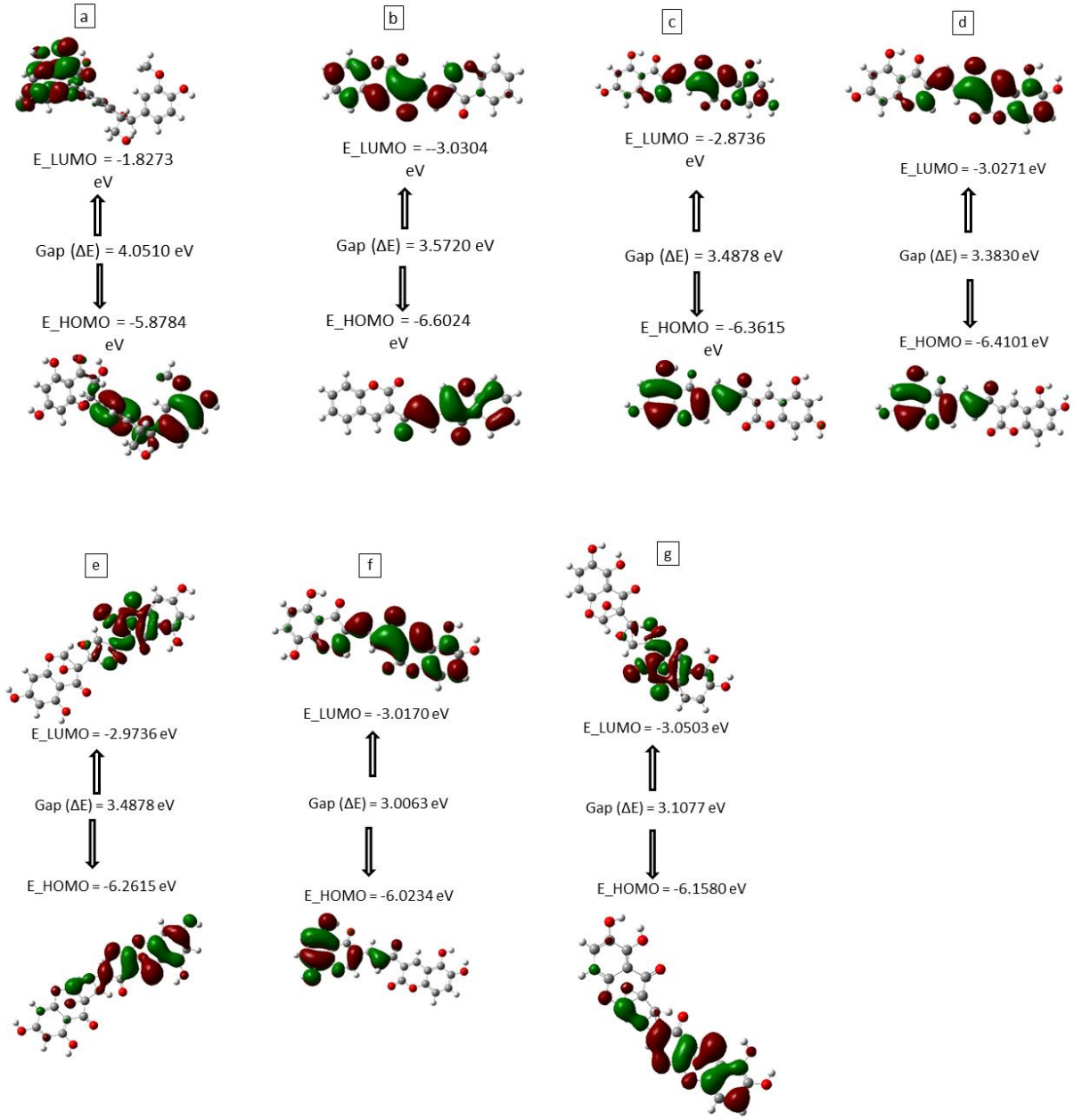


Figure 10: Frontier molecular orbitals for (a) silicristin, (b) parent structure of derivatives, (c) RD1a, (d) RD1c (e) D1a, and (f) RD2c inhibitor (g) D1h

3.8 Thermodynamic Properties of best derivatives

The probability of a reaction taken place, and the stability of the chemical reaction can be anticipated using thermodynamic parameters such as enthalpy and Gibb's free energy (Cohen and Benson, 1993). The sign and quantity of free energy and enthalpy are crucial in expressing the possibility of bimolecular events occurring. Larger negative values imply enhanced thermodynamic characteristics. In the present study, the Gibs free energy and enthalpy values for silicristin and all the best derivatives tend to be negative (Table 5), indicating that the binding of this compounds to PBPs will happen spontaneously without any additional energy consumption (Garbett and Chaires, 2012). Compared to silicristin (Gibs free energy: -1717.83 Hartree; enthalpy: -1717.73 Hartree), the best derivatives against in each case of the PBPs had lesser negative Gibs free energy and enthalpy relative to silicristin (Table 5). This observation suggests that silicristin is energetically and configurationally preferable compared to the best derivatives (Table 5). The best derivatives had relatively similar Gibs free energy and enthalpy values of between -1484.28 and -1484.31 Hartree and -1484.21 and -1484.23 Hartree respectively (Table 5). The relatively similar energy values observed for the derivatives could be due to their relatively similar parent structure with negative Gibs free energy and enthalpy values of -1183.40 Hartree and -1183.33 Hartree respectively (Table 5). Like the Gibs free energy and enthalpy, silicristin had a higher level of dipole moment at 5.62 Debye, compared to the best derivatives [RD1a: 5.16 Debye; RD1c: 3.45 Debye; D1h: 5.16 Debye; RD2c: 3.37 Debye, D1a 5.16 Debye] (Table 5). Higher level of dipole moment might improve the ability of a compound forming hydrogen bond, nonbonding interaction, binding affinity, and polar nature of a molecule (Lien *et al*., 1982). Thus, it can be deduced that the structural optimization of silicristin as done in this study results in the reduction of the thermodynamic properties of the best derivatives.

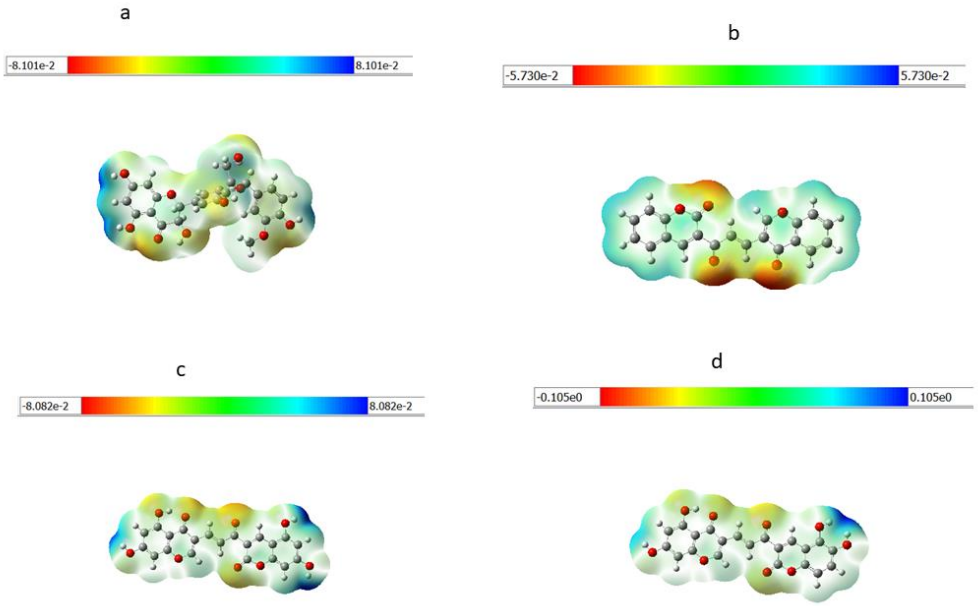
Table 5: Thermodynamic properties of silicristin and best derivatives in each case of the PBP

Thermodynamic Properties	Silicristin	Parent structure of Lead derivatives	Lead derivatives				
			RD1a	RD1c	D1h	RD2c	D1a
Electronic energy (Hartree)	-1718.20	-1183.63	-1484.55	-1484.53	-1484.53	-1484.52	-1484.52
Enthalpy (Hartree)	-1717.73	-1183.33	-1484.23	-1484.22	-1484.21	-1484.21	-1484.22
Gibb's Free energy (Hartree)	-1717.83	-1183.40	-1484.31	-1484.29	-1484.29	-1484.28	-1484.3
Dipole moment (Debye)	5.62	3.035	5.16	3.45	5.16	3.37	5.16
Entropy (cal/mol-kelvin)	206.06	147.85	167.19	164.88	164.23	165.47	166.43
Polarizability (α)	343.12	307.70	341.03	336.10	337.78	337.89	340.03

3.9. Electrostatic potential map of the best derivative

The electrostatic potential of various compounds may be utilized in the modification and development of molecules into viable medications. The primary form of interaction between a compound and a protein is electrostatic interaction, which are mainly hydrogen bonds and halogen bonds. The electrostatic potential function is closely associated with the electrostatic effect and is highly appropriate for the analysis of weak interactions that are induced by electrostatic forces (Politzer *et al.*, 2013). Therefore, to comprehend the charge-dependent characteristics of silicristin and the best derivative, the electrostatic potential function was analyzed. Figure 11 showed electrostatic potential distribution of silicristin and the best derivatives in each case of the PBP displaying the comparative reactivity of the atoms. The negative region is presented in red, and the positive region in blue. The most negative region of silicristin and the best derivatives corresponds to the oxygen in the parent structure of the derivatives while the most positive region was linked to the hydrogen in hydroxyl group of benzene ring of the compound. RD1c, D1h and RD2c had the most negative and positive region at between -0.104 and -0.105 and 0.104 and 0.105 for the negative and positive regions respectively (Figure 11). RD1a and D1a on the other hand had similar negative (-0.0808) and positive regions (0.0808) that compared well with silicristin

[negative region (-0.0810); positive region (0.0810)] (Figure 11). The parent structure had the least negative and positive regions. Studies have shown that even a smaller area of minimal electrostatic potential effect can be very crucial to establishing hydrogen bonds or electrostatic interactions (Rathi *et al*., 2020; Politzer *et al*., 2013). Thus, in this study, it can be deduced that RD1c, RD1h and RD2c had better capabilities of forming enhanced hydrogen bonds or electrostatic interactions compared to silicristin. This observation, while in contrast with the prediction of the dipole moment of this study, is supported by the higher negative docking scores and binding free energy of RD1c, RD1h and RD2c with at least one key PBPs. Generally, it can be concluded that the structural optimization of silicristin as caried out in this study yielded chalcone bis-coumarin derivatives (RD1c, RD1h and RD2c) that have better capability of forming hydrogen bonds or electrostatic interactions with key PBPs.



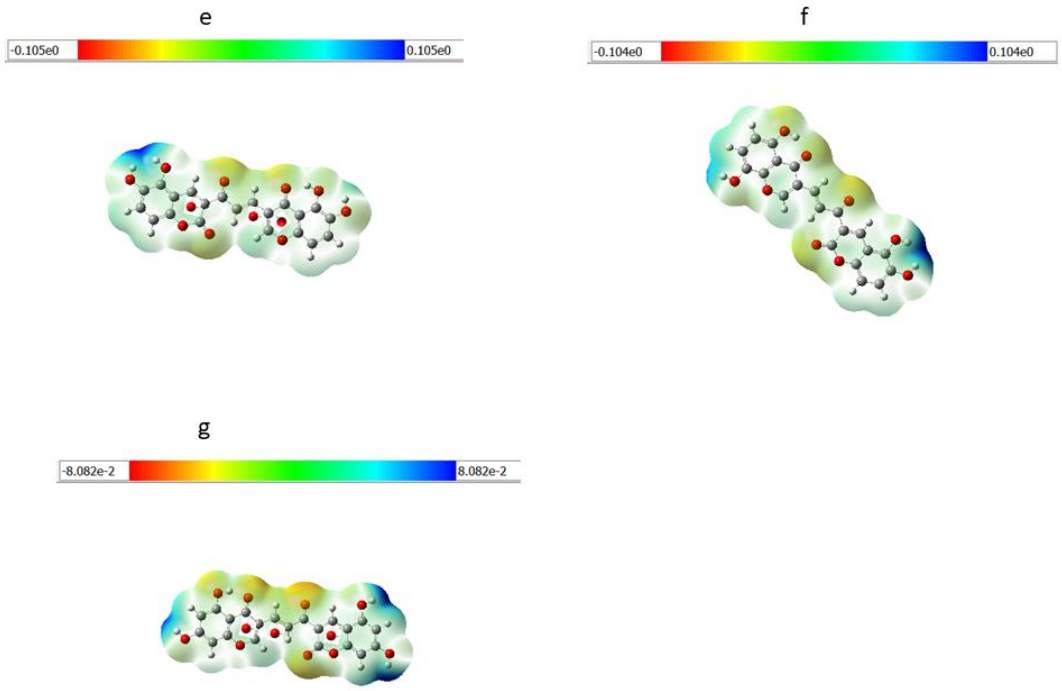


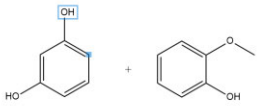
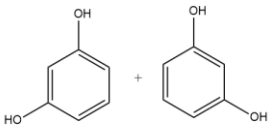
Figure 11: Molecular electrostatic potential map of: (a) silicristin, (b) parent structure of derivatives, (c) RD1a, (d) RD1c (e) D1h, and (f) RD2c (g) D1a

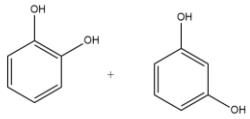
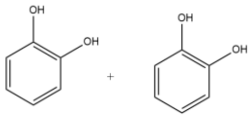
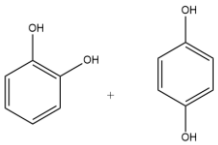
3.10. Evaluation of the positioning of hydroxy group in the observed binding free energy, stability and pharmacokinetics of the best derivatives

Studies have shown that the presence of hydroxyl groups in phenolics enhance strong protein binding (Avila *et al*., 2008). In the study, the influence of the positioning of hydroxyl group in the pharmacodynamics, and pharmacokinetics properties of the best derivatives were evaluated. The presence of a pyrogallol (hydroxy groups at position 1, 2 and 3) at either ends of the derivatives as seen in D1i, D1d, D2h, D2i, D2d, and D2j as well as a benzene with hydroxyl groups at position 1, 2, 3 and 4 as seen in D1j, D1e, D2j, D2e, D3a, D3b, D3c, D3d, D3e instigate a reduction in pharmacokinetics properties. This observation may indicate that the presence of more than two hydroxy groups in the benzene ring of the derivative reduces the likelihood of the derivatives being

used as an oral drug. This finding is further substantiated as derivatives with a combination of phenolic moieties with ≤ two hydroxy group all pass the LRo5. This observation can be seen in D1a, D1b, D1c, D1f, D1, D1g, D2a, D2b, D2c, D2f and D2g. Specifically, the combination of two catechol (hydroxy group in para positions to each other in a benzene ring) at both end of the derivative as seen in D1h enhanced good pharmacokinetic properties, and good protein binding, most especially at the allosteric site of PBP2a of *S. aureus* and PBP2x of *S. pneumoniae* following energy refinement. The combination of two resorcinol (hydroxy group in a benzene ring at position 1 and 3) at both end of the derivative as seen in D1a and RD1a had good pharmacokinetic properties, and enhanced protein binding at the active site of PBP5 of *E. coli* and PBP2a of *S. aureus*. On the other hand, the combination of resorcinol with catechol (as seen D1c and RD1c)) or hydroquinone moieties (D2c and RD2c) promote good pharmacological activities while also increasing their ability of being used as oral drug due to their optimized pharmacokinetics and toxicity profile. Overall, the combination of catechol, resorcinol, and hydroquinone either alone or in combination with each other at either end of the derivatives promote good pharmacological properties relative to silicristin. Silicristin while having a resorcinol at one end had a methoxyl group at the other end. The presence of a methoxyl group instead of a catechol, resorcinol, and hydroquinone could have been the reason for the reduced pharmacodynamic properties of silicristin relative to the best derivatives. On the other hand, the presence of a pyrogallol or a benzene ring with more than two hydroxy group at one or both end of the derivatives caused reduced oral bioavailability relative to silicrsitin.

Table 6: Evaluation of the effect of phenolic moieties in the observed binding free energy, stability, pharmacokinetics, molecular and thermodynamic properties of the best derivatives

Compounds	Different combinations of phenolic moieties	Structures	Effects on binding free energy, stability, and pharmacokinetics relative to silicristin
Silicristin	Resorcinol + methoxyl		Had good docking scores against all the key PBPs. Had good binding free energy against all the key PBPs but can cause significant thermodynamic entropy in most of the PBPs. Had good pharmacokinetics and solubility but can cause drug-drug interactions when co-administer with drug metabolised by CYP3A4. Had good reactivity, thermodynamic properties and electrostatic potential
Best derivatives			
RD1a or D1a	Resorcinol + Resorcinol		Improved docking scores against all the key PBPs relative to silicristin Oxidised and reduced format of D1a had enhanced binding free energy and stability against PBP5 of *E. coli* and PBP2a of *S. aureus* respectively compared to silicristin. RD1a had improvement in pharmacokinetics and toxicology properties while D1a had better solubility. Had better reactivity but with similar electrostatic potential as silicristin

RD1c	Catechol + Resorcinol		Improved docking score against most of the key PBPs relative to silicristin. Subsequent enhanced binding free energy and stability against PBP3 of *P. aeruginosa* and PBP2x of *S. pneumoniae.* Better optimisation of pharmacokinetics and toxicity profile, but with reduced solubility Had better reactivity and electrostatic potential than silicristin
D1h	Catechol + catechol		Improved docking score against most of the key PBPs relative to silicristin. Subsequent enhanced binding free energy and stability against the allosteric site of PBP2a of *S. aureus* and PBP2x of *S. pneumoniae* compared to silicristin. Better optimisation of solubility and toxicity with no effects on pharmacokinetics relative to silicristin Had better reactivity and electrostatic potential than silicristin
RD2c	Catechol + hydroquinone		Improved docking score against most of the key PBPs relative to silicristin. Subsequent enhanced binding free energy and stability against the PBP3 D *E. coli* compared to silicristin. Better optimisation of pharmacokinetics and toxicity profile, but with reduced solubility relative to silicristin Had better reactivity and electrostatic potential than silicristin

3.11. Experimental and computational NMR characterization of parent structure (reduced format) of the best derivatives

To explore the synthetic route of the best derivative, the parent structure which is similar in all the derivative were synthesized and the successful synthesis was characterized using NMR techniques. This is necessary to ensure that the identified lead derivative for each PBP is synthesizable. Using both experimental and theoretical approach the proton (^{1}H) and ^{13}C NMR spectroscopic chemical shifts of the parent compound was explored. The correlation of the experimental and theoretical NMR simulation of the parent structure which took place in tetramethylsilane (TMS) solvent are stated in Supplementary Table S5 and S6 for proton and ^{13}C NMR respectively. According to Pavia *et al*. (2009), the hydrogen atoms attached to benzene aromatic rings should lie between 6 and 8 ppm. In this study while the experimental ^{1}H NMR spectrum of the hydrogen attached to the benzene aromatic rings (4-H, 12-H,14-H, 6-H, 5-H, 7-H,13-H and 15-H) of the parent structure lie between 6 and 8 ppm, the theoretically computed ppm values fall just outside the region basically between 8 and 10 ppm. Although a good correlation exists between atom 27-H (8.38ppm) computed computationally (Figure 12b and supplementary Table S5) which correspond to 3-H (8.43 ppm) obtained experimentally (Figure 12a and supplementary Table S5) lending credence to the successful synthesis of the parent structure. The most pronounced NMR spectrum peak experimentally was detected within the Benzene (aromatic) group, precisely 4-H, 12-H, 14-H, 6-H which form a doublet with a chemical shift of 7.6 ppm and 5-H, 7-H, 13-H and 15-H which form a triplet with a chemical shift of 7.3 ppm. Remarkably, this experimental result closely aligns with the expected nature and range reported in existing literature (Hu *et al*., 2022; Pavia *et al*., 2009), further reinforcing the reliability of the synthesis. It's worth noting that the highest peak observed experimentally was between 8.4 and 8.5 ppm corresponding with 3-H and 10-H hydrogen

atoms found outside the benzene ring respectively which is consistent with the anticipated chemical shift values commonly documented in scientific literature (Hu *et al*., 2022). The ^{13}C NMR spectrum which specify information on the nature of the carbon skeleton that is present, was also explored to ensure confirmation of the successful synthesis of the parent structure. Like the proton NMR, the ^{13}C NMR was obtained experimentally and computationally and unlike the proton NMR, a good correlation exists between the experimentally and computationally obtained ppm for several carbon atoms (supplementary Table S6). Good correlation was obtained experimentally (Figure 13a) and computationally (Figure 13b) for carbon atoms 17-C, 15-C, 15a-C, 10-C, 6-C, and 5-C (supplementary Table S6), further strengthening the reliability of the synthesis of the parent structure of the derivatives. The ^{13}C chemical shifts observed experimentally was within 115 and 195 ppm which correspond fairly with the computationally obtained range between 120 and 190 ppm. While there no observable differences in the peak obtained computationally, the highest pick was obtained at 125 ppm experimentally which correspond with 13-C, 5-C, and 7-C. Experimentally, the aromatic carbons (13-C, 5-C, 7-C, 14-C, 6-C, 4-C, 12-C, 15-C) were generally found within the ranges of 120 and 135 ppm which correspond to the range (120 to 140 ppm) often reported in the literature. Except for 15-C and 4-C, all the aromatic carbons computed computationally were also found within the range reported in the literature. These observations are indication of the successful synthesis of parent structures. Moreso as the ppm computed for ketones (such as 8-C and 11-C at 197ppm) and ester (2-C: 160ppm) in the parent structure fall within the range reported for ketones (200 ppm) and ester (between 160 and 180 ppm) in literature (Hu *et al*., 2022; Pavia *et al*., 2009). Further corroborating the ^{1}H and ^{13}C NMR result is the heteronuclear multiple-bond coherence (HMBC) test which provides correlation between the quaternary carbon and hydrogen atom in a structure (Figure 14).

While 8a-C, 2a-C, 3a-C, and 7-C were observed coupling with 3-H, 8a-C, 11a-C, 15a-C and 10a-C was coupling well with 10-H, 7a-C was coupling with 5-H and 7a-C was coupling greatly with 6-H. This observation is suggestive of the good association that exist between the quaternary carbon and hydrogen atoms in the parent structure and thus an indication of the synthesis of the compound (Figure 14). The heteronuclear single quantum coherence spectroscopy **(**HSQC) (Figure 15) also showed excellent association of the carbon atoms with the hydrogen atoms of the parent structure, with 3-C, 4-C, 6-C, 10-C and 12-C correlating well with 3-H, 4-H, 6-H, 10-H, and 12-H respectively (Figure 15). The correlated spectroscopy (Cosy) test similarly indicate that an excellent relationship exists between the proton-proton atoms in the structure with 3-H associating with 4-H and 5-H; 6-H linking with 7-H, 12-H resonating with 13-H and 14-H, and 14-H associating with 15-H (Figure 16). These observations further reinforced the reliability of the synthesis of the parent structure of the best derivatives.

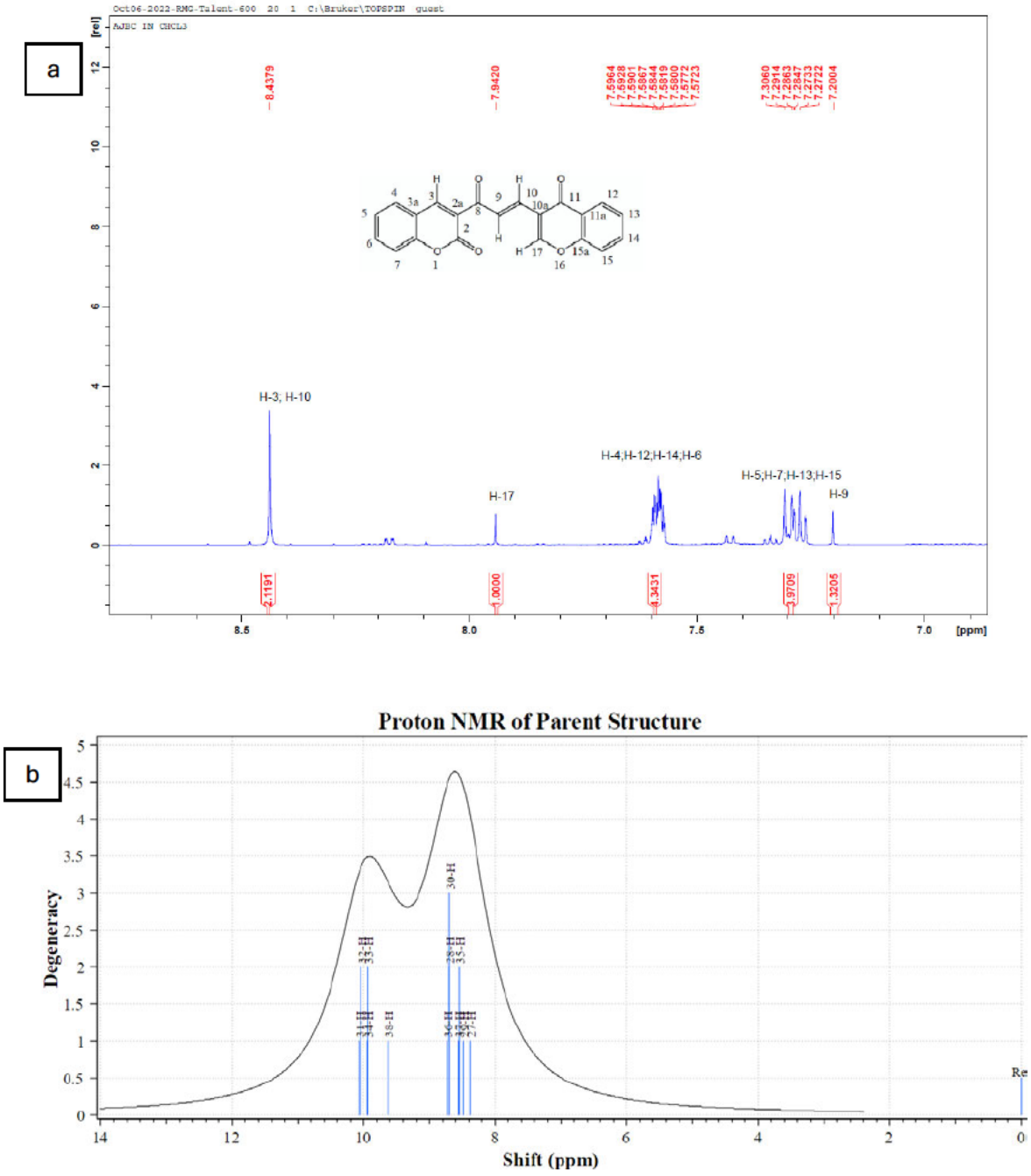


Figure 12: Proton (^{1}H) NMR test of parent structure (a) experimentally obtained spectrum (b) computationally obtained spectrum

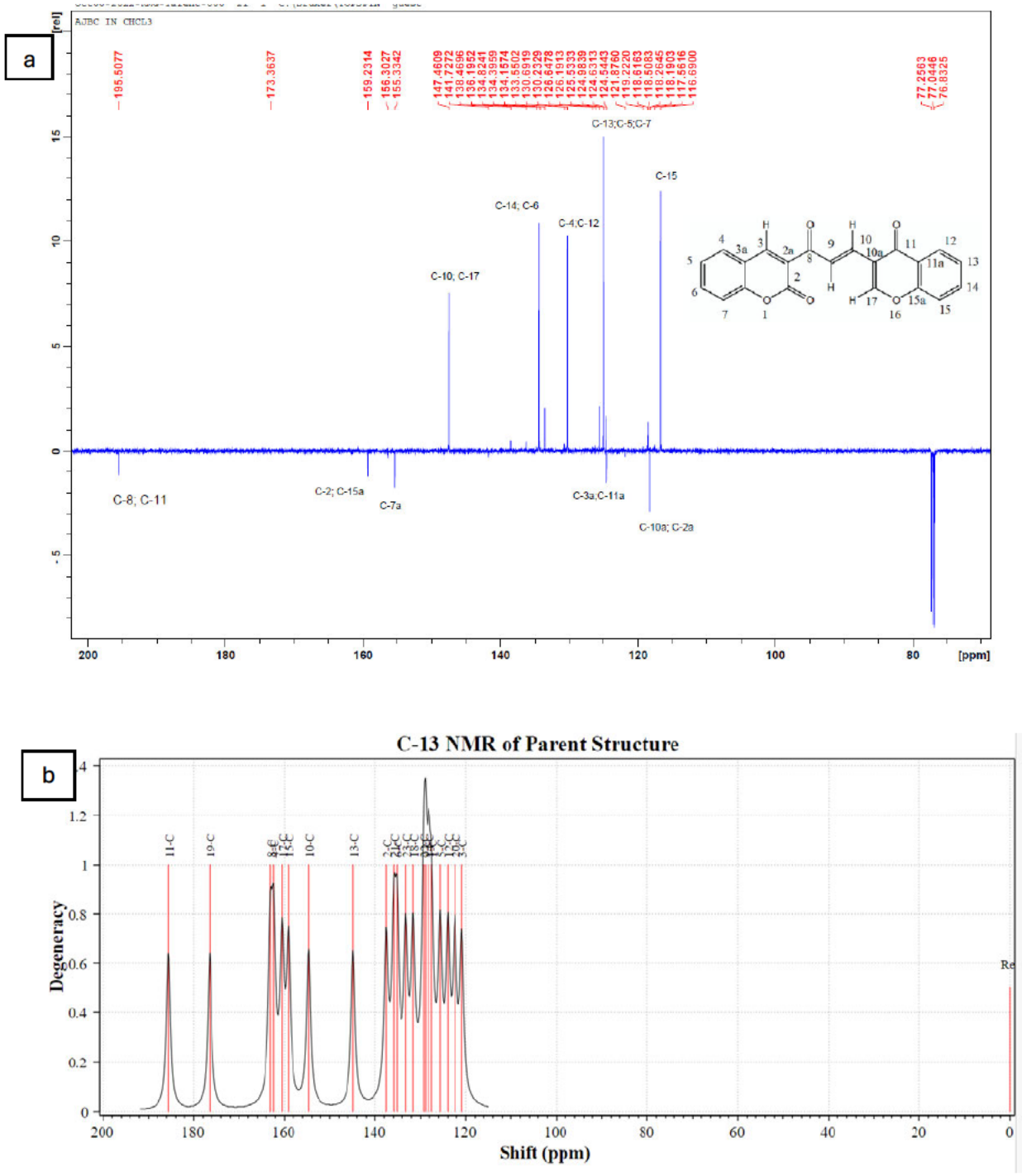


Figure 13: ^{13}C NMR test of parent structure (a) experimentally obtained (b) computationally obtained

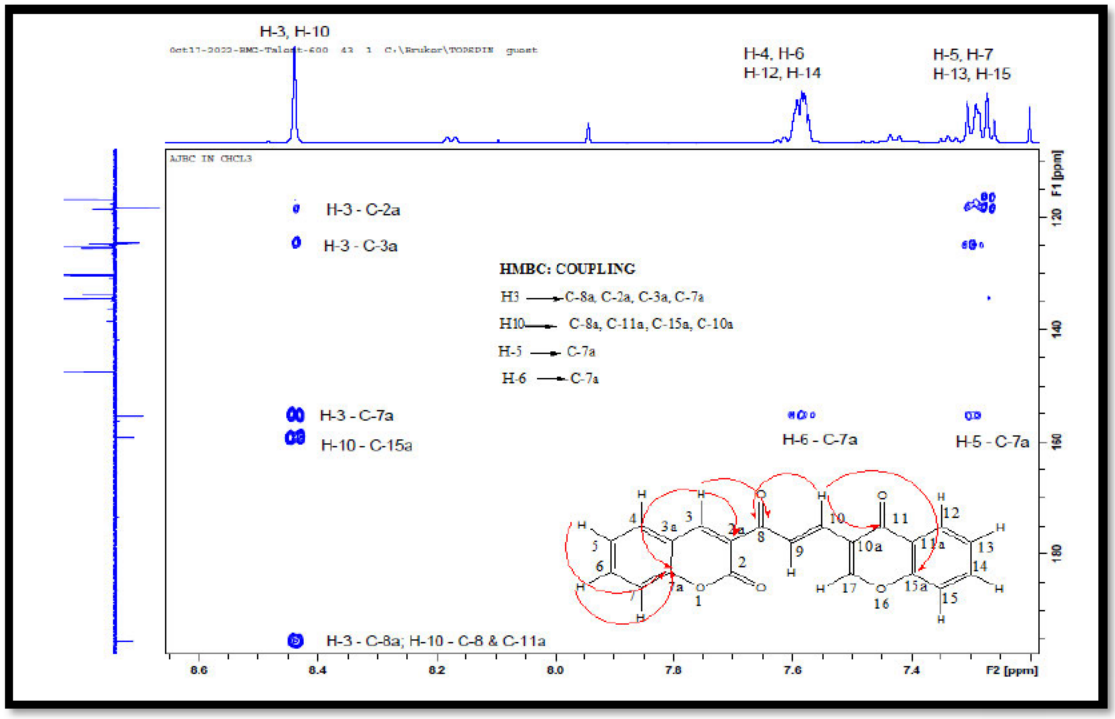


Figure 14: Heteronuclear multiple-bond coherence (HMBC) [correlation of quaternary carbon to hydrogen] of the parent structure

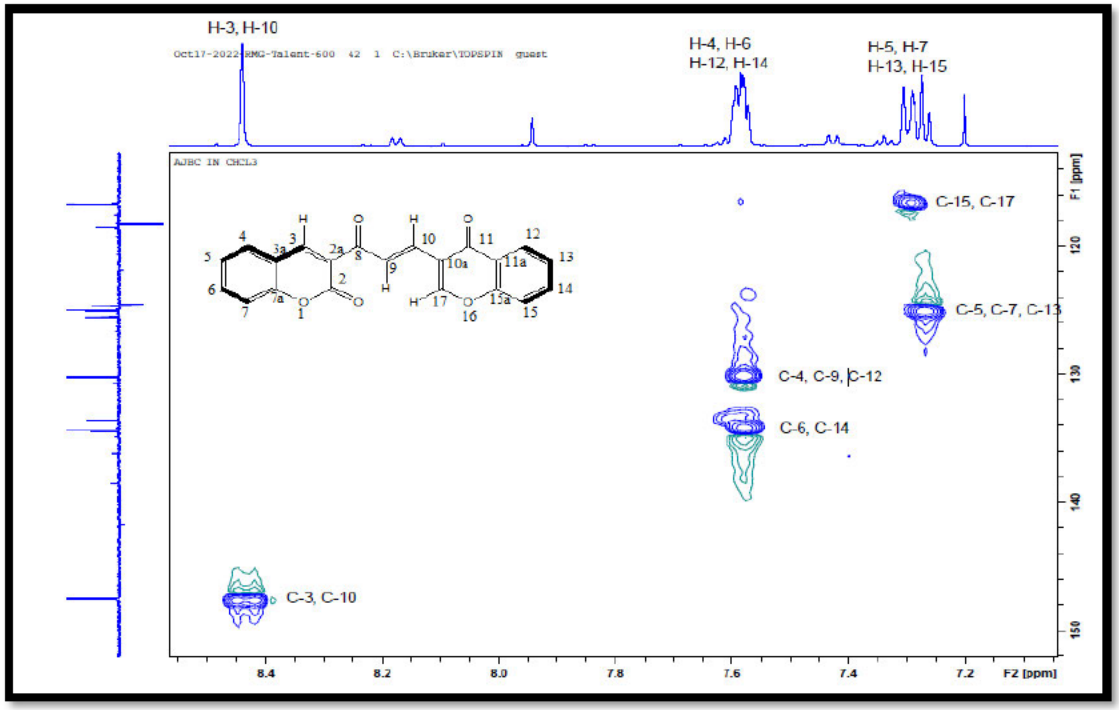


Figure 15: Heteronuclear single quantum coherence spectroscopy (HSQC) [correlation of carbon and hydrogen] of the parent structure

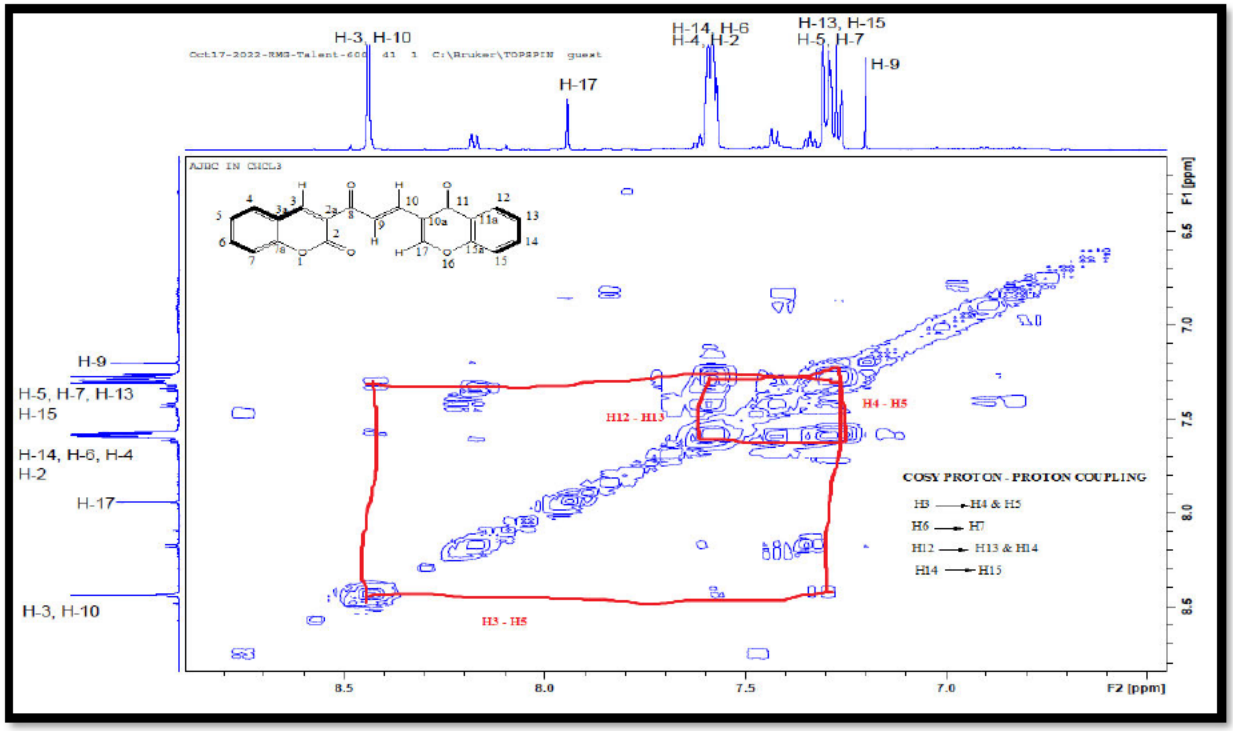


Figure 16: Correlated Spectroscopy (Cosy) (correlation of proton-proton relationship) of the parent structure.

3.12. Computational NMR characterization of the reduced format of the best derivatives (RD1a, RD1c, RD1h and RD2c)

The computational ^{1}H and ^{13}C NMR was computed for the best derivatives (reduced format) to serve as reference for validation when the experimental analysis is done. The proton chemical shifts observed in the tetramethylsilane (TMS) solvent for RD1a (Supplementary Figure S16a), RD1c (Supplementary Figure S16b), RD1h (Supplementary Figure S16c) and RD2c (Supplementary Figure S16d) were between 5.7-14.7 ppm, 3.8-14.2 ppm, 3.8-14.1ppm, and 3.8-13.7ppm respectively (Supplementary Figure S16). Expectedly, the proton chemical shift for the parent structure computationally (between 8 and 10ppm) should falls within the ppm range computed for each of the best derivatives. The observation of the spectra of the parent structure in the spectra observed for each of the best derivative, suggest that the hydrogen atoms are well placed and thus reinforced the validity of the analysis. The spectrum before the 8 ppm and after the 10 ppm represent the hydrogen atoms attached to the characteristic hydroxy groups of the derivative which were absent in the parent structure. On the other hand, a similar pattern in the positioning of carbon atoms and range of ppm for the ^{13}C NMR spectrum was observed for the parent structure (120-190 ppm) and each of the best derivative [(RD1: 100-190 ppm), (RD1c: 100-190 ppm), (RD1h: 115-190 ppm) (RD2c: 110-190 ppm)] (Supplementary Figure S17a-d). This observation could be due to the same nature of carbon atoms (number and positioning of carbon atoms) existing in the parent structure and the best derivatives unlike the hydrogen atoms.

4.0 Conclusion

The results of this study showed significant improvement in the thermodynamic binding free energy, stability and pharmacokinetic properties of the best derivatives [RD2c against PBP3 of *E. coli*, RD1c against PBP3 of *P. aeruginosa*, RD1c against PBP2x active site of *S. pneumoniae*, RD1a against PBP2a active site of *S. aureus*, D1a against PBP5 of *E. coli*, D1h against the allosteric site of PBP2a of *S. aureus* and PBP2x of *S. pneumoniae*] compared to silicristin, an observation that could translate to enhanced potency *in vitro* and *in vivo*. The observed enhanced binding capability of the best derivatives was noted to be due their higher reactivity, better electrostatic potential and improved hydrogen bonding capability with key essential amino acids at the binding pocket of the investigated PBPs. The exploration of catechol, resorcinol, and hydroquinone either alone or in combination with each other at either end of the derivatives promotes good pharmacological properties, while the presence of a pyrogallol and/or a benzene ring with more than two hydroxy group at one or both ends of the derivatives caused reduced oral bioavailability relative to silicristin. The ^{13}C NMR analysis showed a good correlation between the experimentally and computationally obtained ppm for several carbon atoms of the synthesized parent structure of the best derivatives, strengthening the reliability of the synthesis of the parent structure. Since the best derivative in each case of the essential PBPs had a similar synthetic route as the parent compound, it is recommended that the synthetic route be followed in the synthesis of the best derivative to enable the investigation of their *in vitro* and *in vivo* antibacterial activities for the possibility of subsequent development as beta-lactams.

References

Abdelazim, S. Effect of silymarin as natural antioxidants and antimicrobial activity. *Nutri Food Sci Int J*. 2017, 2, 555589. https://doi.org/10.19080/NFSIJ.2017.02.555589

Agamah, F.E.; Mazandu, G.K.; Hassan, R.; Bope, C.D.; Thomford, N.E.; Ghansah, A.; Chimusa, E.R. Computational/in silico methods in drug target and lead prediction. *Brief Bioinform.* 2020, 21, 1663 - 1675. https://doi.org/10.1093/bib/bbz103.

Aihara, J. Reduced HOMO-LUMO Gap as an index of kinetic stability for polycyclic aromatic hydrocarbons. *J. Phys. Chem***.** 1999, 103, 7487 - 7495. https://doi.org/doi/10.1021/jp990092i

Al-Majedy, Y.K.; Kadhum, A.A.; Al-Amiery, A.A.; Mohamad, A.B. Synthesis and characterization of some new 4-hydroxy-coumarin derivatives. *Molecules*. 2014, 8, 11791 - 11799. https:doi.org/10.3390/molecules190811791.

Akoonjee, A.; Lanrewaju, A.A.; Balogun, F.O.; Makunga, N.P.; Sabiu, S. Waste to Medicine: evidence from computational studies on the modulatory role of corn silk on the therapeutic targets implicated in type 2 diabetes mellitus. *Biology*. 2023, 12, 1509. https://doi.org/10.3390/biology12121509.

Aribisala, J. O.; Sabiu, S. Cheminformatics identification of phenolics as modulators of penicillin-binding protein-3 of Pseudomonas aeruginosa towards interventive antibacterial therapy. *J. Biomol Struct Dyn*. 2023, 1, 1 - 16. https://doi.org/10.1080/07391102.2023.2192808.

Aribisala, J.O.; Idowu, K.; Makhanya, T. R.; Sabiu, S. Cheminformatics identification of phenolics as modulators of key penicillin− binding proteins of *Escherichia coli* towards interventive

antibacterial therapy. *Mol Simul*. 2023, 13, 1324 - 1340. https:/doi.org/10.1080/07391102.2023.2192808.

Aribisala, J.O.; Sabiu, S. Cheminformatics Identification of Phenolics as modulators of penicillin − binding protein 2a of *Staphylococcus aureus*: a structure–activity−relationship−based study. *Pharmaceutics*. 2022, 14, 1818. https://doi.org/10.3390/pharmaceutics14091818

Avila, H.P.; Smânia, F.A.; Monache, Smânia, A.J. Structure−activity relationship of antibacterial chalcones. *Bioorg Med Chem.* 2008, 16, 9790 – 9794. https://doi.org/10.1016/j.bmc.2008.09.064.

Ayers, P.W.; Parr, R.G.; Pearson, R.G. Elucidating the hard/soft acid/ base principle: a perspective based on half-reactive ions. *J Chem Phys*. 2006, 124, 194107. https://doi.org/10.1063/1.2196882.

Baig, M.H.; Sudhakar, D.R.; Kalaiarasan, P.; Subbarao, N.; Wadhawa, G.; *et al.* Insight into the effect of inhibitor resistant S130G mutant on physico-chemical properties of SHV type beta-lactamase: a molecular dynamics study. *PLoS ONE*. 2014, 9, e112456. https://doi.org/10.1371/journal.pone. 0112456

Bajorath J. Rational drug discovery revisited: interfacing experimental programs with bio- and chemo-informatics. *Drug Discov Today*. 2001, 6, 989 - 995. https://doi.org/10.1016/s1359-6446(01)01961-4.

Barcelos, M.P. Gomes S.Q.; Fedrico, L.B.; Francischini, I.A.G.; Melim, L.L.D.; Silva, G.M.; Silva, C.H.T. (2022). Lead Optimization in drug discovery. in: Taft, C.A., de Lazaro, S.R. (eds) research topics in bioactivity, environment and energy. engineering materials. *Springer Cham*. 2022, https://doi.org/10.1007/978-3-031-07622-0_19

Belkhir-Talbi, D.; Makhloufi-Chebli, M.; Terrachet-Bouaziz, S.; Hikem-Oukacha, D.; Ghemmit, N.; Ismaili, L. M.S.; Silva, A.; Hamdi, M. Synthesis, characterization, theoretical studies, ADMET and drug-Likeness analysis: electrochemical and biological activities of metal complexes of 3-(2-hydroxybenzoyl)-2H-chromen-2-one. *J Mol Struct*. 2019, 1179, 495 - 505. https://doi.org/10.1016/j.molstruc.2018.11.035.

Biedermann, D.; Buchta, M.; Holečková, V.; Sedlák, D.; Valentová, K.; Cvačka, J.; Bednárová, L.; Křenková. A.; Kuzma, M.; Škuta C.; Peikerová, Ž.; Bartůněk, P.; Křen, V. Silychristin: Skeletal alterations and biological activities. *J Nat Prod.* 2016, 79, 3086 - 3092. https://doi,org/10.1021/acs.jnatprod.6b00750.

BIOVIA. 21.1.0. Dassault Systèmes, San Diego: Dassault Systèmes. 2021. Available at: https://discover.3ds.com/discovery-

Bissantz, C.; Kuhn, B.; Stahl, M.A. Medicinal chemist's guide to molecular interactions. *J Med Chem*. 2010, 14, 5061 - 5084. https://doi.org/10.1021/jm100112j.

Calais, J.L. Density-functional theory of atoms and molecules. RG Parr and W Yang, Oxford University Press, New York, Oxford, 1989. IX + 333 pp. Price £45.00. *Int J Quantum Chem***.** 47: 101. https://doi.org/10.1002/qua.560470107

Cerón-Carrasco, J.P. When virtual screening yields inactive drugs: dealing with false theoretical friends. *ChemMed- Chem*. 2022, 17, e202200278. https://doi.org/10.1002/cmdc.202200278.

Clara, D.; Christ, M.Z.; Jan, M. K. Mining electronic laboratory notebooks: analysis, retrosynthesis, and reaction based enumeration. *J Chem Inf Model*. 2012, 52, 1745 - 1756. https://doi.org/10.1021/ci300116p

Cohen, N.; Benson, S.W. Estimation of heats of formation of organic compounds by additivity methods. *Chem Rev*. 1993, 93, 2419 - 2438. https://doi.org/10.1021/cr00023a005

Dallakyan, S.; Olson, A.J. Small-molecule library screening by docking with PyRx. *Methods mol biol*. 2015, 1263, 243 – 250. https://doi.org/10.1007/978-1-4939-2269-7_19

De Oliveira, D.R.; Tintino, S.R.; Braga, M.F.; Boligon, A.A.; Athayde, M.L.; Coutinho, H.D.; de Menezes, I.R.; Fachinetto, R. *In vitro* antimicrobial and modulatory activity of the natural products silymarin and silibinin. *Biomed Res Int*. 2015, 292797. https://doi.org/10.1155/2015/292797.

Dhaliwal, J.S.; Moshawih, S.; Goh, K.W.; Loy, M.J.; Hossain, M.S.; Hermansyah, A.; Kotra, V.; Kifli, N.; Goh, H.P.; Dhaliwal, S.K.S.; Yassin, H.; Ming, L.C. Pharmacotherapeutics applications and chemistry of chalcone derivatives. *Molecules*. 2022, 19, 7062. https://doi.org/10.3390/molecules27207062.

Du, X.; Li, Y.; Xia, Y.L.; Ai, X.M.; Liang, J.; Sang, P, *et al.* Insights into protein-ligand interactions: mechanisms, models, and methods. *Int J Mol Sci*. 2016, 17, 144. https://doi.org/10.3390/ijms17020144

Ertl, P.; Schuffenhauer, A. Estimation of synthetic accessibility score of drug-like molecules based on molecular complexity and fragment contributions. *J Cheminform.* 2009, 1, 8. https://doi.org/10.1186/1758-2946-1-8

Ertl, P.; Altmann, E.; Racine, S.; Lewis, R. Ring replacement recommender: ring modifications for improving biological activity. *Eur J Med Chem.* 2022, 238, 114483, https://doi.org/10.1016/j.ejmech.2022.114483

Fahad, M.; Al-Khodairy, M.; Kalim, A.; Khan, M.K.; Manogaran, S.P.; Salman, A, *et al*. In Silico prediction of mechanism of erysolin induced apoptosis in human breast cancer cell lines. *American J. Bioinform. Res*. 2013, 3, 62 – 71. https://doi.org/10.5923/j.bioinformatics.20130303.03

Filimonov, D.A.; Lagunin, A.A.; Gloriozova, T.A.; Rudik, A.V.; Druzhilovskii, D.S.; Pogodin, P.V. *et al*. Prediction of the biological activity spectra of organic compounds using the PASS online web resource. *Chem. heterocycl comp*. 2014, 50, 444 – 457. https://doi.org/10.1007/s10593-014-1496-1

Fraipont, C.; Alexeeva, S.; Wolf, B. The integral membrane *FtsW* protein and peptidoglycan synthase PBP3 form a subcomplex in *Escherichia coli*. *Microbiology*. 2011, 157, 251 – 259. https://doi.org/10.1099/mic.0.040071−0

Gao, T.; Zeng, Z.; Wang, G.; Sun, S.; Liu, Y. Synthesis of ethylene tethered isatin-coumarin hybrids and evaluation of their *in vitro* antimycobacterial activities. *J Heterocycl Chem.* 2018, 55, 1484 -1488. https://doi.org/10.1002/jhet.3161

Garbett, N.C.; Chaires, J.B. Thermodynamic studies for drug design and screening. *Expert Opin Drug Discov*. 2012, 7, 299 - 314. https://doi.org/10.1517/17460441.2012.666235

Gordon, E.; Mouz, N.; Duee, E.; Dideberg, O. The crystal structure of the penicillin-binding protein 2x from Streptococcus pneumoniae and its acyl-enzyme form: implication in drug resistance. *J Mol Biol*. 2000, 299, 477 - 485. https://doi.org/10.1006/jmbi.2000.3740.

Hamdi, N.; Bouabdallah, F.; Romerosa, A.; Benhassen, R. Expedious synthesis for α, β-unsaturated coumarin derivatives using boran chelates: a novel class of potential antibacterial and antioxidant agents. *Comptes Rendus Chim.* 2010, 13, 1261 - 1268. https://doi.org/10.1016/j.crci.2009.10.001

Hospital, A.; Goñi, J.R.; Orozco, M.; Gelpí, J.L. Molecular dynamics simulations: advances and applications. *Adv Appl Bioinform Chem*. 2015, 19, 37 - 47. https://doi.org/10.2147/AABC.S70333.

Hu, C-M.; Luo, Y-X.; Wang, W-J.; Li, J-P.; Li, M-Y.; Zhang, Y-F.; Xiao, D.; Lu, L.; Xiong, Z.; Feng, N.; Li, C. Synthesis and evaluation of coumarin- chalcone derivatives as α-glucosidase inhibitors. *Front Chem*. 2022, 10, 926543. https://doi.org/10.3389/fchem.2022.926543

Hu, Y.; Shen, Y.; Wu, X.; Tu, X.; Wang, G.X. Synthesis and biological evaluation of coumarin derivatives containing imidazole skeleton as potential antibacterial agents. *Eur J Med Chem.* 2018, 143, 958 – 969. https://doi.org/10.1016/j.ejmech.2017.11.100

Hughes, J.P.; Rees, S.; Kalindjian, S.B.; Philpott, K.L. Principles of early drug discovery. *Br J Pharmacol*. 2011, 162, 1239 - 1249. https://doi.org/10.1111/j.1476-5381.2010.01127.x.

Jing X.; Zhang, Y.; Huan, Z.; Yang, J., Cheng, J. Catalytic Vilsmeier–Haack reactions for C1-deuterated formylation of indoles. *J Org Chem.* 2022, 87, 15539 - 15546. https://doi.org/10.1021/acs.joc.2c02085

Johannes, J.; Jayarama-Naidu, R.; Meyer, F.; Wirth, E.K.; Schweizer, U.; Schomburg, L.;Köhrle, J.; Renko, K. Silychristin, a flavonolignan derived from the milk thistle, is a potent inhibitor of the

thyroid hormone transporter MCT8. *Endocrinology*. 2016, 157, 1694 -1701. https://doi.org10.1210/en.2015-1933.

Kang, H.K.; Kim, H.Y.; Cha, J.D. Synergistic effects between silibinin and antibiotics on methicillin-resistant *Staphylococcus aureus* isolated from clinical specimens. *Biotechnol J*. 2011, 6, 1397 - 408. https://doi.org/10.1002/biot.201000422

Khumbulani, M.; Alayande, K.A.; Sabiu, S. Orientin Enhances colistin-mediated bacteria lethality through oxidative stress involvement. *Evid Based Complement Alternat Med*. 2022, 3809232. https://doi.org/10.1155/2022/3809232

Koes, D.R.; Camacho, C.J. ZINCPharmer: pharmacophore search of the ZINC database. *Nucleic Acids Res*. 2012, 40, 409 - 414. https://doi.org/10.1093/nar/gks378.

Kren, V.; Walterova, D. Silybin and silymarin-new effects and applications. *Biomed Pap Med. Fac Univ Palacky Olomouc Czech Repub.* 2005, 149, 29 – 41. https://doi.org/10.5507/bp.2005.002.

Kruse, H.; Goerigk, L., Grimme, S. Why the Standard B3LYP/6-31G* MDel Chemistry Should Not Be Used in DFT calculations of molecular thermochemistry: understanding and correcting the problem. *J Org Chem.* 2012, 77, 10824 -10834. https://doi.org/10.1021/jo302156p.

Kumar, V.; Tang, C.; Bethel, C.R.; Papp-Wallace, K.M.; Wyatt, J.; Desarbre, E.; Bonomo, R.A.; Akker, F.V. Structural insights into ceftobiprole inhibition of *Pseudomonas aeruginosa* penicillin-binding Protein 3. *Antimicrob Agents Chemother*. 2020, 64, e00106-20. https://doi.org/10.1128/AAC.00106-20

Land, A.D.; Tsui, H.C.; Kocaoglu, O.; Vella, S.A.; Shaw, S.L.; Keen, S.K. *et al.* Requirement of essential Pbp2x and GpsB for septal ring closure in *Streptococcus pneumoniae* D39. *Mol. Microbiol*. 2013, 90, 939 - 955. https://doi.org/10.1111/mmi.12408

Lanrewaju, A. A.; Enitan-Folami, A. M.; Nyaga, M. M.; Sabiu, S.; Swalaha, F. M. Metabolites profiling and cheminformatics bioprospection of selected medicinal plants against the main protease and RNA-dependent RNA polymerase of SARS-CoV-2. *J. Biomol. Struct. Dyn*. 2023, 1 - 21. https://doi.org/10.1080/07391102.2023.2236718

Lee, D.G.; Kim, H.K.; Park, Y.; Park, S.C.; Woo, E.R.; Jeong, H.G.; Hahm. K.S. Gram-positive bacteria specific properties of silybin derived from *Silybum marianum*. *Arch. Pharm. Res*. 2003b, 26, 597 - 600. https://doi.org/10.1007/BF02976707.

Lee, Y.S.; Jang, K.A; Cha, J.D. Synergistic antibacterial effect between silibinin and antibiotics in oral bacteria. *J Biomed Biotechnol*. 2012, 618081. https://doi.org/10.1155/2012/618081

Liang, Z.; Li, Q.X. π-Cation interactions in molecular recognition: perspectives on pharmaceuticals and pesticides. *J Agric Food Chem*. 2018, 66, 3315 - 3323, https://doi.org/10.1021/acs.jafc.8b00758

Lien, E.J.; Guo, Z.R.; Li, R.L.; Su, C.T. Use of dipole moment as a parameter in drug-receptor interaction and quantitative structure-activity relationship studies. *J. Pharm. Sci.* 1982, 71, 641-655. https://doi.org/10.1002/jps.2600710611.

Lim, P.K.; Julca, I.; Mutwil, M. Redesigning plant specialized metabolism with supervised machine learning using publicly available reactome data. *Comput Struct Biotechnol J*. 2023, 18, 1639 - 1650. https://doi.org/10.1016/j.csbj.2023.01.013

Lipinski, C.A.; Lombardo, F.; Dominy, B.W. Experimental and computational approaches to estimate solubility and permeability in drug discovery and development settings. *Adv Drug Deliv Rev*. 2001, 46, 3 – 26. https://doi.org/10.1016/S0169−409X(00)00129−0

Lobanov, M.Y.; Bogatyreva, N.S.; Galzitskaya, O.V. Radius of gyration as an indicator of protein structure compactness. *Mol Biol.* 2008, 42, 623 – 628. https://doi.org/10.1134/S0026893308040195

Luo J.; Xue, Z.Q.; Liu, W.M.; Wu, J.L.; Yang, Z.Q. Koopmans' theorem for large molecular systems within density functional theory. *J Phys Chem*. 2006, 110, 12005 - 12009. https://doi.org/10.1021/jp063669m

Matteo T.; Degiacomi, S.T.; Chris Greenwell, H.; Valentina E. Assessing convergence of molecular dynamics simulations of interfaces. *Comput Phys Commun*, 2021, 269, 108126, https://doi.org/10.1016/j.cpc.2021.108126.

Mills, N. "ChemDraw Ultra 10.0". *J. Am. Chem. Soc*. 2006, 128, 13649 - 13650. https://doi.org/10.1021/ja0697875.

Murali, M. Ahmed, F.; Gowtham, H.G.; Aribisala, J.O.; Abdulsalam, R.A.; Shati, A.A.; Alfaifi, M.Y.; Sayyed, R.Z.; Sabiu, S.; Amruthesh, K.N. "Exploration of CviR-mediated quorum sensing inhibitors from *Cladosporium* spp. against *Chromobacterium violaceum* through computational studies." *Sci. Rep.* 2023, 13, 15505 - 15505. https://doi.org/10.1038/s41598-023-42833-4.

Nelson, D.E.; Young, K.D. Contributions of PBP 5 and DDcarboxypeptidase penicillin−binding proteins to maintenance of cell shape in *Escherichia coli*. *J Bacteriol.* 2001, 183, 3055 – 3064. https://doi.org/10.1128/JB.183.10.3055-3064.2001

Otero, L. H.; Rojas-Altuve, A.; Llarrull, L. I.; Carrasco-Lopez, C.; Kumarasiri, M.; *et al.* How allosteric control of Staphylococcus aureus penicillin binding protein 2a enables methicillin resistance and physiological function. *Proc Natl Acad Sci.* 2013, 110, 16808 – 16813. https://doi.org/10.1073/pnas.1300118110

Pavia, D.L.; Lampman, G.M.; Kriz, G.S.; Vyvyan, J.R. Introduction to spectroscopy. Saunders Golden Sunburst Series, Brooks/Cole, 2009. Available: https://books.google.com.ng/books?id=6W0QwQEACAAJ.

Pawełczyk, A.; Sowa-Kasprzak, K.; Olender, D.; Zaprutko, L. Molecular consortia—various structural and synthetic concepts for more effective therapeutics synthesis. *Int J Mol Sci.* 2018, 19, 1104. https://doi.org/10.3390/ijms19041104

Pearson, R.G. Absolute electronegativity and hardness correlated with molecular orbital theory. *PNAS*. 1986, 83, 8440 - 8441. https://doi.org/10.1073/pnas.83.22.8440

Pearson, R.G. The HSAB Principle-more quantitative aspects. *Inorganica Chimica Actva.* 1995, 240, 93 - 98. https://doi.org/10.1016/0020-1693(95)04648-8sssss

Perrin, C.L.; Chang, K. the Complete mechanism of an aldol condensation. *J Org Chem*. 2016, 81, 5631 - 5635. https://doi.org/10.1021/acs.joc.6b00959

Pettersen, E.F.; Goddard, T.D.; Huang, C.C.; Couch, G.S.; Greenblatt, D.M.; Meng. E.C.; *et al*. UCSF Chimera–a visualization system for exploratory research and analysis. *J Comput Chem.* 2004; 25: 1605 – 1612. https://doi.org/10.1002/jcc.20084

Politzer, P.; Murray, J.S. Clark, T. Halogen bonding and other σ-hole interactions: a perspective. *Phys Chem Chem Phys*. 2013, 15, 11178 – 11189. httsp://doi.org/10.1039/c3cp00054k.

Ramirex, D.; Caballero, J. Is it reliable to use common molecular docking methods for comparing the binding affinities of enantiomer pairs for their protein target. *Int J Mol Sci*. 2016, 17, 525 − 545. https://doi.org/10.1016/j.biotechadv.2018.11.013

Rathi, P.C.; Ludlow, R.F.; Verdonk, M.L. Practical high-quality electrostatic potential surfaces for drug discovery using a graph-convolutional deep neural network. *J Med Chem*. 2020, 63, 8778 - 8790. https://doi.org/10.1021/acs.jmedchem.9b01129.

Sahoo, C.R.; Paidesetty, S.K.; Padhy, R.M. Norharmane as a potential chemical entity for development of anticancer drugs. *Eur J Med Chem*. 2019, 162, 752 - 764. https://doi.org/10.1016/j.ejmech.2018.11.024

Salih, T.; Pshtiwan, G. A. Rational design of novel compounds to serve as potential NDM-1 inhibitors using molecular docking, molecular dynamics simulation, and physicochemical studies, Mol Simul, 2023, 49, 1373 - 1387. https://doi.org/10.1080/08927022.2023.2232468

Sherif, S.R., Mohamed, A.; Ahmed A.E.; Ayman, M.K. Sweed, Design, synthesis, molecular dynamic simulation studies, and antibacterial evaluation of new spirocyclic aminopyrimidines, *J Mol Struct*. 2023, 1278, 134912. https://doi.org/10.1016/j.molstruc.2023.134912.

Singh, A.; Singh, J.V.; Rana, Kavita Bhagat, H.K.; Gulati, R.K.; Salwan, R.; Kajal Bhagat, G.; Kaur, N.; Singh, Randeep Kumar, H.; Singh, S.; Sharma, P.M.S. Monocarbonyl curcumin based molecular hybrids as potent antibacterial agents. ACS

Omega, 2019, 4, 11673-11684. https://doi.org/10.1021/acsomega.9b01109

Taha, T.Y.; Aboukhatwa, S.M.; Knopp, R.C.; Ikegaki, N.; Abdelkarim, H.; Neerasa, J., *et al.* Design, synthesis, and biological evaluation of tetrahydroisoquinoline-based histone deacetylase 8 selective inhibitors. *ACS Med Chem Lett.* 2017, 8, 824 – 829. https://doi.org/10.1021/acsmedchemlett.9b00336.

Tanwar, S.; Auberger, P.; Gillet, G.; DiPaola, M.; Tsaioun, K.; Villoutreix, B.O. A new ChEMBL dataset for the similarity-based target fishing engine fast target pred: annotation of an exhaustive list of linear tetrapeptides. *DIB.* 2022, 42, 108159. https://doi.org/10.1016/j.dib.2022.108159.

Tyagi, A.; Raina, K.; Singh, R. P.; Gu, M. *et al.*, Chemo preventive effects of silymarin and silibinin on *N*-butyl-*N*-(4-hydroxybutyl) nitrosamine induced urinary bladder carcinogenesis in male ICR mice. *Mol Cancer Ther.* 2007, *6*, 3248 – 3255. https://doi.org/10.1158/1535-7163.MCT-07-2006

Tyagi, A.K.; Agarwal, C.; Chan, D.C.; Agarwal, R. Synergistic anti-cancer effects of silibinin with conventional cytotoxic agents' doxorubicin, cisplatin and carboplatin against human breast carcinoma MCF-7 and MDA-MB468 cells. *Oncol. Rep.* 2004, 11, 493 - 499. https://doi.org/10.3892/or.11.2.493

Uhomoibhi, J.O. ; Shode, F.O. ; Idowu. K.A. *et al.* Molecular modelling identification of phytocompounds from selected African botanicals as promising therapeutics against druggable human host cell targets of SARS−CoV−2. *J Mol Graph Model*. 2022, 114, 108185. https://doi.org/10.1016/j.jmgm.2022.108185

Verdía, P.; Santamarta, F.; Tojo, E. Knoevenagel reaction in [MMIm][MSO_4]: synthesis of coumarins. *Molecules*. 2011, 16, 4379 - 4388. https://doi.org/10.3390/molecules16064379

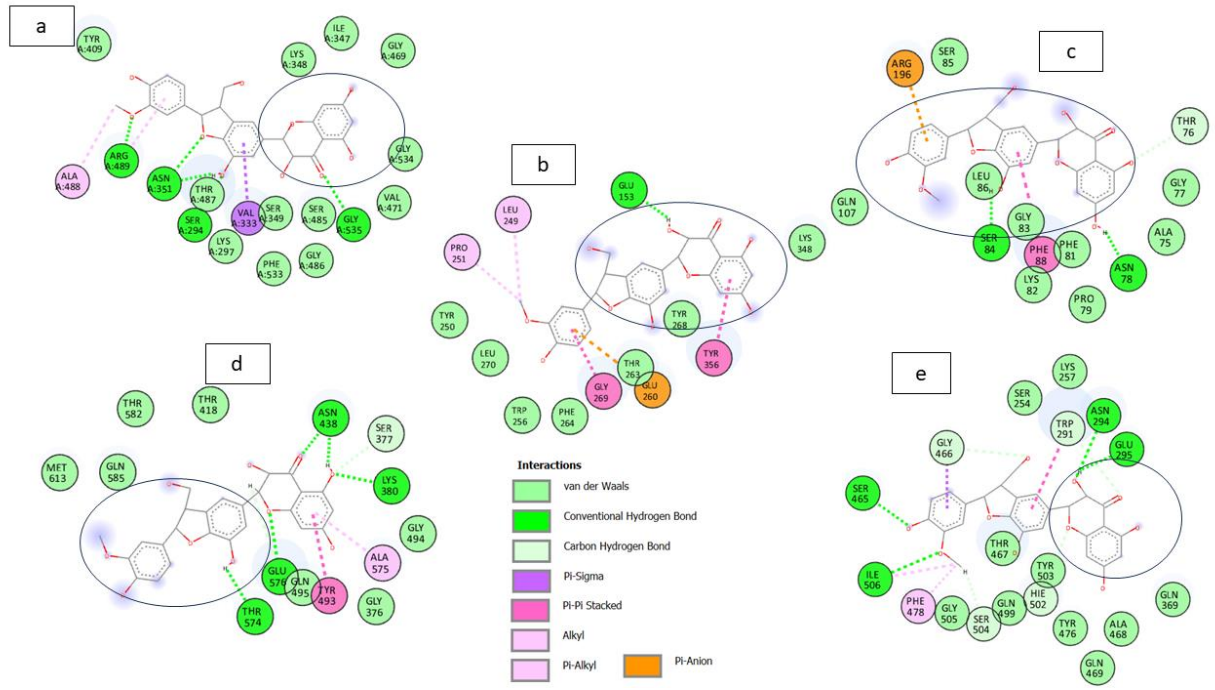
Verma, A.K.; Ahmed, S.F.; Hossain, M.S. Molecular docking and simulation studies of flavonoid compounds against PBP-2a of methicillin-resistant *Staphylococcus aureus*. *J Biomol Struct Dyn*. 2020, 1, 1 – 17. https://doi.org/10.1080/07391102.2021.1944911

Wadhwa, K.; Pahwa, R.; Kumar, M.; Kumar, S.; Sharma, P.C.; Singh, G.; Verma, R.; Mittal, V.; Singh, I.; Kaushik, D.; Jeandet, P. Mechanistic Insights into the Pharmacological Significance of Silymarin. *Molecules*. 2022, 27, 5327. https://doi.org/10.3390/molecules27165327.

Wang, S.; Dong, G.; Sheng, C. Structural simplification: an efficient strategy in lead optimization. *Acta Pharm Sin B*. 2019, 5, 880 - 901. https://doi.org/10.1016/j.apsb.2019.05.004.

Ylilauri, M.; Pentikäinen, O.T. MMGBSA as a tool to understand the binding affinities of filamin-peptide interactions. *J Chem Inf Model*. 2013, 53, 2626 – 2633. https://doi.org/10.1021/ci4002475.

Supplementary information

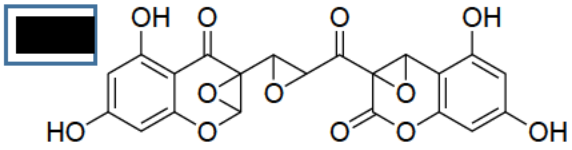


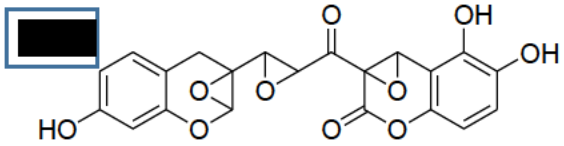
Supplementary Figure S1: Silicristin interactions with key penicillin binding proteins of clinically significant organisms (a) PBP3 of *Pseudomonas aeruginosa*, (b) PBP3 of *Escherichia coli* (c) PBP5 of *E. coli*, (d) PBP2a of *Staphylococcus aureus*, and (e) PBP2x of *Streptococcus pneumoniae.* Regions in black cycle had lesser interactions

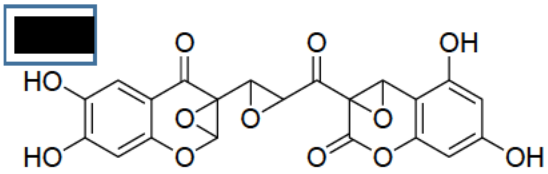
Supplementary Table S1: Numbers of important interactions formed by A, B and C subunits of silicristin with key PBPs of clinically important organisms.

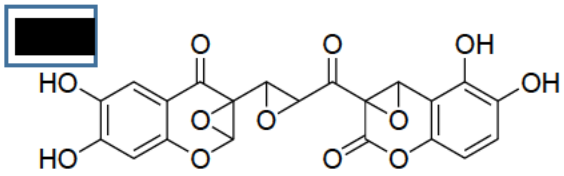
PBPs	Subunit A	Subunit B	Subunit C
PBP3 of *P. aeruginosa*	1 hydrogen bond 9 van der Waals forces	3 hydrogen bonds 1 Pi-Sigma 2 van der Waals forces	1 hydrogen bond 2 Alkyl/Pi-Alkyl
PBP3 of *E. coli*	1 hydrogen bond 1 Pi-Pi Stacked	1 van der Waals forces	2 Alkyl/Pi-Alkyl 1 Pi-Pi Stacked 1 Pi-Anion

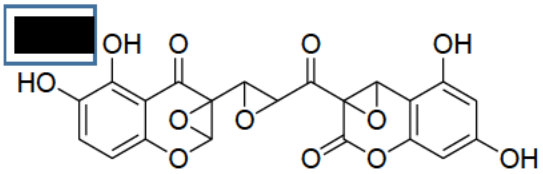
			1 Pi-Pi Stacked
PBP5 of *E coli*	1 hydrogen bond 5 van der Waals forces.	1 hydrogen bond 4 van der Waals forces. 1 Pi-Pi Stacked	1 Pi-Anion 1 Pi-Pi Stacked
PBP2a of *Staphylococcus aureus*	5 hydrogen bonds 1 Pi-Pi Stacked 1 Alkyl/Pi-Alkyl 4 van der Waals forces	1 hydrogen bonds 2 van der Waals forces	2 van der Waals forces
PBP2x of *Streptococcus pneumoniae*	2 hydrogen bonds 6 van der Waals forces	7 van der Waals forces 1 unfavourable bond	2 hydrogen bonds 3 Alkyl/Pi-Alkyl 2 van der Waals forces

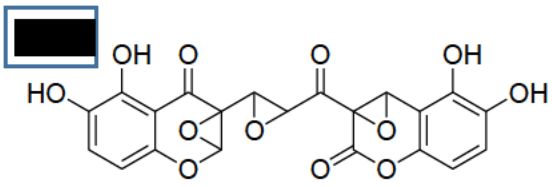


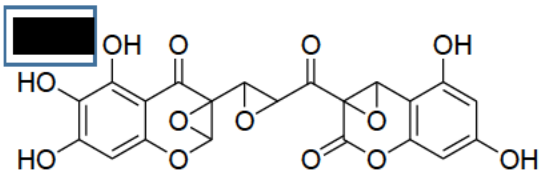


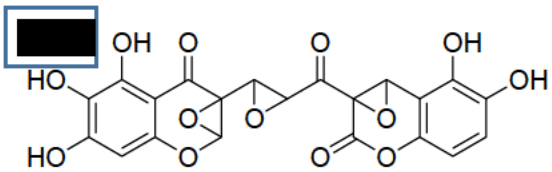


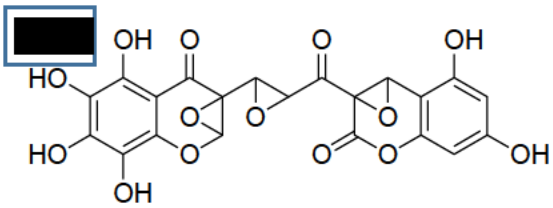


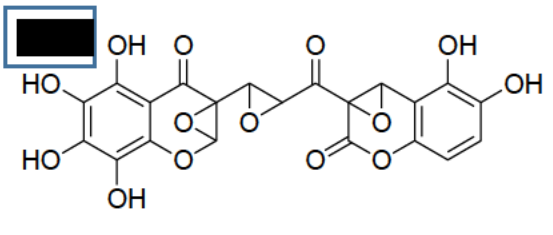


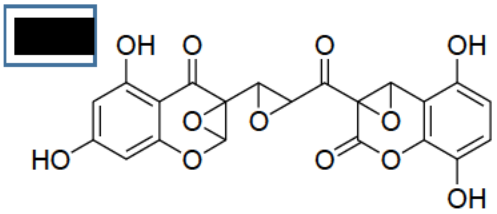


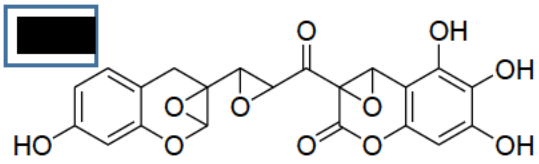


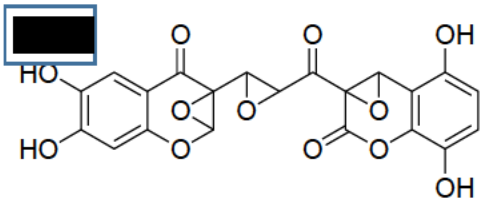


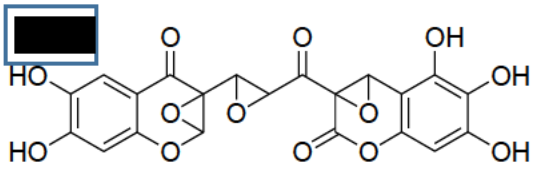


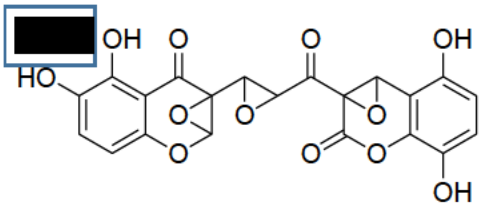


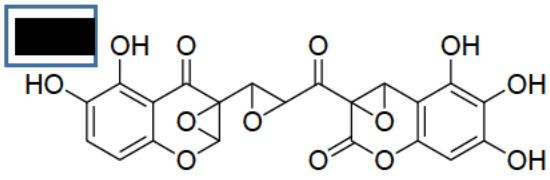


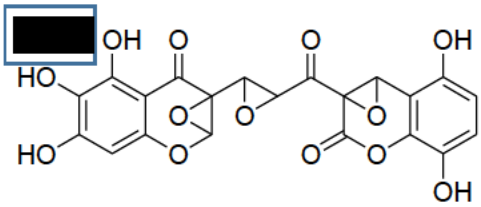


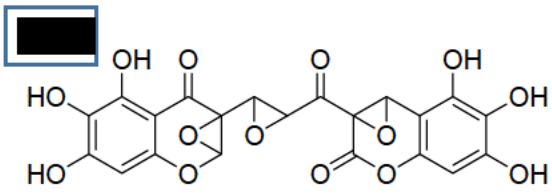


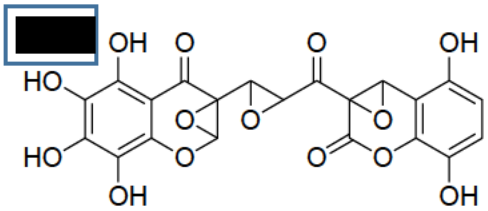


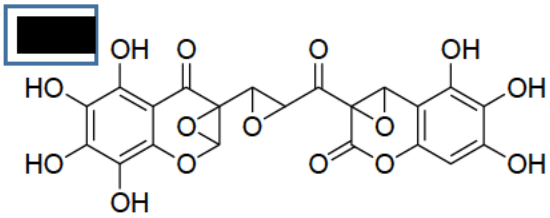


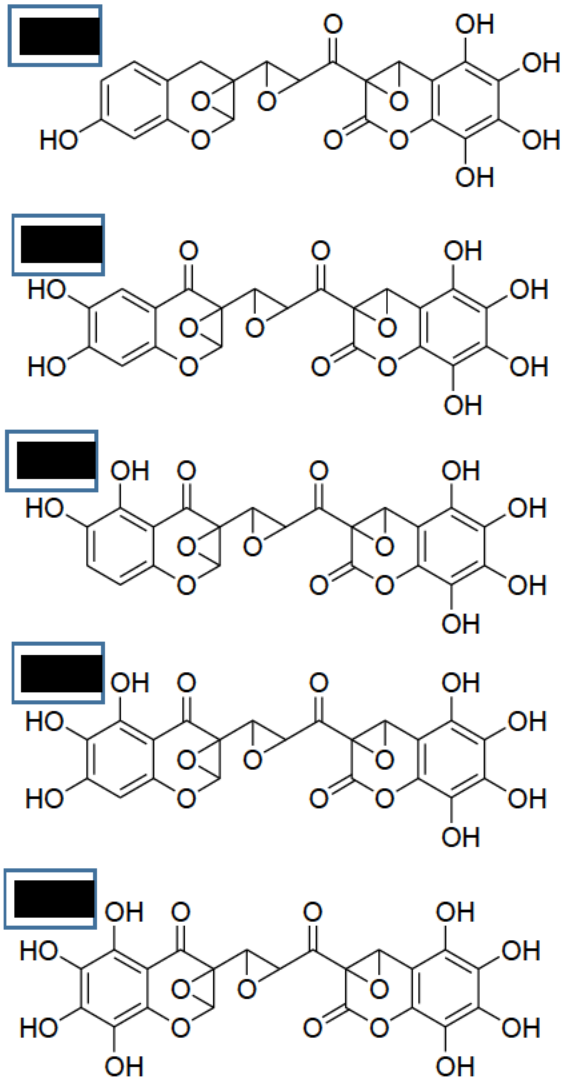




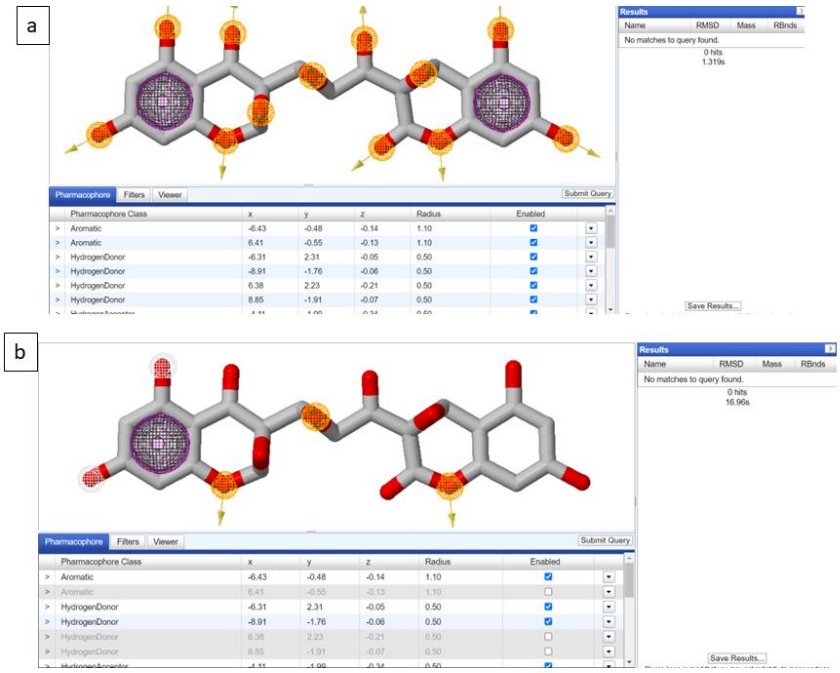




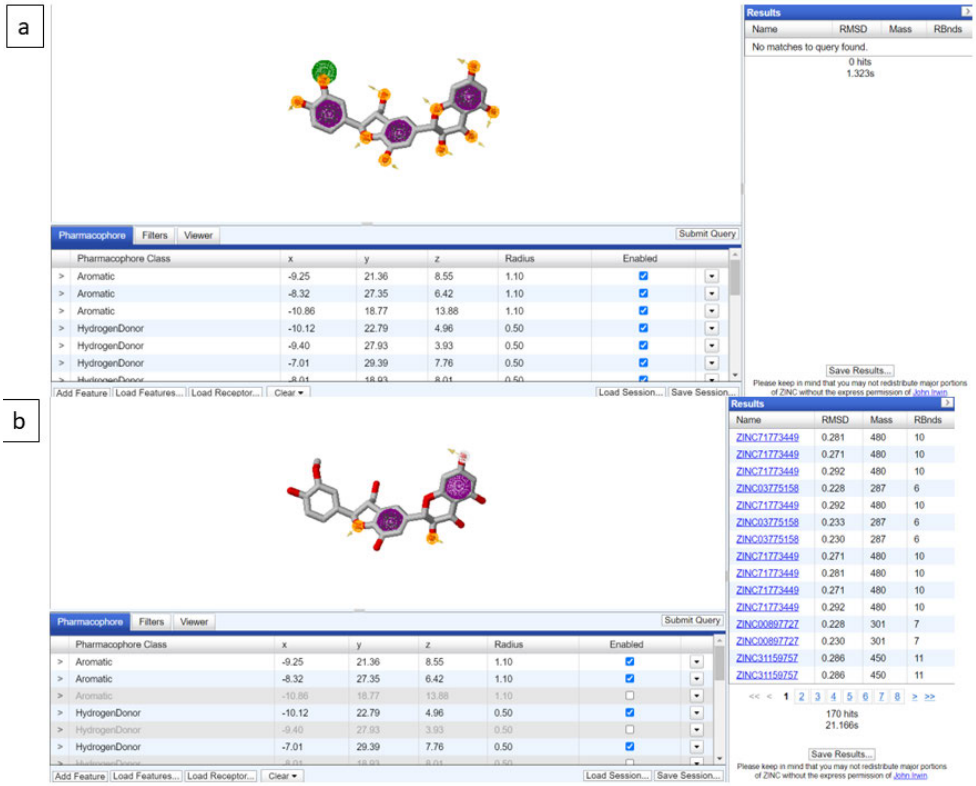




Supplementary Figure S2: 25 newly designed derivatives of chalcone bis-coumarin



Supplementary Figure S3: Similarity search using ligand-based pharmacophore for D1a (a) 100 % (b) 50 % refining.



Supplementary Figure S4: Similarity search using ligand-based pharmacophore for silicristin (a) at 100 % (b) 50 % refining

Supplementary Table S2: Docking scores (kcal/mol) and ADMET properties of derivatives against each of the PBPs

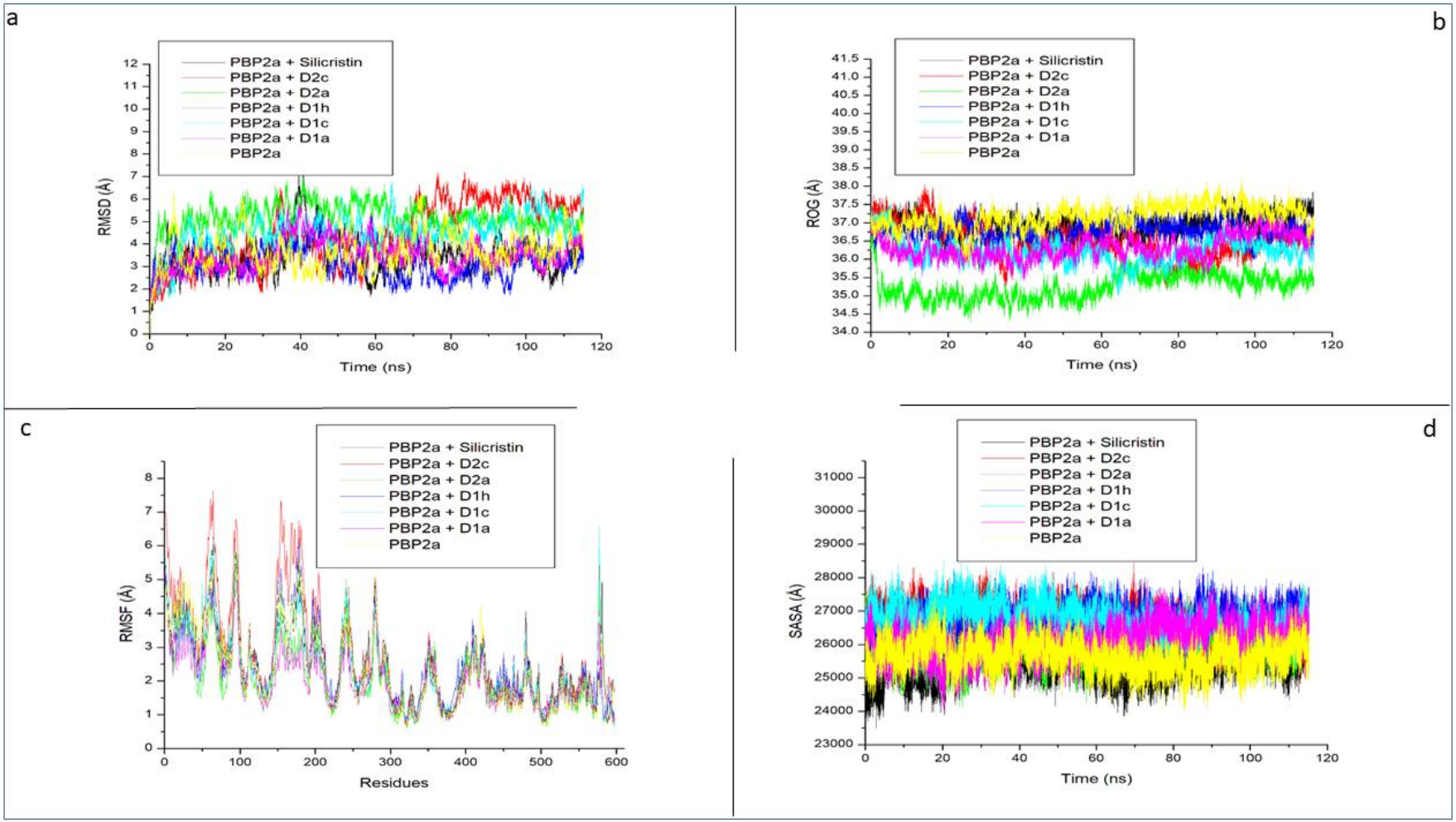
Ligands	*S. pneumonia* PBP2x		*S. aureus* PBP2a		*E. coli*		*P. aeruginosa*	LV < 2	WS	GI-A	BS	pgp	Inhibitor of Cytochrome P450s					TC
	Active	Allosteric	Active	Allosteric	PBP3	PBP5	PBP3						CYP 1A2	CYP 2C19	CYP 2C9	CYP 2D6	CYP 3A4	
Silichristin	-9.9	-9.9	-7.5	-8.4	-8.6	-9.4	-10.5	N(1)	S	L	0.55	N	N	N	N	N	Y	4
Derivatives																		
D1a	-10.5	-10.8	-8.9	-8.3	-9.6	-9.8	-11.1	N(1)	VS	L	0.55	Y	N	N	N	N	Y	4
D1b	-9.4	-10.9	-8.9	-7.4	-9.1	-9.6	-10.3	N(1)	VS	L	0.55	Y	N	N	N	N	N	4
D1c	-9.9	-11.0	-9.3	-7.8	-9.7	-10.3	-10.6	N(1)	VS	L	0.55	Y	N	N	N	N	N	4
D1d	-9.7	-10.5	-8.6	-7	-9.1	-9.7	-10.7	Y(2)	VS	L	0.17	Y	N	N	N	N	N	4
D1e	-9.7	-10.4	-8.8	-7.3	-8.7	-9.3	-10.7	Y(2)	VS	L	0.17	Y	N	N	N	N	N	4
D1f	-9.8	-10.4	-8.9	-7.4	-8.7	-9.8	-11.2	N(0)	VS	L	0.55	Y	N	Y	N	N	N	4
D1g	-10.2	-10.8	-8.8	-10.0	-9.3	-10.0	-11.0	N(1)	VS	L	0.55	Y	N	N	N	N	N	4
D1h	-10.1	-10.4	-9.2	-9.9	-9.6	-11.4	-11.5	N(1)	VS	L	0.55	Y	N	N	N	N	N	4
D1i	-9.7	-10.7	-8.7	-7.2	-9.0	-10.6	-10.5	Y(2)	VS	L	0.17	Y	N	N	N	N	N	4
D1j	-9.3	-10.6	-8.7	-7.4	-8.9	-10	-10.5	Y(2)	VS	L	0.17	Y	N	N	N	N	N	4
D2a	-9.7	-9.9	-9.2	-8.2	-9.2	-9.6	-11.2	N(1)	VS	L	0.55	Y	N	N	N	N	N	4
D2b	-9.8	-10.7	-9.2	-7.5	-8.7	-9.9	-10.6	N(1)	VS	L	0.55	Y	N	N	N	N	N	4
D2c	-10.1	-10.5	-8.9	-7.8	-9.7	-10.7	-11.3	N(1)	VS	L	0.55	Y	N	N	N	N	N	4
D2d	-9.6	-10.3	-9.3	-7.6	-8.9	-10.2	-10.8	Y(2)	VS	L	0.17	Y	N	N	N	N	N	4
D2e	-9.6	-10.8	-8.8	-7.5	-8.5	-9.3	-10.8	Y(2)	VS	L	0.17	Y	N	N	N	N	N	4
D2f	-9.9	-10.7	-8.6	-7.4	-8.9	-9.3	-10.6	N(1)	VS	L	0.55	Y	N	N	N	N	N	4
D2g	-9.8	-10.8	-8.6	-7.5	-9.1	-9.3	-10.4	Y(2)	VS	L	0.17	Y	N	N	N	N	N	4
D2h	-10.0	-10.9	-9	-7.2	-8.9	-10.4	-10.8	Y(2)	VS	L	0.17	Y	N	N	N	N	N	4
D2i	-9.1	-10.7	-8.5	-7.3	-8.6	-9.5	-10.5	Y(2)	VS	L	0.17	Y	N	N	N	N	N	4
D2j	-9.2	-10.5	-9	-7.3	-8.5	-8.7	-10.6	Y(3)	VS	L	0.17	Y	N	N	N	N	N	4
D3a	-10.1	-11.0	-8.9	-7.6	-8.8	-9.2	-11.1	Y(2)	VS	L	0.17	Y	N	N	N	N	N	4
D3b	-9.7	-10.6	-8.8	-7.1	-8.8	-8.8	-10.3	Y(2)	VS	L	0.17	Y	N	N	N	N	N	4
D3c	-9.9	-10.5	-9.3	-7.2	-8.8	-10.3	-10.8	Y(2)	VS	L	0.17	Y	N	N	N	N	N	4
D3d	-9.6	-10.6	-8.8	-7.3	-8.7	-9.4	-10.8	Y(3)	VS	L	0.17	Y	N	N	N	N	N	2
D3e	-9.1	-10.6	-9.2	-7.1	-8.2	-8.6	-10.6	Y(3)	S	L	0.17	Y	N	N	N	N	N	2

Abbreviations: LV: Lipinski violation, MS: water solubility, GI-A: gastrointestinal tract absorption, TC: Toxicity class, pgp: P-glycoprotein, N: No, Y: Yes, L: Low, S: soluble, VS: very soluble, MS: moderately soluble

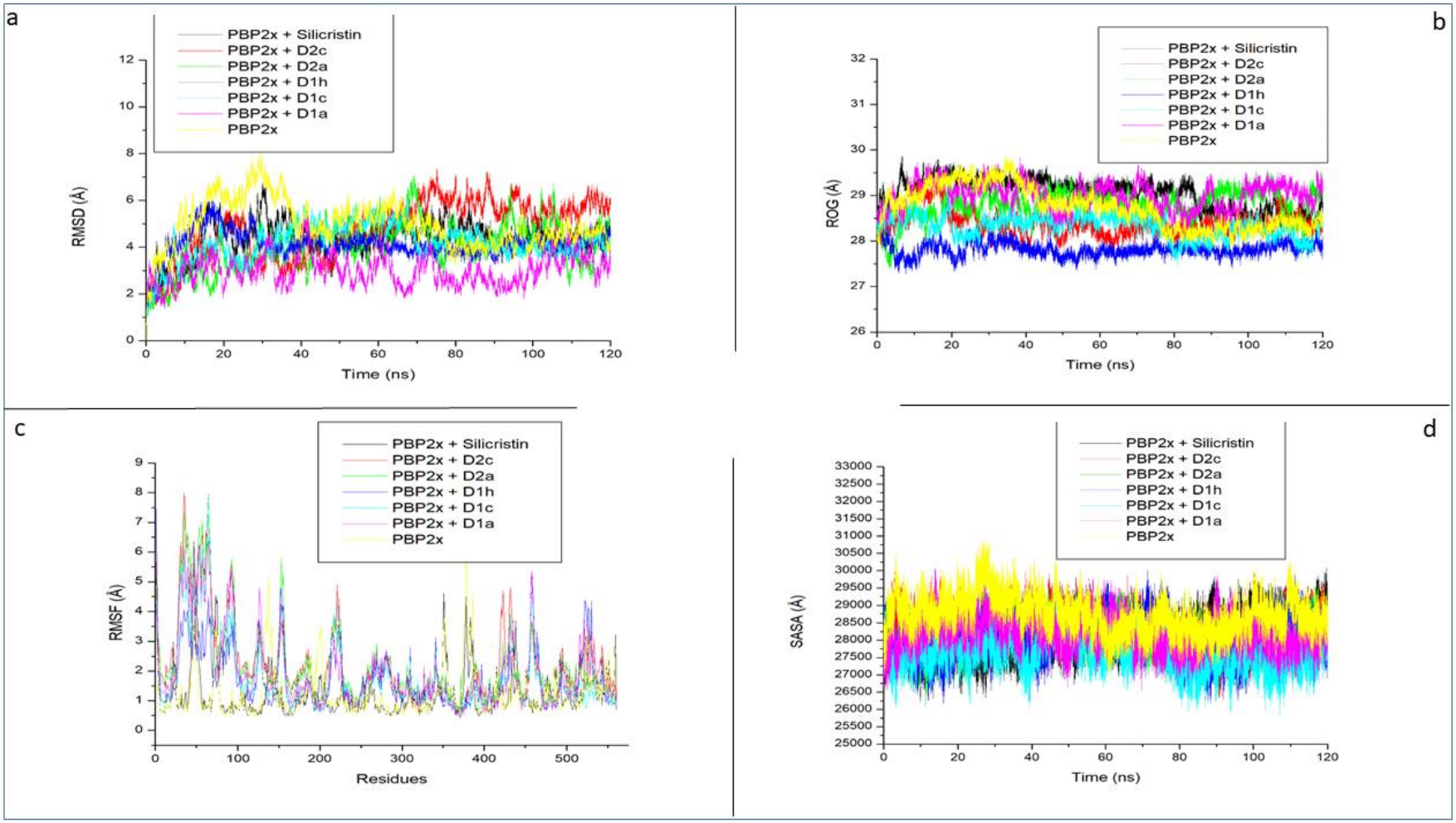
Table S3: Average RMSD, RMSF, ROG and SASA values of top-ranked-ranked derivatives against each of the key PBPs of the investigated bacteria

Targets	Ligands	RMSD (Å)	RMSF (Å)	ROG (Å)	SASA (Å)
E. coli	PBP3				
	Unliganded	3.50 ± 0.79	1.51 ± 1.38	23.39 ± 0.17639	17996.66 ± 383
	D1a	2.67 ± 0.44	1.53 ± 1.29	23.85 ± 0.16	18149.05 ± 314
	D1c	2.55 ± 0.47	1.43 ± 1.24	23.29 ± 0.18	17812.02 ± 493
	D1h	2.21 ± 0.43	1.25 ± 1.08	23.17 ± 0.12	17570.12 ± 345
	D2a	2.55 ± 0.36	1.20 ± 0.86	23.12 ± 0.13	17589.54 ± 357
	D2c	2.31 ± 0.28	1.29 ± 0.99	23.58 ± 0.24	17780.10 ± 330
	Silicristin	3.97 ± 0.70	1.44 ± 1.47	22.95 ± 0.25	18051.17 ± 380
	PBP5				
	Unliganded	2.15 ± 0.48	1.64 ± 0.82	24.54 ± 0.34	15727.36 ± 392
	D1a	2.96 ± 0.51	1.84 ± 0.82	24.96 ± 0.35	15793.42 ± 351
	D1c	2.50 ± 0.58	1.63 ± 1.11	24.93 ± 0.35	15870.72 ± 311
	D1h	3.44 ± 0.78	1.82 ± 0.90	24.64 ± 0.34	16048.53 ± 313
	D2a	2.65 ± 0.52	1.85 ± 0.92	24.29 ± 0.35	15863.10 ± 296
	D2c	3.19 ± 0.59	1.73 ± 0.82	24.66 ± 0.31	16011.95 ± 299
	Silicristin	3.07 ± 0.82	1.92 ± 1.30	25.03 ± 0.54	16306.53 ± 419
P. aeruginosa PBP3 +	Unliganded	2.88 ± 1.10	1.23 ± 0.05	30.39 ± 0.44	23071.92 ± 354
	D1a	3.25 ± 0.67	1.85 ± 1.06	30.46 ± 0.30	24314.68 ± 499
	D1c	2.33 ± 0.39	1.58 ± 0.95	29.96 ± 0.33	23820.46 ± 364
	D1h	4.06 ± 0..80	**1.63** ± 0.90	29.35 ± 0.43	24026.30 ± 417
	D2a	2.34 ± 0..45	1.58 ± 0.95	30.48 ± 0.30	24340.24 ± 445
	D2c	2.73 ± 0.43	1.85 ± 1.09	29.80 ± 0.38	23728.54 ± 376
	Silicristin	2.56 ± 0.50	1.89 ± 0.04	29.89 ± 0.34	23277.40 ± 405
S. pneumoniae PBP2x +	Active site				
	Unliganded	6.32 ± 1.08	1.76 ± 1.02	30.04 ± 0.17	27812.69 ± 465
	D1a	3.41 ± 0.83	1.72 ± 0.97	28.99 ± 0.25	27573.32 ± 476
	D1c	6.18 ± 1.43	2.12 ± 1.53	28.86 ± 0.20	27706.30 ± 588
	D1h	5.22 ± 1.69	2.41 ± 1.50	29.17 ± 0.32	27568.83 ± 546
	D2a	2.95 ± 0.50	1.79 ± 0.99	28.12 ± 0.31	28014.21 ± 398
	D2c	3.13 ± 0.55	2.04 ± 1.14	29.06 ± 0.29	28939.03 ± 449
	Silicristin	4.90 ± 1.72	2.62 ± 2.18	29.63 ± 0.41	28080.16 ± 436
	Allosteric				
	Unliganded	4.36 ± 0.99	1.24 ± 0.79	28.74 ± 0.44	22380.62 ± 352
	D1a	3.01 ± 0.65	1.96 ± 1.25	29.00 ± 0.28	28717.81 ± 460
	D1c	4.17 ± 0.76	1.79 ± 1.18	28.32 ± 0.23	28213.46 ± 454
	D1h	4.12 ± 0.58	1.69 ± 0.96	27.82 ± 0.15	28089.49 ± 539
	D2a	4.00 ± 1.02	2.18 ± 1.29	28.79 ± 0.31	28151.36 ± 443
	D2c	4.72 ± 1.24	2.19 ± 1.32	28.39 ± 0.27	28246.77 ± 458

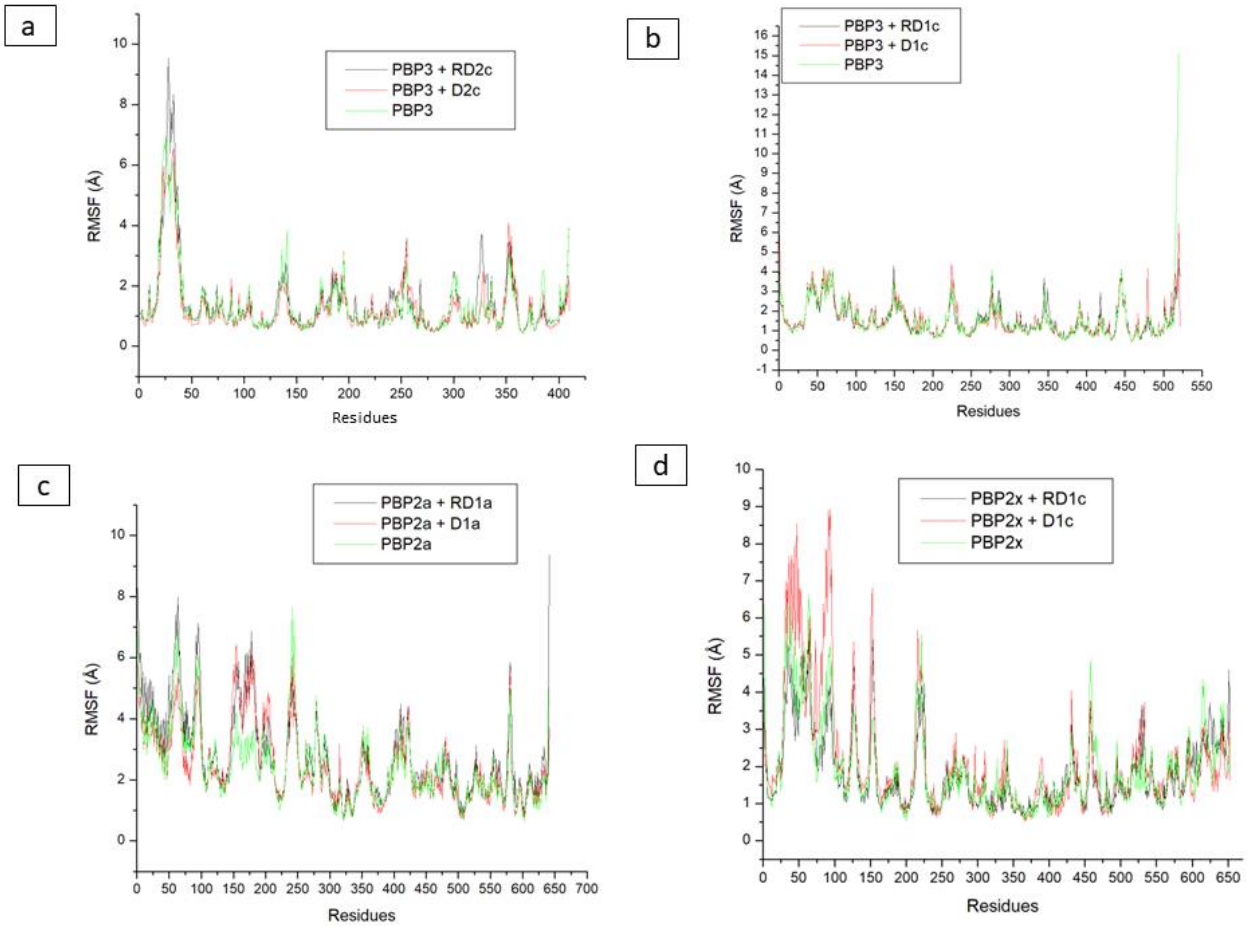
	Silicristin	4.36 ± 0.76	1.22 ± 0.79	29.03 ± 0.33	28094.59 ± 480
S. aureus PBP2a +	Active site				
	Unliganded	6.86 ± 1.18	3.77 ± 0.91	35.37 ± 0.45	26786.05 ± 473
	D1a	5.17 ± 1.21	2.58 ± 1.23	36.57 ± 0.34	26364.22 ± 447
	D1c	4.50 ± 1.21	3.29 ± 1.69	36.59 ± 0.59	27661.33 ± 526
	D1h	4.49 ± 1.14	2.73 ± 1.17	37.56 ± 0.26	27551.52 ± 486
	D2a	3.74 ± 1.01	2.76 ± 1.23	37.46 ± 0.37	27644.41 ± 545
	D2c	3.54 ± 0.89	2.64 ± 1.32	37.37 ± 0.31	27051.17 ± 478
	Silicristin	5.65 ± 2.34	2.26 ± 2.09	36.47 ± 1.15	27160.02 ± 545
	Allosteric site				
	Unliganded	3.66 ± 0.79	2.31 ± 1.17	37.18 ± 0.31	25631.49 ± 414
	D1a	3.49 ± 0.68	2.05 ± 0.90	36.32 ± 0.31	26079.61 ± 497
	D1c	4.52 ± 0.80	2.36 ± 1.08	36.22 ± 0.33	26705.91 ± 468
	D1h	3.18 ± 0.69	2.37 ± 1.03	36.77 ± 0.25	26687.55 ± 402
	D2a	5.18 ± 0.62	2.03 ± 0.93	35.24 ± 0.34	25993.88 ± 460
	D2c	4.41 ± 1.40	2.71 ± 1.51	36.52 ± 0.46	26596.70 ± 440
	Silicristin	3.48 ± 0.80	2.45 ± 1.11	36.93 ± 0.29	25466.88 ± 478



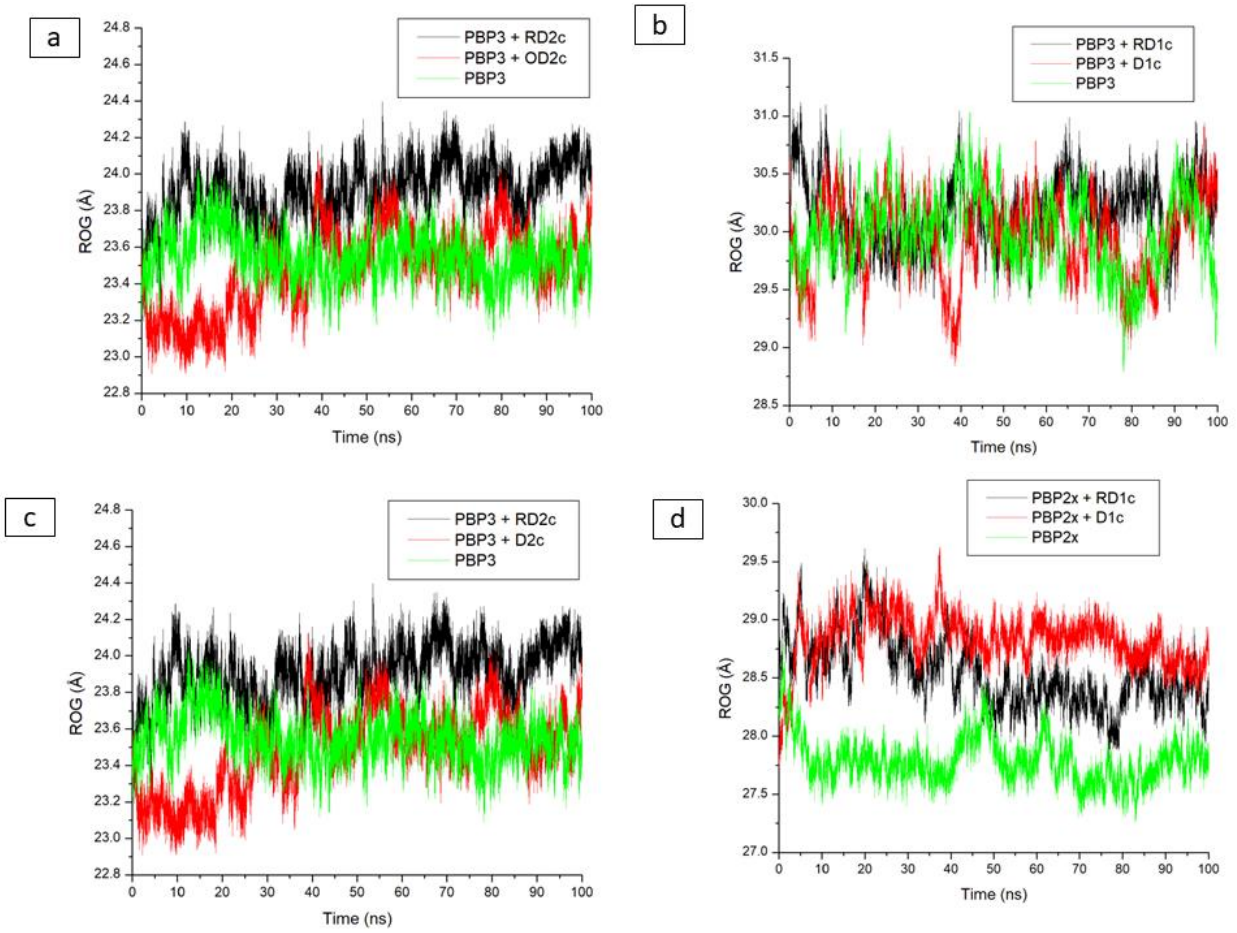
Supplementary Figure S5: Comparative RMSD (a), ROG (b), RMSF (c) and SASA (d) plot of top-ranked derivatives against the allosteric site of PBP2a of *S. aureus*



Supplementary Figure S6: Comparative RMSD (a), ROG (b), RMSF (c) and SASA (d) plot of top-ranked derivatives against the allosteric site of PBP2x of *S. pneumoniae*



Supplementary Figure S7: Comparative root means square fluctuation of reduced and oxidized best derivatives against (a) PBP3 of *E. coli* (b) PBP3 of *P. aeruginosa* (c) PBP2a of *S. aureus* and (d) PBP2x of *S. pneumoniae* over a 100 ns MD simulation

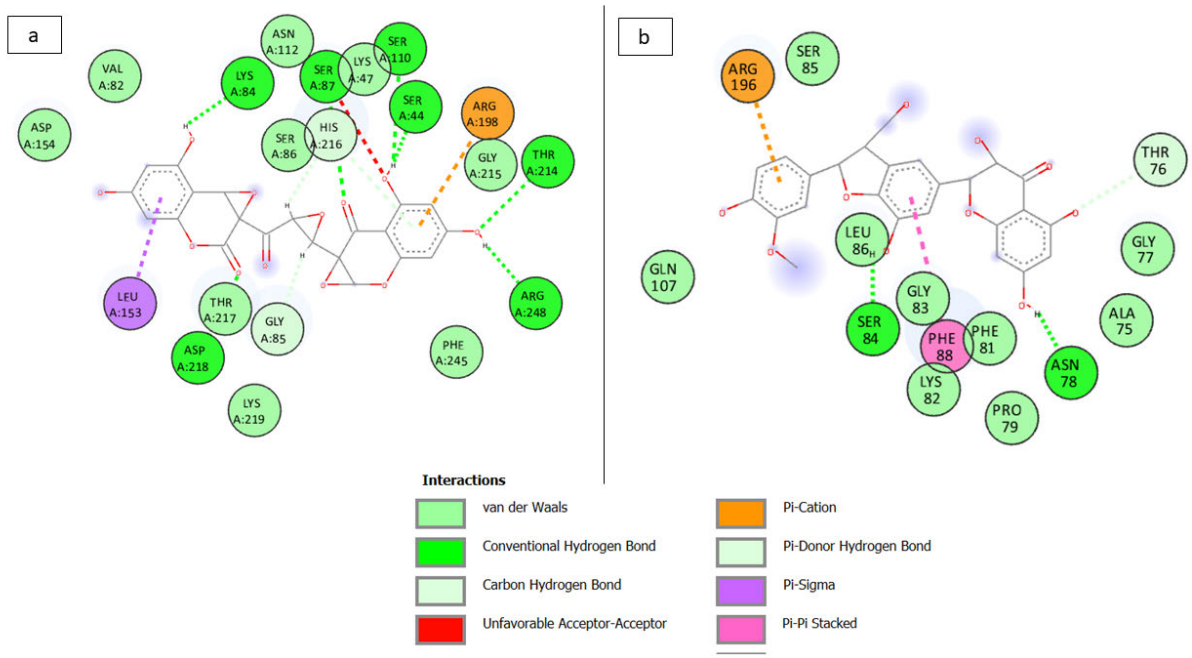


Supplementary Figure S8: Comparative root means square deviation of reduced and oxidized best derivatives against (a) PBP3 of *E. coli* (b) PBP3 of *P. aeruginosa* (c) PBP2a of *S. aureus* and (d) PBP2x of *S. pneumoniae* over a 100 ns MD simulation.

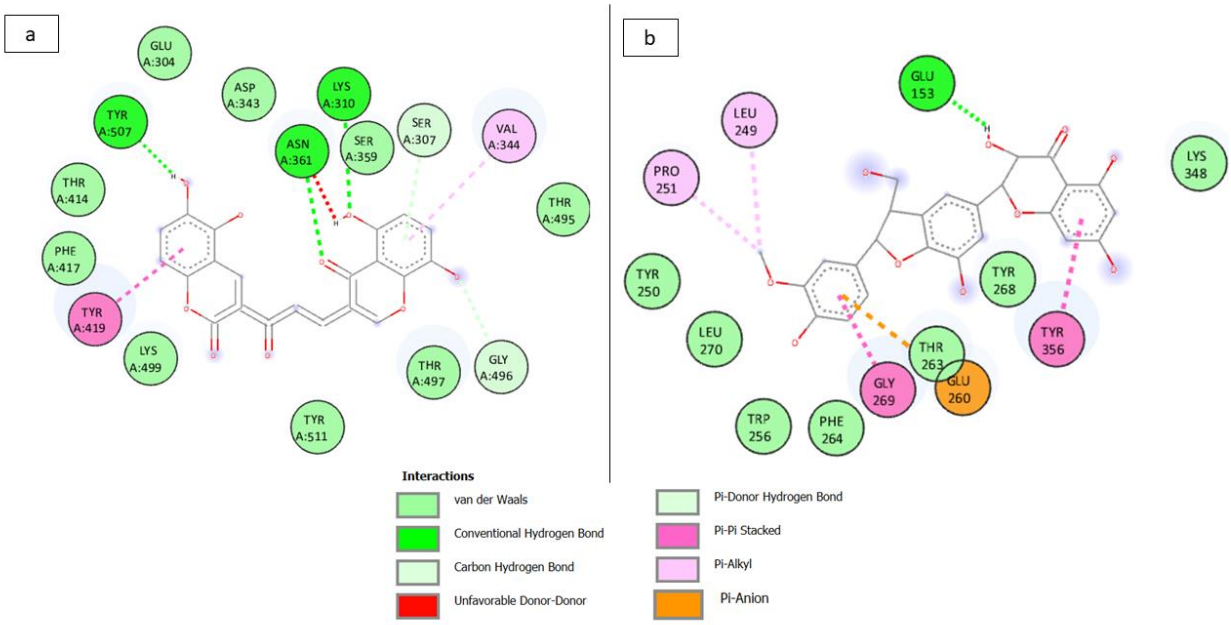
Supplementary Table S4: Effects of parent structure optimization on pharmacokinetics and toxicity properties of best derivatives

	LV < 2	WS	GI-A	BS	pgp	Inhibitor of Cytochrome P450s					TC
						CYP 1A2	CYP 2C19	CYP 2C9	CYP 2D6	CYP 3A4	
RD1a	N (0)	MS	L	0.55	N	N	N	N	N	N	5
RD1c	N (0)	MS	L	0.55	N	Y	N	Y	N	N	5
RD1h	N (0)	MS	L	0.55	N	Y	N	Y	N	N	5
RD2c	N (0)	MS	L	0.55	N	Y	N	Y	N	N	5

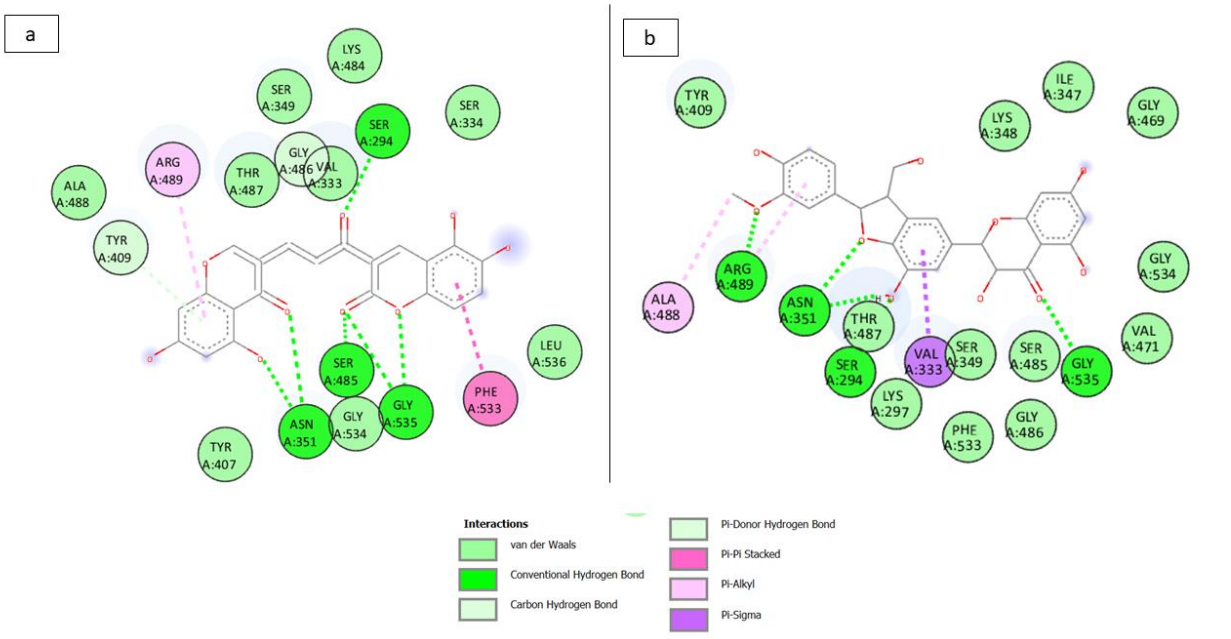
Abbreviations: LV: Lipinski violation, MS: water solubility, GI-A: gastrointestinal tract absorption, TC: Toxicity class, pgp: P-glycoprotein, N: No, Y: Yes, L: Low, S: soluble, VS: very soluble, MS: moderately soluble



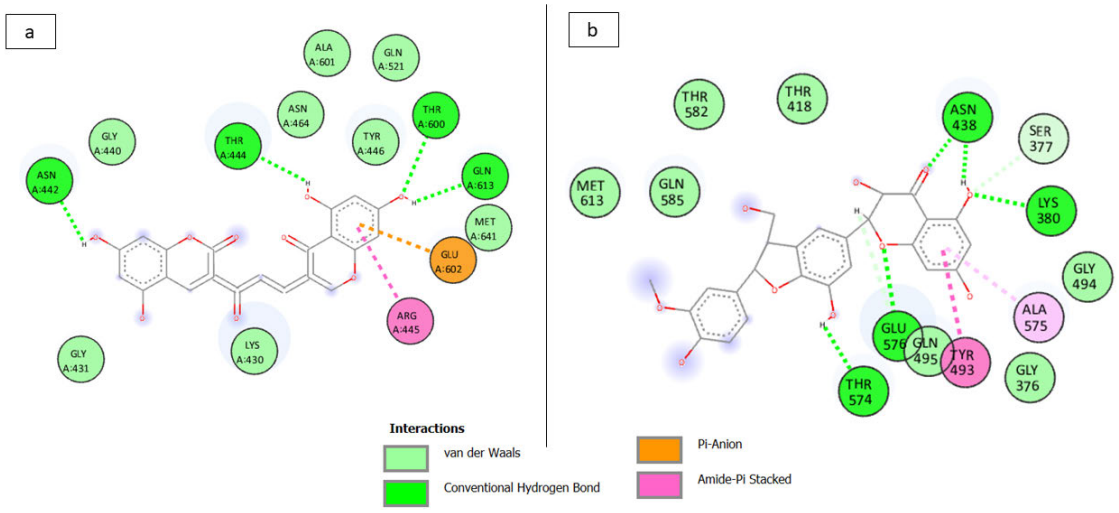
Supplementary Figure S9: Comparative interaction plots of D1a (a) and silicristin (b) against PBP5 of *E. coli* after MD simulation



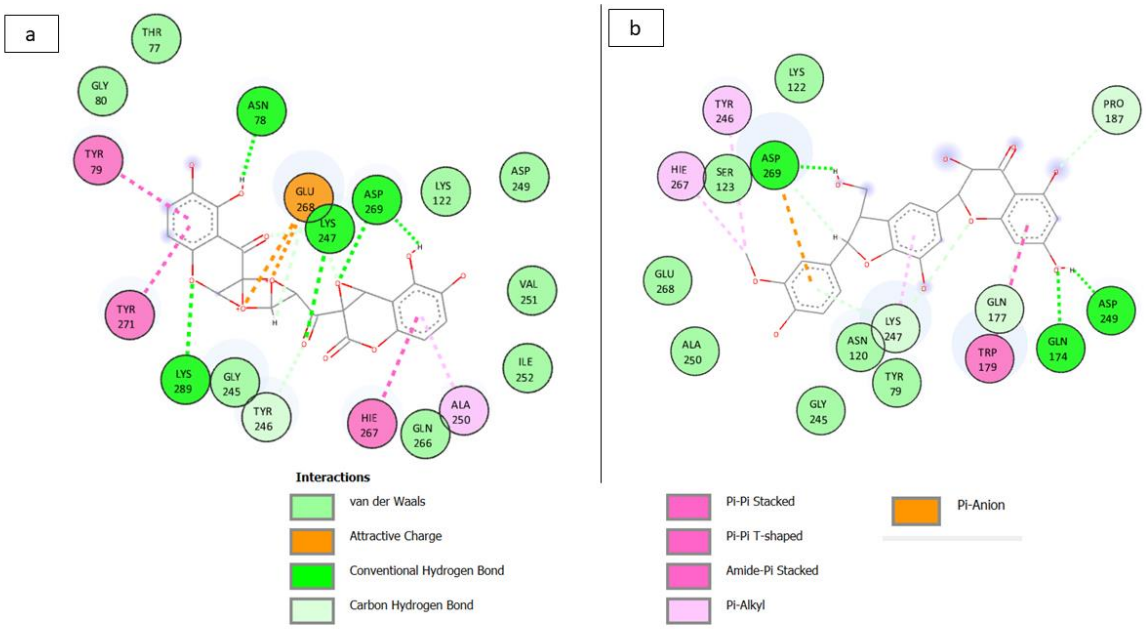
Supplementary Figure S10: Comparative interaction plots of RD2c (a) and silicristin (b) against PBP3 of *E. coli* after MD simulation



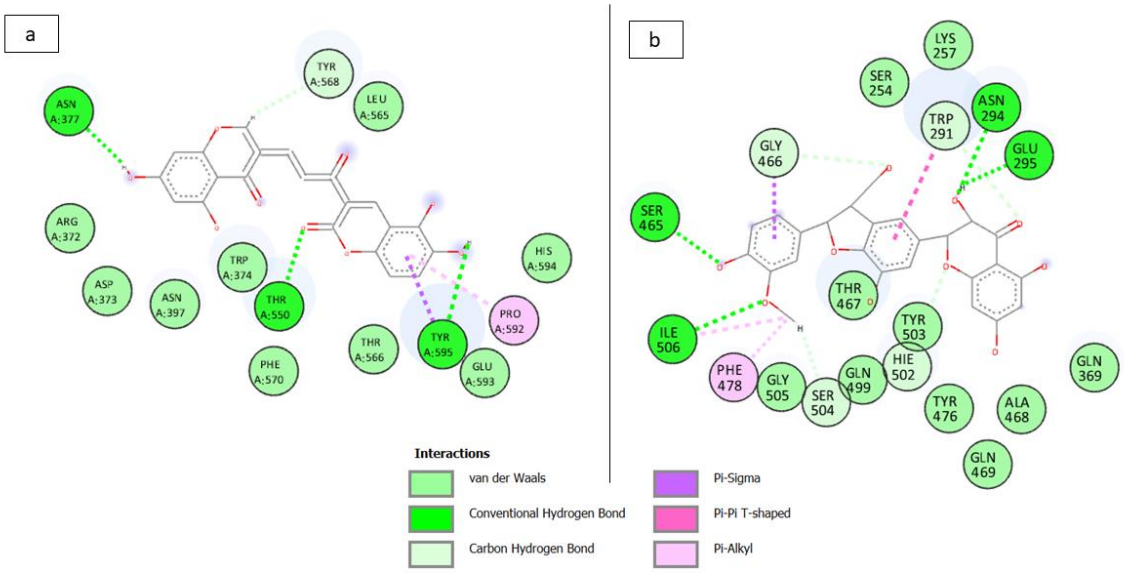
Supplementary Figure S11: Comparative interaction plots of RD1c (a) and silicristin (b) against PBP3 of *P. aeruginosa* after of MD simulation



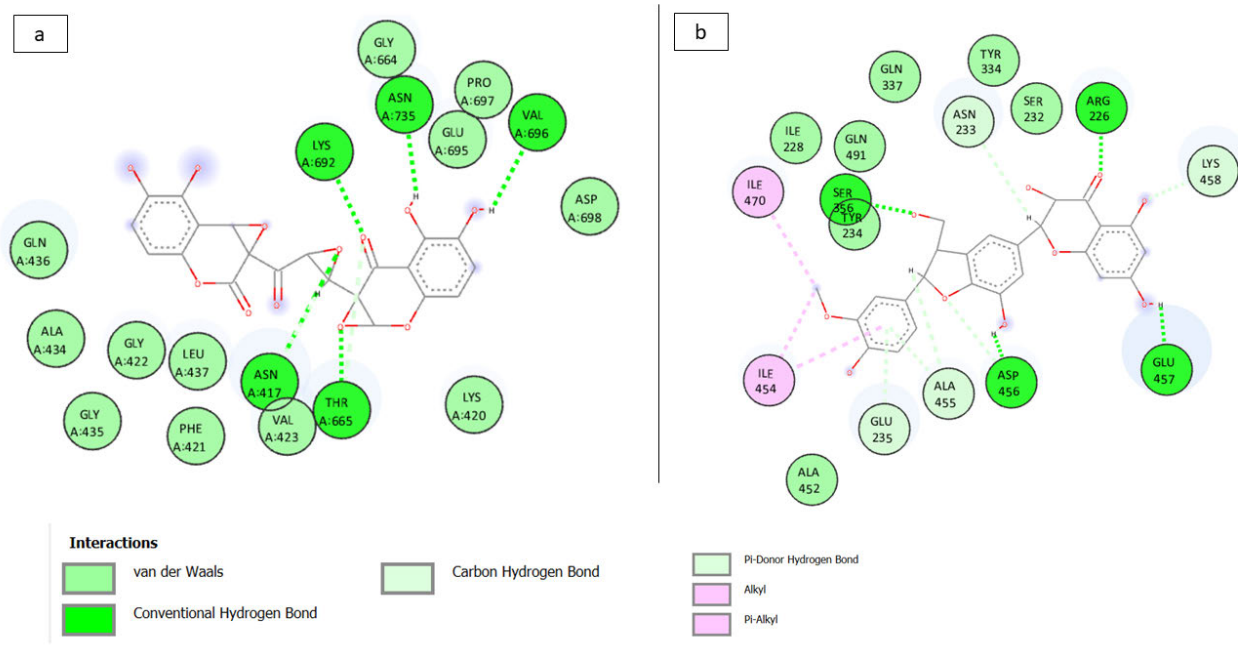
Supplementary Figure S12: Comparative interaction plots of RD2a (a) and silicristin (b) against the active site of PBP2a of *S. aureus* after MD simulation



Supplementary Figure S13: Comparative interaction plots of D1h (a) and silicristin (b) against the allosteric site of PBP2a after MD simulation



Supplementary Figure S14: Comparative interaction plots of RD1c (a) and silicristin (b) against the active site of PBP2x of *S. pneumoniae* after MD simulation



Supplementary Figure S15: Comparative interaction plots of D1h (a) and silicristin (b) against the allosteric site of PBP2a after MD simulation

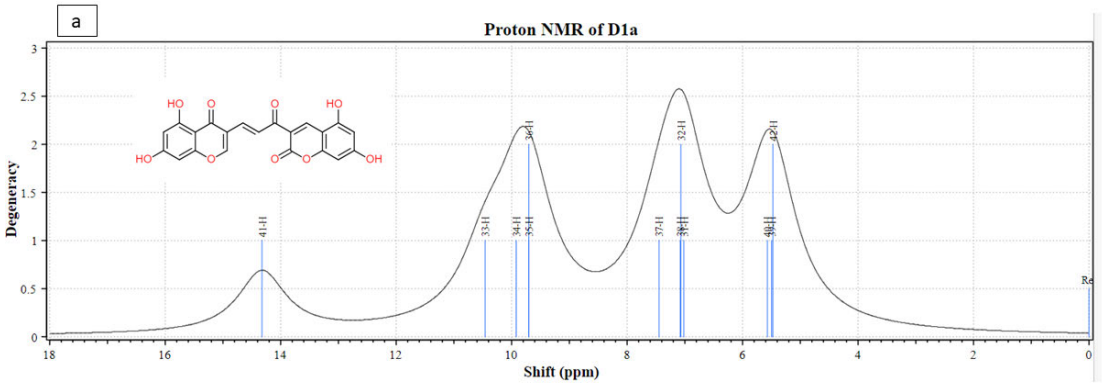
Supplementary Table S5: Correlation of the computationally and experimentally obtained ppm for proton chemical shift of the parent structure.

Parent structure C atoms	DFT computed (ppm)	Experimental computed (ppm)
27-H or 3-H	8.38	8.43
28-H or 4-H	8.69	7.59
29-H or 5-H	8.48	7.30
30-H or 6-H	8.69	7.30
31-H or 7-H	10.07	7.30
32-H or 8-H	10.04	-
33-H or 9-H	9.93	7.20
34-H or 10-H	9.94	8.45
35-H or 11-H	8.54	-
36-H or 12-H	8.73	7.59
37-H or 13-H	8.55	7.30
38-H or 14-H	9.63	7.59
39-H or 15-H	-	7.30

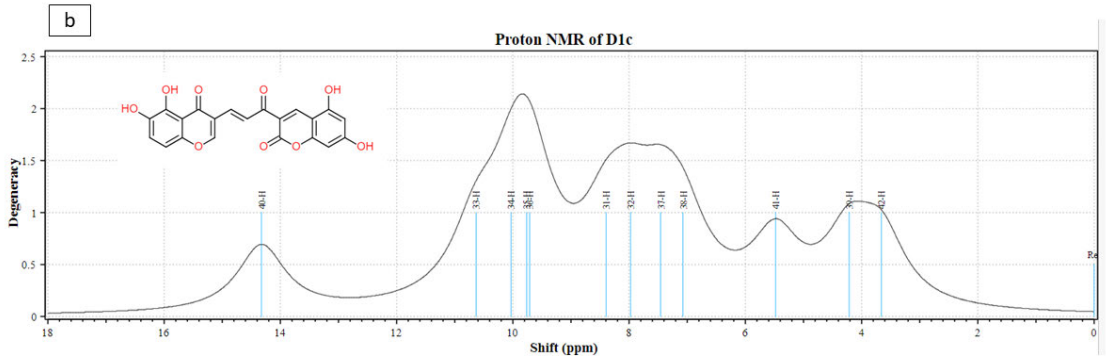
Supplementary Table S6: Correlation of the computationally and experimentally obtained ppm for ^{13}C chemical shift of the parent structure.

Parent structure C atoms	Computationally computed (ppm)	Experimentally obtained (ppm)
11-C and 11a-C	185.6	195 and 124
19-C	176.5	
8-C	163.0	195
4-C	162.3	130
17-C	150.5	149
15-C and15a-C	159.1	117 and 159
10-C and 10a-C	154.7	149 and 117
13-C	140.8	125
2-C and 2a-C	137.5	159 and 119
21-C	135.9	
6-C	135.2	133
23-C	133.2	
18-C	131.6	
22-C	129.3	
9-C	128.9	
14-C	128.1	133
1-C	127.5	
5-C	125.6	125
12-C	123.9	130
20-C	122.4	
3-C	120.8	123
7-C and 7a-C		125 and 155

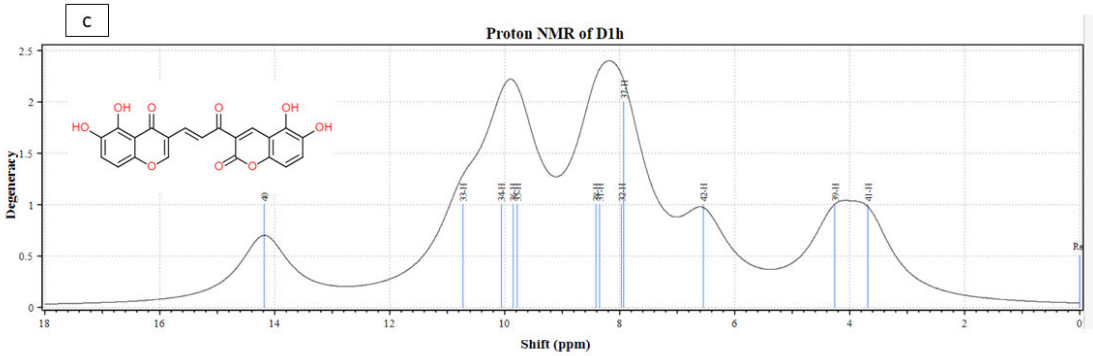
a


Proton NMR of D1a
Degeneracy
Shift (ppm)

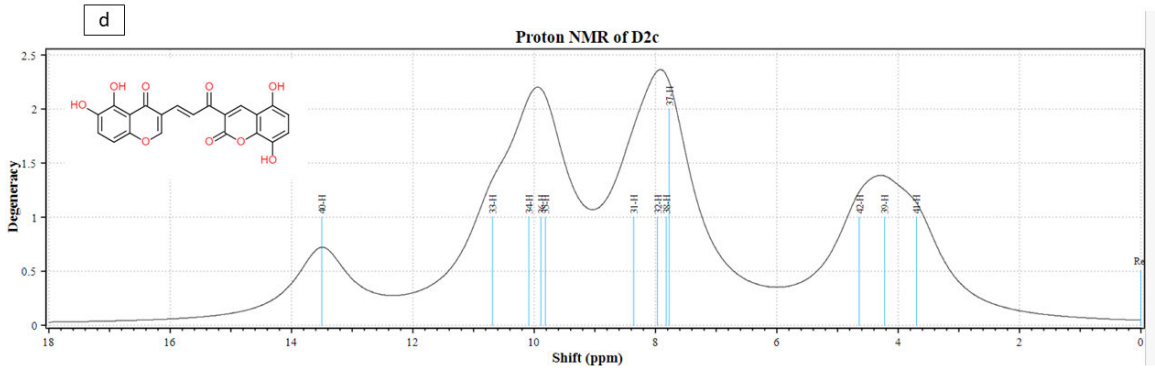
b


Proton NMR of D1c
Degeneracy
Shift (ppm)

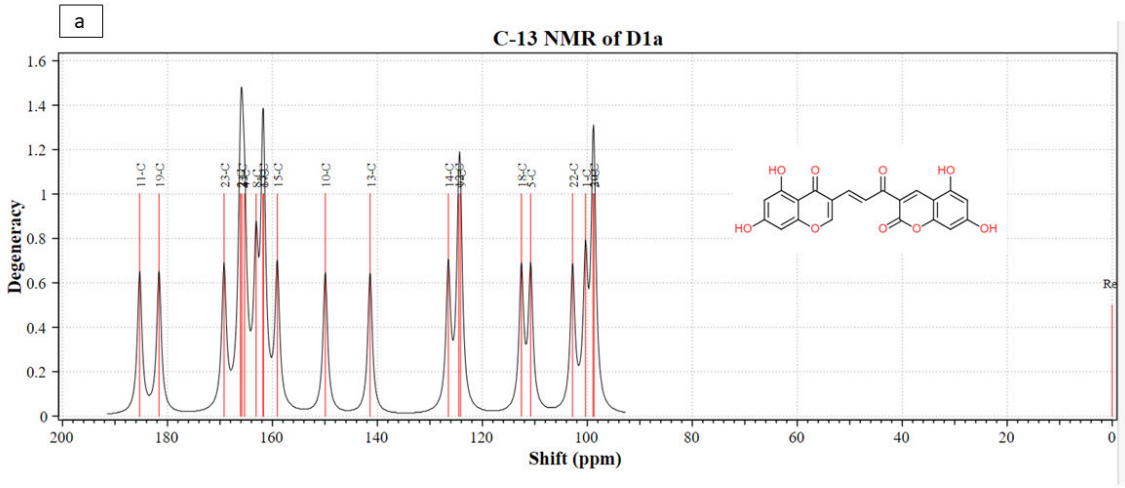
c

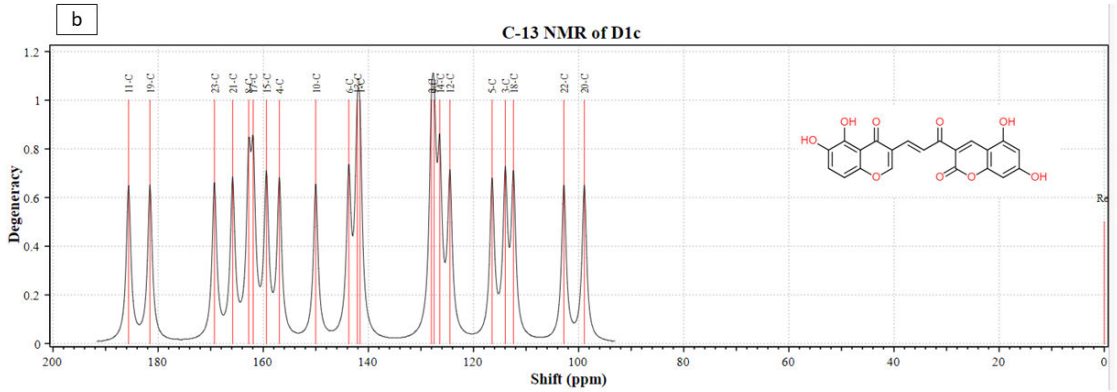

Proton NMR of D1h
Degeneracy
Shift (ppm)

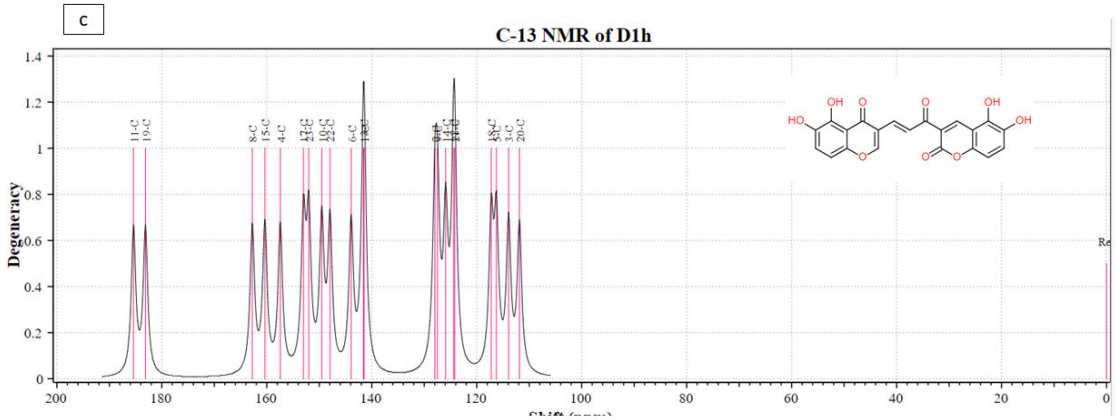
d

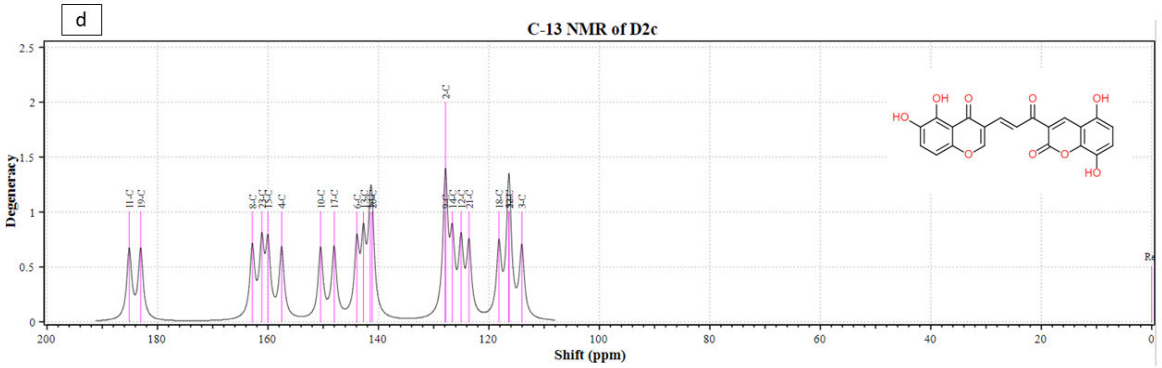

Proton NMR of D2c
Degeneracy
Shift (ppm)

Supplementary Figure S16: Computationally computed ^{1}H NMR proton test for (a) RD1a, (b) RD1c, (c) RD1h and (d) RD2c.









Supplementary Figure S17: Computationally computed ^{13}C NMR for (a) RD1a, (b) RD1c, (c) RD1h and (d) RD2C

CHAPTER FIVE

5.0 *In vitro* antibacterial potential and evaluation of the level of ROS contribution to the antibacterial activity of lead compounds and their derivatives against common and clinically significant pathogenic bacteria using direct ROS quantification and indirect oxidative stress biomarker assays

5.1 Silicristin and parent compound of novel derivatives of chalcone bis coumarin modulate Fenton reaction and facilitate membrane damage in Gram-positive and Gram-negative organisms…….....**324**

Abstract……**324**

1.0 Introduction……**326**

2.0 Materials and Methods……...**329**

3.0 Results and discussion ……...**339**

4.0 Conclusion……..**399**

References……**401**

Supplementary information**……..413**

This chapter has been formatted for submission to Oxidative Medicine and Cellular Longevity

5.1 Silicristin and parent compound of novel derivatives of chalcone bis coumarin (PSCB) modulate Fenton reaction and facilitate membrane damage in Gram-positive and Gram-negative bacteria.

Jamiu Olaseni Aribisala[a], Talent Raymond Makhanya[b] and Saheed Sabiu[a]*

[a]Department of Biotechnology and Food Science, Faculty of Applied Sciences, Durban University of Technology, P.O. Box 1334, Durban 4000, South Africa

[b]Department of Chemistry, Faculty of Applied Sciences, Durban University of Technology, P.O. Box 1334, Durban 4000, South Africa

Correspondence: sabius@dut.ac.za

Abstract

Silicristin is one of the bioactive compounds of silymarin, a standardized extract from the dried seeds of milk thistle which has been reported for its penicillin-binding protein (PBP) modulatory properties *in silico*. To understand its mechanism of action *in vitro*, this study investigates the antibacterial properties of silicristin and parent compounds of novel derivatives of chalcone bis coumarin (PSCB) derived from silicristin against sensitive and resistant strains of Gram-positive (*Staphylococcus aureus* and *Streptococcus pneumoniae*) and Gram-negative (*Escherichia coli* and *Pseudomonas aeruginosa*) bacteria. Also, the possible involvement of reactive oxygen species (ROS) in the lethality of silicristin, PSCB and reference beta-lactams (amoxicillin against Gram-positive organisms and cefotaxime against Gram-negative bacteria) was investigated. The minimum inhibitory concentration (MIC) assessment showed that silicristin, PSCB and reference beta-lactams had higher MIC values against the resistant strains [cefotaxime (2 – 16 µg/mL), amoxicillin (4 – 32 µg/mL, silicristin (8 – 64 µg/mL) and PSCB (16 – 128 µg/mL)]. The highest MIC for silicristin, PSCB and reference beta-lactams was observed against the resistant and

sensitive strains of *P. aeruginosa* [sensitive strains (8 – 64 µg/mL), resistant strains (16 – 128 µg/mL)], while the lowest MIC was observed with *S. pneumoniae* [sensitive strains (0.5 – 8 µg/mL), resistant strains (2 – 16 µg/mL)]. Compared to silicristin (4 – 64 µg/mL), PSCB (8 – 128 µg/mL) had higher MIC values against all the test strains and the observed effects were concentration- and time-dependent. Except against the sensitive and resistant strains of *E. coli* where silicristin had a comparable killing effect as cefotaxime, silicristin showed a better killing rate than PSCB and reference beta-lactams against all the test organisms with the best effect observed between 8 – 14 h post-treatment. Furthermore, silicristin had a synergistic effect with both amoxicillin and cefotaxime against all test organisms, except for the additive effect observed with the combination of silicristin and amoxicillin against the resistant strain of *E. coli*. In contrast, PSCB with cefotaxime and amoxicillin had only synergistic effect against the resistant strains of Gram-positive organisms. A further probe into the ROS generating potential of the antibacterial agents using ROS-specific dyes, showed that while PSCB and reference beta-lactams caused significant ($P < 0.05$) higher generation of superoxide ion ($O_2^{\bullet-}$), silicristin conversely enhanced higher ($P < 0.05$) generation of the most toxic ROS form, the hydroxy radicals ($^{\bullet}OH$), which is often produced via the Fenton reaction. This observation with silicristin suggests its enhanced modulatory effect on Fenton reaction relative to PSCB and the standards and further facilitated increased NAD/NADH ratio, ADP/ATP ratio, lipid peroxidation, carbonyl content, propidium iodide (PI) uptake, and depletion of reduced glutathione as observed with silicristin-treated cells. This observation points to the enhanced involvement of oxidative stress in the modulatory effect of silicristin against all the test organisms compared to PSCB and the reference standards. This enhanced oxidative stress in silicristin-treated cells was substantiated with scanning electron microscopy (SEM) and transmission electron microscopy (TEM) micrographs with cell walls with

more blisters, eruptions, and sores compared to the observed effects with other treatments and the untreated cells. Oxidative stress was also noted to facilitate SOS (Save Our Souls) response in upregulating *SordA* and *SoxR*, with the most prominent effect observed with silicristin in a manner that is more evident in the sensitive strains relative to the resistant strains. Taken together, these observations points to the enhanced redox effect of silicristin on the sensitive and resistant strains of both Gram-positive and Gram-negative organisms relative to PSCB and reference beta-lactams and could be explored to develop novel alternative therapeutics to beta-lactams in the treatment of infections caused by the test organisms.

Keywords: Silicristin, Reactive oxygen species, Oxidative stress, Antibacterial effect, Beta-lactams

1.0 Introduction

The rapid spread of antibiotic resistance has resulted in devastating failure of the present therapeutic procedures against clinically significant pathogens (Salam *et al*., 2023). As a result, there is an urgent need to uncover novel antibacterial compounds and gain a mechanistic understanding of their mode of action to better manage the menace of the bacterial super bugs. Since ancient times, natural products have made enormous contributions as a source of medicines in the treatment of various human diseases, including infectious diseases (Aldulaimi, 2017; Gibbons, 2004). Silymarin, a natural product from milk thistle (*Silybum marianum* L.), has been utilized in a range of nutraceuticals due to its potential chemo- and hepatoprotective effects (El-Sapagh *et al*., 2024). The aqueous extract of silymarin consist of phenolics (silybin A, silybin B, isosilybin A, isosilybin B, silydianin, isosilychristin, silicristin) and flavonoid (taxifolin) and have been shown to have potent antibacterial activities against both Gram-positive and Gram-negative organisms (El-Sapagh *et al*., 2024; Abed *et al*., 2015; de Oliveira *et al*., 2015; Kaur *et al*., 2011).

Silybin, the most abundant metabolite in silymarin, has been intensively explored, and there exists an obvious presumption of attributing all potentially therapeutic qualities of silymarin to silybin, including antibacterial properties (Abed *et al*., 2015; de Oliveira *et al*., 2015). In a study by Radhika *et al*. (2017), where both silymarin and silybin were explored independently against some oral pathogenic bacteria such as *Streptococcus mutans, Lactobacillus acidophilus, Enterococcus faecalis,* and *Staphylococcus aureus,* silymarin exhibited better antimicrobial effect against most of the test pathogens when compared to silybin, suggesting that other lead metabolite different from silybin exist in silymarin that could be responsible for its potent antibacterial effect. Another study by Lee *et al*. (2003), showed that silybin only exhibited antibacterial activity against Gram-positive bacteria. As a result, the strong presumption of attributing the antibacterial activity of silymarin to silybin generally due to its abundance in silymarin may be considered inappropriate, especially considering the paucity of information and investigations on the pure metabolites of other components of silymarin, implying the need to comprehensively investigate their therapeutic potential. Interestingly, recent *in silico* studies on the penicillin-binding protein (PBP) modulatory potential of a library of phenolics identified silicristin, the second most abundant flavonolignan in silymarin, as the most potent against the key PBPs of clinically important Gram-positive and Gram-negative bacteria (Aribisala *et al*., 2024; 2023a; 2023b, Aribisala and Sabiu, 2022). Thus, understanding and validating the antibacterial potential of silicristin and its mechanism of action *in vitro* is imperative

The principal mechanism of action of antibiotics are to disrupt cell wall, protein synthesis and DNA replication (Kohanski *et al*., 2010). However, investigations have shown that antibiotics can also instigate reactive oxygen species (ROS) generation by the overexcitation of electrons through Krebs cycle and electron transport chain (ETC) and the release of iron, which activates Fenton

chemistry (Imlay, 2013). As a result, antibiotics with established primary modes of action have also potentiated common secondary means in the form of ROS production (Paulander *et al*., 2014, Yeom *et al*., 2010), a means which have been explored and deemed relevant in the discovery and development of novel and potent drug candidate. The generation of ROS following treatment with diverse natural products including phenolics has been well documented (Mone *et al*., 2022; Wijesundara *et al*., 2021; Goel *et al*., 2018). Phenolics, aside having the ability to stimulate ROS generation through increased respiration in bacteria, can generate a considerable quantity of ROS through auto-oxidation in the presence of transition metals due to their low redox potential (Wei *et al*., 2022; Ajiboye *et al*., 2017; Eghbaliferiz and Iranshahi, 2016). The ability of ROS generation was initially reported in catechol-containing phenolics; however, studies have since demonstrated the involvement of ROS generation in the bactericidal potential of phenolics containing resorcinol and hydroquinone moieties (Jeyanthi *et al*., 2021; Singh *et al*., 2021; Xiong *et al*., 2017). Thus in this study, the antibacterial mechanism of action of silicristin, a phenolic with a resorcinol moiety (Figure 1), and the parent compound of some novel derivatives of chalcone bis coumarin (PSCB) designed from the optimization of silicristin (Figure 1) were explored *in vitro* against wild (sensitive) and resistant strains of Gram-positive (*S. aureus* and *S. pneumoniae*) and Gram-negative (*Pseudomonas aeruginosa* and *Esherichia coli*) bacteria. The presence of the characteristic hydroxyl groups in phenolics have been demonstrated to instigate ROS generation through auto-oxidation while enhancing strong PBP binding (Ajiboye *et al*., 2017; Avila *et al*., 2008). Thus, in this study, the absence of the characteristic hydroxy group in PSCB (Figure 1) will enable the investigation of the involvement of the characteristic hydroxy group in the ROS generation and potency of silicristin against Gram-positive and Gram-negative bacteria.

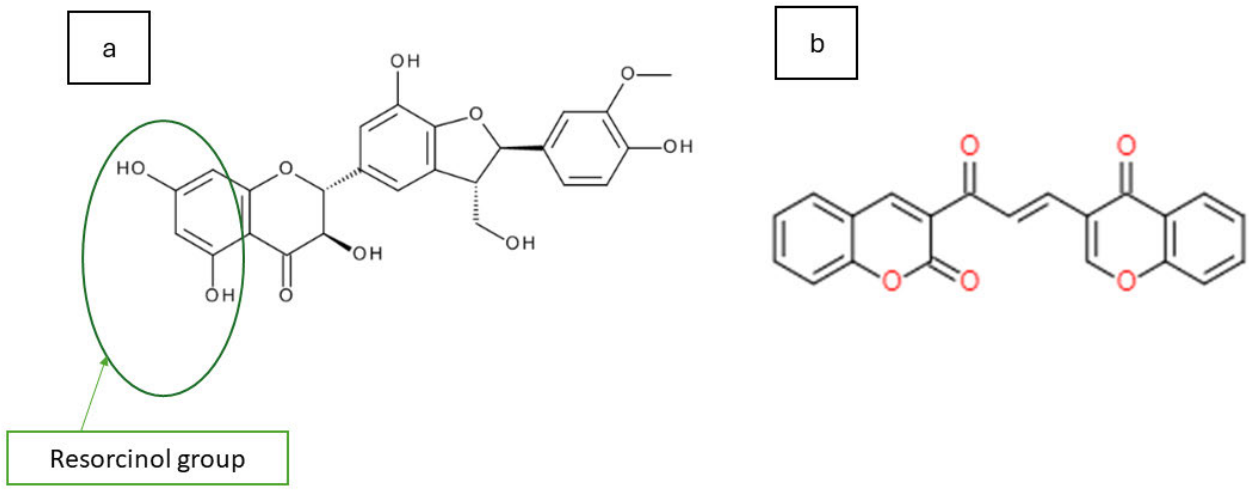


Figure 1: Two-dimensional (2D) structure of (a) silicristin (b) PSCB

2.0 Materials and Methods

2.1 *Materials*

Cefotaxime (Y000420), amoxicillin (A8523-5G), propidium iodide (PI) (P4170-25ML), hydroxyphenyl fluorescein (HPF) solution (H4290-1MG), assay kits [protein carbonyl content (MAK094-1KT), lipid peroxidation (MDA) (MAK085-1KT), ADP/ATP ratio (MAK135-1KT), NAD+/NADH ratio (MAK 037-1KT), cDNA synthesis (5893151001), KAPA SYBR Fast qPCR kit (KK4600), bicinchoninic acid (BCA1-1KT)], silicristin (SML2581-5MG), and glutaraldehyde (G5882-50ML) were procured from Sigma-Aldrich (Pty) Ltd, South Africa, while primers (*SodA*, *SoxR*, and SSRA) were products of Inqaba Biotechnical Industries (Pty) Ltd South Africa. Trizol reagent, 2',7'-dichlorodihydrofluo (OxyBURST™ Green H_2DCFDA), 5-(and-6)-Carboxy-2,7-D (carboxy-H2DCFDA), 6-Chloromethyl-2',7'-Dichlorod and RNA extraction kits were purchased from ThermoFisher Scientific, USA.

2.2. *Bacterial strains, culture growth and drug treatment*

Test organisms including both the wild (sensitive) (*S. pneumoniae* ATCC 49619, *S. aureus* ATCC 25923, *P. aeruginosa* ATCC27853, and *E. coli* ATCC 11775) and resistant strains (*S. pneumoniae* ATCC 700677, *S. aureus ATCC* 43300, *P. aeruginosa* ATCC BAA-3197 *E. coli* ATCC BAA-197) used in this study were acquired from Anatech Instruments (PTY) Ltd, South Africa. Standardization of test organisms was done using 0.5 McFarland turbidity for antibacterial sensitivity, minimum inhibitory concentration (MIC), and checkerboard assay (Balouiri *et al*., 2016). For other assays, cells at Mid log (OD_{600}~0.5) culture were employed (Ajiboye *et al*., 2018). Silicristin and PSCB were dissolved in 1% DMSO and used within one week and the final concentration of DMSO used as negative control in all experiments was 1% (v/v).

2.3. *Minimum inhibitory concentration, minimum bactericidal concentration, sensitivity, and time kinetics assays of antibacterial agents against test organisms*

The lowest concentration of silicristin and PSCB that inhibited the growth of the test organisms was determined as detailed in the CLSI guidelines (Balouiri *et al*., 2016). In brief, 0.2 mL of standardized inoculum of the test organisms was mixed with 2-fold serial dilutions of the antibacterial (0.125 – 128 μg/mL) in 96-well microtiter plates. Plates were incubated for 24 h at 37°C. After incubation, as determined by the well's lack of turbidity, the minimum inhibitory concentration (MIC) was defined as the lowest concentration that prevented bacterial growth. Minimum Bactericidal Concentration (MBC) was established by spotting 0.01 mL from the MIC treatments well and wells after on Mueller-Hinton (MH) agar. After 24 h of incubation, treatment with no visible growth on plate was used as MBC concentration. The susceptibility pattern of test organisms to silicristin and PSCB was determined using the agar well diffusion method as described by Balouiri *et al*. (2016). After standardization of test organisms using 0.5 McFarland,

0.1mL of the standardized test organism's suspension containing $1.5x10^8$ cfu/ml was spread on solidified MH agar using a sterile glass spreader. Wells were made on the plates using a 6 mm sterile cork-borer and antibacterial agents (silicristin, PSCB, amoxicillin and cefotaxime) at median activity concentration (MAC) [(MIC + MBC)/2] was introduced into the wells. The plates were incubated at 37^{o}C for 24 h after which the plates were observed for zones of inhibition. To understand the time-dependent rate of killing of the test organisms by the antibacterial agent, the time-kill kinetics analysis was performed (Ajiboye *et al*., 2018). Briefly, overnight culture of the test organisms in Luria-Bertani (LB) broth was grown at 37°C. Following that, the culture was diluted to OD_{600} of one in LB medium. The resulting culture (1 mL) was inoculated into a 250 mL baffled flask containing 50 mL of LB medium and cultivated aerobically in a shaking incubator (150 rpm) at 37°C. Antibacterial agents were applied when the OD_{600} reached 0.5. The OD_{600} was measured at 2 h intervals throughout an18 h incubation period.

2.4 *Checkerboard assay of silicristin and PSCB when combined with beta-lactams against test organisms*

The ability of silicristin and PSCB to potentiate the activity of amoxicillin and cefotaxime was evaluated using checkerboard assay as described by Ajiboye *et al*. (2018). Briefly, either of amoxicillin or cefotaxime (50 μL) was added to the rows of 96-well microtitre plates in decreasing concentrations (2 MIC – 1/16 MIC) and silicristin and PSCB (50 μL) was added to the columns in decreasing concentration (2 MIC – 1/16 MIC). The microtiter plates were then inoculated with the standardized test organisms (100 μL). The OD600 was measured after 24 h incubation at 37°C. The fractional inhibitory concentration index (FICI) was calculated using the expression. (equation 1):

$$FICI = \frac{\text{MIC of silicristin or PSCB in combination with amoxicillin or cefotaxime}}{\text{MIC of silicristin or PSCB alone}} + \frac{\text{MIC of amoxicillin or cefotaxime in combination with silicristin or PSCB}}{\text{MIC of amoxicillin or cefotaxime alone}} \quad \ldots 1$$

The FICI was interpreted as follows: (1) when FICI ≤ 0.5, there is a synergistic effect; (2) when FICI > 0.5 and < 1, there is an additive effect (3) when FICI > 1 ≤ 4 there is an indifferent effect; and (4) when FICI > 4, the combination is said to be antagonistic.

2.5. *Microscopic evaluations* of *antibacterial-treated cells*

The effects of antibacterial treatment on the cell wall and internal cellular components of the test organisms were established using scanning electron microscope (SEM) and transmission electron microscope (TEM), respectively. The evaluation was done as described by Thiberge *et al*. (2004). Briefly, bacterial cells (OD_{600} = 0.5) were treated with antibacterial agents at MBC concentration and incubated at 37°C for 4 h, after which cells were harvested by centrifugation at 4500 rpm/min for 10 min. After pelleting, cells were washed twice with 1X phosphate buffer solution, and then was re-suspended in 1X phosphate buffer containing 2.5% glutaraldehyde and kept at −4°C for 10 h to fix the cells. After centrifugation, the cells were further dehydrated in water-alcohol solutions at various alcohol concentrations (30, 50, 70, 80, 90, and 100%) for 10 min and then dry using hexamethyldisilazane (> 99% purity). Finally, the samples were fixed on CLSM support, and then sputter-coated with gold under vacuum (Quorum Q150R ES, UK), followed by scanning electron microscopic examination (ZEISS EVO LS 15, Germany). Regarding the transmission electron microscopy, while the above methodology for antibacterial treatment, fixing, dehydration and drying were followed, the samples were processed to resin and embedded in epoxy resin [Low Viscosity Resin (By Dr. Spurr) manufactured by Electron Microscopy Sciences, USA] using a Lynx II Automated Tissue Processor (Electron Microscopy Sciences, USA). Samples were thin sectioned on Leica EM UC7 Ultramicrotome (Leica Microsystems GmbH, Austria). The sections

were examined and photographed on a JEOL JEM 1400 Transmission Electron microscope (JEOL Inc. Japan) with a Tungsten Emitter at 120kV.

2.6. *Quantification of ROS following antibacterial treatment*

The amount of ROS generated following antibacterial treatment was determined using ROS-specific (Table 1) fluorescent dye-based method as described by Dwyer *et al*. (2014). At OD_{600} of 0.5, the test organisms were treated with MBC concentration of either silicristin, PSCB and beta-lactams (cefotaxime or amoxicillin) for 4 h at 37^{o}C. After incubation, cells were pelleted, washed with 1X phosphate buffer twice by centrifuging at 8000 rpm for 10 min at 25^{o}C. Subsequently cells were resuspended in 3 ml 1X phosphate buffer and 200 µL were dispense in 2 mL well of a 96-well plate. The working concentration of each of the dye (HPF, OxyBURST™ Green H_2DCFDA, carboxy-H2DCFDA and 6-Chloromethyl-2',7'-Dichlorod) were added and incubated for 2 h. The mean fluorescence was then read with a fluorescence plate reader (Turner Biosystems Modulus microplate reader, USA) and expressed as specific fluorescence intensity, which is the fluorescence normalized over the absorbance of 600 nm. The excitation/emission wavelengths for HPF, OxyBURST™ Green H_2DCFDA, carboxy-H2DCFDA and 6-Chloromethyl-2',7'-Dichlorod and their ROS target specificity are presented in Table 1.

Table 1: Reactive oxygen species dyes wavelength and their specific ROS targets

Dye	excitation/emission wavelength	Reactive species targets		
		H_2O_2	O_2^-	HO^-
carboxy-H2DCFDA	498/522	X		
6-Chloromethyl-2',7'-Dichlorod	490/520	X		X
OxyBURST™ Green H_2DCFDA	492/520		X	
HPF	490/515			X

2.7. Membrane damage assay following antibacterial treatment

The PI uptake assay for membrane compromise described by Crowley *et al*. (2016) was used in this study. Cells at OD_{600} ~0.5 were washed and resuspended in 1X phosphate buffer solution and treated with antibacterial at MBC for 1 h. Afterward, cells were washed and resuspended in 1X phosphate buffer containing 30 mM PI. After 15 min incubation, cells were washed with phosphate buffer solution and fluorescence was quantified in a plate reader (Turner Biosystems Modulus microplate reader, USA) with excitation 488 nm and emission 536 nm. The absorbance of each sample at 600 nm was also recorded to ensure the same cell density in all samples.

2.8. *Determination of NAD^+/NADH ratio in antibacterial treated cells.*

The ratio of NAD+/NADH in test organisms exposed to different concentrations of silicristin, PSCB, and reference beta-lactams was determined using the NAD+/NADH kit (Sigma-Aldrich, MAK 037) according to manufacturer's instructions. The bacterial cells at OD_{600} ~0.5 were incubated with silicristin, PSCB, and the reference beta-lactams at different concentrations (½ MIC, MIC and 2 MIC) for 30 minutes at 37°C in each case of the treatment. After incubation, bacterial cells were washed with cold phosphate buffer saline (pH 7.5) and centrifuged for 5 minutes at 2000 ×*g*. Treated cells were frozen and thawed twice on dry ice for 20 minutes each, followed by 10 minutes at 25°C in NAD+/NADH extraction buffer. The samples were afterward centrifuged at 13000 ×*g* for 10 minutes to separate the cell-free extract. Afterward, cells were treated with 50 µL of NAD+/NADH extraction buffer, then 100 µL of the master mix (NAD cycling buffer and enzyme). After thorough mixing, the reaction was incubated for 5 minutes at 25°C. The absorbance was read at 450 nm after adding 10 µL of NADH developer and incubating

for 2 hours at 25°C. Using the equation 2 below, the ratio of NAD+/NADH in samples was evaluated:

$$\frac{\text{NAD}^+}{\text{NADH ratio}} = \frac{\text{NADtotal}-\text{NADH}}{\text{NADH}} \quad \ldots\ldots\ldots 2$$

NADtotal = NAD^+ + NADH in the unknown sample (which were treated samples) (pmole) from the standard curve. NADH is the quantity of NADH in treated samples (pmole) from the standard curve.

2.9. *Determination of ADP/ATP ratio in antibacterial treated cells.*

The ratio of ADP/ATP in test organisms exposed to different concentrations of silicristin, PSCB, and reference beta-lactams was determined using the method described in the ADP/ATP ratio quantification kit (Sigma-Aldrich, MAK 135). The bacterial cells at OD_{600} ~0.5 were incubated with silicristin, PSCB, and the reference beta-lactams at different concentrations (½ MIC, MIC and 2 MIC) for 30 minutes at 37°C in each case of the treatment. Subsequently, equal volume of treated cells and ATP reagent (90 µL) was mixed and incubated at 25°C for 1 minute. Using a 3M™ Clean Trace™ luminometer, the luminescence (relative light units) was read for ATP assay (RLU_A). After 10 minutes of incubation, the luminescence for ATP (RLU_B) was again measured. Thereafter, 5 µL of ADP reagent was added and mixed, and the luminescence (RLU_C) after 1 minute was read and recorded as RLU_C. The ADP/ATP ratio was then assessed using the equation 3 below

$$\frac{\text{ADP}}{\text{ATP ratio}} = \frac{\text{RLUC}-\text{RLUB}}{\text{RLUA}} \quad \ldots\ldots\ldots 3$$

2.10 Protein Carbonyl Content Assay

Protein carbonyls content of antibacterial treated cells was evaluated using the procedure specified in the protein carbonyl assay kit (MAK094-1KT). Briefly, following the treatment of test organisms at OD_{600} of 0.5 with 4 MIC concentration of either silicristin, PSCB and novobiocin for

4 h at 37 ^{0}C, 100 µL of DNPH reagent were added to samples, vortexed and incubate for 10 min. Then, 30 µL of 87% TCA reagent was added to the samples, incubated for 5 min, centrifuged at 13,000 g for 2 min, and the supernatant was discarded. Ice acetone (500 µL) was added to each pellet and sonicated for 30 sec in a sonication bath. Subsequently, the samples were incubated at -20 °C for 5 min and centrifuge at 13,000 × *g* for 2 min to remove acetone from pellet. Guanidine solution (200 µL of 6 M) was added and pellet were resolubilize and transferred (100 µL) to the 96 well plate. At absorbance of 375 nm, the protein carbonyl content was analysed on a microplate reader (Thermo Scientific™ Multiskan™ GO Microplate Spectrophotometer, Finland). The protein test on samples to determine the protein concentration was carried out using the bicinchoninic acid kit with absorbance measured at 360 nm. Carbonyl content was calculated using equation 4:

$$\text{Carbonyl content } \left(\frac{\text{nmol}}{\text{mL}}\right) = \frac{\text{C}}{\text{P}} \text{ x } 1000 \text{ x DF} \quad \ldots\ldots 4$$

Where C = Amount of carbonyl in sample well (nmole/well) P = amount of protein, DF = Dilution factor for Sample (DF = 1 for undiluted samples) and 1000 = Conversion factor (µg to mg)

2.11 *Lipid peroxidation assay*

The cellular level of thiobarbituric acid malondialdehyde (TBAMDA) was determined using the procedure outlined in the TBARS assay kit (MAK085-1KT). In brief, after treating test organisms at OD_{600} of 0.5 with 4 MIC concentrations of either silicristin, PSCB, or novobiocin for 4 h at 37 ^{0}C, samples were then spun at 13.000 x *g* for 10 min and the supernatant collected in a vail. After, TBA reagent (600 µl) was introduce into each vial holding the earlier collected supernatant. The samples were subsequently incubated at 95°C for 60 min and iced for 10 min. To calculate the standard curve, 800µl of TBA/sample and standard mix were introduced into 96-well plates. The absorbance of the TBA-MDA conjugate was determined at 532 nm using a plate reader (Thermo

Scientific™ Multiskan™ GO Microplate Spectrophotometer, Finland). The MDA concentration in samples and standard was evaluated from the absorbance as per the manufacturer's instructions using equation 5.

$$\text{Concentration of MDA in sample } \left(\frac{\text{nmol}}{\text{mL}}\right) = \frac{SA}{SV} \text{ x DF} \quad \ldots\ldots\ldots 5$$

Where SA = amount of MDA in sample (nmole) as determined from the standard curve, SV = sample volume (mL) added into the wells, DF = sample dilution factor (DF = 1 for undiluted Samples)

2.12 *Quantification of SoxRS expression by reverse transcription quantitative real time polymerase chain reaction (RT-qPCR)*

Gene transcription of *SoxR*S (*SodA* and *SoxR*) regulons, which have been shown to be sensitive to superoxide radicals (Imlay, 2013) was determined following the method described by Xiong *et al*. (2017). Ribonucleic acid (RNA) was extracted from mid log (OD_{600}~0.5) cells treated with MBC of silicristin, PSCB and beta-lactams for 7 h. The RNA was extracted using the RNA extraction kit (Invitrogen, by ThermoFisher Scientific), as per manufacturer's instructions. Complementary deoxyribonucleic acid (cDNA) was synthesized using the cDNA synthesis kit (5893151001) using 1.0 mg of RNA. The quantitative polymerase chain reaction (qPCR) was performed with 10 ng cDNA using the KAPA SYBR Fast qPCR kit (KK4600) and 0.1 pM of each primer in a 20 mL reaction. The qPCR run and analysis was performed using Quant Studio 5 (Applied Biosystem™ by Thermo Fisher Scientific). The thermocycling conditions included one cycle of denaturation at 95 ^{o}C for 4 minutes, followed by 45 cycles of denaturing at 95^{o}C for 2 s and annealing/extension at 60^{o}C for 40 s. The cycle threshold (Ct) values were normalized against the ssrA gene (housekeeping gene) that codes a multi-functional RNA molecule that perform several diverse roles in the bacterial cell (Julio *et al*., 2000) and the relative gene expression was determined using

the ΔΔCt method (equation 6) (Livak and Schmittgen, 2001). The evaluated genes in this study and their primers are listed in Table 2.

$$RQ=2^{-\Delta\Delta Ct} \quad \text{..... 6}$$

Where: $-\Delta Ct$ (untreated cells) + ΔCt (treated cells) = $\Delta\Delta Ct$

$-\Delta Ct$ (housekeeping genes in treated cells) + Ct (target gene in treated cells) = ΔCt (treated cells)

$-\Delta Ct$ (housekeeping genes in untreated cells) + Ct (target gene in untreated cells) = ΔCt (untreated cells)

Table 2: Primers used for the quantitative RT-PCR

Gene name	Primer sequence
sodA	Forward: GCCTGTTCTGGAAAGGTCTG
	Reverse: CCAGTTTATCGCCTTTCAGC
soxR	Forward: GTATCCGTAACAGCGGCAAT
	Reverse: CATTGGGACGAAAGCTGTTT
ssrA	Forward: TTAGGACGGGGATCAAGAGA
	Reverse: GCGTCCGAAATTCCTACATC

2.13 *Statistical analysis*

All analyses were done in triplicate and are presented as mean ± standard deviation. Post-hoc analysis using Tukey's test for three-group comparisons was performed using SPSS software (version 23, SPSS/IBM). Plots of graphs were done using Origin (version 6.0). Differences between each group were considered statistically significant at $P < 0.05$.

3.0 Results and discussion

3.1 *Antibacterial activity of silicristin and PSCB against investigated test organisms*

The deleterious consequences of antibiotic resistance in bacteria have had a catastrophic impact on current treatment modalities, necessitating the search for an alternative and effective antibacterial chemotherapy. Silicristin is one of the bioactive compounds of silymarin, a standardized extract from the dried seeds of milk thistle (*Silybum marianum* L. Gaertn) (Oliveira *et al*., 2015). Studies have demonstrated the exceptionally antibacterial activities of the extract of milk thistle against both Gram-positives and Gram-negative bacteria attributing the effect mainly to silybin (El-Sapagh *et al*., 2024; de Oliveira *et al*., 2015). Since the mechanism of action of silicristin against bacteria is unclear, and recent *in silico* studies demonstrated the anti-PBP properties of silicristin (Aribisala *et al*., 2024; 2023a; 2023b, Aribisala and Sabiu, 2022), this study evaluates the antibacterial properties of silicristin against the sensitive and drug-resistant strain of four common and clinically significant bacteria (*E. coli*, *P. aeruginosa*, *S. aureus* and *S. pneumoniae*). Also, the antibacterial properties of PSCB designed from the optimization of silicristin with key PBPs of clinically important microorganism were also investigated using conventional beta-lactams [amoxicillin and cefotaxime] as reference standards. The MIC (Table 3) and MBC (Supplementary Table S1) evaluation showed that all the investigated antibacterial agents had higher values against the resistant strains relative to the sensitive strains (Table 3; Supplementary Table S1). This observation substantiates the drug-resistant status of the resistant strains. Compared to silicristin, PSCB (between 8 and 128 µg/mL) had higher MIC values compared to silicristin (4 and 64 µg/mL) against all the strains (Table 3). This observation might be due to the lack of the characteristic hydroxy group of phenolics in PSCB. The characteristic hydroxyl groups of phenolics have been found to promote strong PBP binding and

increase affinity for cytoplasmic membranes, therefore improving antibacterial effect (Avila *et al*., 2008). Amoxicillin and cefotaxime had lesser MIC concentration compared to silicristin and PSCB in all test organisms (Table 3). The observed high MIC values of silicristin and PSCB relative to amoxicillin and cefotaxime in this study are not surprising as amoxicillin and cefotaxime are conventional beta-lactams that have been modified over the years for improved potency while silicristin is a mere plant secondary metabolite that could be further optimized for enhance antibacterial effect. In this regard, while PSCB is a synthesized product from silicristin, the absence of the characteristic hydroxyl groups which is present in silicristin and the main optimized PSCB derivatives might have contributed to its higher MIC value relative to silicristin and the conventional beta-lactams. This observation is consistent with previous *in silico* investigation of this study where PSCB against PBPs of common and clinically important microorganisms had lower negative binding free energy compared to optimized PSCB derivatives and silicristin. According to Ríos and Recio (2005), MIC values of above 1000 µg/ml should be avoided as an antimicrobial, while Simões *et al*. (2009) reported that MIC range of phytocompounds should be between 100 and 1000 µg/ml to be classified as antimicrobials. Thus, the MIC values of silicristin in this study are notable as a potential broad spectrum antibacterial agent while that of PSCB highlights the antibacterial potential of the lead PSCB derivatives. Despite the lower MIC values of amoxicillin and cefotaxime relative to silicristin and PSCB, the sensitivity pattern evaluation showed competitive activities at the median activity concentration (MAC) [(MIC + MBC)/2] (Supplementary Table S 2). Compared to amoxicillin, silicristin and PSCB had higher zone of inhibitions against Gram-negative organisms (both the sensitive and the resistant strain). Against Gram-positive organisms [*S. pneumoniae* ATCC 700677 (12 mm), *S. aureus* ATCC 43300 (10 mm) and *S. aureus* ATCC 25923 (12 mm)], only silicristin had higher zones of inhibition than

cefotaxime (Supplementary Table S2). Consistent with the MIC evaluation, the investigated antibacterial agents had lesser zones of inhibition (Supplementary Table S 2) against the resistant strains compared to the sensitive strain. According to National Committee for Clinical Laboratory Standards (NCCLS), zones of inhibition of < 21 mm are regarded as susceptible, 14 – 20 mm as moderately susceptible, and ≤13 are resistant. In this regard, except for *S. pneumoniae* ATCC 700677 against amoxicillin, all the multidrug resistant strains were resistant to the two conventional beta-lactams used. The Gram-negative sensitive strains (*E. coli* ATCC 11775 and *P. aeruginosa* ATCC*27853*) were susceptible to cefotaxime while moderately susceptible or resistant to amoxicillin. On the other hand, the Gram-positive sensitive strains (*S. aureus* ATCC 25923 and *S. pneumoniae* ATCC 49619) were susceptible to amoxicillin while moderately susceptible or resistant to cefotaxime (Supplementary Table S2). Nevertheless, these observations are not surprising as it is just a confirmation of the test organism status. While silicrsitin had a higher zone of inhibition than either both or one of the beta-lactams against the test organisms, only *P. aeruginosa* ATCC*27853, E. coli* ATCC 11775 and *S. pneumoniae* ATCC 49619 are susceptible or moderately susceptible. Although, little information is known on the antibacterial activity of silicristin, strong antibacterial activities of the standardized ethanolic extract of milk thistle (a plant that has silicristin as one of its active metabolites) have been reported against Gram-positive (*S. aureus*) and Gram-negative bacteria (*Salmonella entirica*) (Basma *et al*., 2020). Thus, the observed antibacterial properties of silicristin in this study might suggest the compound as one of the main antibacterial active metabolites of milk thistle as against most studies that credit the antibacterial properties of the plant mainly to silybin (Wadhwa *et al*., 2022; De Oliver *et al*., 2015). Like silicristin, *P. aeruginosa* ATCC*27853* and *E. coli* ATCC 11775 were moderately susceptible to PSCB, highlighting the antibacterial potential of the lead derivatives designed from PSCB.

Table 3: Minimum inhibitory concentration (µg/mL) of antibacterial agents on test organisms

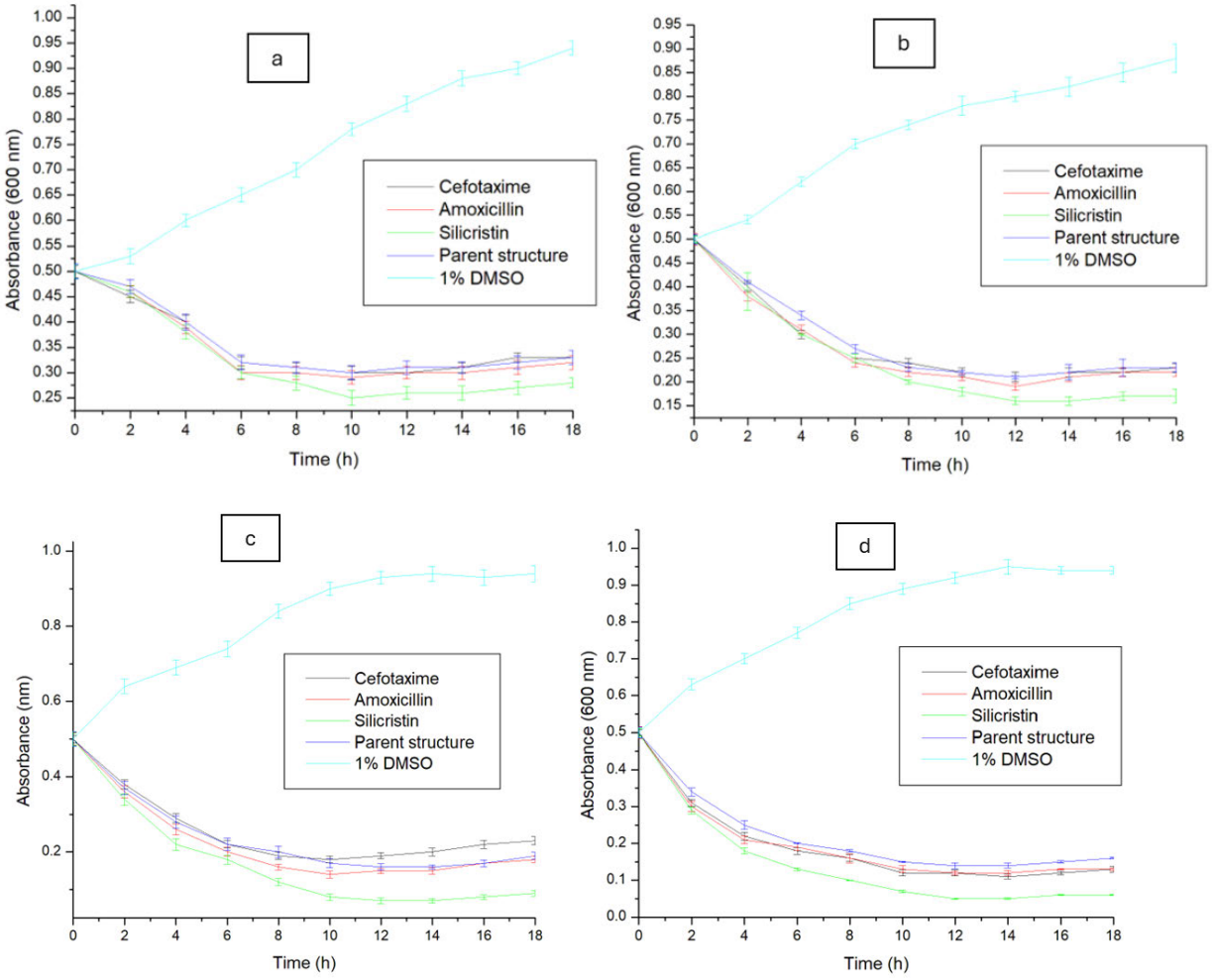
Organisms	Organisms Status	Cefotaxime	Amoxicillin	Silicristin	PSCB
Staphylococcus aureus ATCC 43300	R	16.0	4.0	32.0	128.0
Staphylococcus aureus ATCC 25923	S	2.0	1.0	16.0	32.0
Pseudomonas aeruginosa ATCC BAA-3197	R	16.0	32.0	64.0	128.0
Pseudomonas aeruginosa ATCC27853	S	8.00	16.0	32.0	64.0
Escherichia coli ATCC BAA-197	R	2.0	16.0	32.0	64.0
Escherichia coli ATCC 11775	S	0.5	4.0	16.0	32.0
Streptococcus pneumoniae ATCC 700677	R	4.0	4.0	8.0	16.0
Streptococcus pneumoniae ATCC 49619	S	0.50	0.50	4.0	8.0

Keywords: R: resistant, S: Sensitive

3.2 *Time kills kinetics of silicristin and PSCB against investigated test organisms*

The effect of silicristin and PSCB against the sensitive and multidrug resistant strain of common and clinically significant bacterial was investigated using the time-kill kinetics (Figure 2). The DMSO treated cells had a continuous increase in absorbance in all the strains of the test bacteria, suggesting an increase in cell growth and lack of antibacterial activities. However, silicristin, PSCB and reference beta-lactams (amoxicillin and cefotaxime) had concentration- and time-dependent bacterial killing ability against all the bacteria strains (Supplementary Figure S1-S4). At all concentration, the lowest absorbance for silicristin against multidrug resistant *S. aureus* ATCC 43300, *S. pneumoniae* ATCC 700677, *P. aeruginosa* ATCC BAA-3197, and *E. coli* ATCC BAA-197 was observed at 12h, 14h, 12 h and 10 h respectively after which absorbance value were maintain or slightly increased (Supplementary Figure S1-S4). Except against the resistant (Figure 2c) and sensitive strains (Figure 2d) of *S. pneumoniae* where the lowest absorbance both occur at 14 h, silicristin had longer antibacterial effect against all sensitive strains (*S. aureus* ATCC 25923 at 16h, *P. aeruginosa* ATCC27853 at 14 h, and *E. coli* ATCC 11775 at 14h) (Figure 2b, d, f, h)

relative their resistant strains (Figure 2a, c, e, g). This observation suggests that a shorter interval between medication doses for infection caused by multidrug resistant strains might be required when treating with silicristin. Similar observation was also noted with cells treated with PSCB as antibacterial killing of sensitive strains elapsed longer that the resistant strain. Comparatively at 4MIC, silicristin had the best time-kill effect against Gram-positive organisms (Figure 2a – 2d) relative to PBSB and the beta-lactams with the lowest absorbance observed after the 18 h incubation period. This observation is consistent with the antibacterial susceptibility pattern of this study where silicristin had better effect than both conventional beta-lactams and PSCB. Against Gram-positive organisms, the killing effects of PSCB was not significantly different ($P > 0.05$) from amoxicillin and cefotaxime treated cells (Figure 2a – 2d). This observation suggests the antibacterial potential of PSCB against Gram-positive organisms. Similarly, against Gram-negative organisms (Figure 2e – 2h), silicristin had better time-kill effect after 18 h against *P. aeruginosa* ATCC27853 (Figure 2f), however against *P. aeruginosa* ATCC BAA-3197 (Figure 2e), the effect elicited by silicristin, and cefotaxime was not significantly different ($P > 0.05$) during the incubation period. On the other hand, cefotaxime had better time-kill effect after 18 h of incubation against both strains of *E. Coli* (Figure 2g – 2h). Generally, except for *E. Coli*, the time-kill kinetic investigation of this study points to the better antibacterial effects of silicristin relative to amoxicillin and cefotaxime while that of the PSCB is comparable to both conventional antibiotics against Gram-positive organisms. However, for further analysis, cefotaxime against Gam-negative organisms and amoxicillin against Gram-positive organisms were used as positive control due to their better zone of inhibition and time-kill effects against the respective bacterial classes.


a
Absorbance (600 nm)
Time (h)
Cefotaxime
Amoxicillin
Silicristin
Parent structure
1% DMSO
b
Absorbance (600 nm)
Time (h)
Cefotaxime
Amoxicillin
Silicristin
Parent structure
1% DMSO
c
Absorbance (nm)
Time (h)
Cefotaxime
Amoxicillin
Silicristin
Parent structure
1% DMSO
d
Absorbance (600 nm)
Time (h)
Cefotaxime
Amoxicillin
Silicristin
Parent structure
1% DMSO

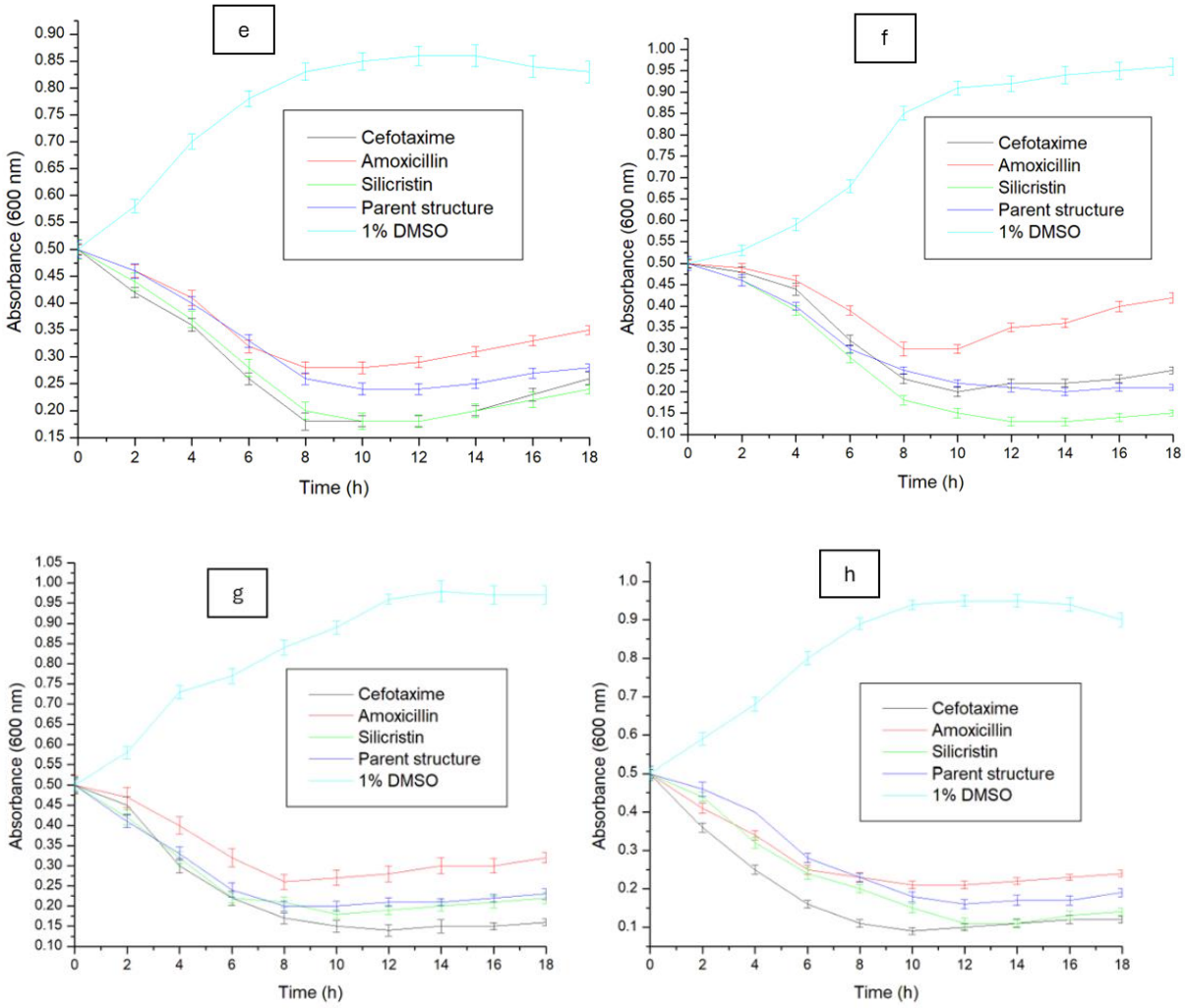


Figure 2: Time-kill curve of silicristin, PSCB (parent structure), and beta-lactams (amoxicillin and cefotaxime) at 4 MIC on resistant (R) [(a) *S. aureus* ATCC 43300, (c) *S. pneumoniae* ATCC 700677 (e) *P. aeruginosa* ATCC BAA-3197 (g) *E. coli* ATCC BAA-197] and sensitive (S) [(b) *S. aureus* ATCC 25923, (d) *S. pneumoniae* ATCC 49619, (f) *P. aeruginosa* ATCC27853, (h) *E. coli* ATCC 11775] strains of test bacteria.

3.3 *Combinatory effects of silicristin and PSCB with beta-lactams against investigated test organisms*

Combination therapy is considered one of the viable strategies to overcome the threat of antibiotic resistance and improve the antibacterial efficacy of antibiotics (Petersen *et al*., 2006). Combination therapy allows the use of lower concentrations and therefore minimizes the occurrence of probable toxicity (Islam *et al*., 2021; Tellis *et al*., 2016). From the checkerboard assay, it was observed that except in the combination of silicristin and amoxicillin against *E. coli* ATCC BAA-197, the combination of silicristin with either cefotaxime or amoxicillin resulted in a synergistic interaction as the FICI was ≤ 0.50 against all the strains (sensitive and multidrug resistant) of the test organisms (Table 4). This observation is an indication that silicristin helped to reduce the MIC value of amoxicillin and cefotaxime in the killing of the test organisms. Except in the combination of silicristin with amoxicillin against *E. coli* ATCC BAA-197 where the MIC reduction of the antibiotic is 8-fold, combination of silicristin with amoxicillin or cefotaxime resulted in >10-fold reduction in MIC of the antibiotic. This observation not only suggests that silicristin enhanced the potency of beta-lactams, but also means that silicristin perhaps has other mechanisms of action that are different from beta-lactams. Other mechanisms of actions that have been reported for phenolics includes their ability to bind to the allosteric site of PBPs of Gram-positive organism (Aribisala and Sabiu, 2022; Aribisala *et al*., 2024), their ability to generate ROS while increasing affinity for cytoplasmic membranes among other (Ajiboye *et al*., 2018; Zeraik *et al*., 2014). The ability of silicristin to enhance the effect of beta-lactam in this study is consistent with a previous study where phenolics such as morin and quercetin enhanced the activity of ciprofloxacin and tetracycline against different strains of *S. aureus* including methicillin resistant strain (Abreu *et al*., 2014). Another recent study by Khumbulani *et al*. (2022), also demonstrated how orientin enhances colistin-mediated bacterial lethality. In both studies (Abreu *et al*., 2014; Khumbulani *et al*., 2022), the existence, amount, and degree of substitution of hydroxyl or methyl groups on the

benzene ring were implicated in the observed effect. Hence, it could be logically inferred that the antibacterial activity of silicristin in this study could also be attributed to the presence of the hydroxyl or methyl groups in its benzene ring structure. This observation was further substantiated as PSCB without this characteristic structure only result in addictive/indifference effect with cefotaxime and amoxicillin with FICI > 0.50 against all the organisms except in the case of multidrug resistant Gram-positive organisms (*S. aureus* and *S. pneumoniae*) (Table 5). An addictive effect means that combining effects of PSCB and cefotaxime/amoxicillin equal the sum of the effects of the two antibacterial acting independently (Hu *et al*, 2002). Except for multidrug resistant Gram-positive organisms, this observation might suggest similar mechanisms of action for PSCB and the beta-lactams in blocking cell wall synthesis. In the case of multidrug resistant Gram-positive organisms, the synergistic effect noted for PSCB and the beta-lactams against these organisms might be due the fact that these strains harbor essential PBPs with allosteric site (PBP2a in *S. aureus* and PBP2x in *S. pneumoniae*) (Acebrón *et al*., 2015) which PSCB could bind to.

Table 4: Checkerboard combinatory effects of silicristin with cefatoxime and amoxicillin against test organisms

	MIC of single agent (µg/mL)		MIC in combination (µg/mL)					Interpretation
Organisms	Silicristin	Cefotaxime	Silicristin	Cefotaxime	FIC_a	FIC_b	FICI ($FIC_a + FIC_b$)	
Staphylococcus aureus ATCC 43300	32.0	16.0	8	2	0.250	0.125	0.375	Synergistic
Staphylococcus aureus ATCC *25923*	16.0	2.0	4	0.25	0.250	0.062	0.312	Synergistic
Pseudomonas aeruginosa ATCC BAA-3197	64.0	16.0	16	4	0.250	0.250	0.500	Synergistic
Pseudomonas aeruginosa ATCC*27853*	32.0	8.00	8	2	0.250	0.250	0.500	Synergistic
Escherichia coli ATCC BAA-197	32.0	2.0	8	0.125	0.250	0.063	0.312	Synergistic
Escherichia coli ATCC 11775	16.0	0.5	4	0.125	0.250	0.250	0.500	Synergistic
Streptococcus pneumoniae ATCC 700677	8.0	4.0	2	0.5	0.250	0.125	0.375	Synergistic
Streptococcus pneumoniae ATCC 49619	4.0	0.50	1	0.125	0.250	0.250	0.500	Synergistic
Organisms	Silicristin	Amoxicillin	Silicristin	Amoxicillin	FIC_a	FIC_b	FICI ($FIC_a + FIC_b$)	
Staphylococcus aureus ATCC 43300	32.0	4.0	8	1	0.250	0.250	0.500	Synergistic
Staphylococcus aureus ATCC *25923*	16.0	1.0	4	0.25	0.250	0.250	0.500	Synergistic
Pseudomonas aeruginosa ATCC BAA-3197	64.0	32.0	8	4	0.125	0.125	0.250	Synergistic
Pseudomonas aeruginosa ATCC*27853*	32.0	16.0	8	4	0.250	0.250	0.500	Synergistic
Escherichia coli ATCC BAA-197	32.0	16.0	16	4	0.500	0.250	0.750	Additive
Escherichia coli ATCC 11775	16.0	4.0	4	1	0.250	0.2500	0.500	Synergistic
Streptococcus pneumoniae ATCC 700677	8.0	4.0	2	1	0.250	0.250	0.500	Synergistic
Streptococcus pneumoniae ATCC 49619	4.0	0.50	1	0.125	0.250	0.250	0.500	Synergistic

Keywords: FICI: fractional inhibitory concentration index, FIC_a (fractional inhibitory concentration a): $\frac{\text{MIC of silicristin in combination with amoxicillin or cefotaxime}}{\text{MIC of silicristin alone}}$,

FIC_b (fractional inhibitory concentration b): $\frac{\text{MIC of amoxicillin or cefotaxime in combination with silicristin}}{\text{MIC of amoxicillin or cefotaxime alone}}$, MIC: minimum inhibitory concentration

Table 5: Checkerboard combinatory effects of PSCB with cefatoxime and amoxicillin against test organisms

	MIC of single agent (µg/mL)		MIC in combination (µg/mL)					Interpretation
Organism	PSCB	Cefotaxime	PSCB	Cefotaxime	FIC_a	FIC_b	FICI (FIC_a + FIC_b)	
Staphylococcus aureus ATCC 43300	128.0	16.0	32	2	0.250	0.125	0.375	Synergistic
Staphylococcus aureus ATCC *25923*	32.0	2.0	16	0.5	0.500	0.250	0.750	Additive
Pseudomonas aeruginosa ATCC BAA-3197	128.0	16.0	32	8	0.250	0.500	0.750	Additive
Pseudomonas aeruginosa ATCC*27853*	64.0	8.00	32	2	0.500	0.250	0.750	Additive
Escherichia coli ATCC BAA-197	64.0	2.0	32	1	0.500	0.500	1.000	Additive
Escherichia coli ATCC 11775	32.0	0.5	16	0.25	0.500	0.500	1.000	Additive
Streptococcus pneumoniae ATCC 700677	16.0	4.0	4	1	0.250	0.25	0.500	Synergistic
Streptococcus pneumoniae ATCC 49619	8.0	0.50	4	0.125	0.500	0.25	0.750	Additive
Organism	PSCB	Amoxicillin	PSCB	Amoxicillin	FIC_a	FIC_b	FICI (FIC_a + FIC_b)	
Staphylococcus aureus ATCC 43300	128.0	4.0	16	1	0.125	0.250	0.375	Synergistic
Staphylococcus aureus ATCC *25923*	32.0	1.0	16	0.5	0.500	0.500	1.000	Additive
Pseudomonas aeruginosa ATCC BAA-3197	128.0	32.0	64	4	0.500	0.125	0.625	Additive
Pseudomonas aeruginosa ATCC*27853*	64.0	16.0	16	8	0.250	0.500	0.750	Additive
Escherichia coli ATCC BAA-197	64.0	16.0	64	8	1.000	0.500	1.500	indifference
Escherichia coli ATCC 11775	32.0	4.0	16	2	0.500	0.500	1.000	Additive
Streptococcus pneumoniae ATCC 700677	16.0	4.0	4	0.5	0.250	0.125	0.375	Synergistic
Streptococcus pneumoniae ATCC 49619	8.0	0.50	4	0.125	0.500	0.500	1.000	Additive

Keywords: FICI: fractional inhibitory concentration index, FIC_a (fractional inhibitory concentration a): $\frac{\text{MIC of PSCB in combination with amoxicillin or cefotaxime}}{\text{MIC of PSCB alone}}$,

FIC_b (fractional inhibitory concentration b): $\frac{\text{MIC of amoxicillin or cefotaxime in combination with PSCB}}{\text{MIC of amoxicillin or cefotaxime alone}}$, MIC: minimum inhibitory concentration

3.4 *Scanning electron microscopy examination of antibacterial treated cells*

The detailed SEM images of test organisms following antibacterial treatment are presented in Figures 3 to 6 for multidrug resistant strain while that of the sensitive strain are presented in Supplementary Figure S5 to S8. SEM examination of the untreated test organisms shows that the cells looked undamaged with normal cell morphology (Figures 3 to 6; Supplementary Figures S 5 to S8). However, for the antibacterial treated cells, alteration in cell morphology was observed in all the test organisms following treatment with MBC concentration (Figures 3 to 6; Supplementary Figures S5 to S8). Specifically, In the sensitive strain of *E. coli* (*E. coli* ATCC 11775) (Supplementary Figure S5), cell elongation with dent formation in cell wall were observed following treatment with silicristin, cefotaxime and PSCB. However, in the multidrug resistant strain of *E. coli* (*E. coli* ATCC BAA-197), the cell looked corrugated, with sores and blisters on the cell wall which is more evident in the silicristin treated cell (Figure 3c) compared to cefotaxime (Figure 3b) and PSCB (Figure 3d) treated cells. According to Spratt (1975), beta-lactams that specifically inhibit cell division binds to PBP3 and the inhibition of cell division might lead to cell elongation or filamentation. Thus, the increased length of cells in *E. coli* ATCC 11775 following antibacterial treatment might suggest the ability of cefotaxime, silicristin and PSCB to inhibit PBP3. This observation is consistent with prior study of Singh *et al*. (2021) where hydroxychavicol (a phenolic) treatment of *E. coli* led to cell elongation. The lack of cell elongation in the resistant strain *E. coli* ATCC BAA-197 might mean that the resistant strain of *E. coli* could overcome inhibition of cell division. However, the presence of sores and blisters on the cell wall of *E. coli* ATCC BAA-197 following antibacterial treatment might suggest cell wall damage, which is more obvious in the silicristin treated cells (Figure 3c). Conversely, uneven cell length, with several blisters in cell wall was observed in both strains of *P. aeruginosa* (Figure 4; Supplementary Figure

S6)following antibacterial treatment and like with *E. coli* treated cells, this observation was more apparent in silicristin treated cells (Figure 4c; Supplementary Figure S6c). This observation while been consistent with previous report (Yi *et al*., 2010), highlight the ability of the antibacterial agent and most especially silicristin to cause cell wall damage. In Gram-positive organisms (strains of *S. aureus* and *S. pneumoniae*), cells with dented cell walls and pores, busted cells and completely lysed cells were observed after antibacterial treatment (Figure 5 and 6; Supplementary Figure S7 and S8). Like Gram-negative organism, the damage caused to cell wall was higher in silicrsitin treated cell (Figure 5c and 6c; Supplementary Figure S7c and S8c). Spratt (1975) showed that binding of PBP2 might cause significant change in cell shape while binding of PBP1 might instigate cell lysis. In this study, the observation that more lysed and busted cells in the sensitive and resistant strain of *S. aureus* and *S. pneumoniae* were observed rather than significant changes in cell shape might suggest more interaction with PBP1 by the antibacterial agents and most especially silicristin.

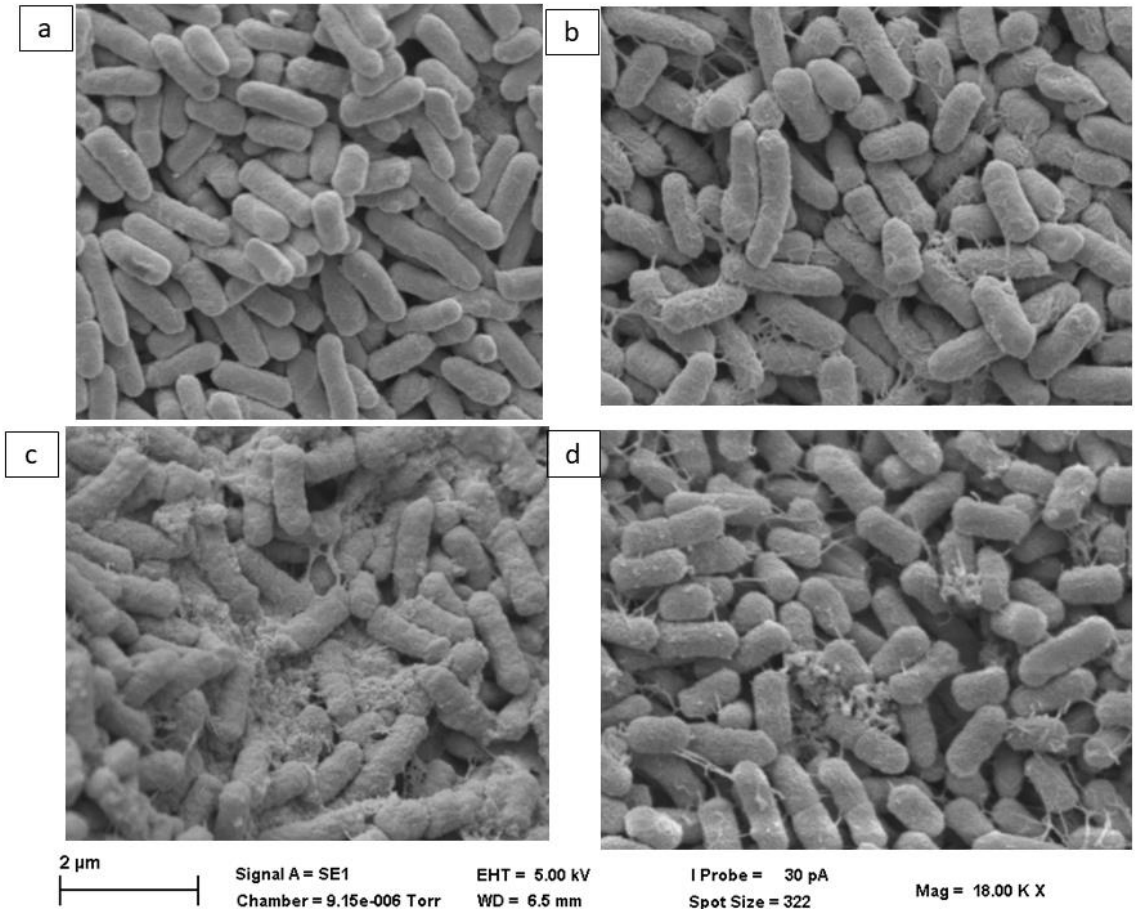


Figure 3: Scanning electron microscopic images of (a) untreated *E. coli* ATCC 11775 and *E. coli* ATCC 11775 treated with MBC concentration of (b) cefotaxime (c) silicristin and (d) PSCB.

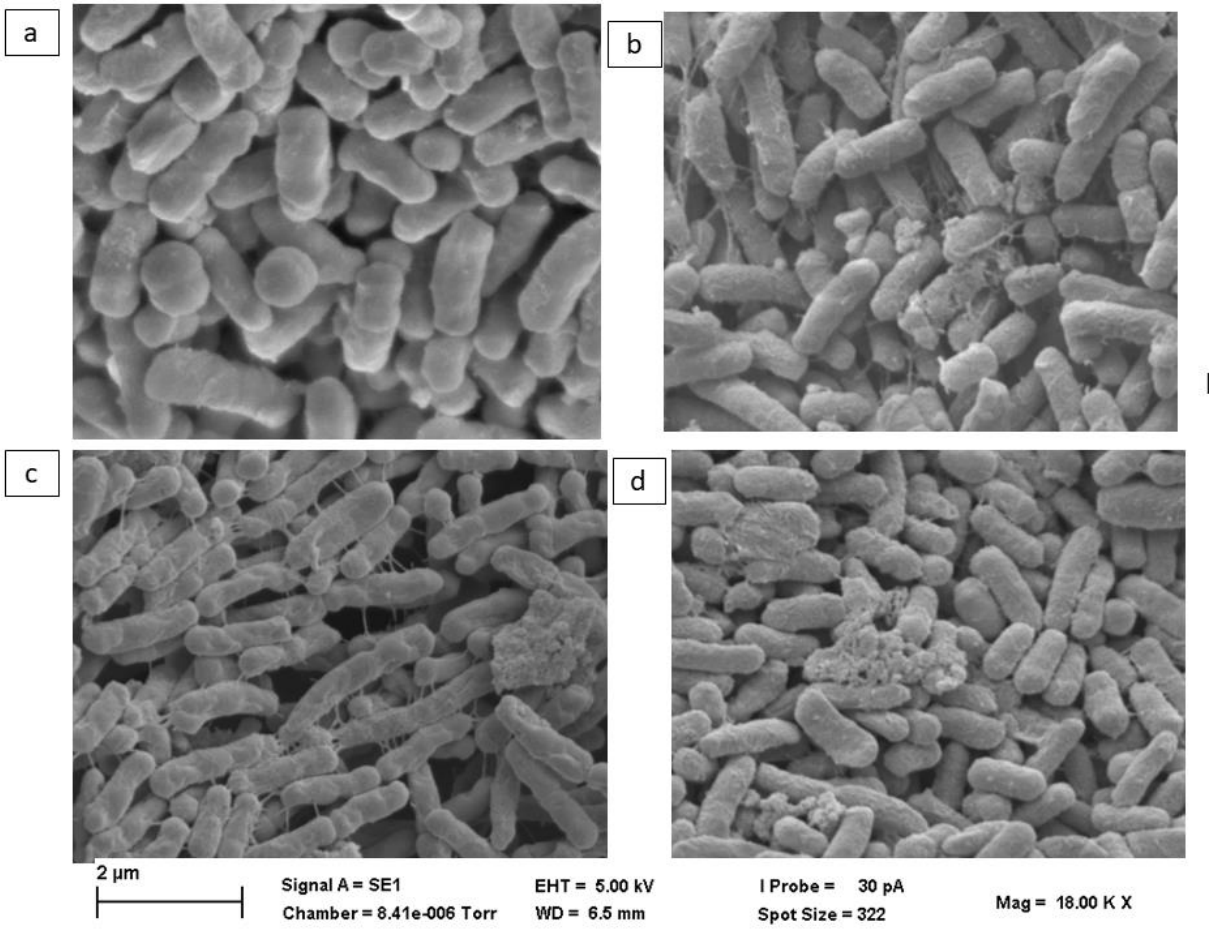


Figure 4: Scanning electron microscopic images of (a) untreated *P. aeruginosa* ATCC BAA-3197 and *P. aeruginosa* ATCC BAA-3197 treated with MBC concentration of (b) cefotaxime (c) silicristin and (d) PSCB.

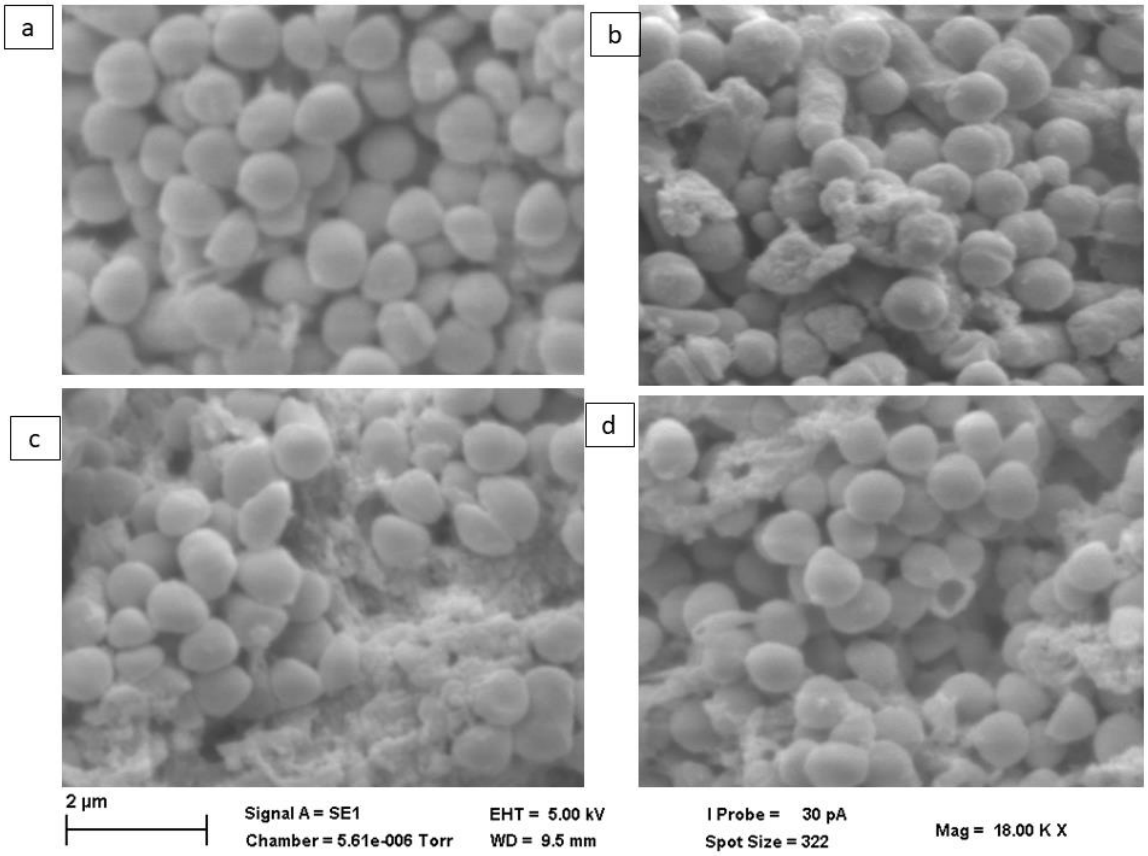


Figure 5: Scanning electron microscopic images of (a) untreated *S. aureus* ATCC 43300 and *S. aureus* ATCC 43300 treated with MBC concentration of (b) cefotaxime (c) silicristin and (d) PSCB.

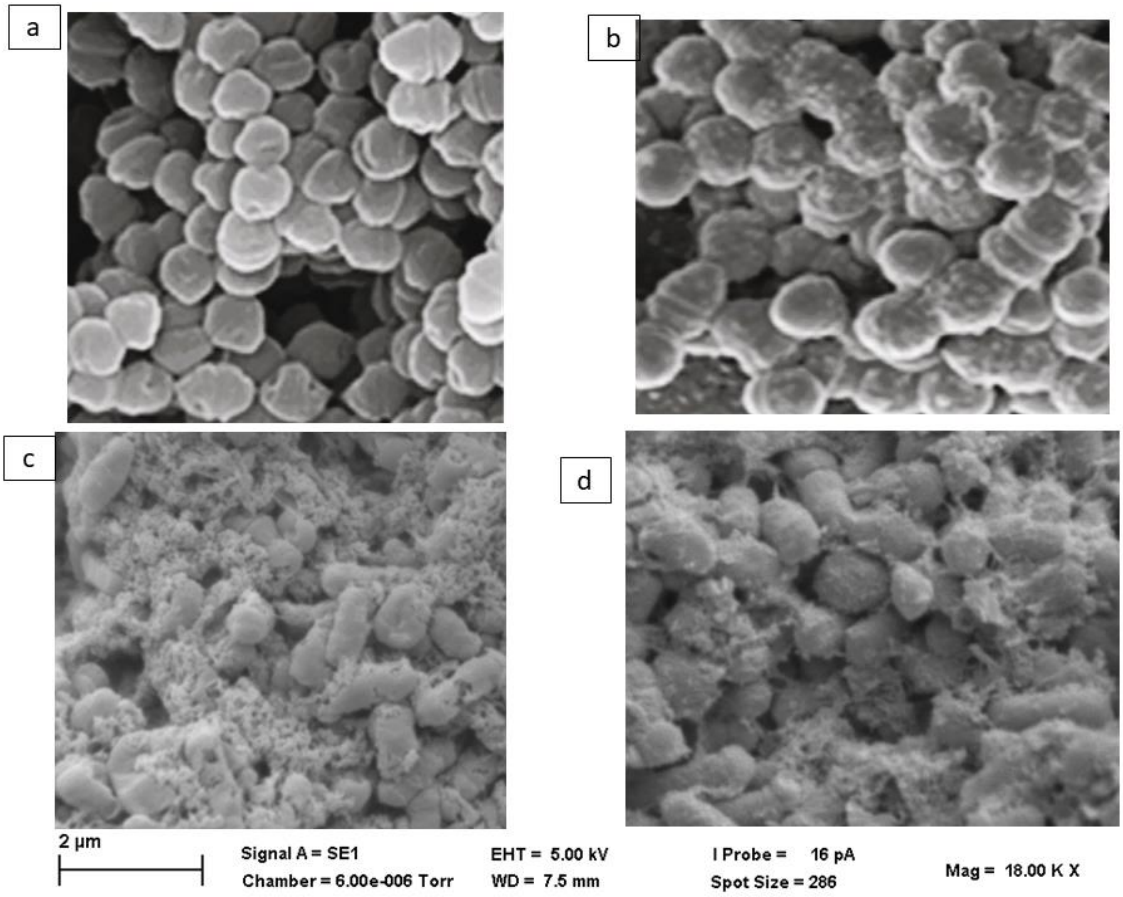


Figure 6: Scanning electron microscopic images of (a) untreated *S. pneumoniae* ATCC 700677 and *S. pneumoniae* ATCC 700677 treated with MBC concentration of (b) cefotaxime (c) silicristin and (d) PSCB.

3.5 *Transmission electron microscopy examination of antibacterial treated cells*

Transmission Electron Microscopy (TEM) was employed to observe the morphological and ultrastructural alterations induced in sensitive and resistant strains of the test organisms upon exposure to MBC concentration of the antibacterial agent relative to the untreated cells. The untreated cells remained intact, with an uninterrupted cell wall, a clearly apparent cell membrane, and a uniform cytoplasm suggesting healthy cells (Figure 7 to 10; Supplementary Figure S9 to S12). In contrast, significant cell deaths (indicated in black arrows) evident from cells with

separated cytoplasmic membrane, broken cell wall, obvious cytoplasmic clear zones and scattering of the intracellular contents were observed in MBC treated cells (Figure 7 to 10; Supplementary Figure S9 to S12). Specifically, while the resistant strains of *S. aureus* (*S. aureus* ATCC 43300) had translucent cell wall (Figure 7), the sensitive strain had cell wall with detached cytoplasmic membrane (Supplementary Figure S9). However, both strains had distorted cell shape relative to the smooth and spherical shape of the untreated group. Unlike the SEM findings where minimal changes in cell shape was observed in *S. aureus* treated cells, the observation of distorted cell shape in the TEM images might suggest the ability of the investigated antibacterial to inhibit PBP2 as previous study have demonstrated that binding of PBP2 cause significant change in cell shape (Spratt, 1975). Translucent cell wall in the resistant strains following antibacterial treatment and the observed detached cytoplasmic membrane from cell wall in the sensitive strain of *S. aureus* highlight the losses of cell wall integrity in both strains. Similar observations were noted in the antibacterial treatment of *S. pneumoniae,* where the resistant strain (*S. pneumoniae* ATCC 700677) had cell wall that are translucent following treatment with MBC concentration of all the antibacterials (silicristin, amoxicillin and PSCB) (Figure 8). On the other hand, membrane merging, degeneration of the cell wall and/or membrane, clumping, cell shape alteration, cytoplasmic disruptions of cells and ruptured indicative of cell death were noted in the sensitive strain of *S. pneumoniae* (*S. pneumoniae* ATCC 49619) following antibacterial treatment with silicristin (Supplementary Figure S10c) and PSCB (Supplementary Figure S10d), a finding that is consistent in the amoxicillin-treated cell (Supplementary Figure S10b). This observation is consistent with the result of Wijesundara *et al*. (2021), where carvacrol, a phenolic monoterpenoid cause cell death in *S. pyogenes* following significant damage to cell wall and cell membrane. TEM analysis of *E. coli*-treated cells showed that the resistant strain (*E. coli* ATCC BAA-197) (Figure

9) exhibited cytoplasmic defects after treatment with amoxicillin and silicristin. This observation could be due to the turgor pressure on the cytoplasm due to damage to the cell wall and cell membrane after antibacterial treatment. Similarly, in the sensitive strain of *E. coli* (*E. coli* ATCC 11775) (Supplementary Figure S11), disintegration of the cell wall and membrane was noted with all the antibacterial treated cells. Against the resistant strain of *P. aeruginosa* (*P. aeruginosa* ATCC BAA-3197), PSCB (Figure 10d) and amoxicillin (Figure 10b) caused significant disintegration of the cell wall and membrane after antibacterial treatment, while cells treated with silicristin (Figure 10c) resulted in cell shape distortion, membrane fusion and cell rupture. In the sensitive strain of *P. aeruginosa* (*P. aeruginosa* ATCC27853) (Supplementary Figure S12), defects such as fusion and disintegration of cell membrane and cell wall were common with all the antibacterial treated cells. However, translucent cytoplasmic which might be due to the turgor pressure on the cytoplasm was specific to silicristin (Supplementary Figure S12c) and PSCB (Supplementary Figure S12d) treated cells. Studies have shown that antibiotics that damage the peptidoglycan owing to the inactivation of essential PBPs in bacteria might cause turgor pressure on the cytoplasmic following disintegration of the cell wall and cell lysis (Silhavy *et al*., 2010). Hence the comparable antibacterial effect of silicristin and PSCB relative to amoxicillin on both Gram-positive and Gram-negative organisms in this study is suggestive of the potential of silicristin and PSCB as broad-spectrum beta-lactams. This observation is consistent with previous studies where silicristin had broad spectrum effects on a wide range of essential PBPs of Gram-positive and Gram-negative organisms *in silico* (Aribisala *et al*., 2023; Aribisala and Sabiu, 2022)

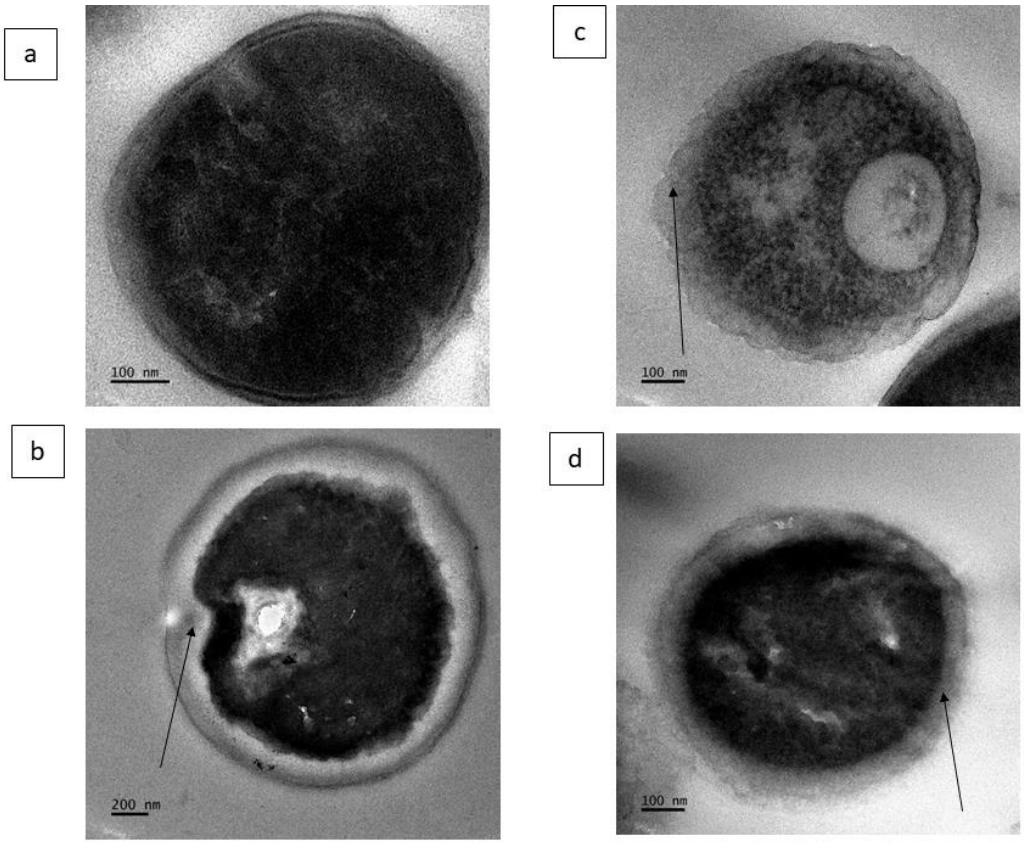


Figure 7: Transmission electron microscopic micrographs of (a) untreated *S. aureus* ATCC 43300 and *S. aureus* ATCC 43300 treated with MBC concentration of (b) cefotaxime (c) silicristin and (d) PSCB.

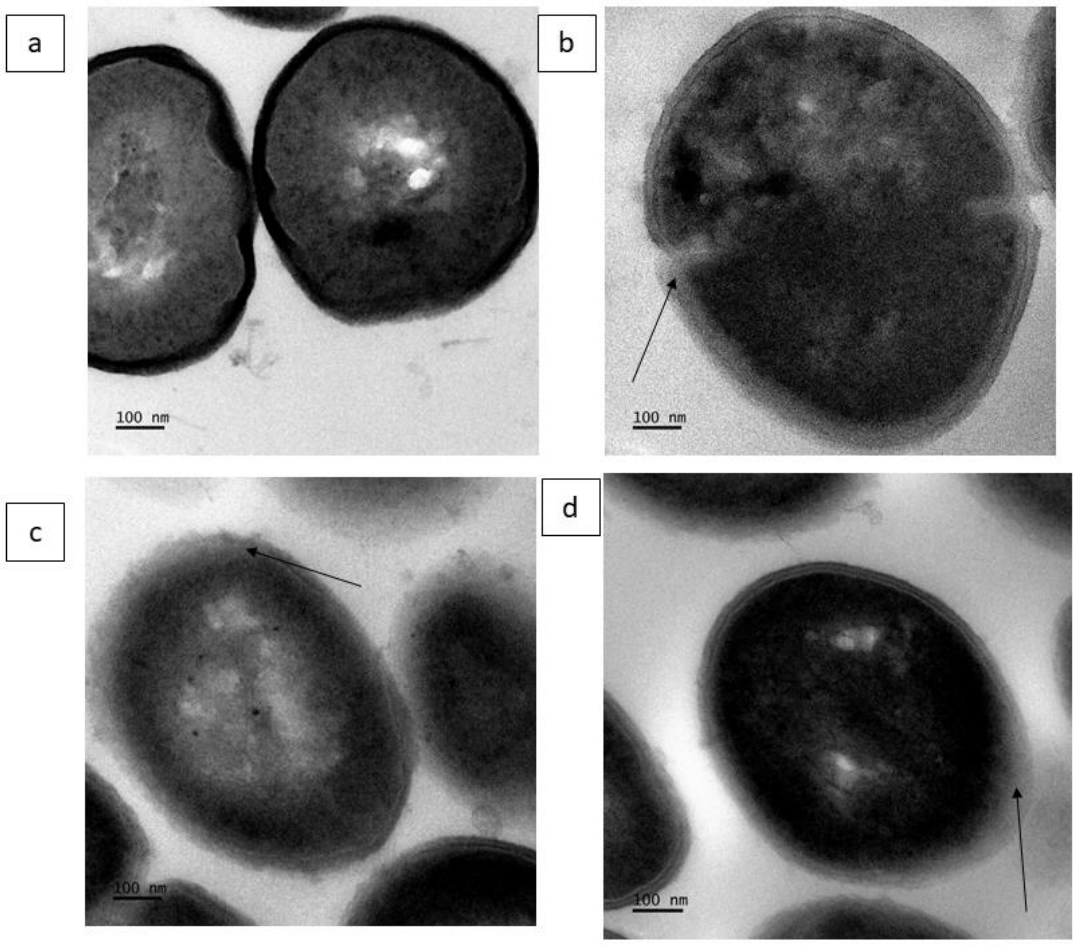


Figure 8: Transmission electron microscopic micrographs of (a) untreated *S. pneumoniae* ATCC 700677 and *S. pneumoniae* ATCC 700677 treated with MBC concentration of (b) cefotaxime (c) silicristin and (d) PSCB.

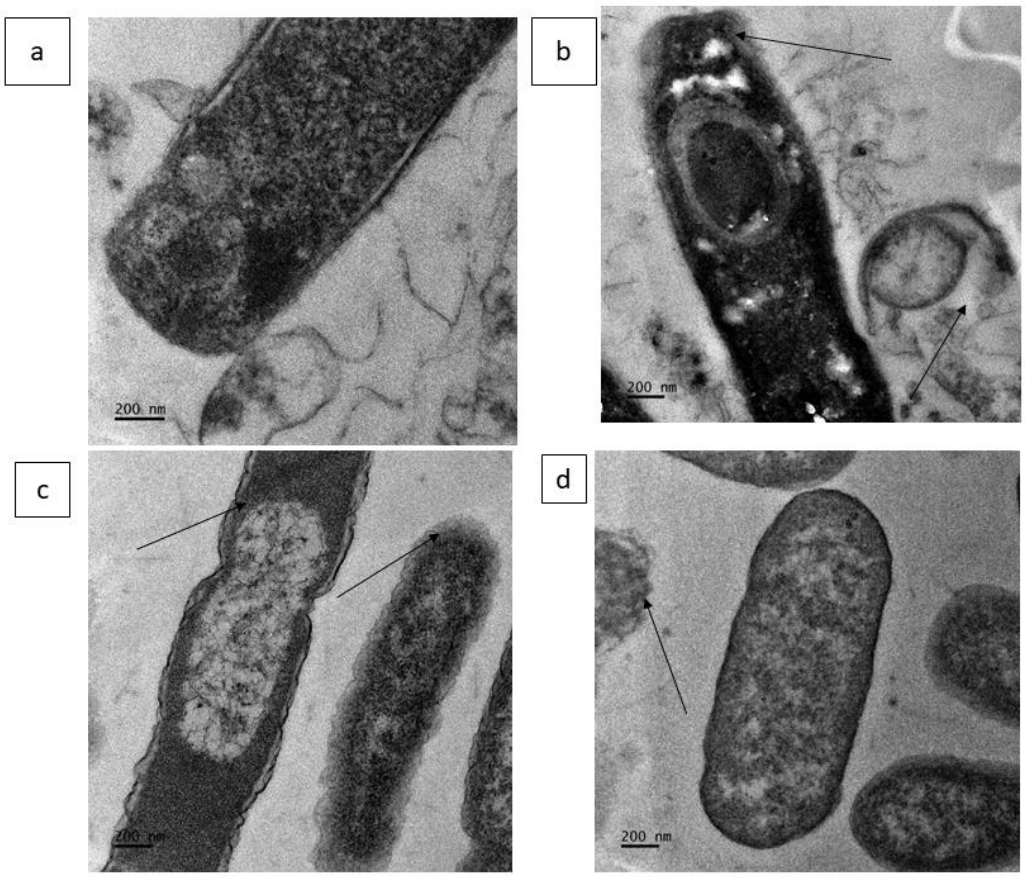


Figure 9: Transmission electron microscopic micrographs of (a) untreated *E. coli* ATCC 11775 and *E. coli* ATCC 11775 treated with MBC concentration of (b) cefotaxime (c) silicristin and (d) PSCB.

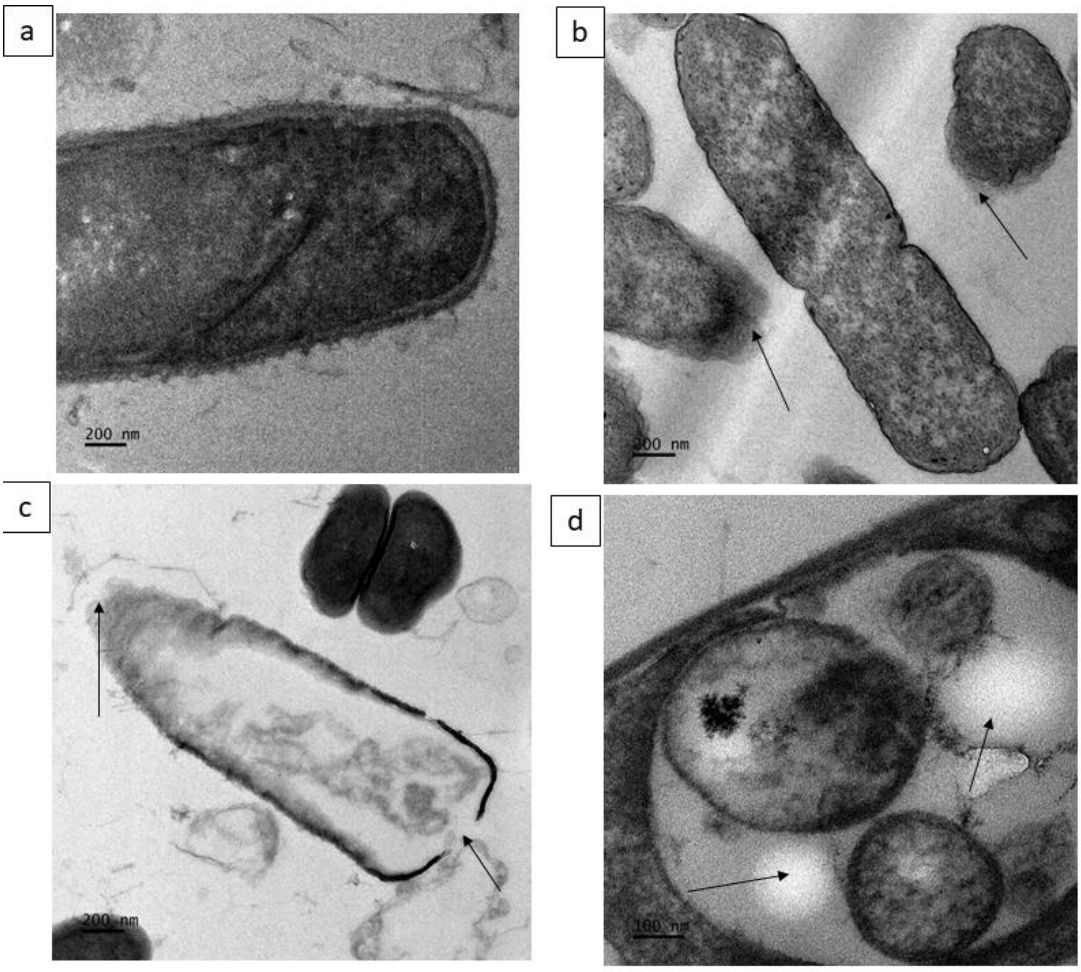


Figure 10: Transmission electron microscopic micrographs of (a) untreated *P. aeruginosa* ATCC BAA-3197 and *P. aeruginosa* ATCC BAA-3197 treated with MBC concentration of (b) cefotaxime (c) silicristin and (d) PSCB.

3.6 *Effects of antibacterial treatments on the level and types of ROS generation*

Several studies have shown that enhanced generation of ROS via redox reactions or due to antibiotic treatment can overcome cellular defense mechanisms, leading to oxidative stress (Lam *et al*., 2020; Mourenza *et al*., 2020; Kim *et al*., 2019). During oxidative stress, small amounts of ROS, against which cells have limited defenses, can quickly become fatal, particularly for bacteria (Mourenza *et al*., 2020). This mechanism of action has been linked to the antibacterial lethality of

most antibiotics such as beta-lactams and fluoroquinolones (Lam *et al*., 2020; Mourenza *et al*., 2020). Some considerations that undermine this hypothesis are the low specificity of dyes for ROS detection and the fact that ROS generated during antibiotic treatment are too small to truly kill bacterial cells (Keren, *et al*., 2014; Liu and Imlay, 2013). To more reliably determine the involvement of ROS in the antibacterial lethality of antibiotics and phenolics *in vitro*, this study employed a high-throughput ROS quantification assay using a diverse group of fluorescent reporter dyes (Table 1) commonly used to detect and quantify ROS following antibacterial treatment (Dwyer *et al*., 2014). A relatively lesser fluorescence was observed for all the dyes in the untreated cells relative to the antibacterial treated cells (Figure 11 to 14; Supplementary Figure S13 to S16). This observation, while consistent with previous studies (Lam *et al*., 2020; Mourenza *et al*., 2020), might mean that the untreated cells generate a relatively lesser concentration of ROS relative to the antibacterial treated cells. The lesser level of ROS generation in the untreated cells could generally be detoxified by the cellular defense mechanisms, leading to no damage to cells as observed in the SEM and TEM micrographs of this study. However, in the antibacterial treated cells, high levels of fluorescence were observed for all the dyes in all the test organisms (Figure 11 to 14; Supplementary Figure S13 - S16). Specifically, except in the sensitive strain of Gram-negative bacteria (*E. coli* and *P. aeruginosa*) (Supplementary Figure S13 - S14), PSCB and the reference standards (cefotaxime in Gram-negative bacteria and amoxicillin in Gram-positive bacteria) caused higher fluorescence of OxyBURST™ Green H_2DCFDA and carboxy-H2DCFDA relative to silicristin in all the strains of the test organisms (Figure 11 to 14; Supplementary Figure S15 to S16). From literature, OxyBURST™ Green H_2DCFDA has been shown to be specific in detecting superoxide ion ($O_2^{\bullet-}$), while carboxy-H2DCFDA is precise for hydrogen peroxide (H_2O_2) detection (Dwyer *et al*., 2014). Hence, the observation that PSCB and the reference

standards caused higher fluorescence of OxyBURST™ Green H_2DCFDA and carboxy-H2DCFDA relative to silicristin might means that both antibacterial agents instigated higher generation of $O_2^{\bullet-}$and H_2O_2 following antibacterial treatment. However, in both strains (sensitive and resistant strain) of the test bacteria, a significantly higher ($P < 0.05$) fluorescence of HPF and 6-Chloromethyl-2',7'-Dichlorod dyes was observed in the silicristin-treated cells relative to reference beta-lactams and PSCB treated cells (Figure 11 to 14; Supplementary Figure S13 to S16). This observation is an indication that silicristin caused higher generation of the hydroxy radical ($^{\bullet}$OH), as HPF dyes has been shown to be specific for the detection of hydroxy radical. Of the four major types of ROS in bacteria including $O2^{\bullet-}$, H_2O_2, $^{\bullet}$OH, and singlet oxygen ($^1O_2$) (Chen *et al*., 2011), studies have shown that $O_2^{\bullet-}$ and H_2O_2 pose fewer risks to bacteria compared to $^{\bullet}$OH and $^1O_2$, because of their lower reactivity and the ability to be detoxified by natural antioxidants in bacteria. Because no enzyme can detoxify •OH, these radicals are very poisonous and can be fatal (Glaeser *et al*., 2011; Altman, 2007). Thus, in this study, it could be deduced that silicristin generated the most fatal species of ROS ($^{\bullet}$OH) against all the test organisms and might explained why its treatments had the most prominent damage on bacteria cell wall/cell membrane in all the test organisms as evident from the SEM and TEM micrographs. This observation could be due to silicristin activating the Fenton reaction ($Fe^{2+} + H_20_2 \rightarrow {}^{\bullet}OH + Fe^{3+}$) faster than amoxicillin and PSCB by causing more damage to the iron-sulphur cluster in bacteria, therefore, generating more independent iron (Fe^{2+}) needed to convert H_2O_2 to •OH radical. This observation is consistent with previous studies where the importance of iron homeostasis was noted to be essential in the activation of Fenton reaction (Li *et al*., 2021; Yeom *et al*., 2010). Superoxide ion and H_2O_2 are however easily convertible by superoxide dismutase (SOD) which catalyses the conversion of $O_2^{\bullet-}$ to H_2O_2 in bacteria and catalase which helps in the conversion of H_2O_2 to water and oxygen

molecule. Thus, suggesting that the type of ROS generated by amoxicillin and PSCB are more easily/readily curbed by innate antioxidants in the cell. This observation is coherent with the findings of Xiong *et al.* (2017), who observed that H_2O_2 only plays a minimal role in the inhibition of *E. coli* following treatment with epigallocatechin gallate. Another important reason why silicristin might generate the most toxic type of ROS could be due to its characteristic hydroxy group which is absent in PSCB and amoxicillin. Studies have shown that phenolics due to their low redox potential, could be excellent pro-oxidants that generate a considerable quantity of ROS through auto-oxidation/redox cycling in the presence of transition metals (Singh *et al*., 2021; Sinsinwar *et al*., 2020, Ajiboye *et al*., 2018; Ajiboye *et al*., 2017, Xiong *et al.*, 2017). This could imply that in addition to the general endogenous mechanisms of ROS generation in bacteria which have been shown to involve the acceleration of tricarboxylic acid (TCA) cycle following antibacterial administration (Ajiboye *et al.*, 2018), treatment with silicristin might generate extra ROS via auto-oxidation, thus instigating a more intense oxidative stress in bacteria. Studies have shown that multidrug resistant strains often possess higher and competent natural antioxidant such as reduced glutathione and catalase needed in detoxifying ROS relative to their sensitive strains (Vila *et al*., 2020). In this study, reduced fluorescence of all the dyes were observed in the resistant strains of both Gram-positive and Gram-negative bacteria (Figure 11 to Figure 14) relative to their sensitive strains (Supplementary Figure S13 to Supplementary Figure S16) for all the antibacterial agents. This observation might mean that lesser $O2^{\bullet-}$, H_2O_2 and $^{\bullet}OH$ were generated in the resistant strain and might explain why silicristin, amoxicillin and PSCB were less effective against them relative to the sensitive strain. The generation of lower ROS in resistant strains of the test organisms in this study is consistent with the findings of Vila *et al*. (2020), who observed that multi-drug-resistant strains of both Gram-positive and Gram-negative bacteria elicited lesser ROS

relative to their sensitive strains following antibacterial treatment with colloidal silver solution. The study however highlighted that the Gram-negative bacteria such as *P. aeruginosa* and *E. coli* generated significantly higher ROS relative to Gram-positive bacteria such as *S.* aureus and *S. epidermidis*. This observation is in contrast with what was obtained in this study as lesser fluorescence of all the dyes were observed in Gram-positive organisms relative to Gram-negative bacteria following treatment with silicristin, PSCB and reference beta-lactams. The observed differences in the antibacterial agents used in both studies might have contributed to the disparity of ROS generated in Gram-positive and Gram-negative bacteria in both studies.

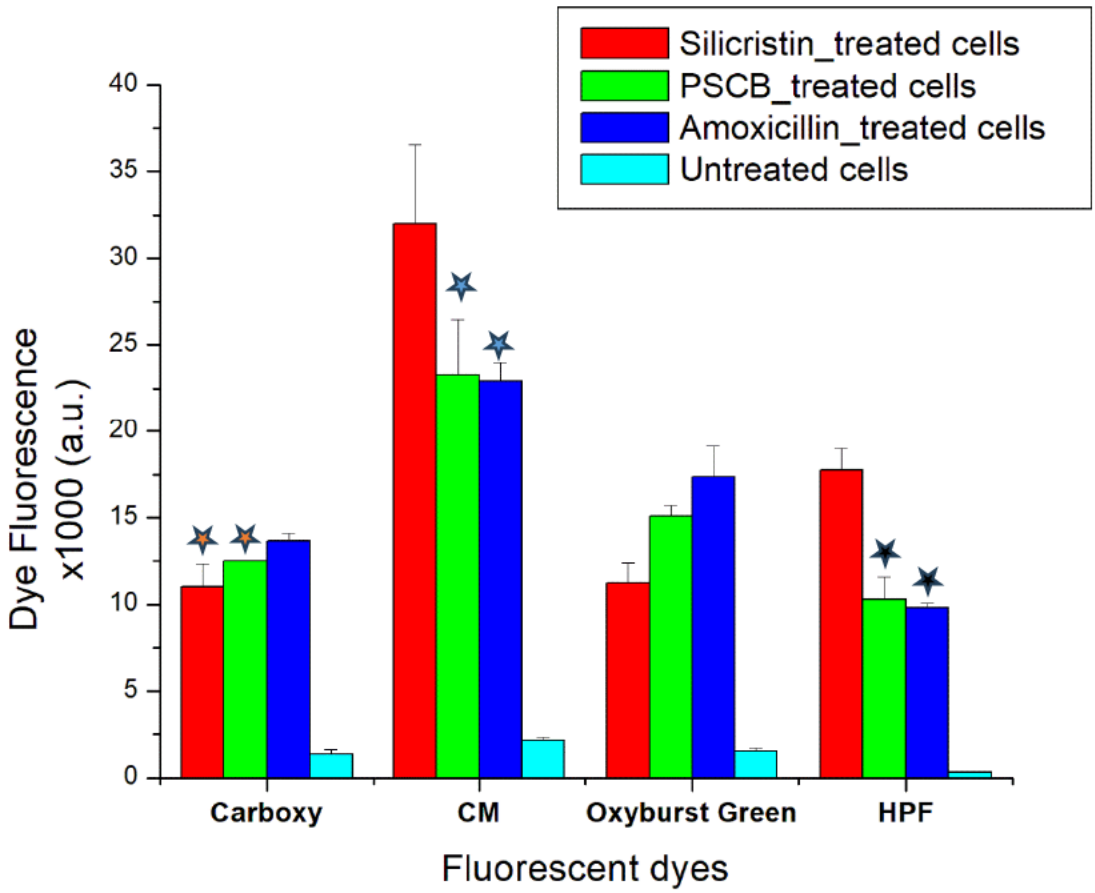


Figure 11: The level of reactive oxygen species (ROS) generated following antibacterial treatment of *S. aureus* ATCC 43300 (resistant strain). The values given are mean ± standard deviation. The same "star sign" colour on the same set of bars in the graph indicates no significant difference at $p > 0.05$.

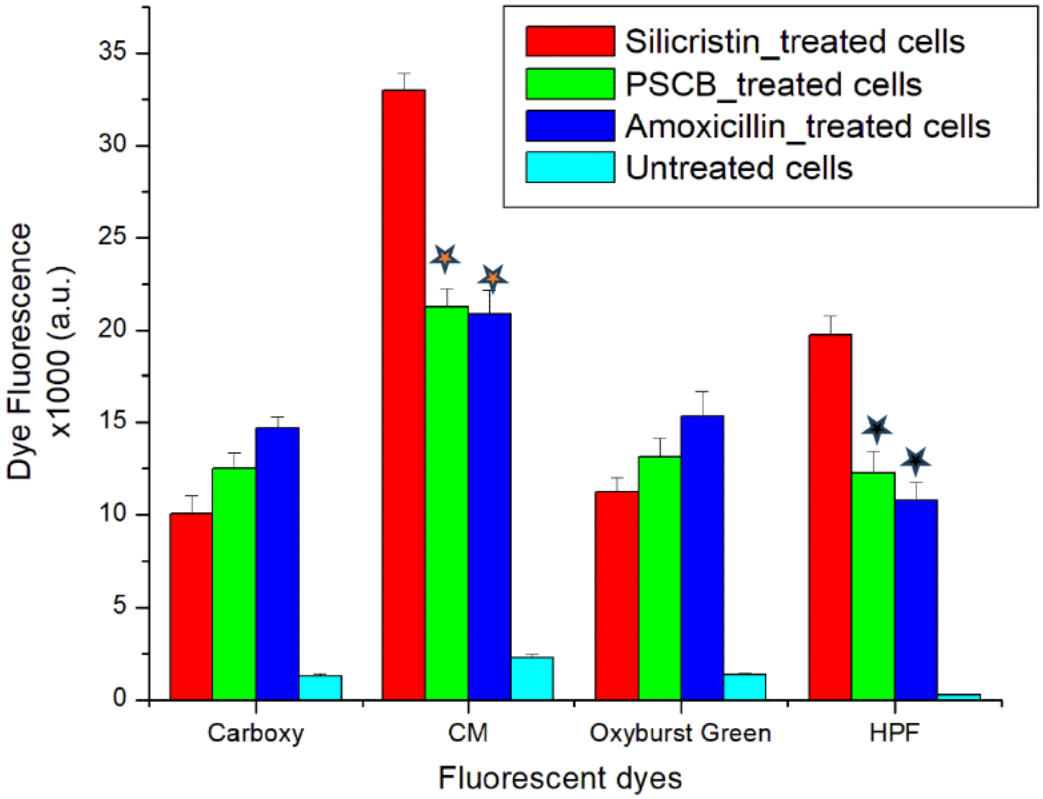


Figure 12: The level of reactive oxygen species (ROS) generated following antibacterial treatment of *S. pneumoniae* ATCC 700677 (resistant strain). The values given are mean ± standard deviation. The same "star sign" colour on the same set of bars in the graph indicates no significant difference at $p > 0.05$.

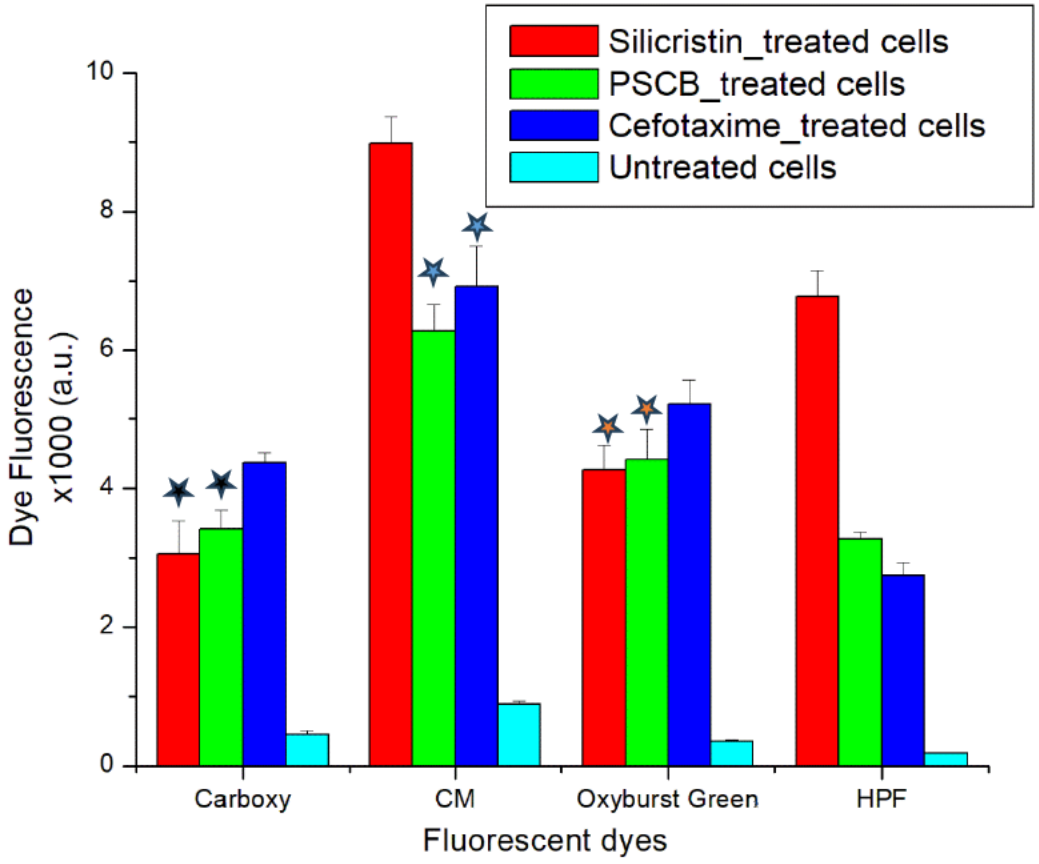


Figure 13: The level of reactive oxygen species (ROS) generated following antibacterial treatment of *E. coli* ATCC BAA-197 (resistant strain). The values given are mean ± standard deviation. The same "star sign" colour on the same set of bars in the graph indicates no significant difference at $p > 0.05$.

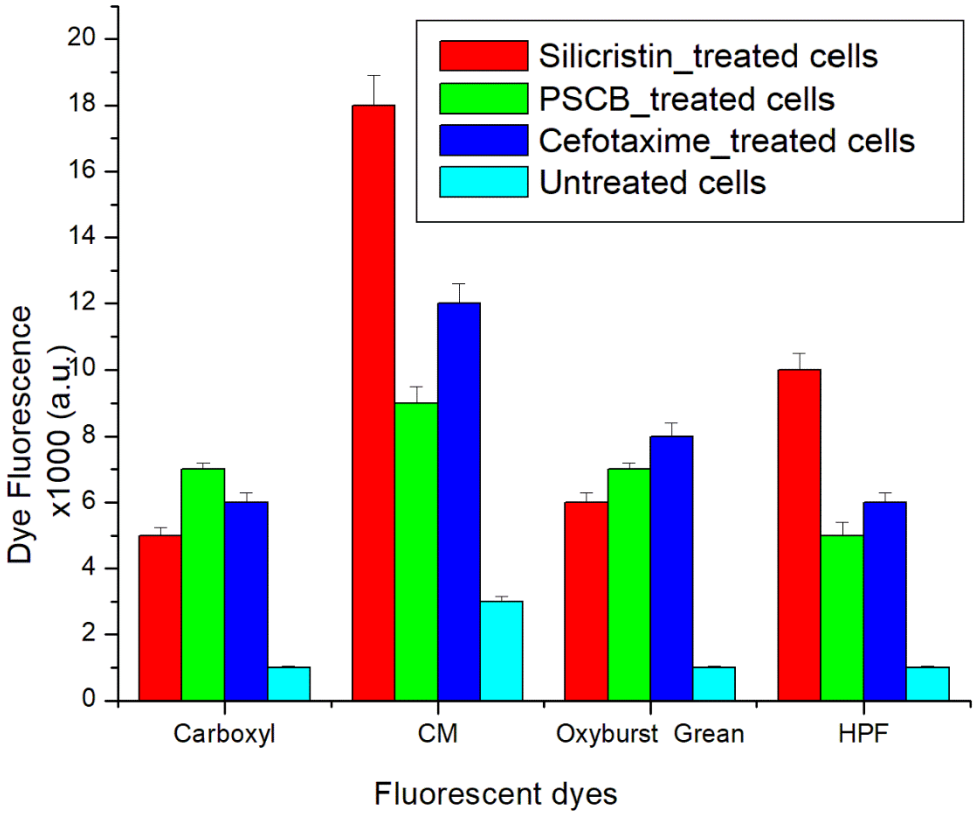


Figure 14: The level of reactive oxygen species (ROS) generated following antibacterial treatment of *P. aeruginosa* ATCC BAA-3197 (resistant strain). The values given are mean ± standard deviation. The same "star sign" colour on the same set of bars in the graph indicates no significant difference at $p > 0.05$.

3.7 *Effects of antibacterial treatment on cell membrane*

Outer membrane permeabilization is one of the strategies to render bacteria susceptible to antibiotics' treatments (Singh *et al*., 2021). In this study, membrane damage and bacterial cell viability were investigated by evaluating the uptake of PI, a cell-impermeable nucleic acid intercalation dye that can selectively stain dead and cell membrane damage cells. The untreated cells in all the test organisms generally had minimal levels of PI uptake after 1 h of incubation, suggesting a relatively higher cell viability with little or no damage to cell membrane (Table 6). On the other hand, silicristin-treated cells had the highest PI uptake in both the sensitive (between 10000 a.u. – 22000 a.u.) and resistant (between 6000 a.u. –16800 a.u.) strains of the test organisms after 1 h of incubation (Table 6). This observation suggests the relatively higher cell membrane damage and cell death in silicristin-treated cells relative to PSCB- and beta-lactams-treated cells, an observation that is consistent with the results of the time-kill assay in this study where silicristin had the highest kill rate against most of the test organisms. The increase cell death and membrane damage following treatment with silicristin in this study is consistent with the findings of Singh *et al.* (2021), where hydroxychavicol, a phenolic, significantly caused higher cell death and cell membrane damage relative to the control. Among the test organisms, the highest uptake of PI following treatment with silicristin was in the sensitive (22000 a.u.) and resistant (16800 a.u.) strains of *S. pneumoniae*, suggesting that the organism is relatively more susceptible to silicristin compared to other test organisms (Table 6). This observation is consistent with the MIC findings of this study where silicristin had the lowest MIC value against the sensitive and resistant strains of *S. pneumoniae*. Comparatively, while PSCB caused significantly higher cell death and cell membrane damage in *S. aureus* ATCC 25923, *S. pneumoniae* ATCC 700677, *E. coli* ATCC BAA-197, *P. aeruginosa* ATCC BAA-3197 and *P. aeruginosa* ATCC27853 relative to reference beta-

lactams, reference beta-lactams and PSCB had competitive effects that are not significantly different (P > 0.05) on *S. aureus* ATCC 43300, *S. pneumoniae* ATCC 49619 and *E. coli* ATCC 11775 (Table 6). Compared to both reference standard and PSCB, the higher cell membrane damage and cell death in silicristin-treated cells in this study might be related to the higher •OH generating potential of silicristin relative to reference beta-lactams and PSCB. Studies have shown higher damage to cellular macromolecule such as cell membrane and cell wall due to the accumulation of •OH (Singh *et al*., 2021). In this study, higher cell death and cell membrane damage were noted in the Gram-positive organisms relative to Gram-negative bacteria (Table 6). This observation is consistent with previous study where poor efficacy of plant derived compounds was observed in Gram-negative bacteria relative to Gram-positive bacteria (Tegos *et al*., 2002). Consistent with previous antibacterial and ROS assays of this study, a significant cell membrane damage was observed in the sensitive strains of the test organisms relative to resistant strains following antibacterial treatment with silicristin, PSCB and beta-lactams (Table 6).

Table 6: Membrane damage induced following treatment of sensitive (S) and resistant (R) strains of test bacteria with silicristin, PSCB and beta-lactams

Organisms	Organisms Status	Dye fluorescence x1000 (a.u.)			
		silicristin	PSCB	Beta-lactams	untreated
Staphylococcus aureus ATCC 43300	R	$11.0^{d} \pm 0.80$	$8.0^{c} \pm 0.50$	$7.0^{b} \pm 0.40$	$1.0^{a} \pm 0.05$
Staphylococcus aureus ATCC 25923	S	$16.0^{d} \pm 1.00$	$13.0^{c} \pm 0.80$	$10.0^{b} \pm 0.60$	$3.0^{a} \pm 0.10$
Pseudomonas aeruginosa ATCC BAA-3197	R	$8.0^{d} \pm 0.70$	$5.0^{c} \pm 0.40$	$4.0^{b} \pm 0.30$	$1.0^{a} \pm 0.06$
Pseudomonas aeruginosa ATCC27853	S	$12.0^{d} \pm 0.80$	$7.0^{c} \pm 0.50$	$5.0^{b} \pm 0.20$	$1.0^{a} \pm 0.05$
Escherichia coli ATCC BAA-197	R	$6.0^{d} \pm 0.50$	$4.0^{c} \pm 0.30$	$3.0^{b} \pm 0.30$	$0.5^{a} \pm 0.05$
Escherichia coli ATCC 11775	S	$10.0^{c} \pm 0.70$	$5.0^{b} \pm 0.30$	$5.0^{b} \pm 0.40$	$0.5^{a} \pm 0.06$
Streptococcus pneumoniae ATCC 700677	R	$16.8^{d} \pm 0.80$	$10.0^{c} \pm 0.50$	$7.5^{b} \pm 0.50$	$2.6^{a} \pm 0.20$
Streptococcus pneumoniae ATCC 49619	S	$22.0^{c} \pm 1.00$	$16.0^{b} \pm 0.80$	$17.0^{b} \pm 0.80$	$3.5^{a} \pm 0.30$

The values given are mean ± standard deviation. Mean values with the same letter across the column indicates no significant difference at $p > 0.05$.

3.8 *Effects of antibacterial treatment on the NAD+/NADH and ADP/ATP ratios of test organisms*

The superoxide anion radicals are generated from the electron transport chains (ETC) and tricarboxylic acid (TCA) cycle activities of the mitochondria and their production are mostly linked with high NAD^+/NADH and ADP/ATP ratios (Akhova and Tkachenko, 2014, Adam-Vizi and Chinopoulos, 2006). Also, a common mechanism of cell death is the stimulation of the Fenton reaction, which consumes ATP and NADH to increases the concentration of hydroxyl radicals, leading to oxidative damage to cells (Kohanski *et al*., 2010). Thus, the evaluation of the NAD^+/NADH and ADP/ ATP ratios following antibacterial treatment may help in the investigation of oxidative stress in bacterial cell. In this study, the untreated cells, had a significantly lower level of NAD+/NADH (Supplementary Figure S17 to S20) and ADP/ATP (Figure 15 to 18) ratios ranging between 1 and 3.2, and 0.1 and 0.3 respectively for all test organisms. This observation might suggest that untreated cells had a balanced redox state due to normal functioning of the ETC and the TCA cycle. In the treated cells however, treatment with silicristin instigated the highest level of NAD^+/NADH and ADP/ ATP ratios. Silicristin treated cells had a NAD^+/NADH (Supplementary Figure S17 to S20) and ADP/ ATP (Figure 15 to 18) ratios raging between 11 and 21, and 1 and 2.2 respectively for all the test organisms with higher ratios observed in the sensitive strains and Gram-positive organisms relative to the resistant strains and Gram-negative organism respectively. The observation might signify that silicristin instigated higher involvement of oxidative stress in the killing of the test organisms and is consistent with the ROS generating assay of this study where silicristin produce higher level of $^{\bullet}OH$ radical via

the Fenton reaction. Studies have shown that higher stimulation of the Fenton reaction consumes ATP and NADH (Kohanski *et al*., 2010). Furthermore, the significant rise in NAD^+/NADH and ADP/ATP ratios in the silicristin-treated cells might indicate that the compound caused ATP buildup by inhibiting energy-consuming activities such as phase 1 glycolysis (Akhova and Tkachenko, 2014). This inhibition may further impede the major electron flow route in the TCA cycle and ETC, causing the production of ROS as previously documented (Khumbulani *et al*., 2022). These observations align with previous studies where phenolic treated cells had increased NAD^+/NADH and ADP/ATP ratios (Khumbulani *et al*., 2022, Ajiboye *et al*., 2016). Comparatively, PSCB and the reference beta-lactams had competitive effects on NAD^+/NADH and ADP/ATP ratios of the test organisms and at $P > 0.05$, PSCB and the reference beta-lactam antibiotics had no significant effects on NAD^+/NADH ratios of the sensitive strains of *E. coli* (Supplementary Figure S17) and *P. aeruginosa* (Supplementary Figure S18) and all Gram-positive strains (Supplementary Figure S19 to S20). Similarly, no significant ($P > 0.05$) exist in the ADP/ATP ratios of the resistant strain of *E. coli* (Figure 15) and both strains of *P. aeruginosa* (Figure 16) and *S. pneumoniae* (Figure 17) following treatment with PSCB and the reference beta-lactam antibiotics. This observation might suggest that PSCB and the reference beta-lactam antibiotics had similar effect on the functioning of the ETC and the TCA cycle and is consistent with previous assays of this study where both compounds had comparable antibacterial killing effects and ROS generation. The NAD^+/NADH (Supplementary Figure S17 to S20) and ADP/ATP (Figure 15 to 18) ratios was higher in the sensitive strains and in Gram-positive organisms relative to the resistant strains and Gram-negative organisms respectively following treatments with silicristin, PSCB and the reference beta-lactams. This observation signifies enhanced functioning of the ETC and the TCA cycle in the sensitive strains and Gram-positive organisms relative to the

resistant strains and the Gram-negative organisms respectively and is consistent with the direct ROS quantification assay of this study and the subsequent membrane damage noted after antibacterial treatment. The enhanced NAD^+/NADH (Supplementary Figure S17 to S20) and ADP/ATP (Figure 15 to 18) ratios observed after antibacterial treatment was noted to be concentration dependent up to 2MIC for all the antibacterial agents. This observation might suggest that enhanced acceleration of the respiratory activities of the test organisms occur at higher concentration of the antibacterial treatment.

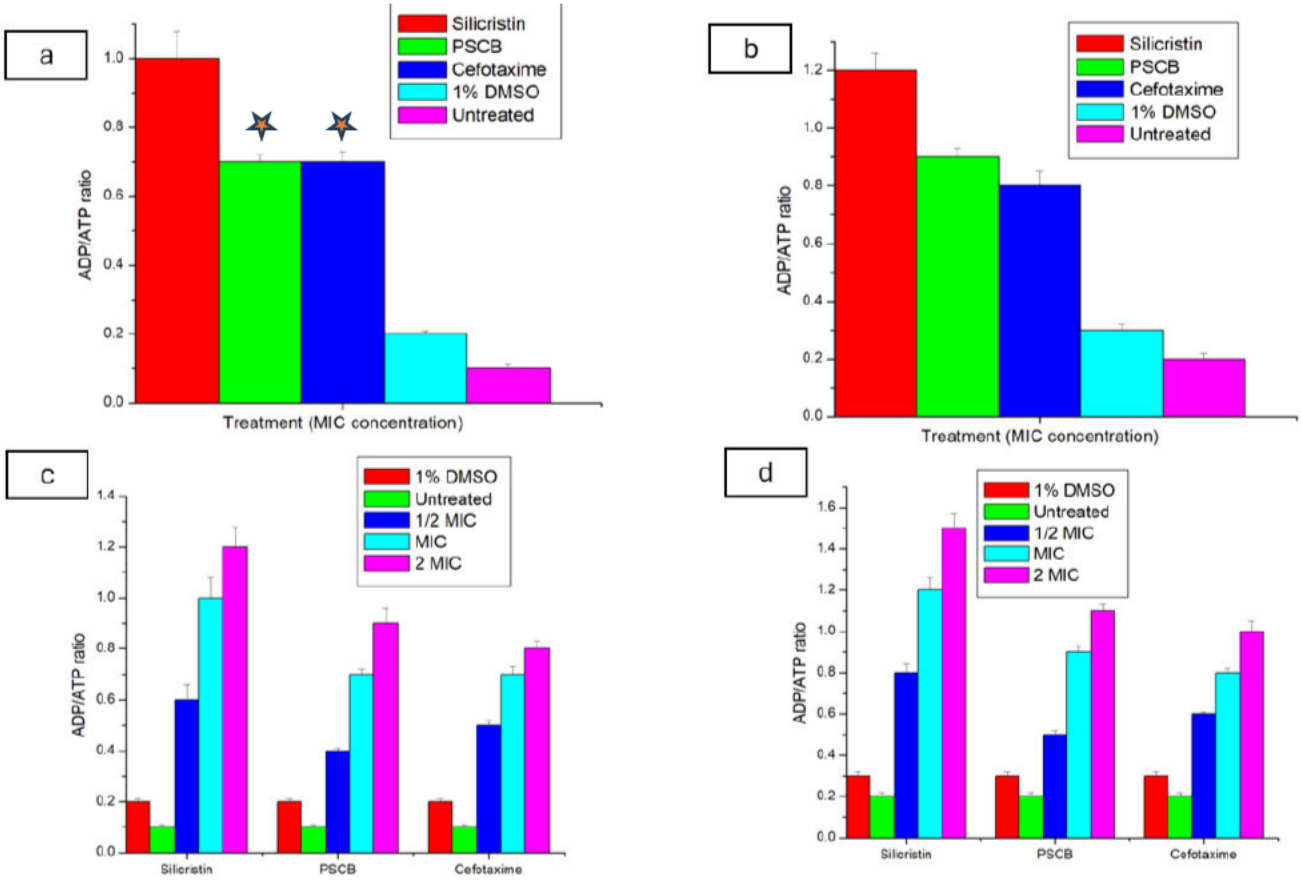


Figure 15: The level of ADP/ATP ratio in (a) *E. coli* ATCC BAA-197 (resistant strain), and (b) *E. coli* ATCC 11775 (sensitive strain) following antibacterial treatment with MIC concentration of silicristin, PSCB and cefotaxime. Effect of different concentrations on the level of ADP/ATP ratio of (c) *E. coli* ATCC BAA-197 (resistant strain), and (d) *E. coli* ATCC 11775 (sensitive strain) following antibacterial treatment with silicristin, PSCB and cefotaxime. The values given are mean ± standard deviation. The same "star sign" colour on the same set of bars in the graph indicates no significant difference at $p > 0.05$.

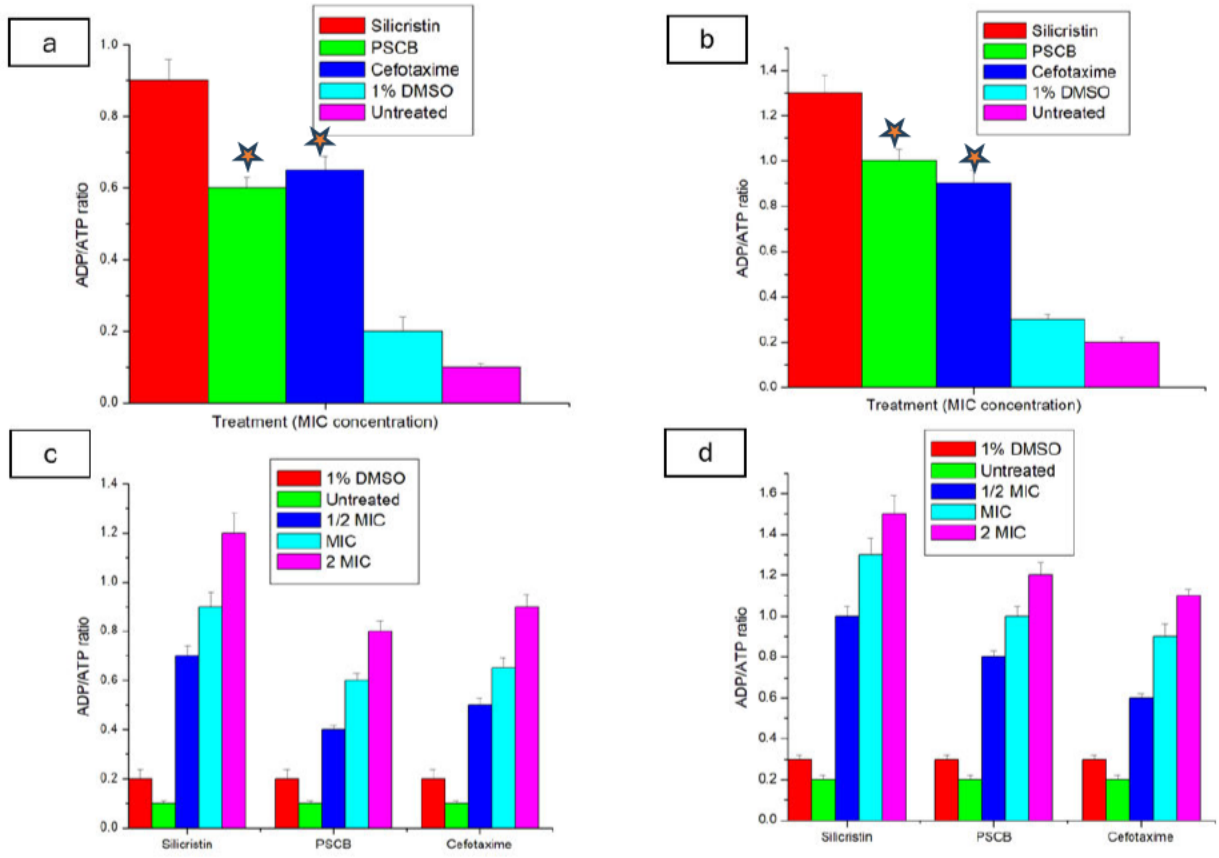


Figure 16: The level of ADP/ATP ratio in (a) *P. aeruginosa* ATCC BAA-3197 (resistant strain), and (b) *P. aeruginosa* ATCC27853 (sensitive strain) following antibacterial treatment with MIC concentration of silicristin, PSCB and cefotaxime. Effect of different concentration on the level of ADP/ATP ratio of (c) *P. aeruginosa* ATCC BAA-3197 (resistant strain), and (d) *P. aeruginosa* ATCC27853 (sensitive strain) following antibacterial treatment with silicristin, PSCB and cefotaxime. The values given are mean ± standard deviation. The same "star sign" colour on the same set of bars in the graph indicates no significant difference at $p > 0.05$.

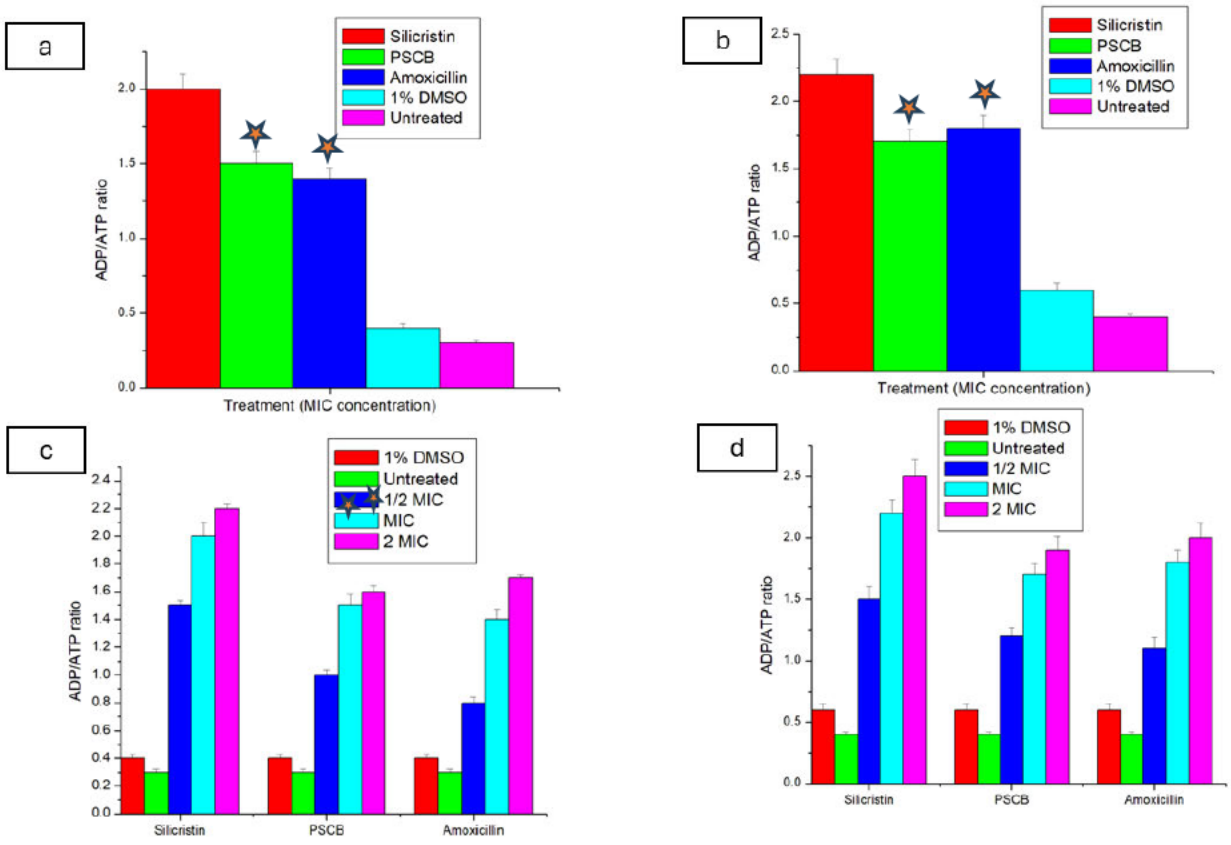


Figure 17: The level of ADP/ATP ratio in (a) *S. pneumoniae* ATCC 700677 (resistant strain), and (b) *S. pneumoniae* ATCC 49619 (sensitive strain) following antibacterial treatment with MIC concentration of silicristin, PSCB and amoxicillin. Effect of different concentrations on the level of ADP/ATP ratio of (c) *S. pneumoniae* ATCC 700677 (resistant strain), and (d) *S. pneumoniae* ATCC 49619 (sensitive strain) following antibacterial treatment with silicristin, PSCB and amoxicillin. The values given are mean ± standard deviation. The same "star sign" colour on the same set of bars in the graph indicates no significant difference at $p > 0.05$.

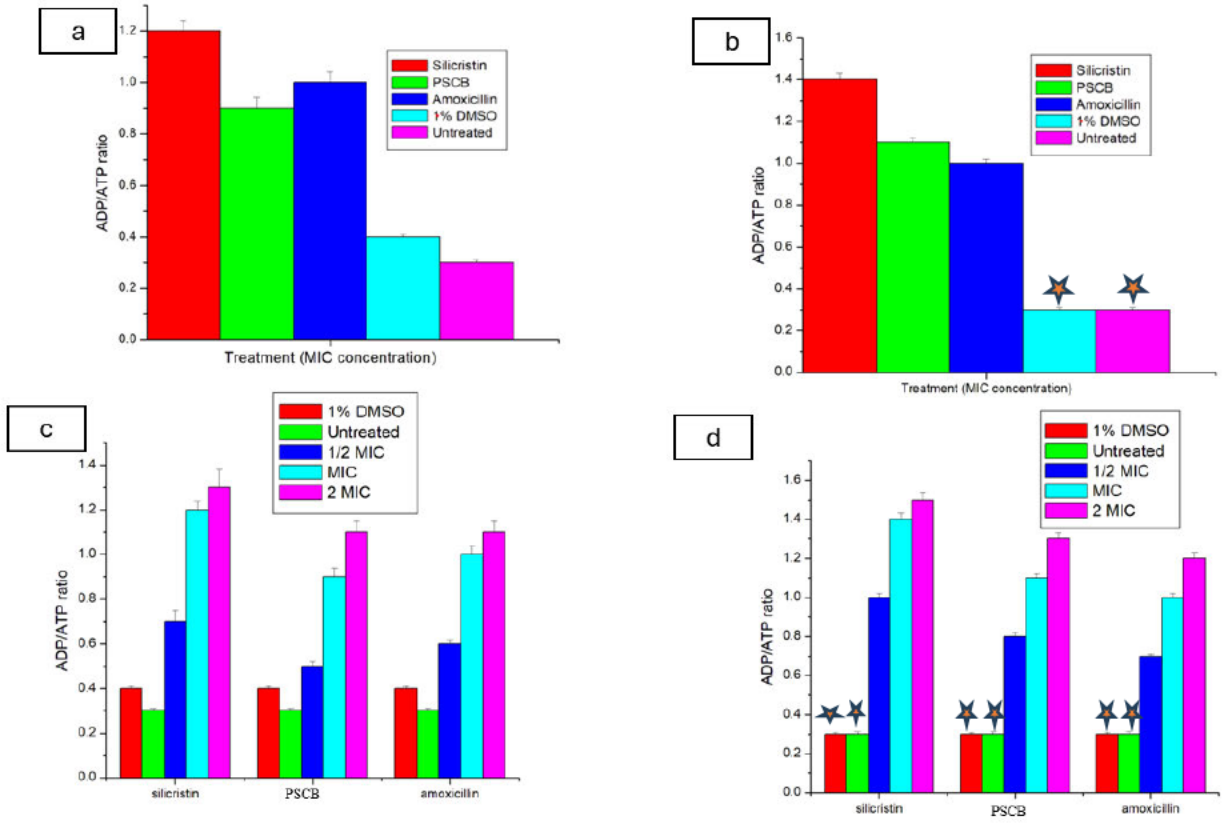


Figure 18: The level of ADP/ATP ratio in (a) *S. aureus* ATCC 43300 (resistant strain), and (b) *S. aureus* ATCC 25923 following antibacterial treatment with MIC concentration of silicristin, PSCB and amoxicillin. Effect of different concentration on the level of ADP/ATP ratio of (c) *S. aureus* ATCC 43300 (resistant strain), and (d) *S. aureus* ATCC 25923 following antibacterial treatment with silicristin, PSCB and amoxicillin. The values given are mean ± standard deviation. The same "star sign" colour on the same set of bars in the graph indicates no significant difference at $p > 0.05$.

3.9 *Effect of antibacterial treatment on the glutathione level of test organisms*

The cellular defense mechanism against ROS includes glutathione, which hampers the oxidation of glutathione (GSH) to Glutathione disulfide (GSSG) (Zitka *et al*., 2012). However, high ROS buildup results in the depletion of glutathione (Zitka *et al*., 2012). Thus, the GSH:GSSG ratio shows the extent of GSH degradation in antibacterial treated cells. The untreated cells had a significantly high level of GSH:GSSG ratios ranging between 3.5 and 5.0 (Figure 19 to 22) for all the test organisms with the resistant strains of the Gram-negative organism (*E. coli* and *P. aeruginosa*) (Figure 19 and 20) having the highest level of GSH:GSSG ratios. Compared to the untreated cells, a significant depletion of GSH was observed in all the test organisms following antibacterial treatment (Figure 19 to 22). The highest reduction of GSH:GSSG ratios was observed in cells treated with silicristin with ratios ranging between 0.75 and 2.0 for all the test organisms (Figure 19 to 22). Depletion of GSH is a hallmark of oxidative damage. GSH plays an important role as a reducing agent and is an important antioxidant, while GSSG is an oxidized form of GSH in bacterial cells (Arteel and Sies, 2001). Therefore, silicristin instigating the highest depletion of GSH might suggest that the compound caused the highest oxidization of the defense system which may trigger cellular dysfunctions (Zitka *et al*., 2012). This observation is not only consistent with the findings of the ROS assay of this study where treatment with silicristin generate the highest amount of ˙OH radical relative to reference beta-lactams and PSCB, but also align with the study of Han *et al*. (2022), where treatment with naringin, a phenolic, instigated higher depletion of GSH relative to norfloxacin and untreated cells. The reference beta-lactams and PSCB on the other hand, had a competitive effect on the test organisms with reference beta-lactams having higher ratio of GSH:GSSG in the resistant strain of *P. aeruginosa* (2.75) (Figure 20) and the sensitive strain of *S. aureus* (2.2) (Figure 22) while PSCB had higher ratio in both strains of *E. coli* (resistant strain:

2.5, sensitive strain: 2.0) (Figure 19) and the sensitive strain of *P. aeruginosa* (2.2) (Figure 20). Against both strains of *S. pneumoniae* (Figure 21), the reference beta-lactams and PSCB had no significant difference ($P > 0.05$) on the ratio of GSH:GSSG. Generally, higher level of GSH:GSSG ratios was observed in the resistant strains and Gram-negative organisms (Figure 19 and 20) relative to the sensitive strains and Gram-positive organisms (Figure 21 and 22) after antibacterial treatments (Figure 19 to 22). As glutathione, not only serves as a cofactor to glutathione peroxidase but also helps in the reversion of other non-enzymatic antioxidants, such as α-tocopherol and ascorbic acid, to their active form (Li *et al*., 2021), the observation of higher level of GSH:GSSG ratios in the resistant strains and Gram-negative organisms might mean that they are more competently equipped in scavenging ROS. This observation might explain why the resistant strains and Gram-negative organisms had relatively reduced ˙OH radical levels and subsequent reduced damage to cell membrane and cell wall relative to the sensitive strains and Gram-positive organisms in this study. Noteworthily, higher reduction in GSH:GSSG ratios increased as the concentration of treatment with silicristin, reference beta-lactams and PSCB increases in all the test organisms (Figure 19 to 22). This observation might imply that the intracellular redox status increased with concentrations of antibacterial treatment, therefore instigating higher ratio of GSH:GSSG to maintain cellular redox homeostasis. This submission is in tandem with a previous study where the change in the intracellular redox status of cells increased following treatment with increased concentration of antibiotics and phenolics (Wei *et al*., 2022). Overall, this study has highlighted that treatment with silicristin caused higher ratio of GSH:GSSG relative to the observations with PSCB- and the beta-lactams-treated cells. Also, the reduction of the GSH:GSSG ratio in the resistant strains and Gram-negative organisms were lesser compared to both the sensitive strains and Gram-positive organisms.

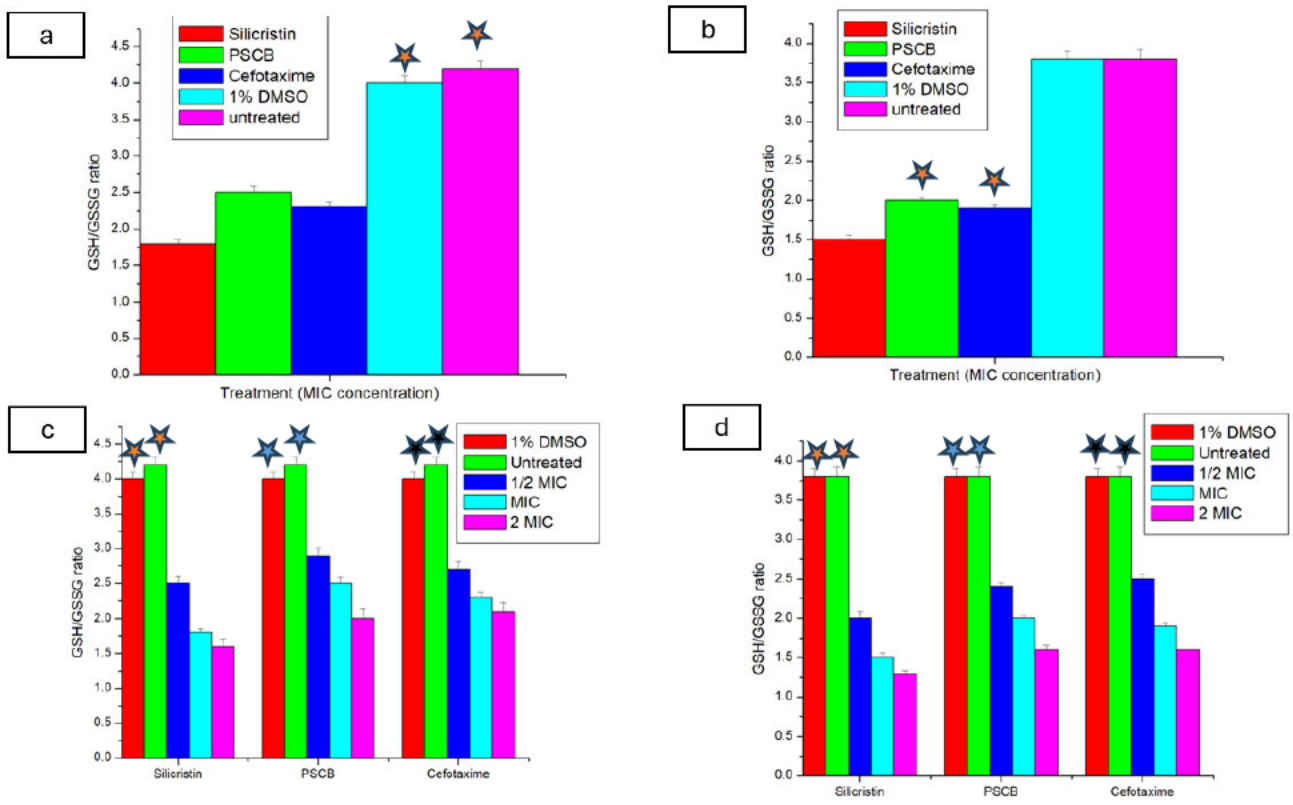


Figure 19: The ratio of reduced (GSH) to oxidized (GSSG) glutathione in (a) *E. coli* ATCC BAA-197 (resistant strain), and (b) *E. coli* ATCC 11775 (sensitive strain) following treatment with MIC concentration of silicristin, PSCB and cefotaxime. Effect of different concentration on ratio of reduced (GSH) to oxidized (GSSG) glutathione in (c) *E. coli* ATCC BAA-197 (resistant strain), and (d) *E. coli* ATCC 11775 (sensitive strain) following antibacterial treatment with silicristin, PSCB and cefotaxime. The values given are mean ± standard deviation. The same "star sign" colour on the same set of bars in the graph indicates no significant difference at $p > 0.05$.

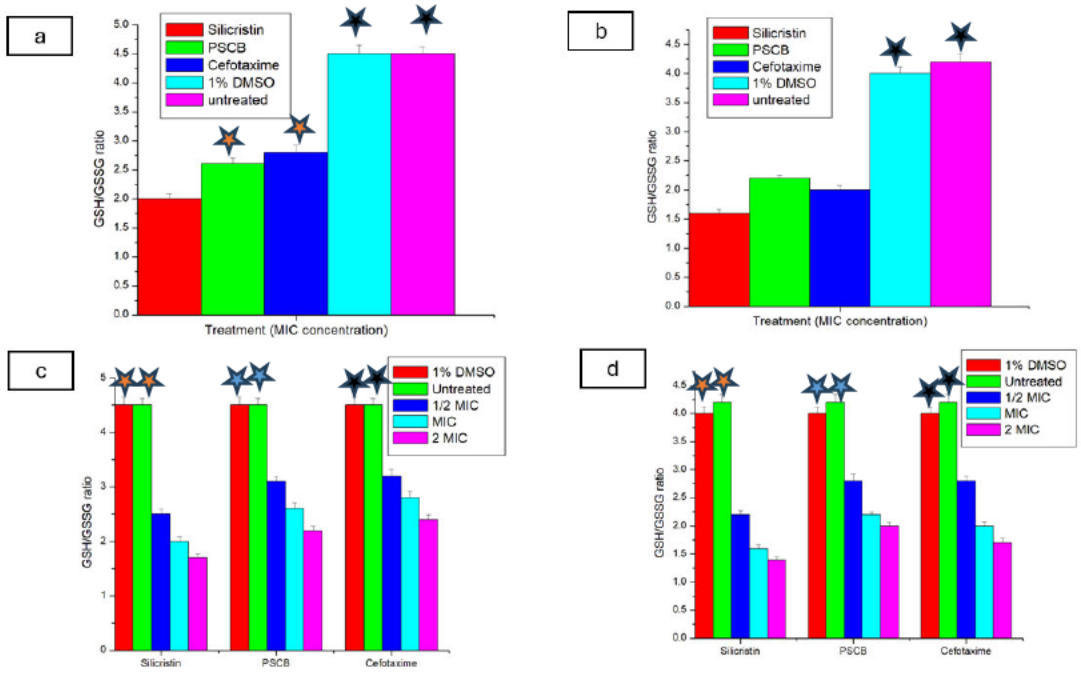


Figure 20: The ratio of reduced (GSH) to oxidized (GSSG) glutathione in (a) *P. aeruginosa* ATCC BAA-3197 (resistant strain), and (b) *P. aeruginosa* ATCC27853 (sensitive strain) following antibacterial treatment with MIC concentration of silicristin, PSCB and cefotaxime. Effect of different concentration on the ratio of reduced (GSH) to oxidized (GSSG) glutathione in (c) *P. aeruginosa* ATCC BAA-3197 (resistant strain), and (d) *P. aeruginosa* ATCC27853 (sensitive strain) following antibacterial treatment with silicristin, PSCB and cefotaxime. The values given are mean ± standard deviation. The same "star sign" colour on the same set of bars in the graph indicates no significant difference at $p > 0.05$.

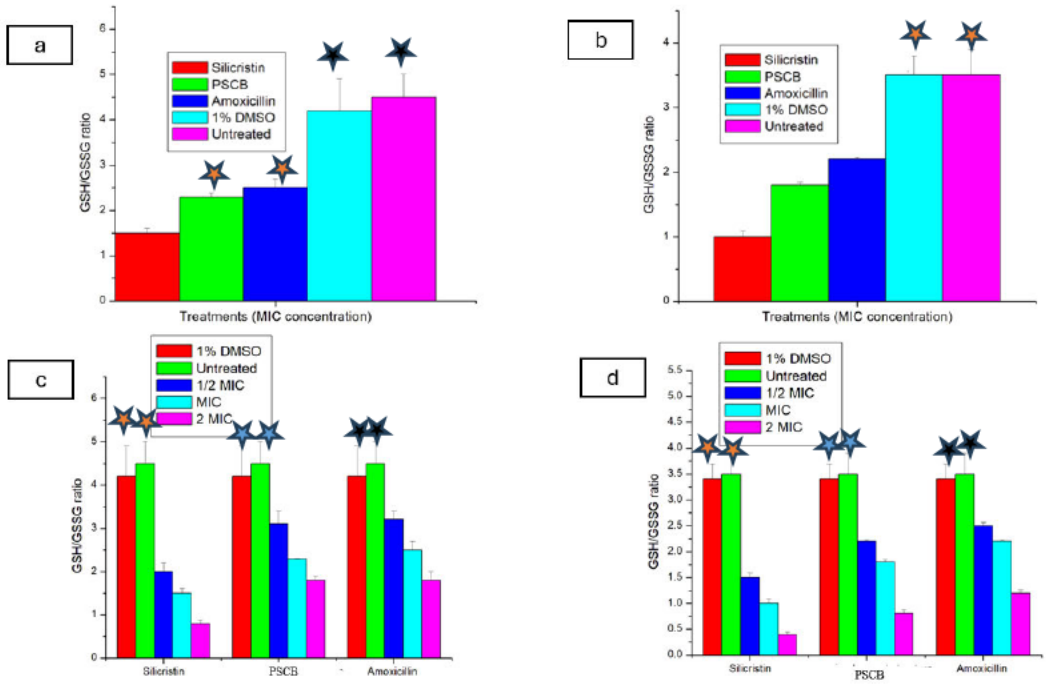


Figure 21: The ratio of reduced (GSH) to oxidized (GSSG) glutathione in (a) *S. aureus* ATCC 43300 (resistant strain), and (b) *S. aureus* ATCC 25923 following antibacterial treatment with MIC concentration of silicristin, PSCB and amoxicillin. Effect of different concentration on the ratio of reduced (GSH) to oxidized (GSSG) glutathione in (c) *S. aureus* ATCC 43300 (resistant strain), and (d) *S. aureus* ATCC 25923 following antibacterial treatment with silicristin, PSCB and amoxicillin. The values given are mean ± standard deviation. The same "star sign" colour on the same set of bars in the graph indicates no significant difference at $p > 0.05$.

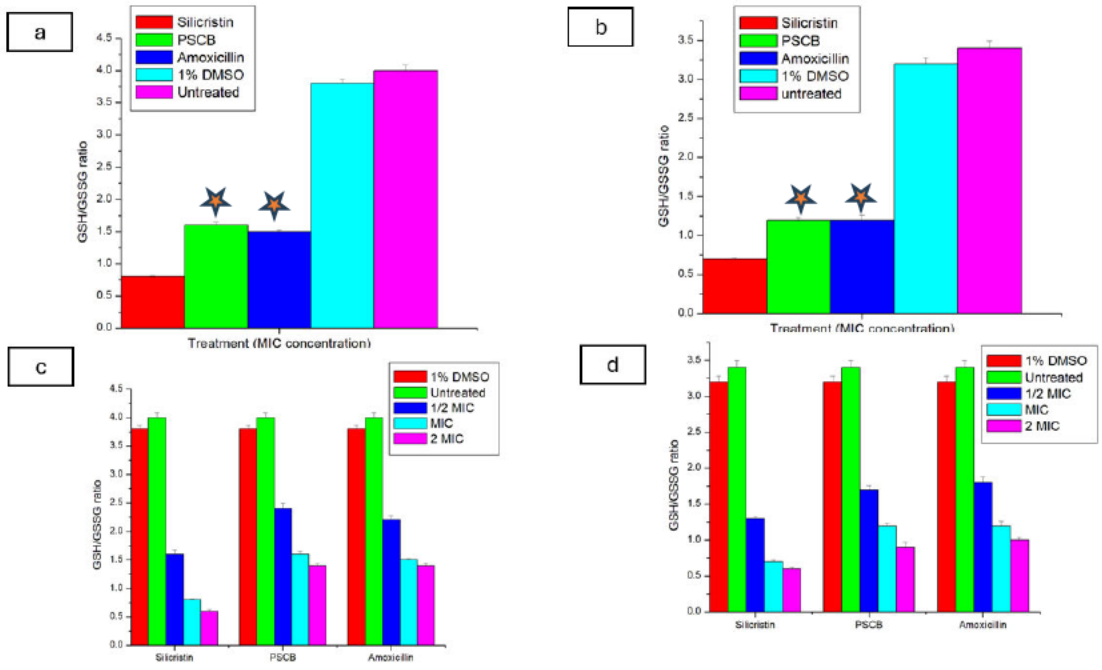


Figure 22: The ratio of reduced (GSH) to oxidized (GSSG) glutathione in (a) *S. pneumoniae* ATCC 700677 (resistant strain), and (b) *S. pneumoniae* ATCC 49619 (sensitive strain) following antibacterial treatment with MIC concentration of silicristin, PSCB and amoxicillin. Effect of different concentration on the ratio of reduced (GSH) to oxidized (GSSG) glutathione in (c) *S. pneumoniae* ATCC 700677 (resistant strain), and (d) *S. pneumoniae* ATCC 49619 (sensitive strain) following antibacterial treatment with silicristin, PSCB and amoxicillin. The values given are mean ± standard deviation. The same "star sign" colour on the same set of bars in the graph indicates no significant difference at $p > 0.05$.

3.10 *Effect of antibacterial treatment on the protein and lipid contents of investigated bacteria*

Autoxidation of cellular macromolecules is a process in which ROS remove electrons from macromolecules and subsequently generate reactive intermediates that can undergo further reactions (Vaishampayan *et al*., 2022). Bacterial macromolecules are particularly susceptible to ROS damage, due to their high levels of polyunsaturated fatty acids and protein. Autooxidation of

macromolecule of the test organisms was evaluated by detecting protein carbonylation and lipid peroxidation following antibacterial treatment. Compared to the untreated cells, a significant increase ($P < 0.05$) in protein carbonylation (Figure 23 to 26) and lipid peroxidation (Figure 27 to 30) was observed in all the test organisms following treatment with silicristin, PSCB and reference beta-lactams. This observation might suggest that antibacterial treatment instigates autoxidation of bacterial macromolecules in both the sensitive and resistant strains of the test bacteria which might be due to the ROS generating potential of the antibacterial agents. This observation is consistent with prior studies which established that normal cells maintain a finely controlled and well-balanced redox state due to the continual generation and detoxification of cellular ROS (Vaishampayan *et al*., 2022; Lam *et al*., 2020). However, in the presence of exogenous stressors, such as antibacterial agents, normal process of respiration and microbial metabolism might lead to increased formation of endogenous ROS and degeneration of defense systems which could be lethal to cellular macromolecules such as lipids, and proteins (Vaishampayan *et al*., 2022; Lam *et al*., 2020; Yoon *et al*., 2002). And like the ROS quantifying assay of this study, silicristin which generate the most toxic type of ROS in the form of $^{\bullet}OH$ radical caused the highest protein carbonylation (Figure 23 to 26) and lipid peroxidation (Figure 27 to 30) in all strains of the test organisms following antibacterial treatment. The reference beta-lactams and PSCB on the other hand with comparable ROS generation in terms of $^{\bullet}OH$ radical are not significant difference ($p > 0.05$) in protein carbonylation (Figure 23 to 26). For lipid peroxidation, except in *P. aeruginosa* (Figure 28) and the resistant strain of *S. pneumoniae* (Figure 29), no significant difference ($p > 0.05$) was observed for the reference beta-lactams and PSCB (Figure 27 to 30). This observation while being consistent with previous studies (Dwyer *et al*., 2014; Wang *et al*., 2009), showed a positive correlation of $^{\bullet}OH$ radical generation and damage to bacterial macromolecules.

Comparatively, a higher level of protein carbonylation and lipid peroxidation was observed in the sensitive strain and Gram-positive (Figures 25 and 26; Figures 29 and 30) organisms relative to the resistant strains and Gram-negative (Figures 23 and 24; Figures 27 and 28) organisms respectively. This observation is consistent with the ROS quantifying assay of this study where higher ROS and most especially ˙OH radical generation was noted with the sensitive and Gram-positive strains relative to the resistant and Gran-negative strains respectively. The variation between strains in this study might be linked to the differences in the composition of the proteome of the selected strains (Vidovic *et al*. 2014). This observation is coherent with the findings of the glutathione assay of this study and with prior study where significant differences in the extent of ROS-induced protein carbonylation between Gram-negative (*E. coli* O157:H7) and Gram-positive (*L. innocua*) strains was associated to the differences in the oxidative resistance of intracellular proteins of the selected strain (Cossu *et al*., 2017). Following antibacterial treatment, a significant difference ($P < 0.05$) exit for protein carbonylation in all cells treated with sub-MIC, MIC and 2 MIC (Figure 23 to 26). Similarly, except for silicristin against *E. coli* ATCC BAA-197 (Figure 27), cefotaxime against *E. coli* ATCC 11775 (Figure 27), silicristin against *P. aeruginosa* ATCC BAA-3197 (Figure 28), silicristin against *S. pneumoniae* ATCC 700677 (Figure 29), amoxicillin against *S. pneumoniae* ATCC 700677 (Figure 29), silicristin against *S. pneumoniae* ATCC 49619 (Figure 29), PSCB against *S. pneumoniae* ATCC 49619 (Figure 29) and amoxicillin against *S. pneumoniae* ATCC 49619 (Figure 29), a significant difference ($P < 0.05$) exist for lipid peroxidation in all cells treated with sub-MIC, MIC and 2 MIC (Figure 26 to 30). This observation suggests that the protein carbonylation and lipid peroxidation observed following antibacterial treatment with silicristin, amoxicillin and PSCB in this study is concentration dependent.

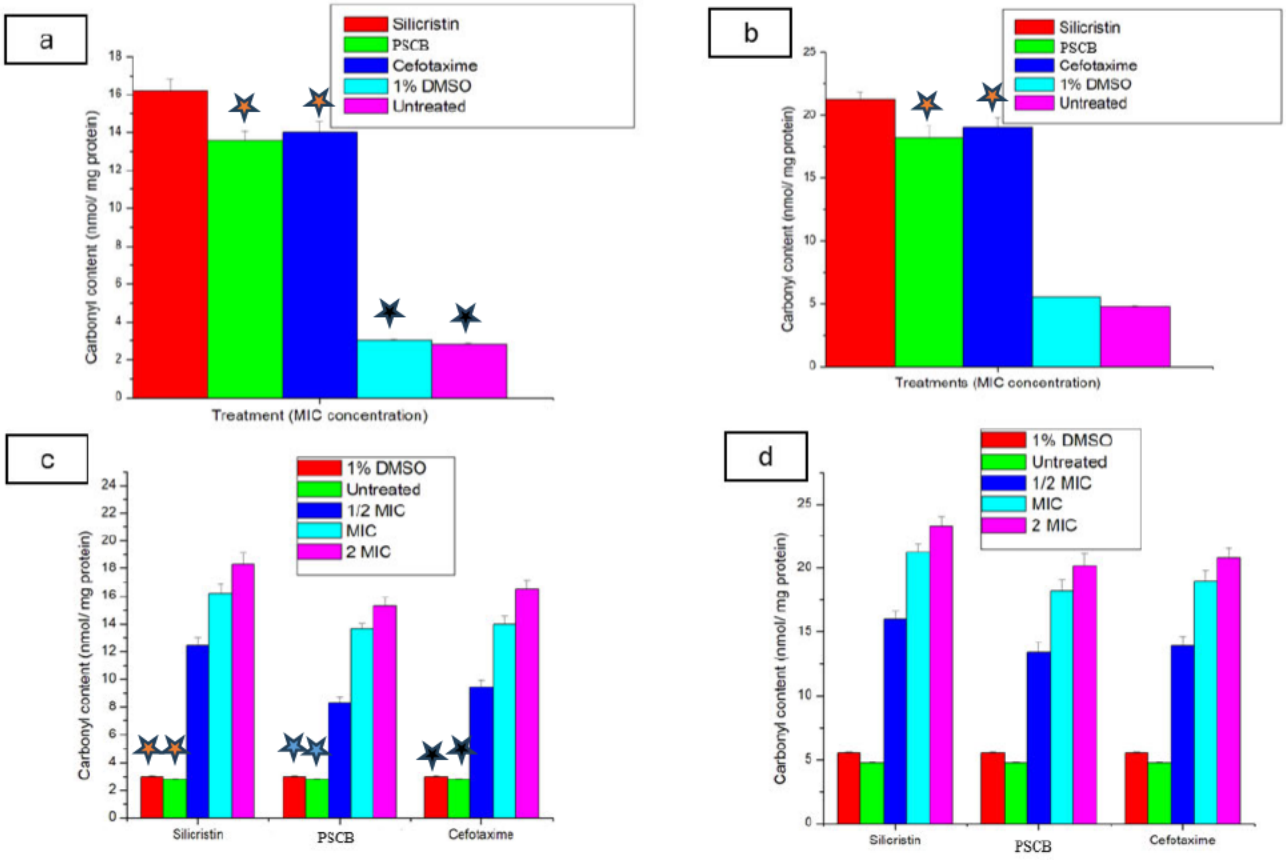


Figure 23: The level of carbonyl content in (a) *E. coli* ATCC BAA-197 (resistant strain), and (b) *E. coli* ATCC 11775 (sensitive strain) following antibacterial treatment with MIC concentration of silicristin, PSCB and cefotaxime. Effect of different concentrations on the level of carbonyl content of (c) *E. coli* ATCC BAA-197 (resistant strain), and (d) *E. coli* ATCC 11775 (sensitive strain) following antibacterial treatment with silicristin, PSCB and cefotaxime. The values given are mean ± standard deviation. The same "star sign" colour on the same set of bars in the graph indicates no significant difference at $p > 0.05$.

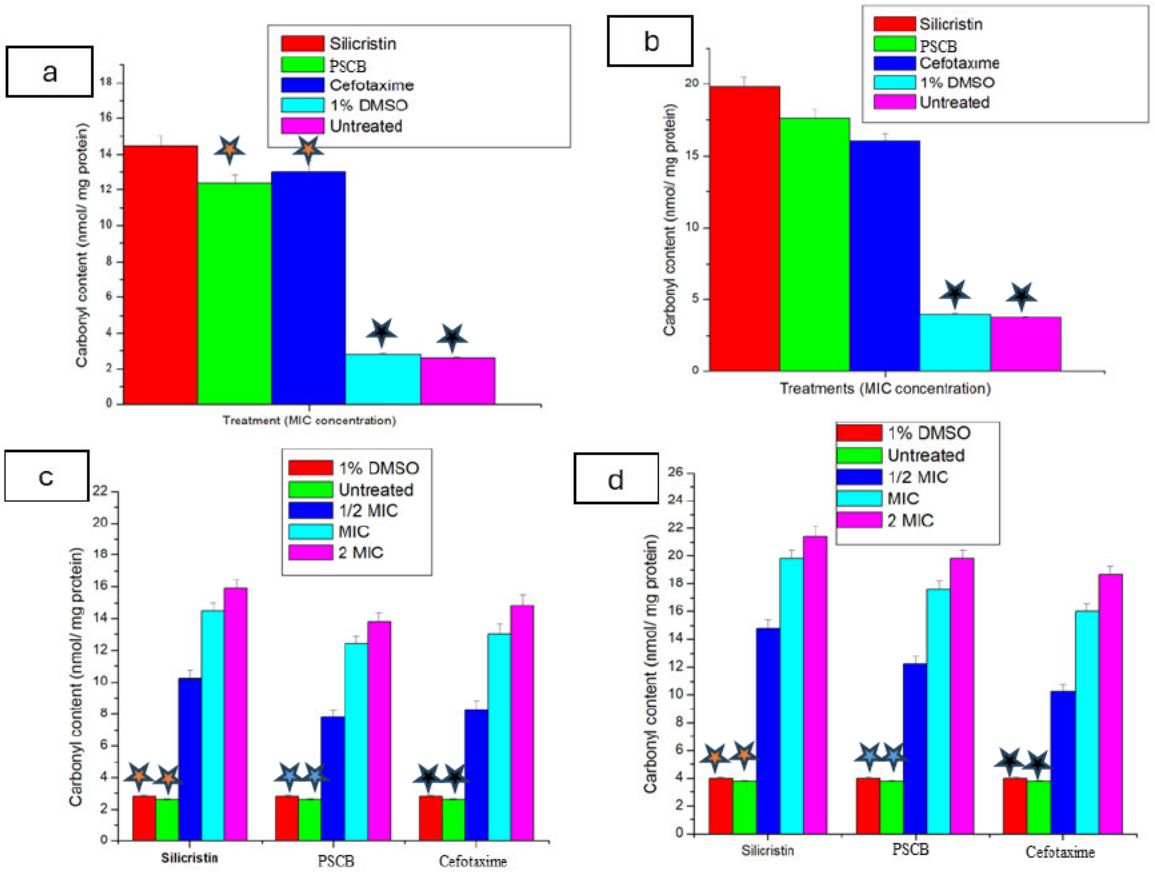


Figure 24: The level of carbonyl content of (a) *P. aeruginosa* ATCC BAA-3197 (resistant strain), and (b) *P. aeruginosa* ATCC27853 (sensitive strain) following antibacterial treatment with MIC concentration of silicristin, PSCB and cefotaxime. Effect of different concentration on the level of carbonyl content of (c) *P. aeruginosa* ATCC BAA-3197 (resistant strain), and (d) *P. aeruginosa* ATCC27853 (sensitive strain) following antibacterial treatment with silicristin, PSCB and cefotaxime. The values given are mean ± standard deviation. The same "star sign" colour on the same set of bars in the graph indicates no significant difference at $p > 0.05$.

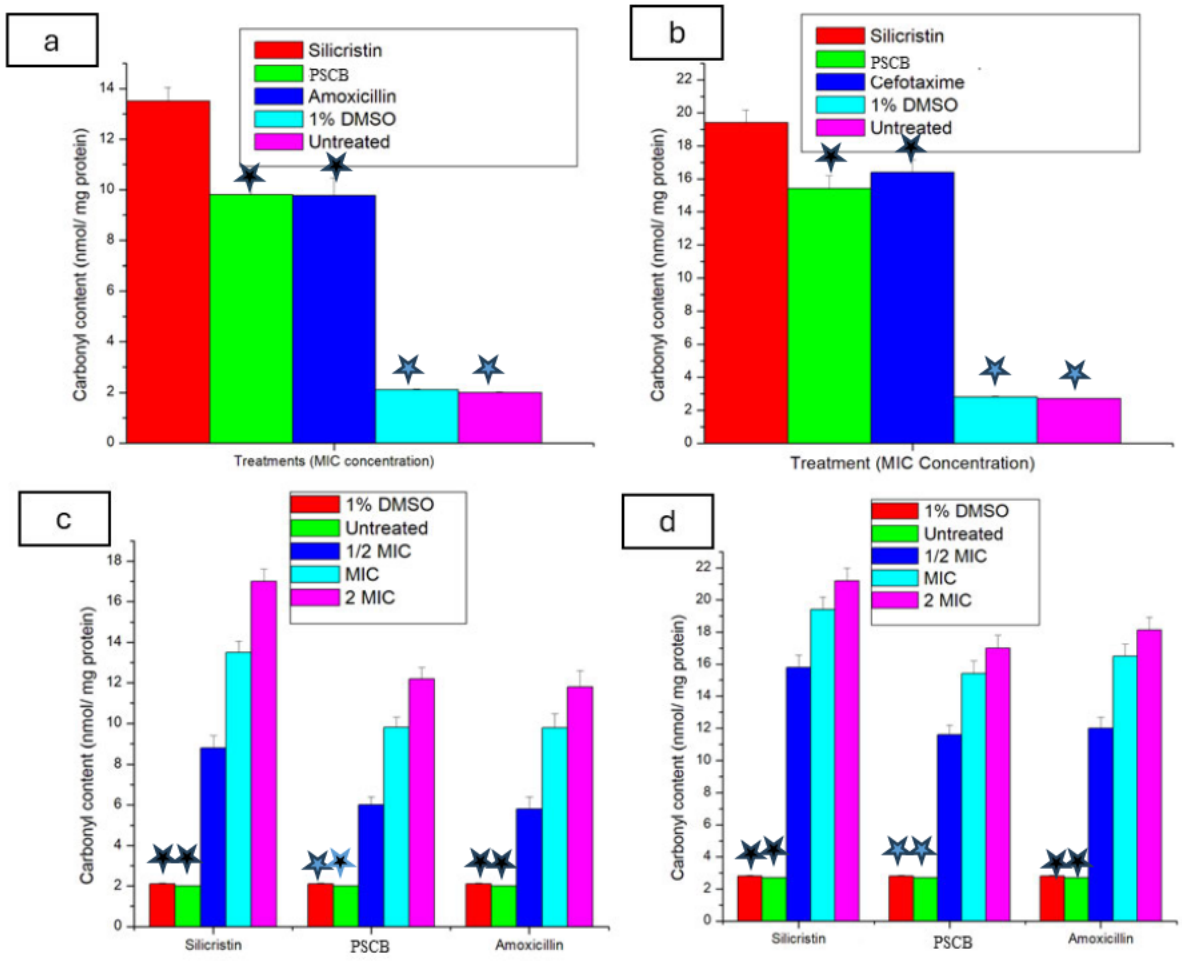


Figure 25: The level of carbonyl content of (a) *S. pneumoniae* ATCC 700677 (resistant strain), and (b) *S. pneumoniae* ATCC 49619 (sensitive strain) following antibacterial treatment with MIC concentration of silicristin, PSCB and amoxicillin. Effect of different concentrations on the level of carbonyl content of (c) *S. pneumoniae* ATCC 700677 (resistant strain), and (d) *S. pneumoniae* ATCC 49619 (sensitive strain) following antibacterial treatment with silicristin, PSCB and amoxicillin. The values given are mean ± standard deviation. The same "star sign" colour on the same set of bars in the graph indicates no significant difference at $p > 0.05$.

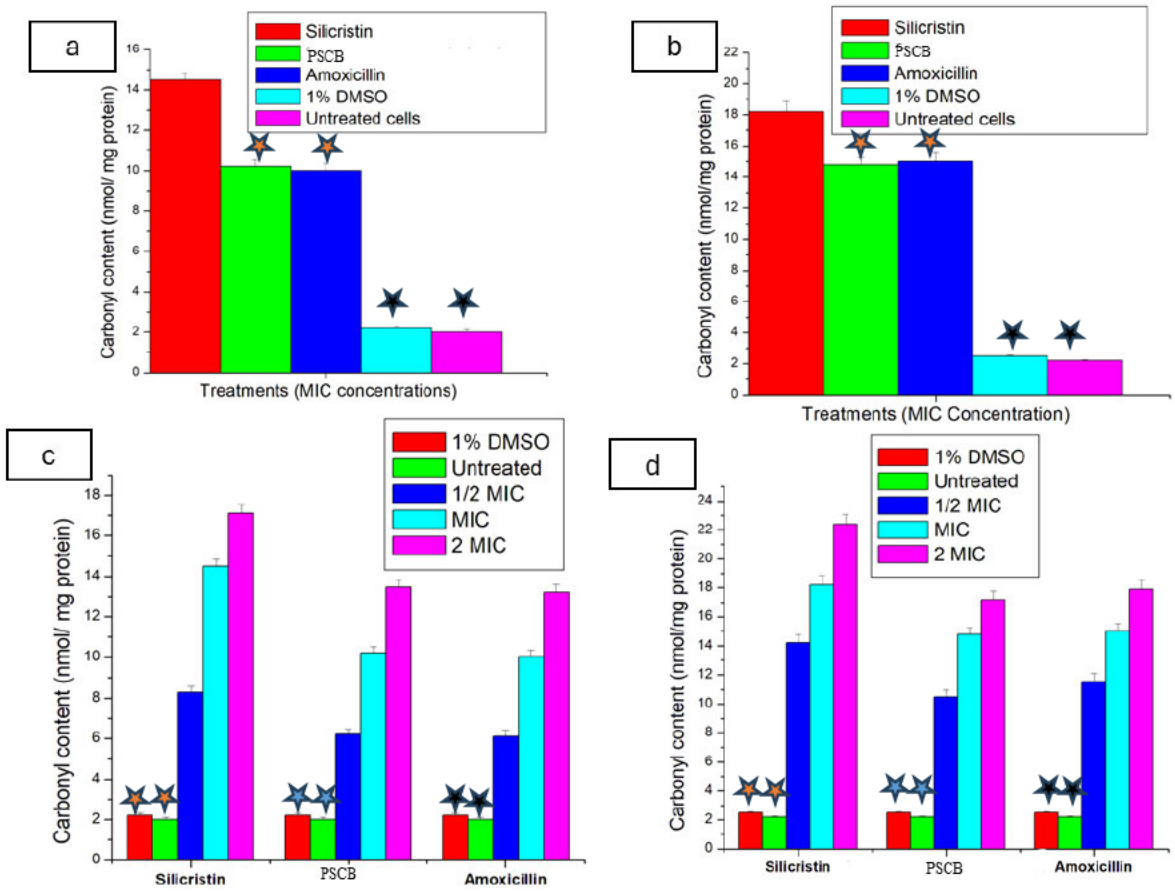


Figure 26: The level of carbonyl content of (a) *S. aureus* ATCC 43300 (resistant strain), and (b) *S. aureus* ATCC 25923 following antibacterial treatment with MIC concentration of silicristin, PSCB and amoxicillin. Effect of different concentrations on the level of carbonyl content of (c) *S. aureus* ATCC 43300 (resistant strain), and (d) *S. aureus* ATCC 25923 following antibacterial treatment with silicristin, PSCB and amoxicillin. The values given are mean ± standard deviation. The same "star sign" colour on the same set of bars in the graph indicates no significant difference at $p > 0.05$.

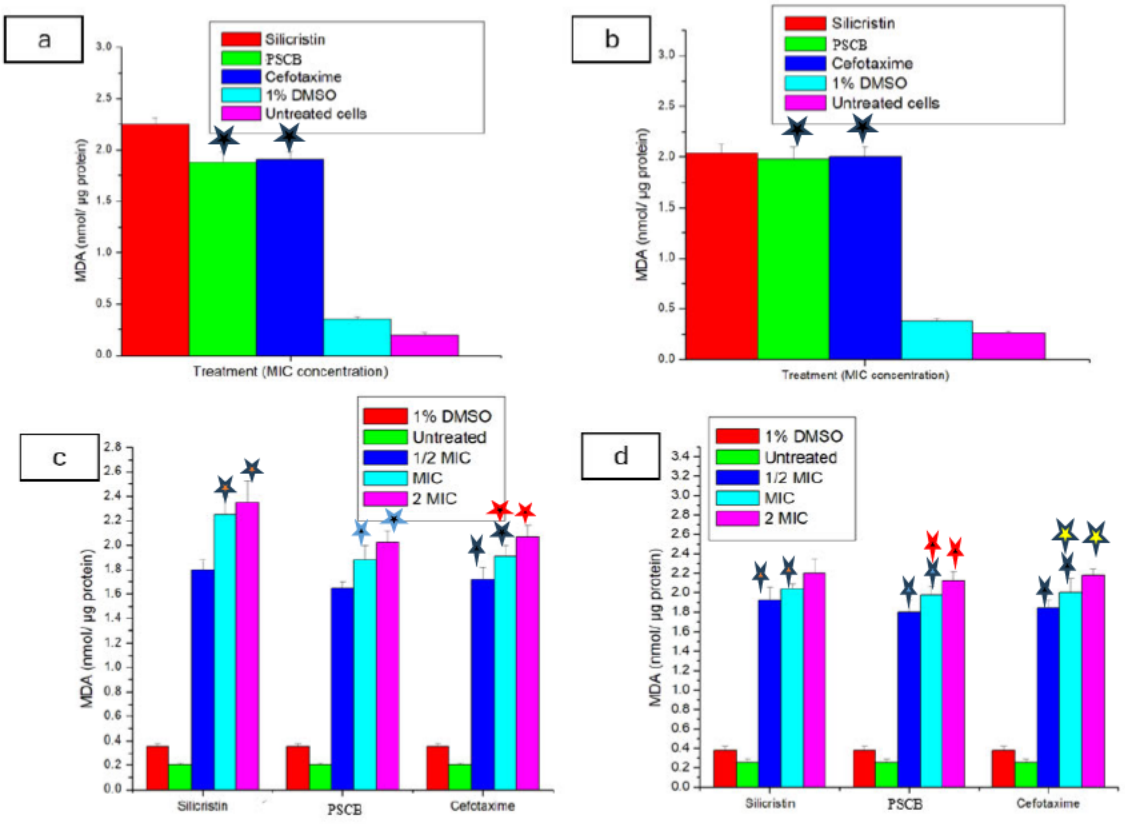


Figure 27: The level of lipid peroxidation in (a) *E. coli* ATCC BAA-197 (resistant strain), and (b) *E. coli* ATCC 11775 (sensitive strain) following antibacterial treatment with MIC concentration of silicristin, PSCB and cefotaxime. Effect of different concentration on the level of lipid peroxidation of (c) *E. coli* ATCC BAA-197 (resistant strain), and (d) *E. coli* ATCC 11775 (sensitive strain) following antibacterial treatment with silicristin, PSCB and cefotaxime. The values given are mean ± standard deviation. The same "star sign" colour on the same set of bars in the graph indicates no significant difference at $p > 0.05$.

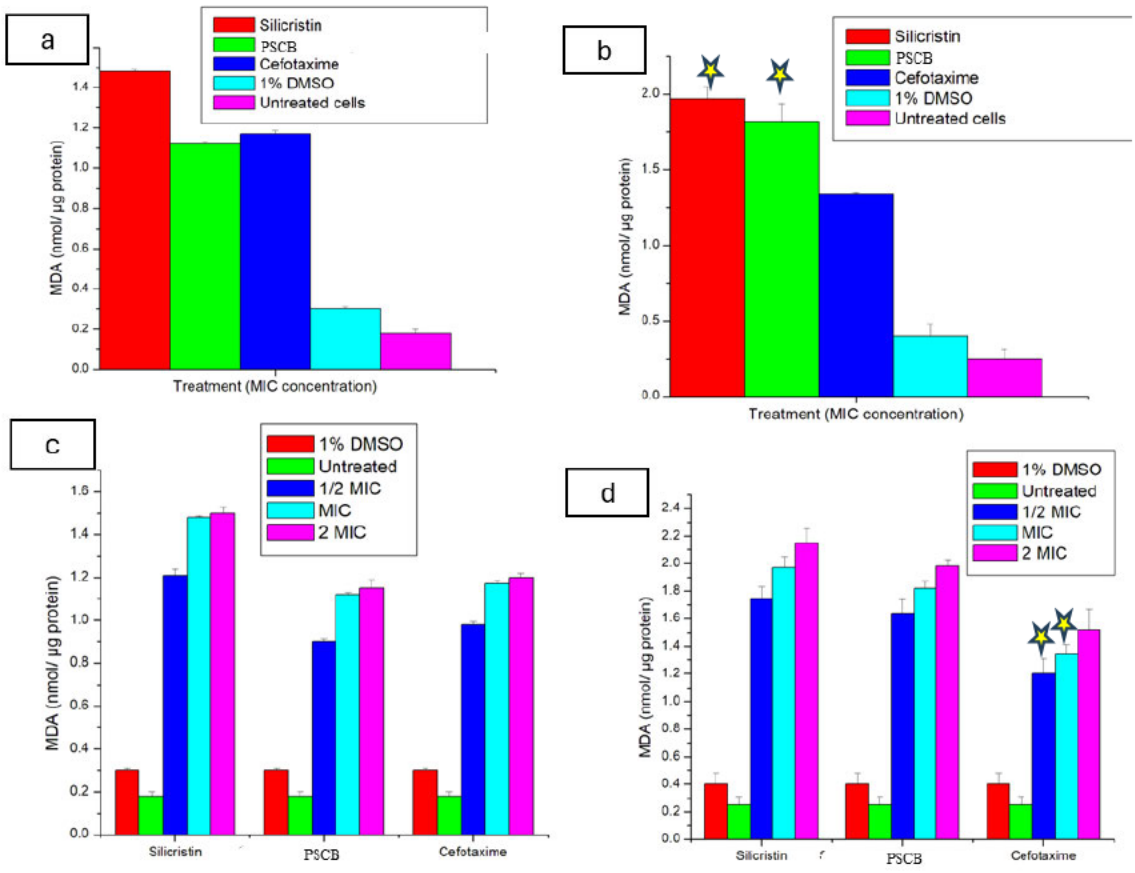


Figure 28: The level lipid peroxidation in (a) *P. aeruginosa* ATCC BAA-3197 (resistant strain), and (b) *P. aeruginosa* ATCC27853 (sensitive strain) following antibacterial treatment with MIC concentration of silicristin, PSCB and cefotaxime. Effect of different concentrations on the level of lipid peroxidation of (c) *P. aeruginosa* ATCC BAA-3197 (resistant strain), and (d) *P. aeruginosa* ATCC27853 (sensitive strain) following antibacterial treatment with silicristin, PSCB and cefotaxime. The values given are mean ± standard deviation. The same "star sign" colour on the same set of bars in the graph indicates no significant difference at $p > 0.05$.

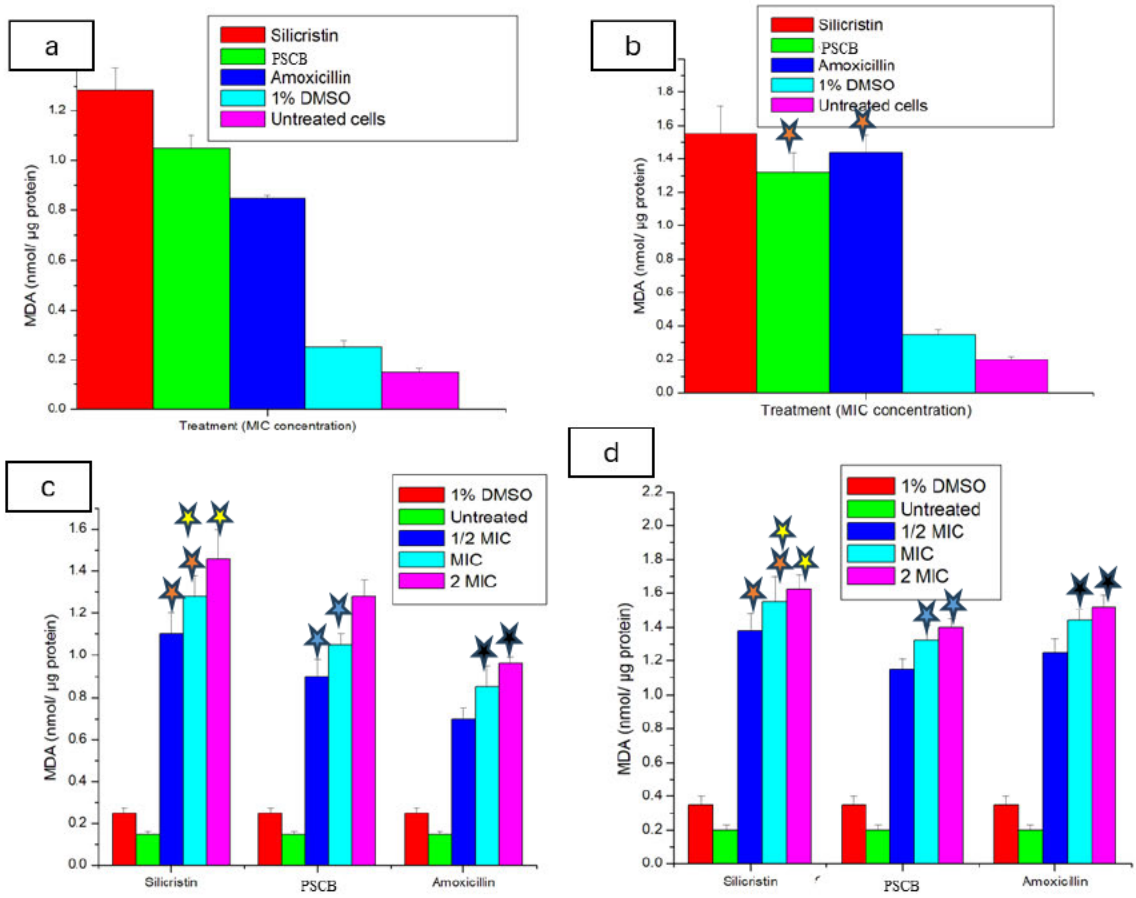


Figure 29: The level of lipid peroxidation in (a) *S. pneumoniae* ATCC 700677 (resistant strain), and (b) *S. pneumoniae* ATCC 49619 (sensitive strain) following antibacterial treatment with MIC concentration of silicristin, PSCB and amoxicillin. Effect of different concentrations on the level of lipid peroxidation of (c) *S. pneumoniae* ATCC 700677 (resistant strain), and (d) *S. pneumoniae* ATCC 49619 (sensitive strain) following antibacterial treatment with silicristin, PSCB and amoxicillin. The values given are mean ± standard deviation. The same "star sign" colour on the same set of bars in the graph indicates no significant difference at $p > 0.05$.

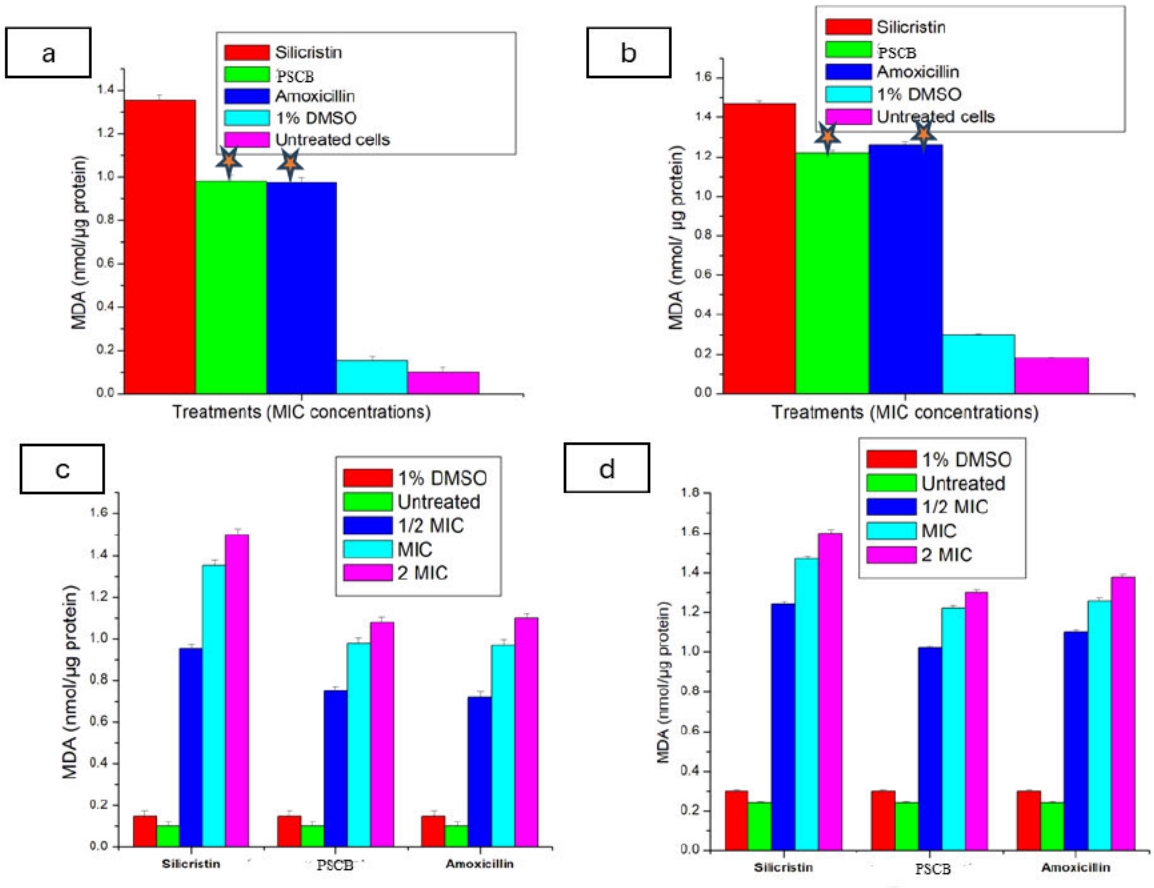


Figure 30: The level of lipid peroxidation in (a) *S. aureus* ATCC 43300 (resistant strain), and (b) *S. aureus* ATCC 25923 following antibacterial treatment with MIC concentration of silicristin, PSCB and amoxicillin. Effect of different concentration on the level of lipid peroxidation of (c) *S. aureus* ATCC 43300 (resistant strain), and (d) *S. aureus* ATCC 25923 following antibacterial treatment with silicristin, PSCB and amoxicillin. The values given are mean ± standard deviation. The same "star sign" colour on the same set of bars in the graph indicates no significant difference at $p > 0.05$.

3.11. *Effects of antibacterial treatment on SoxRS genes of test organisms*

While studies have implicated *SoxRS* to be directly induced by $O_2^{\bullet-}$ (Xiong *et al*., 2017; Imlay, 2013), a study by Gu and Imlay (2011) showed that the redox cycling drugs rather than $O_2^{\bullet-}$ instigate the expression of *SoxRS*. Thus, to elucidate the role of ROS-inducing agent on the expression of *SoxRS* regulons, this study explored the transcription of *SodA* and *SoxR* following antibacterial treatments. Against the sensitive strains of *E. coli* and *S. aureus*, treatment with silicristin, PSCB, and reference beta-lactams significantly induced the upregulation of *SodA* (Figure 31a) and *SoxR* (Figure 31b) relative to the untreated cells (Figure 31). This observation is suggestive of the expression of *SodA* and *SoxR* regulons in response to treatment-induced ROS generation. Except for the expression of *SoxR* in the sensitive strains of *S. aureus* where treatment with amoxicillin enhanced the most significant upregulation, silicristin-treated cells instigated the highest upregulation of *SodA* (Figure 31a, Supplementary Figure S21) and *SoxR* (Figure 31b, Supplementary Figure S22) in the sensitive strains of *E. coli* and *S. aureus.* This observation is consistent with the study of Xiong *et al*. (2017), who demonstrated the upregulation of *SodA* and *SoxR* in *E. coli* following treatment with tea polyphenol epigallocatechin gallate. Although, treatment with silicristin had the highest generation of $^{\bullet}OH$ radical in all the test organisms, PSCB and reference beta-lactams on the other hand generated the highest $O_2^{\bullet-}$. Hence the observation that silicristin instigated the highest upregulation of *SodA* and *SoxR* relative to PSCB and reference beta-lactams in this study could mean that the expression of both regulons is not exclusive to $O_2^{\bullet-}$ production and agrees with the reports of Gu and Imlay (2011) that postulated that redox cycling drugs rather than $O_2^{\bullet-}$ instigated *SoxRS* expression in *E. coli*. More importantly as silicristin belongs to the class of phenolics which have been demonstrated for their remarkable redox cycling

potential in the presence of transition metals and oxygen (Ajiboye *et al*., 2017). Against the resistant strains of both *E. coli* and *S. aureus*, upregulation was observed for *SodA* in *S. aureus* following treatment with silicristin, PSCB and reference beta-lactams. Against *SodA* of the resistant strain of *E. coli*, no significant ($P > 0.05$) expression was observed following treatment with silicristin and reference beta-lactams, while treatment with PSCB caused significant down regulation relative to the untreated cells (Figure 31). Except against *SoxR* of the resistant strain of *S. aureus* where silicristin caused up regulation of the gene, a down regulation of *SoxR* was observed in the resistant strains of *E. coli* and *S. aureus* following treatment with all the antibacterial agents in this study. The relative lesser expression of *SodA* and *SoxR* in the resistant strains of *E. coli* and *S. aureus* relative to the sensitive strains in this study could inferred that lesser ROS is generated in the resistant strain, an observation which align with the ROS quantification assay of this study. Another conclusion from the lesser expression of *SodA* and *SoxR* in the resistant strains of *E. coli* and *S. aureus* relative to the sensitive strain could be that other ROS-induced regulons such as *oxyS, katG, dps* and *ahpF* are expressed in response to the ROS generated by the investigated antibacterial agent. This observation is coherent with the findings of Xiong *et al*. (2017), who noted the upregulation of some ROS-induced genes such as *sodA, soxR, oxyR, oxyS,* and *katG* and the downregulation of *soxS, ahpC, dps*, and *ahpF* in response to treatment with tea polyphenol epigallocatechin gallate.

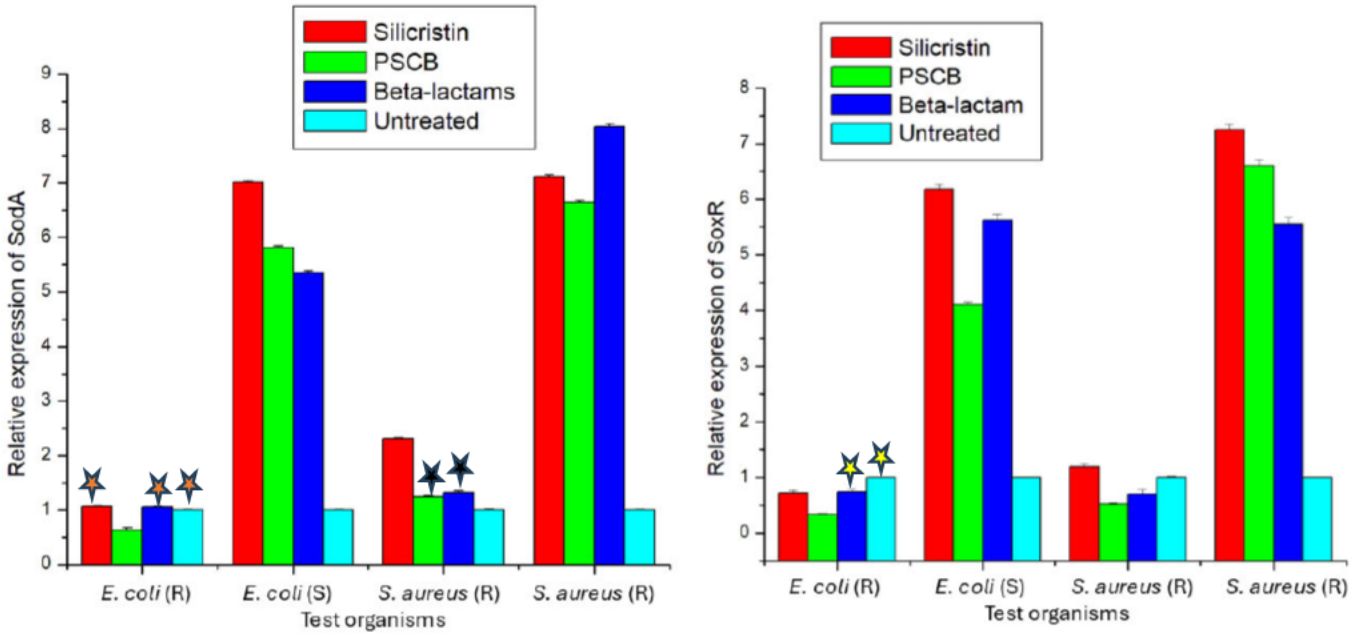


Figure 31: Relative expression of *SodA* (a) and *SoxR* (b) in sensitive and resistant strains of *E. coli* and *S. aureus* following antibacterial treatment with silicristin, PSCB and beta-lactams (cefotaxime for Gram-negative organisms and amoxicillin for Gram-positive organisms). The values given are mean ± standard deviation. The same "star sign" colour on the same set of bars in the graph indicates no significant difference at $p > 0.05$. Beta-lactams (cefotaxime against Gram-negative bacteria and amoxicillin against Gram-positive bacteria)

Taken together and considering the foregoing, a proposed mechanism of antibacterial action of silicristin could be suggested as involving; ROS ($O_2^{\bullet-}$) generated via the over excitation of the activities of the mitochondria (Kreb cycle and ETC) and possibly via autooxidation are being depleted by reduced glutathione (Figure 32). Excess $O_2^{\bullet-}$ are converted to H_2O_2 by superoxide dismutase (SOD) encoded for by the increase expression of *SodA* and *SoxR*. H_2O_2 are similarly scavenged by the reduced glutathione, however excess quantity of H_2O_2 which are not depleted

react with independent iron (possibly generated via damage to iron-sulphur clusters in the cells) in a chemistry known as the Fenton reaction (Figure 32). Increased modulation of the Fenton reaction generally means that an overwhelming amount of H_2O_2 enters the reaction to generate increased quantity of $^{\bullet}OH$ radical which are generally toxic to bacteria macromolecule as evident by the increased lipid peroxidation, protein carbonylation and damage to cell wall and cell membrane (Figure 32).

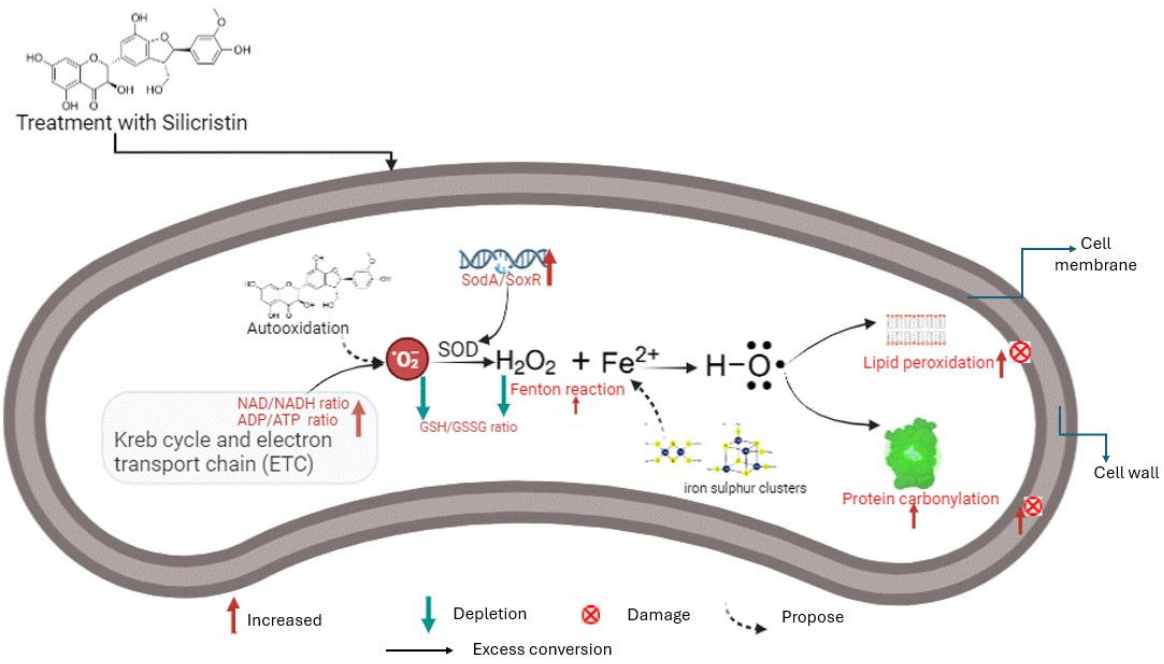


Figure 32: Proposed mechanism of lethality of silicristin on test bacteria.

4.0 Conclusion

The continuous emergence of antibiotic resistance in bacteria has necessitated the need for alternative strategies to overcome this threat. Among the strategies is the identification and development of therapeutics whose mechanism of action would depend primarily on ROS generation. The involvement of ROS in antibacterial lethality is a phenomenon which have been explored and deem relevant in the discovery and development of novel and potent drug candidate. In this study, the antibacterial activity and the possible involvement of oxidative stress in the lethality of silicristin, PSCB and conventional beta-lactam antibiotics (amoxicillin and cefotaxime) were investigated. Silicristin and PSCB showed antibacterial activity against both the sensitive and multidrug resistant strains of *E. coli*, *S. aureus*, *S. pneumoniae* and *P. aeruginosa* in a concentration- and time-dependent manner. Comparatively, except against the sensitive and resistant strains of *E. coli* where treatment with silicristin had a comparable killing effect as cefotaxime, silicristin had a better killing rate than PSCB and reference beta-lactams against all the test organisms. The enhanced killing effect of silicristin over PSCB and reference beta-lactams is hypothesized to be due to its characteristic hydroxyl group, which must have promoted its strong PBP binding and auto-oxidation for enhanced ROS generation. Silicristin with amoxicillin and cefotaxime had synergistic effects against all the test organisms except resistant strain of *E. coli*. In contrast, PSCB with cefotaxime and amoxicillin had only synergistic effect against the resistant strains of Gram-positive bacteria. This observation suggests that silicristin could function in combination therapy with both cefotaxime and amoxicillin in the treatment of infections caused by both the sensitive and resistant strains of *E. coli*, *S. aureus*, *S. pneumoniae* and *P. aeruginosa*. This is of great importance as combinatory therapy is attracting great interest in the treatment of difficult infections as it addresses problems related to resistance while providing broad-spectrum

antibacterial activity with minimal toxicological concerns. PSCB on the other hand only had synergistic effects with cefotaxime and amoxicillin against resistant strains of Gram-positive organism. Probing into the ROS generation potential of the test antibacterials revealed that treatment with PSCB and reference beta-lactams enhanced increased $O_2^{\bullet-}$ generation, while increased level of Fenton reaction-linked $^{\bullet}OH$ radicals, was observed following treatment with silicristin. Hydroxy radicals remain the most toxic ROS to bacteria, and this was evidently demonstrated in this study, where significantly increased levels of NAD^+/NADH ratio, ADP/ATP ratio, MDA, carbonyl content, PI uptake, with concomitant depletion of reduced glutathione were observed with silicristin-treated cells. This clearly suggests that ROS and oxidative stress contributed more to the modulatory effect of silicristin (Figure 36) against the test organisms compared to PSCB and the reference beta-lactams. The enhanced oxidative stress in cells treated with silicristin was further substantiated by SEM and TEM micrographs with cell walls with more blisters, eruptions, and sores compared to both the untreated and cefotaxime-treated cells (Figure 32). Oxidative stress was also noted to facilitate SOS (Save Our Souls) response in the form of upregulation of *SordA* and *SoxR* in the sensitive strains of *E. coli* and *S. aureus* and in this regard silicristin caused the highest upregulation thus linking the expression of the genes to ROS generation in cells. Overall, enhanced oxidative stress was observed more in the sensitive strains and Gram-positive organisms relative to resistant strains and Gram-negative organisms an observation that is consisting with the antibacterial killing effects of this study thus further highlighting the involvement of oxidative stress in the lethality of silicristin, PSCB and reference beta-lactams. The results of this study showed that silicristin had an improved redox effect in killing the sensitive and multi-resistant strains of both Gram-positive and Gram-negative organisms compared to the reference beta-lactams, and it could potentially be used in the

development of new therapeutics whose mechanism of action will be primarily through the generation of ROS to treat infections caused by the test organisms.

References

Abed, I.J.; Al-Moula, R.; Abdulhasan, G. A. Antibacterial effect of flavonoids extracted from seeds of silybum marianum against common pathogenic bacteria. *World J Exp Biosci*. **2015**, 3, 36 - 39. https://doi.org/10.13140/RG.2.1.4632.6240

Abreu, A.C.; Serra, S.C.; Borges, A.; Saavedra, M.J.; Mcbain, A.J.; Salgado, A.J.; Simões, M. Combinatorial activity of flavonoids with antibiotics against drug-resistant *Staphylococcus aureus*. *Microb. Drug Resist*. **2015**, 6, 600 - 609. https:/doi.org/10.1089/mdr.2014.0252.

Acebrón, I.; Chang, M.; Mobashery, S.; Hermoso, J.A. The allosteric site for the nascent cell wall in penicillin-binding protein 2a: An Achilles' Heel of methicillin-resistant *Staphylococcus aureus*. *Curr Med Chem.* **2015**, 22, 1678 - 86. https:/doi.org/10.2174/0929867322666150311150215.

Adam-Vizi, V.; Chinopoulos, C. Bioenergetics and the formation of mitochondrial reactive oxygen species. *Trends Pharmacol. Sci*. 2006, 27, 639 – 645. https:/doi.org/10.1016/j.tips.2006.10.005.

Ajiboye, T.O.; Aliyu, M.; Isiaka, I.; Haliru, F.Z.; Ibitoye, O.B.; Uwazie, J.N.; Muritala, H.F.; Bello, S.A.; Yusuf, I.I.; Mohammed, A.O. Contribution of reactive oxygen species to (+)-catechin-mediated bacterial lethality. *Chem. Biol. Interact*. **2016,** 258, 276– 287, https:/doi.org/10.1016/j.cbi.2016.09.010.

Ajiboye, T.O.; Habibu, R.S.; Saidu, K.; Haliru, F.Z.; Ajiboye, H.O.; Aliyu, N.O.; Ibitoye, O.B.; Uwazie, J.N.; Muritala, H.F.; Bello, S.A.; Yusuf, I.I.; Mohammed, A.O. Involvement of oxidative stress in protocatechuic acid-mediated bacterial lethality. *Microbiologyopen.* **2017**, 6, e00472. https:/doi.org/10.1002/mbo3.472

Ajiboye, T.O.; Skiebe, E.; Wilharm, G. Phenolic acids potentiate colistin-mediated killing of *Acinetobacter baumannii* by inducing redox imbalance. *Biomed. Pharmacother.* **2018**, 101, 737 – 744. https:doi.org/10.1016/j.biopha.2018.02.051

Akhova, A.V., Tkachenko, A.G. ATP/ADP alteration as a sign of the oxidative stress development in *Escherichia coli* cells under antibiotic treatment. *FEMS Microbiol Lett*. **2014**, 353, 69 – 76. https:/doi.org/10.1111/1574-6968.12405.

Aldulaimi, O.A. General overview of phenolics from plant to laboratory, good antibacterials or not?. *Pharmacogn*. **2017**, 11, 123 – 127. https://doi.org/10.4103/phrev.phrev_43_16

Altman, N. The Oxygen Prescription: The miracle of oxidative therapies; *Healing Arts Press*: Rochester, VT, USA, 2007. https://www.amazon.com/Oxygen-Prescription-Miracle-Oxidative-Therapies/dp/1594771774

Aribisala, J.O.; Idowu, K.; Makhanya, T. R.; Sabiu, S. Cheminformatics identification of phenolics as modulators of key penicillin−binding proteins of *Escherichia coli* towards interventive antibacterial therapy. *Mol. Simul*. **2023b,** 49, 1324 – 1340. https://doi.org/10.1080/08927022.2023.2228423

Aribisala, J.O.; S'thebe, N.W.; Sabiu, S. *In silico* exploration of phenolics as modulators of penicillin binding protein (PBP) 2× of *Streptococcus pneumoniae*. *Sci Rep*. **2024**, 14, 8788. https://doi.org/10.1038/s41598-024-59489-3

Aribisala, J.O.; Sabiu, S. Cheminformatics identification of phenolics as modulators of penicillin-Binding Protein 2a of *Staphylococcus aureus*: A Structure–Activity-Relationship-Based Study. *Pharmaceutics.* **2022,** 14, 1818. https://doi.org/10.3390/pharmaceutics14091818

Aribisala, J.O.; Sabiu, S. Cheminformatics identification of phenolics as modulators of penicillin-binding protein-3 of *Pseudomonas aeruginosa* towards interventive antibacterial therapy. *J. Biomol. Struct. Dyn*. **2023a,** 42, 298 – 313. https://doi.org/10.1080/07391102.2023.2192808

Arteel, G.E.; Sies, H. The biochemistry of selenium and the glutathione system, *Environ. Toxicol. Pharmacol.* **2001**, 10, 153 – 158. https:doi.org/10.1016/s1382-6689(01)00078-3.

Avila, H.P.; Smânia, F.A.; Monache, F.D.; Smânia, A. Jr. Structure−activity relationship of antibacterial chalcones. *Bioorg Med Chem*. **2008,** 16, 9790 – 9794. https:/doi.org/10.1016/j.bmc.2008.09.064

Balouiri, M.; Sadiki, M.; Ibnsouda, S.K. Methods for *in vitro* evaluating antimicrobial activity: A review. *J Pharm Anal*. **2016**, 6, 71 – 79. https:/doi.org/10.1016/j.jpha.2015.11.005.

Basma, S.M.A.; Abdelaleim, I.E.; Mahmoud, A.D.; Ahmed, M.A.E.; Ahmad, A. O. Effect of milk thistle (Silybum marianum (L.) Gaertn) seed extract on bacterial activities and growth of human liver cancer cells. *J. Biotech Res.* **2020**, 6, 27 - 33. https:/doi.org/10.32861/jbr.65.27.33

Chen, P.R.; Brugarolas, P.; He, C. Redox signaling in human pathogens. *Antioxid. Redox Signal.* **2011**, 14, 1107 – 1118. https:/doi.org/10.1089/ars.2010.3374.

Cossu, A.; Dou, F.; Young, G.M.; Nitin, N. Biomarkers of oxidative damage in bacteria for the assessment of sanitation efficacy in lettuce wash water. *Appl Microbiol Biotechnol*. **2017**, 101, 5365 - 5375. https:/doi.org/10.1007/s00253-017-8314-5

Crowley, L.C.; Scott, A.P.; Marfell, B.J.; Boughaba, J.A.; Chojnowski, G.; Waterhouse, N.J. Measuring cell death by propidium iodide uptake and flow cytometry. *Cold Spring Harb Protoc*. **2016**, 7. https://doi.org/10.1101/pdb.prot087163.

De Oliveira, D.R.; Tintino, S.R.; Braga, M.F.; Boligon, A.A.; Athayde, M.L.; Coutinho, H.D.; de Menezes, I.R.; Fachinetto, R. *In vitro* antimicrobial and modulatory activity of the natural products silymarin and silibinin. *Biomed Res Int*. **2015,** 292797. https://doi.org/10.1155/2015/292797

Dwyer, D.J.; Belenky, P.A.; Yang, J.H.; MacDonald, I.C.; Martell, J.D.; Takahashi, N.; Chan, C.T.Y.; Michael, A.L.; Braff, D.; Schwarz, E.G.; Ye; J.D.; Pati, M.; Vercruysse, M.; Ralifo, P.S.; Allison, K.R.; Khalil, A.S.; Ting, A.Y.; Walker, G.C.; Collins, J.J. Antibiotics induce redox-related physiological alterations as part of their lethality. *Proc. Natl. Acad. Sci. USA* **2014**, *5*, 100–109. https:/doi.org/10.1073/pnas.1401876111

Eghbaliferiz, S.; Iranshahi, M. Prooxidant activity of polyphenols, flavonoids, anthocyanins and carotenoids: Updated review of mechanisms and catalyzing metals. *Pharmacol. Res.* **2016**, 30, 1379 – 1391. https://doi.org/10.1002/ptr.5643

El-Sapagh, S.; Allam, N.G.; El-Sayed, M.N.E.-D.; El-Hefnawy, A.A.; Korbecka-Glinka, G.; Shala, A.Y. Effects of *Silybum marianum* L. seed extracts on multi drug resistant (MDR) Bacteria. *Molecules.* **2024**, *29*, 64. https://doi.org/10.3390/molecules29010064

Gibbons, S. Anti-staphylococcal plant natural products, *Nat. Prod. Rep*. **2004,** 21, 263e277. https://doi.org/10.1039/B212695H

Glaeser, J.; Nuss, A.M.; Berghoff, B.A.; Klug, G. Singlet oxygen stress in microorganisms. *Adv. Microb. Physiol*. **2011**, 58, 141 – 173. https:/doi.org/10.1016/B978-0-12-381043-4.00004-0.

Goel, S.; Mishra, P. Thymoquinone inhibits biofilm formation and has selective antibacterial activity due to ROS generation. *Appl Microbiol Biotechnol*. **2018**, 4, 1955-1967. https:/doi.org/10.1007/s00253-018-8736-8.

Gu, M.; Imlay, J.A. The *SoxR*S response of *Escherichia coli* is directly activated by redox-cycling drugs rather than by superoxide. *Mol. Microbiol.* **2011**, 5, 1136 - 1150. https:/doi.org/10.1111/j.1365-2958.2010.07520

Han, G.; Lee, D.G. Naringin generates three types of reactive oxygen species contributing differently to apoptosis-like death in *Escherichia coli*. *Life Sci*. **2022**, 1, 304, 120700. https:/doi.org/10.1016/j.lfs.2022.120700.

Hu, Z.Q, Zhao, W.; Yoda, Y.; Asano, N.; Hara, Y.; Shimamura, T. Additive, indifferent and antagonistic effects in combinations of epigallocatechin gallate with 12 non-β-lactam antibiotics against methicillin-resistant *Staphylococcus aureus*, *J Antimicrob Chemother*. **2002,** 50, 1051–1054. https://doi.org/10.1093/jac/dkf250

Imlay, J. A. The molecular mechanisms and physiological consequences of oxidative stress: Lessons from a model bacterium. *Nat Rev Microbiol.* **2013**, 11, 443 – 454. https:/doi.org/10.1038/nrmicro3032.

Islam, N.; Khan, E.; Naveed, U.M.; Shah, A.; Zahoor, M.; Ullah, R.; Bari, A. Enhancing dissolution rate and antibacterial efficiency of azithromycin through drug-drug cocrystals with paracetamol. *Antibiotics*. **2021**, 10, 939. https:/doi.org/10.3390/antibiotics10080939.

Jeyanthi, V.; Velusamy, P.; Kumar, G.V.; Kiruba, K. Effect of naturally isolated hydroquinone in disturbing the cell membrane integrity of *Pseudomonas aeruginosa* MTCC 741 and *Staphylococcus aureus* MTCC 740. *Heliyon*. **2021**, 7, e07021. https:/doi.org/10.1016/j.heliyon.2021.e07021

Julio, S.M.; Heithoff, D.M.; Mahan, M.J. ssrA (tmRNA) plays a role in *Salmonella enterica* serovar Typhimurium pathogenesis. *J Bacteriol*. **2000,** 182, 1558 - 1563. https:/doi.org/10.1128/JB.182.6.1558-1563.2000.

Kaur, A. K.; Wahi, A.; Brijesh, K.; Bhandari, A.; Prasad, N. Milk thistle (*silybum marianum*): A review. *IJPRD.* **2011**, 3, 1-10. https://www.yumpu.com/en/document/view/11591120/milk-thistle-silybum-marianum-a-review-ijprd

Keren, I.; Wu, Y.; Inocencio, J.; Mulchay, L.R.; Lewis, K. Killing by bactericidal antibiotics does not depend on reactive oxygen species. *Science.* **2014**, 339, 1213 – 1216. https:/doi.org/10.1126/science.1232688

Khumbulani, M.; Alayande, K.A.; Sabiu, S. Orientin enhances colistin-mediated bacterial lethality through oxidative stress involvement. *Evid Bas Comp Alternat Med*. **2022**, 9, 3809232. https:/doi.org/10.1155/2022/3809232

Kim, S.Y.; Park, C.; Jang, H.J.; Kim, B.O.; Bae, H.W.; Chung, I.Y.; Kim, E.S.; Cho, Y.H. Antibacterial strategies inspired by the oxidative stress and response networks. *J Microbiol*. **2019**, 57, 203 – 212. https:/doi.org/10.1007/s12275-019-8711-9.

Kohanski, M.A.; Dwyer, D.J.; Collins, J.J. How antibiotics kill bacteria: from targets to networks. *Nat Rev Microbiol*. **2010**, 8, 423 - 435. https:/doi.org/10.1038/nrmicro2333.

Lam, P.L.; Wong, R.S.M.; Lam, K.H.; Hung, L.K.; Wong, M.; Yung, L.H.; Ho, Y.W.; Wong, W.Y.; Hau, D.K.P.; Gambari, R.; Chui CH. The role of reactive oxygen species in the biological activity of antimicrobial agents: an updated Mini Review. *Chem-Biol Interact.* **2020**, 320, 109023. https:/doi.org/10.1016/j.cbi.2020.109023

Lee, D.G.; Kim, H.K.; Park, Y.; Park, S.C.; Woo, E.R.; Jeong, H.G.; Hahm, K.S. Gram-positive bacteria specific properties of silybin derived from *Silybum marianum*. *Arch Pharm Res.* **2003**, 26, 597 - 600. https://doi.org/10.1007/BF02976707.

Li, H.; Zhao, X.; Huang, Y.; Liao, B.; Cheng, L.; Ren, B. Reactive oxygen species in pathogen clearance: the killing mechanisms, the adaption response, and the side effects. *Front Microbiol.* **2021**, 11, 3610. https:/doi.org/10.3389/fmicb.2020.622534.

Liu, Y.; Imlay, J.A. Cell death from antibiotics without the involvement of reactive oxygen species. *Science.* **2013**, 339, 1210 – 1213. https:/doi.org/10.1126/science.1232751.

Livak, K.J.; Schmittgen, T.D. Analysis of relative gene expression data using real-time quantitative PCR and the 2(-Delta Delta C(T)) Method. *Methods*. **2001**, 25, 402 - 408. https:/doi.org/10.1006/meth.2001.1262. PMID: 11846609.

Mone, N.S., Kamble, E.E., Pardesi, K.R. Satpute, S.K. Antibacterial and antibiofilm potency of menadione against multidrug-resistant *S. aureus*. *Curr Microbiol.* **2022**,79, 282. https://doi.org/10.1007/s00284-022-02975-6

Mourenza, A.; Gil, J.A.; Mateos, L.M.; Letek, M. Oxidative stress-generating antimicrobials, a novel strategy to overcome antibacterial resistance. *Antioxidants.* **2020**, 9, 361. https:/doi.org/10.3390/antiox9050361

Paulander, W.; Wang, Y.; Folkesson, A.; Charbon, G.; Løbner-Olesen, A.; Ingmer, H. Bactericidal antibiotics increase hydroxyphenyl fluorescein signal by altering cell morphology. *PLoS ONE.* **2014**, 9, e92231. https:/doi.org/10.1371/journal.pone.0092231

Petersen, P.J.; Labthavikul, P.; Jones, C.H.; Bradford, P.A. *In vitro* antibacterial activities of tigecycline in combination with other antimicrobial agents determined by chequerboard and time-kill kinetic analysis. *J. Antimicrob. Chemother*. **2006**, 57, 573 – 576. https:/doi.org/10.1093/jac/dki477

Radhika, M. I.; Ezhilarasan, D.; Gopinath, P. Comparative antimicrobial efficacy of silymarin and silibinin against oral microbes. *J Microbiol Infect Dis.* **2017,** 3, 139 - 143. https://doi.org/10.5799/jmid.367545

Ríos, J.L.; Recio, M.C. Medicinal plants and antimicrobial activity. *J. Ethnopharmacol*. **2005**, 100, 80 – 84. https:/doi.org/10.1016/j.jep.2005.04.025.

Salam, M.A.; Al-Amin, M.Y.; Salam, M.T.; Pawar, J.S.; Akhter, N.; Rabaan, A.A.; Alqumber, M.A.A. Antimicrobial resistance: a growing serious threat for global public health. *Healthcare.* **2023**, *11*, 1946. https://doi.org/10.3390/healthcare11131946

Silhavy, T.J.; Kahne, D.; Walker, S. The bacterial cell envelope. *Cold Spring Harb Perspect Biol*. **2010**, 2, a000414. https:/doi.org/10.1101/cshperspect.a000414.

Simões M.; Bennett, R.N.; Rosa, E.A.S. Understanding antimicrobial activities of phytochemicals against multidrug resistant bacteria and biofilms. *Nat. Prod. Rep*. **2009**, 26, 746 – 757. https:/doi.org/10.1039/b821648g.

Singh, D.; Majumdar, A.G.; Gamre, S.; Subramanian, M. Membrane damage precedes DNA damage in hydroxychavicol treated *E. coli* cells and facilitates cooperativity with hydrophobic antibiotics. *Biochimie.* **2021,** 180, 158 - 168. https:/doi.org/10.1016/j.biochi.2020.11.008.

Sinsinwar, S.; Vadivel, V. Catechin isolated from cashew nut shell exhibits antibacterial activity against clinical isolates of MRSA through ROS-mediated oxidative stress. *Appl. Microbiol. Biotechnol*. **2020**, 104, 8279 – 8297. https:/doi.org/10.1007/s00253-020-10853-z.

Spratt, B.G. Distinct penicillin binding proteins involved in the division, elongation, and shape of Escherichia coli K12. *Proc Natl Acad Sci*. **1975**, 72, 999 - 3003. https:/doi.org/10.1073/pnas.72.8.2999.

Tegos, G.; Stermitz, F.R.; Lomovskaya, O.; Lewis, K. Multidrug pump inhibitors uncover remarkable activity of plant antimicrobials. *Antimicrob. Agents Chemother*. **2002**, 46, 3133e3141. https:/doi.org/10.1128/AAC.46.10.3133-3141.2002

Tellis, R.C.; Vidyasagar, S., Moosabba, M.; Tellis, R.C. Activity of antibiotic combinations against multidrug resistant *Pseudomonas aeruginosa*: a study from South India. *IJCMAS*. **2016**, 2, 27–34. https://www.academia.edu/71714227/Activity_of_antibiotic_combinations_against_multidrug_resistant_Pseudomonas_aeruginosa_A_study_from_South_India?hb-sb-sw=43032074

Thiberge, S.; Nechushtan, A.; Sprinzak, D.; Gileadi, O.; Behar, V.; Zik, O.; Moses, E. Scanning electron microscopy of cells and tissues under fully hydrated conditions. *PNAS,* **2004,** 101, 3346 - 3351. https:/doi.org/0.1073/pnas.0400088101.

Vaishampayan, A.; Grohmann, E. Antimicrobials functioning through ROS-mediated Mechanisms: Current Insights. *Microrganisms.* **2022**, 10, 61. https:/doi.org/10.3390/microorganisms10010061.

Vidovic, A.; Supek, F.; Nikolic, A.; Krisko, A. Signatures of conformational stability and oxidation resistance in proteomes of pathogenic bacteria. *Cell Rep*. **2014**, 7, 1393 – 1400. https:/doi.org/10.1016/j.celrep.2014. 04.057

Vila Domínguez, A.; Ayerbe Algaba, R.; Miró Canturri, A.; Rodríguez Villodres, Á.; Smani, Y. Antibacterial activity of colloidal silver against Gram-negative and Gram-positive bacteria. *Antibiotics.* **2020**, *9*, 36. https://doi.org/10.3390/antibiotics9010036

Wadhwa, K.; Pahwa, R.; Kumar, M.; Kumar, S.; Sharma, P.C.; Singh, G.; Verma, R.; Mittal, V.; Singh, I.; Kaushik, D.; Jeandet, P. Mechanistic insights into the pharmacological significance of silymarin. *Molecules*. **2022**, 27, 5327. https:/doi.org/10.3390/molecules27165327

Wang, X.; Zhao, X. Contribution of oxidative damage to antimicrobial lethality. *Antimicrob. Agents Chemother.* **2009**, 53, 1395 – 1402. https:/doi.org/10.1128/AAC.01087-08.

Wei, H.; Jin, Z.; Wang, Y.; Yang, F.; Xiao, Y.; Jiang, Y.; Hu, J.; Gao, M.T. antibacterial effect of phenolic acids derived from rice straw and in combination with antibiotics against *Escherichia coli*. *Appl Biochem Biotechnol.* **2022**,194, 2931 - 2945. https:/doi.org/10.1007/s12010-021-03650-5

Wijesundara, N.M.; Lee, S.F.; Cheng, Z.; Davidson, R.; Rupasinghe, H.P.V. Carvacrol exhibits rapid bactericidal activity against *Streptococcus pyogenes* through cell membrane damage. *Sci Rep*. **2021**, 11, 1487. https:/doi.org/10.1038/s41598-020-79713-0.

Xiong, L.G.; Chen, Y.J.; Tong, J.W.; Huang, J.A.; Li, J.; Gong, Y.S.; Liu, Z.H. Tea polyphenol epigallocatechin gallate inhibits *Escherichia coli* by increasing endogenous oxidative stress. *Food Chem.* **2017,** 217, 196 - 204. https:/doi.org/10.1016/j.foodchem.2016.08.098.

Yeom, J.; Imlay, J.A.; Park, W. Iron homeostasis affects antibiotic-mediated cell death in *Pseudomonas* species. *J Biol Chem.* **2010**, 285, 22689 – 22695. https:/doi.org/10.1074/jbc.M110.127456

Yi, S.M.; Zhu, J.L.; Fu, L.L.; Li, J.R. Tea polyphenols inhibit *Pseudomonas aeruginosa* through damage to the cell membrane. *Int J Food Microbiol.* **2010,** 144, 111 - 117. https:/doi.org/10.1016/j.ijfoodmicro.2010.09.005.

Yoon, S.J.; Park, J.E.; Yang, J.H.; Park, J.W. OxyR regulon controls lipid peroxidation-mediated oxidative stress in *Escherichia coli*. *J Biochem Mol Biol.* **2002**, *35*, 297 – 301. https:/doi.org/10.5483/bmbrep.2002.35.3.297.

Zeraik, M.L.; Petrônio, M.S.; Coelho, D.; Regasini, L.O.; Silva, D.H.; da Fonseca, L.M.; Machado, S.A.; Bolzani, V.S.; Ximenes, V.F. Improvement of pro-oxidant capacity of protocatechuic acid by esterification. *PLoS One*. **2014**, 9, e110277. https:/doi.org/10.1371/journal.pone.0110277.

Zitka, O.; Skalickova, S.; Gumulec, J.; Masarik, M.; Adam, V.; Hubalek, J.; Trnkova, L; Kruseova, J.; Eckschlager, T. Kizek, R. Redox status expressed as GSH:GSSG ratio as a marker for oxidative stress in paediatric tumour patients. *Oncol Lett.* **2012**, 6, 1247 - 1253. https:/doi.org/10.3892/ol.2012.931.

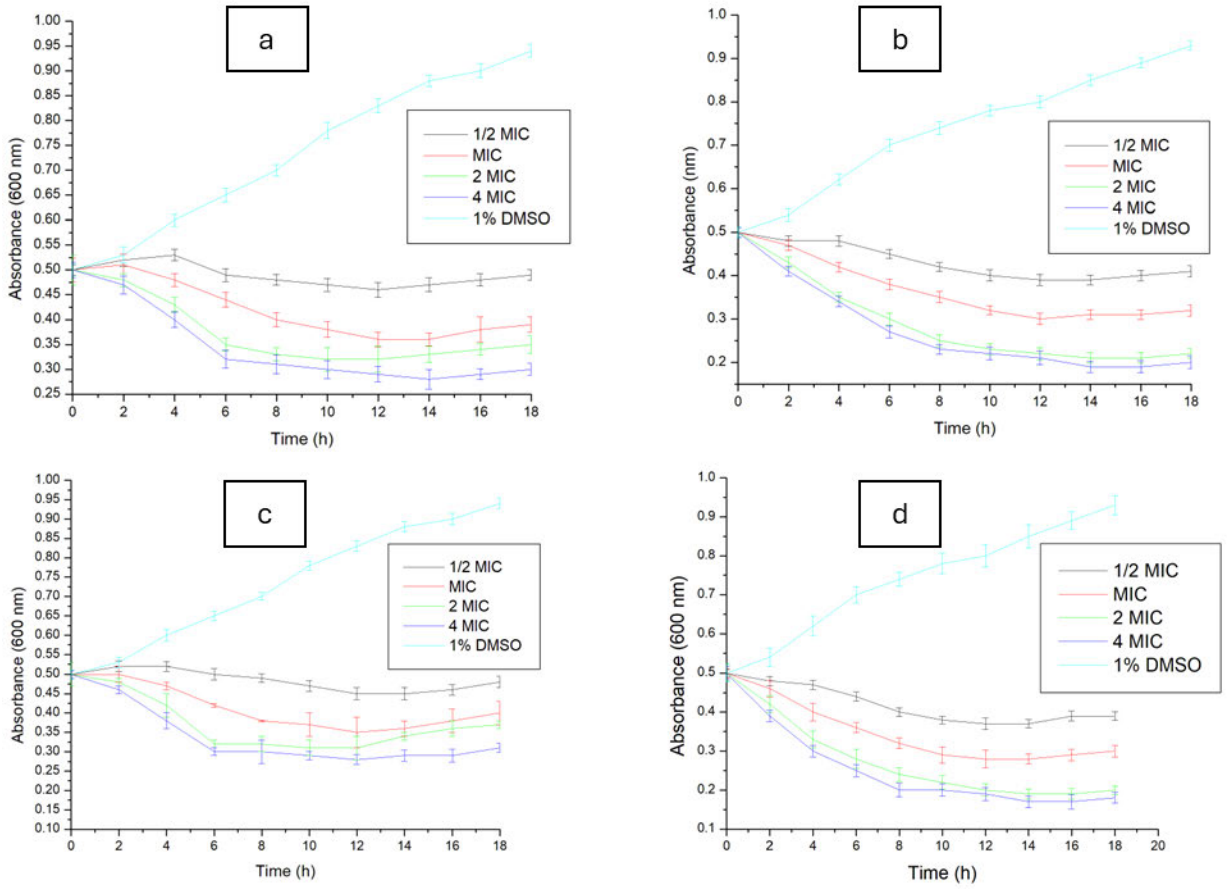
Supplementary information

Supplementary Table S1: Minimum bactericidal concentration (µg/mL) of antibacterial agents on both resistant and sensitive strain of test organisms

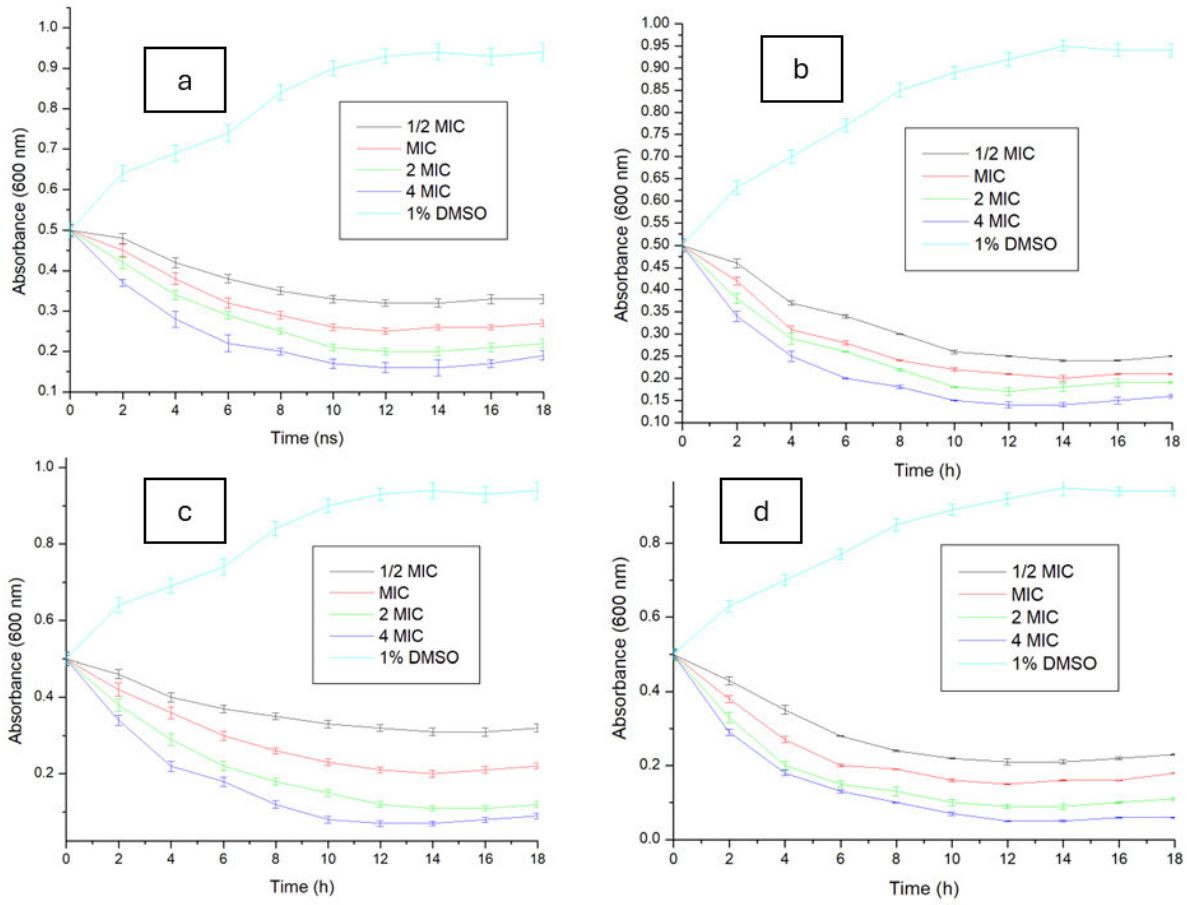
Organisms	Organisms Status	Cefotaxime	Amoxicillin	Silicristin	PSCB
Staphylococcus aureus ATCC 43300	R	32.0	8.0	64.0	128.0
Staphylococcus aureus ATCC *25923*	S	4.0	1.0	32.0	64.0
Pseudomonas aeruginosa ATCC BAA-3197	R	16.0	64.0	128.0	128.0
Pseudomonas aeruginosa ATCC*27853*	S	16.0	32.0	32.0	128.0
Escherichia coli ATCC BAA-197	R	4.0	32.0	32.0	128.0
Escherichia coli ATCC 11775	S	0.5	4.0	32.0	32.0
Streptococcus pneumoniae ATCC 700677	R	4.0	16.0	16.0	16.0
Streptococcus pneumoniae ATCC 49619	S	1.0	1.0	4.0	8.0

Supplementary Table S2: Sensitivity pattern (mm) of sensitive and resistant strains of test organisms at median activity concentration (MAC) [(MIC + MBC)/2]

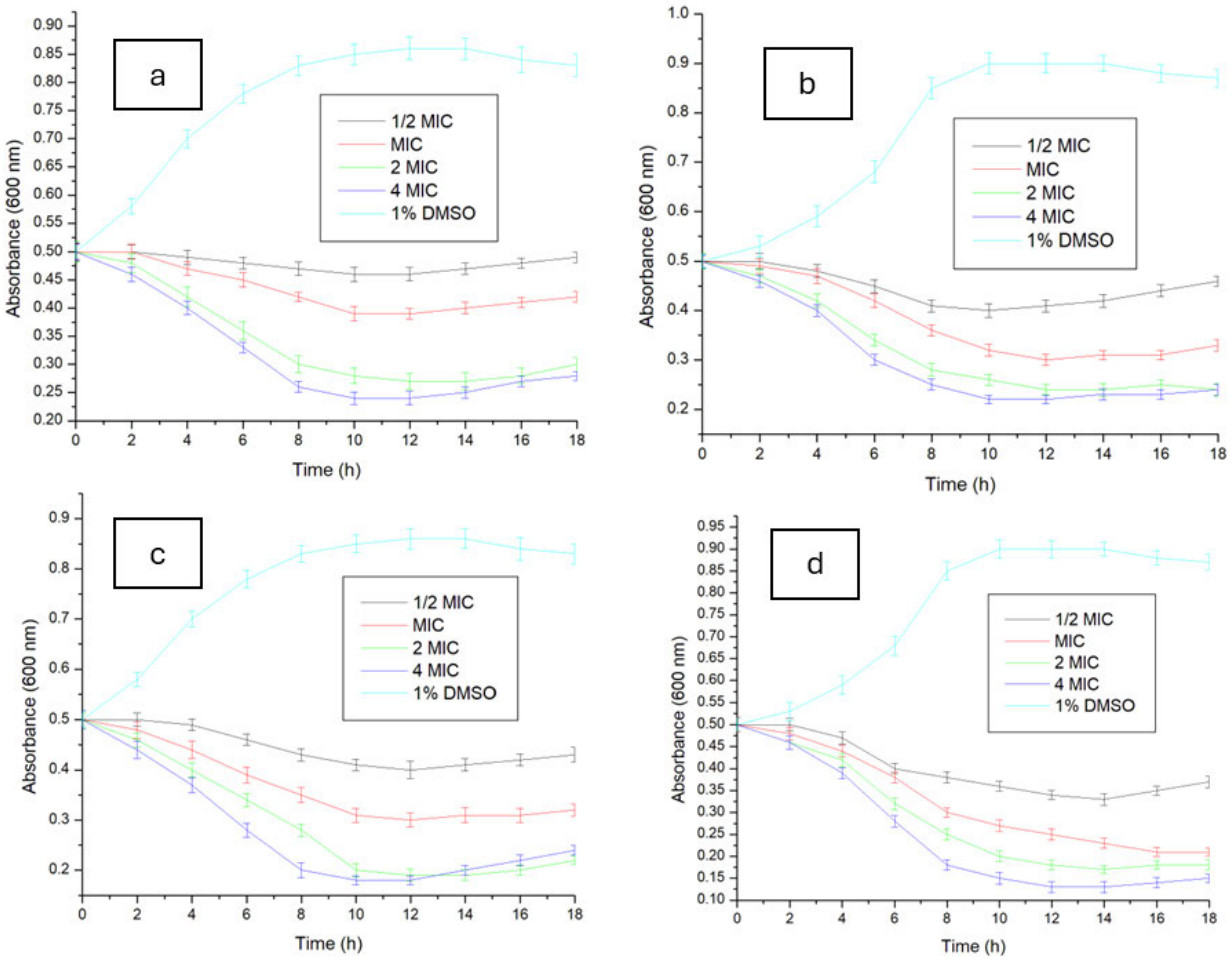
Organisms	Organisms Status	Cefotaxime	Amoxicillin	Silicristin	PSCB
Staphylococcus aureus ATCC 43300	R	7.0 ± 0.10	8.0 ± 0.10	10.0 ± 0.10	7.0 ± 0.3
Staphylococcus aureus ATCC 25923	S	10.0 ± 0.20	15.0 ± 0.30	12.0 ± 0.10	11.0 ± 0.2
Pseudomonas aeruginosa ATCC BAA-3197	R	8.0 ± 0.10	6.0 ± 0.20	10.0 ± 0.20	8.0 ± 1.0
Pseudomonas aeruginosa ATCC*27853*	S	18.0 ± 0.10	10.0 ± 0.20	24.0 ± 0.20	20.0 ± 0.0
Escherichia coli ATCC BAA-197	R	12.0 ± 0.30	5.0 ± 0.30	7.0 ± 0.10	8.0 ± 0.1
Escherichia coli ATCC 11775	S	38.0 ± 1.00	14.0 ± 0.80	20.0 ± 0.10	16.0 ± 0.6
Streptococcus pneumoniae ATCC 700677	R	8.0 ± 0.50	16.0± 0.80	12.0 ± 0.20	6.0 ± 0.4
Streptococcus pneumoniae ATCC 49619	S	15.0 ± 0.30	22.0 ± 0.30	18.0± 0.10	10.0 ± 0.1



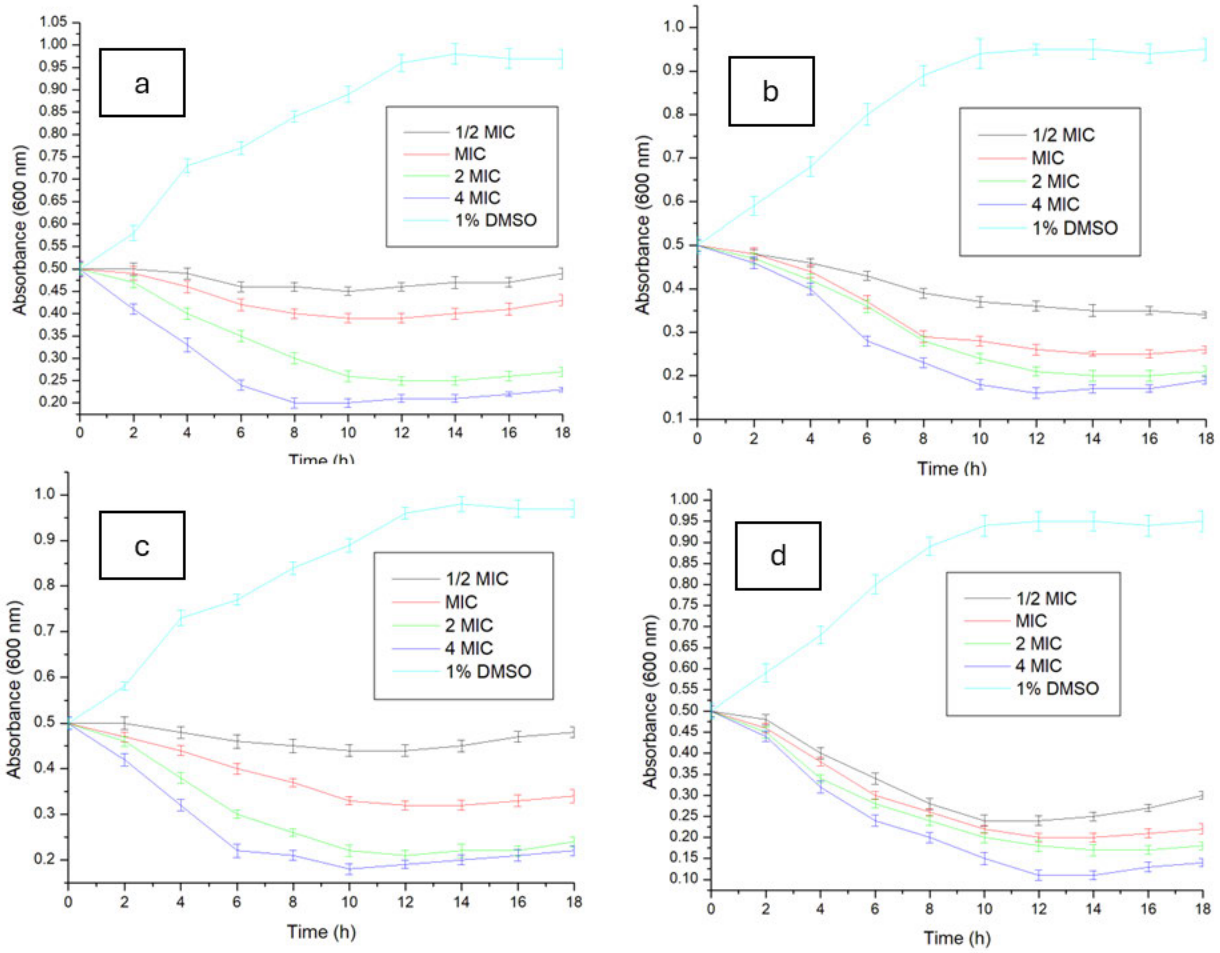
Supplementary Figure S1: Time kill curve of different concentrations of PSCB on (a) resistant strain (*S. aureus* ATCC 43300) and (b) sensitive strain (*S. aureus* ATCC 25923) of *S. aureus*, and silicristin on (c) resistant strain (*S. aureus* ATCC 43300) and (d) sensitive strain of (*S. aureus* ATCC 25923) of *S. aureus*.



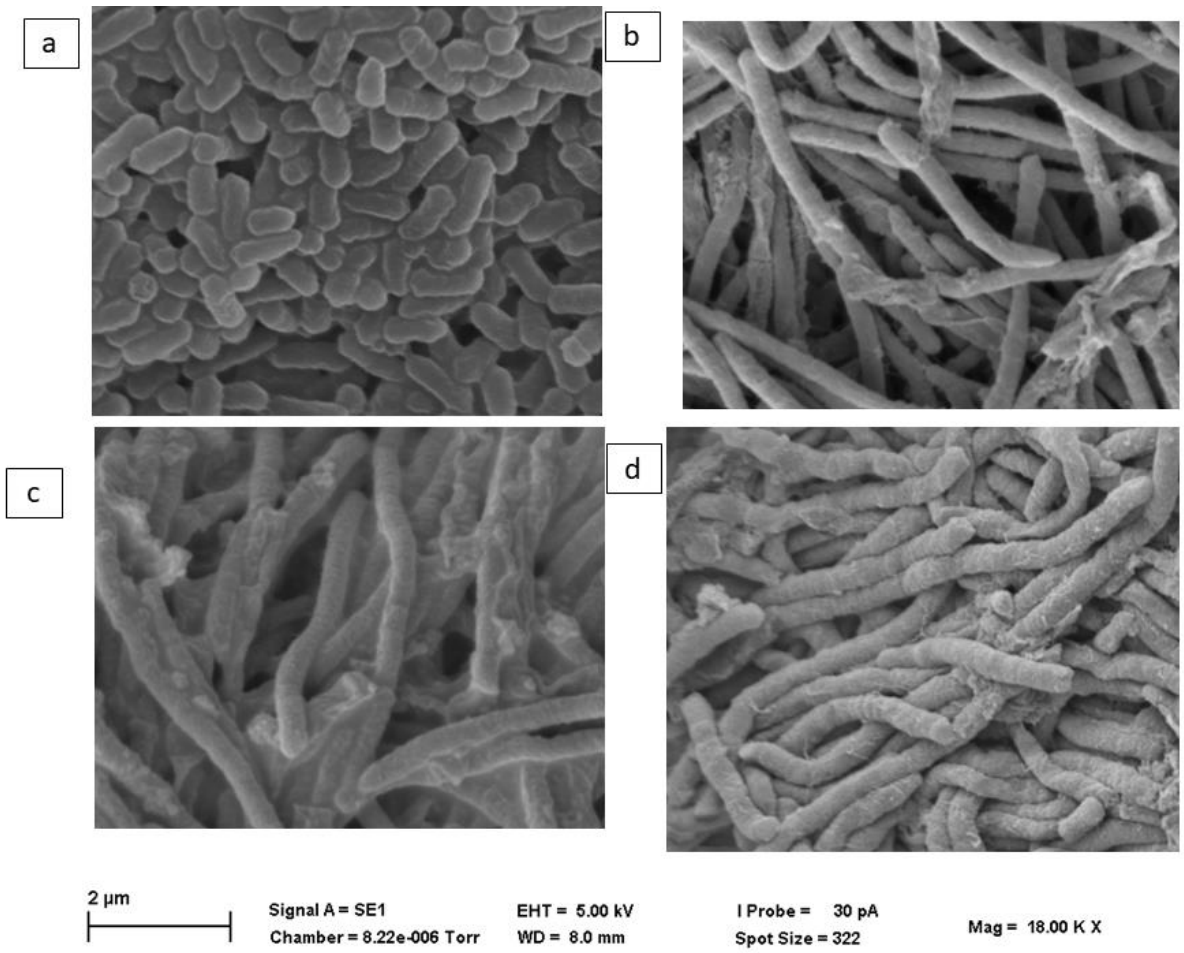
Supplementary Figure S2: Time kill curve of different concentrations of PSCB on (a) resistant strain (*S. pneumoniae* ATCC 700677) and (b) sensitive strain (*S. pneumoniae* ATCC 49619) of *S. pneumoniae*, and silicristin on (c) resistant strain (*S. pneumoniae* ATCC 700677) and (d) sensitive strain of (*S. pneumoniae* ATCC 49619) of *S. pneumoniae*.



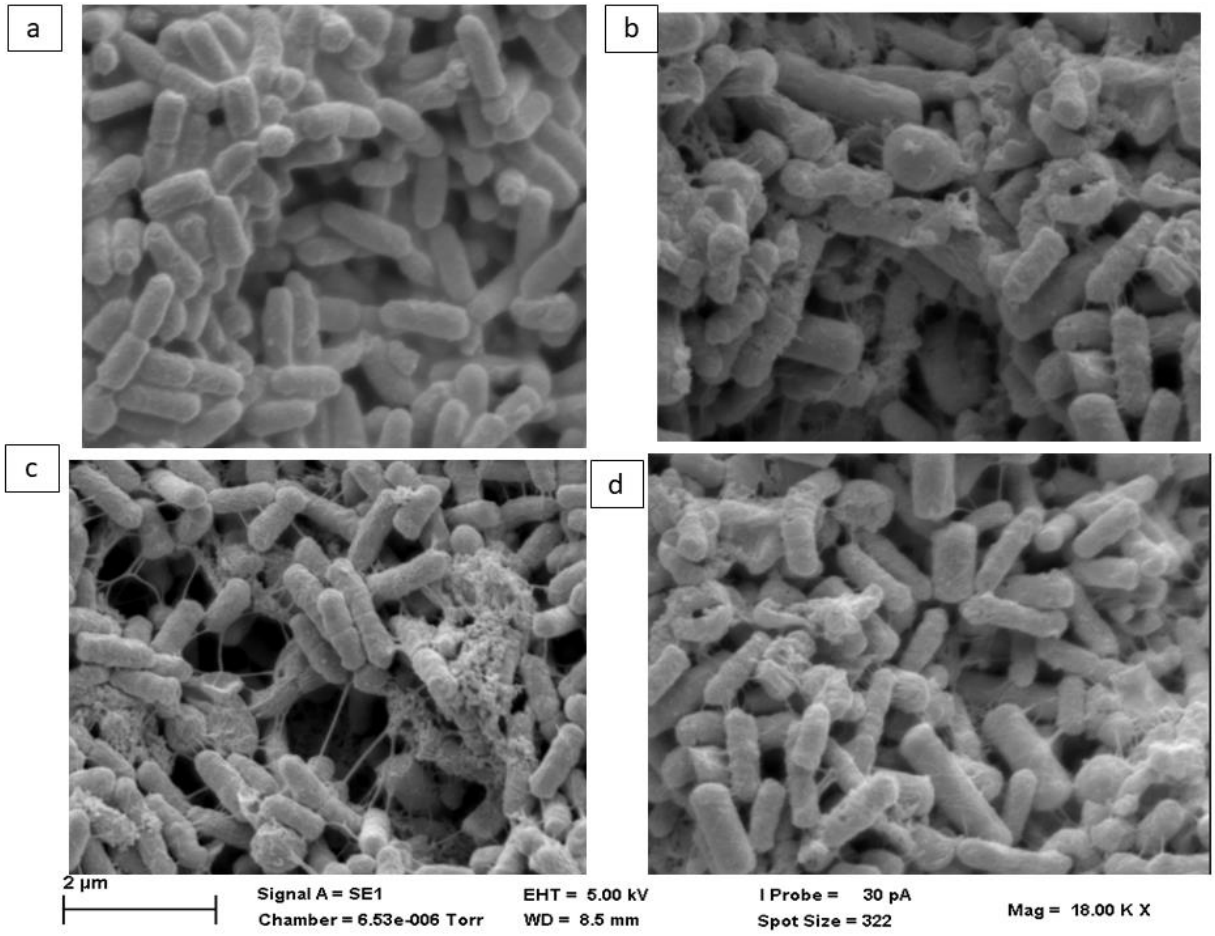
Supplementary Figure S3: Time kill curve of different concentrations of PSCB on (a) resistant strain (*P. aeruginosa* ATCC BAA-3197) and (b) sensitive strain (*P. aeruginosa* ATCC27853) of *P. aeruginosa*, and silicristin on (c) resistant strain (*P. aeruginosa* ATCC BAA-3197) and (d) sensitive strain of (*P. aeruginosa* ATCC27853) of *P. aeruginosa*.



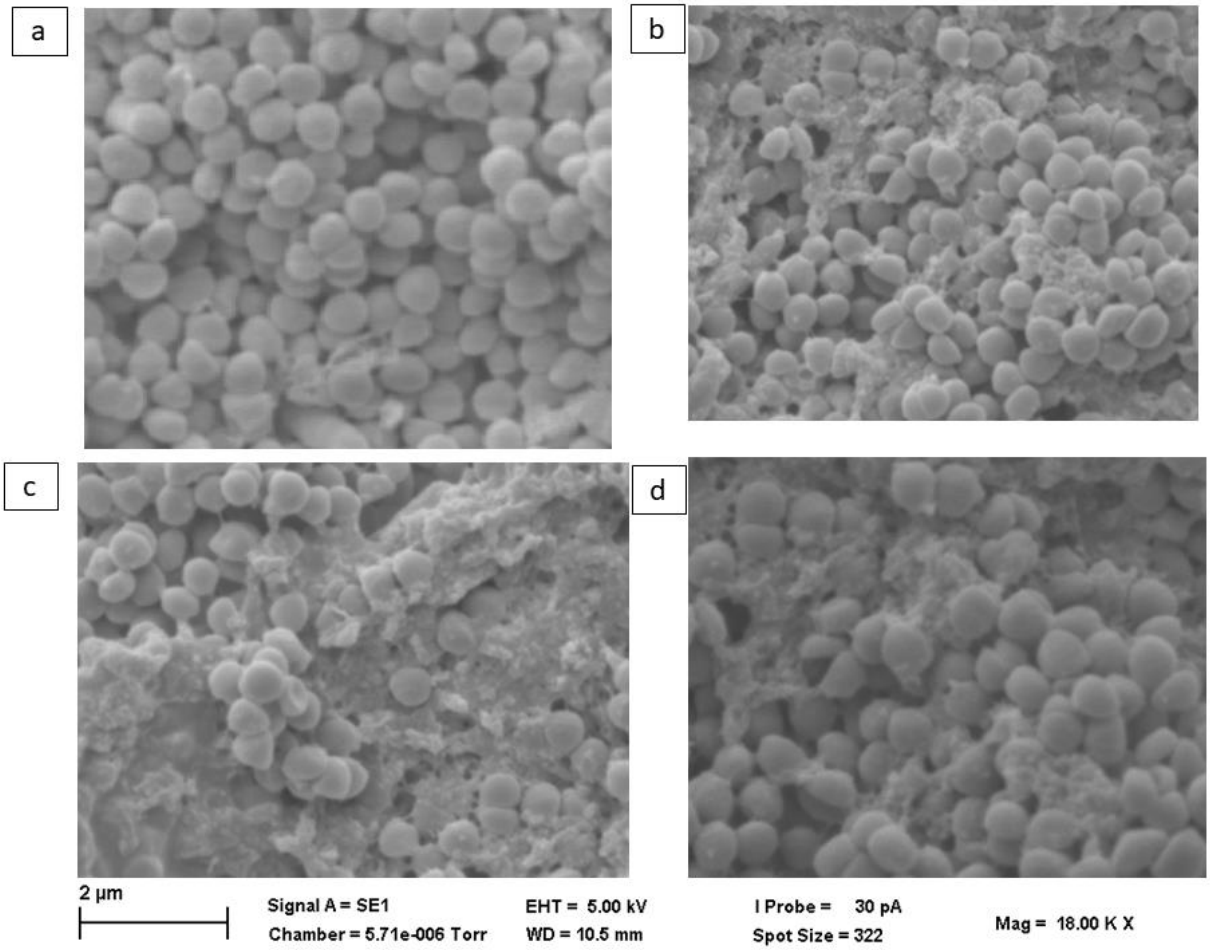
Supplementary Figure S4: Time kill curve of different concentrations of PSCB on (a) resistant strain (*E. coli* ATCC BAA-197) and (b) sensitive strain (*E. coli* ATCC 11775) of *E. coli*, and silicristin on (c) resistant strain (*E. coli* ATCC BAA-197) and (d) sensitive strain of (*E. coli* ATCC 11775) of *E. coli*



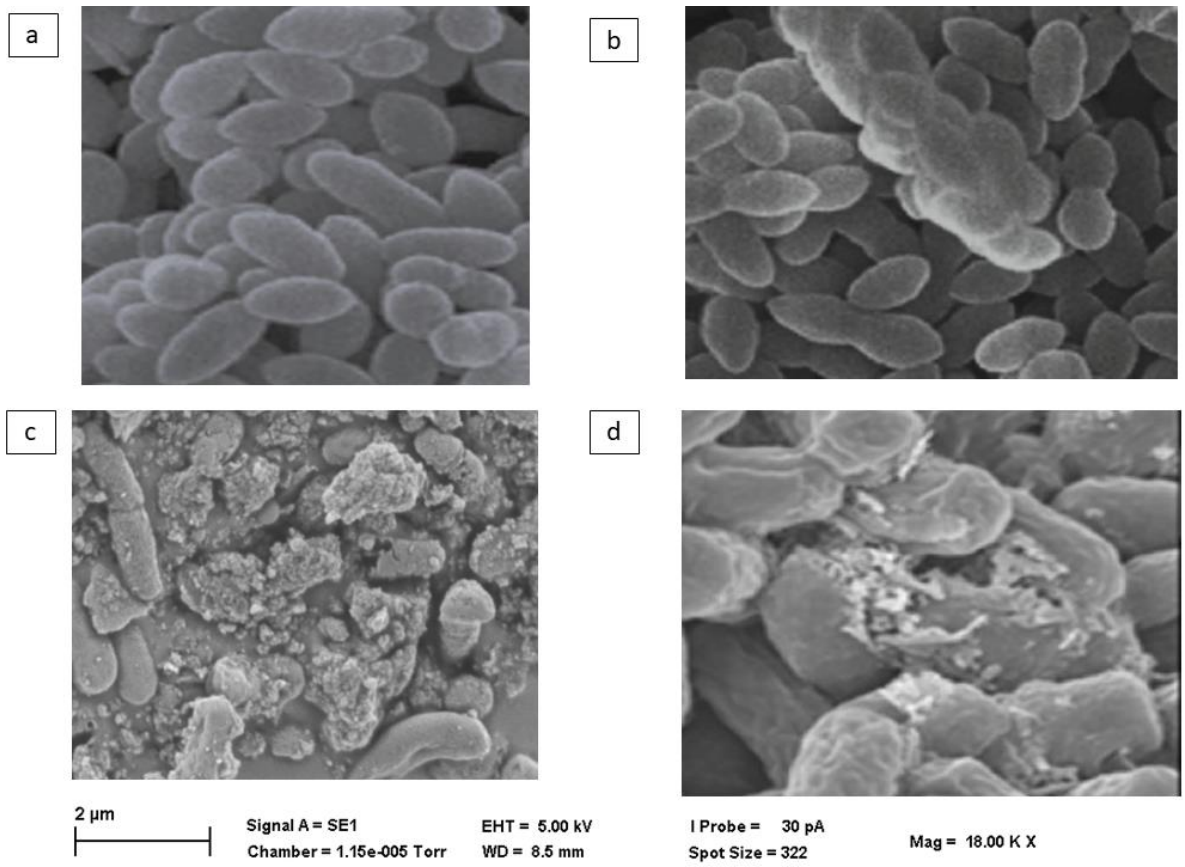
Supplementary Figure S5: Scanning electron microscopic images of (a) untreated *E. coli* ATCC 11775 and *E. coli* ATCC 11775 treated with MBC concentration of (b) cefotaxime (c) silicristin and (d) PSCB.



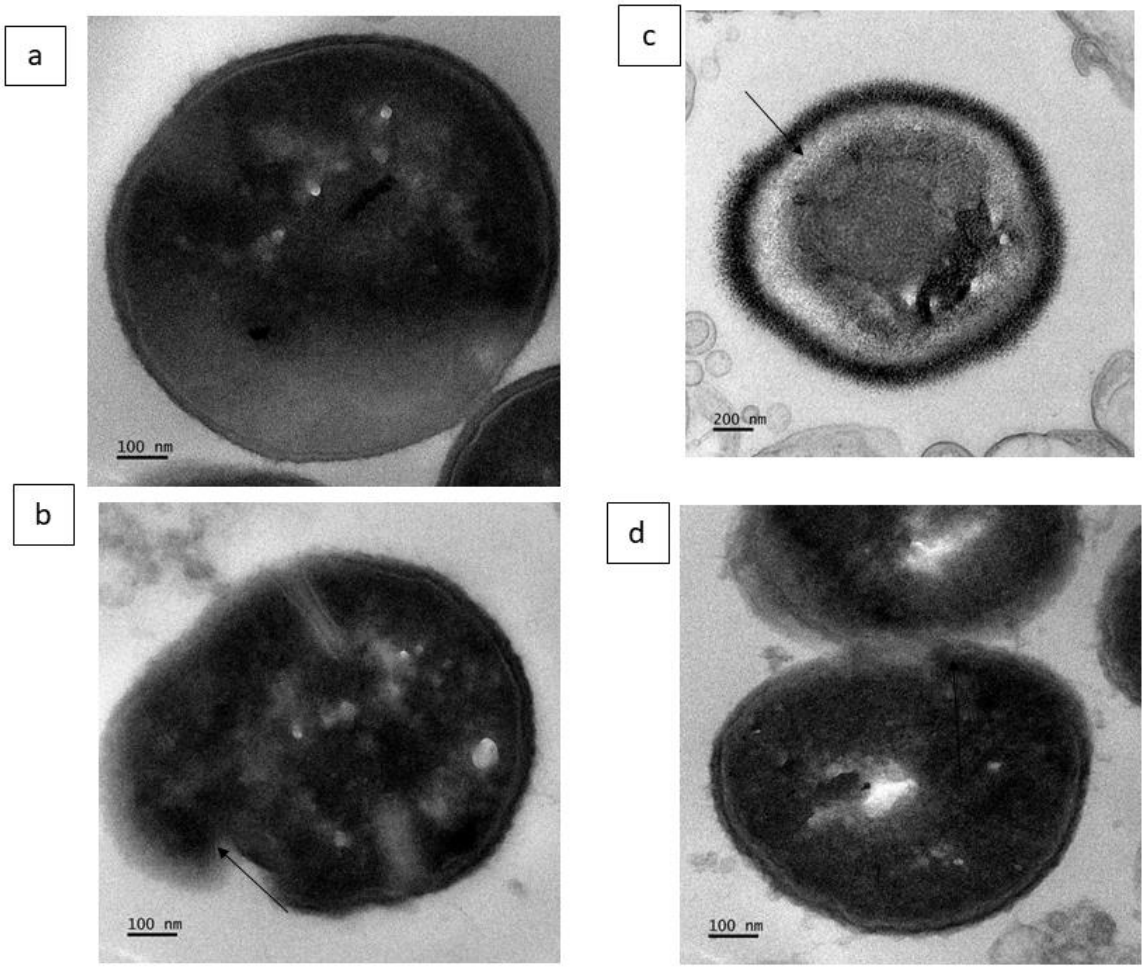
Supplementary Figure S6: Scanning electron microscopic images of (a) untreated *P. aeruginosa* ATCC*27853* and *P. aeruginosa* ATCC27853 treated with MBC concentration of (b) cefotaxime (c) silicristin and (d) PSCB.



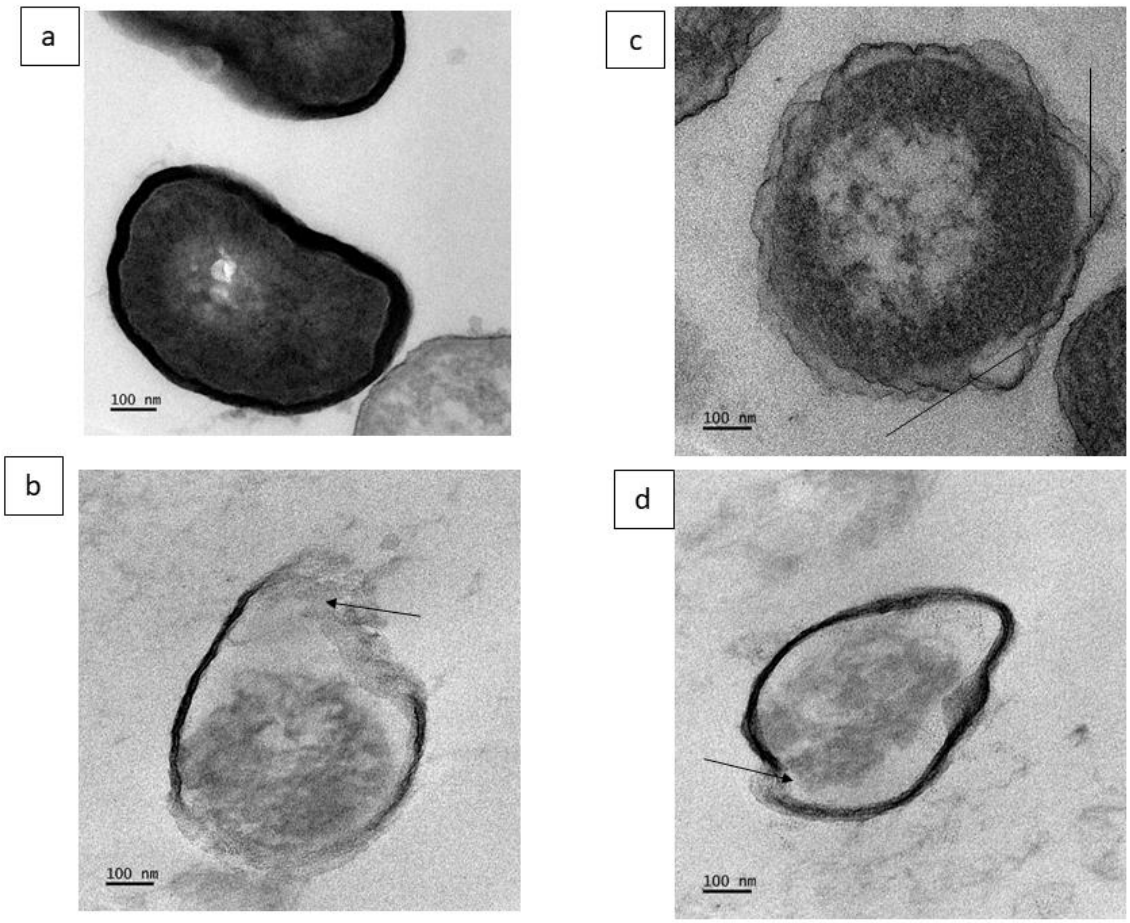
Supplementary Figure S7: Scanning electron microscopic images of (a) untreated *S. aureus* ATCC 25923 and *S. aureus* ATCC 25923 treated with MBC concentration of (b) amoxicillin (c) silicristin and (d) PSCB.



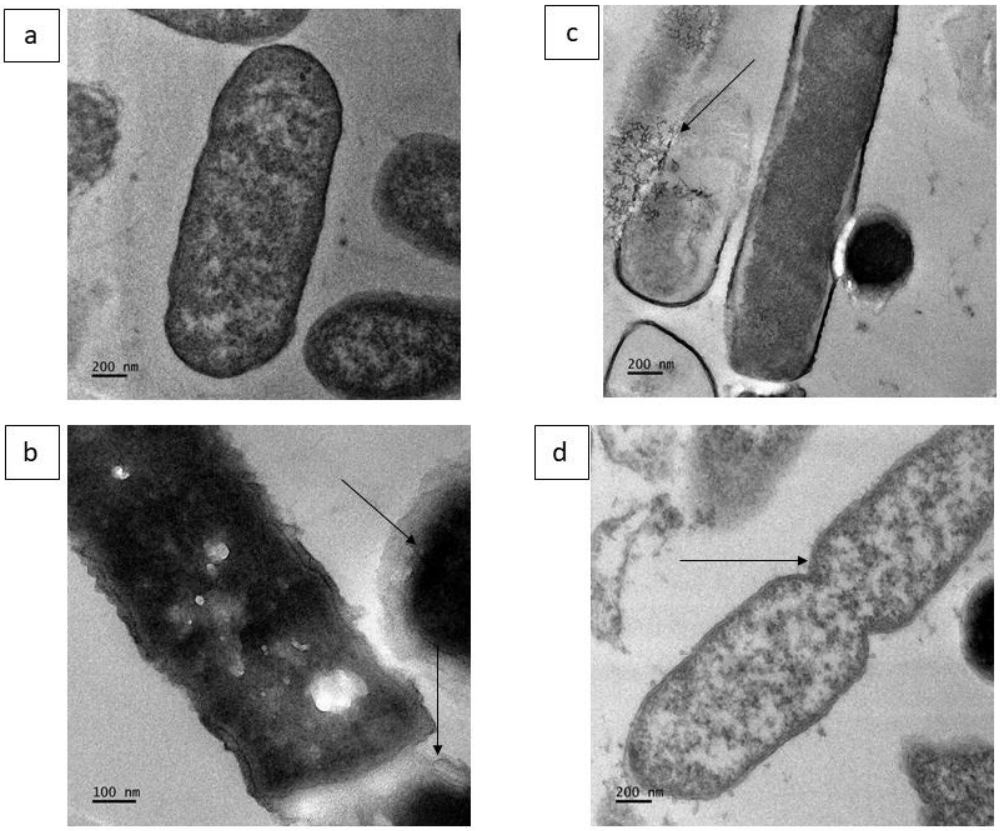
Supplementary Figure S8: Scanning electron microscopic images of (a) untreated *S. pneumoniae* ATCC 49619 and *S. pneumoniae* ATCC 49619 treated with MBC concentration of (b) amoxicillin (c) silicristin and (d) PSCB.



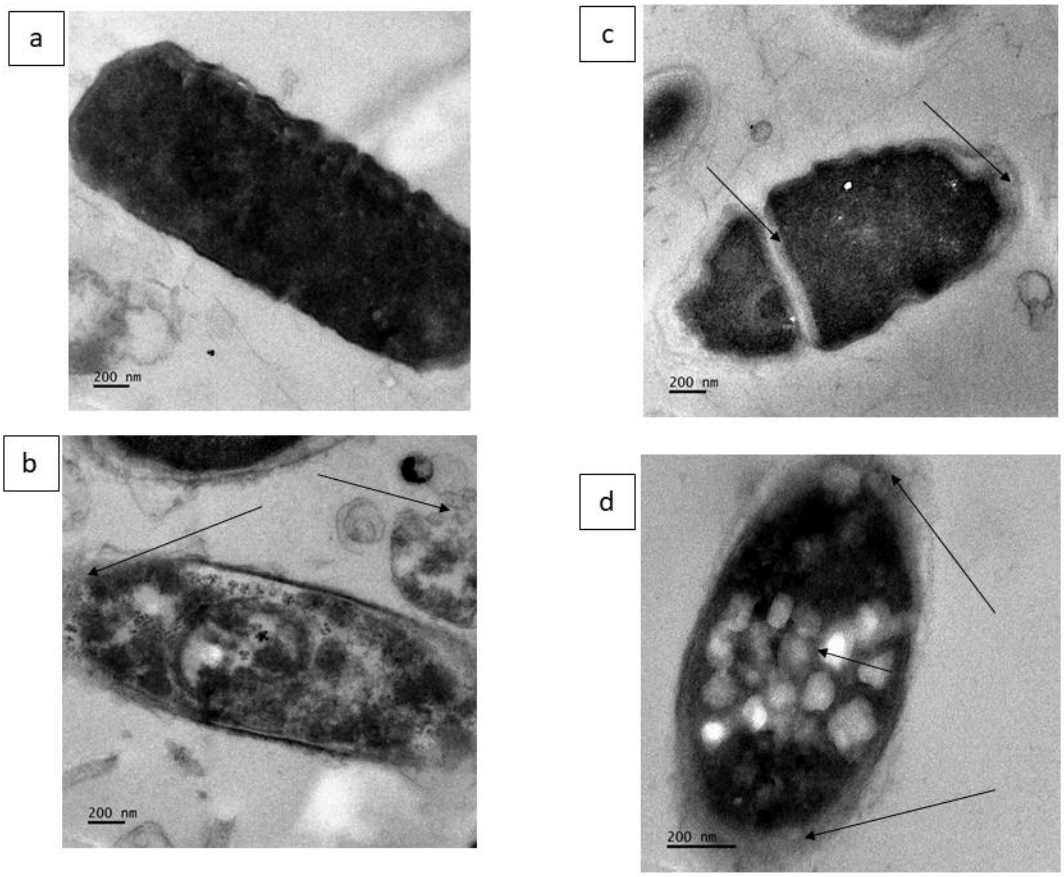
Supplementary Figure S9: Transmission electron microscopic images of (a) untreated *S. aureus* ATCC 25923 and *S. aureus* ATCC 25923 treated with MBC concentration of (b) amoxicillin (c) silicristin and (d) PSCB.



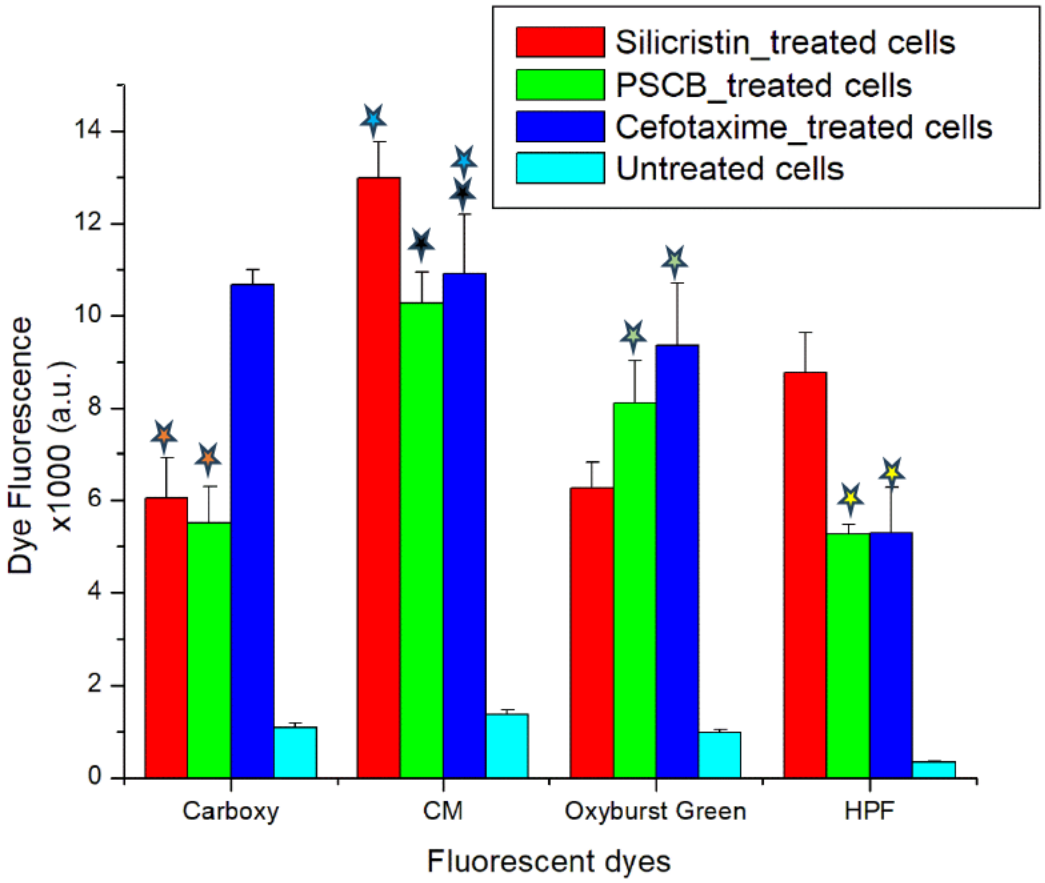
Supplementary Figure S10: Transmission electron microscopic images of (a) untreated *S. pneumoniae* ATCC 49619 and *S. pneumoniae* ATCC 49619 treated with MBC concentration of (b) amoxicillin (c) silicristin and (d) PSCB.



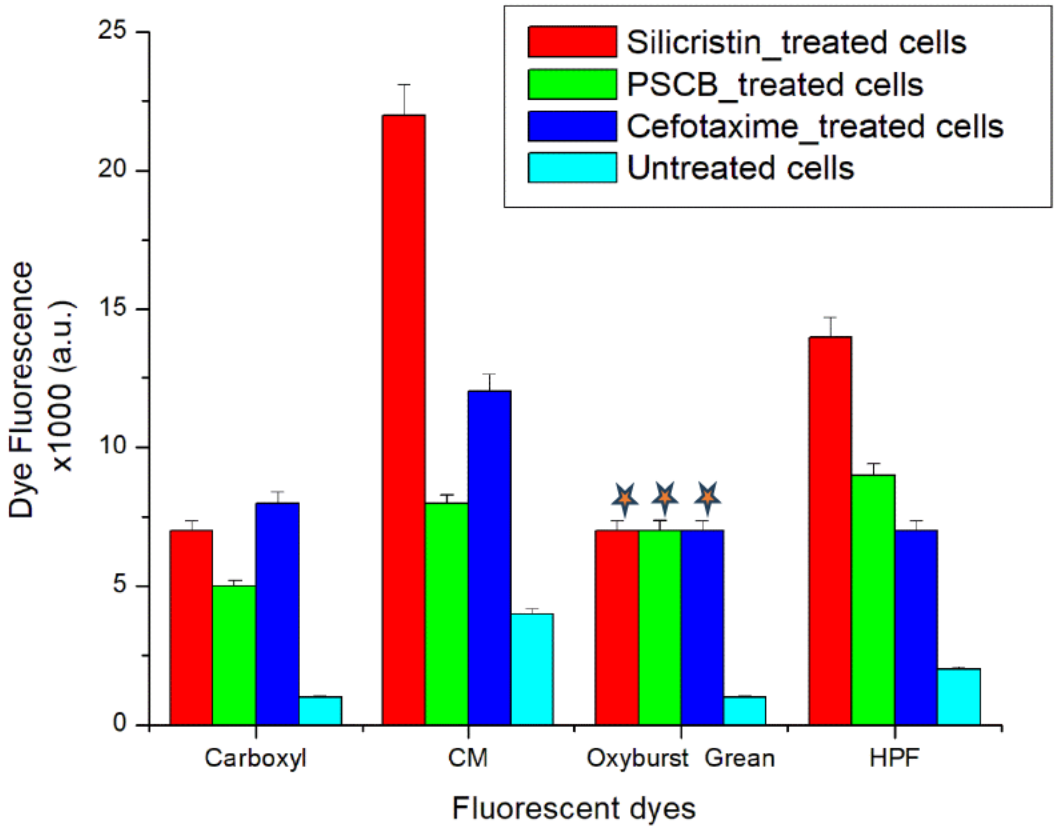
Supplementary Figure S11: Transmission electron microscopic images of (a) untreated *E. coli* ATCC 11775 and *E. coli* ATCC 11775 treated with MBC concentration of (b) cefotaxime (c) silicristin and (d) PSCB.



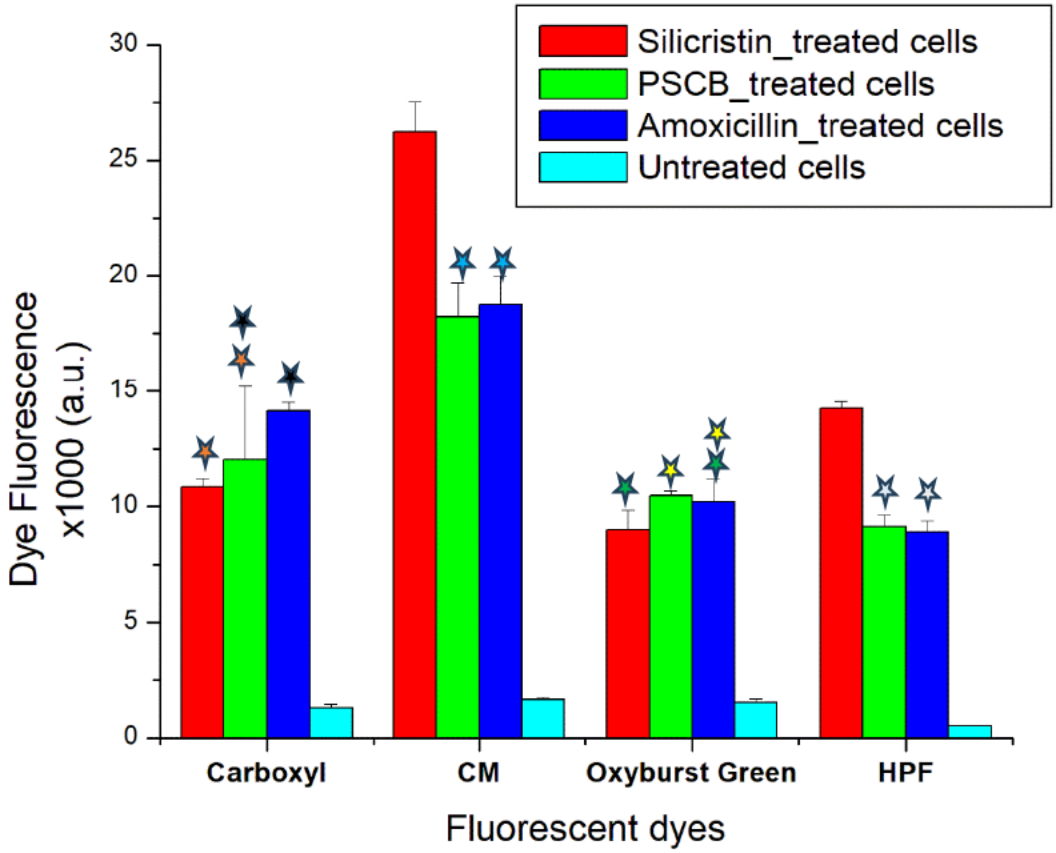
Supplementary Figure S12: Transmission electron microscopic images of (a) untreated *P. aeruginosa* ATCC27853 and *P. aeruginosa* ATCC27853 treated with MBC concentration of (b) cefotaxime (c) silicristin and (d) PSCB.



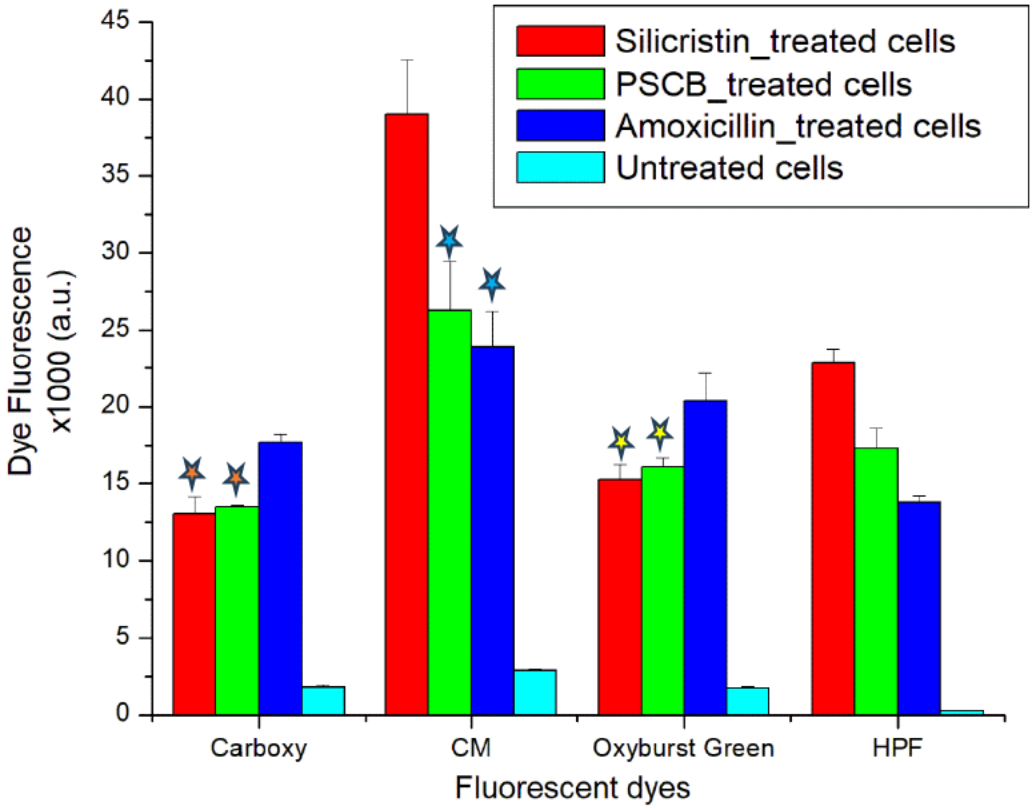
Supplementary Figure S13: The level of reactive oxygen species (ROS) generated following antibacterial treatment of *E. coli* ATCC 11775 (sensitive strain). The values given are mean ± standard deviation. The same "star sign" colour on the same set of bars in the graph indicates no significant difference at $p > 0.05$.



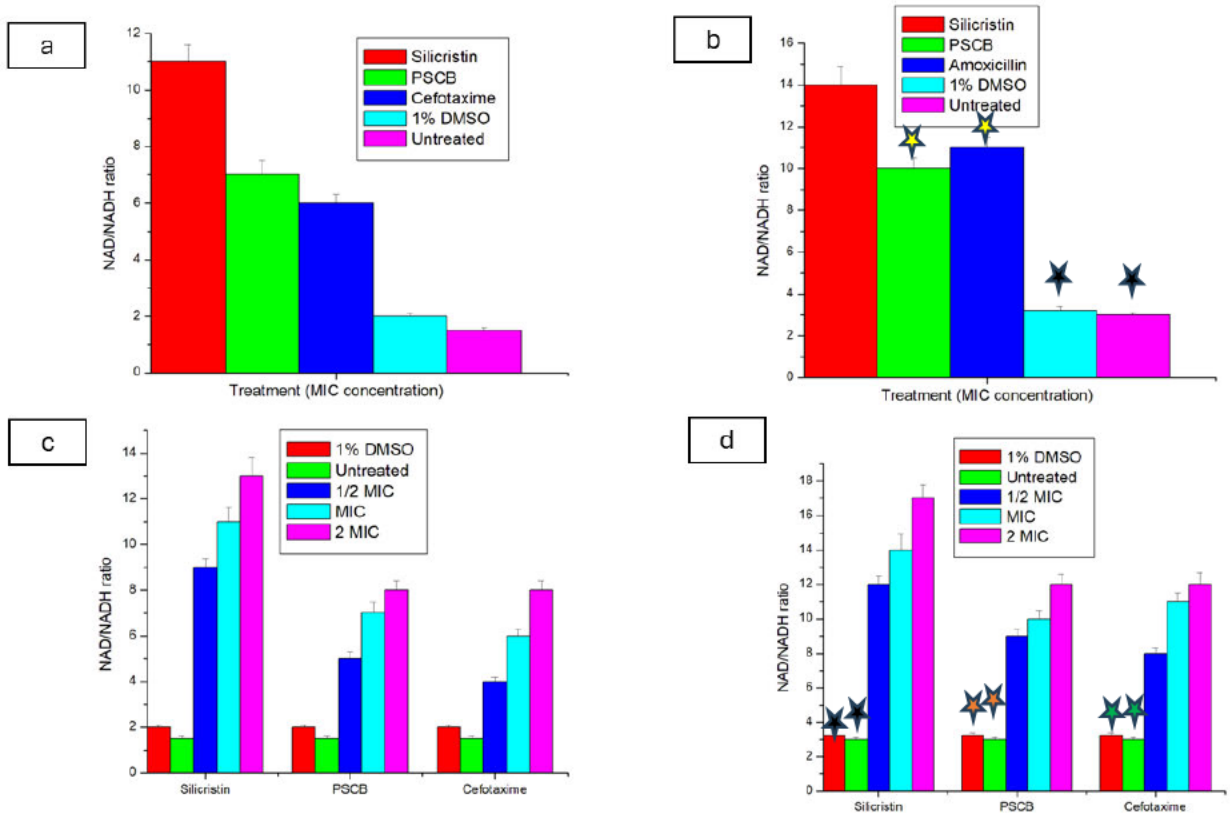
Supplementary Figure S14: The level of reactive oxygen species (ROS) generated following antibacterial treatment of *P. aeruginosa* ATCC27853 (sensitive strain). The values given are mean ± standard deviation. The same "star sign" colour on the same set of bars in the graph indicates no significant difference at $p > 0.05$.



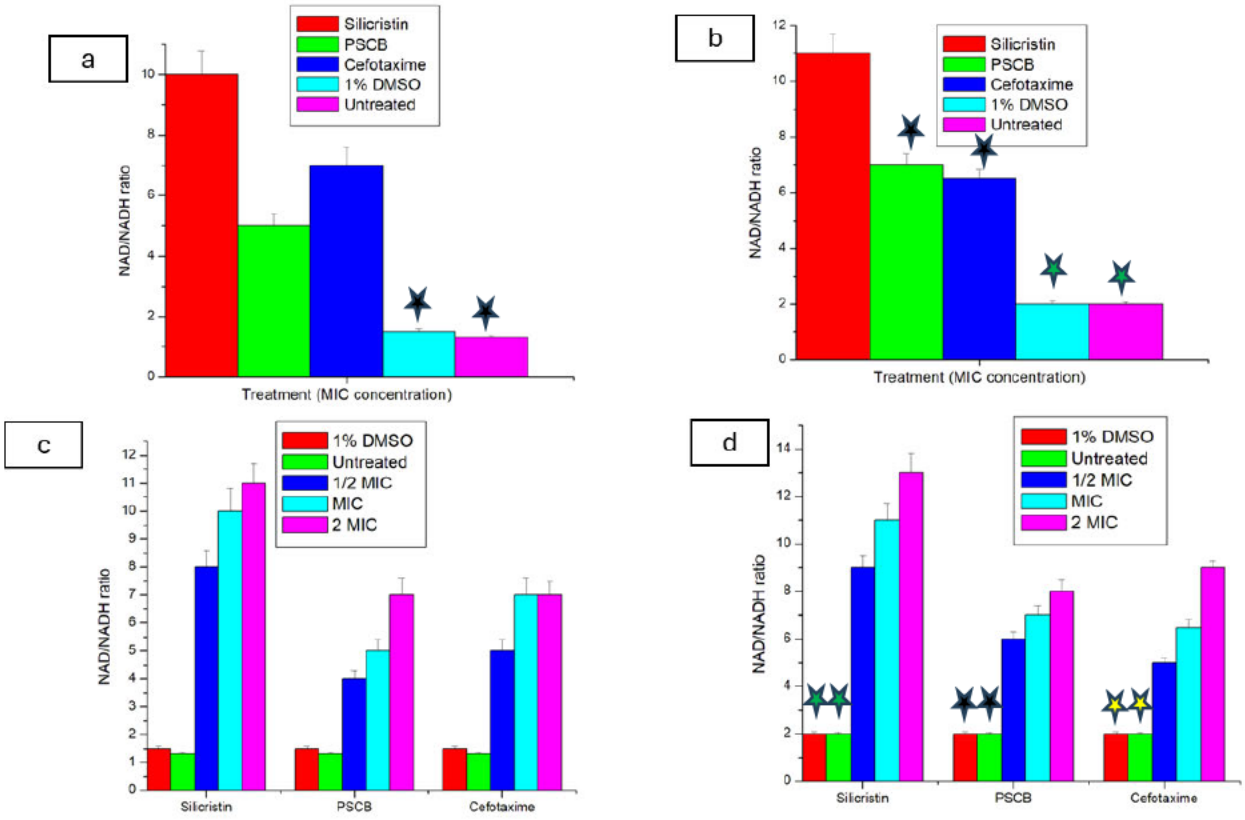
Supplementary Figure S15: The level of reactive oxygen species (ROS) generated following antibacterial treatment of *S. aureus* ATCC 25923 (sensitive strain). The values given are mean ± standard deviation. The same "star sign" colour on the same set of bars in the graph indicates no significant difference at $p > 0.05$.



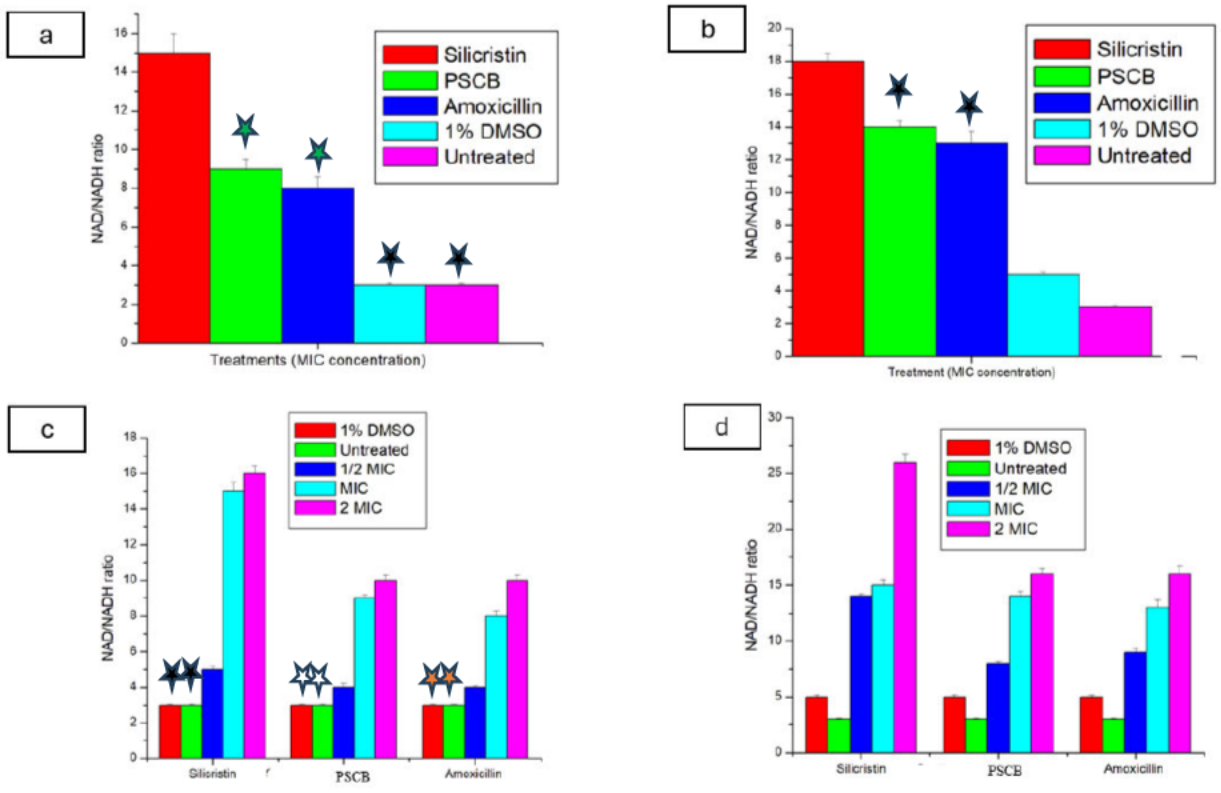
Supplementary Figure S16: The level of reactive oxygen species (ROS) generated following antibacterial treatment of *S. pneumoniae* ATCC 49619 (sensitive strain). The values given are mean ± standard deviation. The same "star sign" colour on the same set of bars in the graph indicates no significant difference at $p > 0.05$.



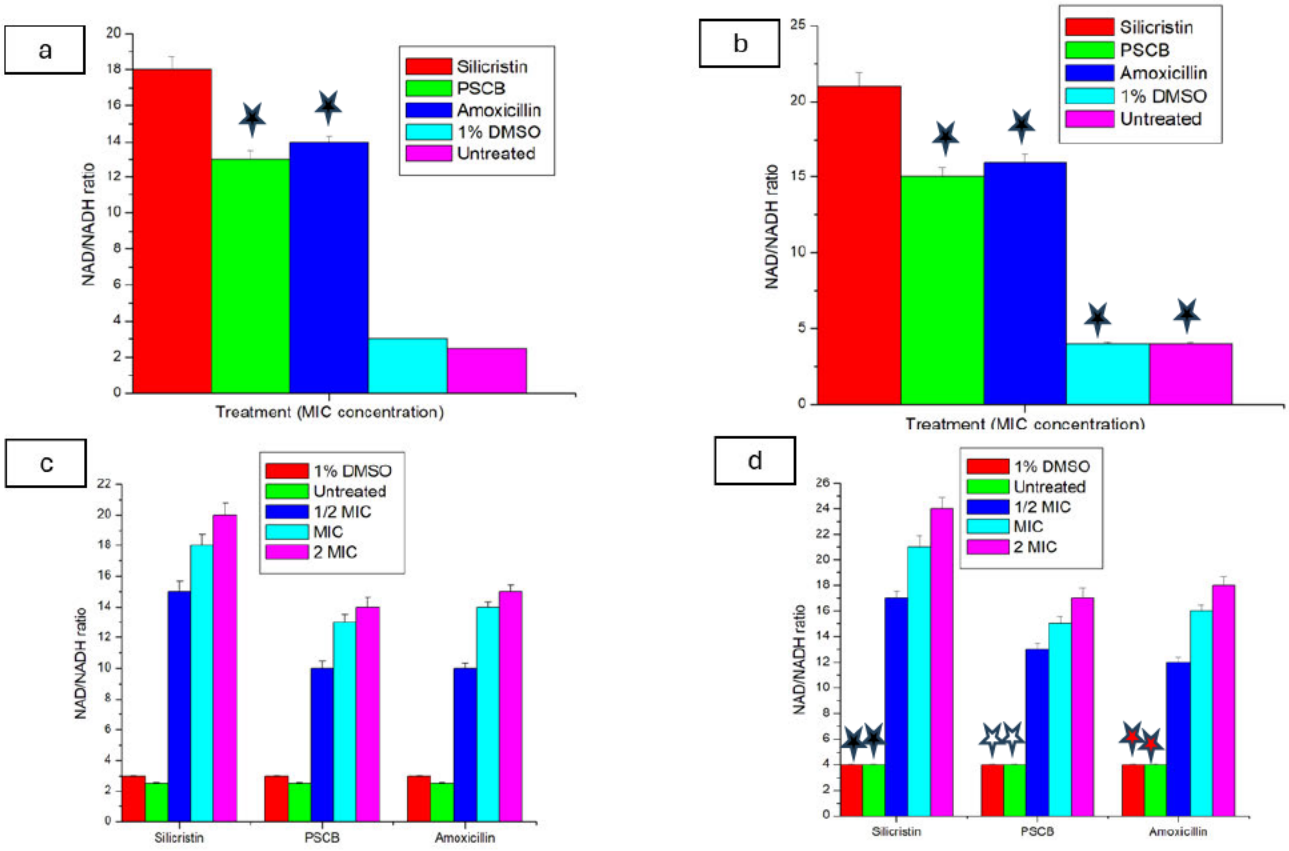
Supplementary Figure S17: Level of NAD/NADH ratio in (a) *E. coli* ATCC BAA-197 (resistant strain), and (b) *E. coli* ATCC 11775 (sensitive strain) following antibacterial treatment with silicristin, PSCB and cefotaxime. Effect of concentration on NAD/NADH ratio of (c) *E. coli* ATCC BAA-197 (resistant strain), and (d) *E. coli* ATCC 11775 (sensitive strain) following antibacterial treatment with silicristin, PSCB and cefotaxime. The values given are mean ± standard deviation. The same "star sign" colour on the same set of bars in the graph indicates no significant difference at $p > 0.05$.



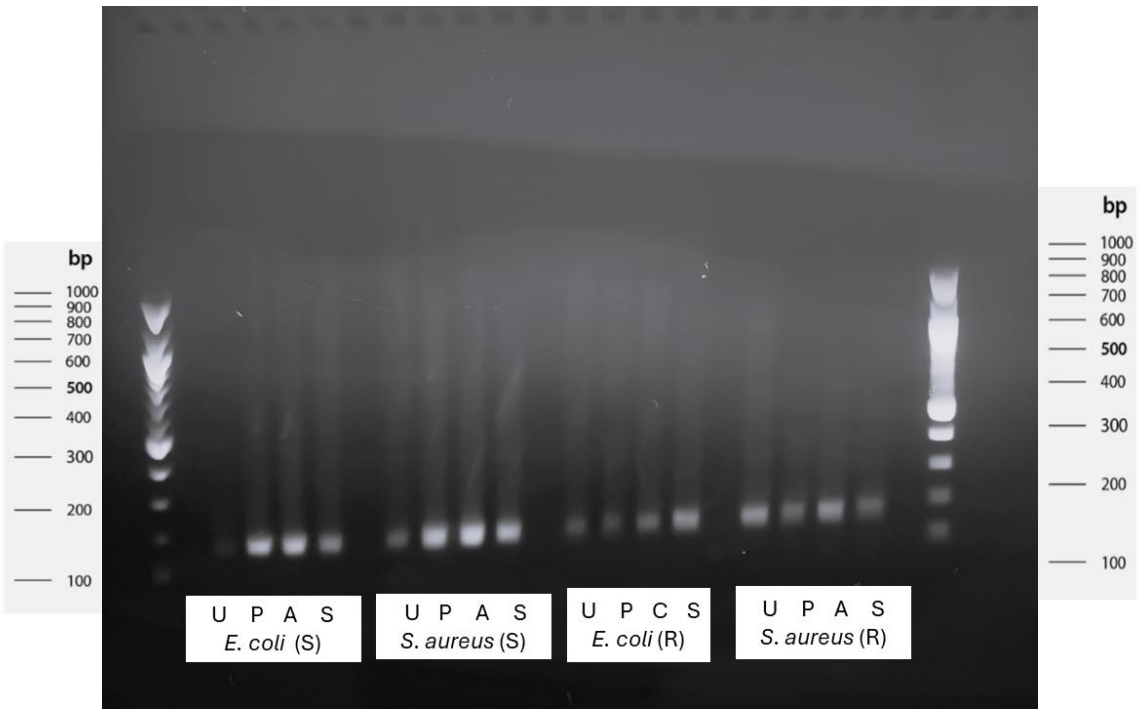
Supplementary Figure S18: Level of NAD/NADH ratio in (a) *P. aeruginosa* ATCC BAA-3197 (resistant strain), and (b) *P. aeruginosa* ATCC27853 (sensitive strain) following antibacterial treatment with silicristin, PSCB and cefotaxime. Effect of concentration on NAD/NADH ratio of (c) *P. aeruginosa* ATCC BAA-3197 (resistant strain), and (d) *P. aeruginosa* ATCC27853 (sensitive strain) following antibacterial treatment with silicristin, PSCB and cefotaxime. The values given are mean ± standard deviation. The same "star sign" colour on the same set of bars in the graph indicates no significant difference at $p > 0.05$.



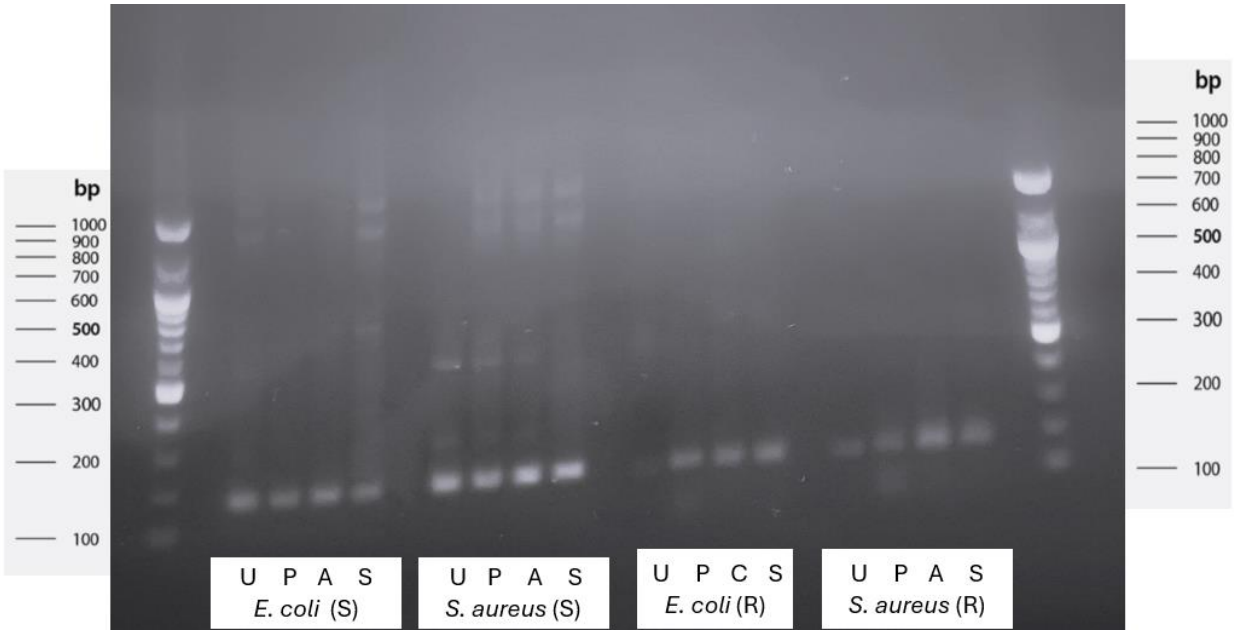
Supplementary Figure S19: Level of NAD/NADH ratio in (a) *S. aureus* ATCC 43300 (resistant strain), and (b) *S. aureus* ATCC 25923 following antibacterial treatment with silicristin, PSCB and amoxicillin. Effect of concentration on NAD/NADH ratio of (c) *S. aureus* ATCC 43300 (resistant strain), and (d) *S. aureus* ATCC 25923 following antibacterial treatment with silicristin, PSCB and amoxicillin. The values given are mean ± standard deviation. The same "star sign" colour on the same set of bars in the graph indicates no significant difference at $p > 0.05$.



Supplementary Figure S20: Level of NAD/NADH ratio in (a) *S. pneumoniae* ATCC 700677 (resistant strain), and (b) *S. pneumoniae* ATCC 49619 (sensitive strain) following antibacterial treatment with silicristin, PSCB and amoxicillin. Effect of concentration on NAD/NADH ratio of (c) *S. pneumoniae* ATCC 700677 (resistant strain), and (d) *S. pneumoniae* ATCC 49619 (sensitive strain) following antibacterial treatment with silicristin, PSCB and amoxicillin. The values given are mean ± standard deviation. The same "star sign" colour on the same set of bars in the graph indicates no significant difference at $p > 0.05$.



Supplementary Figure S21: Expression of *SodA* in sensitive (S) and resistant (R) strains of *E. coli* and *S. aureus* following antibacterial treatment with silicristin (S), PSCB (P) and beta-lactams (cefotaxime (C) for Gram-negative organisms and amoxicillin (A) for Gram-positive organisms) relative to the untreated cells (U).



Supplementary Figure S22: Expression of *SoxR* in sensitive (S) and resistant (R) strains of *E. coli* and *S. aureus* following antibacterial treatment with silicristin (S), PSCB (P) and beta-lactams (cefotaxime (C) for Gram-negative organisms and amoxicillin (A) for Gram-positive organisms) relative to the untreated cells (U).

CHAPTER SIX

6.0 GENERAL DISCUSSION AND RECOMMENDATIONS

6.1 General discussion……..**438**

6.2 Conclusion and recommendation ……...**450**

References…….....**455**

1.0 General Discussion

Beta-lactams are and will continue to be an important agent in the treatment of common and clinically important Gram-positive and Gram-negative bacterial infections (Bush, 2018). Nevertheless, the emergence of resistant isolates complicating the treatment process of many infections is a matter of great concern. Resistance of pathogenic bacteria to beta-lactams is facilitated majorly by two mechanisms, namely the production of beta-lactamases (an enzyme that inactivate beta-lactams) and the modification of key high molecular weight penicillin-binding protein (PBPs) (Bush, 2018). While enzyme modification is most common with Gram-negative organisms, modification of key PBPs is prevalent in Gram-positive organisms and becoming increasingly reported in Gram-negatives organisms (Tooke *et al*., 2019). Modification of PBPs ensures that the interaction with beta-lactams occurs at a considerably higher antibiotic doses than with PBPs from susceptible strains, thus substantially reducing biological activity (Fisher *et al*., 2016; Cho *et al*., 2014). Previous studies have mainly focused on the development of beta-lactamase inhibitors that can be used in combination therapy with beta-lactams (Tooke *et al*., 2019; Hecker *et al*., 2015). However, due to the similar core structure of beta-lactamase inhibitors with beta-lactam, bacterial resistance to this type of combination therapy has developed (Palacios *et al*., 2020; Eiamphungporn *et al*., 2018). Also, the recently discovered beta-lactamase inhibitors with non-beta-lactam scaffolds (diazabicyclooctane derivatives) such as avibactam and relebactam inactivate beta-lactamase, but unlike beta-lactam-based inhibitors, this inactivation is slowly reversible, releasing an intact beta-lactamase and the inhibitor in the process prompting the need for other viable alternative approaches in combating resistance to beta-lactams. Thus, in this study, the identification and development of potent therapeutics from phenolics with a different scaffold from beta-lactams against therapeutically important PBPs was employed as a viable alternative

strategy in ameliorating resistance to beta-lactam. According to Glen *et al*. (2021), identifying and developing novel beta-lactams with different scaffolds that are resistant to beta-lactamases and or have broad-spectrum effect on several PBPs represents a novel approach in overcoming resistance to beta-lactams. Besides having a different scaffold from beta-lactams, phenolics have been demonstrated as potent antibacterial agents against both Gram-positive and Gram-negative pathogens due to their ability to modulate therapeutic targets such as PBPs, beta-lactamase and key quorum sensing systems implicated in biofilm formation (Alhadrami *et al*., 2020; Avila *et al*., 2008). As a result, phenolics have been explored in the identification of drug contenders that can act directly on druggable targets and/or act in synergy with conventional antibiotics, an approach that is encouraged in the treatment of infections caused by multi-drug-resistant bacteria. The presence of hydroxyl groups in phenolics has been shown to enhance strong PBP binding while increasing affinity for cytoplasmic membranes, hence increasing antibacterial action (Avila *et al*., 2008). Additionally, the characteristic hydroxyl group of phenolics are implicated in auto-oxidation in the presence of transition metals (Wei *et al*., 2022; Ajiboye *et al*., 2017; Eghbaliferiz and Iranshahi, 2016), thus generating reactive oxygen species (ROS) which have been implicated in the lethality of most conventional antibiotics as a secondary means of action. These intriguing characteristics of phenolics positioned them as a viable source of drug candidate that can be development as potential beta-lactams. This study used multifaceted *in silico* and *in vitro* approach in bioprespection for phenolics as modulators of PBPs and ROS. The *in silico* approaches including molecular docking, molecular dynamic (MD) simulation, and density functional theory were chosen based on their importance in drug discovery and development in identifying leads from a library of compounds prior to further optimization via retrosynthesis. The *in vitro* techniques used on the other hand allows for the swift validation of the *in silico* results and they

includes the determination of the minimum inhibitory concentration, time kill kinetic assay, checkerboard assay (for synergistic examination), scanning and transmission electron microscopy (for evaluation of binding of PBPs and ROS damage to cell wall, cell membrane and other cell components) and ROS generating potential assay using direct ROS quantification method and several other indirect ROS indicators. The results from the study contribute to the ongoing efforts to tackle the resistant issue faced with the beta-lactams through identification of potent lead phenolics and novel compounds against therapeutically important PBPs of common and clinically important pathogenic bacteria.

1.1 Identification of silicristin as lead phenolics with broad spectrum effects against essential PBPs of common and clinically important bacterial using *in silico* techniques

This aspect of the study focuses on the identification of lead phenolics with a broad-spectrum binding affinity on a wide range of key PBPs (PBP2a of *Staphylococcus aureus*, PBP2x of *Streptococcus pneumoniae,* PBP3 of *Pseudomonas aeruginosa,* and PBP3 and 5 of *Esherichia coli*) of common and clinically important Gram-positive and Gram-negative bacteria. The identification of top-20 phenolics with higher negative docking scores against each of the investigated key PBPs relative to the four beta-lactams references standards (amoxicillin, cefotaxime, aztreonam and doripenem), suggest the effectiveness of the structure-based drug design (SBDD) employed in this study in screening hits from the over 10,000 phenolics currently known. The higher negative docking scores of the top-20 phenolics may mean that the scaffolds of the phenolics fit well at the binding pockets of each of the investigated key PBPs, presenting them as drug candidates that might find use as beta-lactams. The advantage of the identification and development of novel beta-lactams with different scaffolds have been noted by prior study in overcoming resistance to beta-lactams (Glen *et al*., 2021). The top-20 phenolics had a structurally

different scaffolds relative to the beta-lactam ring structure, thus, enzyme modification through beta-lactamase by Gram-negative and some Gram-positive bacteria such as *S. aureus* (e.g. penicillase), may be ineffective against them, thus availing the phenolics to bind and inactivate key PBPs during treatment. Subsequent filtering of the top-20 leads in each case of the key PBPs based on their physicochemical, pharmacokinetic and toxicological profiles afforded top-five phenolics that are chemically diverse, orally bioavailable and with good synthetic feasibility scores (<5) appropriate for drug development. The observation of these characteristics in each case of the top-five phenolics of the key PBPs might suggest that the top-ranked phenolics will be orally bioavailable to reach druggable target (in this case the PBPs) and exert their pharmacological effects while causing lesser toxicity. These observations have been noted by prior studies in molecules that eventually passed the preclinical and clinical stages of drug development (Mousavi *et al*., 2021; Reichel and Lienau, 2016; Lipinski *et al*., 2001). The observation of synthetic feasibility score of < 5 with the top-five phenolics in each case of the key PBPs means that they can be easily derivatized and synthesized in the need for structural modification for toxicity reduction and or potency enhancement as earlier noted by Ertl *et al*. (2021). Additionally, in SBDD studies, virtual screening limitations relating to lack of subsequent refinement (rescoring) and assessment of binding pose stability have contribute to the increased rate of inactive molecules that are certain to fail the next phase of drug development (Cerón-Carrasco, 2022; Acharya *et al.*, 2020). Hence, the use of MD simulations in this study provides insights into the essential biomolecular processes relating to stability, flexibility, and compactness following the top-five phenolics binding of the key PBPs, an approach which have been deem important in drug discovery and development. The observation that at least four of the top-five phenolics had higher negative binding free energy against each of the key PBPs investigated means that the top-ranked phenolics

are structurally and thermodynamically compactible at the binding pockets of the PBPs which again is a pointer to the suitability of the top-ranked phenolics scaffold for beta-lactam development. These submissions are in tandem with prior studies that have reported on the ant-PBPs properties of phenolics (Tabassum *et al*., 2023; Alhadrami *et al*., 2020; Santiago *et al*., 2015). The lead phenolics with the highest negative binding free energy in each case of the key PBPs (silicristin and epicatechin gallate at the active and allosteric site of PBP2a, lysidicichin and epigallocatechin 4-benzylthioether against PBP3 and PBP5 of *E. coli,* catechin 3-rhamside against PBP3 of *P. aeruginosa* and epicatechin 3-O-(3-O-methylgallate and silicristin against active and allosteric site of PBP2x) had higher stability, compactness and flexibility relative to the referenced beta-lactams and other top-ranked phenolics. This observation was noted to be due to the superior hydrogen bonds contact and other important hydrophobic interaction of the lead phenolics at the binding pocket of the key PBPs during the 120-ns MD simulation, which have been noted in previous studies to be important in drug discovery and development (Du *et al.*, 2016; Izadi *et al.*, 2014; Kretschmer *et al.*, 2010). More importantly, the allosteric modulation of Tyr446 (gate keeper residue of PBP2a of *S. aureus*) and Ser337 (critical amino acid residue in PBP2x of *S. pneumoniae*) were noted with the top-ranked phenolic and particularly epicatechin gallate against PBP2a and silicristin against PBP2x following binding at the allosteric sites. These findings might suggest the potential of epicatechin gallate and silicristin as compounds that can function in combinatory therapy for the synergistic treatments of infections caused by *S. aureus* and *S. pneumoniae*. This approach has been noted by previous studies (Ahmad *et al*., 2022; Alhadrami *et al.*, 2020) to not only help in preventing prolonged exposure to antibiotic but also aiding the resuscitation of currently known antibiotics which are no longer effective. Overall, among the top-five phenolics, silicristin remain the only compound with affinity that cut across all the key PBPs suggestive of

its broad-spectrum effects relative to other top-ranked phenolics. According to Glen *et al*. (2021), multiple PBP binding agents compared to agents that target a single PBP might aid the alleviation of PBP modification-based resistance mechanisms. In this study, silicristin aside having affinity for all the key PBPs, had higher negative binding free energy than all the reference beta-lactam used, suggestive of its potent anti-PBPs capability. These properties of silicristin potentiate the compound as drug contender that may succeed in the later stage of drug development. However, despite these intriguing properties of silicristin, the higher root means square deviation (RMSD) of the complexes formed by the compound with three of the key PBPs (silicristin-PBP2a of *S. aureus*, silicristin-PBP2x of *S. pneumoniae*, silicristin-PBP3 of *E. coli*) which was observed to be higher the 3.0 Å limit for good deviation (Ramirex and Caballero, 2016) means that the compound might instigate higher thermodynamic entropy in the proteins. This discovery points to the necessity for further structural modifications of silicristin for stability, which might greatly boost its affinity for the key PBPs. Thus, for subsequent analysis, silicristin was selected for structural optimization against the key PBPs for the possibility of yielding novel drug candidate with enhanced antibacterial efficiency, higher stability, reduced toxicity and favorable pharmacokinetics relative to silicristin.

1.2 Structural optimization of silicristin against key penicillin-binding proteins of selected clinically important bacteria yielded putatively potent chalcone bis-coumarin derivatives

Silicristin although had good potential as a promising PBPs modulator, can also instigate significant thermodynamic disorderliness in essential PBPs of common and clinically important bacteria. In this regard, this study optimizes silicristin by taking understanding from the interactions of silicristin with key PBPs of *S. aureus*, *P. aeruginosa*, *E. coli* and *S. pneumoniae* in designing novel compounds. The hybridization of pharmacophore (coumarin moieties)

(Pawełczyk *et al.,* 2018) and structural simplification of silicristin by shortening unnecessary groups/molecules/ring that are not actively involved in the interactions of the key PBPs were employed in designing novel derivatives. The observation of zero hit following screening of the derivatives through ChEMBL database, might suggest the uniqueness of the 25 newly designed chalcone bis-coumarin derivatives. However, the fact that over 349 hits were observed in the similarity search for silicristin suggests that various metabolites such as silicristin or those with silicristin-like moieties occur in nature and have been profiled and deposited in ChEMBL databases. The significant improvement in the thermodynamic binding free energy, stability and pharmacokinetic properties of the best derivatives [RD2c against PBP3 of *E. coli*, RD1c against PBP3 of *P. aeruginosa*, RD1c against PBP2x active site of *S. pneumoniae*, RD1a against PBP2a active site of *S. aureus*, D1a against PBP5 of *E. coli*, D1h against the allosteric site of PBP2a of *S. aureus* and PBP2x of *S. pneumoniae*] relative to silicristin following *in silico* evaluation, an observation that could translate to enhanced potency *in vitro* and *in vivo*, suggest the effectiveness of the retrosynthetic approaches used. The importance of the retrosynthetic approaches used in this study in the improvement of desired qualities of a compound while also reducing shortcomings have been appreciated by earlier studies as an appealing source of drug candidate for drug discovery (Barcelos *et al.*, 2022, Wang *et al.*, 2019, Pawełczyk *et al.* 2018). Aside the effectiveness of the retrosynthetic techniques used in the derivatization of the novel derivatives, the coumarin moieties used in their build-up may have contributed to their enhanced binding interaction relative to silicristin at the binding pockets of the key PBPs. Prior studies have shown that natural products and synthesized molecules with coumarin structure exhibit good and broad-spectrum biological properties, including antibacterial activities (Singh *et al*., 2019; Hu *et al*., 2018; Hamdi *et al.*, 2010; Gao *et al.*, 2018). Also, aside their reported antibacterial activities, coumarins and their analogues

have been shown to display relatively low cardiotoxicity, cutaneous toxicity, nephrotoxicity, hepatotoxicity, and other adverse effects, making them an attractive contender in drug development (Hamdi *et al.*, 2010; Gao *et al*., 2018). Similarly, the chalcone, which serves as a precursor in hybridizing the coumarin moieties in this study, has been demonstrated to be an effective antibacterial owing to the presence of the reactive αβ-unsaturated system, and the modification at both end of the chalcone using coumarins facilitated increase potency, reduce toxicity, and broaden pharmacological action of the lead derivatives (Dhaliwal *et al*., 2022). The observed enhanced binding capability of the best derivatives was noted to be due to their higher reactivity, better electrostatic potential and improved hydrogen bonding capability with key essential amino acids at the binding pocket of the investigated PBPs. This observation allows for the understanding of the molecular information relevant for the practical applications of the derivatives as therapeutic molecules (Du *et al*., 2016 and Bissantz *et al*., 2010). The exploration of catechol, resorcinol, and hydroquinone either alone or in combination with each other at either end of the derivatives promotes good pharmacological properties, while the presence of a pyrogallol and/or a benzene ring with more than two hydroxy group at one or both ends of the derivatives caused reduced oral bioavailability relative to silicristin. This observation is consistent with earlier studies where the presence and positioning of hydroxyl group of phenolics had influence on the variation of pharmacological properties (Lobiuc *et al*., 2023; Kumar *et al.*, 2019; Maddox *et al*., 2010). As the best derivative in each case of the PBPs are compounds that do not form naturally, their synthesis is therefore paramount to enable further evaluation of their biological activities *in vitro* and *in vivo*. In this study, the good correlation of the ^{13}C Nuclear magnetic resonance spectroscopy (NMR) analysis of the experimentally and computationally obtained ppm for several carbon atoms of the synthesized parent compound of the best derivatives,

confirmed the synthesis of the parent compound. The best derivative in each case of the key PBPs had a similar synthetic route as the parent compound, hence, their successful synthesis using similar approach are achievable, thus enabling their *in vitro* and *in vivo* potency evaluation for the possibility of subsequent development as beta-lactams.

1.3 *In vitro* antibacterial validation and evaluation of the involvement of reactive oxygen species (ROS) in the lethality of silicristin and parent compound of novel derivatives of chalcone bis coumarin (PSCB)

The continuous emergence of antibiotic resistance in bacteria to beta-lactams has necessitated the need for alternative strategies to overcome this threat. Among the strategies is the identification and development of therapeutics whose mechanism of action would depend primarily on ROS generation while having the capability to binds to essential therapeutic targets. The ability of silicristin to bind to key PBPs of common and clinically important bacteria has been demonstrated *in silico,* however, in this aspect of the study, the translation of this binding into antibacterial activities as well as the possibility of ROS involvement in the activities was validated. The observations that silicristin and parent compound of novel derivative of chalcone bis coumarin (PSCB) had antibacterial activity against both the sensitive and multidrug resistant strains of *E. coli*, *S. aureus*, *S. pneumoniae* and *P. aeruginosa* in a concentration- and time-dependent manner validated the broad spectrum *in silico* binding free energy observed in this study against the key PBPs. Based on the MIC assessment, the observation that silicristin, PSCB and reference beta-lactams had higher MIC values against the resistant strains relative to the sensitive strains confirm the resistant status of the resistant bacteria used in the study. The higher resistant of both strains of *P. aeruginosa* to silicristin, PSCB and cefotaxime (reference beta-lactam antibiotic) relative to other organisms in this study attest to the reason while infections caused by the organisms are

relatively very difficult to treat. However, the significant lesser MIC values of silicristin and PSCB against all the investigated bacteria relative to the range (100 -1000 µg/ml) reported by Simões *et al*. (2009) for phytocompounds, suggest the relatively potent antibacterial effects of silicristin and PSCB. Comparatively, except against the sensitive and resistant strains of *E. coli* where treatment with silicristin had a comparable killing effect as cefotaxime, treatment with silicristin had a better killing rate than PSCB and reference beta-lactams against all the test organisms. This observation further demonstrates the antibacterial effects of silicristin and could be attributed to the presence of the characteristic hydroxyl group of the compound which have been implicated in strong PBP binding (Alhadrami *et al*., 2020; Avila *et al*., 2008) and autoxidation for enhanced ROS generation (Ajiboye *et al*., 2017). The lack of the characteristic hydroxyl group in PSCB might have been responsible for the lesser antibacterial effects of PSCB relative to silicritin. Further analysis into the antibacterial action of silicristin and PSCB showed that except in the combination of silicristin and amoxicillin against the resistant strain of *E. coli* where addictive effect was noted, silicristin had synergistic effect with both amoxicillin and cefotaxime against all the test organisms. This observation not only suggests that silicristin enhance the potency of beta-lactams, but also means that silicristin has other mechanisms of actions that is different from beta-lactams, such as its ability to bind to the allosteric site of PBPs of Gram-positive organism as earlier noted in this study. Other mechanism such as the ability to generate ROS while increasing affinity for cytoplasmic membranes have also been reported for phenolics (Ajiboye *et al*., 2017; Zeraik *et al*., 2014). The ability of silicristin to enhance the effect of beta-lactam in this study is consistent with prior study where phenolics such as morin and quercetin enhanced the activity of ciprofloxacin and tetracycline against different strains of *S. aureus* including methicillin resistant strain (Abreu *et al*., 2014). PSCB on the other had only had synergistic effects with cefotaxime and amoxicillin

against resistant strains of *S. aureus* and *S. pneumoniae*, suggestive of the possibility of similar mechanisms of action as beta-lactams. A further probe into the ROS generating potential of the antibacterial agents using ROS-specific dyes, showed that while PSCB and reference beta-lactams caused significant ($P < 0.05$) higher generation of superoxide ion ($O_2^{\bullet-}$), silicristin conversely enhanced higher ($P < 0.05$) generation of the most toxic ROS form, the hydroxy radicals ($^{\bullet}OH$), which is often produced via the Fenton reaction. This observation with silicristin suggests its enhanced modulatory effect on Fenton reaction relative to PSCB and the standards and further facilitated increased NAD/NADH ratio, ADP/ATP ratio, lipid peroxidation, carbonyl content, propidium iodide (PI) uptake, and depletion of reduced glutathione as observed with silicristin-treated cells. This finding points to the enhanced involvement of oxidative stress in the modulatory effect of silicristin against all the test organisms compared to PSCB and the reference standards and is consistent with prior studies which established that normal cells maintain a finely controlled and well-balanced redox state due to the continual generation and detoxification of cellular ROS (Vaishampayan *et al*., 2022; Lam *et al*., 2020). However, in the presence of exogenous stressors, such as antibacterial agents, normal process of respiration and microbial metabolism might lead to increased formation of endogenous ROS and degeneration of defense systems which could be lethal to cellular macromolecules such as lipids, and proteins (Vaishampayan *et al*., 2022; Lam *et al*., 2020; Yoon *et al*., 2002). The observation that the reference beta-lactams and PSCB had comparable ROS generation in terms of $^{\bullet}OH$ radical had effects on their similar rate of depletion of reduced glutathione and damage to cellular macromolecule which further lent credence to the study's earlier observation that the two antibacterial agents might share common mechanism of action. The enhanced oxidative stress in cells treated with silicristin was also complemented by scanning electron microscopy (SEM) and transmission electron microscopy (TEM) micrographs

with cell walls with more blisters, eruptions, and sores compared to the untreated cells, PSCB-treated cells and cefotaxime-treated cells. Oxidative stress was also noted to facilitate SOS (Save Our Souls) response in upregulating *SordA* and *SoxR*, with the most prominent effect observed with silicristin in a manner that is more evident in the sensitive strains relative to the resistant strains. The observation that silicristin instigated the highest upregulation of *SodA* and *SoxR* relative to PSCB and reference beta-lactams could mean that the upregulation of both regulons is not exclusive to superoxide ion $O_2^{\bullet-}$ generation as earlier noted in literature (Xiong *et al*., 2017; Imlay, 2013) since silicristin generated lesser $O_2^{\bullet-}$ compared to PSCB and cefotaxime treated cells in this study. This observation is consistent with the report of Gu and Imlay (2011), that redox cycling drugs rather than $O_2^{\bullet-}$ instigate the upregulation of *SoxRS*. More importantly as silicristin is a phenolic compound which has been demonstrated for their great redox cycling potential in the presence of transition metals and oxygen (Ajiboye *et al*., 2017). The observation that an enhanced oxidative stress was noted in the sensitive strains and Gram-positive organisms relative to resistant strains and Gram-negative organisms is in tandem with the antibacterial killing effects of this study thus further highlighting the involvement of oxidative stress in the lethality of silicristin, PSCB and reference beta-lactams.

Overall, this study showed that silicristin had an enhanced redox effect in the killing of sensitive and multi-resistant strains of both Gram-positive and Gram-negative organisms compared to PSCB and the reference beta-lactams used. Thus, silicritin and its mechanism of action could potentially be exploited in the development of new beta-lactams whose action will be primarily through generation of ROS while having the capability to inactivate key PBPs in the treatment of infections caused by the test organisms.

2.0 Conclusions and recommendations

Beta-lactams are and will continue to be a key agent in the treatment of common and clinically important bacterial infections. Nevertheless, the emergence of resistant isolates due to mutations in cell wall-synthesizing PBPs and other important resistance mechanisms has complicated treatment procedures of many infections, and this has constituted a great concern. Accordingly, this study used a multifaceted *in silico* and *in vitro* approach in screening and identifying potent phenolics and novel compounds with anti-PBPs and ROS generating potentials.

The *in silico* screening of the over 10,000 phenolics currently in existence identified lead phenolics with higher negative binding free energy, better stability and higher capability of forming important hydrogen bond interactions with critical amino acids residues of the key PBPs of the investigated bacterial relative to the reference standards. The filtering of the top-20 leads in each case of the key PBPs based on their physicochemical, pharmacokinetic and toxicological profiles afforded top-five phenolics that are chemically diverse, orally bioavailable and with good synthetic feasibility scores (<5) appropriate for drug development. In PBP2a of *S. aureus* and PBP2x of *S. pneumoniae* with allosteric site that can modulate critical amino acid of the active site, *in silico* investigation of the top-ranked phenolics at this site identified epicatechin gallate and silicristin against PBP2a and PBP2x, respectively, as lead compound. This observation suggests that the compound in each case of the target could function in combinatory therapy with beta-lactams in treating infection caused by *S. aureus* and *S. pneumoniae*. Of the top-five phenolics in each case of the key PBPs, silicristin remain the only compound with affinity that cuts across all the key PBPs, and its higher negative binding free energy relative to the reference standard (amoxicillin), points to its superior PBPs modulatory capability. However, the significant perturbation induced by silicristin as evident from the mean RMSD values in three of the investigated key PBPs (PBP2a

of *S. aureus*, PBP2x of *S. pneumoniae* and PBP3 of *E. coli*) prompted the need for its structural modification for improved stability and affinity of the resulting derivatives for the key PBPs being investigated. While silicristin was selected for further structural modification and subsequent *in vitro* studies, it is recommended that the *in vitro* validation of other lead phenolics including lysidicichin and epigallocatechin 4-benzylthioether against PBP3 and PBP5 of *E. coli*, catechin 3-rhamside against PBP3 of *P. aeruginosa* and epicatechin 3-O-(3-O-methylgallate against the active site of PBP2x, be exploited. The synthetic feasibility scores observed for each of the lead phenolics suggest that further structural modification as done for silicristin in this study could be exploited in the case of moderate or an ineffective activity *in vitro*. Exploration of the lead compounds in this manner may identify novel compounds with well-defined mechanism of action that might help towards the management of resistance to beta-lactams.

The structural alteration of silicritin against the essential PBPs of the investigated bacteria yielded 25 novel derivatives of chalcone bis-coumarin. Subsequent *in silico* screening of the 25 derivatives identified lead derivatives [RD2c against PBP3 of *E. coli*, RD1c against PBP3 of *P. aeruginosa*, RD1c against PBP2x active site of *S. pneumoniae*, RD1a against PBP2a active site of *S. aureus*, D1a against PBP5 of *E. coli*, D1h against the allosteric site of PBP2a of *S. aureus* and PBP2x of *S. pneumoniae*] with significant improvement in thermodynamic binding free energy, stability and pharmacokinetic relative to silicristin. The observed enhanced binding capability of the best derivatives could be attributed to their higher reactivity, better electrostatic potential and improved hydrogen bonding capability with essential amino acids at the binding pocket of the investigated PBPs. The exploration of catechol, resorcinol, and hydroquinone either alone or in combination with each other at either end of the derivatives promoted good pharmacological properties. While the presence of a pyrogallol and/or a benzene ring with more than two hydroxy group at one or

both ends of the derivatives caused reduced oral bioavailability relative to silicrsitin. The ^{13}C NMR analysis showed a good correlation between the experimentally and computationally obtained ppm for several carbon atoms of the synthesized parent compound (PSCB) of the best derivatives, confirming the reliability of the adopted synthetic route. Since the best derivative in each case of the key PBPs had a similar synthetic route as the parent compound, it is recommended that the established synthetic route be followed in the synthesis of the best derivatives to enable the evaluation of their *in vitro* and *in vivo* activities for the possibility of subsequent development as beta-lactam alternatives.

Subsequently, the *in vitro* antibacterial activity and the possible involvement of oxidative stress in the lethality of silicristin, and PSCB were investigated using conventional beta-lactam antibiotic as a reference standard. The antibacterial activity of silicristin and PSCB against both the sensitive and multidrug resistant strains of *E. coli*, *S. aureus*, *S. pneumoniae* and *P. aeruginosa* was concentration- and time-dependent. Comparatively, except against the sensitive and resistant strains of *E. coli* where treatment with silicristin had a comparable killing effect as cefotaxime, silicristin had a better killing rate than PSCB and reference beta-lactams against all the test organisms. The enhanced killing effect of silicristin over PSCB and reference beta-lactams is hypothesized to be due to its characteristic hydroxyl group, which must have promoted its strong PBP binding and auto-oxidation for enhanced ROS generation. Silicristin with amoxicillin and cefotaxime had synergistic effects against all the test organisms except resistant strain of *E. coli*. In contrast, PSCB with cefotaxime and amoxicillin had only synergistic effect against the resistant strains of Gram-positive bacteria. This observation suggests that silicristin could function in combination therapy with both cefotaxime and amoxicillin in the treatment of infections caused by both the sensitive and resistant strains of *E. coli, S. aureus, S. pneumoniae* and *P. aeruginosa.*

This is of great importance as combinatory therapy is attracting great interest in the treatment of difficult infections as it addresses problems related to resistance while providing broad-spectrum antibacterial activity with minimal toxicological concerns. PSCB on the other hand only had synergistic effects with cefotaxime and amoxicillin against resistant strains of Gram-positive organism. Probing into the ROS generation potential of the test antibacterials revealed that treatment with PSCB and reference beta-lactams enhanced increased $O_2^{\bullet-}$ generation, while increased level of Fenton reaction-linked $^{\bullet}OH$ radicals, was observed following treatment with silicristin. Hydroxy radicals remain the most toxic ROS to bacteria and this was evidently demonstrated in this study, where significantly increased levels of NAD/NADH ratio, ADP/ATP ratio, MDA, carbonyl content, PI uptake, with concomitant depletion of reduced glutathione were observed with silicristin-treated cells. This clearly suggests that ROS and oxidative stress contributed more to the modulatory effect of silicristin (Figure 36) against the test organisms compared to PSCB and the reference beta-lactams. The enhanced oxidative stress in cells treated with silicristin was further substantiated by SEM and TEM micrographs with cell walls with more blisters, eruptions, and sores compared to both the untreated and cefotaxime-treated cells (Figure 32). Oxidative stress was also noted to facilitate SOS (Save Our Souls) response in the form of upregulation of *SordA* and *SoxR* in the sensitive strains of *E. coli* and *S. aureus* and in this regard silicristin caused the highest upregulation thus linking the expression of the genes to ROS generation in cells. Overall, enhanced oxidative stress was observed more in the sensitive strains and Gram-positive organisms relative to resistant strains and Gram-negative organisms an observation that is consisting with the antibacterial killing effects of this study thus further highlighting the involvement of oxidative stress in the lethality of silicristin, PSCB and reference beta-lactams. The results of this study showed that silicristin had an improved redox effect in

killing the sensitive and multi-resistant strains of both Gram-positive and Gram-negative organisms compared to the reference beta-lactams, and it could potentially be used in the development of new therapeutics whose mechanism of action will be primarily through the generation of ROS to treat infections caused by the test organisms.

References

Abreu, A.C.; Serra, S.C.; Borges, A.; Saavedra, M.J.; Mcbain, A.J.; Salgado, A.J.; Simões, M. Combinatorial activity of flavonoids with antibiotics against drug-resistant *Staphylococcus aureus*. *Microb. Drug Resist*. **2015**, 6, 600 - 609. https:/doi.org/10.1089/mdr.2014.0252.

Acharya, A.; Agarwal, R.; Baker, M. B. Baudry, J.*et al*. Supercomputer-based ensemble docking drug discovery pipeline with application to Covid-19. *Chem. Inf. Model*. **2020**, 60, 5832 – 5852. https://doi.org/10.1021/acs.jcim.0c01010

Ahmad, N.; Dugad, S.; Chauhan, V.; Ahmed, S.; Sharma, K.; Kachhap, S.; Zaidi, R.; Bishai, W.R.; Lamichhane, G.; Kumar, P. Allosteric cooperation in β-lactam binding to a non-classical transpeptidase. *eLife*. **2022,** 11, e73055. https://doi.org/10.7554/eLife.73055

Ajiboye, T.O.; Habibu, R.S.; Saidu, K.; Haliru, F.Z.; Ajiboye, H.O.; Aliyu, N.O.; Ibitoye, O.B.; Uwazie, J.N.; Muritala, H.F.; Bello, S.A.; Yusuf, I.I.; Mohammed, A.O. Involvement of oxidative stress in protocatechuic acid-mediated bacterial lethality. *Microbiologyopen* **2017**, 6, e00472. https:/doi.org/10.1002/mbo3.472

Alhadrami, H.A.; Hamed, A.A.; Hassan, H.M.; Belbahri, L.; Rateb, M.R.; Sayed, A.M. Flavonoids as potential anti-MRSA agents through modulation of PBP2a: a computational and experimental study. *Antibiotics.* **2020**, 9, 562. https://doi.org/10.3390/antibiotics9090562

Avila, H.P.; Smânia, F.A.; Monache, F.D.; Smânia, A.Jr. Structure−activity relationship of antibacterial chalcones. *Bioorg Med Chem*. **2008,** 16, 9790 – 9794. https:/doi.org/10.1016/j.bmc.2008.09.064

Barcelos, M.P.; Gomes, S.Q.; Fedrico, L.B.; Francischini, I.A.G.; Melim, L.L.D.; Silva, G.M.; Silva, C.H.T. Lead Optimization in Drug Discovery. In: Taft, C.A., de Lazaro, S.R. (eds) Research Topics in Bioactivity, Environment and Energy. Engineering Materials. *Springer, Cham*. **2022,** https://doi.org/10.1007/978-3-031-07622-0_19

Bissantz, C.; Kuhn, B.; Stahl, M.A. Medicinal chemist's guide to molecular interactions. *J Med Chem*. **2010**, 14, 5061 - 5084. https://doi.org/10.1021/jm100112j.

Bush, K. Past and present perspectives on b-lactamases. *Antimicrob Agents Chemother*. **2018**, 62, e01076 - e1118. https://doi.org/10. 1128/AAC.01076-18.

Cerón-Carrasco, J.P. When virtual screening yields inactive drugs: dealing with false theoretical friends. *ChemMedChem*. **2022**, 17, e202200278. https:/doi.org/10.1002/cmdc.202200278.

Cho, H.; Uehara, T.; Bernhardt, T.G. Beta-lactam antibiotics induce a lethal malfunctioning of the bacterial cell wall synthesis machinery. *Cell*. **2014**, 159, 1300 – 1311. https://doi.org/10.1016/j. cell.2014.11.017.

Dhaliwal, J.S.; Moshawih, S.; Goh, K.W.; Loy, M.J.; Hossain, M.S.; Hermansyah, A.; Kotra, V.; Kifli, N.; Goh, H.P.; Dhaliwal, S.K.S.; Yassin, H.; Ming, L.C. Pharmacotherapeutics applications and chemistry of chalcone derivatives. *Molecules*. **2022**, 19, 7062. https:/doi.org10.3390/molecules27207062.

Du, X.; Li, Y.; Xia, Y.L.; Ai, X.M.; Liang, J.; Sang, P.; Ji, X.L.; Liu.S.Q. Insights into protein-ligand interactions: mechanisms, models, and methods. *Int J Mol Sci*. **2016**, 17, 144. https://doi.org/10.3390/ijms17020144

Eghbaliferiz, S.; Iranshahi, M. Prooxidant activity of polyphenols, flavonoids, anthocyanins and carotenoids: updated review of mechanisms and catalyzing metals. *Pharmacol Res.* **2016**, 30, 1379 – 1391. https://doi.org/10.1002/ptr.5643

Eiamphungporn, W., Schaduangrat, N., Malik, A. A., and Nantasenamat, C. Tackling the antibiotic resistance caused by class A beta-lactamases through the use of beta-lactamase inhibitory protein. *Int J Mol Sci.* **2018**, 19, 2222. https://doi.org/10.3390/ijms19082222.

Ertl, P.; Schuffenhauer, A. Estimation of synthetic accessibility score of drug-like molecules based on molecular complexity and fragment contributions. *J. Cheminform.* **2009**, 1, 8–11. https://doi.org/10.1186/1758-2946-1-8

Fisher, J.F.; Mobashery, S. B-Lactam resistance mechanisms: Gram-positive bacteria and Mycobacterium tuberculosis. *Cold Spring Harb Perspect Med*. **2016**, 6, a025221. https://doi.org/10.1101/ cshperspect.a025221.

Gao, T.; Zeng, Z.; Wang, G.; Sun, S.; Liu, Y. Synthesis of ethylene tethered isatin-coumarin hybrids and evaluation of their *in vitro* antimycobacterial activities. *J Heterocycl Chem.* **2018**, 55, 1484-1488. https://doi.org/10.1002/jhet.3161

Glen, K.A.; Lamont, I.L. beta-lactam resistance in *Pseudomonas aeruginosa*: current status, future prospects. *Pathogens.* **2021**, *10*, 1638. https://doi.org/10.3390/pathogens10121638

Gu, M.; Imlay, J.A. The *SoxR*S response of *Escherichia coli* is directly activated by redox-cycling drugs rather than by superoxide. *Mol Microbiol.* **2011**, 5, 1136 - 1150. https:/doi.org/10.1111/j.1365-2958.2010.07520

Hamdi, N.; Bouabdallah, F.; Romerosa, A.; Benhassen, R. Expedious synthesis for α, β-unsaturated coumarin derivatives using boran chelates: a novel class of potential antibacterial and antioxidant agents *Comptes Rendus Chim.* **2010**, 13, 1261 - 1268. https:/doi.org10.1016/j.crci.2009.10.001

Hecker, S.J.; Reddy, K.R.; Totrov, M.; Hirst, G.C.; Lomovskaya, O.; Griffith, D.C.; King, P.; Tsivkovski, R.; Sun. D.; Sabet, M.; Tarazi, Z.; Clifton, M.C.; Atkins, K.; Raymond, A.; Potts, K.T.; Abendroth, J.; Boyer, S.H.; Loutit, J.S.; Morgan, E.E.; Durso, S.; Dudley, M.N. Discovery of a cyclic boronic acid beta-lactamase inhibitor (RPX7009) with utility vs class a serine carbapenemases. *J. Med. Chem.* **2015**, 58, 3682 – 3692. https://doi.org/10.1021/acs.jmedchem.5b00127.

Hu, Y.; Shen, Y.; Wu, X.; Tu, X.; Wang, G.X. Synthesis and biological evaluation of coumarin derivatives containing imidazole skeleton as potential antibacterial agents. *Eur. J. Med. Chem.* **2018**, 143, 958 - 969. 10.1016/j.ejmech.2017.11.100

Imlay, J. A. The molecular mechanisms and physiological consequences of oxidative stress: Lessons from a model bacterium. *Nat Rev Microbiol.* **2013**, 11, 443 – 454. https:/doi.org/10.1038/nrmicro3032.

Izadi, H.; Stewart, K.M.E.; Penlidis. A. Role of contact electrification and electrostatic interactions in gecko adhesion. *J R Soc Interf.* **2014,** 11, 371 - 398. https://doi.org/10.1098/rsif.2014.0371

Kretschmer, R.; Kinzel, D.; Gonza´ Lez, L. The Role of hydrogen bonds in protein – ligand interactions. DFT calculations in 1,3-Dihydrobenzimidazole-2 thione derivatives with

glycinamide as model HIV RT inhibitors. *Int. J. Quantum Chem*. **2010**, 112, 1787 - 1795. https://doi.org/10.1002/qua.23001

Kumar, N.; Goel, N. Phenolic acids: Natural versatile molecules with promising therapeutic applications. *Bio Rep.* **2019**, 24, e00370. https://doi.org/10.1016/j.btre.2019.e00370.

Lam, P.L.; Wong, R.S.M.; Lam, K.H.; Hung, L.K.; Wong, M.; Yung, L.H.; Ho, Y.W.; Wong, W.Y.; Hau, D.K.P.; Gambari, R.; Chui CH. The role of reactive oxygen species in the biological activity of antimicrobial agents: an updated Mini Review. *Chem-Biol Interact.* **2020**, 320, 109023. https:/doi.org/10.1016/j.cbi.2020.109023

Lipinski, C.A.; Lombardo, F.; Dominy, B.W.; Feeney, P.J. Experimental and computational approaches to estimate solubility and permeability in drug discovery and development settings. *Adv Drug Deliv Rev*. **2001**, 46, 3 – 26. https://doi.org/10.1016/s0169-409x(00)00129-0.

Lobiuc, A.; Pavăl, NE.; Mangalagiu, II.; Gheorghiță, R.; Teliban, G.C.; Amăriucăi-Mantu, D.; Stoleru, V. Future antimicrobials: natural and functionalized phenolics. *Molecules*. **2023**, 22, 1114. https:/doi.org/10.3390/molecules28031114.

Maddox, C.E.; Laur, L.M. Tian, L. Antibacterial activity of phenolic compounds against the phytopathogen *Xylella fastidiosa*. *Curr Microbiol.* **2010**, **60**, 53 – 58. https://doi.org/10.1007/s00284-009-9501-0

Mousavi, S.S.; Karami, A.; Haghighi, T.M.; Tumilaar, S.G.; Idroes, R.; Mahmud, S.; Celik, I.; Aˇgagündüz, D.; Tallei, T.E.; Emran, T.B.; Capasso, R. *In Silico* evaluation of Iranian medicinal plant phytoconstituents as inhibitors against main protease and the receptor-binding domain of SARS-CoV-2. *Molecules*, **2021**, 26, 5724. https://doi.org/10.3390/molecules26185724.

Palacios, A.R.; Rossi, M.A.; Mahler, G.S.; Vila, A.J. Metallo-beta-lactamase inhibitors inspired on snapshots from the catalytic mechanism. *Biomolecule.* **2020**, 10, 854. https://doi.org/10.3390/biom10060854.

Pawełczyk, A.; Sowa-Kasprzak, K.; Olender, D.; Zaprutko, L. Molecular consortia—various structural and synthetic concepts for more effective therapeutics synthesis. *Int. J. Mol. Sci.* **2018**, *19*, 1104. https://doi.org/10.3390/ijms19041104

Ramirex, D.; Caballero, J. Is it reliable to use common molecular docking methods for comparing the binding affinities of Enantiomer pairs for their protein target. *Int. J. Mol. Sci*. **2016,** 17, 525 - 545. https://doi.org/10.1016/j.biotechadv.2018.11.013

Reichel, A.; Lienau, P. Pharmacokinetics in Drug Discovery: An exposure-centred approach to optimising and predicting drug efficacy and safety. *Handb Exp Pharmacol.* **2016**, 232, 235 - 260. https://doi.org/10.1007/164_2015_26.

Santiago, C.; Pang, E.L.; Lim, K.H.; Loh, H.S.; Ting, K.N. Inhibition of penicillin-binding protein 2a (PBP2a) in methicillin resistant *Staphylococcus aureus* (MRSA) by combination of ampicillin and a bioactive fraction from *Duabanga grandiflora*. *BMC Complement Altern Med*. **2015**, 10, 178. https:/doi.org/10.1186/s12906-015-0699-z.

Simões M.; Bennett, R.N.; Rosa, E.A.S. Understanding antimicrobial activities of phytochemicals against multidrug resistant bacteria and biofilms. *Nat. Prod. Rep*. **2009**, 26, 746 – 757. https:/doi.org/10.1039/b821648g.

Singh, A.; Singh, J.V.; Rana, A.; Bhagat, K.; Gulati, H.K.; Kumar, R.; Salwan, R.; Bhagat, K.; Kaur, G.; Singh, N.; Kumar, R.; Singh, H.; Sharma, S.; Bedi, P.M.S. Monocarbonyl curcumin-

based molecular hybrids as potent antibacterial agents. *ACS Omega*. **2019,** 4, 11673-11684. https:/doi.org/10.1021/acsomega.9b01109.

Tabassum, R.; Kousar, S.; Mustafa, G.; Jamil, A. Attique SA. *In Silico* method for the screening of phytochemicals against methicillin-resistant *Staphylococcus Aureus*. *Biomed Res Int*. **2023**, 18, 5100400. https:/doi.org/10.1155/2023/5100400.

Tooke, C.L.; Hinchliffe, P.; Bragginton, E.C.; Colenso, C.K.; Hirvonen, V.H.A.; Takebayashi, Y.; Spencer, J. Beta-lactamases and beta-lactamase inhibitors in the 21st century. *J Mol Biol*. **2019**, 431, 3472 – 500. https://doi.org/10.1016/j.jmb.2019.04.002.

Vaishampayan, A.; Grohmann, E. Antimicrobials Functioning through ROS-mediated mechanisms: current insights. *Microrganisms* **2022**, 10, 61, https:/doi.org/10.3390/microorganisms10010061.

Wang, S.; Dong, G.; Sheng, C. Structural simplification: an efficient strategy in lead optimization. *Acta Pharm Sin B*. **2019**, 5, 880 - 901. https:/doi.org/10.1016/j.apsb.2019.05.004.

Wei, H.; Jin, Z.; Wang, Y.; Yang, F.; Xiao, Y.; Jiang, Y.; Hu, J.; Gao, M.T. Antibacterial effect of phenolic acids derived from rice straw and in combination with antibiotics against *Escherichia coli*. *Appl Biochem Biotechnol*. **2022**,194, 2931 - 2945. https:/doi.org/10.1007/s12010-021-03650-5

Xiong, L.G.; Chen, Y.J.; Tong, J.W.; Huang, J.A.; Li, J.; Gong, Y.S.; Liu, Z.H. Tea polyphenol epigallocatechin gallate inhibits *Escherichia coli* by increasing endogenous oxidative stress. *Food Chem.* **2017,** 217, 196 - 204. https:/doi.org/10.1016/j.foodchem.2016.08.098.

Yoon, S.J.; Park, J.E.; Yang, J.H.; Park, J.W. OxyR regulon controls lipid peroxidation-mediated oxidative stress in *Escherichia coli*. *J Biochem Mol Biol.* **2002**, *35*, 297 – 301. https:/doi.org/10.5483/bmbrep.2002.35.3.297.

Zeraik, M.L.; Petrônio, M.S.; Coelho, D.; Regasini, L.O.; Silva, D.H.; da Fonseca, L.M.; Machado, S.A.; Bolzani, V.S.; Ximenes, V.F. Improvement of pro-oxidant capacity of protocatechuic acid by esterification. *PLoS One*. **2014**, 9, e110277. https:/doi.org/10.1371/journal.pone.0110277.